



**HAL**  
open science

# Les aérogels de pectine : matériaux avancés pour l'isolation thermique et la libération de médicaments

Sophie Groult

► **To cite this version:**

Sophie Groult. Les aérogels de pectine : matériaux avancés pour l'isolation thermique et la libération de médicaments. Matériaux. Université Paris sciences et lettres, 2019. Français. NNT : 2019PSLEM016 . tel-02420381

**HAL Id: tel-02420381**

**<https://pastel.hal.science/tel-02420381>**

Submitted on 19 Dec 2019

**HAL** is a multi-disciplinary open access archive for the deposit and dissemination of scientific research documents, whether they are published or not. The documents may come from teaching and research institutions in France or abroad, or from public or private research centers.

L'archive ouverte pluridisciplinaire **HAL**, est destinée au dépôt et à la diffusion de documents scientifiques de niveau recherche, publiés ou non, émanant des établissements d'enseignement et de recherche français ou étrangers, des laboratoires publics ou privés.



**THÈSE DE DOCTORAT**  
**DE L'UNIVERSITÉ PSL**

Préparée à MINES ParisTech

**Pectin-based aerogels:**

Advanced materials for thermal insulation  
and drug delivery applications

**Les aérogels de pectine :**

Matériaux avancés pour l'isolation thermique  
et la libération de médicaments

Soutenue par

**Sophie GROULT**

Le 28 mai 2019

Ecole doctorale n° 364

**Sciences Fondamentales  
et Appliquées**

Spécialité

**Mécanique numérique  
et Matériaux**

**Composition du jury :**

Arnaud RIGACCI Professeur des universités, PERSEE-Mines ParisTech	<i>Président du jury</i>
Orlando ROJAS Professor, Aalto University	<i>Rapporteur</i>
Didier LE CERF Professeur des universités, Université de Rouen	<i>Rapporteur</i>
Kirsi S. MIKKONEN Assistant Professor, University of Helsinki	<i>Examineur</i>
Jacques MAZOYER Doctor, Principal scientist at Cargill	<i>Examineur</i>
Tatiana BUDTOVA Directeur de recherche, CEMEF-Mines ParisTech	<i>Directrice de thèse</i>



## Remerciements

Ce travail de thèse a été réalisé au Centre de Mise en Forme des Matériaux (CEMEF) de Mines ParisTech (France). Une partie de ces travaux a été menée en collaboration avec l'institut de chimie macromoléculaire P. Poni (Iasi, Roumanie) dans le cadre du projet BIOGELS (projet n° 38322XD) au sein du programme bilatéral France-Roumanie PHC BRANCUSI 2017.

En premier lieu, je souhaite remercier ma directrice de thèse, Tatiana Budtova. Tania, je ne sais comment résumer avec de simples mots l'ensemble de ce que tu m'as apportée, tant du point de vue professionnel que personnel. Merci pour ta bienveillance, ta patience, ta compréhension et gentillesse infinies. Plus important encore, pour avoir perpétuellement encouragé ma curiosité scientifique, avoir cru en moi et m'avoir fait confiance. Merci pour m'avoir si bien comprise et guidée, à tantôt me rebooster, me tempérer ou me rassurer, pour au final me permettre de pleinement m'épanouir autant scientifiquement qu'humainement. A tes côtés, je suis passée de la doctorante peu assurée à une jeune chercheuse courageuse et passionnée, et à la fin je crois que tu as réussi, je me suis surprise à croire en moi-même. Je me plais à le répéter car j'en suis intimement convaincue, ces années de thèse ont été sincèrement les plus belles de ma vie et c'est aussi grâce à toi.

Je remercie les membres de mon jury pour avoir accepté d'évaluer mon travail de thèse : Pr. Orlando Rojas et Pr. Didier Le Cerf d'avoir été mes rapporteurs, ainsi que Pr. Arnaud Rigacci, Dr. Kirsi Mikkonen et Dr. Jacques Mazoyer d'avoir été mes examinateurs. Merci pour votre bienveillance, votre considération et vos commentaires positifs qui m'ont beaucoup touchée. Et merci pour les nombreuses questions initiant des discussions riches et passionnantes via des prismes variés : scientifique, technologique, industriel, écologique, éthique ou lié à la santé.

Du plus profond de mon cœur, je adresse ma reconnaissance infinie à mes proches, mes ami-e-s et ma famille qui m'ont accompagnée et soutenue durant ce périple :

Tout particulièrement Lucile Druel, ma co-bureau, mon binôme de thèse et avant tout mon amie. Comment exprimer mon infinie gratitude avec des mots ? Comme nous nous le sommes répété pendant 3 ans : « Nous avons commencé ensemble et nous allons terminer (avec brio) ensemble ! ». Jamais l'une sans l'autre ! Nous avons immédiatement formé notre petit duo de choc (Team BIO represent), complémentaire et fusionnel, connu et reconnu dans tout le centre. Merci à toi pour ton amitié, ta gaieté spontanée, ta gentillesse, ton grain de folie qui ont rendu cette aventure des bio-aérogels encore plus merveilleuse. Merci pour ta présence permanente et ton soutien sans faille, et ce, jusqu'à la dernière minute sur scène avant la soutenance. Pour ta lumière et ton aide, si précieuses quand j'en ai eu besoin et que je n'oublierai jamais. Spéciale dédicace à nos coffee/tea time, nos craquages nerveux inévitables passés 19h, nos sessions gros câlins réconforts, aux millions de post-it « feel good » et de mots gentils que tu déposais absolument partout à mon intention, aux afterworks à base de gossips et de mojitos pour décompresser, aux peluches et origamis qui ont fleuris en masse dans le bureau, à nos heures passées ensemble méga-concentrées sur un calculs de maths/physique ou sur des

enquêtes « policières » dans le labo pour rétablir l'ordre et la propreté... Bref, tu le sais bien, sans toi RIEN n'aurait pas été pareil <3.

Je souhaite remercier mon compagnon Antoine, pour m'avoir accompagnée malgré la distance et le temps, pour m'avoir permis de trouver le courage d'oser un doctorat à 28 ans et m'avoir prodiguée de la force aux moments où je n'en avais plus une goutte. Pour avoir écouté chaque craquage nerveux, chaque challenge scientifique et doute sur lequel je buttais. Mais aussi et surtout d'avoir partagé et vécu en direct mes explosions de joies et de fierté, mes moments d'euphorie et d'enthousiasme, de mes petites victoires aux plus grandes réussites !

Je remercie ma famille : papa, maman, ma sœur, mes tata chéries, mes grands-parents de la terre et du ciel, et ma belle-famille d'amour pour avoir qui m'ont soutenue avec tendresse et confiance dans ce périple. Merci pour avoir cru en moi et encouragé cette petite fille qui depuis toute petite voulait être une scientifique « quand elle serait grande ». En particulier, je dédicace ce manuscrit à ma petite sœur Clara, mon étoile brillante qui me guide et m'inspire au quotidien.

Je remercie également tous mes collègues du CEMEF qui m'ont appris de leurs discipline ou expertise, m'accompagnant ainsi jusqu'au grade de chercheuse, notamment Suzanne Jacomet, Patrick Navard, Edith Peuvrel-Disdier, Rudy Valette, Gabriel Monge, Alain Burr, Frédéric Georgi, Gilbert Fiorucci et Marc Bouyssou. Mention très spéciale à Sélim Kraria et Hallen Ben Aissa pour avoir sauvé mes données (et ma vie) après que mon PC ait rendu l'âme brutalement 15 j avant la soutenance (argh). Je souhaite également remercier mes collègues du centre PERSEE pour leur collaboration et leur soutien, en particulier à Pierre Ilbizian pour son accompagnement bienveillant et nos discussions amicales qui m'offraient une grande bouffée d'air frais, à Laurent Schiatti de Monza pour son aide si précieuse et sa patience infinie à tenter de m'apprendre à coder, et à Arnaud Rigacci pour nos discussions et échanges chaleureux.

Un grand merci à toute la joyeuse bande de copains : à Oona K. et ton amitié sincère et dont le rire franc résonne encore dans les couloirs du CEMEF, à Romain C. mon allié, à cette porte toujours ouverte et à nos heures à discuter rhéologie, et surtout de mille autres choses, à Erika G., pour ton amitié et nos moments confidences dans le labo, à Gerry A. et ta bonne humeur, ta générosité et ton sourire, à Vincent M. pour ta bienveillance adorable, ta présence et ta main tendue dans les moments plus difficiles, à Romain F. et nos encouragements mutuels pour tenir le gouvernail du doctorat, à Ben G. l'archéo qui a amené un vent de nouveauté et de jeux de mots de haut vol dans la troupe, à Gabriella P. et Dragos P. mes amis en Roumanie pour leur générosité, à Katrina C. ma toute première stagiaire ! Et aussi toutes celles et ceux qui ont croisé ma route : Feng, Lucie, Thibault, Emilie, Catheline, Manon, Antoine, Fabien, Christophe, Danaï, Suzanne, Corentin, Geneviève, Marie-Françoise et Sylvie...

Enfin, reconnaissance éternelle à mon amour de chat Léon qui m'a supportée au quotidien, boostée et consolée à coup de ronrons et de câlins. Spéciales cassdédi au sacro-saint café soluble (par tonnes !), à la magie des licornes et évidemment à cette merveilleuse pectine (que j'ai autant aimée que boudée, selon les jours) sans quoi rien n'aurait été possible ! 😊

**C'est une page qui se tourne et croyez-moi, c'est un vrai bonheur que j'ai vécu.**





# Contents

ABBREVIATIONS AND SYMBOLS .....	10
GENERAL INTRODUCTION.....	13
ARTICLES AND COMMUNICATIONS.....	22
RESUME DES TRAVAUX DE THESE.....	25
<b>CHAPTER I. STATE OF THE ART .....</b>	<b>39</b>
<b>INTRODUCTION.....</b>	<b>42</b>
<b>1. PECTIN: STRUCTURE AND PROPERTIES .....</b>	<b>43</b>
1.1. SOURCES AND EXTRACTION OF PECTIN .....	43
1.2. CHEMICAL AND MACROMOLECULAR STRUCTURES.....	44
1.3. PHYSICO-CHEMICAL PROPERTIES OF PECTINS .....	46
1.3.1. <i>Physical acid-gelation</i> .....	47
1.3.2. <i>Ionic gelation in presence of divalent cations (called ionic gelation)</i> .....	49
1.3.3. <i>Food and pharmaceutical uses of pectin</i> .....	52
1.4. CONCLUSION ON PECTIN .....	53
<b>2. AEROGELS .....</b>	<b>54</b>
2.1. GENERALITIES ON AEROGELS .....	54
2.1.1. <i>Network formation via sol-gel route</i> .....	54
2.1.2. <i>General aspects of the drying methods</i> .....	55
2.2. CLASSICAL INORGANIC AND SYNTHETIC POLYMER AEROGELS: A BRIEF OVERVIEW.....	57
2.2.1. <i>First generation of aerogels: silica aerogels</i> .....	58
▪ The synthesis of silica aerogels.....	58
▪ Hydrophobization treatment.....	59
2.2.2. <i>Synthetic organic polymers aerogels</i> .....	60
2.2.3. <i>Applications of classical aerogels</i> .....	62
2.3. BIO-AEROGELS: THE THIRD GENERATION OF AEROGELS.....	64
2.3.1. <i>Synthesis routes of bio-aerogels: similarities and differences with inorganic and synthetic polymer aerogels</i> .....	67
▪ Network formation by polymer gelation or by direct coagulation .....	67
▪ Solvent exchange and supercritical drying .....	68
2.3.2. <i>Aerogels based on neutral polysaccharides</i> .....	70
▪ Cellulose II aerogels.....	70
▪ Starch aerogels .....	71
2.3.3. <i>Aerogels based on polyelectrolyte polysaccharides</i> .....	72

▪	Pectin aerogels .....	72
▪	Alginate aerogels .....	73
▪	Chitosan aerogels .....	74
2.3.4.	<i>From bio-polymers to the diversity of bio-aerogels:</i> .....	75
2.3.5.	<i>Modifications of bio-based aerogels</i> .....	76
2.4.	BIO-AEROGELS FOR THERMAL INSULATION APPLICATIONS .....	78
2.4.1.	<i>Context</i> .....	78
2.4.2.	<i>Thermal conductivity of aerogels</i> .....	79
2.4.3.	<i>Aerogels used as thermal insulating materials: issues and open questions</i> .....	81
2.5.	THE USE OF BIO-AEROGELS AND SILICA AEROGELS FOR DRUG DELIVERY APPLICATIONS .....	83
2.5.1.	<i>Drug delivery systems: introductive concepts and principles</i> .....	84
▪	Modified drug release behaviors .....	84
▪	Drug release mechanisms from polymer matrix systems .....	85
2.5.2.	<i>Aerogels used as drug delivery systems</i> .....	87
▪	Production of drug loaded aerogels .....	87
▪	Factors influencing drug loading .....	89
▪	Case studies of silica-based and polysaccharide-based aerogels .....	90
➤	Effect of aerogel composition on the release properties .....	91
➤	Effect of preparation conditions on aerogels' release properties .....	94
➤	Effect of hydrophobization on aerogels release properties .....	95
➤	Creation of complex matrix systems by production of composite aerogels .....	96
	<b>CONCLUSIONS</b> .....	<b>99</b>
	<b>REFERENCES</b> .....	<b>100</b>

## CHAPTER II. MATERIALS AND METHODS..... 123

	<b>INTRODUCTION</b> .....	<b>124</b>
	<b>1. STARTING MATERIALS:</b> .....	<b>125</b>
1.1.	PECTINS.....	125
1.2.	CELLULOSE .....	126
1.3.	SILICA-SOLS .....	126
1.4.	SOLVENTS AND OTHER CHEMICALS .....	126
1.4.1.	<i>Solvents for aerogels preparation</i> .....	126
1.4.2.	<i>Chemicals and preparations specific to drug release experiments</i> .....	127
	<b>2. METHODS</b> .....	<b>127</b>
2.1.	PREPARATION OF PECTIN AEROGELS .....	127
2.1.1.	<i>Pectin dissolution</i> .....	128
2.1.2.	<i>Solvent-exchange step</i> .....	129
2.1.3.	<i>Supercritical drying using CO<sub>2</sub></i> .....	131
2.1.4.	<i>Alternative drying methods</i> .....	132
▪	Freeze drying .....	132
▪	Evaporative drying.....	132

2.2.	CHARACTERIZATION METHODS .....	132
2.2.1.	Viscometry .....	132
2.2.2.	Rheology .....	133
2.2.3.	Fourier Transformed Infrared spectroscopy (FTIR).....	133
2.2.4.	Sample shrinkage and aerogel apparent density.....	133
2.2.5.	Porosity and pore specific volume.....	134
2.2.6.	Specific surface area measurement (BET method) .....	135
2.2.7.	Scanning electron microscopy.....	138
2.2.8.	ESD analysis .....	138
2.2.9.	Contact angle.....	138
2.2.10.	Uniaxial compression measurements .....	139
2.2.11.	Thermal conductivity.....	140
2.3.	PREPARATION AND CHARACTERIZATION OF DRUG-LOADED PECTIN AEROGELS.....	141
2.3.1.	Drug incorporation into pectin matrices .....	141
	▪ Loading of theophylline into aerogels, xerogels and cryogels.....	141
2.3.2.	Aerogels' drug loading capacity and specific loading .....	142
2.3.3.	Determination of the crystalline form of theophylline incorporated into pectin matrices by X-ray diffraction .....	144
2.3.4.	In vitro drug release experiments.....	144
	▪ Determination of theophylline absorbance properties .....	145
	▪ In vitro drug release experiments.....	146
2.3.5.	Cytotoxicity profile of different solid matrices .....	148
	▪ Sample preparation .....	148
	▪ MTS assay method .....	149
	<b>REFERENCES.....</b>	<b>151</b>

## **CHAPTER III. TUNING STRUCTURE AND PROPERTIES OF PECTIN AEROGELS. 155**

### **INTRODUCTION: IMPORTANCE OF AEROGELS' STRUCTURAL PROPERTIES 157**

#### **1. CHARACTERIZATION OF PECTINS..... 159**

1.1.	CHARACTERIZATION OF PECTINS' DEGREE OF ESTERIFICATION.....	159
1.2.	DETERMINATION OF PECTIN MOLECULAR WEIGHTS.....	161

#### **2. TUNING STRUCTURE AND PROPERTIES OF LOW METHYLATED PECTIN AEROGELS ..... 162**

2.1.	INFLUENCE OF NON-SOLVENT TYPE AND PECTIN P35 CONCENTRATION ON AEROGEL STRUCTURE AND PROPERTIES .....	163
2.2.	INFLUENCE OF PH ON LOW-METHYLATED PECTIN AEROGEL STRUCTURE AND PROPERTIES.....	167
2.3.	EFFECT OF CALCIUM IONS ON LOW-METHYLATED PECTIN AEROGEL STRUCTURE AND PROPERTIES .....	172
2.4.	EFFECT OF MONOVALENT IONS (NaCl) ON LOW-METHYLATED PECTIN AEROGEL STRUCTURE AND PROPERTIES	175
2.5.	DISCUSSION ON THE CORRELATIONS BETWEEN THE PROCESSING PARAMETERS AND THE AEROPECTIN PHYSICAL PROPERTIES.....	178
2.6.	MECHANICAL PROPERTIES OF LOW-METHYLATED PECTIN AEROGELS .....	182

2.6.1.	<i>Effect of pectin concentration</i> .....	182
2.6.2.	<i>Effect of pH of starting pectin solution on the mechanical properties</i> .....	184
2.6.3.	<i>Effect of addition of calcium into pectin solution</i> .....	186
2.7.	CONCLUSIONS ON THE PROPERTIES OF LOW-METHYLATED PECTIN AEROGELS .....	191
<b>3.</b>	<b>EFFECTS OF PECTIN DEGREE OF ESTERIFICATION ON PECTIN AEROGELS STRUCTURAL PROPERTIES</b> .....	<b>191</b>
3.1.	IMPACT OF DE ON AEROPECTIN STRUCTURAL PROPERTIES VARYING THE PH.....	192
3.1.1.	<i>Impact of pectin DE on the viscosity of pectin solutions while varying the pH</i> .....	193
3.1.2.	<i>Impact of pectin DE on aéropectin properties while varying the pH</i> .....	194
3.2.	IMPACT OF DE ON AEROPECTIN STRUCTURAL PROPERTIES VARYING R(CA) RATIO .....	198
3.2.1.	<i>Effect of DE on gel state at different R(Ca)</i> .....	199
3.2.2.	<i>Effect of pH on calcium sensitivity for various DE</i> .....	199
3.3.	CONCLUSIONS ON THE INFLUENCE OF PECTIN DE ON AEROPECTINS PROPERTIES .....	204
	<b>CONCLUSIONS</b> .....	<b>205</b>
	<b>REFERENCES</b> .....	<b>206</b>

#### CHAPTER IV. THERMAL CONDUCTIVITY-STRUCTURE PROPERTIES

	<b>CORRELATIONS OF PECTIN AEROGELS</b> .....	<b>215</b>
	<b>INTRODUCTION</b> .....	<b>217</b>
<b>1.</b>	<b>THERMAL CONDUCTIVITY AS A FUNCTION OF PECTIN AEROGEL DENSITY: SUMMARY OF ALL RESULTS</b> .....	<b>218</b>
<b>2.</b>	<b>INFLUENCE OF PECTIN CONCENTRATION AND NON-SOLVENT TYPE ON AEROGEL THERMAL CONDUCTIVITY</b> .....	<b>222</b>
2.1.	INFLUENCE OF PECTIN CONCENTRATION .....	222
2.2.	INFLUENCE OF NON-SOLVENT TYPE ON AEROGEL THERMAL CONDUCTIVITY .....	226
<b>3.</b>	<b>INFLUENCE OF CA-INDUCED CROSS-LINKING AND PH ON PECTIN AEROGEL PROPERTIES</b> .....	<b>228</b>
3.1.	INFLUENCE OF PH AT R(CA) = 0 AND 0.2 .....	228
3.2.	INFLUENCE OF CALCIUM CONCENTRATION AT PH 3 .....	232
	<b>CONCLUSIONS</b> .....	<b>236</b>
	<b>REFERENCES</b> .....	<b>237</b>

#### CHAPTER V. PECTIN AEROGELS AS DRUG DELIVERY SYSTEMS .....

	<b>INTRODUCTION</b> .....	<b>241</b>
--	---------------------------	------------

<b>1. PRODUCTION AND CHARACTERIZATION OF THE DRUG-LOADED AEROPECTINS.....</b>	<b>242</b>
1.1. METHOD OF INCORPORATION OF THEOPHYLLINE INTO AEROGEL PRECURSORS .....	242
1.2. CHARACTERIZATION OF LOADED AEROPECTINS.....	244
1.2.1. <i>Aeropectins drug loading efficiency</i> .....	244
1.2.2. <i>Structural characterization of theophylline loaded aeropectins</i> .....	247
1.2.3. <i>Determination of crystalline structure of theophylline incorporated in pectin aerogels, xerogels and cryogels by X-rays diffraction</i> .....	248
<b>2. STUDY OF THEOPHYLLINE RELEASE FROM PECTIN, AEROGELS, CRYOGELS AND XEROGELS .....</b>	<b>251</b>
2.1. STRUCTURAL PROPERTIES OF PECTIN MATRIX MADE WITH DIFFERENT DRYINGS .....	252
2.2. THEOPHYLLINE RELEASE PROFILES AS A FUNCTION OF DRYING METHOD.....	254
2.3. COMPARISON OF RELEASE PROPERTIES OF PECTIN HYDROGELS AND AEROGELS .....	259
<b>3. BACKGROUND ANALYSIS OF AEROPECTIN BEHAVIOUR AND THEOPHYLLINE RELEASE.....</b>	<b>261</b>
3.1. INFLUENCE OF PH OF RELEASE MEDIUM ON AEROPECTIN EROSION, SWELLING AND DRUG RELEASE .....	261
3.2. SELECTION OF A MODEL TO DESCRIBE RELEASE KINETICS.....	264
3.2.1. <i>Mathematical models fitting drug release profiles</i> .....	265
3.2.2. <i>Overview of drug release from aeropectins</i> .....	269
<b>4. CASE STUDIES: INFLUENCE OF VARIOUS PARAMETERS ON THE KINETICS OF THEOPHYLLINE RELEASE FROM PECTIN AEROGELS.....</b>	<b>272</b>
4.1. INFLUENCE OF PH OF PECTIN SOLUTIONS ON RELEASE KINETICS OF THEOPHYLLINE FROM AEROPECTIN .....	272
4.2. IMPACT OF CALCIUM CONCENTRATION ON RELEASE KINETICS OF THEOPHYLLINE FROM AEROPECTIN.....	278
<b>CONCLUSIONS .....</b>	<b>284</b>
<b>REFERENCES .....</b>	<b>286</b>

## **CHAPTER VI. ORGANIC-ORGANIC AND ORGANIC-INORGANIC PECTIN-BASED COMPOSITE AEROGELS FOR DRUG RELEASE APPLICATIONS .....**

<b>INTRODUCTION.....</b>	<b>294</b>
<b>1. CELLULOSE-PECTIN COMPOSITE AEROGELS .....</b>	<b>295</b>
1.1. PRODUCTION AND CHARACTERIZATION OF CELLULOSE-PECTIN COMPOSITES.....	296
1.1.1. <i>Production of cellulose-pectin composites</i> .....	296
▪ Production of cellulose matrix samples.....	296
▪ Impregnation of cellulose matrix by pectin solution .....	296
1.1.2. <i>Structure and properties of cellulose-pectin composite aerogels</i> .....	299
▪ Formation of interpenetrated network cellulose-pectin and density of composite aerogels.....	299
▪ Morphology of composite aerogels.....	304
1.2. CELLULOSE-PECTIN COMPOSITES AS DRUG DELIVERY SYSTEM .....	306

1.2.1.	<i>Characteristics of drug-loaded composite cellulose-pectin aerogels</i> .....	306
1.2.2.	<i>Theophylline release profiles from cellulose-pectin aerogels</i> .....	309
	▪ Comparison of theophylline release from neat reference pectin-based versus neat reference cellulose-based aerogel matrices .....	310
	▪ Influence of pectin/cellulose composition on release kinetics of theophylline from composite aerogels.....	315
	➤ Cellulose-pectin composite aerogels without calcium .....	315
	➤ Cellulose-pectin composite aerogels with calcium .....	322
1.3.	CONCLUSIONS ON PECTIN-CELLULOSE COMPOSITE AEROGELS.....	326
<b>2.</b>	<b>PECTIN-SILICA COMPOSITE AEROGELS.....</b>	<b>328</b>
2.1.	PRODUCTION AND CHARACTERIZATION OF PECTIN-SILICA COMPOSITES .....	329
2.1.1.	<i>Materials</i> .....	329
2.1.2.	<i>Sol-gel synthesis of neat silica aerogels using either TEOS or PEDS</i> .....	329
	▪ Production of silica aerogels made from TEOS.....	329
	▪ Production of silica aerogels made from PEDS.....	330
1.1.1.	<i>Production of pectin-silica composite aerogels</i> .....	330
	▪ Process route of pectin-silica composite aerogels .....	330
	▪ Calculation of silica diffusion time inside pectin matrix .....	332
	▪ Estimation of the silica impregnation efficiency into pectin matrices.....	333
2.2.	CHARACTERIZATION OF PECTIN-SILICA COMPOSITE AEROGELS .....	334
2.2.1.	<i>Influence of the type of silica sol on the properties of neat silica aerogels (TEOS vs PEDS)</i> .....	334
2.2.2.	<i>Distribution and impregnation efficiency of silica in pectin matrix</i> .....	339
2.2.3.	<i>Structural properties of pectin-silica composite aerogels and loading with theophylline ..</i> .....	342
2.2.4.	<i>Theophylline loading in pectin-silica composite aerogels</i> .....	346
2.3.	THEOPHYLLINE RELEASE PROFILES FROM PECTIN-SILICA AEROGEL MATRICES.....	348
2.3.1.	<i>Comparison of theophylline release from neat silica and pectin aerogels matrices</i> .....	349
2.3.2.	<i>Theophylline release from pectin-silica composite aerogels</i> .....	354
	➤ Without calcium crosslinking .....	355
	➤ Pectin cross-linked with calcium .....	358
2.4.	CONCLUSIONS ON PECTIN-SILICA COMPOSITE AEROGELS .....	369
<b>3.</b>	<b>CYTOXOCITY PROFILE OF DIFFERENT AEROGELS AND CRYOGELS MATRICES .....</b>	<b>371</b>
	<b>CONCLUSIONS .....</b>	<b>373</b>
	<b>REFERENCES .....</b>	<b>374</b>
	<b>GENERAL CONCLUSIONS AND PERSPECTIVES.....</b>	<b>377</b>

## **ANNEX. FUNDAMENTALS AND CONCEPTS FOR DRUG DELIVERY**

<b>APPLICATIONS.....</b>	<b>385</b>
<b>1. DRUG RELEASE MECHANISMS FROM POLYMER MATRIX SYSTEMS .....</b>	<b>387</b>
1.1. WATER DIFFUSION AND POLYMER RELAXATION (SWELLING) .....	387
1.2. MATRIX EROSION .....	388
1.3. DRUG DISSOLUTION .....	389
1.4. DRUG DIFFUSION.....	390
<b>2. MATHEMATICAL MODELS OF RELEASE KINETICS .....</b>	<b>391</b>
2.1. ZERO-ORDER KINETICS .....	393
2.2. FIRST-ORDER RELEASE KINETICS .....	394
2.3. HIGUCHI RELEASE MODEL .....	394
2.4. HIXSON-CROWELL RELEASE MODEL .....	396
2.5. HOPFENBERG MODEL .....	397
2.6. RITGER-KORSMEYER-PEPPAS (POWER LAW) MODEL .....	397
2.7. PEPPAS-SAHLIN MODEL.....	400
2.8. GALLAGHER-CORRIGAN MODEL .....	401
<b>REFERENCES.....</b>	<b>402</b>

# ABBREVIATIONS AND SYMBOLS

---

## ➤ Experimental parameters

wt%: weight percent

$\rho_{\text{bulk}}$  (g/cm<sup>3</sup>): bulk density

$\rho_{\text{skeletal}}$  (g/cm<sup>3</sup>): skeletal (or solid) density

$\varepsilon$  (%): porosity

$S_{\text{BET}}$  (m<sup>2</sup>/g): specific surface area

$E$  (MPa): Young modulus  $\sigma_{\text{yield}}$

$\varepsilon_{\text{yield}}$  (%): yield strain

$\varepsilon_{\text{d}}$  (%): densification strain

$\lambda_{\text{effective}}$  (W.m<sup>-1</sup>.K<sup>-1</sup>): total or effective thermal conductivity

$\lambda_{\text{solid}}$  (W.m<sup>-1</sup>.K<sup>-1</sup>): thermal conductivity of the solid phase

$\lambda_{\text{gas}}$  (W.m<sup>-1</sup>.K<sup>-1</sup>): thermal conductivity of the gaseous phase

$\lambda_{\text{radiative}}$  (W.m<sup>-1</sup>.K<sup>-1</sup>): thermal conductivity of radiative transfer

$Q(t)$ : cumulative theophylline release over time in liquid release media

$\eta$  (Pa.s): viscosity

$[\eta]$  (mL/g): intrinsic viscosity

$G'$  (Pa): elastic modulus

$G''$  (Pa): viscous modulus

$\lambda_{271}$  (nm): wavelength of 271 nm

$A$  (u.a.): Absorbance

$\varepsilon_{\text{mol}}$  (M<sup>-1</sup>.cm<sup>-1</sup>): Molar extinction coefficient

## ➤ **Materials**

DE (or DM) (%): Degree of Esterification (or Degree of Methylation) of pectin in %

Gal.A: Galacturonic acid

HM pectin: High-methylated pectin

LM pectin: Low-methylated pectin

P35, P56, P59, P70: Pectins with methylation degree of 35%, 56%, 59%, 70%, respectively.

%P and C%: Mass fraction of pectin and cellulose within a composite, respectively.

TEOS: Tetraethyl orthosilicate

PEDS: Polyethoxydisiloxane

SGF: Simulated Gastric Fluid

SIF: Simulated Intestinal Fluid

## ➤ **Techniques**

BET: method of Brunauer-Emmett-Teller for specific surface area

BJH: method of Barrett, Joyner and Halenda for pore size distribution

EDS: Energy-dispersive X-ray spectroscopy

FTIR: Fourier Transform InfraRed spectroscopy

SEM: Scanning Electron Microscope

Sc-drying: Supercritical drying

UV: Ultraviolet



# **GENERAL INTRODUCTION**

---

The design of new advanced materials which are versatile and multi-functional has become a key research focus to meet tomorrow's engineering applications. Nowadays, polymer technology and material engineering fields are facing new challenges in assimilating the rapid technological advances coupled with a more sustainable approach. Indeed, the integration of environmental sustainability by the development of bio-based materials produced by "greener" processes is essential in future technologies to decrease environmental footprints and harmonize with our living environment for today and tomorrow.

In particular, both academic and industrial research areas aim to achieve breakthroughs in the development of bio-based materials (*i.e.* materials made from natural resources) as they represent renewable and environmentally-friendly alternatives to "classical" materials made from non-renewable fossil resources. Bio-based materials are made from natural polymers such as polysaccharides (cellulose, starch, pectin, alginate, chitosan...), proteins (gelatin, silk fibroin, egg albumin, casein...), or lipids (vegetal oil, fatty acids...). Polysaccharides are natural sugar-based polymers extracted from various biomass sources. These bio-polymers present many attractive properties as they are widely available, renewable, non-toxic, biocompatible and can be easily functionalized due to a large amount of hydroxyl groups on polymer backbone. Besides, as they are part of our daily food diet and are commonly used for food & feed, polysaccharides thus appear as "human-friendly" polymers. Due to these characteristics, bio-based materials made from polysaccharides are suitable for a wide range of life science applications such as biomedical, pharmaceutical, biotechnological, cosmetic and food. The application domain of bio-based materials is vast and versatile and also includes bio-based plastics, textile and fabric sectors or construction and building industry.

In the recent past, the design of new "smart" materials presenting similar or better functional properties than "classical" or synthetic materials has become a key research focus in materials science as evident from publications and patents. Aerogels, which are highly porous and ultra-light materials obtained by supercritical drying of wet gels, are one example of materials for advanced applications. Indeed, they present outstanding structural properties with a very fine porous structure (solid network) and numerous pores of few tens to a few hundreds of nanometres. Aerogels are extremely versatile materials due their wide range of textural and morphological properties combined to the possibility to tune and functionalize them by varying the process route. As a result, there are numerous potential applications of aerogels in many different technological fields (such as for thermal/acoustic insulations, as catalyst, adsorbents, filtration systems, as carrier-materials for release/adsorption of compounds, as sensor materials... *etc.*).

In this thesis, we used pectin, a polysaccharide extracted from fruits and widely used as a thickening or gelling agent in food industry, to make bio-aerogels. The topic of the thesis concerns structure-properties correlations in pectin aerogels as advanced materials for i)

thermal insulation and ii) drug delivery. As it will be shown all along the manuscript, pectin aerogels are perfectly fitting the request of smart bio-based multifunctional material.

Here, we first present how bio-aerogels used as thermal insulating materials can be promising sustainable alternatives to classical aerogels made from silica or synthetic polymers, and then how bio-based aerogels can present major advantages compared to hydrogels used for life sciences applications.

## ➤ **Bio-aerogels for thermal insulation**

The continuous increase of global energy consumption and its associated environmental side-effects have become major ecological issues. In addition to the environmental aspects, there is also a huge economic issue with a high potential of energy cost saving (Narbel & Hansen, 2014). Since the building sector is the most energy consuming sector, the building insulation is a main focus in order to decrease both energy consumption and CO<sub>2</sub> emissions (Baetens, Jelle, & Gustavsen, 2011).

In order to reduce energy loss, research was performed both by academia and industry to design and develop lower-energy-consuming buildings, mostly by applying wall insulation. In order to provide good insulation properties, wall insulation generally is performed by thick and/or multilayers of thermal insulating materials which are able to strongly reduce heat conduction. This can be done either by vacuum insulation panels or by “intrinsically” insulating materials. Thanks to their extraordinary structural and physical characteristics, aerogels present very low thermal conductivity, generally in the super-insulation domain (*i.e.* with thermal conductivity below that of air), which makes them suitable as very efficient thermal insulating materials. “Classical” aerogels are often either inorganic (*e.g.* silica aerogels (Kistler, 1931)) or organic (*e.g.* resorcinol-formaldehyde aerogels (Pekala, 1989)). However, they have either poor mechanical properties (non chemically-modified silica aerogels) or their process route includes toxic compounds (organic aerogels).

One promising solution that combines high material performances and ecological aspects is to develop a new generation of super-insulating materials, which would be bio-based and obtained via a “green” process route. The development of bio-based aerogels made from natural polymers with thermal super-insulating properties is a “hot research topic”. Compared to silica aerogels which are extremely fragile, polymer-based aerogels, and bio-aerogels in particular, do not break under compression (Rudaz et al., 2014). Moreover, the synthesis of bio-aerogels does not involve any toxic compounds which is the case of many synthetic polymer aerogels (for example, based on resorcinol formaldehyde or polyurethanes cross-linked with isocyanate).

The first bio-aerogels made from cellulose and derivatives did not show super-insulating properties (see, for example (Rudaz, 2013)) contrary to aerogels based on pectin (Rudaz et al., 2014), nanofibrillated cellulose (Jiménez-Saelices, Seantier, Cathala, & Grohens, 2017; Kobayashi, Saito, & Isogai, 2014; Seantier, Bendahou, Bendahou, Grohens, & Kaddami, 2016), alginate (Gurikov, Raman, Weinrich, Fricke, & Smirnova, 2015) and starch (Druel, Bardl, Vorweg, & Budtova, 2017). However, the relationships between the thermal conductivity, the structure and the properties of bio-aerogels remain open.

### ➤ **Bio-aerogels for life sciences applications**

Hydrogels are self-standing water-swollen 3D-dimensional polymer networks which allow the diffusion of liquids and molecules (absorption and release). Their use has become very popular in life science applications due their many attractive properties such as high water-content, swelling/contraction ability, easy moldability in shape, versatility in fabrication, flexibility and soft consistency close to physiological living tissues (Caló & Khutoryanskiy, 2015). Moreover, hydrogels are highly valued thanks to the possibility to finely adjust their physico-chemical characteristics to address specific applications. Indeed, tuning of their nanostructures (polymer composition, functionalization, degree of crosslinking, nature of junction zones...) and the ability to encapsulate active compounds allow tailoring material macromolecular properties and thus offering the opportunity for the development of advanced and innovative properties. As a result, hydrogels are commonly used for different applications in various areas such as in food industry (food additives and viscosity modifiers), cosmetics (facial mask, gels ...), biomedical (regenerative tissue engineering, plastic surgery, contact lens, wound dressing, hygienic products...), pharmaceutical (drug encapsulation and delivery systems), agricultural or environmental fields (water retention, pesticide delivery systems, pollutant adsorbents) (Popa & Volf, 2018).

However, hydrogels have disadvantages that limit their widespread applications. As hydrogels are “wet” and usually mechanically weak systems, they may not be easy to handle. Besides, their use is limited in terms of transportation without breakage and of storage issues over time (microbiological stability). Due to all these limitations, it appears not easy to use hydrogels as already prefabricated matrices (Caló & Khutoryanskiy, 2015; Zhao et al., 2015).

One potential solution to solve these technical drawbacks would be to dry wet gels to obtain dry porous materials *i.e.* aerogels (via supercritical drying) or cryogels (via freeze-drying). Indeed, compared to hydrogels, porous dry materials present major advantages related to their manufacturing. First, thanks to enhanced mechanical properties resulting from the drying, they are more easily handled and transportable than soft hydrogels. Besides, as aerogels and cryogels are light-weight materials, transport saving can be huge, impacting industrial costs

and environmental aspects. Then, contrary to hydrogels that may be hard to sterilize, dry materials do not require antimicrobial additives to ensure their stability over time, which makes them suitable for long-term storage. As a result, the drying of wet gels opens the possibility to an upstream production (as pre-fabricated materials) at a large scale. Finally, as it will be shown in this manuscript, the use of supercritical drying preserves the physico-chemical and functional properties of the initial hydrogels, and can even lead to better controlled drug release properties when used as drug-carriers.

### ➤ **Goals of the thesis and overview of the manuscript**

Lately, pectin aerogels were found to be promising bio-based materials for high added-values application such as thermal insulation (Demilecamps, 2015; Rudaz, 2013). As pectin has gastro-resistant properties, pectin aerogels might have high potential for life sciences applications such as used as oral drug-carriers (García-González, Alnaief, & Smirnova, 2011; García-González, Jin, Gerth, Alvarez-Lorenzo, & Smirnova, 2015; Gonçalves et al., 2016; Tkalec, Knez, & Novak, 2015; Veronovski, Tkalec, Knez, & Novak, 2014).

Despite the importance of aerogel morphology control regarding to applications' performances, very little is known about the relationships between the type of polysaccharide, processing conditions and aerogel structure and properties.

The overall goal of this thesis is double:

- First, we want to understand and correlate the characteristics of the initial polymer (pectin), the preparation conditions, the internal structure of aerogel and the final application properties. The open questions we ask here are first: “How can we control and tune the textural properties of bio-aerogels?” and then “What are the structure-properties correlations for bio-aerogels developed for either thermal insulation or for drug release applications?”.
- Second, we would like to evaluate, develop, and show the high potential of pectin aerogels as advanced biomaterials for the two different applications: thermal insulation and drug delivery.

To answer these questions, pectin, a versatile polysaccharide from fruits, was selected as it allows numerous variations of conditions that influence solution viscosity and gelation, potentially leading to a wide range of aerogel morphologies and properties. We produced pectin aerogels with different internal structure and morphological properties and tested them for the two applications mentioned above.

This manuscript is divided into six chapters and includes an annex part:

**Chapter I** gives a state of the art on bio-aerogels focusing on what is known about the correlations between initial polysaccharide characteristics, aerogels' internal structure and application properties. The structure and physico-chemical characteristics of pectin will be presented in order to understand how we can tune the properties of pectin solutions/gels and thus of pectin aerogels. We will introduce the concept of aerogel and will review the state of the art on bio-aerogels, from their synthesis to their potential applications with a special focus on aerogels made from polysaccharides. We will detail two particular potential applications of aerogels: as thermal insulating materials and as matrices for drug release, and highlight the scientific issues and technical challenges which remain open.

**Chapter II** describes the starting materials and the experimental preparation and characterization methods used during the thesis. We will present the main steps of preparation of pectin aerogels via dissolution, coagulation and supercritical drying using CO<sub>2</sub>. Rheological studies of pectin solutions and structural characterisation techniques of aerogels (such as nitrogen adsorption, scanning electron microscopy, contact angle and X-rays diffraction...) will be presented. The mechanical properties of pectin aerogels will be studied by uniaxial compression measurements and their effective thermal conductivity will be investigated via steady-state method using a heat flowmeter. Finally, we will present in detail the preparation and characterization methods of drug-loaded aerogels used as drug delivery systems. The process of drug incorporation into aerogel precursors prior to supercritical drying to produce drug loaded aerogels will be detailed, and we will describe the methods to characterise aerogels' drug loading properties and their *in vitro* drug release properties over time in gastro-intestinal media.

**Chapter III** investigates the correlations between the initial polymer characteristics - processing parameters –aerogel structural and mechanical properties in order to show why and how pectin aerogel morphology and properties vary as a function of pectin intrinsic parameters and external conditions. For this purpose, pectin aerogels will be studied in a systematic way by varying the type of pectin (with different degree of methylation), pectin concentration, solution pH, type and concentration of metal salts (CaCl<sub>2</sub> and NaCl) and nature of non-solvent.

**Chapter IV** focuses on the correlations between thermal conductivity, morphology and physical properties of pectin aerogels in order to understand how to obtain a thermal super-insulating material with the lowest possible conductivity. The influence of pectin concentration, the type of non-solvent, pH conditions and of Ca-induced cross-linking by increasing calcium concentration on aerogel density and morphology, and then on the resulting thermal properties will be studied.

**Chapter V** explores the potential use of pectin hydrogels, aerogels, cryogels and xerogels as oral drug delivery systems. We will study the release of a model drug (theophylline) from different pectin matrices in order to find out structure-properties correlations explaining

drug release mechanisms and kinetics. The impact of the drying methods (supercritical, evaporative or freeze drying) on release properties of the different pectin matrices (hydrogel, aerogels, cryogels, xerogels) will be investigated. Then, the influence of aeropectins' preparation conditions on their drug release properties will be examined. Matrix swelling, erosion and drug release profiles of different aerogels matrices will be characterized and compared. Kinetics models based on mathematical functions will be used to identify the main mechanism governing the release (*e.g.* diffusion, dissolution, erosion, swelling...*etc.*).

**Chapter VI** deals with the production and use of organic-organic and organic-inorganic pectin-based composite aerogels as drug delivery systems, with one component being pectin and the other either cellulose or silica. Indeed, the synergy of properties brought by the different components is expected to result in new physical and chemical properties of composite aerogels and to offer new prospects in composite aerogels used as drug carrier. First, the processes routes to produce theophylline-loaded pectin-cellulose and pectin-silica composite aerogels will be presented. Then, we will explore the influence of the “second component” on drug release kinetics and matrix behaviour. In this chapter, the focus will be made on the relationships between the intrinsic characteristics of each component of aerogel, the structural and physical properties of the composite network, and the properties of the composite materials used as drug carriers. The impact of the composition of the composite aerogels on their matrix swelling ability, erosion properties, drug loading characteristics and release profile will be discussed.

**The annex** section contains an overview of drug release fundamentals and concepts. The main drug release mechanisms from polymer matrix (dissolution, diffusion, matrix erosion and swelling, polymer relaxation...*etc.*) and the most used kinetics mathematical models applicable for solid matrix systems (Zero-order, First-order, Higushi, Korsmeyer-Peppas, Hixson-Crowell, Hopfenberg, Gallagher–Corrigan release models) will be presented in details.

Finally, conclusions are drawn and suggestions for further work are proposed.

Part of the work on pectin aerogels for drug delivery applications (Chapter V) was performed within “Biogels” project in the frame of BRANCUSI program sponsored by Campus France and CNCS - UEFISCDI, Romania (PN-III-P3-3.1-PM-RO). We thank all the partners from the "Petru Poni" Institute of Macromolecular Chemistry (Iasi, Romania) that were involved in the project.

We wish to thank Pierre Ilbizian (from PERSEE, Mines ParisTech, France) for supercritical drying with CO<sub>2</sub>. We warmly thank Laurent SCHIATTI DE MONZA (from PERSEE, Mines ParisTech, France) for helping in computer programming to automatically control the spectrophotometer device over time. We are also grateful to Cargill for providing pectins and their characteristics. Spectrophotometric measurements over time were automatically conducted

## References

- Baetens, R., Jelle, B. P., & Gustavsen, A. (2011). Aerogel insulation for building applications: A state-of-the-art review. *Energy and Buildings*, 43(4), 761-769. <https://doi.org/10.1016/j.enbuild.2010.12.012>
- Caló, E., & Khutoryanskiy, V. V. (2015). Biomedical applications of hydrogels: A review of patents and commercial products. *European Polymer Journal*, 65, 252-267. <https://doi.org/10.1016/j.eurpolymj.2014.11.024>
- Cuce, E., Cuce, P. M., Wood, C. J., & Riffat, S. B. (2014). Toward aerogel based thermal superinsulation in buildings: A comprehensive review. *Renewable and Sustainable Energy Reviews*, 34, 273-299. <https://doi.org/10.1016/j.rser.2014.03.017>
- Demilecamps, A. (2015). *Synthesis and characterization of polysaccharides-silica composite aerogels for thermal superinsulation*. (PhD Thesis, Ecole Nationale Supérieure des Mines de Paris).
- Druel, L., Bardl, R., Vorweg, W., & Budtova, T. (2017). Starch Aerogels: A Member of the Family of Thermal Superinsulating Materials. *Biomacromolecules*, 18(12), 4232-4239. <https://doi.org/10.1021/acs.biomac.7b01272>
- García-González, C. A., Alnaief, M., & Smirnova, I. (2011). Polysaccharide-based aerogels—Promising biodegradable carriers for drug delivery systems. *Carbohydrate Polymers*, 86(4), 1425-1438. <https://doi.org/10.1016/j.carbpol.2011.06.066>
- García-González, C. A., Jin, M., Gerth, J., Alvarez-Lorenzo, C., & Smirnova, I. (2015). Polysaccharide-based aerogel microspheres for oral drug delivery. *Carbohydrate Polymers*, 117, 797-806. <https://doi.org/10.1016/j.carbpol.2014.10.045>
- Gonçalves, V. S. S., Gurikov, P., Poejo, J., Matias, A. A., Heinrich, S., Duarte, C. M. M., & Smirnova, I. (2016). Alginate-based hybrid aerogel microparticles for mucosal drug delivery. *European Journal of Pharmaceutics and Biopharmaceutics: Official Journal of Arbeitsgemeinschaft Fur Pharmazeutische Verfahrenstechnik e.V.*, 107, 160-170. <https://doi.org/10.1016/j.ejpb.2016.07.003>
- Gurikov, P., Raman, S. P., Weinrich, D., Fricke, M., & Smirnova, I. (2015). A novel approach to alginate aerogels: carbon dioxide induced gelation. *RSC Advances*, 5(11), 7812-7818. <https://doi.org/10.1039/C4RA14653K>
- Jiménez-Saelices, C., Seantier, B., Cathala, B., & Grohens, Y. (2017). Spray freeze-dried nanofibrillated cellulose aerogels with thermal superinsulating properties. *Carbohydrate Polymers*, 157, 105-113. <https://doi.org/10.1016/j.carbpol.2016.09.068>
- Kistler, S. S. (1931). Coherent Expanded-Aerogels. *The Journal of Physical Chemistry*, 36(1), 52-64. <https://doi.org/10.1021/j150331a003>

- Kobayashi, Y., Saito, T., & Isogai, A. (2014). Aerogels with 3D Ordered Nanofiber Skeletons of Liquid-Crystalline Nanocellulose Derivatives as Tough and Transparent Insulators. *Angewandte Chemie International Edition*, 53(39), 10394-10397. <https://doi.org/10.1002/anie.201405123>
- Narbel, P. A., & Hansen, J. P. (2014). Estimating the cost of future global energy supply. *Renewable and Sustainable Energy Reviews*, 34, 91-97. <https://doi.org/10.1016/j.rser.2014.03.011>
- Pekala, R. W. (1989). Organic aerogels from the polycondensation of resorcinol with formaldehyde. *Journal of Materials Science*, 24(9), 3221-3227. <https://doi.org/10.1007/BF01139044>
- Popa, V. I., & Volf, I. (2018). *Biomass as Renewable Raw Material to Obtain Bioproducts of High-Tech Value*. Elsevier.
- Rudaz, C. (2013). *Cellulose and Pectin Aerogels: Towards their nano-structuration* (PhD Thesis, Ecole Nationale Supérieure des Mines de Paris). Consulté à l'adresse <https://pastel.archives-ouvertes.fr/pastel-00957296/document>
- Rudaz, C., Courson, R., Bonnet, L., Calas-Etienne, S., Sallée, H., & Budtova, T. (2014). Aeropectin: Fully Biomass-Based Mechanically Strong and Thermal Superinsulating Aerogel. *Biomacromolecules*, 15(6), 2188-2195. <https://doi.org/10.1021/bm500345u>
- Seantier, B., Bendahou, D., Bendahou, A., Grohens, Y., & Kaddami, H. (2016). Multi-scale cellulose based new bio-aerogel composites with thermal super-insulating and tunable mechanical properties. *Carbohydrate Polymers*, 138, 335-348. <https://doi.org/10.1016/j.carbpol.2015.11.032>
- Tkalec, G., Knez, Ž., & Novak, Z. (2015). Fast production of high-methoxyl pectin aerogels for enhancing the bioavailability of low-soluble drugs. *The Journal of Supercritical Fluids*, 106, 16-22. <https://doi.org/10.1016/j.supflu.2015.06.009>
- Veronovski, A., Tkalec, G., Knez, Ž., & Novak, Z. (2014). Characterisation of biodegradable pectin aerogels and their potential use as drug carriers. *Carbohydrate Polymers*, 113, 272-278. <https://doi.org/10.1016/j.carbpol.2014.06.054>
- Zhao, F., Yao, D., Guo, R., Deng, L., Dong, A., & Zhang, J. (2015). Composites of Polymer Hydrogels and Nanoparticulate Systems for Biomedical and Pharmaceutical Applications. *Nanomaterials*, 5(4), 2054-2130. <https://doi.org/10.3390/nano5042054>

# ARTICLES AND COMMUNICATIONS

---

This work has led to two articles published in international journals and several are in preparation. Several communications (oral presentations and posters) were given at national and international conferences.

## ➤ Articles

Sophie Groult, Tatiana Budtova (2018). Thermal conductivity/structure correlations in thermal super-insulating pectin aerogels *Carbohydrate Polymers*, Volume 196, Pages 73-81

Sophie Groult, Tatiana Budtova (2018). Tuning structure and properties of pectin aerogels. *European Polymer Journal*, Volume 108, Pages 250-261

## ➤ Oral presentations

Sophie Groult, Tatiana Budtova

“Pectin aerogels: structure-properties correlations and use for drug controlled-release”. 5th EPNOE International Polysaccharide Conference, Jena, Germany, 20–24 August 2017

Sophie Groult, Gabriela Pricope, Dragos Peptanariu, Diana Ciolacu, Tatiana Budtova

“Bio-aerogels for controlled release”, Polysaccharides as Sweet Spot for Innovation, Leuven, Belgium, September 17-18th, 2018

Sophie Groult, Lucile Druel, Cyrielle Rudaz, Richard Bardl, Tatiana Budtova

“Thermal conductivity of bio-aerogels”, 4<sup>th</sup> International seminar on aerogels  
“Properties-Manufacture-Applications”, Hamburg, Germany, 24 – 26 September 2018.

Sophie Groult, Gabriela Pricope, Dragos Peptanariu, Diana Ciolacu, Tatiana Budtova

“Pectin aerogels: structure-properties correlations and use for drug controlled-release”. The 4th International Conference on Bioinspired and Biobased. Chemistry & Materials (N.I.C.E. 2018), Nice, France, 14-17 October 2018.

Sophie Groult, Gabriela Pricope, Dragos Peptanariu, Diana Ciolacu, Tatiana Budtova

"Pectin aerogels for controlled release". American Chemical Society meeting, 31 March - 4 April 2019, Orlando, USA.

## ➤ Posters

Sophie Groult, Tatiana Budtova

“Pectin aerogels”. International Seminar on Aerogels; Sophia Antipolis, France, 22-23 September 2016

Sophie Groult, Tatiana Budtova

“Pectin aerogels”. 2nd EPNOE Junior Scientists Meeting, Sophia-Antipolis, France, 13-14 October 2016

Sophie Groult, Tatiana Budtova

“Pectin and pectin composite aerogels- structure-properties correlations and use for drug-controlled release”. Fourth International Seminar on aerogels, Hamburg, Germany, 24-26 September 2018



# **RESUME DES TRAVAUX DE THESE**

---

## ➤ Introduction

La conception de nouveaux matériaux versatiles, multifonctionnels et couplée à des procédés de fabrication « plus verts », est devenue un axe d'innovation majeur tant pour la recherche académique qu'industrielle. On observe en particulier un fort intérêt pour les matériaux biosourcés (ou « bio-matériaux ») (*i.e.* issus de ressources naturelles) qui offrent des alternatives plus respectueuses de l'environnement aux matériaux dits "classiques" issus de ressources non-renouvelables. Les matériaux biosourcés sont fabriqués à partir de polymères naturels tels que les polysaccharides (cellulose, amidon, pectine, alginate, ...), les protéines (gélatine, fibroïne de soie, ovalbumine, ...), ou les lipides. Les polysaccharides, en particulier, polymères naturels à base de sucre couramment utilisés dans l'agroalimentaire, présentent des propriétés particulièrement attractives dans la mesure où ils sont largement disponibles et accessibles, non-toxiques, biocompatibles, biodégradables et peuvent être aisément "fonctionnalisés" du fait de la présence de nombreux groupements hydroxyles. De ce fait, les matériaux à base de polysaccharides conviennent à un large éventail d'applications notamment à l'interface avec le vivant (*e.g.* biomédical, cosmétique ou alimentaire) mais inclut également les secteurs des bio-plastiques, du textile ou encore l'ingénierie du bâtiment.

Dans ce contexte, une classe particulière de matériaux avancés connaît un récent engouement, comme en attestent les nombreuses publications et dépôt de brevets sur le sujet : les aérogels. Les aérogels sont des matériaux hautement poreux et ultralégers obtenus par un type de séchage supercritique d'un gel, durant lequel la phase liquide du gel est remplacé par du gaz. Le séchage en conditions supercritiques permet en effet de préserver la microstructure du gel, conférant ainsi aux aérogels des propriétés physiques et structurales exceptionnelles. En effet, les aérogels sont constitués d'une fine structure poreuse, formé par un réseau polymère en 3-D et comportant de nombreux pores de diamètres allant de quelques dizaines à quelques centaines de nanomètres. Il en résulte une très forte porosité (> 90%), une faible densité (typiquement 0.05-0.025 g/cm<sup>3</sup>), et une très grande surface spécifique (200-1000 m<sup>2</sup>/g). Pour illustration, différentes morphologies d'aérogels de pectine d'agrumes sont présentées en Fig. 1.

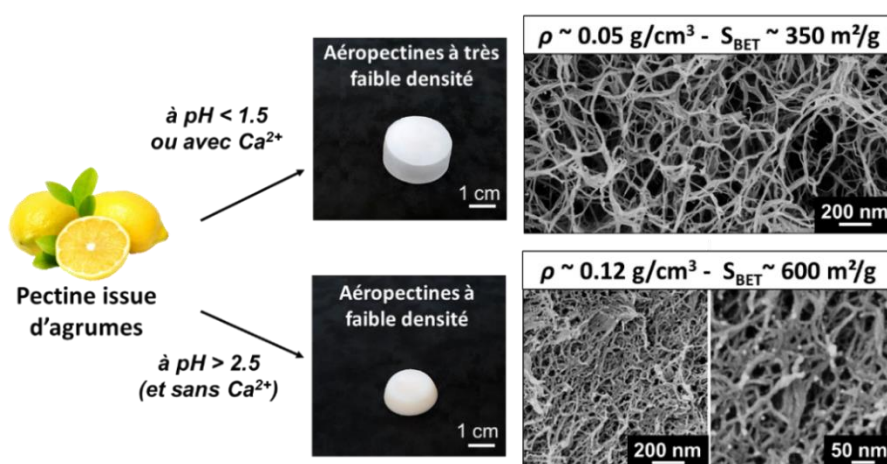


Figure 1. Différentes photographies et images MEB d'aéropectines obtenues en variant le procédé de fabrication (pH des solutions et ajout d'ions calcium  $\text{Ca}^{2+}$ ). Leur densités  $\rho$  ( $\text{g}/\text{cm}^3$ ) ainsi que leur surface spécifiques  $S_{\text{BET}}$  ( $\text{m}^2/\text{g}$ ) respectives sont précisées.

En outre, les aérogels présentent une très faible conductivité thermique et propagation du son du fait de leur structure méso-poreuse, ce qui en fait d'excellents isolants thermiques et phoniques et offre de grandes perspectives dans le secteur du bâtiment, leur application la plus connue à ce jour (Baetens et al. 2011). En réalité, les aérogels sont extrêmement versatiles du fait leur large gamme en termes de propriétés structurales, combinée à la possibilité de les ajuster et de les fonctionnaliser "à la demande" en variant le procédé de fabrication. Les applications potentielles des aérogels sont donc extrêmement nombreuses et concernent de domaines technologiques variés (isolation thermique et acoustique, support de catalyseurs, adsorbants, systèmes de filtration, matrices pour la libération/adsorption de composés, matériaux "capteurs"... etc.).

Les aérogels classiques à base de silice sont les plus connus (Kisler et al., 1931), notamment car ils font partie des super-isolants thermiques, c'est-à-dire ayant un conductivité thermique inférieure à celui de l'air en conditions ambiantes ( $< 0.025 \text{ W}/(\text{m.K})$ ). D'autres type d'aérogels ont émergé dans les années 1980 à base de polymères synthétiques organiques comme les aérogels à base de résorcinol-formaldéhyde (Pekala et al. 1989) ou de polyuréthane. Cependant, les aérogels de silice (non modifiés chimiquement) sont extrêmement fragiles et cassants, ce qui limite leurs potentialités d'application et génère une pollution de nanoparticules de silice. Les aérogels de polymères organiques synthétiques, quant à eux, intègrent des composés toxiques ou nocifs pour l'environnement dans leurs procédés de fabrication.

Plus récemment, la recherche s'est concentrée sur une nouvelle génération d'aérogels biosourcés : les « bio-aérogels ». Ces derniers sont généralement fabriqués à partir de polysaccharides via un procédé de dissolution-échange de solvant-séchage au  $\text{CO}_2$  supercritique (voir Figure 2), comme par exemple les aérogels de cellulose, d'amidon, d'alginate ou de pectine pour les plus connus.

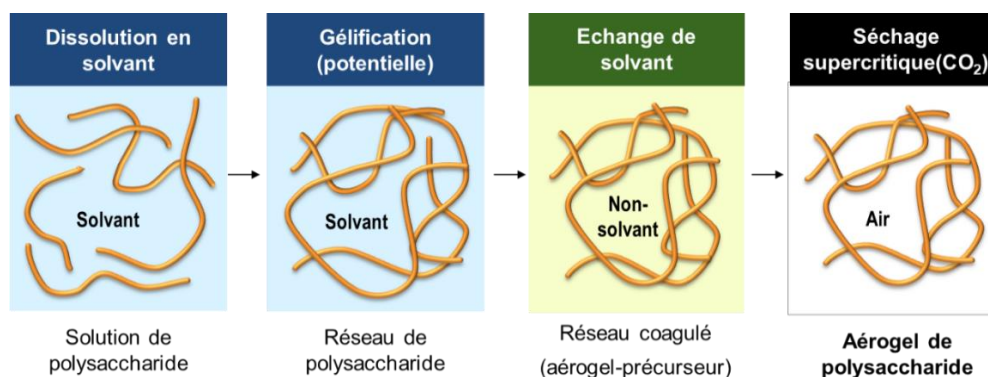


Figure 2. Illustration schématique du procédé de fabrication des aérogels de polysaccharide.

Les aérogels de polysaccharides montrent de réels avantages comparés aux aérogels classiques car ils sont ductiles et compressibles (Rudaz et al. 2014) et de ce fait, présentent potentiellement de meilleures propriétés mécaniques que les fragiles aérogels de silice. Issus de ressources naturelles renouvelables, résultants de procédés de fabrication plus respectueux de l'environnement et n'intégrant pas de composé toxique, ils sont aussi des alternatives plus durables aux aérogels synthétiques. Enfin, du fait de leurs biodégradabilité, biocompatibilité et de la grande possibilité de fonctionnalisation inhérentes aux polysaccharides, ces aérogels biosourcés pourraient offrir de nouvelles perspectives pour d'autres types d'applications, notamment en lien avec les sciences du vivant (biomédical, alimentaire, cosmétique, pharmaceutique, etc.).

Dans le cadre de cette thèse de doctorat, nous avons utilisé la pectine, un polysaccharide extrait de fruits et couramment utilisé comme agent épaississant/gélifiant dans l'agro-alimentaire, pour fabriquer des bio-aérogels. Le sujet de cette thèse porte sur les corrélations structure-propriétés des aérogels de pectine utilisés en tant que matériaux de pointe pour i) l'isolation thermique et ii) la libération de médicaments. Dans les sections suivantes, nous expliquons d'abord en quoi les bio-aérogels utilisés en tant qu'isolants thermiques peuvent être une alternative durable et prometteuse aux aérogels "classiques" fabriqués à partir de silice ou de polymères synthétiques, puis dans un second temps en quoi les bio-aérogels pourraient présenter des avantages majeurs par rapport aux hydrogels utilisés dans les sciences du vivant.

### ➤ Les bio-aérogels pour l'isolation thermique

Afin de réduire les pertes en énergie, de nombreuses études ont été menées afin de concevoir des bâtiments à basse consommation d'énergie, principalement via l'isolation thermique des murs grâce à l'application de matériaux isolants épais et/ou multicouches. De par leurs caractéristiques physiques exceptionnelles, les aérogels présentent une très faible conductivité thermique, généralement dans le domaine de la super-isolation (c'est-à-dire avec une conductivité thermique inférieure à celle de l'air), et se prêtent donc parfaitement à des applications d'isolation thermique. Les aérogels "classiques" présentent cependant soit de faibles propriétés mécaniques (aérogels de silice), soit leurs procédés de fabrication intègrent des composés toxiques (aérogels organiques).

Une alternative prometteuse, alliant hautes performances des matériaux et aspects écologiques, consiste à développer une nouvelle génération d'aérogels super-isolants, biosourcés et issus de procédés plus "verts", et présentant de propriétés mécaniques satisfaisantes. Le développement de bio-aérogels à base de polymères naturels aux propriétés thermiques super-isolantes est un sujet de recherche d'actualité. (voir par exemple les travaux de Rudaz et al., 2014). Les premiers bio-aérogels à base de cellulose (et dérivés) n'ont pas fait preuve de propriétés super-isolantes (voir, par exemple (Rudaz, 2013)) contrairement aux

aérogels de pectine (Rudaz et al, 2014), de cellulose nano-fibrillée (Jiménez-Saelices, Seantier, Cathala, & Grohens, 2017 ; Kobayashi, Saito, & Isogai, 2014 ; Seantier, Bendahou, Bendahou, Grohens, & Kaddami, 2016), d'alginate (Gurikov, Raman, Weinrich, Fricke, & Smirnova, 2015) et d'amidon (Druel, Bardl, Vorwerg, & Budtova, 2017). Néanmoins, les relations entre la conductivité thermique, les caractéristiques structurales et les propriétés des bio-aérogels demeurent encore largement méconnues.

### ➤ Les bio-aérogels pour les sciences du vivant

Les hydrogels sont constitués d'un réseau 3D de polymères interconnectés maintenant une phase aqueuse liquide en leur sein. Leur utilisation est devenue très populaire dans les sciences du vivant du fait de leurs multiples propriétés attractives telles que leur forte teneur en eau, leur capacité de gonflement/contraction, leur perméabilité permettant la diffusion de liquides et molécules (absorption et relargage), la capacité à encapsuler des composés actifs, ou enfin une flexibilité et consistance souple se rapprochant des tissus physiologiques vivants. De ce fait, les hydrogels sont couramment utilisés pour diverses applications et dans de nombreux domaines tels que les industries alimentaire (additifs alimentaires et modificateurs de viscosité), cosmétique (masque facial, gels...), biomédicale (ingénierie de réparation tissulaire, chirurgie plastique, lentilles de contact, pansements, produits d'hygiène...), pharmaceutique (encapsulation et distribution de médicaments), agricole ou environnementale (rétention d'eau, systèmes de distribution des pesticides, adsorption de polluants) (Popa et Volf, 2018). Cependant, les hydrogels présentent quelques inconvénients techniques qui restreignent leurs possibilités d'usage en tant matrices déjà préfabriquées (Caló & Khutoryanskiy, 2015 ; Zhao et al., 2015). Les hydrogels étant des systèmes mécaniquement faibles, ils sont généralement fragiles et difficiles à manipuler. De plus, leur usage est limité en termes de transport (sans rupture du gel) mais également en termes de stockage dans le temps (stabilité microbiologique).

Pour pallier la fragilité intrinsèque des hydrogels, une solution envisageable serait de les sécher pour en obtenir des matériaux poreux secs, comme par exemple des aérogels (par séchage supercritique) ou des cryogels (par lyophilisation). Après séchage, il a été constaté une véritable amélioration des propriétés mécaniques permettant de manipuler et de transporter ces derniers plus facilement (et certainement à moindre coût du fait de leur grande légèreté). Ensuite, à la différence des hydrogels, difficiles à stériliser, les matériaux secs ne requièrent pas d'additifs antimicrobiens pour assurer leur stabilité en vue d'un stockage à long terme. Enfin, comme il sera démontré dans ce manuscrit, non seulement le recours au séchage supercritique préserve les propriétés physico-chimiques et fonctionnelles des hydrogels "initiaux", mais peut aussi permettre de mieux contrôler la libération des médicaments quand les aérogels sont utilisés en tant que matrices de libération de médicaments comparativement aux hydrogels.

## ➤ Objectifs de la thèse

Récemment, les aérogels de pectine se sont révélés être des biomatériaux prometteurs et à haute valeur ajoutée pour l'isolation thermique (Demilecamps, 2015 ; Rudaz, 2013). Ils présentent également un potentiel élevé pour les applications en lien avec les sciences du vivant. En effet, la pectine présente des propriétés gastro-résistantes, ce qui ouvre des perspectives d'utilisation des aéropectines en tant que matrice de libération de médicaments pour une administration orale (García-González, Alnaief et Smirnova, 2011 ; García-González, Jin, Gerth, Alvarez-Lorenzo, et Smirnova, 2015 ; Gonçalves et al., 2016 ; Tkalec, Knez, & Novak, 2015 ; Veronovski, Tkalec, Knez, & Novak, 2014). Toutefois, malgré l'importance du contrôle de la morphologie de l'aérogel au regard des performances des applications, nos connaissances concernant les relations entre le type de polysaccharide, les conditions de préparation et les propriétés structurales et d'application des aérogels sont encore très réduites.

L'objectif global de cette thèse est double :

- Tout d'abord, nous nous sommes intéressés à la compréhension des corrélations existantes entre les caractéristiques du polymère initial (pectine), le procédé de fabrication, la structure interne de l'aérogel et les propriétés d'application finale. Les questionnements que nous nous posons sont d'abord : " Comment contrôler et ajuster les propriétés texturales des bio-aérogels ", puis " Quelles sont les corrélations structure-propriétés des bio-aérogels dédiés que ce soit pour l'isolation thermique ou pour la libération de médicaments " ?
- Deuxièmement, nous avons cherché à évaluer, développer et illustrer le potentiel des aérogels de pectine utilisés comme biomatériaux pour les deux applications différentes : pour l'isolation thermique et la libération de médicaments.

Pour répondre à ces questions, la pectine (un polysaccharide issu d'agrumes), a été sélectionnée car elle permet de multiples variations de formulation/procédé influençant la viscosité des solutions et leur gélification, et ainsi pouvant conduire à une grande diversité morphologique d'aérogels. Une partie des travaux sur les aérogels de pectine utilisés pour la libération de médicaments (Chapitre V) a été réalisée dans le cadre du projet "Biogels" dans le cadre du programme BRANCUSI parrainé par Campus France et CNCS - UEFISCDI, Roumanie (PN-III-P3-3.1-PM-RO).

Dans ce cadre, nous avons préparé, caractérisé et étudié différents types d'aérogels de pectine et d'aérogels composites aux caractéristiques variées et nous les avons testés pour les deux applications. La variation systématique des paramètres externes (composition, pH, concentration en polymère, type de non-solvant, concentration d'ions métalliques mono- et divalents) nous a permis une modulation fine de la viscosité des solutions, des mécanismes de

gélification qui, en retour, ont grandement affecté les structures internes et les propriétés d'application finale des aérogels.

### ➤ Principales conclusions et perspectives des travaux de thèse

Tout au long de ce travail de thèse, nous avons fait la démonstration que les bio-aérogels de pectine (et composites) peuvent être utilisés pour des applications distinctes : comme matrices de libération de médicaments et pour l'isolation thermique.

Dans le premier chapitre décrivant les résultats obtenus dans ces travaux (**Chapitre III**), nous avons réalisé une étude complète sur l'ajustement des propriétés structurales, physiques et morphologiques des aérogels de pectine en adaptant finement les procédés de fabrication. Plus précisément, nous avons expliqué pourquoi et comment les propriétés intrinsèques de la pectine (comme le degré de méthylation) et les paramètres extrinsèques (comme le pH, le type de non-solvant, le type de sel et la concentration) influent sur les caractéristiques des aérogels de pectine. Le mécanisme de structuration du réseau, i. e. par gélification ou par séparation de phases, s'est avéré être la clé du contrôle de leur structure interne. Les corrélations multi-échelles entre les aspects macromoléculaires (ionisation des polymères avec pH, sensibilité au calcium et liaison) et les propriétés morphologiques, structurelles et mécaniques des aérogels de pectine sont maintenant établies. Les résultats obtenus constituent des lignes directrices permettant la production d'autres aérogels matrices (notamment à partir d'autres polyélectrolytes) aux caractéristiques parfaitement maîtrisées.

Dans le **Chapitre IV**, nous avons étudié en détail les propriétés thermiques des aérogels de pectine. Le procédé de fabrication a été modifié de manière systématique afin de moduler la densité et la morphologie des aérogels et ainsi de déterminer leur influence sur la conductivité thermique de l'aérogel. Pour la première fois, il a été possible d'obtenir une courbe en U entre la conductivité thermique et la densité pour des bio-aérogels synthétisés via dissolution-échange de solvants - séchage supercritique. Nous avons démontré que le type d'interactions des chaînes de pectine et l'état physique de la matière (solution ou gel) sont essentiels pour comprendre et prédire la morphologie et les propriétés finales des aérogels. Un compromis délicat entre la morphologie de l'aéropectine (taille des pores) et sa densité est nécessaire pour optimiser l'effet Knudsen tout en minimisant la conduction thermique via le squelette solide afin d'obtenir la plus basse conductivité thermique possible. Cette valeur minimale de  $0,0147 \pm 0,0002 \text{ W/(m.K)}$  a été obtenue pour une aéropectine produite à partir d'une solution non-gélifiée de pectine à une concentration de 2 wt% et au pH = 2, ce qui est très proche de la conductivité minimale reportée pour les aérogels de silice ( $\sim 0.012 \text{ W/(m.K)}$ ) (Baetens et al. 2011). Par conséquent, les aérogels de pectine présentent un potentiel élevé pour les applications d'isolation thermique dans la mesure où ils sont super-isolants, entièrement biosourcés et mécaniquement robustes.

Dans le **Chapitre V**, nous avons exploré et évalué le potentiel des aérogels de pectine comme système de libération orale de médicaments en utilisant la théophylline comme médicament modèle. Il a été démontré que l'efficacité et la capacité de charge de la substance médicamenteuse dans l'aérogel dépendaient de la structure et des propriétés de la matrice (surface spécifique et densité). Une fois immergée dans des milieux physiologiques artificiels, les aérogels de pectine ont présenté un comportement de libération prolongée du médicament, caractérisée par une phase de résistance à l'érosion en milieu gastrique suivie par une phase de dissolution rapide en milieu intestinal. Il est apparu que la libération du médicament était régie par des transports diffusifs à travers le système, associés à des phénomènes de relaxation induits par le gonflement et l'érosion de la matrice, en corrélation avec les caractéristiques de polyélectrolytes et hydrosolubles de la pectine. En ajustant la formulation et de la méthode de séchage des échantillons, nous avons pu déterminer l'impact des paramètres structuraux des aéropectines (surface spécifique, densité et degré de réticulation ionique avec le calcium) sur la cinétique de libération et de charge en médicaments. Dans l'ensemble, nos résultats mettent en évidence la possibilité d'adapter les propriétés de libération des médicaments des aérogels par la modification du procédé dans le but de cibler le plus précisément possible les indications thérapeutiques. Les aéropectines présentent un potentiel très prometteur pour les applications de libération de médicaments en tant que matrices biodégradables, biocompatibles et biosourcés.

Enfin, dans le dernier chapitre (**Chapitre VI**), nous sommes allés encore plus loin en montrant que la cinétique de libération des aérogels de pectine pouvait être modifiée par la préparation d'aérogels composites organique-organique et organique-inorganique basés sur la pectine. Nous avons proposé des méthodes originales permettant d'interpénétrer les réseaux de pectine avec la cellulose et la silice en vue de produire des aérogels composites chargés en médicaments. Les aérogels de pectine-cellulose ont été fabriqués par imprégnation d'une solution de pectine dans une matrice de cellulose, tandis que les aérogels de pectine-silice ont été produits par imprégnation de particules de silice organique dans un réseau de pectine. La formulation et le procédé ont été modifiées afin de moduler les propriétés structurales, physiques et physico-chimiques des aérogels composites pectine-cellulose et pectine-silice, ce qui s'est répercuté sur leurs propriétés de libération de médicaments. Puis, nous avons démontré que la charge en médicament dans l'aérogel, les paramètres cinétiques ainsi que les mécanismes physiques impliqués dans la libération du médicament (diffusion et/ou érosion) pouvaient être contrôlés en adaptant la composition et le procédé de des composites. En particulier, nous avons réussi à obtenir des profils différents de libération du médicament en combinant finement les propriétés physico-chimiques, structurelles et physiques apportées par chaque composant du composite : d'un relargage immédiat, à une libération prolongée pendant plusieurs heures, et même, jusqu'à une libération prolongée pendant plus de 24 heures. L'ensemble des travaux présenté et discuté dans les chapitres V et VI contribue à la compréhension des phénomènes

physiques impliqués dans la libération de médicaments à partir d'aérogels, et permet de mettre en lumière les corrélations composition – structure-propriétés des matrices aérogels.

En tant que conclusion générale, comme cela a été démontré tout au long de ces travaux de thèse, les aérogels de pectine peuvent être des bio-matériaux versatiles et performants à fort potentiel tant pour l'isolation thermique que la libération de médicaments. Ils répondent ainsi parfaitement aux attentes et spécificités des matériaux avancés dont les propriétés physico-chimiques, structurelles et morphologiques peuvent être adaptées avec précision en vue de répondre spécifiquement à une application donnée. Cependant, l'ensemble des travaux réalisés au cours de ces trois années de thèse sur les aérogels de pectine ne constitue pas une "solution clé en main" directement applicable, le domaine des bio-aérogels étant encore très récent. C'est pourquoi, nous tenons à faire part de perspectives éventuelles susceptibles d'inspirer les recherches futures sur les aérogels de polysaccharides.

#### ➤ Perspectives en lien avec l'isolation thermique

- Premièrement, les raisons pour lesquelles les aérogels de pectine et certains autres bio-aérogels sont des matériaux super-isolants contrairement à d'autres (ex. aérogels de cellulose) demeurent inexplicables. Nous mettons en évidence ici l'influence de la structure chimique des chaînes des polysaccharides sur la morphologie des aérogels et donc sur leurs propriétés thermiques finales. La modélisation des phénomènes moléculaires au cours de la coagulation serait particulièrement intéressante pour mieux appréhender (et piloter) la formation du réseau en milieu liquide lors de l'étape d'échange des solvants.
- De plus, un défi technique particulièrement attractif serait celui de l'hydrophobisation des bio-aérogels (hydrophiles) afin de réduire l'adsorption d'humidité et prévenir le vieillissement des matériaux. En outre, afin de conserver un procédé « vert », l'utilisation de composés naturellement hydrophobe (cire, acide gras végétaux) constituerait une bien meilleure option pour les bio-aérogels que les techniques classiques d'hydrophobisation des aérogels de silice par silylation (*e.g.* au trichlorométhylsilane ou méthyltriméthoxysilane).

#### ➤ Perspectives pour des applications biomédicales

- Comme nous l'avons montré dans cette thèse, les propriétés de libération de médicaments des aérogels "matrices" peuvent être modifiées en fabriquant des aérogels composites de divers composants (organiques ou inorganiques). Le " mixage " des

propriétés apportés par les différents constituants de la matrice engendre de nouvelles caractéristiques physiques et chimiques au composite et ouvre de nouvelles perspectives aux aérogels polysaccharidiques utilisés comme vecteurs médicamenteux. Il peut être intéressant d'aller plus loin, par exemple en enrobant un "coeur" de polysaccharide peu soluble par d'une enveloppe externe d'un polysaccharide gastro-résistant (pectine ou alginate, par.ex.) (technique du « core-shell »). Cela atténuerait à la fois la forte phase de "burst " observée en début de cinétique, protégerait le médicament de toute dégradation acide dans l'estomac et différerait sa libération dans le tractus intestinal.

- Enfin, la technologie d'impression 3D des gels ouvre la voie à la synthèse de tissus bio-artificiels (ingénierie de réparation tissulaire) (Markstedt et al., 2015). Du fait de sa gélification ionique rapide avec le calcium, l'alginate (un autre polysaccharide polyélectrolyte) est déjà couramment utilisé comme « bio-encre » pour produire des hydrogels imprimés en 3-D (Axpe & Oyen, 2016 ; Song et al., 2011). Récemment, les gels de pectine se sont également avérés être des matériaux imprimables, citons par exemple les travaux de (Vancauwenberghe, Baiye Mfortaw Mbong, et al, 2017) concernant l'impression 3D d'une matrice de pectine encapsulant des cellules végétales vivantes en son sein. Le séchage supercritique d'hydrogels de pectine imprimés en 3D permettrait de concevoir sur mesure des aérogels hautement poreux aux structures spécifiques, pour produire des supports cellulaires pour la médecine régénérative.

## Références

- Axpe, E., & Oyen, M. L. (2016). Applications of Alginate-Based Bioinks in 3D Bioprinting. *International Journal of Molecular Sciences*, 17(12). <https://doi.org/10.3390/ijms17121976>
- Baetens, R., Jelle, B. P., & Gustavsen, A. (2011). Aerogel insulation for building applications: A state-of-the-art review. *Energy and Buildings*, 43(4), 761-769. <https://doi.org/10.1016/j.enbuild.2010.12.012>
- Caló, E., & Khutoryanskiy, V. V. (2015). Biomedical applications of hydrogels: A review of patents and commercial products. *European Polymer Journal*, 65, 252-267. <https://doi.org/10.1016/j.eurpolymj.2014.11.024>
- Demilecamps, A. (2015). *Synthesis and characterization of polysaccharides-silica composite aerogels for thermal superinsulation*. (PhD Thesis, Ecole Nationale Supérieure des Mines de Paris).
- Druel, L., Bardl, R., Vorweg, W., & Budtova, T. (2017). Starch Aerogels: A Member of the Family of Thermal Superinsulating Materials. *Biomacromolecules*, 18(12), 4232-4239.
- García-González, C. A., Alnaief, M., & Smirnova, I. (2011). Polysaccharide-based aerogels—Promising biodegradable carriers for drug delivery systems. *Carbohydrate Polymers*, 86(4), 1425-1438. <https://doi.org/10.1016/j.carbpol.2011.06.066>
- García-González, C. A., Jin, M., Gerth, J., Alvarez-Lorenzo, C., & Smirnova, I. (2015). Polysaccharide-based aerogel microspheres for oral drug delivery. *Carbohydrate Polymers*, 117, 797-806. <https://doi.org/10.1016/j.carbpol.2014.10.045>
- Gonçalves, V. S. S., Gurikov, P., Poejo, J., Matias, A. A., Heinrich, S., Duarte, C. M. M., & Smirnova, I. (2016). Alginate-based hybrid aerogel microparticles for mucosal drug delivery. *European Journal of Pharmaceutics and Biopharmaceutics: Official Journal of Arbeitsgemeinschaft Fur Pharmazeutische Verfahrenstechnik e.V*, 107, 160-170. <https://doi.org/10.1016/j.ejpb.2016.07.003>
- Gurikov, P., Raman, S. P., Weinrich, D., Fricke, M., & Smirnova, I. (2015). A novel approach to alginate aerogels: carbon dioxide induced gelation. *RSC Advances*, 5(11), 7812-7818. <https://doi.org/10.1039/C4RA14653K>
- Jiménez-Saelices, C., Seantier, B., Cathala, B., & Grohens, Y. (2017). Spray freeze-dried nanofibrillated cellulose aerogels with thermal superinsulating properties.

- Carbohydrate Polymers*, 157(Supplement C), 105-113.  
<https://doi.org/10.1016/j.carbpol.2016.09.068>
- Kistler, S. S. (1931). Coherent Expanded-Aerogels. *The Journal of Physical Chemistry*, 36(1), 52-64. <https://doi.org/10.1021/j150331a003>
- Kobayashi, Y., Saito, T., & Isogai, A. (2014). Aerogels with 3D Ordered Nanofiber Skeletons of Liquid-Crystalline Nanocellulose Derivatives as Tough and Transparent Insulators. *Angewandte Chemie International Edition*, 53(39), 10394-10397. <https://doi.org/10.1002/anie.201405123>
- Markstedt, K., Mantas, A., Tournier, I., Martínez Ávila, H., Hägg, D., & Gatenholm, P. (2015). 3D Bioprinting Human Chondrocytes with Nanocellulose–Alginate Bioink for Cartilage Tissue Engineering Applications. *Biomacromolecules*, 16(5), 1489–1496. <https://doi.org/10.1021/acs.biomac.5b00188>
- Pekala, R. W. (1989). Organic aerogels from the polycondensation of resorcinol with formaldehyde. *Journal of Materials Science*, 24(9), 3221-3227. <https://doi.org/10.1007/BF01139044>
- Popa, V. I., & Volf, I. (2018). *Biomass as Renewable Raw Material to Obtain Bioproducts of High-Tech Value*. Elsevier.
- Rudaz, C. (2013). *Cellulose and Pectin Aerogels: Towards their nano-structuration* (PhD Thesis, Ecole Nationale Supérieure des Mines de Paris). Consulté à l'adresse <https://pastel.archives-ouvertes.fr/pastel-00957296/document>
- Rudaz, C., Courson, R., Bonnet, L., Calas-Etienne, S., Sallée, H., & Budtova, T. (2014). Aeropectin: Fully Biomass-Based Mechanically Strong and Thermal Superinsulating Aerogel. *Biomacromolecules*, 15(6), 2188-2195. <https://doi.org/10.1021/bm500345u>
- Seantier, B., Bendahou, D., Bendahou, A., Grohens, Y., & Kaddami, H. (2016). Multi-scale cellulose based new bio-aerogel composites with thermal super-insulating and tunable mechanical properties. *Carbohydrate Polymers*, 138, 335-348. <https://doi.org/10.1016/j.carbpol.2015.11.032>
- Tkalec, G., Knez, Ž., & Novak, Z. (2015). Fast production of high-methoxyl pectin aerogels for enhancing the bioavailability of low-soluble drugs. *The Journal of Supercritical Fluids*, 106, 16-22. <https://doi.org/10.1016/j.supflu.2015.06.009>
- Vancauwenberghe, V., Baiye Mfortaw Mbong, V., Vanstreels, E., Verboven, P., Lammertyn, J., & Nicolai, B. (2017). 3D printing of plant tissue for innovative food manufacturing:

Encapsulation of alive plant cells into pectin-based bio-ink. *Journal of Food Engineering*.  
<https://doi.org/10.1016/j.jfoodeng.2017.12.003>

Veronovski, A., Tkalec, G., Knez, Ž., & Novak, Z. (2014). Characterisation of biodegradable pectin aerogels and their potential use as drug carriers. *Carbohydrate Polymers*, 113, 272-278. <https://doi.org/10.1016/j.carbpol.2014.06.054>

Zhao, F., Yao, D., Guo, R., Deng, L., Dong, A., & Zhang, J. (2015). Composites of Polymer Hydrogels and Nanoparticulate Systems for Biomedical and Pharmaceutical Applications. *Nanomaterials*, 5(4), 2054-2130. <https://doi.org/10.3390/nano5042>



## **CHAPTER I. STATE OF THE ART**

---

### **PECTIN AND OTHER BIO-AEROGELS: PREPARATION, PROPERTIES AND SELECTED APPLICATIONS**

## CONTENTS

### CHAPTER I. STATE OF THE ART

INTRODUCTION.....	42
<b>1. PECTIN: STRUCTURE AND PROPERTIES .....</b>	<b>43</b>
1.1. SOURCES AND EXTRACTION OF PECTIN .....	43
1.2. CHEMICAL AND MACROMOLECULAR STRUCTURES.....	44
1.3. PHYSICO-CHEMICAL PROPERTIES OF PECTINS .....	46
1.3.1. <i>Physical acid-gelation</i> .....	47
1.3.2. <i>Ionic gelation in presence of divalent cations (called ionic gelation)</i> .....	49
1.3.3. <i>Food and pharmaceutical uses of pectin</i> .....	52
1.4. CONCLUSION ON PECTIN .....	53
<b>2. AEROGELS .....</b>	<b>54</b>
2.1. GENERALITIES ON AEROGELS .....	54
2.1.1. <i>Network formation via sol-gel route</i> .....	54
2.1.2. <i>General aspects of the drying methods</i> .....	55
2.2. CLASSICAL INORGANIC AND SYNTHETIC POLYMER AEROGELS: A BRIEF OVERVIEW.....	57
2.2.1. <i>First generation of aerogels: silica aerogels</i> .....	58
▪ The synthesis of silica aerogels.....	58
▪ Hydrophobization treatment.....	59
2.2.2. <i>Synthetic organic polymers aerogels</i> .....	60
2.2.3. <i>Applications of classical aerogels</i> .....	62
2.3. BIO-AEROGELS: THE THIRD GENERATION OF AEROGELS.....	64
2.3.1. <i>Synthesis routes of bio-aerogels: similarities and differences with inorganic and synthetic polymer aerogels</i> .....	67
▪ Network formation by polymer gelation or by direct coagulation .....	67
▪ Solvent exchange and supercritical drying .....	68
2.3.2. <i>Aerogels based on neutral polysaccharides</i> .....	70
▪ Cellulose II aerogels.....	70
▪ Starch aerogels .....	71
2.3.3. <i>Aerogels based on polyelectrolyte polysaccharides</i> .....	72
▪ Pectin aerogels .....	72
▪ Alginate aerogels.....	73
▪ Chitosan aerogels .....	74
2.3.4. <i>From bio-polymers to the diversity of bio-aerogels:</i> .....	75
2.3.5. <i>Modifications of bio-based aerogels</i> .....	76
2.4. BIO-AEROGELS FOR THERMAL INSULATION APPLICATIONS .....	78
2.4.1. <i>Context</i> .....	78
2.4.2. <i>Thermal conductivity of aerogels</i> .....	79
2.4.3. <i>Aerogels used as thermal insulating materials: issues and open questions</i> .....	81
2.5. THE USE OF BIO-AEROGELS AND SILICA AEROGELS FOR DRUG DELIVERY APPLICATIONS.....	83
2.5.1. <i>Drug delivery systems: introductive concepts and principles</i> .....	84

CHAPTER I.  
State of the art

---

▪ Modified drug release behaviors.....	84
▪ Drug release mechanisms from polymer matrix systems.....	85
2.5.2. <i>Aerogels used as drug delivery systems</i> .....	87
▪ Production of drug loaded aerogels .....	87
▪ Factors influencing drug loading .....	89
▪ Case studies of silica-based and polysaccharide-based aerogels .....	90
➤ Effect of aerogel composition on the release properties.....	91
➤ Effect of preparation conditions on aerogels' release properties.....	94
➤ Effect of hydrophobization on aerogels release properties .....	95
▪ Creation of complex matrix systems by production of composite aerogels .....	96
<b>CONCLUSIONS .....</b>	<b>99</b>
<b>REFERENCES.....</b>	<b>100</b>

## Introduction

Recently, pectin aerogels turned out to be extremely promising bio-based materials for high added-values application such as thermal insulation (Demilecamps, 2015; Rudaz et al., 2014), they also present a high potential for life sciences applications. Despite the importance of aerogel structure control regarding to applications' performances, very little is known about the relationships between the type of polysaccharide, processing conditions and aerogel texture and properties.

In this work we produced pectin aerogels with different internal structure and morphological properties and tested them for two applications: thermal insulation and drug delivery. The goal of our work was to understand and correlate the characteristics of the initial polymer (pectin), the preparation conditions, the internal structure of aerogel and the final application properties. The open questions we are asking here are first: "How can we control and tune the textural properties of bio-aerogels?" and then "What are the structure-properties correlations for bio-aerogels developed for either thermal insulation or for drug release applications?". To answer these questions we selected pectin, a versatile polysaccharide from fruits, as it allows numerous variations of conditions that influence solution viscosity and gelation, potentially leading to a wide range of aerogel morphologies and properties.

This chapter is a review of the state of the art on bio-aerogels focusing on what is known about the correlations between initial polysaccharide characteristics, aerogels' internal structure and application properties.

- The first part is dedicated to pectin: its structure, physico-chemical characteristics and different gelling mechanisms either in acidic conditions or using cations. The goal is to understand how we can tune the properties of pectin solutions/gels (and thus of pectin aerogels) based on the characteristics and specificity of the starting polymer.
- In the second part we introduce the concept of aerogel, a special class of highly porous materials obtained by supercritical drying. We review the state of the art on bio-aerogels, from their synthesis to their potential applications with a special focus on aerogels made from polysaccharides. We discuss the major advantages and drawbacks for industrial applications of bio-aerogels compared to classical ones taking silica aerogels as a reference. Finally, we present and detail two particular potential applications of aerogels: as thermal insulating materials and as matrices for drug release, and highlight the scientific issues and technical challenges which remain open.

The overall goal of this chapter is first to highlight the importance in aerogel structure control and then to question on what is known about structure-properties correlations of bio-aerogels.

## 1. Pectin: structure and properties

Polysaccharides (or polyosides) are natural carbohydrate polymers composed of long chains of repeating units of either monosaccharides (*e.g.*, glucose, mannose, fructose, galactose) or oligosaccharides (*e.g.*, cellobiose, sucrose, lactose) bounded together by glycosidic linkages. Polysaccharides regroup very different polymers whose physico-chemical properties depend on composition, structure (conformation) and molecular weight: they can be homo- or heteropolysaccharides, linear or highly branched, neutral or charged (anionic or cationic), hydrophilic or lipophilic, *etc.* Polysaccharides are extracted or produced by various natural sources: from marine sources (agar, alginates, and carrageenans), animals (glycogen, chitin), plants cell walls (cellulose, pectins), tuber and roots (starch), plant seeds (guar, locust bean gum) and microorganisms (xanthan, gellan gum, bacterial cellulose). In nature, they perform different functions, such as a structural role (*e.g.* cellulose or chitin), energy storage (*e.g.* starch or glycogen) or water regulation (*e.g.* pectin), depending on their composition, chemical structure, and ionic character (if any).

### 1.1. Sources and extraction of pectin

Pectin is a structural polysaccharide present in the middle lamella, the primary and secondary cell walls of non-woody plants, allowing cell wall expansion during plant growth and rigidity of plant tissue (F. Voragen, Schols, & Visser, 2013). Due to their anionic nature, pectins also play a role in the regulation of ion transport and water holding capacity (A. G. J. Voragen, Coenen, Verhoef, & Schols, 2009). Pectin content and chemical structure highly differ depending on plant type, age and source, but commercial pectins are mainly extracted from citrus peel (25 – 30% of dry matter or apple pomace (15 – 18 % of dry matter) (Walter, 2012) and are widely used in food industry as thickening and gelling agent. Sugar beets, sunflower heads and mango are pectin alternative sources, but with lower gelling abilities (BeMiller & Whistler, 2012).

Pectin is obtained by hot acid extraction (~ pH 2.0) from the raw vegetal material (apple pomace, citrus peel). The liquid pectin extract is filtered to eliminate solid residues and purified. Pectin extracts are then concentrated under vacuum before being precipitated using alcohols or aluminum salts. Pectin is then pressed and washed after being dried and grounded into powder. These processes lead to commercial High Methylation (HM) pectins of around 70% esterification, additional demethylation treatments are needed to produce other types of pectin (May, 1990).

## 1.2. Chemical and macromolecular structures

Pectin is a complex ramified hetero-polysaccharide composed of more than 17 different monosaccharides with more than 20 different linkages. It is essentially composed of linear blocks of  $\alpha$ -1,4-linked D-galacturonic acids (Gal.A) (see Figure 1) (called “smooth regions”), partly esterified, and blocks of highly ramified rhamnogalacturonan regions (called “hairy regions”) (Ridley, O’Neill, & Mohnen, 2001). The Gal.A content strongly varies with pectin source, but “industrial” pectins usually consist of high Gal.A content with a minimum requirement of 65% to be used as gelling and thickening agent (May, 1990).

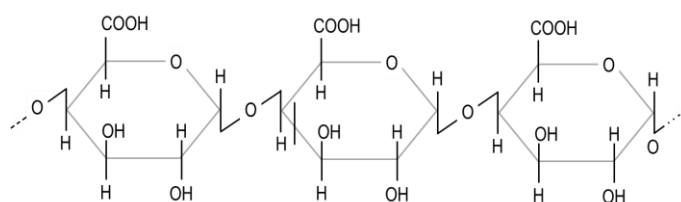


Figure 1. Chemical structure of pectin D-galacturonic acids linked by  $\alpha$ (1-4) glycosidic bonds

As illustrated in Figure 2, the linear homogalacturonan segments are frequently interrupted by rhamnose insertions causing chain “elbows” on which are branched side chains which are mainly composed of neutral sugars such as arabinose, galactose, arabinogalactose or xylose (Comstock, 1986; D. G. Oakenfull, 1991). Side chains and rhamnose elbows play a role in molecule rigidity and chains interaction due to steric hindrance (F. Voragen et al., 2013). In aqueous solutions, pectin forms helices, most probably right-handed, with three subunits per turn and an identity period of 1.31 nm (Walkinshaw & Arnott, 1981).

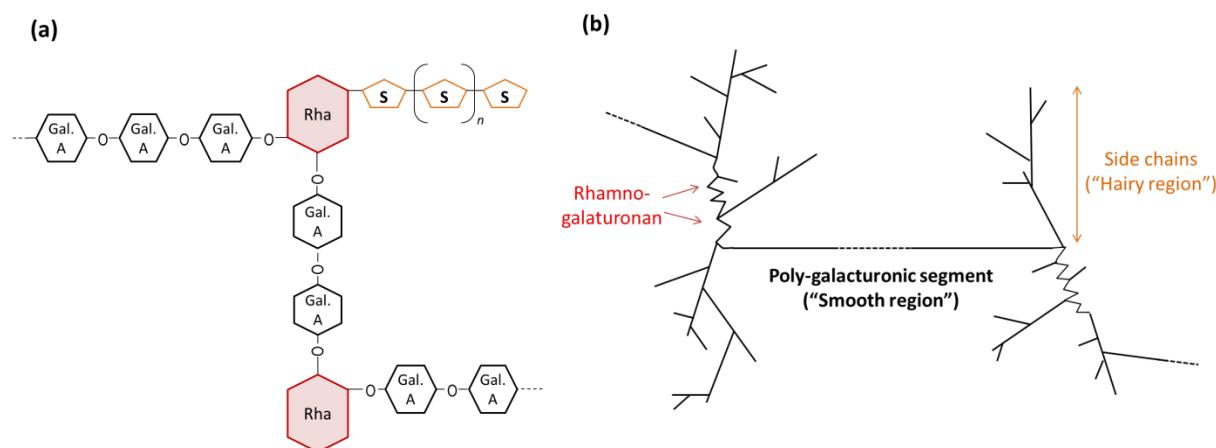


Figure 2. Schematic chemical structure of pectin chain

(a) The rhamosyl groups (Rha) induce elbows within the polygalacturonic acid chains (Gal.A) allowing the insertion of neutral sugars side chains (S)

(b) Homogalacturonans segments (smooth regions) branched by side chains (hairy regions)  
(adapted from (Axelos & Thibault, 1991))

Depending on pectin source and/or chemical treatments, Gal.A units are partly methyl-esterified at C<sub>6</sub>, and can be amidated at C<sub>6</sub> or acetylated at O<sub>2</sub> or O<sub>4</sub> positions, as illustrated in Figure 3. These chemical variations are known to strongly impact pectin physico-chemical properties and gelling abilities; in this chapter we will detail only the impact of methyl-esterification of pectin (the esterification degree and distribution) as it is the most common variation between commercial pectins.

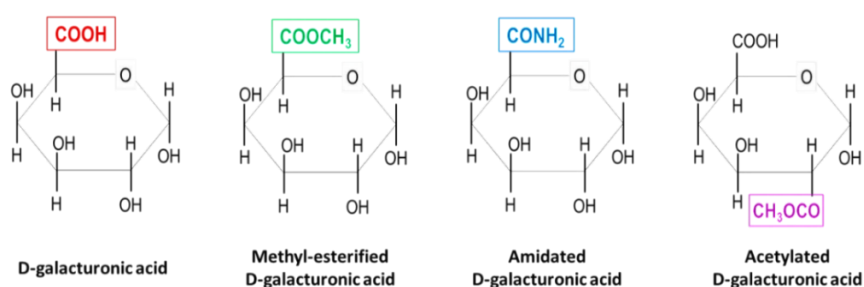


Figure 3. Chemical structure of D-galacturonic of pectin acids which can be either methyl-esterified, amidated or acetylated.

Pectin Degree of Esterification (DE) defines the proportion of Gal.A units that are methyl-esterified, and is commonly used to classify pectin into two groups: High-Methylated pectin (HM) for DE > 50% and Low-Methylated pectin (LM) for DE < 50% (see a schematic example in Figure 4). It is commonly admitted that HM and LM pectins have different macromolecular properties and gelling abilities. Indeed, HM pectin chains are more likely to form hydrophobic interactions due to the high proportion of methyl-esterified Gal.A, while LM pectin are more likely to interact with divalent cations via carboxylate functions of their non-esterified Gal.A (Sriamornsak, 2003). The impacts of pectin DE on their gelation mechanisms are detailed in the next Section 1.3.

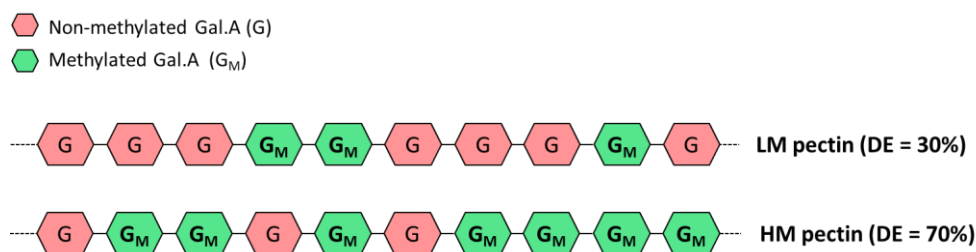


Figure 4. Schematic representation of the homogalacturonan segment of Low Methylated pectin (LM) and High Methylated pectin (HM) based on the Degree of Esterification (DE) (%) of their galacturonic acids (Gal.A).

Pectins with lower DE are obtained by industrial demethylation processes and consist of

the replacement of methyl-ester groups of HM pectins by carboxylic acid functions (hydrolysis). This is carried out using either enzymatic treatment (methyl-esterase) or more commonly by chemical process in alkaline or neutral conditions and low temperature. Alkaline treatments are known to induce pectin  $\beta$ -depolymerization even at low temperature, and lead to reduction of the neutral sugars content and molecular weight (Ilse Fraeye, Duvetter, Doungra, Van Loey, & Hendrickx, 2010; Garnier, Axelos, & Thibault, 1993; Thakur, Singh, Handa, & Rao, 1997). Using ammonia hydrolysis for pectin demethylation results in conversion of some ester groups into amide groups, leading to amidated pectins with different gel forming ability.

Finally, it has to be noted that large differences may exist between pectins due to natural polydispersity (plant source, species, tissue, and maturity), acid extraction process and additional demethylation treatment. This leads to highly different pectin intrinsic characteristics (such as the degree of esterification, of amidation or acetylation, structural distribution of methyl-ester group, pectin molecular weight ...etc.) which in turn strongly impacts pectin physico-chemical properties and gelling abilities. Depending on the intrinsic properties of the polymer and external conditions (pH, temperature, ionic strength, presence of multivalent metal ions, sugars, etc.) pectin chains in aqueous solutions may associate in different ways leading to the formation of various types of gels.

### 1.3. Physico-chemical properties of pectins

Pectin is water-soluble polyelectrolyte polysaccharide with  $pK_a$  around 2.9 – 3.5 (Ralet, Bonnin, & Thibault, 2002; Ralet, Dronnet, Buchholt, & Thibault, 2001) depending on pectin DE. Pectins are relatively stable in water at pH  $\sim$  3 – 4, however prolonged heating in a strongly acidic media may lead to pectin degradation by acid hydrolysis, while neutral to alkaline conditions can lead to  $\beta$ -depolymerization and de-methoxylation (I Fraeye et al., 2007; Krall & McFeeters, 1998; Renard & Thibault, 1996).

As a consequence of their polyelectrolyte nature, pectins present a high sensitivity to ionization/protonation of carboxyl functions induced by pH change. This is known to strongly impact their chain charge density, their water binding capacity and chains interactions abilities. Dissolved pectin can interact in aqueous solvent by joining their homogalacturonan domains into intermolecular junction zones involving successive physical bonds. These physical bonds can be based on different chains interactions depending on the conditions: chain entanglements, hydrogen bonds, hydrophobic interactions or ionic bonds with multivalent cations. If the number of efficient interactions is sufficient, pectin 3D-network is formed within the aqueous phase, resulting in a physical gel. Pectin solution viscosity and ability to gel are governed by chains interactions, the latter being influenced by various external parameters (*e.g.* temperature, polymer concentration, soluble solids content, pH and presence of ions, the ionic strength and

type of ions, etc.) as well as a large number of pectin intrinsic characteristics (*e.g.* chemical structure, molecular weight, degree of esterification / amidation / acetylation, branching degree, charge distribution along the chain, etc.) (Axelos & Thibault, 1991; Thakur et al., 1997). Depending on the main type of chains interactions involved in the gelation process, two different physical gelation mechanisms are reported for pectin: acid-induced gelation (or “acid gelation”) in acidic media ( $\text{pH} < 3.0$ ) or ionic gelation in the presence of polyvalent cations.

### 1.3.1. Physical acid-gelation

It is known that dissolved pectin, being a polyelectrolyte, is very sensitive to pH. Indeed, pH lower than pectin  $\text{pK}_a$  ( $\sim 2.9 - 3.5$ ) favors the protonation of carboxylic acids functions of pectin ( $-\text{COOH}$ ) while pH above  $\text{pK}_a$  favors their dissociation into carboxylate ( $\text{COO}^-$ ). At low pH chains associate and are stabilized by successive hydrogen bonding between un-dissociated free carboxylic acids and secondary alcohol groups and by hydrophobic interactions between methyl esters (D. G. Oakenfull, 1991; D. Oakenfull & Scott, 1984), as illustrated in Figure 5. This is reflected by change of solution viscosity and may lead to acid gelation if the number of junction zones is sufficient, the latter depending on solution’s temperature and pectin concentration (Garnier et al., 1993; Kar & Arslan, 1999; F. Voragen et al., 2013).

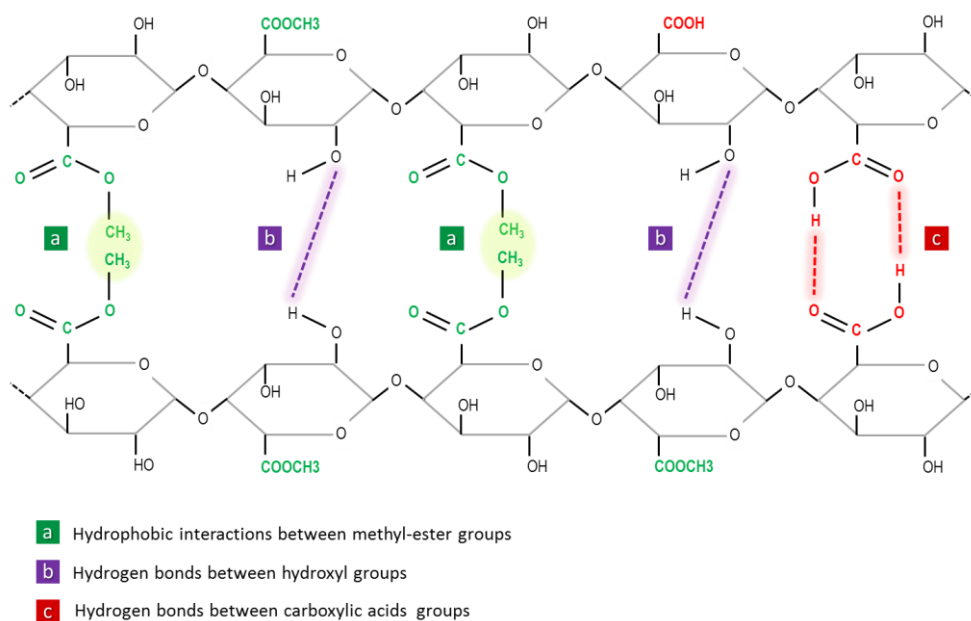


Figure 5. Schematic illustration of pectin acid gelation involving hydrogen bonding between un-dissociated free carboxylic acids and secondary alcohol groups and by hydrophobic interactions between methyl esters. (Adapted from (Basu, Shivhare, & Chakraborty, 2017)).

Pectin acid-gelation is known to be temperature dependent as it is based on junction zones subject to thermal conditions: hydrogen bonds are destabilized with temperature, while

hydrophobic interactions are becoming more stable (F. Voragen et al., 2013). Overall, when pectin solutions are heated, thermal energy of pectin molecules is augmented which lower the viscosity of pectin solutions, and intermolecular distances increase due to thermal expansion. As a result, acid gels are formed during cooling when adverse thermal effects are overcompensated by chains interactions and other factors that reduce molecules mobility (*e.g.* pectin concentration, pH, ionic strength, co-solute, interactions with cations...) (Garnier et al., 1993; Kar & Arslan, 1999; D. G. Oakenfull, 1991). Hence, gelation time strongly decreases when interactions are favored between chain (*i.e.* by lowering temperature, increasing pectin concentration, adding cations or lowering pH). As a direct consequence of its thermal dependence, pectin acid gelation is thermo-reversible and pectin acid-gel becomes a solution by increasing temperature.

On the opposite, the increase of pH above  $pK_a$  leads to progressive dissociation of carboxylic acids into carboxylates. The increase of negative charges along pectin backbone results in chain repulsion due to coulombic repulsion and increase of the osmotic pressure of counterions which lead to a high hydration of pectin macromolecules. In this case, ionized pectin chains are hydrated, extended, and independent from each other, leading to the decrease of solution viscosity and preventing polymer aggregation and gelation (Paoletti, Cesaro, Delben, & Ciana, 1986).

It is known that HM and LM pectins have different macromolecular properties impacting their gelling abilities. Indeed, HM pectin chains are more likely to form hydrophobic interactions due to the high proportion of esterified Gal.A, while LM pectin are more likely to create ionic bonds with divalent cations using the carboxylate functions of their non-esterified Gal.A. As a result, for a long time it was commonly admitted that HM and LM pectins were presenting opposite gelling mechanisms. Due to the high proportion of methylated groups, it was admitted that HM pectin was only able to acid-gel in an acidic environment (typically  $pH < 3.5$ ) and in the presence of large amount of low molecular weight co-solutes (typically sucrose  $> 55 - 60$  wt%). Indeed, the presence of a high concentration of sugar reduces water activity and stabilizes junction zones by promoting hydrophobic interactions between methyl-esters groups (Evageliou, 2000; D. G. Oakenfull, 1991).

In contrast, LM pectin was thought to gel only by ionic gelation in the presence of divalent cations (Axelos & Thibault, 1991) (as it will be explained in the next paragraph). However, several recent works reported the ability of LM pectins to also be able to gel under cooling in very acidic conditions ( $pH < 3.0$ ) thanks to the high proportion of non-methyl-esterified carboxyl groups (Capel, Nicolai, Durand, Boulenguer, & Langendorff, 2006; Dobies, Kempka, Kuśmia, & Jurga, 2008; Fishman & Cooke, 2009; Gilsenan, Richardson, & Morris, 2000, 2003; Lootens et al., 2003; Ström et al., 2007; Yuliarti, Hoon, & Chong, 2017). Acid gelation mechanism of LM pectins are not clearly identified but contemporary theories assume that it is attributed to the suppression of electrostatic repulsion at low  $pH (< pK_a)$ , which allows

numerous carboxyl groups to act as hydrogen bond donor (Gilsenan et al., 2000). Successive and stable hydrogen bonds between adjacent chains are then created between protonated carboxylic acid groups of the Gal.A and also between the hydroxyl groups of neighboring molecules (Vincent, Mansel, Kramer, Kroy, & Williams, 2013). Gilsenan et al. and *Dobies* et al. proved that decreasing pH below  $pK_a$  leads to pectin chain conformation change from an extended two-fold to a more compact threefold helical structure (Dobies et al., 2008; Gilsenan et al., 2003). According to them, LM pectin chains undergo a conformational ordering that would allow their aggregation and possibly their gelation. Another theory is based on a “cooperative zipping interactions” effect from hydrogen bonding between LM pectin chains (Kjøniksen, Hiorth, & Nyström, 2005).

### 1.3.2. Ionic gelation in presence of divalent cations (called ionic gelation)

Pectin ionic gelation is based on electrostatic interactions involving ionized carboxylates of pectin galacturonic acids units and added metal ions. This gelling mechanism is generally attributed to LM pectin gels due to a higher proportion of non-methylated Gal.A able to interact with cations when dissociated, as compared to HM pectins ((Gilsenan et al., 2000; Löfgren, Walkenström, & Hermansson, 2002; Lootens et al., 2003; Morris, Gidley, Murray, Powell, & Rees, 1980). The cross-linking formed by ionic bonds between carboxylate functions and polyvalent cations such as calcium produce strong, brittle and less elastic pectin gels than those formed by hydrogen and hydrophobic interactions in acidic condition (Sriamornsak, 2003; Ström et al., 2007).

The ability of pectin to form complexes with polyvalent cations is based on strong electrostatic interactions between the cations and the free dissociated carboxyl groups of pectin, *i.e.* at pH close to or higher than  $pK_a$  (~ 2.9 -3.5). More precisely, the ionic bonding results from specific non-covalent electrostatic interactions between polyvalent cations and the oxygen atoms of the hydroxyl groups, the oxygen atoms of the glucosidic ring and the bridging oxygen atoms of dissociated galacturonic acids through their free-electron pairs (Rudolf Kohn, 1987) as shown in Figure 6a. This leads to the formation of an ionic “egg box” cavity and gives rise to a cross-linking of two different chains in close proximity. The lifetime of the ionic junction depends on the strength of the electrostatic bonds and becomes more stable in the presence of 7 to 20 consecutive ionic cross-links (Braccini & Pérez, 2001; Powell, Morris, Gidley, & Rees, 1982). Successive ionic bonds can form junction zones only between unbranched non-esterified galacturonan segments of two pectin chains in a twofold helical conformation, retaining metal ions in between.

As described by the so-called “egg-box model” developed for divalent metal ions such as calcium, the whole gelation mechanism is a two-step process with the formation of strongly linked dimers associating two crosslinked pectin chains (Figure 6b), followed by weak inter-

dimers associations governed by electrostatic interactions leading to an aggregate of several pectin chains (Figure 6c) (Grant, Morris, Rees, Smith, & Thom, 1973).

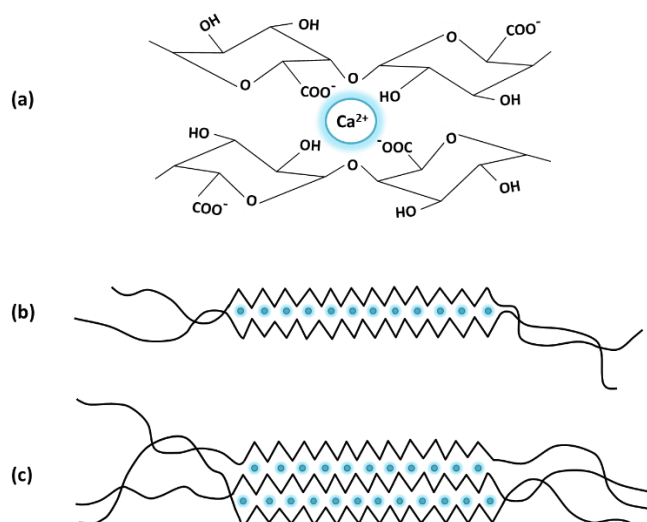


Figure 6. Schematic representation of calcium binding to polygalacturonate segment of pectin: (a) an "egg-box" cavity; (b) egg-box dimer; (c) aggregation of dimers. (Adapted from (Axelos & Thibault, 1991)).

This gelation mechanism depends on multiple intrinsic and extrinsic factors including pectin concentration and DE, type and concentration of cations, pH conditions, temperature and the type and concentration of soluble solid content (Axelos & Thibault, 1991). Generally, most of the works on LM pectins deal with their ionic gelation with calcium ions, but the affinity and binding capacity of LM pectin chains towards divalent cations was found to depend on the type and the valency of the cations. As an illustration, Dronnet et al. showed that pectin affinity toward cations increases as follows:  $\text{Cu}^{2+} \sim \text{Pb}^{2+} \ll \text{Zn}^{2+} < \text{Cd}^{2+} \sim \text{Ni}^{2+} \leq \text{Ca}^{2+}$  (Dronnet, Renard, Axelos, & Thibault, 1996) and Guo et al. showed it increased as follows  $\text{K}^+ < \text{Na}^+ < \text{Mg}^{2+} < \text{Ca}^{2+}$  (Guo et al., 2016).

If focusing on the ionic interactions between pectin and  $\text{Ca}^{2+}$  ions, it was found that pectin affinity towards calcium increases and pectin gelation was more pronounced by i) lowering pectin DE (R. Kohn & Luknár, 1975; Ström et al., 2007; Thibault & Rinaudo, 1985), ii) increasing calcium concentration (I Fraeye et al., 2007; Löfgren et al., 2002; Ström et al., 2007), iii) increasing polymer concentration (Garnier, Axelos, & Thibault, 1994), and iv) when solution pH is close and higher than  $\text{pK}_a$  ( $\sim 2.9 - 3.5$  depending on DE) (I Fraeye et al., 2007; Gidley, Morris, Murray, Powell, & Rees, 1980; Guo et al., 2016; Ström et al., 2007).

The effects of pH conditions and pectin DE on pectin gelling abilities are easily understood as they both influence the fraction of ionized free carboxylic groups of pectin that are available to interact with cations. Indeed, increasing the pH of pectin solutions above  $\text{pK}_a$  induces ionization of pectin and promotes ions binding by dissociated acid functions

(carboxylate). In the same way, lowering pectin DE increases its affinity towards cations as it directly increases the fraction of non-methylated functions able to be dissociated to interact with cations (R. Kohn & Luknár, 1975; Ström et al., 2007; Thibault & Rinaudo, 1985).

To reflect the impact of calcium concentration on pectins taking into account their respective intrinsic sensitivity toward cations due to different DE, the molar ratio  $R$  of metal cation ( $Me$ ) is commonly used (instead of only ions concentration), as an indicator of the ratio of cations per pectin carboxyl group ( $RCOO^-$ ) (expressed in  $\text{mol L}^{-1}$ ), the later directly depending on pectin DE and concentration. It is calculated as follows (Equation (1.1)):

$$R(Me) = \frac{[Me]}{[RCOO^-]} \quad (1.1)$$

It was shown that increasing  $R(\text{Ca})$  ratio by increasing calcium concentration up to a certain value reinforces pectin network by the formation of large amount of strong ionic junction zones, leading to denser and firmer pectin gels (Cárdenas, Goycoolea, & Rinaudo, 2008; I Fraeye et al., 2007; Grosso & Rao, 1998; Löfgren et al., 2002; Ström et al., 2007). However, there is a maximum amount of calcium which can bind pectin: it is around stoichiometric ratio, 0.3–0.6, depending on pectin degree of methylation (Dronnet et al., 1996; Garnier et al., 1994; Siew, Williams, & Young, 2005), which corresponds to molar ratio  $R(\text{Ca})$  from 0.15 to 0.3. “High” calcium level promotes gel syneresis and can even lead to pectin precipitation (BeMiller & Whistler, 2012; May, 1990).

Finally, in addition to the direct impact of pectin DE on its gelling abilities, the distribution pattern of methyl-esterified groups also strongly affects the rheological and gelling properties (BeMiller & Whistler, 2012). The distribution of methyl ester groups along the backbone chain can be either block-wise or random-like (Winning, Viereck, Nørgaard, Larsen, & Engelsen, 2007). Daas et al. introduced the term ‘Degree of Blockiness’ which is quantified by enzymatic digestion of the percentage of Gal.A which are distributed in blocks (*i.e.* contiguous Gal.A units  $\geq 4$ ). The higher the degree of blockiness of pectins with similar DE, the more block-wise the distribution of the methyl esters groups in the pectin. It is now known that a demethylation process via alkaline treatment or using fungus-pectin methyl esterase results in random distribution, while plant pectin methyl esterase results in block-wise distribution (Daas, Meyer-Hansen, Schols, De Ruiter, & Voragen, 1999). Like pectin DE, the degree of blockiness also strongly influences the functionality, the internal charge distribution and gelling ability of pectins. Compared to random-distributed pectins, block-wise pectins show stronger calcium-binding behavior with greater interchain associations in the presence of calcium, and are often referred to as “ $\text{Ca}^{2+}$ -sensitive” pectins (Powell et al., 1982; Thibault & Rinaudo, 1986). Several authors showed that pectins with similar DE but different internal distributions of methoxy groups responded completely differently to calcium addition and pH

changes (Löfgren, Guillotin, Evenbratt, Schols, & Hermansson, 2005; Löfgren & Hermansson, 2007; Lutz, Aserin, Wicker, & Garti, 2009).

### 1.3.3. Food and pharmaceutical uses of pectin

Like the majority of polysaccharides, pectin is part of our daily food diet and thus appears as a “human-friendly” polymer. Thanks to its high-water binding capacity and gelling abilities, pectin is widely used as a thickening or gelling agent, or as a stabilizer additive in food industry. Pectin is commonly added into various food preparations such as jams, jellies, bakery and dessert filling, soft drinks and fruit-based preparations and dairy products. Depending on the formulation and final targeted “sensorial texture” of the food product, either HM or LM pectins can be used. HM pectins are usually chosen for sweet acid preparations (juices, jams and desserts) as the latter present high sucrose concentration, promoting pectin thickening or gelling properties. LM pectins are especially useful in low-sugar food products or when gels need to be thermostable (during bakery cooking step, for example).

Thanks to its biodegradability and its safe toxicity profile which are required for medical and pharmaceuticals applications, pectin is particularly attractive for both its bio-active effects and/or its gelling properties.

As bio-active compound, pectin is known to be a natural hypocholesterolemic agent (Keys, Grande, & Anderson, 1961), a prophylactic substance against noxious effects of toxic cations such as mercury (Rudolf Kohn, 1982). Pectin has been extensively used to treat gastrointestinal disorders, and may present a small antimicrobial effect against *Escherichia Coli*, and antiviral activity (United States Patent No. US3485920A, 1969; Thakur et al., 1997).

The use of pectin is also interesting for wound healing preparations, as it is bio-active compound or for its gelling properties. Applied upon a wound, pectin can form adhesives and occlusive preparations with hemostatic properties (United States Patent No. US4292972A, 1981), while when administrated intravenously pectin shortens blood coagulation time which may be useful to restrain hemorrhage or wound local bleeding (Sriamornsak, 2003).

Besides its bioactive effects, pectin appears to be an interesting candidate for pharmaceutical applications, used as a binding agent, or as an excipient in pharmaceutical formulations. Around 1950, pectin was shown to be able to delay drug absorption, which reveals its high potential value for drug-controlled release (United States Patent No. US4199560A, 1980; Murray & Finland, 1946; Welch & Welch, 1949). Up to now, literature reports a large number of publications about pectin-based matrix formulations used as a sustained-release drug delivery system which allow a slow drug release in the body over an extended period of time, reducing side-effects and drug intake (see, for example, the work of

(Krusteva, Lambov, & Velinov, 1990)).

Due to its low solubility when crosslinked with calcium, and because it resists to gastric and intestinal enzymes but not to colonic pectinolytic ones (Englyst, Hay, & Macfarlane, 1987), pectin presents gastro-resistant properties (Sandberg, Ahderinne, Andersson, Hallgren, & Hultén, 1983) which are required to protect some drugs which are sensitive to degradation in gastric conditions. These properties also enable specific drug delivery to the lower gastrointestinal tract for a local or systemic action, and are particularly suitable for colon targeting in case of ulcerative colitis, Crohn's disease and colon carcinomas (Ashford, Fell, Attwood, Sharma, & Woodhead, 1993; Rubinstein, Radai, Ezra, Pathak, & Rokem, 1993). A wide range of pectin-based dosage forms are reported in literature such as hydrogel beads, compressed tablets, or film gel coating, and combinations with other polysaccharides (alginate (Pillay & Fassihi, 1999), chitosan (Macleod, Fell, Collett, Sharma, & Smith, 1999), and hydroxypropylmethyl cellulose (Orlu, Cevher, & Araman, 2006)). Their pharmaceutical properties may be tuned by adjusting formulation parameters such as the type of pectin, gelation conditions, addition of excipients, coating agents, or dosage forms.

#### **1.4. Conclusion on pectin**

As we have shown in this part, pectin is a versatile natural polymer sensitive to a wide range of intrinsic (molecular weight, DE, branching degree, ...) and extrinsic (pH, ionic strength, concentration of multivalent cations, presence of co-solute) parameters. Besides its interesting bio-active effects and gelling abilities, pectin presents attractive properties such as its biodegradability, non-toxicity and renewability: a "human-friendly" image which is required for life sciences applications.

In this PhD work we used different pectins from citrus presenting various DE (from 35% to 70%) to produce pectin-based aerogels, also called "aeropectins". Pectin was selected because it allows numerous variations of conditions that influence solution viscosity and gelation, hoping this would also allow obtaining wide range of pectin aerogel morphologies and properties. Through their wide range of physical and textural characteristics, pectin gels and aerogels were used as a model system to build some preparation-structure-properties correlations that were missing in the field of bio-aerogel.

## 2. Aerogels

In this second part, we mostly focus on supercritically dried aerogels. The first section is dedicated to the state of the art in area of aerogels and, in particular, of bio-based aerogels. Bio-based aerogels' properties, applications and open questions are then presented.

### 2.1. Generalities on aerogels

A gel is defined as a solid-liquid biphasic stable system, made of a solid percolating tridimensional network maintaining a liquid phase. The term “aerogel” was first introduced by Kistler to describe a gel whose liquid phase is replaced by a gas without collapsing the structure of the solid network (S. S. Kistler, 1931).

#### 2.1.1. Network formation via sol-gel route

“Classical” aerogels are usually synthesized via sol-gel route either from inorganic (*e.g.* silica (Pajonk et al., 1995)) or synthetic organic (*e.g.* resorcinol-formaldehyde (R. W. Pekala, 1989)) compounds (Pierre & Pajonk, 2002). Their general preparation takes place in three steps: gelation by sol gel process, aging of the gel (if needed) and supercritical drying, as schematized in Figure 7.

The sol-gel process is a method for producing solid materials from small molecules (monomers or particles). It involves the conversion of a solution into a colloidal suspension (the “sol”) which is gradually “transformed” into a network by polymerization.

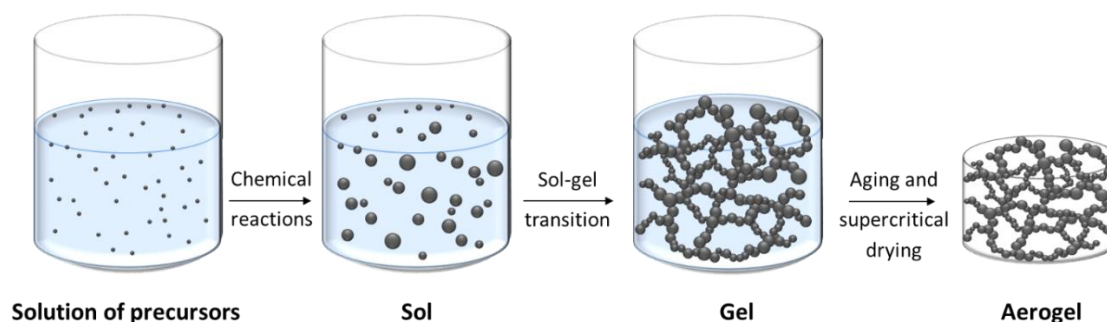


Figure 7. Schematic illustration of aerogel preparation via sol-gel process route

After sol-gel transition, an aging step may take place during which significant time-dependent changes occur such as completion of polymerization, potentially crystallization, aggregation, syneresis, phase changes, network scission or formation of junction zones. All

these processes contribute to the chemical and/or physical structure and properties of the gel. After aging, the wet gels are extensively washed with fresh solvent to remove excess of catalyst and non-polymerized entities from the pores. Finally, the removal of the liquid phase requires a drying process, and supercritical drying remains the “reference” technique for making aerogels. Currently, three main drying methods are considered to obtain dry porous materials: evaporative drying, freeze drying and supercritical drying (Pierre & Pajonk, 2002).

### 2.1.2. General aspects of the drying methods

During classical evaporative drying the liquid phase contained within the pores of the network forms a concave meniscus inside the gel pore due to lower cohesive intermolecular forces between liquid-liquid molecules than between liquid-solid (pore walls), as illustrated in Figure 8.

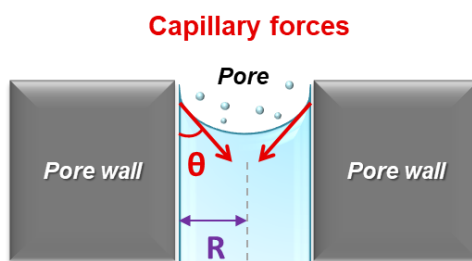


Figure 8. Illustration of capillary forces during evaporative drying.

With evaporation of a liquid, the meniscus curvature increases inducing a stress applied to pore’s walls termed as capillary forces. The capillary pressure is defined by Young-Laplace equation (see equation (1.2)):

$$P_c = \frac{2\gamma \cos \theta}{R} \quad (1.2)$$

with  $P_c$  the capillary pressure inside the pores (Pa),  $\gamma$  the surface tension between the evaporating liquid and the gas phase ( $\text{N}\cdot\text{m}^{-1}$ ),  $\theta$  the meniscus angle formed between the solid (pore walls) and the liquid phase (in  $^\circ$ ), and  $R$  the characteristic pore radius (m).

As the liquid phase evaporates, capillary pressure increases, pore walls collapse and the network starts to shrink. Capillary pressure can be high enough to provoke cracks, densification and complete destruction of the gel network structure. Thus, drying process route is a critical step if willing to produce low density open pores nanostructured material. To avoid capillary forces, it is necessary to either suppress the liquid-gas surface tension, or perform chemical treatment of pore surface to make meniscus angle as high as possible (close to  $90^\circ$ ) or for pores to re-open

as in the case of silylated silica ambient dried aerogels. Figure 9 shows the state of the matter phase diagram with three main ways of drying: by evaporative drying, by freeze-drying and by supercritical drying.

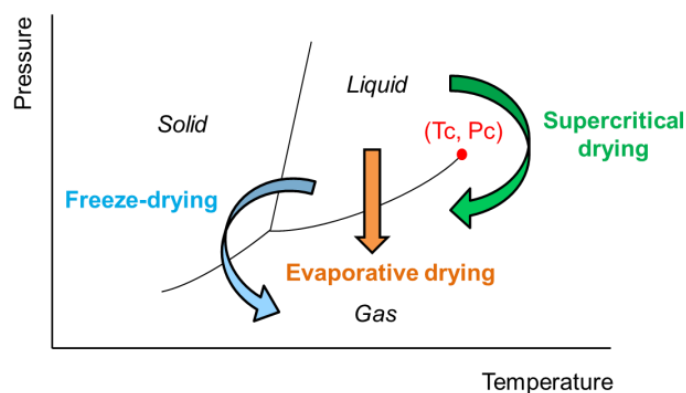


Figure 9. Schematic illustration of different drying processes: freeze-drying, evaporative drying and supercritical drying (above the critical temperature ( $T_c$ ) and pressure ( $P_c$ )).

Conventional evaporation, *i.e.* drying directly from liquid to gas, usually ends with dense and low-porosity materials, which we will call for simplicity “xerogels”. If using freeze-drying technique (also known as lyophilization), the liquid phase is frozen and then sublimated by lowering the pressure. However, freeze-dried samples, which will be termed as “cryogels” for simplicity, generally suffer from strong mechanical damages and pore walls densification due to ice crystals growth within the material.

In supercritical conditions *i.e.* above the critical temperature and pressure, densities of the liquid and vapor phases become equal leading to only one-phase supercritical fluid within the network. As there is no physical distinction between the liquid and vapor phases and thus, no vapor-liquid interface anymore, no capillary forces are exerted, which prevents from network collapsing, volume shrinkage and gel cracking (Brinker & Scherer, 1990). This drying process is termed as supercritical drying (sc-drying), and  $\text{CO}_2$  is commonly used due to its “mild” supercritical conditions ( $T_{\text{critical}} \sim 31^\circ\text{C}$  and  $P_{\text{critical}} \sim 75$  bars) suitable for the majority of polymers and also for polysaccharides.

Supercritical drying using  $\text{CO}_2$  starts from liquid  $\text{CO}_2$  at low pressure, which is then compressed and heated beyond its critical point in order to mix with the liquid phase in the gel pores. As a consequence, the fluid in the pores of the gel has to be miscible with the supercritical fluid used. Finally, slow and isothermal depressurization of the supercritical phase (mostly  $\text{CO}_2$  after supercritical extraction is complete) is performed until it is gaseous at ambient pressure. The gaseous  $\text{CO}_2$  is then replaced by air through simple molecular diffusion. The resulting aerogels are lightweight nanostructured materials composed of a solid open pores network.

Classical aerogels, known since the pioneering work of Kistler, are based on silica (Kistler, 1931) or synthetic polymers (for example, resorcinol-formaldehyde) (REF). They have outstanding properties such as a very low density (typically lower than  $0.2 \text{ g/cm}^3$ ) and a high specific surface area (noted  $S_{\text{BET}}$ ) which is the accessible (or detectable) area of solid surface per unit mass of a material, and can reach up to several hundreds of  $\text{m}^2/\text{g}$  due to the internal structure of aerogel.

As an illustration, a comparison of the visual aspect and microstructure of aerogel, cryogel and xerogel obtained in this work from the same initial pectin gel crosslinked with calcium is shown in Figure 10.

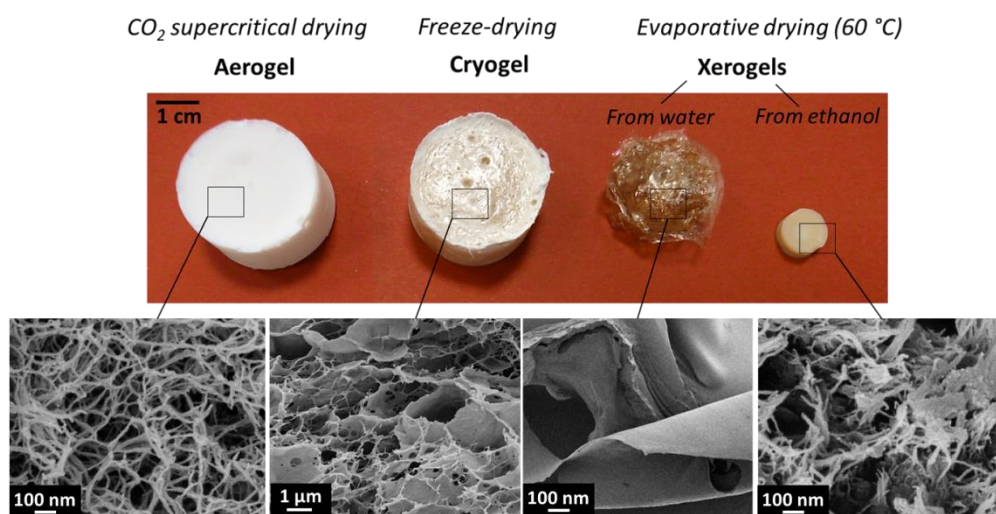


Figure 10. Visual aspect and network morphology observed by SEM of the same “dry” pectin hydrogel made from 3 wt% pectin (with 35% of degree of methylation) dissolved at pH 2.0 with calcium ( $R(\text{Ca}) = 0.2$  see Equation (1.1)) dried in different ways: with supercritical  $\text{CO}_2$ , by freeze-drying, or by evaporative drying (at  $60^\circ\text{C}$  under vacuum) of either a pectin hydrogel or a coagulated pectin gel in ethanol.

## 2.2. Classical inorganic and synthetic polymer aerogels: a brief overview

Classical aerogels are usually produced via sol-gel route either from inorganic (*e.g.* silica or metal, metal oxide, graphene, carbon nanotubes, clay) or organic (*e.g.* resorcinol-formaldehyde, phenol-formaldehyde, polyurethanes, polyvinyl alcohol dialdehyde) compounds (Pierre & Pajonk, 2002). Silica aerogels (the “first generation” of aerogels (S. S. Kistler, 1931)) were extensively studied, so we will use them as an example of how classical inorganic aerogels are prepared and of their potential applications.

### 2.2.1. First generation of aerogels: silica aerogels

#### ▪ The synthesis of silica aerogels

Silica aerogels are by far the most known and commercially most important class of aerogel materials. They are prepared by silica gelation via “sol-gel” route followed by supercritical drying. The “silica sol” is a colloidal suspension of silica alkoxides dispersed in a solvent (usually ethanol, methanol, isopropanol or 1- or 2-propanol). The most known examples are tetraethyl orthosilicate (TEOS), tetramethyl orthosilicate (TMOS) and polyethoxydisiloxane (PEDS), the latter being pre-polymerized silica sol developed to optimize aerogel properties. Using aqueous acid- or base-catalyst, the colloidal silica suspension undergoes sol-gel transition, leading to the formation of a 3D-network termed as a “gel”.

The gelation of silica by sol-gel process is actually divided into two reactions steps; the first one is acid-catalyzed hydrolysis step leading to the production of hydrolyzed reactive monomers silanol (SiOH) with hydroxyl function bound to silicon (Figure 11).

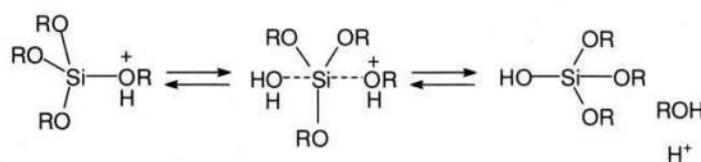


Figure 11. Acid-catalyzed hydrolysis reaction. Reprinted with permission from (Buckley & Greenblatt, 1994). Copyright (2019) American Chemical Society.

This step is then followed by acid- or base-catalyzed polycondensation reactions of two silanol (Si-OH) groups, leading to the creation of silicon-oxygen-silicon bridges (-Si-O-Si-) and further polymerization (Figure 12). The obtained silica gel consists of a three-dimensional solid network of silicon oxide (SiO<sub>2</sub>) filled with solvent.

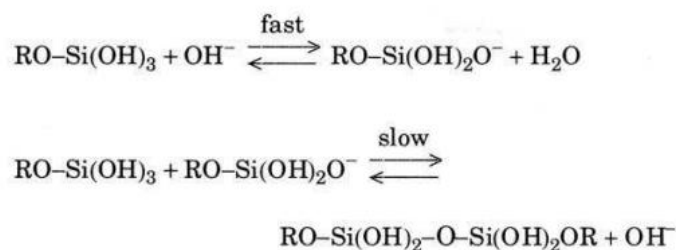


Figure 12. Base-catalyzed condensation reactions. Reprinted with permission from (Buckley & Greenblatt, 1994). Copyright (2019) American Chemical Society.

In silica aerogel production, hydrolysis and condensations reactions can be performed simultaneously through one-step procedure, or separately via two-steps procedure. After sol-gel transition, silica gels are usually aged (at various temperature and duration) as this leads to smaller pore sizes and network finer structuration. After washing steps, silica gels are supercritically dried to obtained aerogels. The type and concentration of silica in the sol and of

acid/base catalysts, temperature and time for hydrolysis, gelation and aging steps are known to impact the textural properties of silica gels and aerogels (Davis, Deshpande, Smith, Brinker, & Assink, 1994; Pierre & Pajonk, 2002; Soleimani Dorcheh & Abbasi, 2008).

Silica aerogels present many outstanding properties (Aegerter, Leventis, & Koebel, 2011); they present a high open porosity above 90% and a low bulk density (typically 0.05 - 0.25 g/cm<sup>3</sup>). Silica aerogels display a high specific surface area (800 - 1000 m<sup>2</sup>/g and higher) due to a mesoporous network (average pore size from 10 to 50 nm). Examples of morphologies of silica aerogels are shown in Figure 13, using different types of silica sol precursors (TEOS, TMOS, and PEDS). To cope with the high brittleness inherent to silica aerogels, highly bendable silica aerogels can be obtained by chemical modifications of the network during the sol-gel process as described in the work of (Hayase et al., 2013; Hayase, Kanamori, & Nakanishi, 2011; Shimizu, Kanamori, Maeno, Kaji, & Nakanishi, 2016). Such chemically modified silica aerogels present significantly improved mechanical properties as compared to original silica aerogels and exhibit a flexible deformation behavior against compression without collapse.

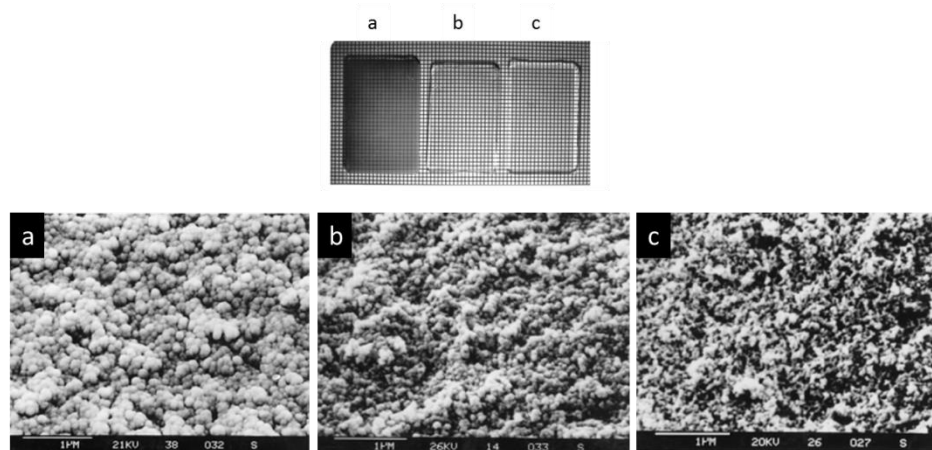


Figure 13. Visual aspects and network morphologies observed by SEM of silica aerogels made from different silica sources: TEOS (a), TMOS (b) and PEDS (c) (Adapted from (Wagh, Begag, Pajonk, Rao, & Haranath, 1999)).

### ▪ **Hydrophobization treatment**

Due to the remaining reactive groups (such as alkoxy and hydroxyl groups), silica aerogels present a certain hydrophilicity and suffer from subsequent water vapour adsorption which limits the range of applications. Thus, hydrophobization of silica aerogels has been widely studied the past decades and two main approaches are reported to increase their hydrophobic character (Aegerter et al., 2011):

- **by the addition of a silylating agent during the sol-gel step.** For instance,

Schwertfeger et al. produced hydrophobic silica aerogels by adding methyltrimethoxysilane (MTMS) to TMOS hydrolyzed in basic conditions, followed by supercritical drying (Schwertfeger, Glaubitt, & Schubert, 1992; Schwertfeger, Hüsing, & Schubert, 1994; Venkateswara Rao & Haranath, 1999). In this case, after TMOS reacted, MTMS was grafted through the silanol groups, as shown in Figure 14(ref). Similar results were obtained by co-gelling TMOS as silica-precursor with trimethylethoxysilane (TMES) (Rao, Kulkarni, Pajonk, Amalnerkar, & Seth, 2003), or by adding dimethyldiethoxysilane (DMDES) to TEOS (Cao & Zhu, 1999).

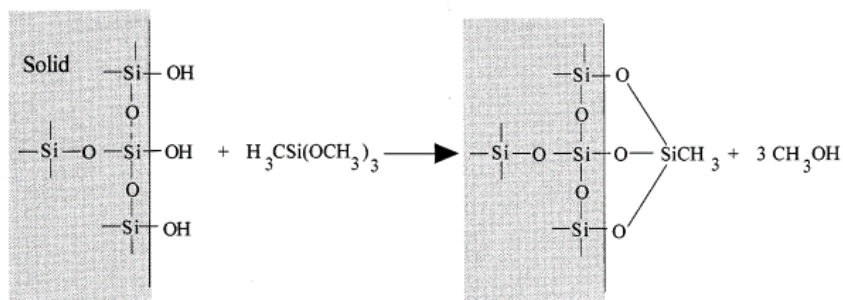


Figure 14. The reaction of hydrophobization of silica aerogels (from TMOS) with MTMS, Reprinted with permission from (Pierre & Pajonk, 2002). Copyright (2019) American Chemical Society.

- **By surface modification after sc-drying**, *i.e.* by post-treatment of the silica aerogels (two-steps procedure). The principle is to let the aerogels in contact with vapors of a surface modifying agent such as trimethylchlorosilane (TMCS) (United States Patent No. US6005012A, 1999) or hexamethyldisilazane (HMDS). In the same way, the modifying agent react by forming Si-O-Si bonds with the silanol groups on pores' surface, which results in the formation a protective hydrophobic "layer" of methyl groups.

### 2.2.2. Synthetic organic polymers aerogels

Neat synthetic organic aerogels were first described by (R. W. Pekala, 1989), and they were based on resorcinol–formaldehyde (RF) resin. RF aerogels are the most known synthetic organic aerogels; a wide range of other organic aerogels were developed in the last decades, either based on other type of resins (*e.g.* phenol-formaldehyde, melamine-formaldehyde, cresol- formaldehyde, phenol-furfural *etc.*), or organic compounds (*e.g.* polyimides, polyacrylamides, polyacrylonitriles, polyacrylates, polystyrenes, polyurethanes, *etc.*) (Pierre & Pajonk, 2002).

As an illustrative example of a synthetic organic aerogel, we detail the chemical process to synthesize RF aerogel. Although the mechanism of RF polycondensation via sol-gel route is

different from the reaction to make inorganic gels such as silica from alkoxy silanes (presented in the Section 2.2.1), the general approach is quite similar. Indeed, RF aerogels are synthesized by the aqueous polycondensation of resorcinol with formaldehyde under alkaline or acid conditions, with different variations of essentially the same procedure. In this case, resorcinol and formaldehyde serve as a trifunctional and difunctional monomers, respectively, and the RF polymer obtained is classified as a phenolic resin.

- First, resorcinol reacts with formaldehyde to form hydroxymethylated resorcinol (substituted resorcinol derivatives).
- Then, the hydroxymethylated groups (-CH<sub>2</sub>OH) condense with each, resulting in the formation of a sol composed of nanometer-sized polymer “clusters”. The structure of a polymer crosslinked cluster resulting from the reaction of resorcinol with formaldehyde is shown in Figure 15.

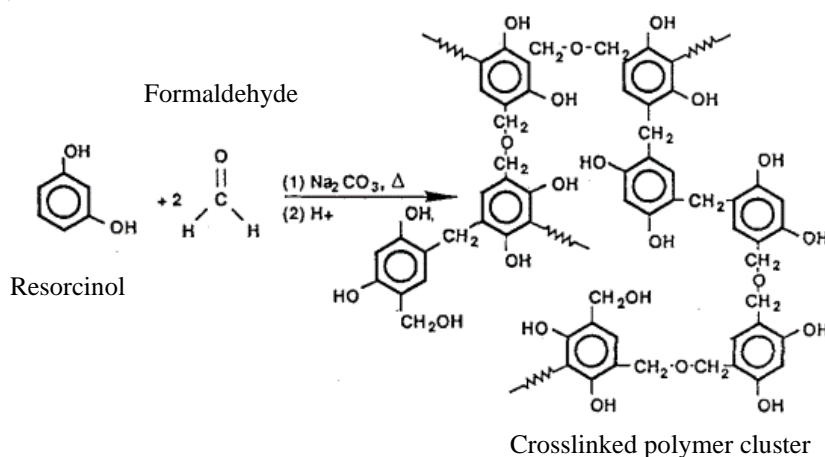


Figure 15. Polymer crosslinked cluster resulting from the reaction of resorcinol with formaldehyde, adapted from (R. Pekala & Kong, 1989).

- Then, the sol is usually heated for a sufficient time allowing the "nano-clusters" to form covalent bridges with each other through the polycondensation of surface functional groups (*e.g.* hydroxymethyl species), leading to the production of stable gels with high cross-linking densities. The gelation mechanism of RF gels is illustrated in Figure 16. In the case of basic catalysis, the reaction is carried out in aqueous alkaline solution with the use of sodium carbonate as catalyst (or similar). Generally, the gelation reaction in alkaline conditions requires heating at elevated temperatures (generally 80-100°C) for prolonged time periods (few days to several weeks). With acid catalysts, the monomers are mixed with the acid catalyst (*e.g.* hydrochloric acid, acetic acid, and perchloric acid) in aqueous

or non-aqueous media, leading to a much faster gelation which can even take place at room conditions. The size of the "clusters" and their interpenetration are known to be influenced by the typical sol–gel parameters such as the pH of the sol, temperature, concentration and ratio of reactants and type of catalyst (Aegerter et al., 2011; R. Pekala & Kong, 1989).

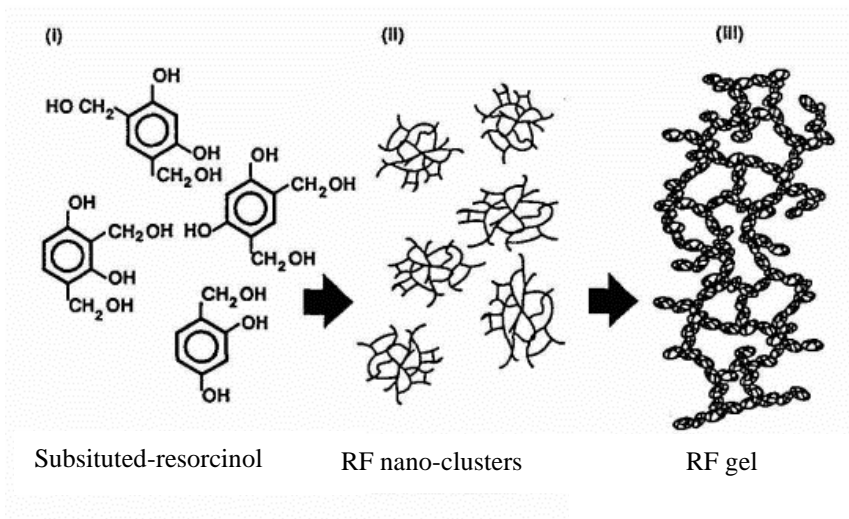


Figure 16. Schematic illustration of the RF gelation mechanism, adapted from (R. Pekala & Kong, 1989).

- The gels are then aged (using different organic solvent) in order to increase the crosslinking density.
- Finally, the RF gels are subsequently solvent-exchanged with fresh suitable solvent, and then supercritically dried to obtain RF aerogels.

The resulting RF aerogels are dark red in color and transparent, they present typical aerogels properties: lightweight and highly porous with an open mesoporosity and a high specific surface area (300 – 1000 m<sup>2</sup>/g). As the formation of the “nano-cluster”, and thus the final structural properties of RF aerogels, can be controlled by the reaction conditions, the physical properties of RF aerogels can be finely tuned to target specific application (Aegerter et al., 2011; R. Pekala & Kong, 1989; United States Patent No. US4873218A, 1989).

### 2.2.3. Applications of classical aerogels

Silica aerogels present many attractive properties such as a very low thermal conductivity, a low refractive index, a low sound speed, a low dielectric constant and an optical transparency (as shown in Figure 17). One of the most famous application properties of silica aerogels is their thermal conductivity in ambient conditions, which can be as low as 0.012–

0.015 W/(m·K), significantly lower than that of ambient air (0.025 W/m·K) (M. Koebel, Rigacci, & Achard, 2012).



Figure 17. Example of silica aerogel monolith (from TEOS) presenting a density of  $0.13 \text{ g cm}^{-3}$  and an effective thermal conductivity of  $0.015 \text{ W/(m.K)}$ . Reprinted by permission from [Springer Nature] [Journal of Sol-Gel Science and Technology] [from (M. Koebel et al., 2012)], [COPYRIGHT] (2019).

Concerning RF aerogels, they became very popular thanks to the controllability of their internal structure combined to attractive physical and mechanical properties. When compared to silica aerogels, RF aerogels exhibit similar very low thermal conductivity of ( $\sim 0.012 \text{ W/m K}$  under ambient conditions) but with improved mechanical properties as RF aerogels are much stiffer and stronger than silica aerogels (Aegerter et al., 2011). Thus, RF aerogels can be used as performant materials for acoustic and thermal insulation, with easy machinability. In addition to that, RF aerogels received great attention as they can serve as precursors to produce electrically conductive carbon aerogels after pyrolysis (usually at  $600^{\circ}\text{C}$ – $2000^{\circ}\text{C}$ ), as shown in Figure 18.

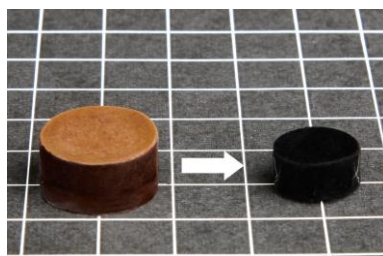


Figure 18. RF polymer aerogels and RF-carbon aerogels (obtained after pyrolysis under inert atmosphere) produced by BuyAerogel.com. Picture taken from BuyAerogel.com.

Carbon aerogels are particularly attractive for a wide variety of applications (filtration/adsorption support, catalysis, fuel cell applications, as electrode supercapacitors or anode for battery, energy storage...etc.) as they combine a high electrical conductivity with outstanding structural properties (low density, open mesoporosity, very high surface area) (Horikawa, Hayashi, & Muroyama, 2004). Figure 19 shows an example of the very fine structure of RF-carbon aerogels. More generally, the increasing popularity of synthetic organic aerogels (and their carbonized derivatives) is largely due to their unique and controllable properties by varying the process route.

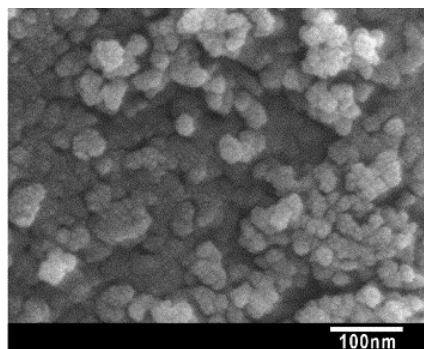


Figure 19. Morphology of the RF carbon aerogel made with  $K_2CO_3$  catalyst and pyrolyzed at 1073 K for 30 min. Reprinted from (Horikawa et al., 2004), Copyright (2019), with permission from Elsevier.

More generally, “classical” aerogels are extremely versatile materials due their wide range of textural and morphological properties combined with the possibility to tune and functionalize them by varying the process route. Currently, the most promising commercial application of classical aerogels seems to be in thermal and acoustic insulations. But other potential applications fields of classical aerogels include (not exhaustive): chemistry (as catalyst, adsorbents, extracting agents, filtration systems for gas or liquid purification, filler additives, as a carrier-materials for release/adsorption of compounds...), for electrical/electronic applications (batteries, capacitor electrodes, sensor materials, dielectric/piezoelectric materials), for shock absorption, for space industry (space dust particles collectors - “Stardust” project )...*etc.*(Pierre & Pajonk, 2002).

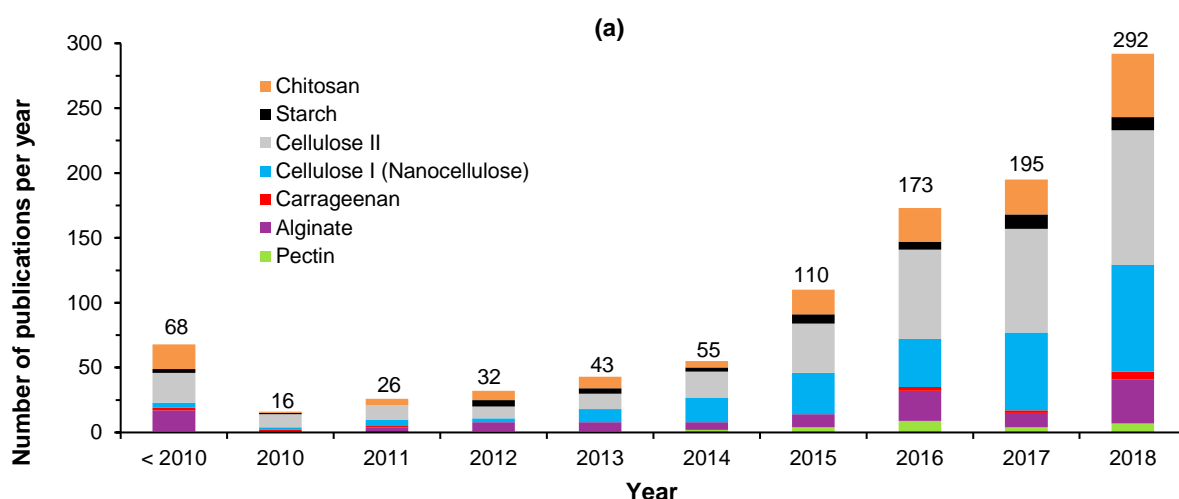
However, the range of applications of non chemically-modified silica aerogels is strongly limited because of their poor mechanical properties and release of very small particles; the price of the starting material is also rather expensive for mass production applications as insulating materials. In addition, the organic compounds used for the production of synthetic organic aerogels (*e.g.* RF-based) or for post-gelation modifications and/or the hydrophobization treatments of aerogels (silylation) can be highly toxic. This has to be taken into considerations not only for health and safety during applications, but also as they generate toxic wastes (liquids and streams) with undesirable environmental properties. In the light of these limitations, the search for greener and human-friendly alternatives to classical aerogels has become a key aspect.

### 2.3. Bio-aerogels: the third generation of aerogels

A new generation of aerogels was developed during the 21st century: they are biomass-based and thus are called “bio-aerogels”. Bio-aerogels are made of natural polymers such as polysaccharides and proteins (Chtchigrovsky et al., 2009; Druel, Bardl, Vorweg, & Budtova,

2017; P. Gurikov, Raman, Weinrich, Fricke, & Smirnova, 2015; Gabrijela Horvat, Fajfar, Uzunalić, Knez, & Novak, 2017; Jiménez-Saelices, Seantier, Cathala, & Grohens, 2017; Kobayashi, Saito, & Isogai, 2014; Quignard, Valentin, & Di Renzo, 2008; Rudaz et al., 2014; Seantier, Bendahou, Bendahou, Grohens, & Kaddami, 2016; Selmer, Kleemann, Kulozik, Heinrich, & Smirnova, 2015; Sescousse, Gavillon, & Budtova, 2011). Kistler first reported the possibility of making aerogels from gelatin, cellulose, nitrocellulose, agar and egg albumin (S. S. Kistler, 1931), but their properties were not studied.

Since the last decade and due to many attractive properties of biopolymers, we are observing a growing interest in bio-aerogels. The annual number of publications on polysaccharide-based aerogels per type of polysaccharide in Figure 20a shows a continuous increase starting from 2010. The most frequent polysaccharides used to make bio-aerogels are cellulose (both based on various types of nanocelluloses and on cellulose II.), then chitosan (obtained by deacetylation of chitin extracted from exoskeleton of arthropods), alginate (from brown algae), starch (from potato, pea, maize, rice, wheat ...etc.), carrageenans (from red seaweeds) and pectins (from fruits such as citrus peel or apple pomace and vegetables) as illustrated in Figure 20b.



(b) Share of publications on aerogels in 2018 by type of polysaccharide

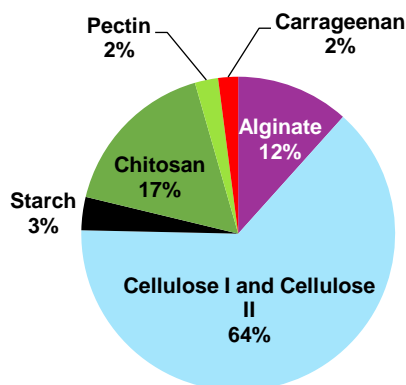


Figure 20. (a) Number of publications per year and (b) distribution percentage (%) by the type of polysaccharide in bio-aerogels: chitosan, starch, cellulose (I and II), carrageenans, alginate, and pectin. Data were taken from Web of science website (<https://webofknowledge.com>) - consulted the 03/20/2019.

Bio-aerogels usually have densities from 0.02 to 0.25 g/cm<sup>3</sup> and present lower specific surface areas than those of silica aerogels, from 200 to 700 m<sup>2</sup>/g. Bio-aerogels display a wide range of network morphologies and pore sizes (from a few tens of nanometers to a few microns), depending on the bio-polymer and the process route. Compared to extremely fragile silica aerogels, polysaccharide aerogels tend to display much better mechanical properties with plastic deformation until a strain of 60–80% before complete pore wall collapse (Kobayashi et al., 2014; Rudaz et al., 2014; Sescousse et al., 2011).

As compared to their inorganic and synthetic polymer counterparts, bio-aerogels present an important advantage: they are biodegradable, based on renewable polymers and with low or non-toxicity profile. Bio-aerogels also possess a large variety of chemical functional group (hydroxyl-, carboxyl-, amino groups...etc.) allowing targeted functionalization. Moreover, the synthesis of bio-aerogels does not involve any toxic compounds which is the case of many synthetic polymer aerogels (for example, based on resorcinol formaldehyde or polyurethanes cross-linked with isocyanate). Thus, polysaccharide aerogels are perceived as sustainable and “human-friendly” materials, in adequacy with the change in people “consumption trend/awareness”. All these attractive properties make them promising bio-based materials for a wide range of potential applications as of “classical” aerogels (thermal insulation, as matrices for catalysis when functionalized (Budarin et al., 2006; Chtchigrovsky et al., 2009), in electrochemical applications when pyrolyzed (Vitaliy L. Budarin, Clark, Luque, Macquarrie, & White, 2008; Guilminot et al., 2008), and in adsorption and/or separation (P. Gurikov et al., 2015).

Thanks to their bio-compatibility and biodegradability, bio-aerogels are suitable for all variety of life science applications (*e.g.* medical devices, pharmaceuticals, cosmetics, food ...). In particular, they recently have received significant attention from both academic and industrial researchers to be used as biodegradable solid matrices as drug delivery systems (Comin, Temelli, & Saldaña, 2012; De Cicco et al., 2016; C. A. García-González, Jin, Gerth, Alvarez-Lorenzo, & Smirnova, 2015; Lovskaya, Lebedev, & Menshutina, 2015; Mehling, Smirnova, Guenther, & Neubert, 2009; Tkalec, Knez, & Novak, 2015a; Veronovski, Tkalec, Knez, & Novak, 2014) and as 3D cellular scaffolds (Goimil et al., 2017; G. Horvat et al., 2017; Martins et al., 2015; Quraishi et al., 2015) for tissue engineering or wound dressing devices (De Cicco et al., 2016). Despite the recent increase of polysaccharide aerogels’ studies in the academic field, their transition to pilot and industrial applications is still pending (S. Zhao, Malfait, Guerrero-Alburquerque, Koebel, & Nyström, 2018).

### 2.3.1. Synthesis routes of bio-aerogels: similarities and differences with inorganic and synthetic polymer aerogels

Bio-aerogels can be produced either i) from polymer solutions (*e.g.* cellulose, alginate, pectin, starch, chitosan...) or ii) from nanoparticles in suspension (cellulose, chitin, or protein aggregates). In this section, we will present only the case of the use of polysaccharides in solution to make aerogels. We will show the similarities and differences in terms of synthesis route between the most known bio-aerogels and classical ones (from inorganic components or synthetic polymers).

The synthesis of bio-aerogels is inspired by that of classical aerogels: usually starting from polymer dissolution to solution, gelation (which can be omitted) followed by solvent exchange and drying with super-critical (sc) carbon dioxide, as illustrated in Figure 21.

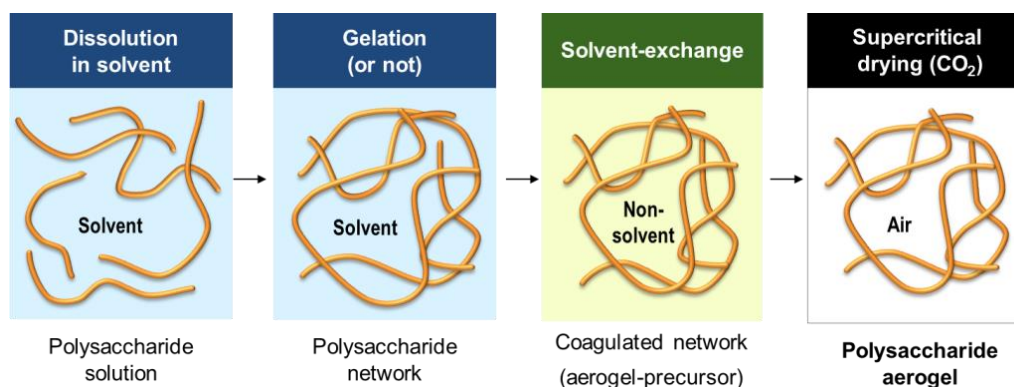


Figure 21. General process route of making bio-aerogels from polysaccharides.

- **Network formation by polymer gelation or by direct coagulation**

Like classical aerogels, the network formation is crucial as it will determine future properties of aerogel after supercritical drying. The “wet” bio-polymer network can be formed either via conventional gelation or via non-solvent phase separation during solvent-exchange step:

- A major difference between “classical” and bio-polymer aerogels stands in their process routes, as the gelation bio-polymers is rather different from the sol-gel route and does not include a polymerization step. Indeed, bio-polymers are already polymers and the gel network can be formed either by physical interactions by chain entanglements or weak forces (*e.g.* hydrogen bonds, ionic bonds, hydrophobic interactions...) between polymeric chains which is termed

as “physical gelation”; or by chemical crosslinking between chains by cross-linkers or cross-linker promoters which is termed as “chemical gelation”. Gelation depends on the intrinsic properties of the bio-polymer (molecular weight, chemical structure, functionalization...etc.) and the external processing conditions (polymer concentration, pH, temperature, crosslinker concentration...etc.).

- However, for some polysaccharides there may even be no gelation at all or this step can be just omitted. Instead of conventional gelation, another way of forming polysaccharide network is via non-solvent induced phase separation (also known as “immersion precipitation”) during solvent-exchange step from solvent to non-solvent. During this process, the progressive addition of a non-solvent to polysaccharide solution results in phase separation phenomena: the solubility of the polysaccharide decreases as non-solvent proportion increases, leading to polymer coagulation and contraction. The particularity of polysaccharides is that above the overlap concentration, the coagulated polymers are not precipitating even if solutions were not-gelled. Thanks to a certain chain rigidity of polysaccharides, the coagulated polymers keep 3D structure, forming the network of aerogel precursors. Literature reports few cases of bio-aerogels whose aerogel precursors were obtained from non-gelled solutions of cellulose, alginate and pectin (Buchtová & Budtova, 2016; Gurikov & Smirnova, 2018; G. Horvat et al., 2017; Innerlohinger, Weber, & Kraft, 2006; Pircher et al., 2016; Sescousse et al., 2011; Tkalec et al., 2015a).

#### ▪ **Solvent exchange and supercritical drying**

As the polymers used to make bio-aerogels are mostly polysaccharides, the dissolution step often occurs in aqueous solvents. In order to dry using scCO<sub>2</sub>, water has to be replaced by a non-polar fluid miscible with CO<sub>2</sub>, usually acetone or ethanol, which are non-solvents for polysaccharides.

The final properties of bio-aerogels (porosity, morphology, density) logically depend on the structure formation of the polymer network all along the process route. The latter are impacted i) by the characteristics of the starting biopolymer (*e.g.* functional groups, molecular length, chemical functionalization (Cheng, Lu, Zhang, Shi, & Cao, 2012; Takeshita, Konishi, Takebayashi, Yoda, & Otake, 2017)), ii) the typical gelation parameters (*e.g.* polymer concentration, pH/temperature of polymer solution, the nature and concentration of cross-linkers (C. A. García-González, Alnaief, & Smirnova, 2011; Tkalec, Knez, & Novak, 2016)) and iii) the process route (*e.g.* type of non-solvent, drying procedure...).

As an illustration, Figure 22 shows the network morphologies of various bio-aerogels made from different composition and concentration of polysaccharides (starch, pectin, alginate).

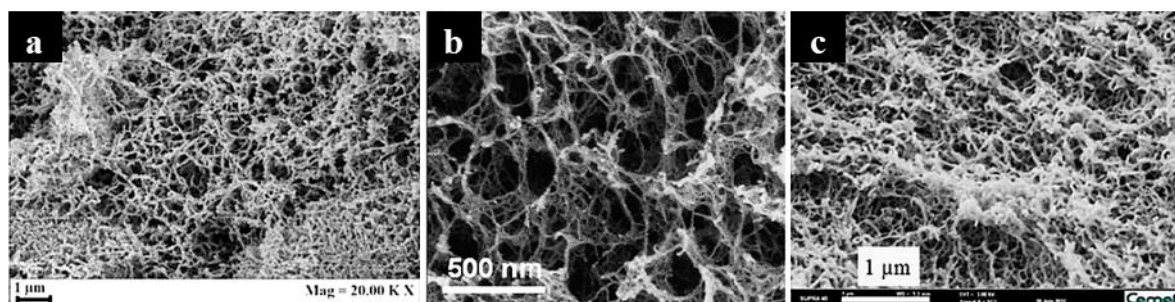


Figure 22. SEM images of bio-aerogels made from: (a) 5 wt% starch (adapted from (De Marco, Baldino, Cardea, & Reverchon, 2015)); (b) 1 wt% alginate cross-linked by calcium (adapted from (Robitzer, David, Rochas, Renzo, & Quignard, 2008)); (c) 5 wt% pectin (w/w) (adapted from (Rudaz et al., 2014))

In order to target a specific application, the shape of polysaccharide aerogels can be customized by different processes (such as emulsion-gelation method, jet cutting, dropping, molding, grinding, extrusion...) to obtain aerogels as monoliths, fibers or particles (from macroscopic to micrometric size). An example of shaping starch aerogels into particles of different size (from millimeters to micrometers) is shown in Figure 23.

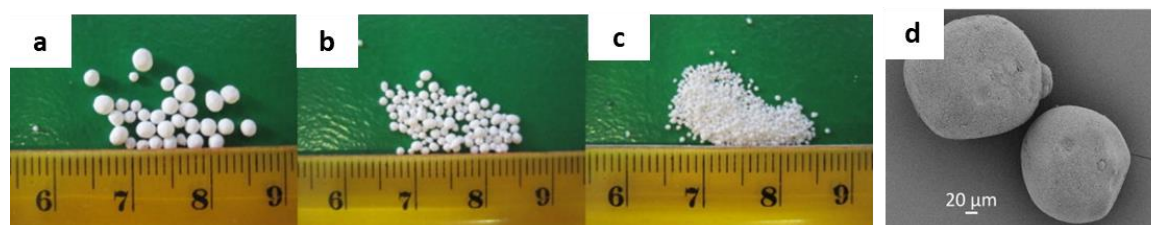


Figure 23. Examples of shaping starch aerogels into particles of different sizes (from millimeters to micrometers) using emulsion-gelation method with different mixing parameters. Adapted from (C.A. García-González, Uy, Alnaief, & Smirnova, 2012).

Polysaccharides used to make aerogels can be separated into two main groups depending on their physico-chemical characteristics: “neutral” polysaccharides (*e.g.* cellulose, starch, guar, ...*etc.*) and polyelectrolytes (*e.g.* pectin, alginate, chitosan, carrageenans, xanthan... *etc.*). The polyelectrolyte nature of a polysaccharide greatly impacts the gelling abilities, structuration and the overall aerogel process route.

In the following, we present the process routes and the general characteristics of the most known polysaccharide aerogels based on cellulose II, starch, alginate and pectin. A special attention is paid on the specificity of the initial polymer to produce bio-aerogel.

### 2.3.2. Aerogels based on neutral polysaccharides

#### ▪ Cellulose II aerogels

Cellulose aerogels are the most studied bio-aerogels (Aaltonen & Jauhiainen, 2009; Gavillon & Budtova, 2008; Liebner, Potthast, Rosenau, Haimer, & Wendland, 2008; Rege, Schestakow, Karadagli, Ratke, & Itskov, 2016; Sescousse et al., 2011; Tsiptsias, Stefopoulos, Kokkinomalis, Papadopoulou, & Panayiotou, 2008). As mentioned above, they can be prepared either from a cellulose solution by dissolution of pulps or of micro-crystalline cellulose resulting in aerogels based on cellulose II such as in (Aaltonen & Jauhiainen, 2009; Hoepfner, Ratke, & Milow, 2008; Innerlohinger et al., 2006; Rege et al., 2016), or from a suspension of nanocellulose particles or fibers (*i.e.* nanofibrillated cellulose and cellulose nanocrystals such as in (Carlsson et al., 2012; Heath & Thielemans, 2010; Jin et al., 2011; Olsson et al., 2010; Sehaqui, Zhou, & Berglund, 2011)). In this section, we will only present the case of cellulose aerogels obtained from dissolved cellulose.

Cellulose is the most abundant organic polymer on earth. It is a linear carbohydrate polymer made of repeated D-glucose bounded by  $\beta(1-4)$  glycosidic bounds. Its general formula is  $(C_6(H_{10}O)_5)_n$ , with  $n$  the degree of polymerization. It is a structural polysaccharide and the major component of cell walls of plants. Cellulose can be extracted from various lignocellulosic sources (such as cotton linters, wood, flax, hemp...*etc.*) but can be produced as well by bacteria (*Acetobacter xylinum*) and also by marine invertebrate animal tunicate. The origin of cellulose and the extraction mode have a strong influence on the purity of cellulose (potential presence of lignin and hemicellulose) and degree of polymerization and thus on its physical-chemical properties. Cellulose is usually organized in a semi-crystalline structure with low ordered amorphous region coexisting with crystalline regions, due to numerous intra- and inter-molecular hydrogen bonds between hydroxyl groups (Itagaki, Tokai, & Kondo, 1997). This also impact cellulose physico-chemical properties and its solubility.

Cellulose II aerogels are prepared through dissolution-solvent-exchange-supercritical drying route. Different solvents can be used to dissolve cellulose such as N-Methylmorpholine N-oxide (NMMO) monohydrate, NaOH-water (with or without additives), ionic liquids (*e.g.* 1-Ethyl-3-methylimidazolium acetate (EmimAc), 1-Allyl-3-methylimidazolium chloride (AMIMCl), 1-Butyl-3-methylimidazolium chloride (BMIMCl) ...), molten salt hydrates such as zinc chloride ( $ZnCl_2 \cdot 6H_2O$ ) and calcium thiocyanate,  $Ca(SCN)_2 \cdot 6H_2O$ , etc. After the dissolution, non-solvents are used to coagulate cellulose (sometimes called “regeneration” for historical reasons) including water, acids, ethanol, propanol, butanol and acetone. The type of solvent and non-solvent may have a strong impact on the final structural properties of the obtained cellulose II aerogel. In general, two types of network morphologies can be distinguished, either more “fibrous-like” (Figure 24a) and “globular-like” (Figure 24 b, c).

Cellulose II aerogels typically present bulk density varying from 0.05 to 0.2 g/cm<sup>3</sup> and specific surface area from 200 to 400 m<sup>2</sup>/g depending on cellulose concentration and process route parameters (Druel, Niemeyer, Milow, & Budtova, 2018; Gavillon & Budtova, 2007, 2008; Innerlohinger et al., 2006; Sescousse, 2010; Tsiptsias et al., 2008).

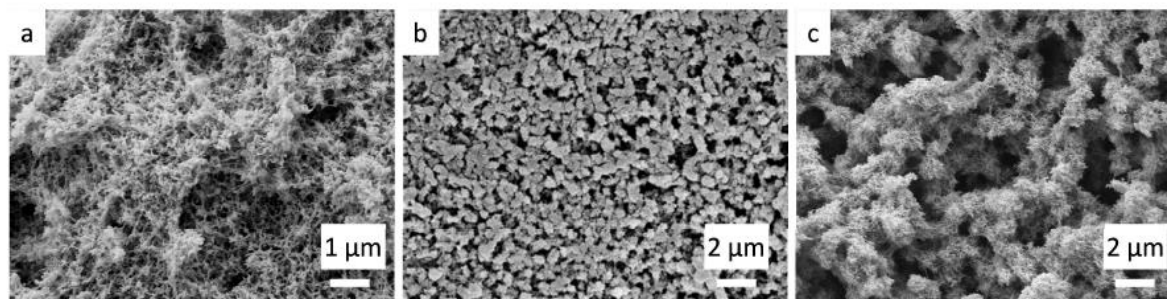


Figure 24. Various morphologies of cellulose aerogels from cellulose solutions in different solvents: (a) 8%NaOH adapted from (Sescousse et al., 2011); (b) NMMO adapted from (Gavillon & Budtova, 2008); and (c) ionic liquid (EMIMAc) (adapted from (Sescousse et al., 2011)).

### ▪ Starch aerogels

Starch is an energy-storage matter extracted from green plants (potato, wheat, pea, maize, rice, corn, tapioca...). It consists of two polysaccharides made of D-glucose units joined by glycosidic bonds: linear amylose and branched amylopectin chains. The proportion of amylose/amylopectin is known to depend on starch source.

Starch aerogels are typically made via dissolution–retrogradation-solvent exchange–sc CO<sub>2</sub> drying route. The process starts with the destruction of starch granules in water under heating and mixing which induces so-called gelatinization of starch. The dissolution can be complete or partial, followed by retrogradation under cooling during which gelation and partial recrystallization occurs. Solvent exchange is then performed prior to sc-drying.

Starch aerogels usually present specific surface area lower than that of cellulose II aerogels (typically 50 – 150 m<sup>2</sup>/g but can also reach 200 – 250 m<sup>2</sup>/g) and bulk densities from 0.05 to 0.35 g/cm<sup>3</sup> depending on starch source and processing route ((Druel et al., 2017; C. A. García-González et al., 2011; Garcia-Gonzalez & Smirnova, 2013; C.A. García-González et al., 2012; Mehling et al., 2009; Starbird, García-González, Smirnova, Krautschneider, & Bauhofer, 2014; Ubeyitogullari & Ciftci, 2016). More generally, intrinsic properties of starch such as the amylose/amylopectin ratio (which depends on starch source and treatment) (Druel et al., 2017; C.A. García-González et al., 2012; Kenar, Eller, Felker, Jackson, & Fanta, 2014; Ubeyitogullari & Ciftci, 2016) and external parameters such as cooling rate, temperature and non-solvent used (Druel et al., 2017; Hoover & Vasanthan, 1994) were reported to influence the final properties

of starch aerogels (network morphology, density and specific surface area), as well as thermal conductivity values (from 0.021 - 0.024 W/(m.K) (Druel et al., 2017; Glenn & Irving, 1995) and higher).

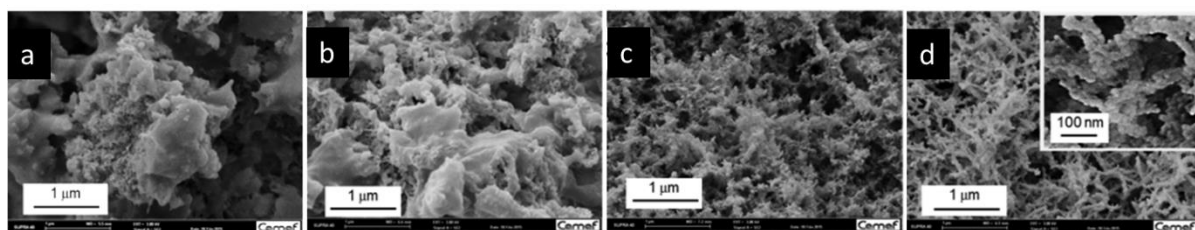


Figure 25. SEM images of starch aerogels from different starch sources and amylose/amylopectin ratio: (a) waxy potato, (b) regular potato, (c) pea, and (d) high amylose corn starch. Reprinted with permission from (Druel et al., 2017), Copyright (2019) American Chemical Society.

### 2.3.3. Aerogels based on polyelectrolyte polysaccharides

Pectin, alginate, chitosan and carrageenans are polyelectrolytes, *i.e.* they present significant proportion of ionizable functions depending on pH conditions. As a consequence, physico-chemical properties and chains' interactions mechanisms of these polysaccharides are impacted by ionization/protonation phenomena induced by pH. We present here the cases of aerogels made from pectin and alginate (polyanions) and chitosan (polycation).

#### ▪ Pectin aerogels

The details on pectin structure and gelling properties are presented in Section 1 of this chapter. Pectin aerogels are usually obtained through dissolution in water – gelation (in some cases, this step is omitted) – solvent-exchange – sc drying using CO<sub>2</sub>. Literature reports aerogels made from pectins gelled in various conditions (pH, cations concentrations) and from pectins of different concentrations and DE.

However, a systematic study of the influence of all extrinsic and intrinsic parameters on the final properties of pectin aerogels have not been conducted yet. For instance, pectin aerogels were produced from either LM pectins (Tkalec, Knez, & Novak, 2015b; Veronovski et al., 2014; White, Budarin, & Clark, 2010) or HM pectins (C. A. García-González et al., 2015; Carlos A. García-González, Carenza, Zeng, Smirnova, & Roig, 2012; Rudaz et al., 2014; Tkalec et al., 2015b, 2015a) and through different process route: either via physical gelation in acidic media (Rudaz et al., 2014), via ionic gelation using different cations (calcium, zinc, strontium) of various concentrations (Demilecamps, 2015; C. A. García-González et al., 2015; Tkalec, Knez, et al., 2016; Veronovski et al., 2014) or by non-solvent phase separation (G. Horvat et

al., 2017; Tkalec et al., 2015b, 2015a; White, Budarin, et al., 2010; H.-B. Zhao, Chen, & Chen, 2017).

Figure 26 shows an example of network morphology of pectin aerogels made from the same starting pectin but acid-gelled (in HCl 1M) (Figure 26a) or ionic-gelled with calcium (Figure 26b). Besides, few studies report the preparation of pectin-based composite aerogels with xanthan (G. Horvat et al., 2017), alginate (Tkalec, Knez, et al., 2016), polyaniline (H.-B. Zhao et al., 2017), silica (Demilecamps, 2015) or with magnetic nanoparticles (TiO<sub>2</sub>) (Carlos A. García-González et al., 2012).

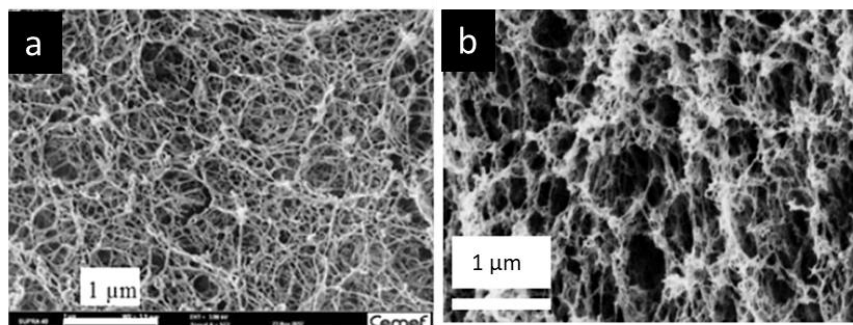


Figure 26. SEM images of pectin aerogels from 3 wt% of the same starting citrus pectin (DE = 56%). Pectin gelation was induced either (a) by physical gelation in acid media at pH = 0.5 (HCl 1M), adapted from (Rudaz et al., 2014) and (b) by calcium-induced gelation (R(Ca) = 0.2 at pH 6.0). adapted from (Demilecamps, 2015).

In general, pectin aerogels have a low bulk density around 0.05-0.15 g/cm<sup>3</sup>, a quite homogenous fibrillar network morphology with pore size from 50 to 300 nm of diameter and a high specific surface area usually from 350 to 500 m<sup>2</sup>/g. Due to small pore size and low density, some pectin aerogels were found to be thermal super-insulating materials with thermal conductivity varying from 0.016 - 0.021 W/(m.K) (Gabrijela Horvat et al., 2017; Rudaz et al., 2014; Tkalec et al., 2015b). Probably due to their polyelectrolyte nature and pH-sensitivity, pectin aerogels and also alginate and chitosan aerogels have received specific attention for biomedical applications. Indeed, they were suggested to be used as carriers for drug delivery via oral or mucosal administration as their release ability can be influenced by pH change within the body (*e.g.* acid gastric media and neutral intestinal media). These cases studies are detailed in the following Section 2.5.

#### ▪ **Alginate aerogels**

Alginate is produced by brown algae and consists of a copolymer of 1,4-β-D-mannuronic acid and α-L-guluronic acid of various ratios and sequences. Similarly to pectin, alginate can undergo ionic gelation by crosslinking with multivalent cations following the egg-box model or by physical acid-gelation via hydrogen bonds at pH lower than pK<sub>a</sub> (~3.4 - 3.7) (Dumitriu,

2004).

Alginate aerogels were widely studied the past decade due to the “easy” ionic gelation process which allows shaping of alginate gels and aerogels as beads (Alnaief, Alzaitoun, García-González, & Smirnova, 2011; Deze, Papageorgiou, Favvas, & Katsaros, 2012; Silva, Ribeiro, Ferreira, & Veiga, 2006) or monoliths (Mehling et al., 2009). In most of the cases, alginate aerogels were obtained via ionic gelation using different cations (generally  $\text{Ca}^{2+}$  but also  $\text{Zn}^{2+}$ ,  $\text{Ba}^{2+}$ ) (Escudero, Robitzer, Renzo, & Quignard, 2009; Tkalec, Knez, et al., 2016; Trens, Valentin, & Quignard, n.d.), or, more rarely, by physical gelation via hydrogen bonds at pH lower than  $\text{pK}_a$  (~3.4 - 3.7) (White, Antonio, et al., 2010). The structure of alginate gel and aerogel was found to depend on cation concentration in alginate solution and the guluronate/mannuronate (C. A. García-González et al., 2011; Ingar Draget, Østgaard, & Smidsrød, 1990; Quignard et al., 2008; Subrahmanyam, Gurikov, Dieringer, Sun, & Smirnova, 2015). Alternatively, alginate aerogels were also produced via non-solvent phase separation process (without gelation step) (Tkalec et al., 2015b; Tkalec, Kranvogel, Uzunalić, Knez, & Novak, 2016).

Alginate aerogels present very attractive structural properties close to synthetic polymer aerogels: homogeneous network morphology, high specific surface area (usually between 350 to 700  $\text{m}^2/\text{g}$ ) and variable bulk density (usually from 0.05 to 0.2  $\text{g}/\text{cm}^3$ ) depending on alginate concentration and the way and parameters of wet network formation (*i.e.* acid gelation, ionic gelation, non-solvent phase separation) (Alnaief et al., 2011; Mehling et al., 2009; Quignard et al., 2008; Robitzer et al., 2008; Robitzer, Renzo, & Quignard, 2011; Trens et al., n.d.). Finally, in the work of Gurikov et al. alginate aerogels were reported to present thermal super-insulating properties (P. Gurikov et al., 2015).

#### ▪ **Chitosan aerogels**

Chitosan is a linear polysaccharide composed of  $\beta$ -(1→4)-linked D-glucosamine (deacetylated unit) and N-acetyl-D-glucosamine (acetylated unit). It is obtained by deacetylation treatment of chitin (extracted from exoskeleton of arthropods such as sea crustaceans) with different the degree of deacetylation (usually 60-95 %). Due to the protonation of the amino groups on the backbone (from  $\text{NH}_2$  to  $\text{NH}_3^+$ ) at pH below  $\text{pK}_a$  (~ 6.5), chitosan is a cationic polyelectrolyte in acidic medium, with charge density depending on the degree of deacetylation and pH conditions. As a result, chitosan is particularly soluble in acidic aqueous medium and can interact with negatively charged compounds by electrostatic interaction. Gelation of chitosan can occur either by physical gelation via hydrogen bonding at  $\text{pH} > \text{pK}_a$  (Kadib, Molvinger, Cacciaguerra, Bousmina, & Brunel, 2011; Quignard et al., 2008; Valentin, Bonelli, Garrone, Di Renzo, & Quignard, 2007), or by chemical crosslinking usually with aldehydes (Chang, Chen, & Jiao, 2008; Takeshita & Yoda, 2015, 2015).

Chitosan is widely used in pharmaceuticals as a delivery matrix with fast dissolution in gastric acid media, and in biomedical applications thanks to its antibacterial properties and ability to form polyelectrolyte complexes with other bio-based polyanions (including alginate, pectin, carrageenan, xanthan gum, carboxymethyl cellulose, chondroitin sulphate, hyaluronic acid... *etc.*).

Chitosan aerogels typically present specific surface area of 300-550 m<sup>2</sup>/g (but can vary from 50 - 800 m<sup>2</sup>/g) and are often combined with cellulose, alginate or pectin (polyelectrolyte complex) (ref) or silica (ref) (ref) to produce composite aerogels. The structural properties of chitosan aerogels were found to be influenced by the viscosity of chitosan starting solutions and their gelling properties. The latter depends on chitosan deacetylation degree, crystallinity, molecular weight and chemical sequence of the polymer (which are all impacted by the chitin natural source and chemical treatment), as well as the type of medium to induce chitosan gelation (Lamarque, Viton, & Domard, 2004; Quignard et al., 2008).

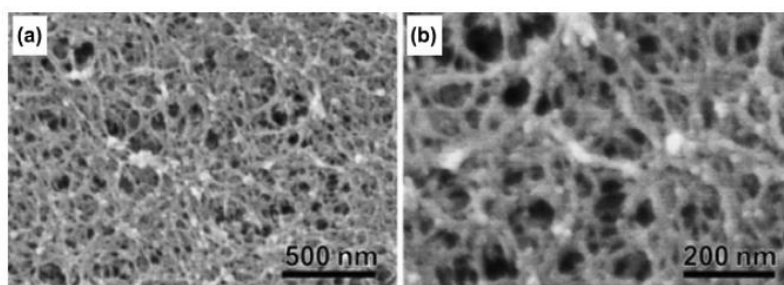


Figure 27. SEM images of cross-section at different magnifications of chitosan aerogel prepared using 4 wt% chitosan and 7.2 wt% formaldehyde solutions. Reprinted with permission from (Takeshita & Yoda, 2015). Copyright (2019) American Chemical Society.

#### 2.3.4. From bio-polymers to the diversity of bio-aerogels:

Bio-aerogels have also been produced from other polysaccharides such as carrageenan (C. A. García-González et al., 2011; Hoover & Vasanthan, 1994; Quignard et al., 2008), agar (Brown, Fryer, Norton, & Bridson, 2010; C. A. García-González et al., 2011; Robitzer et al., 2011), xanthan (G. Horvat et al., 2017; Gabrijela Horvat et al., 2017; Robitzer et al., 2011; L. Wang, Schiraldi, & Sánchez-Soto, 2014), guar (Campia et al., 2017; Ghafar et al., 2017; G. Horvat et al., 2017; Ponzini et al., 2019) and pullulan (Deuber, Mousavi, Federer, & Adlhart, 2017), but they were not studied as much as those based on cellulose, starch, pectin, alginate or chitosan.

In addition to polysaccharides, bio-aerogels are also produced from proteins and amino-acids, such as bovine serum albumin (Kimmich et al., 1993), whey (Betz, García-González, Subrahmanyam, Smirnova, & Kulozik, 2012), soy protein (Arboleda et al., 2013) and egg white

protein (Selmer et al., 2015) and silk fibroin (Mallepally et al., 2015; Marin, Mallepally, & McHugh, 2014). The process route of protein aerogels often includes a heat treatment or pH change to coagulate the protein network; another possibility is the addition of crosslinkers to induce chemical gelation by covalent bonds.

Another approach to make bio-based aerogels is the mixing different starting materials to produce composite aerogels either in order to reinforce the overall aerogel material (Demilecamps, Beauger, Hildenbrand, Rigacci, & Budtova, 2015; Markevicius, Jaxel, Budtova, & Rigacci, 2016; S. Zhao et al., 2016), or to combine their properties and create new functionalities (De Cicco et al., 2016; El Kadib & Bousmina, 2012; R. Wang et al., 2017). Indeed, a significant number of publications report on inorganic/organic (polysaccharide) and polysaccharide/polysaccharide composites aerogels. The most known examples are bio-polymer/silica composite aerogels, which combine the ultralow thermal conductivity (0.012 – 0.015 W/(m.K)) and very high specific surface area (800 - 1100 m<sup>2</sup>/g) of silica aerogels and better mechanical properties provided by polysaccharide addition (*e.g.* cellulose, pectin...) in order to reinforce the inherent brittleness of silica network (Demilecamps, Reichenauer, Rigacci, & Budtova, 2014; M. M. Koebel, Huber, Zhao, & Malfait, 2016; S. Zhao et al., 2015).

All these bio-polymers have specific chemical structure and different physico-chemical properties leading to a wide variety of gelation mechanisms (if any) and process routes. This results in various bio-aerogels (and their composites) with different internal structure and application properties.

### 2.3.5. Modifications of bio-based aerogels

Chemical modification of bio-aerogels is a way to optimize a specific property and extend the range of potential applications. For instance, surface functionalization of a polysaccharide can be performed to modify gelation mechanism by cross-linking (He, Zhang, & Batchelor, 2016; Pushpamalar, Veeramachineni, Owh, & Loh, 2016; Rinaudo, 2006; Takeshita & Yoda, 2015; Zhang, Ren, Tong, & Deng, 2016), to use bio-aerogels as catalyst support (Quignard et al., 2008) or as supercapacitor material (Hao et al., 2015).

Examples of post-gelation surface modification of the main chemical functions of polysaccharides to create new chemical functionalities are presented in Figure 28.

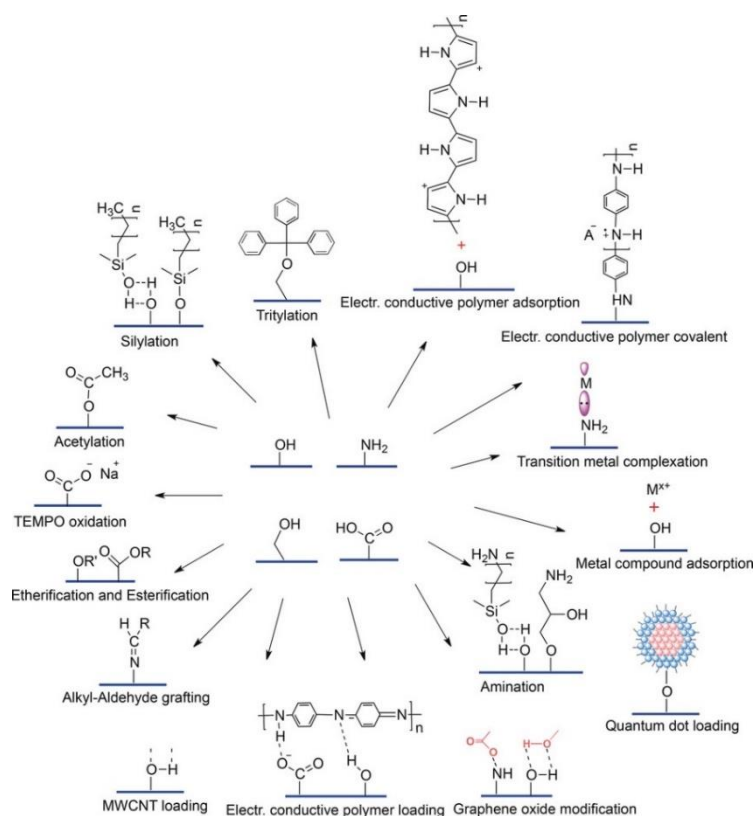


Figure 28. Typical functionalization strategies for biopolymer aerogels. Reprinted from (S. Zhao et al., 2018), Copyright (2019), with permission from Wiley.

The inherent hydrophilicity of polysaccharides might lower long-term stability or limit the range of potential applications of bio-aerogels. Thus, similarly to silica aerogels, bio-aerogels were often hydrophobized using alkyl-siloxanes (*e.g.* octyl-trichlorosilane, methyl-trimethoxysilane...) by hydrogen bonding, electrostatic interactions or covalent bonds (Hayase et al., 2014). Some works report non-silane based hydrophobization approaches such as the work of Takeshita et al. based on the reaction of alkylaldehydes with the amino groups of chitosan -Figure 29) or the work of Pour et al. via trityl- groups grafting on cellulose (Pour, Beauger, Rigacci, & Budtova, 2015).

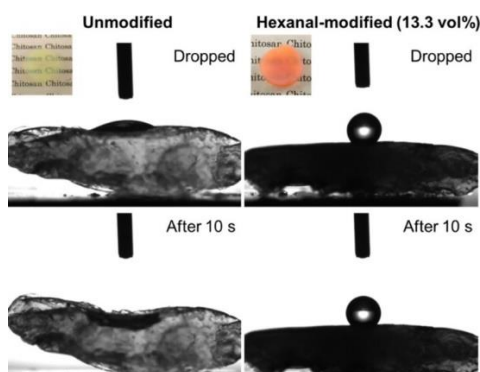


Figure 29. Photographs of water droplets of unmodified and hexanal-modified chitosan aerogel samples at time 0 and after 10 s. Reprinted with permission from (Takeshita et al., 2017). Copyright (2019) American Chemical Society.

The references (Cunha & Gandini, 2010a) and (Cunha & Gandini, 2010b) report other strategies to hydrophobize polysaccharides (which were not tried yet in bio-aerogel production): either by chemical modifications (*e.g.* amidation with fatty acids, (trans)-esterification, grafting of various hydrophobic groups...) or physical treatments (*e.g.* plasma treatment, polymeric coating without covalent attachment...).

Aerogels are extremely versatile materials due their wide range of textural and morphological properties combined to the possibility to tune and functionalize them by varying the process route. As a result, there are numerous potential applications of aerogels in many different technological fields (such as for thermal/acoustic insulations, as catalyst, adsorbents, filtration systems, as carrier materials for release/adsorption of compounds, as sensor materials... etc.). In the following, we will focus on the use of bio-aerogels for two different applications: i) for thermal insulation and ii) for drug delivery applications.

## 2.4. Bio-aerogels for thermal insulation applications

### 2.4.1. Context

Global energy consumption is continuously increasing due to population growth and technological modernization of society, in particular, the major energy consuming sectors are building sector (including heating, ventilation and air conditioning), followed by transport and agriculture (Cuce, Cuce, Wood, & Riffat, 2014). Building insulation is a major ecological issue to consider in order to decrease both energy consumption and CO<sub>2</sub> emissions (Baetens, Jelle, & Gustavsen, 2011). In addition to the ecological aspect, there is also a huge economic issue with a high potential of energy cost saving (Narbel & Hansen, 2014; Rühl, Appleby, Fennema, Naumov, & Schaffer, 2012). In order to reduce energy lost, research was performed from both academia and industry to design and develop lower-energy-consuming building, mostly by applying wall insulation. In order to provide good insulation properties, wall insulation generally is performed by thick and/or multilayers of thermal insulating materials.

A thermally conducting material is able to easily transfer heat flow through it, while a thermal insulator is a material that is able to stop (or at least strongly reduce) heat flow. In order to describe the ability of a material to transfer heat, we use its thermal conductivity (in W/(m.K)) in ambient conditions which is an intrinsic property of a material that quantifies the heat flow passing through its area and thickness. Conventional insulating materials for house and buildings are usually glass wool or mineral wool ( $\lambda \approx 0.03\text{-}0.05$  W/(m.K)) and expanded polystyrene/extruded polystyrene ( $\lambda \approx 0.029\text{-}0.055$  W/(m.K)). For comparison, some existing thermal insulating materials are presented in Table 1.

Table 1. Thermal conductivities in ambient conditions of some existing insulating materials.

Thermal insulating materials	Range of thermal conductivity ( $\lambda$ ) (W/(m.K))	References
<b>Silica aerogels</b>	0.012-0.020	(Aegerter et al., 2011; Cuce et al., 2014)
<b>Silica aerogel blankets</b>	0.010-0.023	("BuyAerogel.com," n.d.)   (accessed 26 march 2019).
<b>Silica aerogels particles/granulates</b>	0.012-0.015	("BuyAerogel.com," n.d.)   (accessed 26 march 2019).
<b>Synthetic organic aerogels</b>	0.012-0.020	(Aegerter et al., 2011)
<b>Polyurethane foams</b>	0.020-0.029	(Aegerter et al., 2011; Cuce et al., 2014)
<b>Expanded or extruded polystyrene</b>	0.029-0.055	(Aegerter et al., 2011; Cuce et al., 2014)
<b>Glass wool</b>	0.031-0.43	(Aegerter et al., 2011; Cuce et al., 2014)
<b>Glass foam</b>	0.040-0.045	(Aegerter et al., 2011; Cuce et al., 2014)
<b>Mineral wool</b>	0.033-0.05	(Aegerter et al., 2011; Cuce et al., 2014)
<b>Vacuum glazing</b>	0.010-0.023	(Aegerter et al., 2011; Cuce et al., 2014)

#### 2.4.2. Thermal conductivity of aerogels

In the first approximation the thermal conductivity  $\lambda$  of a porous material can be described by a model equivalent to an additive sum of the conductions of the solid  $\lambda_{\text{solid}}$  and gas  $\lambda_{\text{gas}}$  phases and of the radiative heat transfer  $\lambda_{\text{rad}}$  (see equation 1.3):

$$\lambda = \lambda_{\text{solid}} + \lambda_{\text{gas}} + \lambda_{\text{rad}} \quad (1.3)$$

Heat conduction via the solid backbone  $\lambda_{\text{solid}}$  results from thermal transport between atoms by lattice vibrations through chemical bonds between them. Gas thermal conductivity  $\lambda_{\text{gas}}$  is due to thermal energy transfer from one gas molecule to the other by collision between them. The radiative heat transfer  $\lambda_{\text{rad}}$  is linked to the emittance of electromagnetic radiation in the infrared wavelength region from the surface of the material.  $\lambda_{\text{rad}}$  is not significant at room temperatures and for optically thick materials (which is the case of the majority of bio-aerogels). A schematic representation of heat conduction via the solid network and heat transfer via the gaseous phase within the pores of an aerogel is shown in Figure 30.

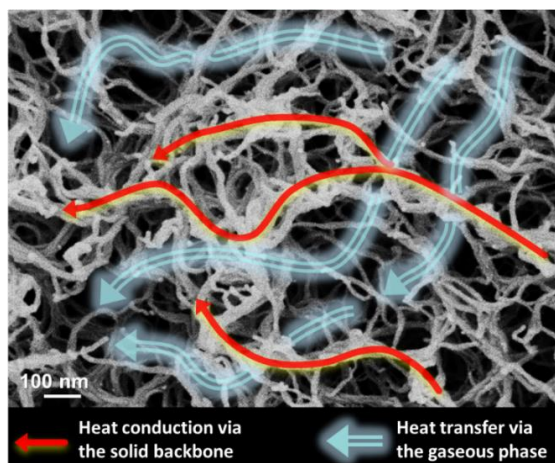


Figure 30. Schematic illustration of heat transfer mechanisms in an aerogel: by the solid backbone (red arrows) and by the gaseous phase present in the porous structure (blue arrows). The picture sample is a pectin aerogel made from 3 wt% of pectin of DE = 35% with calcium added ( $R(\text{Ca}) = 0.2$ , see Equation (1.1)), prepared in this work.

Solid phase conduction logically increases with density increase and is decreased in a material of high porosity and solid skeleton of high tortuosity. To minimize the conduction of the gaseous phase two options are possible: either evacuation the gas (air), or decrease of pores' sizes down to mesoporous region to reduce the contact between gas molecules. In the latter case pore size is below the mean free path of air molecules, which is around 70 nm at 25 °C and 1 atm, leading to  $\lambda_{\text{gas}}$  lower than that of ambient air according to Knudsen effect. As an illustration, Figure 31 shows the variation of thermal conductivity of air in porous materials while decreasing the average pore size.

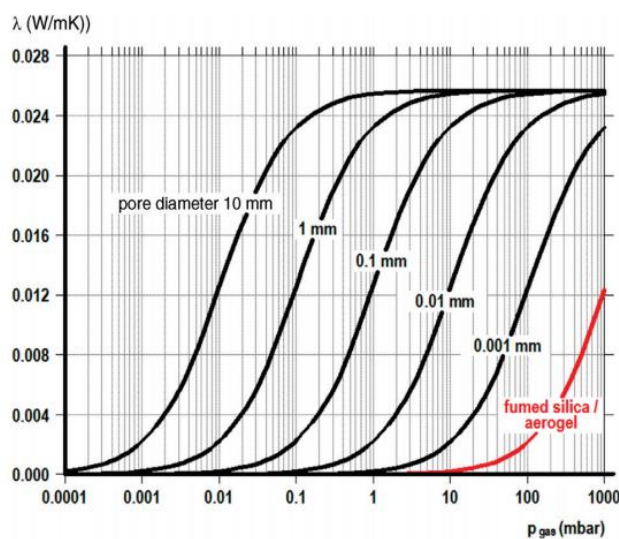


Figure 31. Variation of the thermal conductivity of air contained in porous material with different average pore diameters and as a function of pressure, Reprinted from (Baetens et al., 2011). Copyright (2019), with permission from Elsevier.

Due to the Knudsen effect and heat conduction via the solid backbone, the control of the aerogel pore sizes and density is extremely important to obtain super-insulating materials by significantly reducing both gas and solid thermal conductivities (Baetens et al., 2011). Intuitively it is thus clear that the lowest thermal conductivity can be reached for low-density mesoporous materials.

For silica and synthetic polymer aerogels it was demonstrated that the dependence of thermal conductivity on density has a U-shape as shown in Figure 32 (Hüsing & Schubert, 1998; Lu et al., 1992): higher density leads to conductivity increase because of  $\lambda_{\text{solid}}$  input, and lower density leads to  $\lambda_{\text{gas}}$  increase because of the presence of large pores which do not contribute to Knudsen effect.

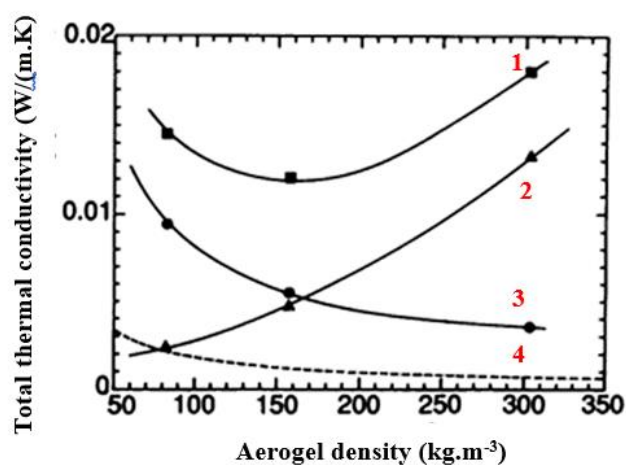


Figure 32. Total thermal conductivity (1), solid conductivity (2), gaseous conductivity (3) and calculated radiative conductivity (4) of resorcinol-formaldehyde aerogels as a function of density at ambient conditions. Adapted from (Lu et al., 1992).

Aerogels may present a very low density (0.05 - 0.1 g/cm<sup>3</sup>), meso- and small macroporosity, and very high specific surface area (> 500 m<sup>2</sup>/g). Thanks to these properties, both gaseous and solid thermal conductivity are drastically reduced allowing silica and some synthetic polymer aerogels to be thermal super-insulating materials, *i.e.* with thermal conductivity below that of air in ambient conditions, 0.012 – 0.015 (M. Koebel et al., 2012) vs 0.025 W/m.K. Till now, silica aerogels are known to be materials with the lowest thermal conductivity.

### 2.4.3. Aerogels used as thermal insulating materials: issues and open questions

The extremely low thermal conductivity and good transparency of silica aerogels make them very promising materials for insulation of windows and buildings and other structures

such as cooling or heating systems, pipelines, food storage... *etc.* Among existing inorganic thermal insulating materials, silica aerogel was one of the most extensively studied the past years (Baetens et al., 2011). The sector of classical aerogels has now matured resulting in the production and commercialization of aerogels blankets and particles (Table 1).

Despite of their extraordinary textural and thermal properties, silica aerogels are still not widely used because of their high mechanical brittleness, the release of silica “dust” because of their poor mechanical properties, and a relatively high raw materials and production costs. Technical solutions were proposed to improve the mechanical properties of silica aerogels, one possibility being making silica-based composites with another polymer or with fibers that bring a mechanical reinforcement. As an example, fiber reinforced composite aerogels were produced by adding natural fibers to silica sol (Markevicius, Ladj, Niemeyer, Budtova, & Rigacci, 2017). However, silica-based composite aerogels usually present higher conductivity than neat silica aerogels due to either material densification or higher heat conduction via the added fibers.

Some synthetic polymer aerogels showed excellent thermal insulation characteristics, such as RF aerogels with thermal conductivity around 0.012 W/(m.K) (Lu et al., 1992). Other examples are polyurethane aerogels which are also super-insulating materials but with slightly higher conductivity, around 0.017 W/(m.K) (Biesmans, Randall, Francais, & Perrut, 1998; Diascorn, Calas, Sallee, Achard, & Rigacci, 2015). Taking into account the actual ecological and sustainability issues, there is still a need of renewable alternatives avoiding toxic chemistry process of synthetic polymer aerogels synthesis, in order to develop new cost-effective and mechanically robust aerogels with thermal super-insulating properties.

In this context, bio-based materials and especially bio-aerogels had logically received considerable attention the past 15 years as they may combine low thermal conductivities (from 0.016 to 0.05 W/(m.K) depending on the type of bio-polymer used), good mechanical properties and are environmentally friendly. It would be extremely attractive to develop bio-aerogels presenting similar thermal insulation properties as silica even if the processing costs of bio-aerogels are hard to evaluate as they were never transferred to pilot scale process up to now. However, very few is known about the thermal conductivity of bio-aerogels as it is a very recent field, and practically nothing on conductivity-structure correlations.

Up to date, only few and recent works on bio-aerogels with thermal super-insulating properties are reported: with the conductivity around 0.016–0.020 W/m.K for aerogels based on pectin (Rudaz et al., 2014), around 0.018 W/(m.K) based on nanofibrillated cellulose (cellulose I cryogels and aerogels) (Jiménez-Saelices et al., 2017; Kobayashi et al., 2014; Seantier et al., 2016), 0.018-0.022 W/(m.K) based on alginate (P. Gurikov et al., 2015) and 0.021 – 0.023 W/(m.K) based on starch (Druel et al., 2017; Glenn & Irving, 1995). Although starch and cellulose have D-glucose as repeating units (but linked differently), up to now, no

cellulose II aerogels with thermal super-insulating properties were reported (with the lowest value of thermal conductivity being around 0.026 W/(m.K) (Rudaz, 2013)), most probably because of the presence of large macropores promoting thermal conduction of the gaseous phase within the material. Why some bio-aerogels present super-insulating properties and some do not? What are the correlations between polysaccharide type, aerogel preparation conditions, morphology and final properties? How can we control bio-aerogel structure to vary aerogel thermal properties?

In this context, Rudaz et al. produced pectin aerogels from high-methylated pectins and polymer concentration was varied to modify aerogel morphology and density (from 0.05 to 0.15 g/cm<sup>3</sup>) which led to increase conductivity from 0.018 W/(m.K) to 0.03 W/(m.K) but no U-shape curve was obtained (Rudaz, 2013). Similar results but with slightly higher conductivity values were recorded for starch aerogels (Druel et al., 2017). Seantier et al. reported a U-curve of conductivity vs density for freeze-dried bleached cellulose fibers “filled” with nanofibrillated cellulose: density was varied by sample compression and the lowest thermal conductivity was 0.023 W/(m.K) (Seantier et al., 2016). The same approach by uniaxial densification was applied to nanocellulose aerogels to decrease their thermal conductivity in the super-insulation domain (Plappert, Nedelec, Rennhofer, Lichtenegger, & Liebner, 2017). The correlations between the conductivity and structure and properties of bio-aerogels made via dissolution-solvent exchange route remain open.

Finally, as future prospects and technical challenge, hydrophobization of hydrophilic bio-aerogels would be particularly attractive in order to decrease moisture adsorption and avoid aging. Classical hydrophobization techniques of silica aerogels consist in the coverage of surface hydrophilic functions by non-polar functions such as methyl groups during “wet steps” prior to drying (*e.g.* by silylation with trichloromethylsilane or methyltrimethoxysilane) (United States Patent No. US2589705A, 1952; Schwertfeger et al., 1992) or by aerogel post-treatment after sc-drying (*e.g.* using hexamethyldisilazane (HMDS) (Rao et al., 2003)). However, using natural compound would be a much better option for bio-aerogels in adequation with their low-toxicity profile, environmentally-friendly and human friendly characteristics.

## **2.5. The use of bio-aerogels and silica aerogels for drug delivery applications**

In this section, the case of an oral drug administration from a solid drug delivery system will be considered. A detailed information of the fundamental concepts and the common mathematical models used for drug delivery applications is presented in the Annex to the

manuscript.

### 2.5.1. Drug delivery systems: introductive concepts and principles

#### ▪ **Modified drug release behaviors**

After oral administration, the release of a drug occurs in the gastro-intestinal tract. In addition to the dose administered and the release profile over time, the drug concentration and kinetics of exposure to the organism are regulated by continuous biological phenomena (absorption, distribution, metabolism and elimination). The equilibrium between the drug absorption and elimination rate determines the actual level of drug distributed in the plasma.

If drug concentration in plasma is above toxic Maximum Safe Concentration (MSC), the patient can exhibit side effects due to over-dosage. On the contrary, a concentration below the Minimum Effective Concentration (MEC) conducts to under-dosage and the drug is therapeutically ineffective (Bruschi, 2015; Siepmann, Siegel, & Rathbone, 2012). The therapeutic range or window of a drug refers to the range of drug concentrations between MSC and MEC, which are expected to achieve therapeutic efficiency with minimal toxicity, as illustrated in Figure 33.

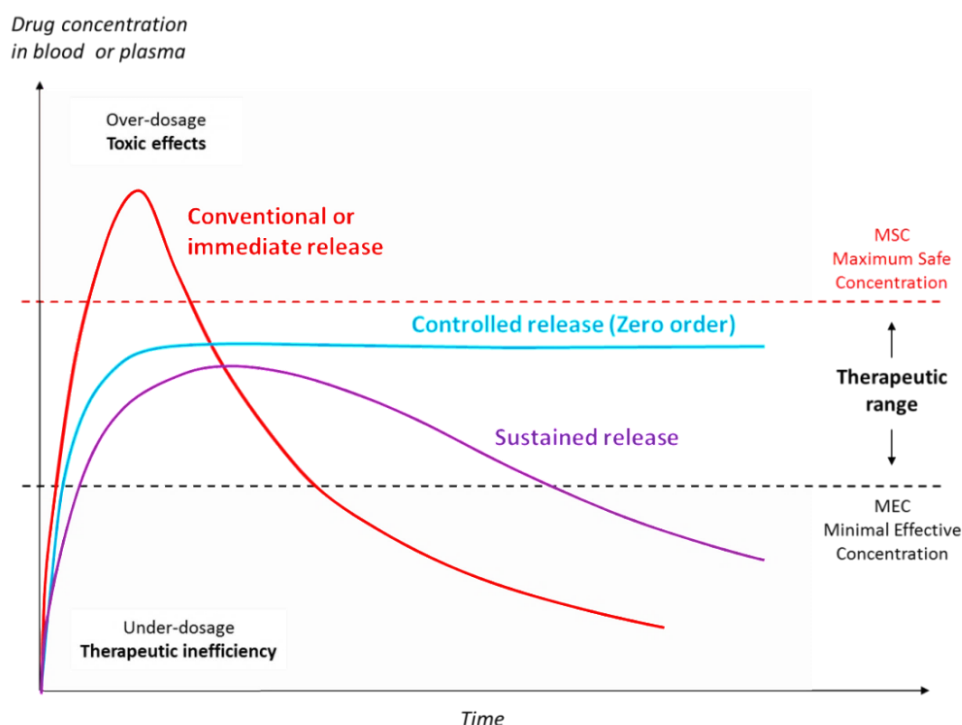


Figure 33. Schematic representation of drug concentrations in blood/plasma as a function of time for different types of release: conventional drug intake (or immediate release), sustained release and controlled release.

An optimal Drug Delivery System (DDS) will deliver the drug at a precise rate determined by the therapeutic indications over a specified period of time. Ideally, the dose delivered in blood should be maintained constant inside the therapeutic window to be therapeutically effective and non-toxic, which corresponds to Zero-order kinetics (Bruschi, 2015; Siepmann et al., 2012).

An immediate-release DDS releases the drug within a short period of time, typically less than 30 minutes, resulting in a rapid burst of drug concentration in blood. In contrast, modified release dosage forms deliver the drug either with a delay after administration, during an extended period of time, or to specific locations in the body (targeted release) (Bruschi, 2015; Siepmann et al., 2012). These systems provide many benefits such as avoidance of local and systemic side effects due to over-dosage, maintenance of drug therapeutic concentration without fluctuation, allow therapeutic efficiency with diminution of the administered dose, minimization of dose intake frequency and protection of the compound against degradation by biological fluids (Chien, 1991). The most common modified release DDS includes:

- **Delayed release** DDS are designed to deliver a drug therapeutic dosage at a later time after administration. They are typically enteric-coated to be stable at gastric pH in order to prevent immediate release in the stomach. These systems are needed in order to protect the drug from acid degradation, to prevent gastric irritation, or to target specific intestinal or colonic site.
- **Sustained release or extended release** DDS are expected to achieve prolonged therapeutic effect by releasing drug at a sufficient initial therapeutic dose then followed by a gradual release (possibly at variable rates) over an extended period of time after administration.
- **Controlled release** DDS release the drug at a nearly constant rate for an extended period of time after administration. It corresponds to the ideal case or Zero order kinetics.

In the design of a modified release DDS, it is necessary to know the exact mass transport phenomena mechanism involved in drug release, in order to provide a specific drug release profile.

#### ▪ **Drug release mechanisms from polymer matrix systems**

A large variety of solid oral dosage forms exist to modify and control drug release such as encapsulation, reservoir, membrane or matrix systems. When studying drug delivery from a solid device, different mass transport phenomena are involved successively or simultaneously: water diffusion inside the device, system swelling, system dissolution and/or erosion, drug dissolution and diffusion through the hydrated system.

Usually, the slowest physical phenomenon is the determining step as it plays a significant controlling role on the release (Bruschi, 2015; Siepmann et al., 2012). The classification of DDS is based on their main mechanism that drives drug release including *inter alia*:

- Diffusion-controlled systems
- Matrix erosion-controlled systems
- Swelling-controlled systems
- Osmotic pressure-controlled systems (drug with solution core)
- Chemically controlled systems
- Ion-exchange systems ...

In the case of matrix systems, the drug is dispersed into a solid carrier, generally polymer-based, from which it is extracted by a liquid media. Matrix systems are more prone to **diffusion-controlled release** *i.e.* when the release rate is dependent on drug diffusion through the liquid media within a non-soluble and non-swellable matrix, or to **matrix erosion-controlled release** *i.e.* when the release rate is dependent of the progressive degradation of the matrix by chemical, physical or biological reactions. A schematic illustration of the most diffusion-controlled and matrix erosion-controlled releases of the drug are shown in Figure 34. “Matrix erosion” refers to all physical or chemical mechanisms that lead to matrix “degradation” with the loss of its structural integrity. Erosion can be due to polymer dissolution, breakage, or detachments of particles. It should be noted that a combination of mechanisms is often involved such as **diffusion-erosion controlled release**, or **diffusion-swelling controlled release**, for the most known systems (Bruschi, 2015; Siepmann et al., 2012).

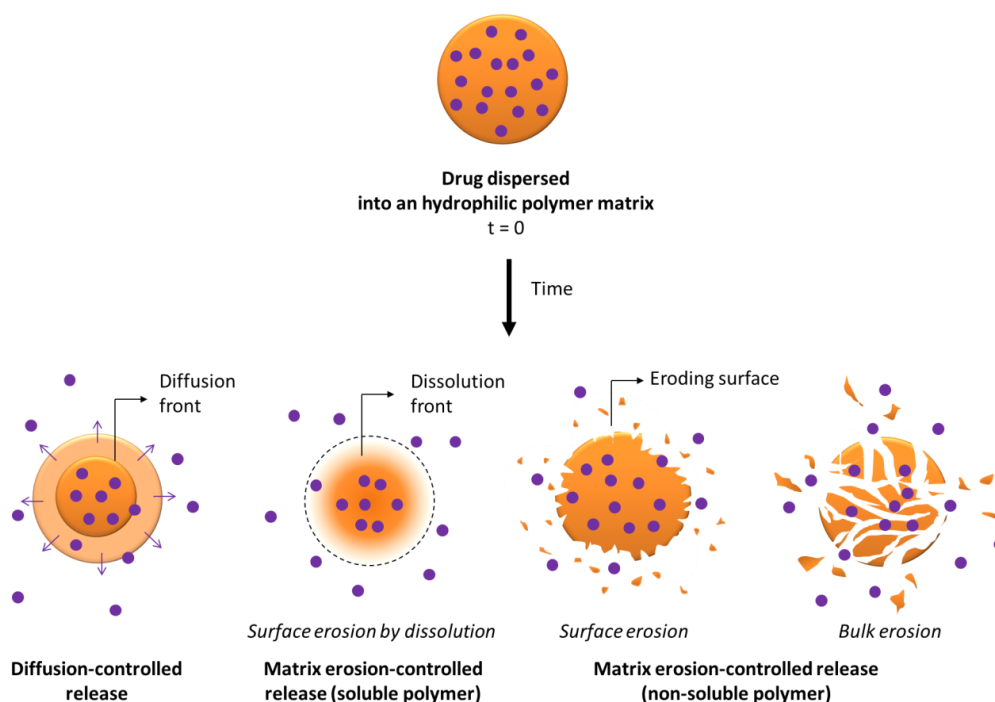


Figure 34. Most frequent drug release mechanisms from solid polymer matrix

Mass transport phenomena, description of drug release mechanisms from a polymeric matrix, and the usual mathematical models are presented in the Annex.

### 2.5.2. Aerogels used as drug delivery systems

#### ▪ **Production of drug loaded aerogels**

Biocompatible aerogels, such as polysaccharide-based, are suitable materials for a wide range of life science applications such as biomedical, pharmaceutical, biotechnological, cosmetic and food. Silica aerogels were first investigated for biomedical and pharmaceutical applications (I. Smirnova, Mamic, & Arlt, 2003; I. Smirnova, Suttiruengwong, & Arlt, 2004; I. Smirnova, 2011; I. Smirnova, Suttiruengwong, Seiler, & Arlt, 2004), however, their poor mechanical properties and their non-biodegradability are limiting factors for some requirements. The use of aerogels and especially polysaccharide-aerogels as porous DDS present several advantages (I. Smirnova, 2011) :

- i) their high inner surface area which optimizes drug loading,
- ii) their open porosity and quite homogeneous pore size distribution,
- iii) low toxicity profile and biodegradability,
- iv) avoidance of drug agglomerates as they are dispersed through the network of the matrix,
- v) the aerogel backbone is as chemically stable as original biopolymer,
- vi) provide physical protection of the drug from oxidation and moisture,
- vii) might allow chemical stabilization of the drug in case of interactions with the matrix,
- viii) increase of bio-availability of the drug in case of amorphous state (precipitated drug) and
- ix) ease for chemical modification and adjustment of release profile. To target different administration routes and therapeutic indications, the size and morphology of aerogels can be customized using different techniques (molding, dropping, emulsion-gelation, milling...) by shaping aerogels as monoliths, beads, spheres and particles of different size, membranes, powders etc.

Incorporation of the drug within the aerogels depends on drug physico-chemical and solubility properties, and can be realized before or after sc-drying as illustrated in Figure 35:

- **Drug loading before sc-drying:** by addition of the drug into the sol or polymer solution before gelation (Figure 35a) (United States Patent No. US6994842B2, 2006; Tkalec, Knez, et al., 2016) or by dissolution in polymer non-solvent and impregnation by diffusion into the aerogel precursor before the drying step (Figure 35b) ((Haimer et

al., 2010; Mehling et al., 2009; Tkalec et al., 2015a). In these cases, the drug should present low solubility in the supercritical fluid used for drying, to avoid drug removal. It was shown that impregnation during solvent-exchange step led preferentially to deposition of the drug by precipitation during sc-drying (Haimer et al., 2010; Mehling et al., 2009). Haimer et al. found that drug loading of bacterial cellulose aerogels by drug diffusion during solvent-exchange was directly dependent on drug concentration in the loading bath (Haimer et al., 2010).

- **Drug loading after sc-drying (post-treatment):** by diffusion of the drug through a liquid (Buisson, Hernandez, Pierre, & Pierre, 2001), gaseous or supercritical fluid phase (Figure 35c) (I. Smirnova et al., 2003), leading to drug adsorption/precipitation in the already dried aerogel. Supercritical fluid-assisted drug loading leads preferentially to drug deposition in the amorphous state.

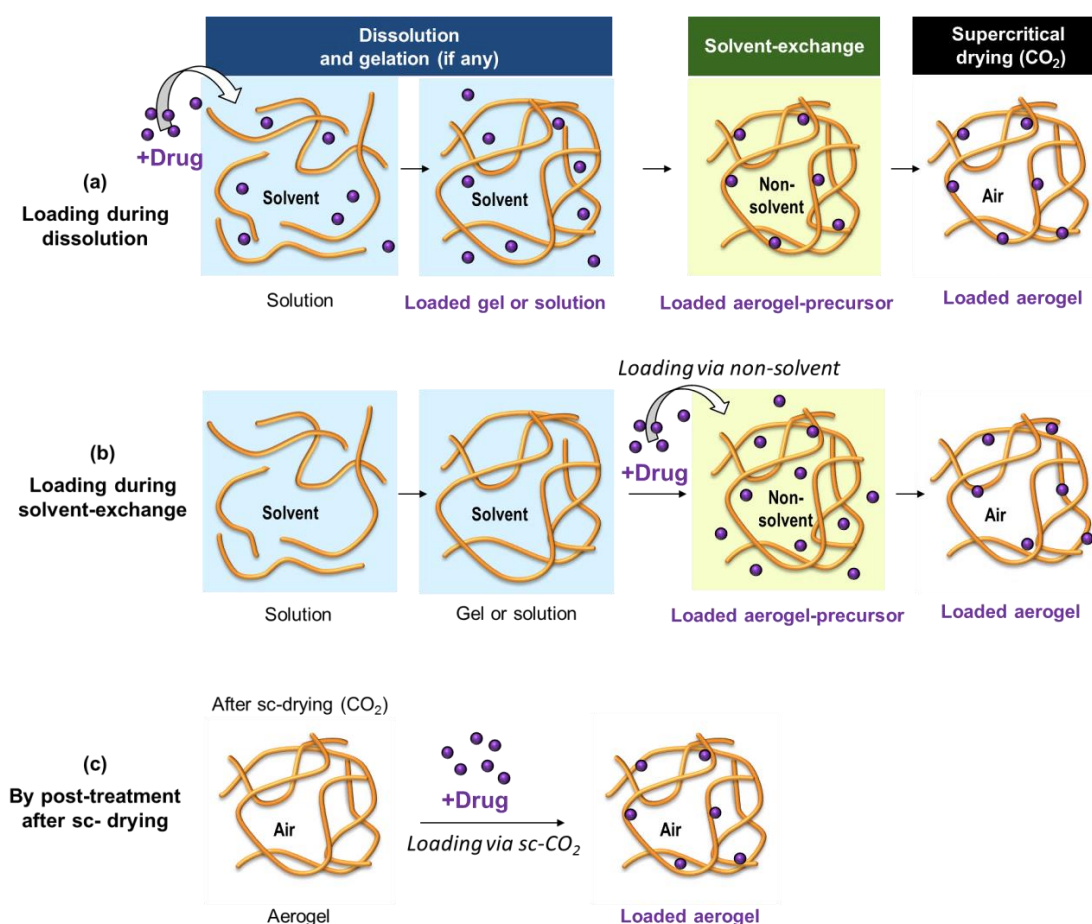


Figure 35. Drug loading of aerogels: (a) during dissolution step (before gelation); (b) during solvent exchange step by diffusion via non-solvent; (c) in the aerogel matrix by supercritical impregnation post-treatment method.

It has to be noted that the precipitation or crystallization of the drug on the walls of aerogel precursor or aerogel can be controlled by the incorporation method, the process

parameters during sc-drying (pressure, temperature) as well as the physico-chemical interactions with the aerogel carrier. For example, Gorle et al. pointed out strong interactions of the drug with the matrix which favored amorphous state of the drug which can be stabilized in multilayers, whereas weak interactions with matrix led preferentially to drug crystallization (Gorle, Smirnova, & Arlt, 2010).

### ▪ **Factors influencing drug loading**

When using aerogels as DDS, the most important parameters to take in account are the kinetics of drug release over time and the drug loading within the aerogel. The maximum drug loading depends on drug solubility in the medium used for drug impregnation and on the area of the active surface of the aerogel (Haimer et al., 2010). The latter depends on aerogel specific surface area, total mesopores volume and surface functionality that impact the affinity of the drug to a given matrix.

For a given system [drug-aerogel], it was shown that loading increased with aerogel specific surface area and with mesopores volume which enables better diffusion than in micropores (Alnaief & I. Smirnova, 2010; Haimer et al., 2010; I. Smirnova et al., 2003; I. Smirnova, 2011; I. Smirnova, Suttiruengwong, & Arlt, 2005). Smirnova et al. observed that drug loading was also increased with aerogel density assuming that the explanation would be the increase of  $S_{BET}$  with density, but underlined that  $S_{BET}$  was not the only factor (I. Smirnova et al., 2004). Garcia et al. suggested that apart specific surface area, other parameters might play a significant role in drug loading such as surface chemistry and drug-matrix interactions (Garcia-Gonzalez & Smirnova, 2013).

Mehling et al. showed that drug loading of starch aerogels (by diffusion in non-solvent) increased when specific surface area was higher and pore size smaller (Mehling et al., 2009). They assumed that smaller pore sizes led to increased drug loading due to capillary forces holding drug molecules inside the porous matrix.

Finally, Tkalec et al. showed that aerogel composition (pectin, alginate, or composite pectin-alginate) and gelation conditions (crosslinking with  $Ca^{2+}$ ,  $Sr^{2+}$  or  $Zn^{2+}$  ions) may drastically change of drug entrapment efficiency (%) (*i.e.* the mass of drug experimentally extracted from the carrier toward the mass of drug that was theoretically incorporated) and drug loading (*i.e.* the mass of drug towards aerogel mass) (Tkalec, Knez, et al., 2016). Surprisingly, these authors found that the loading as well as the entrapment efficiency of Diclofenac into bio-aerogels were varying from around 40 % to 80 %, and were inversely related which the variation of aerogel specific surface area (from 260  $m^2/g$  to 440  $m^2/g$ ) resulting from different composition and ionic cross-linking, as shown in Figure 36. On the opposite, Veronovski et al. observed higher theophylline and nicotinic acid loadings ( $\sim + 50\%$ ) within citrus pectin-

aerogels than within apple pectin-aerogels in correlation with their inherent higher specific surface area ( $\sim + 15\%$ ) (Veronovski et al., 2014).

Sample <sup>a</sup>	Drug loading (%)	Entrapment efficiency (%)	Surface area <sub>BET</sub> (m <sup>2</sup> g <sup>-1</sup> )
AZ	79.6	80.72	261
AS	49.8	51.78	287
AC	40.5	42.30	437
PZ	79.0	68.07	272
PS	58.7	40.45	292
PC	44.2	36.52	407
APZ	56.9	70.59	299
APS	39.4	50.07	332
APC	35.9	44.98	417

<sup>a</sup> A: alginate, P: pectin, AP: alginate-pectin, Z: zinc, S: strontium, C: calcium.

Figure 36. Drug loadings in wt% (mass of drug towards aerogel mass) and entrapment efficiency of diclofenac (or drug loading efficiency in %) and specific surface area (m<sup>2</sup>/g) of different bio-aerogels varying polysaccharide composition (alginate and/or pectin) and the nature of cation (Ca<sup>2+</sup>, Zn<sup>2+</sup>, S<sup>2+</sup>) used to induce ionic gelation. Adapted from (Tkalec, Knez, et al., 2016)

### ▪ Case studies of silica-based and polysaccharide-based aerogels

Aerogels can be used as carriers for different strategies: enhancing the bioavailability of low-soluble drugs (Hentzschel, Alnaief, Smirnova, Sakmann, & Leopold, 2012; I. Smirnova et al., 2004; Tkalec et al., 2015a) or prolonging their release over time (C. A. García-González et al., 2015; Marin et al., 2014; Mehling et al., 2009; I. Smirnova et al., 2005). In the first case, the use of immediate-release delivery systems is particularly desirable in case of poorly water-soluble drugs, as their dissolution rates and bioavailability are limited. On the contrary, delayed- or extended-release of drug which are highly soluble and bioavailable is required to target therapeutic window with minimum toxic effects (Bruschi, 2015).

Drug release kinetics from aerogel into a liquid media is known to be affected by several parameters such as the properties of the releasing media, of the drug and the aerogel carrier. For a given drug, the most important parameters were shown to be as follows:

- The physical state of the adsorbed drug (amorphous or crystalline form) determined by the drug incorporation method and drug properties. Drug in the amorphous state leads to faster dissolution rate and faster release than that of drugs in the crystalline form ((I. Smirnova et al., 2004; I. Smirnova, Türk, Wischumerski, & Wahl, 2005; I. Smirnova et al., 2004).
- Size and geometry of the aerogel carrier (United States Patent No. US6994842B2, 2006; I. Smirnova et al., 2005; I. Smirnova et al., 2004) as they directly determine the surface contact with the releasing fluid and time needed for the drug to diffuse out of the carrier

(Haimer et al., 2010).

- Chemical and physical properties of the aerogel matrix (Mehling et al., 2009). Tuning of these parameters drastically changes the mechanical and structural properties of the porous matrix, which in turn influences the diffusion mass transport and matrix erosion phenomena governing drug release (Mehling 2009). Besides, chemical interactions between the drug and the matrix carrier and functionalization may also influence the release rate.

Literature reports that drug release profiles from bio-aerogels are strongly influenced by aerogels' composition, physico-chemical properties as well as the type of releasing medium as it largely affects mass transport mechanisms (diffusion, dissolution, aerogel swelling and erosion) and the chemical interactions with the drug (Maleki et al., 2016; Stergar & Maver, 2016). Data fitting with the most common mathematical models such as First-order, Higushi, Korsmeyer–Peppas, and Gallagher–Corrigan models are often used to identify the main release mechanism governing drug release from aerogels (C. A. García-González et al., 2015; Haimer et al., 2010; G. Horvat et al., 2017; Marin et al., 2014; Obaidat, Tashtoush, Bayan, T. Al Bustami, & Alnaief, 2015; R. Wang et al., 2017).

Below we discuss the correlations known from literature between the physico-chemical properties of aerogel carrier and its release properties. Different strategies to tailor release properties are reported in literature such as varying aerogel matrix composition, employing different preparation conditions and processing parameters, varying matrix hydrophilicity by surface modification/functionalization or by producing composite aerogels.

➤ *Effect of aerogel composition on the release properties*

Bio-polymers and silica aerogels display different properties such as hydrophilicity, solubility and mechanical properties in a given releasing media. Thus, for a given drug, the composition of the aerogel carrier has to be set considering that it will drive matrix swelling and erosion and thus, drug release properties.

Several comparative studies were carried out on the release properties of drugs from aerogels made from different substances: silica, starch, sodium alginate and pectin (C. A. García-González et al., 2015; Lovskaya et al., 2015; Mehling et al., 2009) Mehling et al. Lovskaya et al. Garcia et al. They showed that drug release profile from aerogel was mainly dependent on the physical “stability” of the aerogel matrix in the release media (*i.e.* the matrix resistance to erosion and/or dissolution by the liquid media) as well as affinity towards the drug, both determined by aerogel's composition and process route (*e.g.* gelation method). The illustrations of the impact of aerogels' composition on their release properties *in vitro* are shown in Figure 37(A and B), and *in vivo* Figure 38.

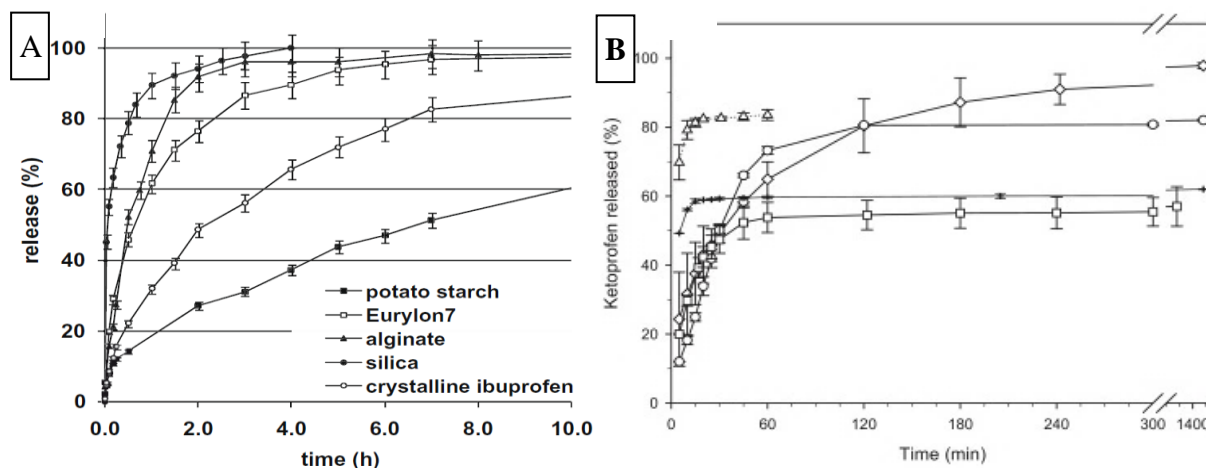


Figure 37. (A) Release of ibuprofen from polysaccharide and silica aerogels in comparison to the dissolution of the crystalline drug form. Release conditions: paddle method, 37°C, 0.2 M phosphate buffer at pH 7.2. Adapted from (Mehling et al., 2009).

(B) In vitro release profiles of ketoprofen in phosphate buffer (pH 6.8) from, alginate (1), pectin (2) silica (3) and starch (4) aerogel microspheres. The dissolution of the same amount of free drug (5) is also plotted for comparison. Adapted from (C. A. García-González et al., 2015).

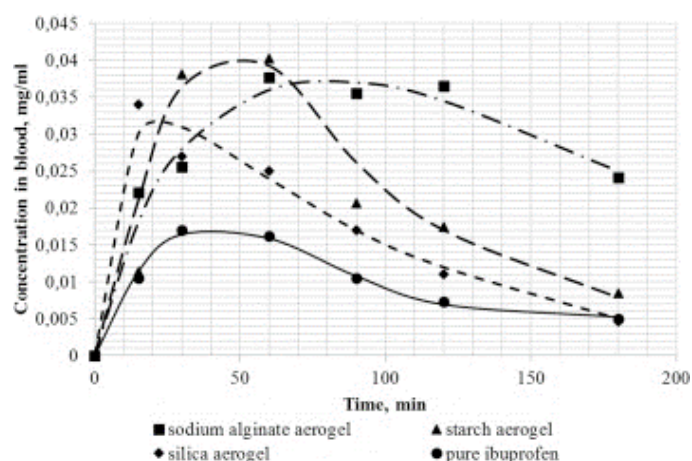


Figure 38. Results of *in-vivo* release test of ibuprofen from various aerogels compared to the pure substance. Reprinted from (Lovskaya et al., 2015). Copyright (2019), with permission from Elsevier.

Depending on the physico-chemical properties of the aerogel carrier (*i.e.* swellable, soluble/erodible), the drug release from polysaccharide aerogels were reported to be either diffusion-controlled or diffusion-erosion controlled.

#### Diffusion-controlled polysaccharide aerogels:

Haimer et al. showed that drug release from bacterial cellulose aerogels was due to pure Fickian diffusion as the matrix was found to be stable (no erosion) in aqueous media. Hence, drug release is controlled by varying the thickness of the gel as it is directly impacted by the

distance to be covered to diffuse out of the matrix (Haimer et al., 2010). Similarly, Marin et al. demonstrated the ability of silk fibroin aerogels to deliver ibuprofen for an extended period of time, and suggested that release was governed by slow Fickian diffusion within the system as it was not subjected to matrix erosion (Marin et al., 2014).

#### **Diffusion and erosion-controlled polysaccharide aerogels:**

Due to their slow erosion in aqueous media, drug release from chitosan (Obaidat et al., 2015) or starch aerogels (C. A. García-González et al., 2015; Garcia-Gonzalez & Smirnova, 2013) were found to be governed by a combined effect of both diffusion and erosion processes. Besides, drug release from starch aerogels is usually not complete, and suggestions were made about the formation of insoluble drug-amylose inclusion complexes (Garcia-Gonzalez & Smirnova, 2013).

Aerogels made from polyelectrolyte polysaccharides such as alginate (C. A. García-González et al., 2015; Gonçalves et al., 2016; Mehling et al., 2009), pectin (De Cicco et al., 2016; C. A. García-González et al., 2015; Gonçalves et al., 2016; Lovskaya et al., 2015; Veronovski et al., 2014) and  $\kappa$ -carrageenan (Gonçalves et al., 2016) were found to have similar drug release behavior governed by diffusion-controlled strongly assisted by matrix erosion. This stems from polyelectrolyte sensitivity to the pH of the aqueous medium (pH 1-1.2 or close to neutral condition). Indeed, while release due to matrix erosion is slow in acidic conditions, much faster matrix erosion was observed at pH close to neutral which promoted drug release in buffer solution. Rapid matrix erosion by dissolution process was attributed to high hydrophilicity and physico-chemical “instability” of polyelectrolyte aerogels in aqueous media, especially with the formation of charges when pH is above  $pK_a$ .

In addition to the nature of the polysaccharide aerogels, the polysaccharide source was reported to slightly modify the physico-chemical characteristics of the polymer, impacting its release properties. As an illustration, Mehling et al. observed that starch source had a significant impact on matrix “resistance” to erosion. Indeed, aerogels based on modified starch (Eurylon7) disaggregated relatively fast in liquid because of poor mechanical properties, providing quite fast drug release.

On the contrary, potato starch aerogels were found to be more stable in liquid media resulting in slower drug release (Mehling et al., 2009). In the same way, pectin aerogels were produced from different amidated low-methylated pectin sources (citrus and apple) by (Veronovski et al., 2014). Citrus pectin aerogel was found to be more stable in terms of dissolution in phosphate buffer (pH 6.5) than apple pectin aerogel, which resulted in slower and more controlled drug release behavior as shown in Figure 39. These results were attributed to lower degree of methylation of citrus pectin (23–28%) than of apple pectin (27–32%).

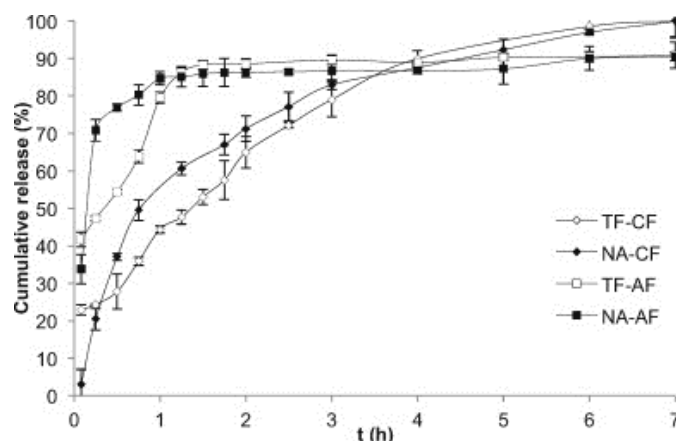


Figure 39. Theophylline (TF) and nicotinic acid (NA) release kinetics in phosphate buffer solution (pH 6.5) from spherical multi-membrane aerogels based on citrus pectin (CF) or apple pectin (AF) and using 0.2 M  $\text{CaCl}_2$  for cross-linking. Reprinted from (Veronovski et al., 2014). Copyright (2019), with permission from Elsevier.

➤ Effect of preparation conditions on aerogels' release properties

Del Gaudio et al. noticed that ketoprofen-lysinate release from alginate aerogels was dependent on matrix structural parameters which resulted from different network formation processes (ionic gelation in calcium aqueous solutions or coagulation in ethanol) and drying methods (supercritical or evaporative drying). They assumed that high porosity and high specific surface area of the aerogels compared to xerogels might have induced faster release (Gaudio et al., 2013). Tkalec et al. produced pectin and alginate aerogels by cross-linking with three different ions, zinc, strontium and calcium. They assumed that the type of divalent cation might have impacted the strength of the ionotropic cross-linking and aerogel density. Once in the release media, the aerogel swelling ability and matrix erosion were different depending on the type of ionic junctions, which influenced drug release profile (Tkalec, Knez, et al., 2016), as shown in Figure 40.

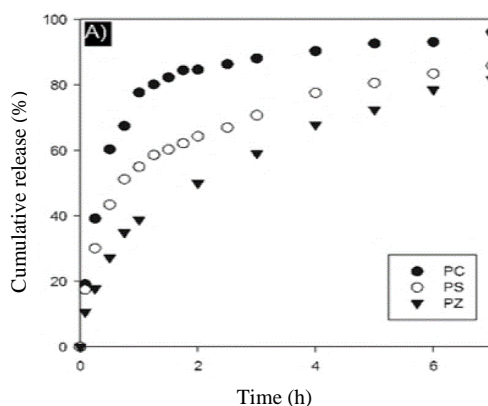


Figure 40. Cumulative drug release from pectin (P) aerogels cross-linked with three different ions Z: zinc, S: strontium, C: calcium. Reprinted from (Tkalec, Knez, et al., 2016). Copyright (2019), with permission from Elsevier.

In the work on chitosan aerogel microparticles loaded with salbutamol, (Obaidat et al., 2015) highlighted that increasing chitosan molecular weight, polymer concentration and the crosslinker concentration (tripolyphosphate) decreased the swelling ability and erosion of the matrix, which in turn slowed down drug diffusion and release. Chang et al. studied the adsorption and removal kinetics of a surfactant from aqueous solutions (sodium dodecylbenzene-sulfonate) within different chitosan-based aerogels. Structural properties of chitosan aerogels were strongly varied with different cross-linkers (glutaraldehyde, glyoxal or formaldehyde) and water/chitosan/cross-linker ratios during gel preparation. They found that the adsorption capacity and rate increase as the specific surface area and pore diameter of the aerogels increases (Chang et al., 2008).

Betz et al. carried out a comparative study of drug release properties of whey protein-based aerogels with different physical properties due to various levels of network crosslinking governed by the pH of hydrogels. The differences in aerogels' structural and mechanical properties were found to govern matrix swelling properties upon contact with gastric and intestinal release media. However, drug release behavior from different aerogels was not found impacted. In contrast with slow dissolution of pure ketoprofen, the release from whey protein aerogels was attributed to complex anomalous transport involving diffusion overlaid by gel relaxation due to matrix swelling, according to Korsmeyer-Peppas model (Betz et al., 2012).

➤ *Effect of hydrophobization on aerogels release properties*

Varying matrix hydrophilicity/hydrophobicity by changing matrix composition or by surface modification with hydrophobic groups is known to have a major impact on the release (I. Smirnova et al., 2004). Indeed, reducing aerogel hydrophilicity results in the decrease of the matrix wettability and solvent penetration rate within the system thus slowing down the release.

As an illustration, Smirnova et.al was able to tune drug release profile from immediate release to prolonged release only by tuning hydrophobicity of silica aerogels by surface modification. Hydrophilic silica aerogels demonstrated fast matrix disintegration upon contact with the liquid due to capillary forces inside the pores. Because of its high hydrophilicity and its brittle characteristics, hydrophilic silica network was rapidly fractured and completely collapses into particles. As the hydrophilic silica aerogel lost its matrix integrity, drug molecules got surrounded by the liquid media and dissolved, leading to their rapid release, also confirmed by (Caputo, Scognamiglio, & De Marco, 2012) and (Mehling et al., 2009). On the opposite, hydrophobic silica aerogels appeared much more stable in aqueous media as compared to their hydrophilic counterparts. Their lower network wettability prevented from structure collapse and restricted liquid influx inside the system. Thus, drug prolonged release occurred by slow drug diffusion through the hydrophobic silica network. An example of

different release properties from either hydrophilic or hydrophobic silica aerogels is shown in Figure 41.

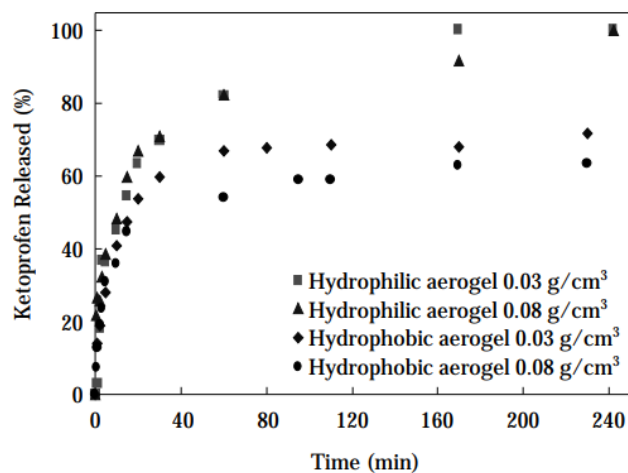


Figure 41. Release of ketoprofen from hydrophilic and hydrophobic aerogels of different densities. Release conditions: 0.1 M HCl at 37 °C. Reprinted from (I. Smirnova et al., 2004). Copyright (2019), with permission from Elsevier.

➤ Creation of complex matrix systems by production of composite aerogels

Finally, the release properties of polysaccharide-based aerogels as drug matrix can be varied by creating composite aerogels from different components (organic or inorganic). The “mixture” of properties brought by the different components in the same matrix will result in new physical and chemical properties and offer new perspectives to polysaccharide-based aerogels used as drug carrier (Gonçalves et al., 2016; Kadib, Molvinger, Guimon, Quignard, & Brunel, 2008; Molvinger, Quignard, Brunel, Boissière, & Devoisselle, 2004; Tkalec, Knez, et al., 2016; Péter Veres et al., 2017; Peter Veres, López-Periago, Lázár, Saurina, & Domingo, 2015; R. Wang et al., 2017).

Composite aerogels can be produced either i) by making interpenetrated networks of different polymers (*i.e.* by co-gelation or by network impregnation) (Molvinger et al., 2004; Tkalec, Knez, et al., 2016; Péter Veres et al., 2017), ii) or by coating of a gel by another polymer layer, the latter acting as a barrier (skin) to drug release (Alnaief et al., 2012; De Cicco et al., 2016; Giray, Bal, Kartal, Kızılel, & Erkey, 2012; Murillo-Cremaes, Subra-Paternault, Saurina, Roig, & Domingo, 2014; Peter Veres et al., 2015).

For instance, Tkalec et al. produced diclofenac loaded pectin aerogels, alginate aerogels and pectin-alginate hybrid aerogels by mixing dissolved polymer in water. They observed that varying aerogel composition and making hybrid aerogels changed the swelling ability and erosion of the matrix, and thus impacted its release properties (Tkalec, Knez, et al., 2016). In the same way, Veres et al. produced silica-gelatin composite aerogels by impregnation method,

and loaded them with low water-soluble drugs (ibuprofen, ketoprofen and triflusal). Composite aerogels were differently functionalized with phenyl, long hydrocarbon chain or methyl moiety in order to tune their surface hydrophobization and interactions with drugs (Péter Veres et al., 2017). The authors correlated drug release profiles with the properties of the drug, aerogel composition and its functionalization, and thus demonstrated the possibility of tailoring drug release profile from immediate to semi-retarded release based on relationship between matrix structure and release kinetics.

Applying a polymeric coating layer on aerogel surface to produce composite aerogels can also be performed to slow down release from immediate-release to extended-release as illustrated in Figure 42 for silica aerogels coated with PEG, or to delay release to avoid drug delivery in the stomach (Alnaief et al., 2012).

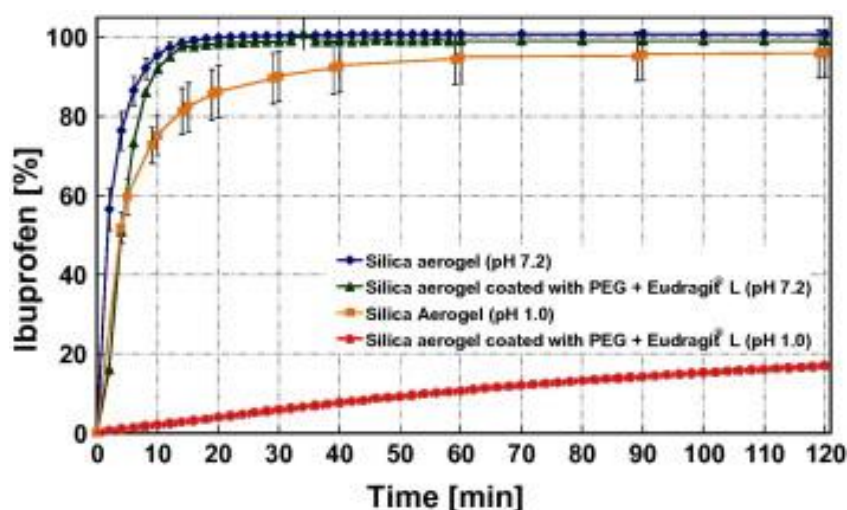


Figure 42. Drug release profiles of ibuprofen-loaded silica aerogel microspheres: un-coated or coated with PEG and Eudragit, at different pH values. Reprinted from (Alnaief et al., 2012). Copyright (2019), with permission from Elsevier.

De Cicco et al. produced core-shell composite aerogels beads by coating a core made of pectin hosting doxycycline with an external layer of alginate (De Cicco et al., 2016). They showed that drug diffusion from the core-shell aerogel matrix was mainly governed by the swelling properties of alginate external hydrogel layer which acted as a barrier to drug diffusion. As a result, drug release profile was dependent on both drug/pectin ratio and alginate concentration as shown in Figure 43, and governed by polymer chains relaxation during water diffusion into the matrix, according to Korsmeyer-Peppas model.

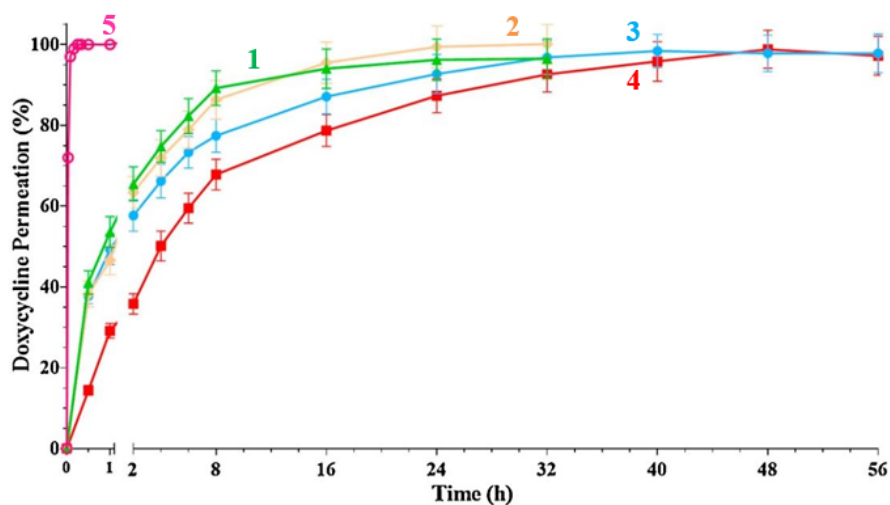


Figure 43. Doxycycline released profiles (%) in simulated wound fluid, as a function of alginate shell concentration (1.50 or 1.75 wt%) and pectin to drug ratio (0.1 or 0.2): alginate layer of 1.50 wt % with pectin-drug ratio of 0.2 (1) or 0.1 (2), or alginate layer of 1.75 wt% with pectin/drug ratio of 0.2 (3) or 0.1 (4) in comparison with pure crystalline doxycycline (5). Adapted from (De Cicco et al., 2016).

Another example is the work of Fagundes et al. on atenolol loaded collagen-silica hybrid aerogels; it was found that the presence of collagen in the silica matrix prevented rapid release by acting as a temporary barrier to drug diffusion (Fagundes, Sousa, Sousa, Silva, & Sousa, 2006).

## Conclusions

In this chapter, we pointed out that the design of advanced versatile materials coupled with a more sustainable approach had become a key research focus to meet tomorrow's engineering applications. In this context, the development of new bio-based aerogels appeared extremely attractive as an alternative to "classical" inorganic or synthetic organic aerogels. The latter are limited in terms of application because of either poor mechanical properties (silica aerogels) or the use of toxic compounds during their process route (*e.g.* RF aerogels) or functionalization treatments (organic modifications, hydrophobization). Thus, we suggest that polysaccharides such as pectin, is attractive polymer candidates to produce bio-aerogels, as they present many advantages: widely available and commonly used for food & feed ("human friendly"), renewable, non-toxic, biocompatible and easily functionalized due to a large amount of hydroxyl groups on polymer backbone. Thanks to these characteristics, bio-based materials made from polysaccharides are suitable for a wide range of life science applications such as biomedical, pharmaceutical, biotechnological, cosmetic and food. Recently, pectin aerogels turned out to be promising bio-based materials for high added-values application such as thermal insulation (Demilecamps, 2015; Rudaz, 2013). As pectin is a biodegradable and biocompatible polysaccharide with gastro-resistant properties, they also have high potential for life sciences applications, which opens prospects in using pectin aerogels as oral drug-carriers.

It is well known that the internal structure and physical characteristics of aerogels determine their final application properties. Thus, the understanding of how formulation and external conditions (polymer ionization and concentration, solution pH, presence of ions, *etc.*) influence aerogel properties is a key issue. In this chapter, we reported in detail what is known (or not) on the structure-properties relationships for aerogels either used as thermal insulator materials, or used as drug-carriers. However, in spite of the importance of morphology control regarding to applications' performances, not many systematic studies provide the correlations between the type of polysaccharide, processing conditions and bio-aerogel structure and final application properties.

## References

- Aaltonen, O., & Jauhiainen, O. (2009). The preparation of lignocellulosic aerogels from ionic liquid solutions. *Carbohydrate Polymers*, 75(1), 125–129. <https://doi.org/10.1016/j.carbpol.2008.07.008>
- Aegerter, M. A., Leventis, N., & Koebel, M. M. (Eds.). (2011). *Aerogels Handbook*. Retrieved from <http://link.springer.com/10.1007/978-1-4419-7589-8>
- Alnaief, M., Alzaitoun, M. A., García-González, C. A., & Smirnova, I. (2011). Preparation of biodegradable nanoporous microspherical aerogel based on alginate. *Carbohydrate Polymers*, 84(3), 1011–1018. <https://doi.org/10.1016/j.carbpol.2010.12.060>
- Alnaief, M., Antonyuk, S., Hentschel, C. M., Leopold, C. S., Heinrich, S., & Smirnova, I. (2012). A novel process for coating of silica aerogel microspheres for controlled drug release applications. *Microporous and Mesoporous Materials*, 160, 167–173. <https://doi.org/10.1016/j.micromeso.2012.02.009>
- Alnaief, M., & Smirnova, I. (2010). Effect of surface functionalization of silica aerogel on their adsorptive and release properties. *Journal of Non-Crystalline Solids*, 356(33), 1644–1649. <https://doi.org/10.1016/j.jnoncrysol.2010.06.027>
- Arboleda, J. C., Hughes, M., Lucia, L. A., Laine, J., Ekman, K., & Rojas, O. J. (2013). Soy protein–nanocellulose composite aerogels. *Cellulose*, 20(5), 2417–2426. <https://doi.org/10.1007/s10570-013-9993-4>
- Ashford, M., Fell, J., Attwood, D., Sharma, H., & Woodhead, P. (1993). An evaluation of pectin as a carrier for drug targeting to the colon. *Journal of Controlled Release*, 26(3), 213–220. [https://doi.org/10.1016/0168-3659\(93\)90188-B](https://doi.org/10.1016/0168-3659(93)90188-B)
- Axelos, M. A. V., & Thibault, J.-F. (1991). CHAPTER 6 - The Chemistry of Low-Methoxyl Pectin Gelation. In R. H. Walter (Ed.), *The Chemistry and Technology of Pectin* (pp. 109–118). <https://doi.org/10.1016/B978-0-08-092644-5.50011-X>
- Baetens, R., Jelle, B. P., & Gustavsen, A. (2011). Aerogel insulation for building applications: A state-of-the-art review. *Energy and Buildings*, 43(4), 761–769. <https://doi.org/10.1016/j.enbuild.2010.12.012>
- Basu, S., Shivhare, U. S., & Chakraborty, P. (2017). Chapter 14 - Influence of Sugar Substitute in Rheology of Fruit Gel. In J. Ahmed, P. Ptaszek, & S. Basu (Eds.), *Advances in Food Rheology and Its Applications* (pp. 355–376). <https://doi.org/10.1016/B978-0-08-100431-9.00014-0>
- BeMiller, J. N., & Whistler, R. L. (2012). *Industrial Gums: Polysaccharides and Their Derivatives*. Academic Press.

- Bender, W. A. (1969). *United States Patent No. US3485920A*. Retrieved from <https://patents.google.com/patent/US3485920/en>
- Betz, M., García-González, C. A., Subrahmanyam, R. P., Smirnova, I., & Kulozik, U. (2012). Preparation of novel whey protein-based aerogels as drug carriers for life science applications. *The Journal of Supercritical Fluids*, 72, 111–119. <https://doi.org/10.1016/j.supflu.2012.08.019>
- Biesmans, G., Randall, D., Francais, E., & Perrut, M. (1998). Polyurethane-based organic aerogels' thermal performance. *Journal of Non-Crystalline Solids*, 225, 36–40. [https://doi.org/10.1016/S0022-3093\(98\)00103-3](https://doi.org/10.1016/S0022-3093(98)00103-3)
- Braccini, I., & Pérez, S. (2001). Molecular Basis of Ca<sup>2+</sup>-Induced Gelation in Alginates and Pectins: The Egg-Box Model Revisited. *Biomacromolecules*, 2(4), 1089–1096. <https://doi.org/10.1021/bm010008g>
- Brinker, C. J., & Scherer, G. W. (1990). *Sol-gel Science: The Physics and Chemistry of Sol-gel Processing*. Academic Press.
- Brown, Z. K., Fryer, P. J., Norton, I. T., & Bridson, R. H. (2010). Drying of agar gels using supercritical carbon dioxide. *The Journal of Supercritical Fluids*, 54(1), 89–95. <https://doi.org/10.1016/j.supflu.2010.03.008>
- Bruschi, M. L. (2015). *Strategies to Modify the Drug Release from Pharmaceutical Systems*. Woodhead Publishing.
- Buchtová, N., & Budtova, T. (2016). Cellulose aero-, cryo- and xerogels: towards understanding of morphology control. *Cellulose*, 23(4), 2585–2595. <https://doi.org/10.1007/s10570-016-0960-8>
- Buckley, A. M., & Greenblatt, M. (1994). The Sol-Gel Preparation of Silica Gels. *Journal of Chemical Education*, 71(7), 599. <https://doi.org/10.1021/ed071p599>
- Budarin, Vitaliy L., Clark, J. H., Luque, R., Macquarrie, D. J., & White, R. J. (2008). Palladium nanoparticles on polysaccharide-derived mesoporous materials and their catalytic performance in C-C coupling reactions. *The Royal Society of Chemistry*, 10, 382–387.
- Budarin, Vitaly L., Clark, J. H., Hardy, J. J. E., Luque, R., Milkowski, K., Tavener, S. J., & Wilson, A. J. (2006). *Starbons: New starch-derived mesoporous carbonaceous materials with tunable properties*. (45), 3782–3786.
- Buisson, P., Hernandez, C., Pierre, M., & Pierre, A. C. (2001). Encapsulation of lipases in aerogels. *Journal of Non-Crystalline Solids*, 285(1), 295–302. [https://doi.org/10.1016/S0022-3093\(01\)00470-7](https://doi.org/10.1016/S0022-3093(01)00470-7)
- BuyAerogel.com. (n.d.). Retrieved March 26, 2019, from <http://www.buyaerogel.com/>

- Campia, P., Ponzini, E., Rossi, B., Farris, S., Silveti, T., Merlini, L., ... Galante, Y. M. (2017). "Aerogels of enzymatically oxidized galactomannans from leguminous plants: Versatile delivery systems of antimicrobial peptides and enzymes." *Carbohydrate Polymers*, 158, 102–111. <https://doi.org/10.1016/j.carbpol.2016.11.089>
- Cao, B., & Zhu, C. (1999). Sol–gel derived self-supporting film. *Journal of Non-Crystalline Solids*, 246(1), 34–38. [https://doi.org/10.1016/S0022-3093\(99\)00047-2](https://doi.org/10.1016/S0022-3093(99)00047-2)
- Capel, F., Nicolai, T., Durand, D., Boulenger, P., & Langendorff, V. (2006). Calcium and acid induced gelation of (amidated) low methoxyl pectin. *Food Hydrocolloids*, 20(6), 901–907. <https://doi.org/10.1016/j.foodhyd.2005.09.004>
- Caputo, G., Scognamiglio, M., & De Marco, I. (2012). Nimesulide adsorbed on silica aerogel using supercritical carbon dioxide. *Chemical Engineering Research and Design*, 90(8), 1082–1089. <https://doi.org/10.1016/j.cherd.2011.11.011>
- Cárdenas, A., Goycoolea, F. M., & Rinaudo, M. (2008). On the gelling behaviour of 'nopal' (*Opuntia ficus indica*) low methoxyl pectin. *Carbohydrate Polymers*, 73(2), 212–222. <https://doi.org/10.1016/j.carbpol.2007.11.017>
- Carlsson, D. O., Nyström, G., Zhou, Q., Berglund, L. A., Nyholm, L., & Strømme, M. (2012). Electroactive nanofibrillated cellulose aerogel composites with tunable structural and electrochemical properties. *Journal of Materials Chemistry*, 22(36), 19014–19024. <https://doi.org/10.1039/C2JM33975G>
- Chang, X., Chen, D., & Jiao, X. (2008). Chitosan-Based Aerogels with High Adsorption Performance. *The Journal of Physical Chemistry B*, 112(26), 7721–7725. <https://doi.org/10.1021/jp8011359>
- Cheng, Y., Lu, L., Zhang, W., Shi, J., & Cao, Y. (2012). Reinforced low density alginate-based aerogels: Preparation, hydrophobic modification and characterization. *Carbohydrate Polymers*, 88(3), 1093–1099. <https://doi.org/10.1016/j.carbpol.2012.01.075>
- Chien, Y. (1991). *Novel Drug Delivery Systems*. <https://doi.org/10.1201/b14196>
- Chtchigrovsky, M., Primo, A., Gonzalez, P., Molvinger, K., Robitzer, M., Quignard, F., & Taran, F. (2009). Functionalized chitosan as a green, recyclable, biopolymer-supported catalyst for the [3+2] Huisgen cycloaddition. *Angewandte Chemie (International Ed. in English)*, 48(32), 5916–5920. <https://doi.org/10.1002/anie.200901309>
- Comin, L. M., Temelli, F., & Saldaña, M. D. A. (2012). Barley  $\beta$ -glucan aerogels as a carrier for flax oil via supercritical CO<sub>2</sub>. *Journal of Food Engineering*, 111(4), 625–631. <https://doi.org/10.1016/j.jfoodeng.2012.03.005>
- Comstock, M. J. (1986). Chemistry and Function of Pectins, Copyright, ACS Symposium Series, FOREWORD. In Comstock M. Joan (Ed.), *Chemistry and Function of Pectins*

- (pp. i–vi). <https://doi.org/10.1021/bk-1986-0310.fw001>
- Cuce, E., Cuce, P. M., Wood, C. J., & Riffat, S. B. (2014). Toward aerogel based thermal superinsulation in buildings: A comprehensive review. *Renewable and Sustainable Energy Reviews*, *34*, 273–299. <https://doi.org/10.1016/j.rser.2014.03.017>
- Cunha, A. G., & Gandini, A. (2010a). Turning polysaccharides into hydrophobic materials: a critical review. Part 1. Cellulose. *Cellulose*, *17*(5), 875–889. <https://doi.org/10.1007/s10570-010-9434-6>
- Cunha, A. G., & Gandini, A. (2010b). Turning polysaccharides into hydrophobic materials: a critical review. Part 2. Hemicelluloses, chitin/chitosan, starch, pectin and alginates. *Cellulose*, *17*(6), 1045–1065. <https://doi.org/10.1007/s10570-010-9435-5>
- Daas, P. J. H., Meyer-Hansen, K., Schols, H. A., De Ruiter, G. A., & Voragen, A. G. J. (1999). Investigation of the non-esterified galacturonic acid distribution in pectin with endopolygalacturonase. *Carbohydrate Research*, *318*(1), 135–145. [https://doi.org/10.1016/S0008-6215\(99\)00093-2](https://doi.org/10.1016/S0008-6215(99)00093-2)
- Davis, P. J., Deshpande, R., Smith, D. M., Brinker, C. J., & Assink, R. A. (1994). Pore structure evolution in silica gel during aging/drying. IV. Varying pore fluid pH. *Journal of Non-Crystalline Solids*, *167*(3), 295–306. [https://doi.org/10.1016/0022-3093\(94\)90252-6](https://doi.org/10.1016/0022-3093(94)90252-6)
- De Cicco, F., Russo, P., Reverchon, E., García-González, C. A., Aquino, R. P., & Del Gaudio, P. (2016). Prilling and supercritical drying: A successful duo to produce core-shell polysaccharide aerogel beads for wound healing. *Carbohydrate Polymers*, *147*, 482–489.
- De Marco, I., Baldino, L., Cardea, S., & Reverchon, E. (2015). Supercritical Gel Drying for the Production of Starch Aerogels for Delivery Systems. *Chemical Engineer Ing Transaction*, (43), 307–312.
- Demilecamps, A. (2015). *Synthesis and characterization of polysaccharides-silica composite aerogels for thermal superinsulation*. (PhD Thesis, Ecole Nationale Supérieure des Mines de Paris).
- Demilecamps, A., Beauger, C., Hildenbrand, C., Rigacci, A., & Budtova, T. (2015). Cellulose–silica aerogels. *Carbohydrate Polymers*, *122*, 293–300. <https://doi.org/10.1016/j.carbpol.2015.01.022>
- Demilecamps, A., Reichenauer, G., Rigacci, A., & Budtova, T. (2014). Cellulose–silica composite aerogels from “one-pot” synthesis. *Cellulose*, *21*(4), 2625–2636. <https://doi.org/10.1007/s10570-014-0314-3>
- Deuber, F., Mousavi, S., Federer, L., & Adlhart, C. (2017). Amphiphilic Nanofiber-Based Aerogels for Selective Liquid Absorption from Electrospun Biopolymers. *Advanced*

- Materials Interfaces*, 4(12), 1700065. <https://doi.org/10.1002/admi.201700065>
- Deze, E. G., Papageorgiou, S. K., Favvas, E. P., & Katsaros, F. K. (2012). Porous alginate aerogel beads for effective and rapid heavy metal sorption from aqueous solutions: Effect of porosity in Cu<sup>2+</sup> and Cd<sup>2+</sup> ion sorption. *Chemical Engineering Journal*, 209, 537–546. <https://doi.org/10.1016/j.cej.2012.07.133>
- Diascorn, N., Calas, S., Sallee, H., Achard, P., & Rigacci, A. (2015). Polyurethane aerogels synthesis for thermal insulation – textural, thermal and mechanical properties. *Journal of Supercritical Fluids*, 106, 76–84. <https://doi.org/10.1016/j.supflu.2015.05.012>
- Dobies, M., Kempka, M., Kuśmia, S., & Jurga, S. (2008). Acid-Induced Gelation of Low-Methoxyl Pectins Studied by <sup>1</sup>H NMR and Rheological Methods. *Applied Magnetic Resonance*, 34(1–2), 71–84. <https://doi.org/10.1007/s00723-008-0107-7>
- Dronnet, V. M., Renard, C. M. G. C., Axelos, M. A. V., & Thibault, J.-F. (1996). Characterisation and selectivity of divalent metal ions binding by citrus and sugar-beet pectins. *Carbohydrate Polymers*, 30(4), 253–263. [https://doi.org/10.1016/S0144-8617\(96\)00107-5](https://doi.org/10.1016/S0144-8617(96)00107-5)
- Druel, L., Bardl, R., Vorweg, W., & Budtova, T. (2017). Starch Aerogels: A Member of the Family of Thermal Superinsulating Materials. *Biomacromolecules*, 18(12), 4232–4239. <https://doi.org/10.1021/acs.biomac.7b01272>
- Druel, L., Niemeyer, P., Milow, B., & Budtova, T. (2018). Rheology of cellulose-[DBNH][CO<sub>2</sub>Et] solutions and shaping into aerogel beads. *Green Chemistry*, 20(17), 3993–4002. <https://doi.org/10.1039/C8GC01189C>
- Dumitriu, S. (2004). *Polysaccharides: Structural Diversity and Functional Versatility, Second Edition*. CRC Press.
- El Kadib, A., & Bousmina, M. (2012). Chitosan bio-based organic-inorganic hybrid aerogel microspheres. *Chemistry (Weinheim an Der Bergstrasse, Germany)*, 18(27), 8264–8277. <https://doi.org/10.1002/chem.201104006>
- Englyst, H. N., Hay, S., & Macfarlane\*, G. T. (1987). Polysaccharide breakdown by mixed populations of human faecal bacteria. *FEMS Microbiology Letters*, 45(3), 163–171. <https://doi.org/10.1111/j.1574-6968.1987.tb02352.x>
- Escudero, R. R., Robitzer, M., Renzo, F. di, & Quignard, F. (2009). Alginate aerogels as adsorbents of polar molecules from liquid hydrocarbons: hexanol as probe molecule. *Carbohydrate Polymers*, 75(1), 52–57.
- Evageliou, V. (2000). Effect of pH, sugar type and thermal annealing on high-methoxy pectin gels. *Carbohydrate Polymers*, 42(3), 245–259. [https://doi.org/10.1016/S0144-8617\(99\)00191-5](https://doi.org/10.1016/S0144-8617(99)00191-5)

- Fagundes, L. B., Sousa, T. G. F., Sousa, A., Silva, V. V., & Sousa, E. M. B. (2006). SBA-15-collagen hybrid material for drug delivery applications. *Journal of Non-Crystalline Solids*, 352(32), 3496–3501. <https://doi.org/10.1016/j.jnoncrysol.2006.03.111>
- Fishman, M. L., & Cooke, P. H. (2009). The structure of high-methoxyl sugar acid gels of citrus pectin as determined by AFM. *Carbohydrate Research*, 344(14), 1792–1797. <https://doi.org/10.1016/j.carres.2008.09.031>
- Fraeye, I., Deroeck, A., Duvetter, T., Verlent, I., Hendrickx, M., & Vanloey, A. (2007). Influence of pectin properties and processing conditions on thermal pectin degradation. *Food Chemistry*, 105(2), 555–563. <https://doi.org/10.1016/j.foodchem.2007.04.009>
- Fraeye, Ilse, Duvetter, T., Dounsla, E., Van Loey, A., & Hendrickx, M. (2010). Fine-tuning the properties of pectin–calcium gels by control of pectin fine structure, gel composition and environmental conditions. *Trends in Food Science & Technology*, 21(5), 219–228. <https://doi.org/10.1016/j.tifs.2010.02.001>
- García-González, C. A., Alnaief, M., & Smirnova, I. (2011). Polysaccharide-based aerogels—Promising biodegradable carriers for drug delivery systems. *Carbohydrate Polymers*, 86(4), 1425–1438. <https://doi.org/10.1016/j.carbpol.2011.06.066>
- García-González, C. A., Jin, M., Gerth, J., Alvarez-Lorenzo, C., & Smirnova, I. (2015). Polysaccharide-based aerogel microspheres for oral drug delivery. *Carbohydrate Polymers*, 117, 797–806. <https://doi.org/10.1016/j.carbpol.2014.10.045>
- Garcia-Gonzalez, C. A., & Smirnova, I. (2013). Use of supercritical fluid technology for the production of tailor-made aerogel particles for delivery systems. *Journal of Supercritical Fluids*, 79, 152–158. <https://doi.org/10.1016/j.supflu.2013.03.001>
- García-González, C.A., Uy, J. J., Alnaief, M., & Smirnova, I. (2012). Preparation of tailor-made starch-based aerogel microspheres by the emulsion-gelation method. *Carbohydrate Polymers*, 88(4), 1378–1386. <https://doi.org/10.1016/j.carbpol.2012.02.023>
- García-González, Carlos A., Carezza, E., Zeng, M., Smirnova, I., & Roig, A. (2012). Design of biocompatible magnetic pectin aerogel monoliths and microspheres. *RSC Advances*, 2(26), 9816–9823. <https://doi.org/10.1039/C2RA21500D>
- Garnier, C., Axelos, M. A. V., & Thibault, J.-F. (1993). Phase diagrams of pectin-calcium systems: Influence of pH, ionic strength, and temperature on the gelation of pectins with different degrees of methylation. *Carbohydrate Research*, 240, 219–232. [https://doi.org/10.1016/0008-6215\(93\)84185-9](https://doi.org/10.1016/0008-6215(93)84185-9)
- Garnier, C., Axelos, M. A. V., & Thibault, J.-F. (1994). Selectivity and cooperativity in the binding of calcium ions by pectins. *Carbohydrate Research*, 256(1), 71–81. [https://doi.org/10.1016/0008-6215\(94\)84228-0](https://doi.org/10.1016/0008-6215(94)84228-0)

- Gaudio, P. D., Auriemma, G., Mencherini, T., Porta, G. D., Reverchon, E., & Aquino, R. P. (2013). Design of alginate-based aerogel for nonsteroidal anti-inflammatory drugs controlled delivery systems using prilling and supercritical-assisted drying. *Journal of Pharmaceutical Sciences*, *102*(1), 185–194. <https://doi.org/10.1002/jps.23361>
- Gavillon, R., & Budtova, T. (2007). Kinetics of cellulose regeneration from cellulose--NaOH-water gels and comparison with cellulose--N-methylmorpholine-N-oxide--water solutions. *Biomacromolecules*, *8*(2), 424–432. <https://doi.org/10.1021/bm060376q>
- Gavillon, R., & Budtova, T. (2008). Aerocellulose: new highly porous cellulose prepared from cellulose-NaOH aqueous solutions. *Biomacromolecules*, *9*(1), 269–277. <https://doi.org/10.1021/bm700972k>
- Ghafar, A., Gurikov, P., Subrahmanyam, R., Parikka, K., Tenkanen, M., Smirnova, I., & Mikkonen, K. S. (2017). Mesoporous guar galactomannan based biocomposite aerogels through enzymatic crosslinking. *Composites Part A: Applied Science and Manufacturing*, *94*, 93–103. <https://doi.org/10.1016/j.compositesa.2016.12.013>
- Gidley, M. J., Morris, E. R., Murray, E. J., Powell, D. A., & Rees, D. A. (1980). Evidence for two mechanisms of interchain association in calcium pectate gels. *International Journal of Biological Macromolecules*, *2*(5), 332–334. [https://doi.org/10.1016/0141-8130\(80\)90060-4](https://doi.org/10.1016/0141-8130(80)90060-4)
- Gilsenan, P. M., Richardson, R. K., & Morris, E. R. (2000). Thermally reversible acid-induced gelation of low-methoxy pectin. *Carbohydrate Polymers*, *41*(4), 339–349. [https://doi.org/10.1016/S0144-8617\(99\)00119-8](https://doi.org/10.1016/S0144-8617(99)00119-8)
- Gilsenan, P. M., Richardson, R. K., & Morris, E. R. (2003). Associative and segregative interactions between gelatin and low-methoxy pectin: Part 1. Associative interactions in the absence of Ca<sup>2+</sup>. *Food Hydrocolloids*, *17*(6), 723–737. [https://doi.org/10.1016/S0268-005X\(03\)00094-8](https://doi.org/10.1016/S0268-005X(03)00094-8)
- Giray, S., Bal, T., Kartal, A. M., Kızılel, S., & Erkey, C. (2012). Controlled drug delivery through a novel PEG hydrogel encapsulated silica aerogel system. *Journal of Biomedical Materials Research Part A*, *100A*(5), 1307–1315. <https://doi.org/10.1002/jbm.a.34056>
- Glenn, G. M., & Irving, D. W. (1995). Starch-based microcellular foams. *Cereal Chemistry*, *72*(2), 155–161.
- Goimil, L., Braga, M. E. M., Dias, A. M. A., Gómez-Amoza, J. L., Concheiro, A., Alvarez-Lorenzo, C., ... García-González, C. A. (2017). Supercritical processing of starch aerogels and aerogel-loaded poly( $\epsilon$ -caprolactone) scaffolds for sustained release of ketoprofen for bone regeneration. *Journal of CO<sub>2</sub> Utilization*, *18*, 237–249. <https://doi.org/10.1016/j.jcou.2017.01.028>

- Gonçalves, V. S. S., Gurikov, P., Poejo, J., Matias, A. A., Heinrich, S., Duarte, C. M. M., & Smirnova, I. (2016). Alginate-based hybrid aerogel microparticles for mucosal drug delivery. *European Journal of Pharmaceutics and Biopharmaceutics: Official Journal of Arbeitsgemeinschaft Fur Pharmazeutische Verfahrenstechnik e.V.*, *107*, 160–170. <https://doi.org/10.1016/j.ejpb.2016.07.003>
- Gorle, B. S. K., Smirnova, I., & Arlt, W. (2010). Adsorptive crystallization of benzoic acid in aerogels from supercritical solutions. *The Journal of Supercritical Fluids*, *52*(3), 249–257. <https://doi.org/10.1016/j.supflu.2010.01.006>
- Grant, G. T., Morris, E. R., Rees, D. A., Smith, P. J. C., & Thom, D. (1973). Biological interactions between polysaccharides and divalent cations: The egg-box model. *FEBS Letters*, *32*(1), 195–198. [https://doi.org/10.1016/0014-5793\(73\)80770-7](https://doi.org/10.1016/0014-5793(73)80770-7)
- Grosso, C. R. F., & Rao, M. A. (1998). Dynamic rheology of structure development in low-methoxyl pectin+Ca<sup>2+</sup>+sugar gels. Based on a paper presented at the 3rd International Hydrocolloids Conference, 11–16 August 1996, Sydney, Australia. *Food Hydrocolloids*, *12*(3), 357–363. [https://doi.org/10.1016/S0268-005X\(98\)00034-4](https://doi.org/10.1016/S0268-005X(98)00034-4)
- Guilminot, E., Gavillon, R., Chatenet, M., Berthon-Fabry, S., Rigacci, A., & Budtova, T. (2008). New nanostructured carbons based on porous cellulose: Elaboration, pyrolysis and use as platinum nanoparticles substrate for oxygen reduction electrocatalysis. *Journal of Power Sources*, *185*(2), 717–726. <https://doi.org/10.1016/j.jpowsour.2008.08.030>
- Guo, X., Meng, H., Tang, Q., Pan, R., Zhu, S., & Yu, S. (2016). Effects of the precipitation pH on the ethanolic precipitation of sugar beet pectins. *Food Hydrocolloids*, *52*, 431–437. <https://doi.org/10.1016/j.foodhyd.2015.07.013>
- Gurikov, P., Raman, S. P., Weinrich, D., Fricke, M., & Smirnova, I. (2015). A novel approach to alginate aerogels: carbon dioxide induced gelation. *RSC Advances*, *5*(11), 7812–7818. <https://doi.org/10.1039/C4RA14653K>
- Gurikov, P., & Smirnova, I. (2018). Non-Conventional Methods for Gelation of Alginate. *Gels*, *4*(1), 14. <https://doi.org/10.3390/gels4010014>
- Gyarmati, L., Racz, I., Szentmiklosi, P., & Plachy, J. (1980). *United States Patent No. US4199560A*. Retrieved from <https://patents.google.com/patent/US4199560A/de>
- Haimer, E., Wendland, M., Schlufte, K., Frankenfeld, K., Miethe, P., Potthast, A., ... Liebner, F. (2010). Loading of Bacterial Cellulose Aerogels with Bioactive Compounds by Antisolvent Precipitation with Supercritical Carbon Dioxide. *Macromolecular Symposia*, *294*(2), 64–74. <https://doi.org/10.1002/masy.201000008>
- Hao, P., Zhao, Z., Leng, Y., Tian, J., Sang, Y., Boughton, R. I., ... Yang, B. (2015). Graphene-based nitrogen self-doped hierarchical porous carbon aerogels derived from chitosan for

- high performance supercapacitors. *Nano Energy*, 15, 9–23. <https://doi.org/10.1016/j.nanoen.2015.02.035>
- Hayase, G., Kanamori, K., Abe, K., Yano, H., Maeno, A., Kaji, H., & Nakanishi, K. (2014). Polymethylsilsesquioxane–Cellulose Nanofiber Biocomposite Aerogels with High Thermal Insulation, Bendability, and Superhydrophobicity. *ACS Applied Materials & Interfaces*, 6(12), 9466–9471. <https://doi.org/10.1021/am501822y>
- He, Z., Zhang, X., & Batchelor, W. (2016). Cellulose nanofibre aerogel filter with tuneable pore structure for oil/water separation and recovery. *RSC Advances*, 6(26), 21435–21438. <https://doi.org/10.1039/C5RA27413C>
- Heath, L., & Thielemans, W. (2010). Cellulose nanowhisiker aerogels. *Green Chemistry*, 12(8), 1448–1453. <https://doi.org/10.1039/C0GC00035C>
- Hentzschel, C. M., Alnaief, M., Smirnova, I., Sakmann, A., & Leopold, C. S. (2012). Enhancement of griseofulvin release from liquid compact. *European Journal of Pharmaceutics and Biopharmaceutics*, 80(1), 130–135. <https://doi.org/10.1016/j.ejpb.2011.08.001>
- Hoepfner, S., Ratke, L., & Milow, B. (2008). Synthesis and characterisation of nanofibrillar cellulose aerogels. *Cellulose*, 15(1), 121–129. <https://doi.org/10.1007/s10570-007-9146-8>
- Hoover, R., & Vasanthan, T. (1994). Effect of heat-moisture treatment on the structure and physicochemical properties of cereal, legume, and tuber starches. *Carbohydrate Research*, 252, 33–53. [https://doi.org/10.1016/0008-6215\(94\)90004-3](https://doi.org/10.1016/0008-6215(94)90004-3)
- Horikawa, T., Hayashi, J., & Muroyama, K. (2004). Controllability of pore characteristics of resorcinol–formaldehyde carbon aerogel. *Carbon*, 42(8), 1625–1633. <https://doi.org/10.1016/j.carbon.2004.02.016>
- Horvat, G., Xhanari, K., Finšgar, M., Gradišnik, L., Maver, U., Knez, Ž., & Novak, Z. (2017). Novel ethanol-induced pectin-xanthan aerogel coatings for orthopedic applications. *Carbohydrate Polymers*, 166, 365–376. <https://doi.org/10.1016/j.carbpol.2017.03.008>
- Horvat, G., Fajfar, T., Uzunalić, A. P., Knez, Ž., & Novak, Z. (2017). Thermal properties of polysaccharide aerogels. *Journal of Thermal Analysis and Calorimetry*, 127(1), 363–370. <https://doi.org/10.1007/s10973-016-5814-y>
- Hrubesh, L. W., Poco, J. F., & Coronado, P. R. (1999). *United States Patent No. US6005012A*. Retrieved from <https://patents.google.com/patent/US6005012A/en>
- Hüsing, N., & Schubert, U. (1998). Aerogels—Airy Materials: Chemistry, Structure, and Properties. *Angewandte Chemie International Edition*, 37(1–2), 22–45. [https://doi.org/10.1002/\(SICI\)1521-3773\(19980202\)37:1/2<22::AID-](https://doi.org/10.1002/(SICI)1521-3773(19980202)37:1/2<22::AID-)

ANIE22>3.0.CO;2-I

- Ingar Draget, K., Østgaard, K., & Smidsrød, O. (1990). Homogeneous alginate gels: A technical approach. *Carbohydrate Polymers*, 14(2), 159–178. [https://doi.org/10.1016/0144-8617\(90\)90028-Q](https://doi.org/10.1016/0144-8617(90)90028-Q)
- Innerlohinger, J., Weber, H. K., & Kraft, G. (2006). Aerocellulose: Aerogels and Aerogel-like Materials made from Cellulose. *Macromolecular Symposia*, 244(1), 126–135. <https://doi.org/10.1002/masy.200651212>
- Itagaki, H., Tokai, M., & Kondo, T. (1997). Physical gelation process for cellulose whose hydroxyl groups are regioselectively substituted by fluorescent groups. *Polymer*, 38(16), 4201–4205. [https://doi.org/10.1016/S0032-3861\(96\)01007-5](https://doi.org/10.1016/S0032-3861(96)01007-5)
- Jiménez-Saelices, C., Seantier, B., Cathala, B., & Grohens, Y. (2017). Spray freeze-dried nanofibrillated cellulose aerogels with thermal superinsulating properties. *Carbohydrate Polymers*, 157, 105–113. <https://doi.org/10.1016/j.carbpol.2016.09.068>
- Jin, H., Kettunen, M., Laiho, A., Pynnönen, H., Paltakari, J., Marmur, A., ... Ras, R. H. A. (2011). Superhydrophobic and superoleophobic nanocellulose aerogel membranes as bioinspired cargo carriers on water and oil. *Langmuir: The ACS Journal of Surfaces and Colloids*, 27(5), 1930–1934. <https://doi.org/10.1021/la103877r>
- Kadib, A. E., Molvinger, K., Cacciaguerra, T., Bousmina, M., & Brunel, D. (2011). Chitosan templated synthesis of porous metal oxide microspheres with filamentary nanostructures. *Microporous and Mesoporous Materials*, 142(1), 301–307. <https://doi.org/10.1016/j.micromeso.2010.12.012>
- Kadib, A. E., Molvinger, K., Guimon, C., Quignard, F., & Brunel, D. (2008). Design of Stable Nanoporous Hybrid Chitosan/Titania as Cooperative Bifunctional Catalysts. *Chemistry of Materials*, 20(6), 2198–2204. <https://doi.org/10.1021/cm800080s>
- Kar, F., & Arslan, N. (1999). Effect of temperature and concentration on viscosity of orange peel pectin solutions and intrinsic viscosity–molecular weight relationship. *Carbohydrate Polymers*, 40(4), 277–284. [https://doi.org/10.1016/S0144-8617\(99\)00062-4](https://doi.org/10.1016/S0144-8617(99)00062-4)
- Kenar, J. A., Eller, F. J., Felker, F. C., Jackson, M. A., & Fanta, G. F. (2014). Starch aerogel beads obtained from inclusion complexes prepared from high amylose starch and sodium palmitate. *Green Chemistry*, 16(4), 1921–1930. <https://doi.org/10.1039/C3GC41895B>
- Keys, A., Grande, F., & Anderson, J. T. (1961). Fiber and pectin in the diet and serum cholesterol concentration in man. *Proceedings of the Society for Experimental Biology and Medicine. Society for Experimental Biology and Medicine (New York, N.Y.)*, 106, 555–558.

- Kimmich, R., Klammler, F., Skirda, V. D., Serebrennikova, I. A., Maklakov, A. I., & Fatkullin, N. (1993). Geometrical restrictions of water diffusion in aqueous protein systems. A study using NMR field-gradient techniques. *Applied Magnetic Resonance*, 4(4), 425–440. <https://doi.org/10.1007/BF03162458>
- Kistler, S. S. (1931). Coherent Expanded-Aerogels. *The Journal of Physical Chemistry*, 36(1), 52–64. <https://doi.org/10.1021/j150331a003>
- Kistler, Samuel S. (1952). *United States Patent No. US2589705A*. Retrieved from <https://patents.google.com/patent/US2589705A/en>
- Kjønliksen, A.-L., Hiorth, M., & Nyström, B. (2005). Association under shear flow in aqueous solutions of pectin. *European Polymer Journal*, 41(4), 761–770. <https://doi.org/10.1016/j.eurpolymj.2004.11.006>
- Kobayashi, Y., Saito, T., & Isogai, A. (2014). Aerogels with 3D Ordered Nanofiber Skeletons of Liquid-Crystalline Nanocellulose Derivatives as Tough and Transparent Insulators. *Angewandte Chemie International Edition*, 53(39), 10394–10397. <https://doi.org/10.1002/anie.201405123>
- Koebel, M. M., Huber, L., Zhao, S., & Malfait, W. J. (2016). Breakthroughs in cost-effective, scalable production of superinsulating, ambient-dried silica aerogel and silica-biopolymer hybrid aerogels: from laboratory to pilot scale. *Journal of Sol-Gel Science and Technology*, 79(2), 308–318. <https://doi.org/10.1007/s10971-016-4012-5>
- Koebel, M., Rigacci, A., & Achard, P. (2012). Aerogel-based thermal superinsulation: an overview. *Journal of Sol-Gel Science and Technology*, 63(3), 315–339. <https://doi.org/10.1007/s10971-012-2792-9>
- Kohn, R., & Luknár, O. (1975). Calcium and strontium ion activity in solutions of the corresponding pectinates and its dependence on their degree of esterification. *Collection of Czechoslovak Chemical Communications*, 40(4), 959–970. <https://doi.org/10.1135/cccc19750959>
- Kohn, Rudolf. (1982). Binding of toxic cations to pectin, its oligomeric fragments and plant tissues. *Carbohydrate Polymers*, 2(4), 273–275. [https://doi.org/10.1016/0144-8617\(82\)90030-3](https://doi.org/10.1016/0144-8617(82)90030-3)
- Kohn, Rudolf. (1987). Binding of divalent cations to oligomeric fragments of pectin. *Carbohydrate Research*, 160, 343–353. [https://doi.org/10.1016/0008-6215\(87\)80322-1](https://doi.org/10.1016/0008-6215(87)80322-1)
- Krall, S. M., & McFeeters, R. F. (1998). Pectin Hydrolysis: Effect of Temperature, Degree of Methylation, pH, and Calcium on Hydrolysis Rates. *Journal of Agricultural and Food Chemistry*, 46(4), 1311–1315. <https://doi.org/10.1021/jf970473y>
- Krusteva, S., Lambov, N., & Velinov, G. (1990). [Biopharmaceutic studies of a bioerodible

- nystatin unit]. *Die Pharmazie*, 45(3), 195–197.
- Lamarque, G., Viton, C., & Domard, A. (2004). Comparative study of the first heterogeneous deacetylation of alpha- and beta-chitins in a multistep process. *Biomacromolecules*, 5(3), 992–1001. <https://doi.org/10.1021/bm034498j>
- Lee, K. P., & Gould, G. L. (2006). *United States Patent No. US6994842B2*. Retrieved from <https://patents.google.com/patent/US6994842B2/en>
- Liebner, F., Potthast, A., Rosenau, T., Haimer, E., & Wendland, M. (2008). Cellulose aerogels: Highly porous, ultra-lightweight materials. *Holzforschung*, 62(2), 129–135. <https://doi.org/10.1515/HF.2008.051>
- Löfgren, C., Guillotin, S., Evenbratt, H., Schols, H., & Hermansson, A.-M. (2005). Effects of Calcium, pH, and Blockiness on Kinetic Rheological Behavior and Microstructure of HM Pectin Gels. *Biomacromolecules*, 6(2), 646–652. <https://doi.org/10.1021/bm049619+>
- Löfgren, C., & Hermansson, A.-M. (2007). Synergistic rheological behaviour of mixed HM/LM pectin gels. *Food Hydrocolloids*, 21(3), 480–486. <https://doi.org/10.1016/j.foodhyd.2006.07.005>
- Löfgren, C., Walkenström, P., & Hermansson, A.-M. (2002). Microstructure and Rheological Behavior of Pure and Mixed Pectin Gels. *Biomacromolecules*, 3(6), 1144–1153. <https://doi.org/10.1021/bm020044v>
- Lootens, D., Capel, F., Durand, D., Nicolai, T., Boulenguer, P., & Langendorff, V. (2003). Influence of pH, Ca concentration, temperature and amidation on the gelation of low methoxyl pectin. *Food Hydrocolloids*, 17(3), 237–244. [https://doi.org/10.1016/S0268-005X\(02\)00056-5](https://doi.org/10.1016/S0268-005X(02)00056-5)
- Lovskaya, D. D., Lebedev, A. E., & Menshutina, N. V. (2015). Aerogels as drug delivery systems: In vitro and in vivo evaluations. *The Journal of Supercritical Fluids*, 106, 115–121. <https://doi.org/veron>
- Lu, X., Arduini-Schuster, M. C., Kuhn, J., Nilsson, O., Fricke, J., & Pekala, R. W. (1992). Thermal conductivity of monolithic organic aerogels. *Science (New York, N.Y.)*, 255(5047), 971–972. <https://doi.org/10.1126/science.255.5047.971>
- Lutz, R., Aserin, A., Wicker, L., & Garti, N. (2009). Structure and physical properties of pectins with block-wise distribution of carboxylic acid groups. *Food Hydrocolloids*, 23(3), 786–794. <https://doi.org/10.1016/j.foodhyd.2008.04.009>
- Macleod, G. S., Fell, J. T., Collett, J. H., Sharma, H. L., & Smith, A. M. (1999). Selective drug delivery to the colon using pectin:chitosan:hydroxypropyl methylcellulose film coated tablets. *International Journal of Pharmaceutics*, 187(2), 251–257.

- Maleki, H., Durães, L., García-González, C. A., del Gaudio, P., Portugal, A., & Mahmoudi, M. (2016). Synthesis and biomedical applications of aerogels: Possibilities and challenges. *Advances in Colloid and Interface Science*, 236, 1–27. <https://doi.org/10.1016/j.cis.2016.05.011>
- Mallepally, R. R., Marin, M. A., Surampudi, V., Subia, B., Rao, R. R., Kundu, S. C., & McHugh, M. A. (2015). Silk fibroin aerogels: potential scaffolds for tissue engineering applications. *Biomedical Materials*, 10(3), 035002. <https://doi.org/10.1088/1748-6041/10/3/035002>
- Marin, M. A., Mallepally, R. R., & McHugh, M. A. (2014). Silk fibroin aerogels for drug delivery applications. *Journal of Supercritical Fluids*, 91, 84–89. <https://doi.org/10.1016/j.supflu.2014.04.014>
- Markevicius, G., Jaxel, J., Budtova, T., & Rigacci, A. (2016). *Cellulose fibre – silica aerogel thermal superinsulation composites*. Retrieved from <https://hal-mines-paristech.archives-ouvertes.fr/hal-01436060>
- Markevicius, G., Ladj, R., Niemeyer, P., Budtova, T., & Rigacci, A. (2017). Ambient-dried thermal superinsulating monolithic silica-based aerogels with short cellulosic fibers. *Journal of Materials Science*, 52(4), 2210–2221. <https://doi.org/10.1007/s10853-016-0514-3>
- Martins, M., Barros, A. A., Quraishi, S., Gurikov, P., Raman, S. P., Smirnova, I., ... Reis, R. L. (2015). Preparation of macroporous alginate-based aerogels for biomedical applications. *The Journal of Supercritical Fluids*, 106, 152–159. <https://doi.org/10.1016/j.supflu.2015.05.010>
- May, C. D. (1990). Industrial pectins: Sources, production and applications. *Carbohydrate Polymers*, 12(1), 79–99. [https://doi.org/10.1016/0144-8617\(90\)90105-2](https://doi.org/10.1016/0144-8617(90)90105-2)
- Mehling, T., Smirnova, I., Guenther, U., & Neubert, R. H. H. (2009). Polysaccharide-based aerogels as drug carriers. *Journal of Non-Crystalline Solids*, 355(50–51), 2472–2479. <https://doi.org/10.1016/j.jnoncrysol.2009.08.038>
- Molvinger, K., Quignard, F., Brunel, D., Boissière, M., & Devoisselle, J.-M. (2004). Porous Chitosan-Silica Hybrid Microspheres as a Potential Catalyst. *Chemistry of Materials*, 16(17), 3367–3372. <https://doi.org/10.1021/cm0353299>
- Morris, E. R., Gidley, M. J., Murray, E. J., Powell, D. A., & Rees, D. A. (1980). Characterization of pectin gelation under conditions of low water activity, by circular dichroism, competitive inhibition and mechanical properties. *International Journal of Biological Macromolecules*, 2(5), 327–330. [https://doi.org/10.1016/0141-8130\(80\)90058-6](https://doi.org/10.1016/0141-8130(80)90058-6)
- Murillo-Cremaes, N., Subra-Paternault, P., Saurina, J., Roig, A., & Domingo, C. (2014).

- Compressed antisolvent process for polymer coating of drug-loaded aerogel nanoparticles and study of the release behavior. *Colloid and Polymer Science*, 292(10), 2475–2484. <https://doi.org/10.1007/s00396-014-3260-6>
- Murray, R., & Finland, M. (1946). Pectin adjuvant for oral penicillin. *Proceedings of the Society for Experimental Biology and Medicine*. Society for Experimental Biology and Medicine (New York, N.Y.), 62(2), 240–242.
- Narbel, P. A., & Hansen, J. P. (2014). Estimating the cost of future global energy supply. *Renewable and Sustainable Energy Reviews*, 34, 91–97. <https://doi.org/10.1016/j.rser.2014.03.011>
- Oakenfull, D. G. (1991). CHAPTER 5 - The Chemistry of High-Methoxyl Pectins. In R. H. Walter (Ed.), *The Chemistry and Technology of Pectin* (pp. 87–108). <https://doi.org/10.1016/B978-0-08-092644-5.50010-8>
- Oakenfull, D., & Scott, A. (1984). Hydrophobic Interaction in the Gelation of High Methoxyl Pectins. *Journal of Food Science*, 49(4), 1093–1098. <https://doi.org/10.1111/j.1365-2621.1984.tb10401.x>
- Obaidat, R. M., Tashtoush, B. M., Bayan, M. F., T. Al Bustami, R., & Alnaief, M. (2015). Drying Using Supercritical Fluid Technology as a Potential Method for Preparation of Chitosan Aerogel Microparticles. *AAPS PharmSciTech*, 16(6), 1235–1244. <https://doi.org/10.1208/s12249-015-0312-2>
- Olsson, R. T., Azizi Samir, M. a. S., Salazar-Alvarez, G., Belova, L., Ström, V., Berglund, L. A., ... Gedde, U. W. (2010). Making flexible magnetic aerogels and stiff magnetic nanopaper using cellulose nanofibrils as templates. *Nature Nanotechnology*, 5(8), 584–588. <https://doi.org/10.1038/nnano.2010.155>
- Orlu, M., Cevher, E., & Araman, A. (2006). Design and evaluation of colon specific drug delivery system containing flurbiprofen microsponges. *International Journal of Pharmaceutics*, 318(1–2), 103–117. <https://doi.org/10.1016/j.ijpharm.2006.03.025>
- Pajonk, G. M., Elaloui, E., Achard, P., Chevalier, B., Chevalier, J.-L., & Durant, M. (1995). Physical properties of silica gels and aerogels prepared with new polymeric precursors. *Journal of Non-Crystalline Solids*, 186, 1–8. [https://doi.org/10.1016/0022-3093\(95\)00210-3](https://doi.org/10.1016/0022-3093(95)00210-3)
- Paoletti, S., Cesaro, A., Delben, F., & Ciana, A. (1986). Ionic Effects on the Conformation, Equilibrium, Properties, and Rheology of Pectate in Aqueous Solutions and Gels. In *ACS Symposium Series: Vol. 310. Chemistry and Function of Pectins* (Vol. 310, pp. 73–87). <https://doi.org/10.1021/bk-1986-0310.ch007>
- Pawelchak, J. M., Wang, Y. J., & LaVia, A. L. (1981). *United States Patent No. US4292972A*. Retrieved from <https://patents.google.com/patent/US4292972A/en>

- Pekala, R., & Kong, F. (1989). A synthetic route to organic aerogels - mechanism, structure and properties. *Journal de Physique Colloques*, 50(C4), C4-33-C4-40. <https://doi.org/koebel> 2012
- Pekala, R. W. (1989). Organic aerogels from the polycondensation of resorcinol with formaldehyde. *Journal of Materials Science*, 24(9), 3221–3227. <https://doi.org/10.1007/BF01139044>
- Pekala, Richard W. (1989). *United States Patent No. US4873218A*. Retrieved from <https://patents.google.com/patent/US4873218A/en>
- Pierre, A. C., & Pajonk, G. M. (2002). Chemistry of Aerogels and Their Applications. *Chemical Reviews*, 102(11), 4243–4266. <https://doi.org/10.1021/cr0101306>
- Pillay, V., & Fassihi, R. (1999). In vitro release modulation from crosslinked pellets for site-specific drug delivery to the gastrointestinal tract: II. Physicochemical characterization of calcium–alginate, calcium–pectinate and calcium–alginate–pectinate pellets. *Journal of Controlled Release*, 59(2), 243–256. [https://doi.org/10.1016/S0168-3659\(98\)00197-7](https://doi.org/10.1016/S0168-3659(98)00197-7)
- Pircher, N., Carbajal, L., Schimper, C., Bacher, M., Rennhofer, H., Nedelec, J.-M., ... Liebner, F. (2016). Impact of selected solvent systems on the pore and solid structure of cellulose aerogels. *Cellulose*, 23(3), 1949–1966. <https://doi.org/10.1007/s10570-016-0896-z>
- Plappert, S. F., Nedelec, J.-M., Rennhofer, H., Lichtenegger, H. C., & Liebner, F. W. (2017). Strain Hardening and Pore Size Harmonization by Uniaxial Densification: A Facile Approach toward Superinsulating Aerogels from Nematic Nanofibrillated 2,3-Dicarboxyl Cellulose. *Chemistry of Materials*, 29(16), 6630–6641. <https://doi.org/10.1021/acs.chemmater.7b00787>
- Ponzini, E., Natalello, A., Usai, F., Bechmann, M., Peri, F., Müller, N., & Grandori, R. (2019). Structural characterization of aerogels derived from enzymatically oxidized galactomannans of fenugreek, sesbania and guar gums. *Carbohydrate Polymers*, 207, 510–520. <https://doi.org/10.1016/j.carbpol.2018.11.100>
- Pour, G., Beauger, C., Rigacci, A., & Budtova, T. (2015). Xerocellulose: lightweight, porous and hydrophobic cellulose prepared via ambient drying. *Journal of Materials Science*, 50(13), 4526–4535. <https://doi.org/10.1007/s10853-015-9002-4>
- Powell, D. A., Morris, E. R., Gidley, M. J., & Rees, D. A. (1982). Conformations and interactions of pectins: II. Influence of residue sequence on chain association in calcium pectate gels. *Journal of Molecular Biology*, 155(4), 517–531. [https://doi.org/10.1016/0022-2836\(82\)90485-5](https://doi.org/10.1016/0022-2836(82)90485-5)
- Pushpamalar, J., Veeramachineni, A. K., Owh, C., & Loh, X. J. (2016). Biodegradable Polysaccharides for Controlled Drug Delivery. *ChemPlusChem*, 81(6), 504–514.

<https://doi.org/10.1002/cplu.201600112>

- Quignard, F., Valentin, R., & Di Renzo, F. (2008). Aerogel materials from marine polysaccharides. *New Journal of Chemistry*, 32(8), 1300. <https://doi.org/10.1039/b808218a>
- Quraishi, S., Martins, M., Barros, A. A., Gurikov, P., Raman, S. P., Smirnova, I., ... Reis, R. L. (2015). Novel non-cytotoxic alginate–lignin hybrid aerogels as scaffolds for tissue engineering. *The Journal of Supercritical Fluids*, 105, 1–8. <https://doi.org/10.1016/j.supflu.2014.12.026>
- Ralet, M.-C., Bonnin, E., & Thibault, J.-F. (2002). Pectins. In *Polysaccharides II: Polysaccharides of Eukaryotes* (Wiley-VCH, Vol. 6). Weinheim: A. Steinbüchel, S. De Baets, E.J. Vandamme.
- Ralet, M.-C., Dronnet, V., Buchholt, H. C., & Thibault, J.-F. (2001). Enzymatically and chemically de-esterified lime pectins: characterisation, polyelectrolyte behaviour and calcium binding properties. *Carbohydrate Research*, 336(2), 117–125. [https://doi.org/10.1016/S0008-6215\(01\)00248-8](https://doi.org/10.1016/S0008-6215(01)00248-8)
- Rao, A. V., Kulkarni, M. M., Pajonk, G. M., Amalnerkar, D. P., & Seth, T. (2003). Synthesis and Characterization of Hydrophobic Silica Aerogels Using Trimethylethoxysilane as a Co-Precursor. *Journal of Sol-Gel Science and Technology*, 27(2), 103–109. <https://doi.org/10.1023/A:1023765030983>
- Rege, A., Schestakow, M., Karadagli, I., Ratke, L., & Itskov, M. (2016). Micro-mechanical modelling of cellulose aerogels from molten salt hydrates. *Soft Matter*, 12(34), 7079–7088. <https://doi.org/10.1039/C6SM01460G>
- Renard, C. M. G. C., & Thibault, J.-F. (1996). Degradation of pectins in alkaline conditions: kinetics of demethylation. *Carbohydrate Research*, 286, 139–150. [https://doi.org/10.1016/0008-6215\(96\)00056-0](https://doi.org/10.1016/0008-6215(96)00056-0)
- Ridley, B. L., O'Neill, M. A., & Mohnen, D. (2001). Pectins: structure, biosynthesis, and oligogalacturonide-related signaling. *Phytochemistry*, 57(6), 929–967.
- Rinaudo, M. (2006). Chitin and chitosan: Properties and applications. *Progress in Polymer Science*, 31(7), 603–632. <https://doi.org/10.1016/j.progpolymsci.2006.06.001>
- Robitzer, M., David, L., Rochas, C., Renzo, F. D., & Quignard, F. (2008). Nanostructure of Calcium Alginate Aerogels Obtained from Multistep Solvent Exchange Route. *Langmuir*, 24(21), 12547–12552. <https://doi.org/10.1021/la802103t>
- Robitzer, M., Renzo, F. D., & Quignard, F. (2011). Natural materials with high surface area. Physisorption methods for the characterization of the texture and surface of polysaccharide aerogels. *Microporous and Mesoporous Materials*, 140(1–3), 9–16.

<https://doi.org/10.1016/j.micromeso.2010.10.006>

- Rubinstein, A., Radai, R., Ezra, M., Pathak, S., & Rokem, J. S. (1993). In vitro evaluation of calcium pectinate: a potential colon-specific drug delivery carrier. *Pharmaceutical Research*, *10*(2), 258–263.
- Rudaz, C. (2013). *Cellulose and Pectin Aerogels: Towards their nano-structuration* (PhD Thesis, Ecole Nationale Supérieure des Mines de Paris). Retrieved from <https://pastel.archives-ouvertes.fr/pastel-00957296/document>
- Rudaz, C., Courson, R., Bonnet, L., Calas-Etienne, S., Sallée, H., & Budtova, T. (2014). Aeropectin: Fully Biomass-Based Mechanically Strong and Thermal Superinsulating Aerogel. *Biomacromolecules*, *15*(6), 2188–2195. <https://doi.org/10.1021/bm500345u>
- Rühl, C., Appleby, P., Fennema, J., Naumov, A., & Schaffer, M. (2012). Economic development and the demand for energy: A historical perspective on the next 20 years. *Energy Policy*, *50*, 109–116. <https://doi.org/10.1016/j.enpol.2012.07.039>
- Sandberg, A. S., Ahderinne, R., Andersson, H., Hallgren, B., & Hultén, L. (1983). The effect of citrus pectin on the absorption of nutrients in the small intestine. *Human Nutrition. Clinical Nutrition*, *37*(3), 171–183.
- Schwertfeger, F., Glaubitt, W., & Schubert, U. (1992). Hydrophobic aerogels from Si(OMe)<sub>4</sub>/MeSi(OMe)<sub>3</sub> mixtures. *Journal of Non-Crystalline Solids*, *145*, 85–89. [https://doi.org/10.1016/S0022-3093\(05\)80435-1](https://doi.org/10.1016/S0022-3093(05)80435-1)
- Schwertfeger, F., Hüsing, N., & Schubert, U. (1994). Influence of the nature of organic groups on the properties of organically modified silica aerogels. *Journal of Sol-Gel Science and Technology*, *2*(1), 103–108. <https://doi.org/10.1007/BF00486221>
- Seantier, B., Bendahou, D., Bendahou, A., Grohens, Y., & Kaddami, H. (2016). Multi-scale cellulose based new bio-aerogel composites with thermal super-insulating and tunable mechanical properties. *Carbohydrate Polymers*, *138*, 335–348. <https://doi.org/10.1016/j.carbpol.2015.11.032>
- Sehaqui, H., Zhou, Q., & Berglund, L. A. (2011). High-porosity aerogels of high specific surface area prepared from nanofibrillated cellulose (NFC). *Composites Science and Technology*, *71*(13), 1593–1599. <https://doi.org/10.1016/j.compscitech.2011.07.003>
- Selmer, I., Kleemann, C., Kulozik, U., Heinrich, S., & Smirnova, I. (2015). Development of egg white protein aerogels as new matrix material for microencapsulation in food. *The Journal of Supercritical Fluids, Complete*(106), 42–49. <https://doi.org/10.1016/j.supflu.2015.05.023>
- Sescousse, R. (2010). *Nouveaux matériaux cellulose ultra-poreux et leurs carbones à partir de solvants verts* (Phdthesis, École Nationale Supérieure des Mines de Paris). Retrieved

from <https://pastel.archives-ouvertes.fr/pastel-00618528/document>

- Sescousse, R., Gavillon, R., & Budtova, T. (2011). Aerocellulose from cellulose–ionic liquid solutions: Preparation, properties and comparison with cellulose–NaOH and cellulose–NMMO routes. *Carbohydrate Polymers*, 83(4), 1766–1774. <https://doi.org/10.1016/j.carbpol.2010.10.043>
- Siepmann, J., Siegel, R. A., & Rathbone, M. J. (Eds.). (2012). *Fundamentals and Applications of Controlled Release Drug Delivery*. Retrieved from [//www.springer.com/us/book/9781461408802](http://www.springer.com/us/book/9781461408802)
- Siew, C. K., Williams, P. A., & Young, N. W. G. (2005). New Insights into the Mechanism of Gelation of Alginate and Pectin: Charge Annihilation and Reversal Mechanism. *Biomacromolecules*, 6(2), 963–969. <https://doi.org/10.1021/bm0493411>
- Silva, C. M., Ribeiro, A. J., Ferreira, D., & Veiga, F. (2006). Insulin encapsulation in reinforced alginate microspheres prepared by internal gelation. *European Journal of Pharmaceutical Sciences*, 29(2), 148–159. <https://doi.org/10.1016/j.ejps.2006.06.008>
- Smirnova, I., Mamic, J., & Arlt, W. (2003). Adsorption of Drugs on Silica Aerogels. *Langmuir*, 19(20), 8521–8525. <https://doi.org/10.1021/la0345587>
- Smirnova, I., Suttiruengwong, S., & Arlt, W. (2004). Feasibility study of hydrophilic and hydrophobic silica aerogels as drug delivery systems. *Journal of Non-Crystalline Solids*, 350, 54–60. <https://doi.org/10.1016/j.jnoncrysol.2004.06.031>
- Smirnova, I., Türk, M., Wischumerski, R., & Wahl, M. A. (2005). Comparison of Different Methods for Enhancing the Dissolution Rate of Poorly Soluble Drugs: Case of Griseofulvin. *Engineering in Life Sciences*, 5(3), 277–280. <https://doi.org/10.1002/elsc.200500081>
- Smirnova, I. (2011). Pharmaceutical Applications of Aerogels. In M. A. Aegerter, N. Leventis, & M. M. Koebel (Eds.), *Aerogels Handbook* (pp. 695–717). [https://doi.org/10.1007/978-1-4419-7589-8\\_31](https://doi.org/10.1007/978-1-4419-7589-8_31)
- Smirnova, I., Suttiruengwong, S., & Arlt, W. (2005). Aerogels: Tailor-made Carriers for Immediate and Prolonged Drug Release. *KONA Powder and Particle Journal*, 23, 86–97. <https://doi.org/10.14356/kona.2005012>
- Smirnova, I., Suttiruengwong, S., Seiler, M., & Arlt, W. (2004). Dissolution rate enhancement by adsorption of poorly soluble drugs on hydrophilic silica aerogels. *Pharmaceutical Development and Technology*, 9(4), 443–452.
- Soleimani Dorcheh, A., & Abbasi, M. H. (2008). Silica aerogel; synthesis, properties and characterization. *Journal of Materials Processing Technology*, 199(1), 10–26. <https://doi.org/10.1016/j.jmatprotec.2007.10.060>

- Sriamornsak, P. (2003). Chemistry of pectin and its pharmaceutical uses: A review. *Silpakorn University International Journal*, 3(1–2), 206–228.
- Starbird, R., García-González, C. A., Smirnova, I., Krautschneider, W. H., & Bauhofer, W. (2014). Synthesis of an organic conductive porous material using starch aerogels as template for chronic invasive electrodes. *Materials Science and Engineering: C*, 37, 177–183. <https://doi.org/10.1016/j.msec.2013.12.032>
- Stergar, J., & Maver, U. (2016). Review of aerogel-based materials in biomedical applications. *Journal of Sol-Gel Science and Technology*, 77(3), 738–752. <https://doi.org/10.1007/s10971-016-3968-5>
- Ström, A., Ribelles, P., Lundin, L., Norton, I., Morris, E. R., & Williams, M. A. K. (2007). Influence of Pectin Fine Structure on the Mechanical Properties of Calcium–Pectin and Acid–Pectin Gels. *Biomacromolecules*, 8(9), 2668–2674. <https://doi.org/10.1021/bm070192r>
- Subrahmanyam, R., Gurikov, P., Dieringer, P., Sun, M., & Smirnova, I. (2015). On the Road to Biopolymer Aerogels—Dealing with the Solvent. *Gels*, 1(2), 291–313. <https://doi.org/10.3390/gels1020291>
- Takeshita, S., Konishi, A., Takebayashi, Y., Yoda, S., & Otake, K. (2017). Aldehyde Approach to Hydrophobic Modification of Chitosan Aerogels. *Biomacromolecules*, 18(7), 2172–2178. <https://doi.org/10.1021/acs.biomac.7b00562>
- Takeshita, S., & Yoda, S. (2015). Chitosan Aerogels: Transparent, Flexible Thermal Insulators. *Chemistry of Materials*, 27(22), 7569–7572. <https://doi.org/10.1021/acs.chemmater.5b03610>
- Thakur, B. R., Singh, R. K., Handa, A. K., & Rao, M. A. (1997). Chemistry and uses of pectin — A review. *Critical Reviews in Food Science and Nutrition*, 37(1), 47–73. <https://doi.org/10.1080/10408399709527767>
- Thibault, J. F., & Rinaudo, M. (1985). Interactions of mono- and divalent counterions with alkali- and enzyme-deesterified pectins in salt-free solutions. *Biopolymers*, 24(11), 2131–2143.
- Thibault, J. F., & Rinaudo, M. (1986). Chain association of pectic molecules during calcium-induced gelation. *Biopolymers*, 25(3), 455–468.
- Tkalec, G., Knez, Ž., & Novak, Z. (2015a). Fast production of high-methoxyl pectin aerogels for enhancing the bioavailability of low-soluble drugs. *The Journal of Supercritical Fluids*, 106, 16–22. <https://doi.org/10.1016/j.supflu.2015.06.009>
- Tkalec, G., Knez, Ž., & Novak, Z. (2015b). Formation of polysaccharide aerogels in ethanol. *RSC Advances*, 5(94), 77362–77371. <https://doi.org/10.1039/C5RA14140K>

- Tkalec, G., Knez, Ž., & Novak, Z. (2016). PH sensitive mesoporous materials for immediate or controlled release of NSAID. *Microporous and Mesoporous Materials*, 224, 190–200. <https://doi.org/10.1016/j.micromeso.2015.11.048>
- Tkalec, G., Kranvogel, R., Uzunalić, A. P., Knez, Ž., & Novak, Z. (2016). Optimisation of critical parameters during alginate aerogels' production. *Journal of Non-Crystalline Solids*, C(443), 112–117. <https://doi.org/10.1016/j.jnoncrsol.2016.04.014>
- Trens, P., Valentin, R., & Quignard, F. (n.d.). Cation enhanced hydrophilic character of textured alginate gel beads. *Colloids and Surfaces A: Physicochemical and Engineering Aspects*, 296(1–3), 230–237.
- Tsiptsias, C., Stefopoulos, A., Kokkinomalis, I., Papadopoulou, L., & Panayiotou, C. (2008). Development of micro- and nano-porous composite materials by processing cellulose with ionic liquids and supercritical CO<sub>2</sub>. *Green Chemistry*, 10(9), 965–971. <https://doi.org/10.1039/B803869D>
- Ubeyitogullari, A., & Ciftci, O. N. (2016). Formation of nanoporous aerogels from wheat starch. *Carbohydrate Polymers*, 147, 125–132. <https://doi.org/10.1016/j.carbpol.2016.03.086>
- Valentin, R., Bonelli, B., Garrone, E., Di Renzo, F., & Quignard, F. (2007). Accessibility of the Functional Groups of Chitosan Aerogel Probed by FT-IR-Monitored Deuteration. *Biomacromolecules*, 8(11), 3646–3650. <https://doi.org/10.1021/bm070391a>
- Venkateswara Rao, A., & Haranath, D. (1999). Effect of methyltrimethoxysilane as a synthesis component on the hydrophobicity and some physical properties of silica aerogels. *Microporous and Mesoporous Materials*, 30(2), 267–273. [https://doi.org/10.1016/S1387-1811\(99\)00037-2](https://doi.org/10.1016/S1387-1811(99)00037-2)
- Veres, Péter, Kéri, M., Bányai, I., Lázár, I., Fábián, I., Domingo, C., & Kalmár, J. (2017). Mechanism of drug release from silica-gelatin aerogel—Relationship between matrix structure and release kinetics. *Colloids and Surfaces B: Biointerfaces*, 152, 229–237. <https://doi.org/10.1016/j.colsurfb.2017.01.019>
- Veres, Peter, López-Periago, A. M., Lázár, I., Saurina, J., & Domingo, C. (2015). Hybrid aerogel preparations as drug delivery matrices for low water-solubility drugs. *International Journal of Pharmaceutics*, 496(2), 360–370. <https://doi.org/10.1016/j.ijpharm.2015.10.045>
- Veronovski, A., Tkalec, G., Knez, Ž., & Novak, Z. (2014). Characterisation of biodegradable pectin aerogels and their potential use as drug carriers. *Carbohydrate Polymers*, 113, 272–278. <https://doi.org/10.1016/j.carbpol.2014.06.054>
- Vincent, R. R. R., Mansel, B. W., Kramer, A., Kroy, K., & Williams, M. A. K. (2013). Micro-rheological behaviour and nonlinear rheology of networks assembled from

- polysaccharides from the plant cell wall. *New Journal of Physics*, 15(3), 035002. <https://doi.org/10.1088/1367-2630/15/3/035002>
- Voragen, A. G. J., Coenen, G.-J., Verhoef, R. P., & Schols, H. A. (2009). Pectin, a versatile polysaccharide present in plant cell walls. *Structural Chemistry*, 20(2), 263. <https://doi.org/10.1007/s11224-009-9442-z>
- Voragen, F., Schols, H., & Visser, R. G. F. (2013). *Advances in Pectin and Pectinase Research*. Springer.
- Wagh, P. B., Begag, R., Pajonk, G. M., Rao, A. V., & Haranath, D. (1999). Comparison of some physical properties of silica aerogel monoliths synthesized by different precursors. *Materials Chemistry and Physics*, 57(3), 214–218. [https://doi.org/10.1016/S0254-0584\(98\)00217-X](https://doi.org/10.1016/S0254-0584(98)00217-X)
- Walkinshaw, M. D., & Arnott, S. (1981). Conformations and interactions of pectins: II. Models for junction zones in pectinic acid and calcium pectate gels. *Journal of Molecular Biology*, 153(4), 1075–1085. [https://doi.org/10.1016/0022-2836\(81\)90468-X](https://doi.org/10.1016/0022-2836(81)90468-X)
- Walter, R. H. (2012). *The Chemistry and Technology of Pectin*. Academic Press.
- Wang, L., Schiraldi, D. A., & Sánchez-Soto, M. (2014). Foamlike Xanthan Gum/Clay Aerogel Composites and Tailoring Properties by Blending with Agar. *Industrial & Engineering Chemistry Research*, 53(18), 7680–7687. <https://doi.org/10.1021/ie500490n>
- Wang, R., Shou, D., Lv, O., Kong, Y., Deng, L., & Shen, J. (2017). pH-Controlled drug delivery with hybrid aerogel of chitosan, carboxymethyl cellulose and graphene oxide as the carrier. *International Journal of Biological Macromolecules*, 103, 248–253. <https://doi.org/10.1016/j.ijbiomac.2017.05.064>
- Welch, H., & Welch, H. (1949). *Pectin penicillin preparation*. Retrieved from <https://www.google.com/patents/US2603583>
- White, R. J., Antonio, C., Budarin, V. L., Bergström, E., Thomas-Oates, J., & Clark, J. H. (2010). Polysaccharide-Derived Carbons for Polar Analyte Separations. *Advanced Functional Materials*, 20(11), 1834–1841. <https://doi.org/10.1002/adfm.201000169>
- White, R. J., Budarin, V. L., & Clark, J. H. (2010). Pectin-Derived Porous Materials. *Chemistry – A European Journal*, 16(4), 1326–1335. <https://doi.org/10.1002/chem.200901879>
- Winning, H., Viereck, N., Nørgaard, L., Larsen, J., & Engelsen, S. B. (2007). Quantification of the degree of blockiness in pectins using <sup>1</sup>H NMR spectroscopy and chemometrics. *Food Hydrocolloids*, 21(2), 256–266. <https://doi.org/10.1016/j.foodhyd.2006.03.017>
- Yuliarti, O., Hoon, A. L. S., & Chong, S. Y. (2017). Influence of pH, pectin and Ca concentration on gelation properties of low-methoxyl pectin extracted from *Cyclea barbata* Miers. *Food Structure*, 11, 16–23. <https://doi.org/10.1016/j.foostr.2016.10.005>

- Zhang, F., Ren, H., Tong, G., & Deng, Y. (2016). Ultra-lightweight poly (sodium acrylate) modified TEMPO-oxidized cellulose nanofibril aerogel spheres and their superabsorbent properties. *Cellulose*, 23(6), 3665–3676. <https://doi.org/10.1007/s10570-016-1041-8>
- Zhao, H.-B., Chen, M., & Chen, H.-B. (2017). Thermally Insulating and Flame-Retardant Polyaniline/Pectin Aerogels. *ACS Sustainable Chemistry & Engineering*, 5(8), 7012–7019. <https://doi.org/10.1021/acssuschemeng.7b01247>
- Zhao, S., Malfait, W. J., Demilecamps, A., Zhang, Y., Brunner, S., Huber, L., ... Koebel, M. M. (2015). Strong, Thermally Superinsulating Biopolymer-Silica Aerogel Hybrids by Cogelation of Silicic Acid with Pectin. *Angewandte Chemie (International Ed. in English)*, 54(48), 14282–14286. <https://doi.org/10.1002/anie.201507328>
- Zhao, S., Malfait, W. J., Guerrero-Alburquerque, N., Koebel, M. M., & Nyström, G. (2018). Biopolymer Aerogels and Foams: Chemistry, Properties, and Applications. *Angewandte Chemie (International Ed. in English)*, 57(26), 7580–7608. <https://doi.org/10.1002/anie.201801247>
- Zhao, S., Malfait, W. J., Jeong, E., Fischer, B., Zhang, Y., Xu, H., ... Koebel, M. M. (2016). Facile one-pot synthesis of mechanically robust biopolymer–silica nanocomposite aerogel by cogelation of silicic acid with chitosan in aqueous media. *ACS Sustainable Chemistry and Engineering*, 4(10), 5674–5683. <https://doi.org/10.1021/acssuschemeng.6b01574>



# CHAPTER II. MATERIALS AND METHODS

---

## CONTENTS

### CHAPTER II. MATERIALS AND METHODS

<b>INTRODUCTION.....</b>	<b>125</b>
<b>1. STARTING MATERIALS: .....</b>	<b>125</b>
1.1. PECTINS.....	125
1.2. CELLULOSE .....	126
1.3. SILICA-SOLS .....	126
1.4. SOLVENTS AND OTHER CHEMICALS .....	126
1.4.1. <i>Solvents for aerogels preparation</i> .....	126
1.4.2. <i>Chemicals and preparations specific to drug release experiments</i> .....	127
<b>2. METHODS .....</b>	<b>127</b>
2.1. PREPARATION OF PECTIN AEROGELS .....	127
2.1.1. <i>Pectin dissolution</i> .....	128
2.1.2. <i>Solvent-exchange step</i> .....	129
2.1.3. <i>Supercritical drying using CO<sub>2</sub></i> .....	131
2.1.4. <i>Alternative drying methods</i> .....	132
▪ Freeze drying .....	132
▪ Evaporative drying.....	132
2.2. CHARACTERIZATION METHODS .....	132
2.2.1. <i>Viscometry</i> .....	132
2.2.2. <i>Rheology</i> .....	133
2.2.3. <i>Fourier Transformed Infrared spectroscopy (FTIR)</i> .....	133
2.2.4. <i>Sample shrinkage and aerogel apparent density</i> .....	133
2.2.5. <i>Porosity and pore specific volume</i> .....	134
2.2.6. <i>Specific surface area measurement (BET method)</i> .....	135
2.2.7. <i>Scanning electron microscopy</i> .....	138
2.2.8. <i>ESD analysis</i> .....	138
2.2.9. <i>Contact angle</i> .....	138
2.2.10. <i>Uniaxial compression measurements</i> .....	139
2.2.11. <i>Thermal conductivity</i> .....	140
2.3. PREPARATION AND CHARACTERIZATION OF DRUG-LOADED PECTIN AEROGELS.....	141
2.3.1. <i>Drug incorporation into pectin matrices</i> .....	141
▪ Loading of theophylline into aerogels, xerogels and cryogels.....	141
2.3.2. <i>Aerogels' drug loading capacity and specific loading</i> .....	142
2.3.3. <i>Determination of the crystalline form of theophylline incorporated into pectin matrices by X-ray diffraction</i> .....	144
2.3.4. <i>In vitro drug release experiments</i> .....	144
▪ Determination of theophylline absorbance properties.....	145
▪ <i>In vitro</i> drug release experiments.....	146
2.3.5. <i>Cytotoxicity profile of different solid matrices</i> .....	148
▪ Sample preparation .....	148
▪ MTS assay method .....	149
<b>REFERENCES.....</b>	<b>151</b>

## Introduction

In this chapter, the preparation and characterization of pectin aerogels are described in detail.

- First, we present the starting raw materials including pectins, cellulose, silica-sols, and different solvents and chemicals used.
- Then we describe the main steps of preparation of neat pectin aerogels: dissolution, coagulation and supercritical drying. It has to be noted that the process route to make pectin-cellulose and pectin-silica composite aerogels are directly presented in the Methods section of Chapter VI. “Pectin-cellulose and pectin-silica composite aerogels for drug release applications”.
- The rheological properties of pectin solutions in various conditions are characterized using viscometry in dilute state and rheology.
- Methods to characterize polysaccharide and silica aerogels are then presented; aerogel physical and morphological properties are evaluated by their skeletal and bulk densities, their specific surface area, by SEM observations, by contact angle and X-rays. Their mechanical properties are characterized by uniaxial compression measurements. Aerogels effective thermal conductivity is determined using heat flowmeter.
- Finally, the last section is dedicated to the preparation and characterization of drug-loaded aerogels used as drug delivery systems. Thus, we present the process of drug incorporation into aerogel precursors prior to sc drying to produce drug loaded aerogels. Then we describe the methods to characterize aerogels’ drug loading properties and their drug release properties over time in gastro-intestinal media during *in vitro* dissolution testing. Finally, we detail the *in vitro* method to evaluate the cytotoxicity of aerogels regarding to human cells culture.

### 1. Starting materials:

#### 1.1. Pectins

Pectins used in the work were all from citrus, with different degrees of esterification (DE, %): 35% (named as P35), 56 % (P56), 59 % (P59) and 70 % (P70). P35, P59 and P70 were kindly provided by Cargill, and P56 was purchased from Sigma Aldrich.

Their actual DE (%) and molecular weight were determined using FITR and viscometry measurements, respectively, as detailed in the following Sections 2.2.1 and 2.2.3.

## 1.2. Cellulose

Microcrystalline cellulose Avicel® PH101 was purchased from Sigma-Aldrich and will be called “cellulose” in the following. Avicel was obtained from wood pulps by acid treatments. It is a purified and partially depolymerized  $\alpha$ -cellulose with a degree of polymerization of 180, given by the manufacturer.

## 1.3. Silica-sols

In order to produce silica aerogels and pectin-silica composite aerogels, we synthesized silica alcogels by sol-gel polymerization of two different silica-sols:

- Tetraethylorthosilicate (TEOS) (98 wt%) from ACROS Organics.
- Polyethoxydisiloxane (PEDS, called P75E20 by the producer), 20 w/w.% SiO<sub>2</sub> content in ethanol, kindly provided by ENERSENS (France). It consists of pre-polymerized oligomers of TEOS. These partially hydrolyzed precursors are therefore very prone to acid- or base-catalyzed condensation reactions as described in Ref. (Malfait et al., 2015; Strøm et al., 2007).

Solutions of hydrochloric acid (HCl) (32%, Analysis Grade, Certified Analytical Reagent) from Fisher Scientific and of ammonium hydroxide (NH<sub>4</sub>OH) (30wt%, ACS reagent grade) from Sigma-Aldrich were used as catalysts for hydrolysis and condensation reactions, respectively.

All solvents and chemicals were used as received. TEOS and PEDS were diluted with ethanol when needed.

## 1.4. Solvents and other chemicals

### 1.4.1. Solvents for aerogels preparation

Sodium hydroxide pellets (NaOH) (certified analytical reagent), potassium hydroxide pellets (KOH) (>99%, certified extra pure), hydrochloric acid (HCl) (32%, analysis grade, certified analytical reagent) were from Fisher Scientific and used as received. Potassium

phosphate monobasic ( $\text{KH}_2\text{PO}_4$ ) (> 99%, certified extra pure) and sodium chloride salt ( $\text{NaCl}$ ) (99.5%, certified analysis grade) were from Acros Organics. Calcium chloride anhydrous powder (96% extra pure) from Acros Organics was used to make  $\text{CaCl}_2$  aqueous solutions. Water was distilled.

Ethanol (purity > 99%, laboratory reagent grade), acetone (> 99%, laboratory reagent grade) were used as non-solvent for solvent-exchange steps during aerogel preparation.

### 1.4.2. Chemicals and preparations specific to drug release experiments

Theophylline anhydrous powder ( $\geq 99\%$ ) was from Sigma Aldrich and used as drug model. Theophylline was dissolved in ethanol to make 2.5 g/L solutions or 3.4 g/L suspensions and used as impregnation baths of aerogel precursors.

Buffer pharmacopeial solutions suitable for drug release experiments within simulated gastro-intestinal fluids are described in the United States Pharmacopeia (USP) following the guidelines of the USA Food and Drug Administration (FDA) and the Division of Bioequivalence of the Office of Generic Drugs (OGD) in Refs. (FDA/Center for Drug Evaluation and Research, 2019) and (U.S. FDA S, Center for Drug Evaluation and Research, 1997; U.S. FDA S, Center for Drug Evaluation and Research, 2018)

- Simulated Gastric Fluid (SGF) without enzyme was made from HCl solution (0.1N, pH 1.0)
- Simulated Intestinal Fluid without enzyme (SIF) (pH 6.8) was made using NaOH at 0.0112M (0.65 g/L) and  $\text{KH}_2\text{PO}_4$  at 0.05M (6.8 g/L).

## 2. Methods

### 2.1. Preparation of pectin aerogels

Pectin aerogels were prepared via dissolution – gelation (in some cases gelation did not occur) – solvent exchange with acetone or ethanol – drying with supercritical  $\text{CO}_2$  ( $\text{scCO}_2$  in the following) as illustrated in Figure 44.

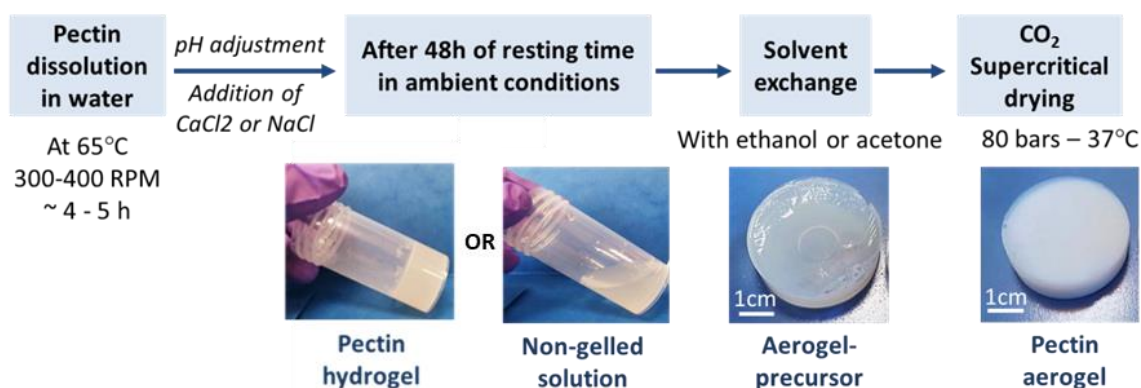


Figure 44. Preparation of pectin aerogels via dissolution – gelation (in some cases gelation did not occur) – solvent exchange – drying with sc CO<sub>2</sub>. From (Groult & Budtova, 2018)

In the following, each step is described and detailed.

The preparation of pectin-cellulose and pectin-silica aerogel composite are presented in the Chapter VI.

### 2.1.1. Pectin dissolution

Pectin aqueous solutions were prepared by dissolution of pectin powder in distilled water (with different concentrations that will be specified for each case) at 65 °C under stirring at around 300 to 400 rpm during several hours (usually 4 to 5 h depending on pectin concentration). Pectin concentrations are given in weight percent (wt %) unless otherwise mentioned. After complete dissolution, solution pH was adjusted<sup>[1]</sup> by addition of small quantity of HCl or KOH. pH was varied from 0.5 to 5 because at  $\text{pH} \geq 5$  solutions were of so low viscosity that solvent exchange was not possible. Pectin solutions were then poured into plastic molds of 27.5 mm of diameter. Specific larger cylindrical molds of 70 mm diameter were used for thermal analysis measurements in order to fit the size requirement of the Heat Flow meter device.

In certain cases, sodium (NaCl) or calcium solution (CaCl<sub>2</sub>) was added to pectin solution under stirring. The molar ratio R of metal cation (Me), Na<sup>+</sup> or Ca<sup>2+</sup>, to pectin carboxyl groups, expressed in mol.L<sup>-1</sup>, was varied from 0.05 to 2 and calculated as follows (Equation (2.1)):

---

<sup>[1]</sup> Some degradation may be possible at very low and high pH due to acid hydrolysis or  $\beta$ -depolymerization and demethoxylation in neutral to alkaline conditions (Fraeye et al., 2007; Krall & McFeeters, 1998; Renard & Thibault, 1996). This resulted in aerogel poor mechanical properties, especially at pH 0.5, and texture deterioration, as it will be shown in the Chapter III.

$$R = \frac{[Me]}{[RCOO^-]} \quad (2.1)$$

Pectin solutions were let gelling for 48 h at room temperature. Depending on the conditions (concentration, pH, presence of CaCl<sub>2</sub> or NaCl), solutions were gelling or not as determined by a simple “tilting test” (solution flowing or not); the state of the matter of pectin samples before solvent-exchange, *i.e.* solution (noted “S” for the matter flowing) or gel (noted “G” for the matter not flowing) will be given for each aerogel studied.

### 2.1.2. Solvent-exchange step

In order to perform drying with sc CO<sub>2</sub>, water has to be replaced by a fluid which is miscible with CO<sub>2</sub>. Two were used; ethanol and acetone, and both are pectin non-solvents. Solvent exchange was performed by progressively decreasing water/non-solvent (v/v) ratio to 50/50, 25/75 and 0/100, followed by the final extensive washing with pure non-solvent. At each “washing step”, pectin samples were immersed into 5 times higher volume of non-solvent than sample volume. In general, the solvent was changed every day (once or twice a day depending on sample thickness).

For the case when the state of matter was “gel”, the sample was placed in water-non-solvent baths as described above. When the state of matter was “solution”, a mixture of water-ethanol 50/50 (v/v) was gently put on the top of the solution (see Figure 45a), the principle is the same when using acetone as non-solvent. This led to a non-solvent induced phase separation (Figure 45b) also known as “immersion precipitation” process in membranes’ preparation (Wijmans, Altena, & Smolders, 1984): the solubility of the polymer decreases as non-solvent proportion increases.

This process had already been reported for making bio-aerogels from cellulose-ionic liquid (1-ethyl-3-methylimidazolium acetate (EmimAc) (Buchtová & Budtova, 2016), hot cellulose-N-methyl morpholine-N-oxide monohydrate (NMMO) (Innerlohinger, Weber, & Kraft, 2006), alginate (Gurikov & Smirnova, 2018; Horvat et al., 2017; Tkalec, Knez, & Novak, 2015b) and pectin solutions ((Tkalec et al., 2015b; Tkalec, Knez, & Novak, 2015a)ref).

In both cases, solution or gel, pectin coagulated during solvent exchange step resulting in a pectin “alco-gel” also called aerogel precursor: a 3D network composed of coagulated pectin with non-solvent in the pores. To ensure complete solvent-exchange, washing steps with non-solvent were performed in order to obtain at least a total 1/75 000 dilution factor before sc drying.

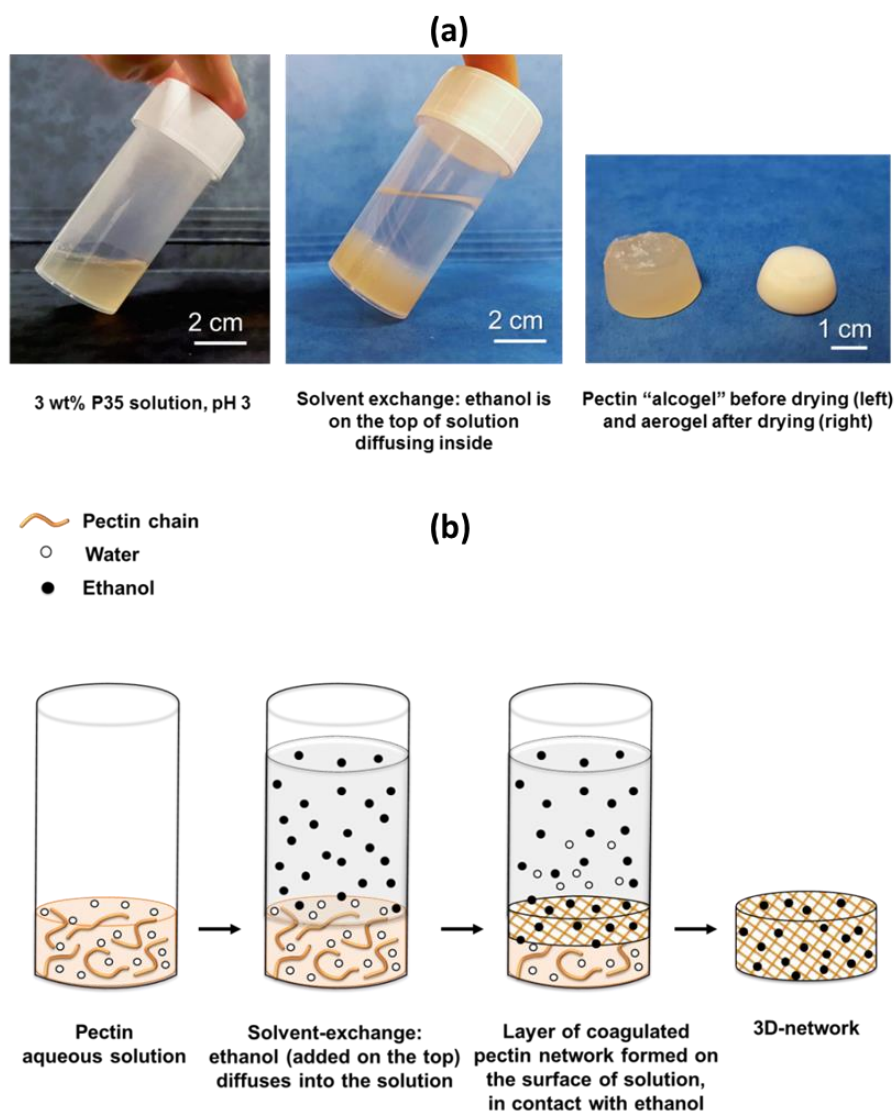


Figure 45. Illustration of solvent exchange using ethanol for non-gelled pectin solutions. The principle is the same when using acetone as non-solvent. From (Groult & Budtova, 2018)

a) pictures of non-gelled pectin P35 solution (3 wt%, pH 3), solvent exchange using ethanol, "alcogel" and aerogel;

b) schematic presentation of the phase separation occurring during solvent exchange from water to ethanol. The 3D network coagulated samples were then dried with sc CO<sub>2</sub>.

### 2.1.3. Supercritical drying using CO<sub>2</sub>

The aerogel precursors were then dried with supercritical CO<sub>2</sub>. The scCO<sub>2</sub> drying was performed in the center PERSEE of Mines ParisTech in Sophia Antipolis. The laboratory-scale device is shown in Figure 46. ScCO<sub>2</sub> was obtained with a pressure P=72.8 bar and temperature T=31.1°C. First, aerogel precursors coagulated in ethanol or acetone were placed in a 1L autoclave. The system is closed and pressurized at 50 bars and 37°C with gaseous CO<sub>2</sub>. Then pressure is increased to 80 bars. CO<sub>2</sub> becomes supercritical and solubilizes the residual solvent inside sample porosity. A dynamic washing step at 80 bars, 37°C with an output of 5 kg CO<sub>2</sub>/h is carried out for 1 hour. The system is let on a static mode at the same pressure and temperature conditions to allow scCO<sub>2</sub> to diffuse and solubilizes solvent even in the nanometric pores for 1-2 hours. The dynamic washing is then starting over with the same CO<sub>2</sub> output for 2 hours. Afterwards, the system is slowly depressurized overnight at 4 bar/h and 37°C and cooled down to room temperature. The autoclave is then opened, and samples collected. Pectin aerogels were placed into desiccator to protect them against moisture.

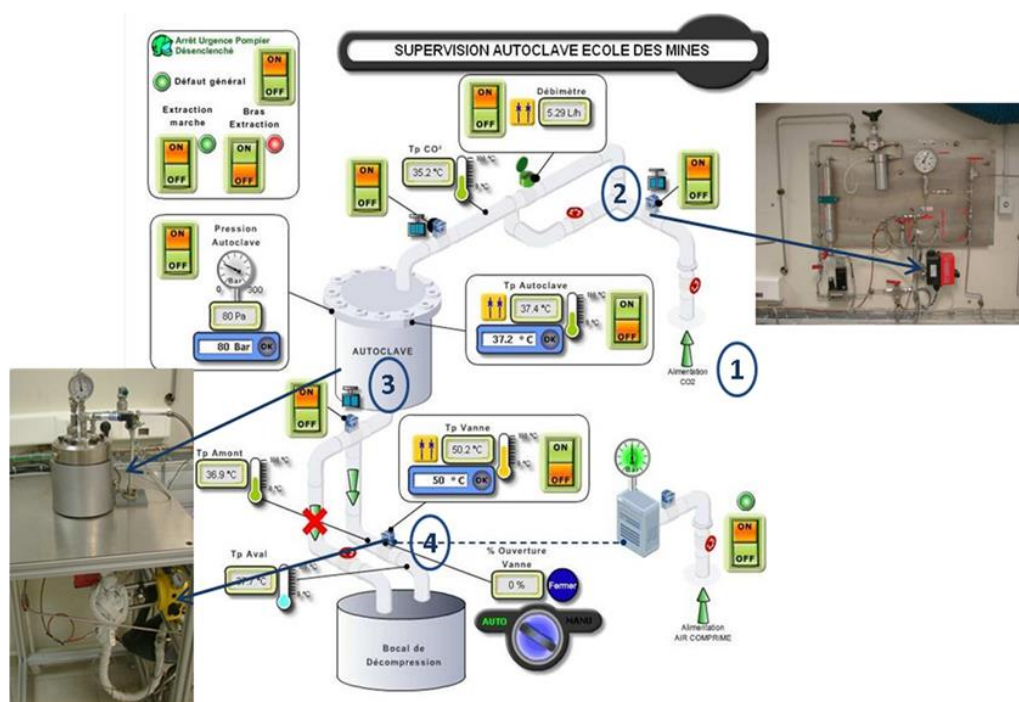


Figure 46. Laboratory-scale supercritical CO<sub>2</sub> drying device in Persée-Mines ParisTech; (1) CO<sub>2</sub> alimentation, (2) feeding valve, (3) autoclave, (4) depressurization valve. Courtesy of Pierre Ibizian, Persée-Mines ParisTech.

Generally, the final shape of dried samples were disks with diameter around 15-25 mm and thickness around 6-10 mm depending on sample shrinkage which in turn is controlled by pectin concentration and state of the matter before solvent exchange (solution or gel), presence of CaCl<sub>2</sub>, etc.

Alternatively, other types of drying were performed: freeze-drying technique to produce pectin cryogels and evaporative drying to make pectin xerogels.

#### 2.1.4. Alternative drying methods

##### ▪ **Freeze drying**

When freeze-drying procedure was chosen, pectin solutions and gels obtained after 48 h of resting time were directly used, and no solvent exchange with ethanol or acetone was performed. To freeze-dry samples, pectin hydrogels or aqueous solutions in plastic tubes were immersed in liquid nitrogen (-196°C) for around 5 minutes. Once completely frozen, the samples were placed into the freeze-dryer Cryotec Cosmos 80. First, vacuum was slowly made in the chamber, and then water vapor was condensed in the refrigerating unit. Samples were let drying for 48 hours to obtain pectin cryogels.

##### ▪ **Evaporative drying**

When evaporative drying was chosen, pectin samples were coagulated in ethanol or acetone prior to drying. Pectin coagulated samples were placed in oven at 60°C under vacuum and let dry for at least 4 days to obtain pectin xerogels. The duration of drying can be prolonged until the mass of samples is constant to remove all water traces from samples.

## 2.2. Characterization methods

### 2.2.1. Viscometry

Viscometry was used to determine pectins' intrinsic viscosities and molecular weights using a iVisc from LAUDA and capillary Ubbelohde Dilution Viscometer Type I with capillary diameter 0.63 mm. Huggins method was used to determine pectin intrinsic viscosity  $[\eta]$  by measuring kinematic viscosity of diluted pectin solutions (dilutions in series from 0.15 wt% to 0.05 wt%) in saline conditions (0.01 mol/ L of NaCl) at 26.6°C according to (Masuelli, 2014). These conditions were used as far as they allow the calculation of pectin molecular weight  $M$  according to Mark-Houwink equation (Equation (2.2)):

$$[\eta] = KM^\alpha \quad (2.2)$$

where  $K = 0.0234$  and  $\alpha = 0.8221$  (Masuelli, 2014).

### 2.2.2. Rheology

The rheological measurements were performed on Gemini rotational rheometer with Peltier temperature control system, using cone-plate geometry, both of 60 mm of diameter and cone with an angle of 2°. Solutions were let at rest for 1 h at room temperature prior the analysis. A pre-shear at 20 s<sup>-1</sup> was applied for 120 s before performing rheological measurements.

Steady state viscosity as a function of shear rate was measured with increasing shear rate from 0.1 to 600 s<sup>-1</sup> for 0.9 % pectin solutions at 20 °C and various pH. In these conditions, solutions are not gelling.

### 2.2.3. Fourier Transformed Infrared spectroscopy (FTIR)

FTIR spectroscopy is based on the interaction of infrared radiation with the matter. When excited by infrared beam, the molecules absorb at specific resonant frequencies that are characteristic to their own structure in relation with the mass of the atoms and the strength of the bond. In practice, a beam of infrared light is passing through the sample, and a then a transmittance or absorbance spectrum as a function of frequency is generated. The chemical structure of the sample can be identified by analyzing the characteristic absorption bands (in terms of intensity and frequency) as they are specifically related to functional groups.

FTIR spectroscopy was carried out on a Bruker Tensor 27 spectrometer in PERSEE (Mines ParisTech) with OPUS 7.8 software. Pectin powders were analyzed in attenuated total reflectance mode (ATR) using a Pike MIRacle accessory equipped with a Ge crystal (Pike Technology). The spectrum has been collected 100 times with a resolution of 4 cm<sup>-1</sup> and corrections for CO<sub>2</sub> and H<sub>2</sub>O were applied to correct the background noise. A smoothing curve treatment and offset correction were applied. Baseline was corrected and set at 1900 cm<sup>-1</sup>.

### 2.2.4. Sample shrinkage and aerogel apparent density

Volume shrinkage  $\Delta V$  of samples was determined before drying (*i.e.* at the end of solvent exchange) and after drying (Equation (2.3)):

$$\text{Volume shrinkage, \%} = \frac{V_i - V_f}{V_i} \times 100 \% \quad (2.3)$$

where  $V_i$  is the volume of the gel before solvent exchange and  $V_f$  is sample volume at the corresponding step.

Bulk density  $\rho_{bulk}$  was determined as the ratio of sample mass to volume. The mass of the aerogel was measured with digital analytical balance with a precision of 0.01 mg. The sample volume was measured with digital caliper with a precision of 0.01 mm.

### 2.2.5. Porosity and pore specific volume

Porous materials such as aerogels and foams are materials containing cavities or channels filled with air, called pores, and a solid backbone. The porosity of a material is defined as the ratio between the volume of pores and the total volume of the material (solid + pore volume). It can be estimated from bulk and skeletal densities as follows (Equation (2.4)):

$$\varepsilon, \% = \frac{V_{pores}}{V_{material}} = 1 - \frac{\rho_{bulk}}{\rho_{skeletal}} \times 100\% \quad (2.4)$$

where the skeletal density of pectin aerogels ( $\rho_{skeletal}$ ) is 1.5 g/cm<sup>3</sup>. Skeletal densities of different pectin aerogels were determined using helium pycnometry in the Charles Coulomb laboratory of the university of Montpellier, France.

Pore specific volume was estimated using bulk and skeletal densities (Equation (2.5)):

$$V_{pores} = \frac{1}{\rho_{bulk}} - \frac{1}{\rho_{skeletal}} \quad (2.5)$$

Materials with open pores and closed pores should be distinguished. Contrary to open pores, closed pores are not accessible from the outside by liquid or gases (see Figure 47). The total volume of pores is the sum of open and closed pores volumes.

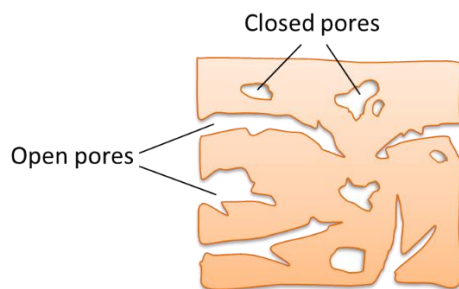


Figure 47. Schematic representation of a porous sample with open and closed pores.

The properties of a porous material strongly depend on the geometry and size of pores as well as their size (width) distribution. IUPAC classification (“IUPAC Gold Book,” 2017) divides pores sizes in three groups (Sing, 1985) (Sing et al., 1985):

- Macropores are pores with an internal width above 50 nm
- Mesopores with an internal width between 2 and 50 nm
- Micropores with an internal width below 2 nm

### 2.2.6. Specific surface area measurement (BET method)

Specific surface area is an important structural characteristic for porous materials and corresponds to the total open pore surface per gram of matter. It is strongly related to pore diameters and size distribution as well as their surface rugosity.

The Brunauer, Emmett and Teller (BET) method was developed to determine the specific surface area of porous solids based on multilayer gas physical and reversible adsorption, *i.e.* the accumulation of gas molecules over the available surface of a material at the gas-solid interface by weak physical interactions (physisorption) such as Van der Waals interactions (see Figure 48). The BET method assumes an absence of interactions between adsorption layers, with the number of adsorption layers on a solid being theoretically infinite, and thus the Langmuir theory can be applied to each layer.

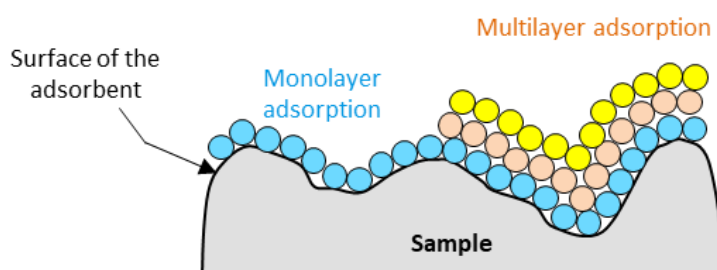


Figure 48. Schematic illustration of monolayer and multilayer adsorptions of gas molecules over the surface of a sample (the adsorbent).

Physisorption experiments are conducted at the boiling point of liquid nitrogen (-196 °C) at atmospheric pressure. The nitrogen adsorption isotherm plots the adsorbed quantity of gas per gram of adsorbate as a function of equilibrium relative pressure  $p/p_0$ , where  $p$  is the equilibrium pressure of adsorbate gas and  $p_0$  the vapor pressure of nitrogen at saturation. The adsorption/desorption isotherms are a way to evaluate the porosity of materials.

In the range  $p/p_0$  between 0.05 and 0.3, adsorption isotherm is quasi-linear, and a simplified equation is known as BET equation (Equation 2.6):

$$\frac{p/p_0}{n^a(1-p/p_0)} = \frac{1}{n_m^a c} + \left[ \frac{c-1}{n_m^a c} \right] \left( \frac{p}{p_0} \right) \quad (2.6)$$

where  $n_m$  is the amount of gas absorbed at the relative pressure  $p/p_0$ ,  $p/p_0$  is the equilibrium relative pressure,  $n_m^a$  is the monolayer capacity (*i.e.* the amount of adsorbate needed to cover the surface with a complete monolayer of molecules).

When the available surface of the material is totally covered by adsorbed molecules, specific surface area  $S_{BET}$  may be determined by Equation (2.7):

$$S_{BET} = \left( \frac{v_m^a}{m_s} \right) \frac{N_A \sigma_m}{v_i} \quad (2.7)$$

with  $v_m^a$  the monolayer adsorbed gas volume,  $m_s$  mass of the adsorbent,  $N_A$  the Avogadro constant,  $\sigma_m$  is the cross section occupied by each nitrogen molecule (fixed by IUPAC at  $\sigma_m = 0.162 \text{ nm}^2$ ) and  $v_i$  molar volume of perfect gas equals to  $22\,414 \text{ cm}^3 \cdot \text{mol}^{-1}$ .

Specific surface area was determined by nitrogen adsorption using Micromeritics ASAP 2020 and BET method. Prior to analysis, samples were degassed in a high vacuum at  $70 \text{ }^\circ\text{C}$  for 10 h.

It should be noted that standard methods for measuring pore size distribution and pore volume such as Barrett, Joyner and Halenda method (or BJH method) with nitrogen adsorption or mercury porosimetry cannot be applied to bio-aerogels. BJH method considers pores sizes below 200 nm, which takes in account around 10-20% of the total pore volume of the majority of bio-aerogels (Robitzer, Renzo, & Quignard, 2011; Rudaz et al., 2014). The classical formula for calculating average pore size  $D$  within the approximation of cylindrical pores is given by equation (2.8):

$$D = \frac{4V_{p,BJH}}{S_{BET}} \quad (2.8)$$

where  $V_{p,BJH}$  is pore volume measured by nitrogen adsorption/desorption method. Equation (2.8) gives strongly underestimated values of  $D$  as far as  $S_{BET}$  considers only mesopores and small macropores.

If replacing  $V_{p,BJH}$  by  $V_{pores}$  calculated from skeletal and bulk densities (section 2.2.4),  $D$  is strongly overestimated. It may also be possible that bio-aerogel is compressed at higher nitrogen pressure. An example of BHJ analysis of one of aeropectins obtained in this work is shown in Figure 49. It shows that  $V_{p,BJH}$  is around 8 % of  $V_p$ , as pore volume  $V_p$  calculated using equation (2.5) is around  $18.3 \text{ cm}^3/\text{g}$ .

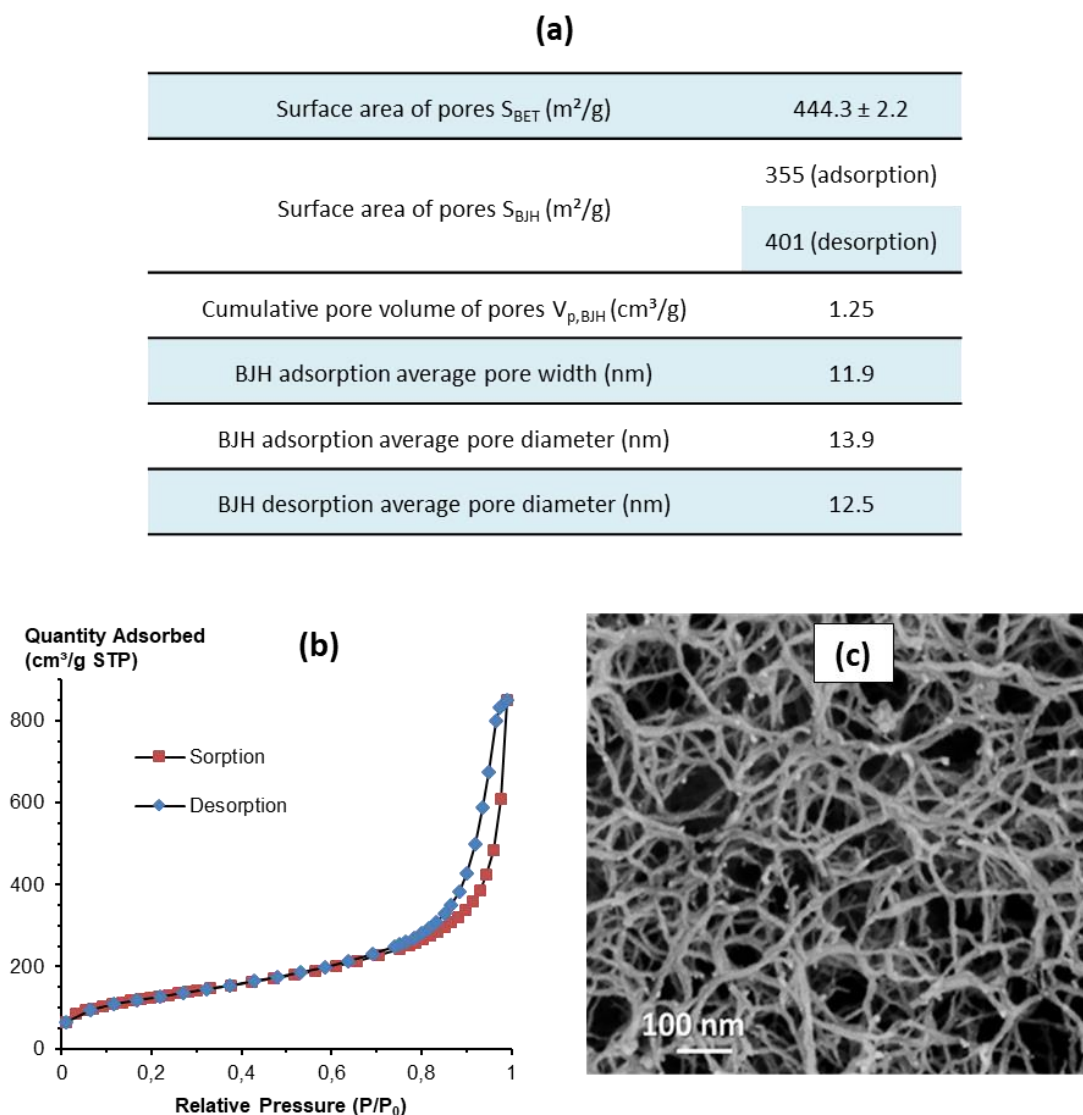


Figure 49. Example of BJH analysis of pectin aerogel made from 3 wt% of P35 at pH 3.0 with calcium at  $R = 0.2$ : (a) structural parameters obtained, (b) adsorption/desorption curves (b) and (c) SEM image of this sample. Total pore volume calculated using equation (2.5) is around  $18.3 \text{ cm}^3/\text{g}$ . Adapted from (Groult & Budtova, 2018)

When mercury porosimetry is used, bio-aerogels are compressed without mercury penetration in the pores, and thus the "value" given by the machine is an artefact (Rudaz, 2013; Rudaz et al., 2014). Thus, in this manuscript total pore volume will be based on bulk and skeletal density values, and only specific surface area will be reported from nitrogen adsorption measurements.

### 2.2.7. Scanning electron microscopy

A scanning electron microscope (SEM) gives images of a sample surface (topography) by scanning it with a focused beam of electrons. Beam electrons interact with the electrons on the surface, producing various signals (electrons, photons, phonons...) that can be detected. The position of the electron beam is combined with the detected signal to produce a SEM image.

Scanning electron microscopy observations of aerogel morphology were performed on a ZeissSupra™ 40 FEG (Field Emission Gun) at an acceleration voltage of 3 KeV and a diaphragm of 10  $\mu\text{m}$  or 20  $\mu\text{m}$ . Prior to observations, a fine layer of about 7 nm of platinum was sputtered onto the sample surface with Q150T Quarum rotating metallizer.

### 2.2.8. ESD analysis

Energy diffractive spectroscopy (EDS) analyses the elemental composition of sample surface, by detecting X-rays emitted during the interaction with electron beam from a SEM. The beam excites atoms in the sample, and they release energy in the form of X-rays. The energy of emitted X-rays is characteristic for the atoms that produced them. Thus, a spectrum can be obtained, where different elements in the sample are identified by peaks at characteristic energy values. As the electron beam can be precisely controlled, and EDS spectrum can be collected from a selected area of the sample. This technique gives an elemental analysis of a few cubic microns of material.

EDS analysis was carried out on a XL30 FEI Philipps ESEM (Environmental Scanning Electron Microscopy) in Cemef, Mines ParisTech, with an acceleration voltage of 12 keV and a vacuum pressure in the chamber of at low vacuum (0.1 to 1.3 mbar). Non-metallized, electrically insulating samples were studied with an environmental electron microscope as this type of SEM does not require the samples to be metallized.

### 2.2.9. Contact angle

The simplest way to assess the hydrophobicity of a material is the measurement of the contact angle of the material with water. When a drop of water is placed on the surface of a material, a thermodynamic equilibrium between the solid, liquid and gas phases is reached (Figure 50).

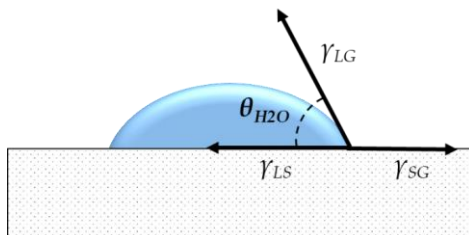


Figure 50. Contact angle with water drop and surface tensions at a sample surface.

The surface tensions between the different phases are noted  $\gamma_{SG}$  for the solid-gas interface,  $\gamma_{LG}$  for the liquid-gas interface and  $\gamma_{LS}$  for the liquid-solid interface; the contact angle  $\theta_{H2O}$  can be theoretically determined from Young-Dupré equation (Equation (2.9))

$$\gamma_{SG} - \gamma_{LG} - \gamma_{LS} \cdot \cos \theta_{H2O} = 0 \quad (2.9)$$

Samples showing contact angles with water superior to  $90^\circ$  are considered hydrophobic. Generally, the contact angle is measured directly on the surface of the sample.

For all aerogels studied in this work, water contact angle measurements were performed with a Krüss DropAnalyzer DSA 100 goniometer in controlled atmosphere ( $20^\circ\text{C}$ , 50% RH). Droplets of  $50 \text{ mm}^3$  were deposited on sample flat and horizontal surface. The contact angle was measured from pictures of the droplets using Drop Shape Analysis software.

### 2.2.10. Uniaxial compression measurements

The mechanical properties of pectin aerogels were characterized by uniaxial compression measurements. Samples with cylindrical shape and a ratio length/diameter around 1 were compressed up to high deformations (strain up to 90%) to obtain full stress-strain curves.

A schematic illustration of stress-strain curve is shown in Figure 51. Young's modulus (E) (obtained in the linear viscoelastic regime), yield stress ( $\sigma_{\text{yield}}$ ) (beginning of plasticity), and densification strain  $\varepsilon_d$  (corresponding to the end of the plastic region with high increase of the stress) were determined from the compression strain-stress curves.

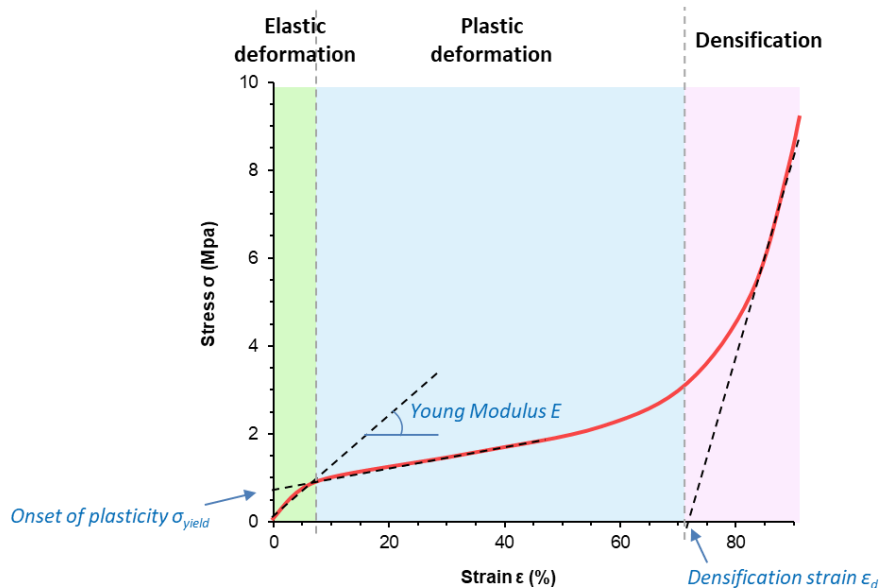


Figure 51. Schematic representation of a stress-strain curve with the three different domains: elastic deformation, plastic deformation and densification.

The experiments were carried out on the Instron EM17 testing machine. The samples were placed between two parallel plates. Before measurements, samples were polished to make upper and lower surfaces planar and parallel. The measurements were performed at room temperature (22-24°C) and ambient conditions. A pre-loading test of 1 N was performed before compression. Compression was performed at a displacement rate of 1 mm/min, until 90% deformation, with a maximum force of 30 kN. 20 points/sec were recorded. At least three samples per formulation were tested to ensure reproducibility.

### 2.2.11. Thermal conductivity

Thermal conductivity ( $\lambda$ ) of pectin aerogels was measured at ambient pressure using heat flow meter Fox 150 equipped with a custom “micro flow meter cell” developed for small samples (see details in (Rudaz et al., 2014)) at 20 °C. Spaceloft<sup>®</sup> aerogel from Aspen (thickness of 3.70 mm) with thermal conductivity of 0.0133 W/(m.K) at 20 °C according to the European Norm EN 12667 was used as a standard for calibration.

Aerogel disk is placed between two plates, one heated at  $T_h = 25^\circ\text{C}$  (called “Hot Plate”) and the other cooled at  $T_c = 15^\circ\text{C}$  (called “Cold Plate”) (see Figure 52).

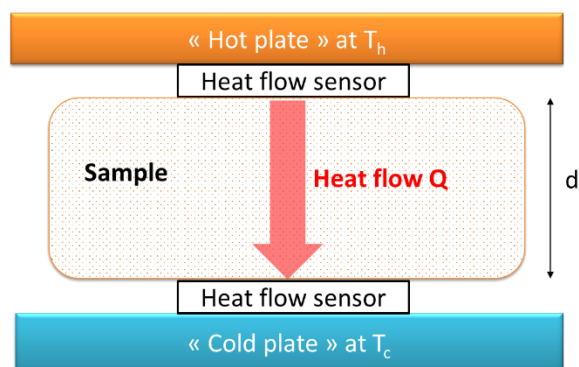


Figure 52. Schematic presentation of Heat Flow meter device.

Temperature of the plates is monitored until they are constant (steady state). Determination of the heat flow through the sample from the “Hot plate” towards the “Cold plate” is achieved by means of a heat flux sensor (meter). Thermal conductivity is calculated according to Equation (2.10):

$$\lambda = \frac{Q \cdot d}{A (T_h - T_c)} \quad (2.10)$$

with Q quantity of heat passing through the sample (W), A area of the sample (m<sup>2</sup>), d thickness of the sample (m).

## 2.3. Preparation and characterization of drug-loaded pectin aerogels

### 2.3.1. Drug incorporation into pectin matrices

In this work, we prepared drug-loaded hydrogels, aerogels, cryogels and xerogels made from different compositions (pectin, cellulose, silica) using theophylline as drug model. The goal is to evaluate the potential of different solid matrices and their composites used as drug-carriers for gastro-intestinal drug release applications.

In this section, we explain the general drug incorporation method to load pectin aerogels, cryogels and xerogels with theophylline. Then, we explain the characterization methods specific to drug-loaded pectin matrices.

- **Loading of theophylline into aerogels, xerogels and cryogels**

Theophylline is moderately soluble in ethanol (3.5 g/L at 25 °C) allowing its impregnation into pectin aerogel precursor (pectin coagulated in ethanol) through diffusion. Due to its high

polarity and low octanol-water partition coefficient  $K_{ow}$  from -0.02 (experimental value) (M. Grassi, Colombo, & Lapasin, 2001) to -0.7 (predicted value) (“ChemAxon,” n.d.; Mario Grassi et al., 2006) theophylline is practically insoluble in non-polar solvent such as supercritical  $CO_2$ , with solubility lower than 0.04 g/kg at 313 K and 19.9 MPa (Johannsen & Brunner, 1994), thus avoiding its wash out during  $CO_2$  sc drying. To minimize the dilution effect due to the presence of ethanol within the aerogel precursors, the samples were immersed in theophylline solution 25 to 30 times larger than the volume of pectin, and ethanol solution bath was changed for fresh one after 48 h. As shown in Figure 53, pectin aerogel precursors were immersed for 7 days into ethanol solution at a concentration of theophylline of either 2.5 g/L or 3.4 g/L, depending on the case. This duration of impregnation ensures a complete diffusion of theophylline within the samples in ambient conditions taking in account sample thickness, as it will be demonstrated in Chapter V.

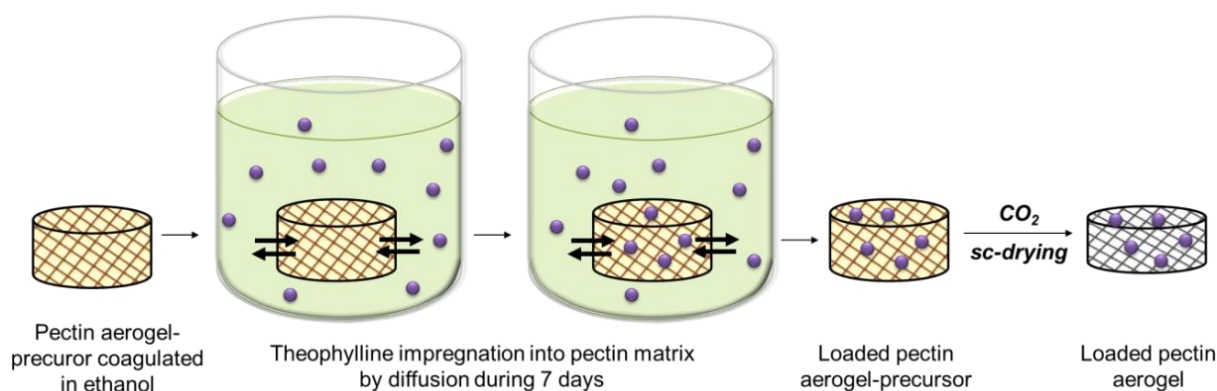


Figure 53. Schematic representation of the impregnation method of theophylline into pectin aerogel precursor by diffusion.

To produce drug-loaded xerogels and aerogels, theophylline was impregnated into the coagulated samples as shown in Figure 53. To obtain theophylline loaded hydrogels and cryogels, the drug was added to pectin aqueous solution at 3.4 g/L which was gelled for 48 h. Pectin cryogel was made by freeze-drying of a drug-loaded hydrogel (without any solvent-exchange step).

### 2.3.2. Aerogels' drug loading capacity and specific loading

For clarity, we take the example of an aerogel to present different drug loading properties of a sample.

A theoretical estimation of maximum drug loading can be given based on the volume of aerogel precursor (“alcogel”) during impregnation and theophylline concentration in ethanol used for impregnation.

Assuming that:

- Aerogel precursor volume is mainly ethanol (pectin concentration is low):  $V_{alcogel} \sim V_{ethanol}$
- The diffusion of theophylline into alcogel is complete, thus the theophylline concentration in ethanol (in the impregnation bath) is the same as in the alcogel:  $C_{alcogel} = C_{ethanol}$

If 100% of theophylline present in the loaded alcogel volume remained after CO<sub>2</sub> sc-drying, a theoretical maximum drug mass (or dose inside an aerogel) can be expressed as follow:

$$\text{Aerogel maximum drug dose (g)} = V_{alcogel}(\text{cm}^3) \times C_{ethanol} (\text{g} \cdot \text{cm}^{-3}) \quad (2.11)$$

It has to be noted that for hydrogels and cryogels, the theoretical maximum drug mass dose is simply given by the theophylline concentration set during sample preparation. Indeed, contrary to aerogels and xerogels, drug loading of hydrogels and cryogels is conducted by direct drug dissolution into pectin solution and not by diffusion through ethanol into a pre-existing sample.

*Actual theophylline doses (g)* in aerogels are obtained after dissolution testing using spectrophotometric characterization, knowing the total theophylline released after complete dissolution (or after matrix destruction in case of non-soluble matrix).

Thus, *drug loading efficiency (%)* can be defined as:

$$\text{Drug loading efficiency (\%)} = \frac{\text{Aerogel actual drug dose (g)}}{\text{Aerogel maximum drug dose (g)}} \times 100 \% \quad (2.12)$$

Finally, knowing the theophylline actual dose, aerogels' *loading capacity* and *specific loading* are defined as the weight percent of drug (wt% of drug) and mass of drug per specific surface area unit (g/ m<sup>2</sup>), respectively:

$$\text{Aerogel loading capacity (wt\%)} = \frac{\text{Aerogel actual drug dose (g)}}{\text{Loaded aerogel mass (g)}} \times 100\% \quad (2.13)$$

$$\text{Aerogel specific loading (g/m}^2\text{)} = \frac{\text{Aerogel loading capacity (wt\%)}}{\text{Specific surface area (m}^2\text{/g)}} \quad (2.14)$$

### 2.3.3. Determination of the crystalline form of theophylline incorporated into pectin matrices by X-ray diffraction

X-ray crystallography is a technique used for the identification of unknown crystalline structures by determination of the atomic and molecular structure of a crystal. Crystalline materials are characterized by a three-dimensional structure defined by regular and repeating planes of atoms that form a crystal lattice. When X-ray beam interacts with these planes of atoms a part is diffracted. X-rays are diffracted differently depending on the atomic organization and spatial arrangement in the lattice of the crystalline structure. The diffraction from crystalline substances are characterized by well-defined Bragg peaks as atoms are periodically arranged, while for amorphous materials it is characterized either by a broad peak or background hump due to the random orientation of atoms scattering the incident beam in all directions.

To determine the crystalline form of the drug incorporated into pectin aerogels, cryogels and xerogels, wide-angle X-ray diffraction (XRD) analysis was conducted on the external surface and in the core of the drug loaded samples. XRD was performed with diffractometer “XPRT-PRO” from PANalytical equipped with measurement program “ScanPixcel”. The patterns with Cu K $\alpha$  radiation ( $\lambda = 1.5406 \text{ \AA}$ ) were recorded in the range from 6° to 80°. Samples were dried overnight at 50 °C under vacuum to remove humidity. Additional X-ray diffraction analysis on drug-loaded aerogels, xerogels and cryogels were also carried out using a BRUKER AD8 Advance X-ray Diffractometer at the “Petru Poni” Institute of Macromolecular Chemistry, Iasi, Romania.

### 2.3.4. *In vitro* drug release experiments

To evaluate the potential of aerogels, cryogels, xerogels and hydrogels to be used as oral drug delivery systems, theophylline-loaded samples were immersed into simulated gastrointestinal fluids at 37.0 °C under soft stirring, in order to mimic the physiological conditions in case of an oral drug intake.

The release of the drug out of the solid matrices was followed in time by spectrophotometric measurements as theophylline has a specific signal in UV. *In vitro* drug release experiments were conducted for aerogels, cryogels, xerogels and hydrogels of different composition (pectin, cellulose, silica). We first present the absorbance properties of theophylline, then we present and detail the *in vitro* method of drug release experiments. For clarity and simplicity, we detail the methods taking a drug-loaded pectin aerogel as an example.

## ▪ Determination of theophylline absorbance properties

Every chemical compound absorbs or transmits light over a certain range of wavelength. Spectrophotometry is a quantitative method which measures the intensity of light absorbed by a chemical after it passes through sample solution. As Beer-Lambert Law states that there is a linear relationship between the absorbance and the concentration of a matter in solution, this measurement can be used to determine the amount of a known chemical substance based on its absorbance. In order to follow the release of the drug out of the matrices by spectrophotometry, the absorbing properties of theophylline dissolved in Simulated Gastric Fluid (SGF) (HCl at 0.1N - pH1.0) and in Simulated Intestinal Fluids (SIF) (NaOH at 0.0112M, KH<sub>2</sub>PO<sub>4</sub> at 0.05M - pH 6.8) were characterized.

As shown in Figure 54, theophylline absorbs in the UV range (190nm – 400 nm) with two distinct absorption peaks at wavelengths around 204 nm and 271 nm, as reported in literature (Lide et al., 2005). As the peak obtained at 271 nm is better defined and not close to the limit of detection of the spectrophotometer compared to that at 204 nm, the wavelength of 271 nm was chosen to detect the drug in liquid media.

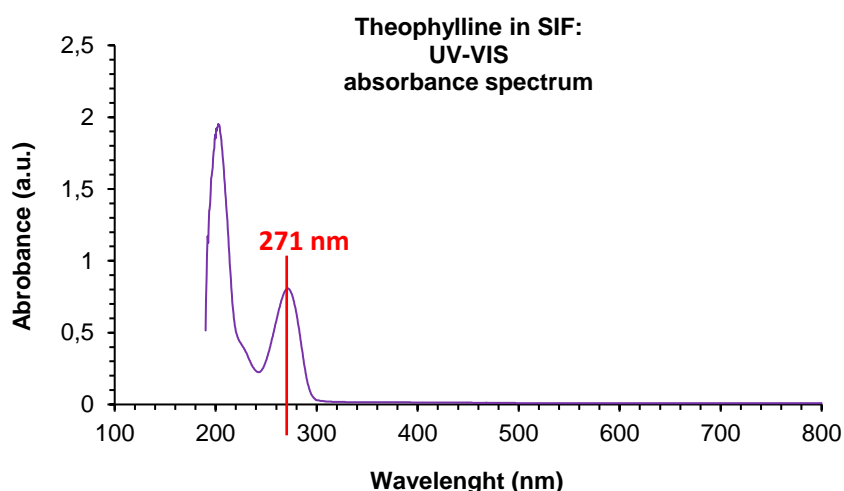


Figure 54. Example of theophylline's absorbance UV-VIS spectrum as a function of wavelength. In this case, theophylline was dissolved at a concentration of 0.0125 g/L into simulated intestinal fluid (NaOH at 0.0112M, KH<sub>2</sub>PO<sub>4</sub> at 0.05M - pH 6.8) at 37.0°C.

Theophylline was dissolved at various concentrations (between 0.0025 g/L up to 0.0375 g/L) in SGF (pH 1.0) and in SIF (pH 6.8), both at 37.0 °C. The absorbance at 271 nm vs concentration were found to be in the relationship as expressed by the Beer-Lambert's Law.

$$A = C_i \cdot l \cdot \varepsilon_i \quad (2.15)$$

where  $A$  is the measured absorbance at a given wavelength;  $\varepsilon_i$  is the molar attenuation coefficient or absorptivity of the attenuating species  $i$  in the material sample;  $C_i$  the

concentration of the attenuating species in the material sample and  $l$  is the path length of the beam of light through the material sample.

The molar extinction coefficients of theophylline were determined to be  $\sim 57.4$   $\text{L mol}^{-1} \text{cm}^{-1}$  in SGF (pH 1.0) at  $37.0^\circ\text{C}$  ( $R^2 \geq 0.997$ ) and  $\sim 59.1$   $\text{L mol}^{-1} \text{cm}^{-1}$  in SIF (pH 6.8) at  $37.0^\circ\text{C}$  ( $R^2 \geq 0.99$ ). The absorbance calibrations (absorbance vs concentration) for theophylline in SGF and in SIF are shown in Figure 55.

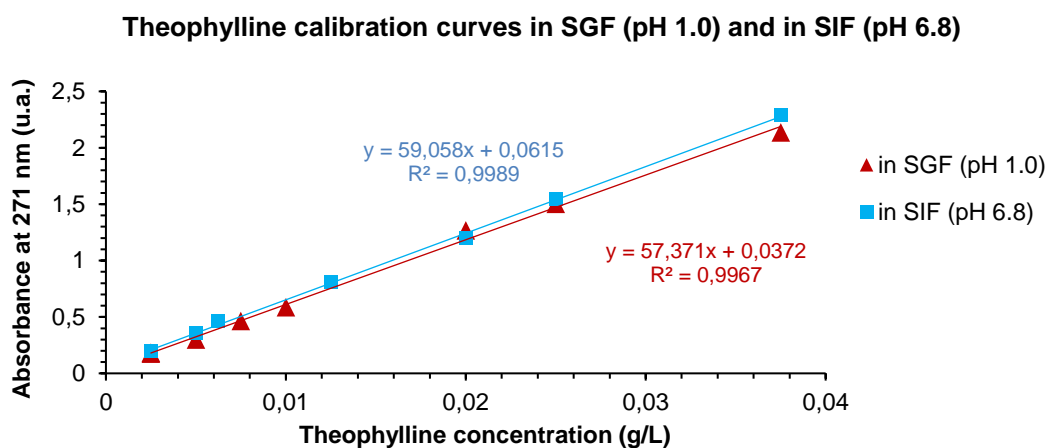


Figure 55. Absorbance calibration curves (at 271 nm) for theophylline dissolved in SGF (pH 1.0) and in SIF (pH 6.8). Straight lines are linear regressions of the data and give equations  $y = 57.371x + 0.0372$  ( $R^2 = 0.9967$ ) for theophylline in SGF ( $37.0^\circ\text{C}$ ) and  $y = 59.058x + 0.0615$  ( $R^2 = 0.9989$ ) for theophylline in SIF ( $37.0^\circ\text{C}$ ).

### ▪ *In vitro* drug release experiments

The *in vitro* drug release experiments followed the Food and Drug Administration (FDA) Dissolution Methods specific for theophylline extended-release tablets (updated 10/06/2008) (FDA/Center for Drug Evaluation and Research, 2019) recommended by the FDA's Division of Bioequivalence of the Office of Generic Drugs (OGD). Guidelines concerning the Dissolution Testing experiments can be found in the FDA's guidance for industry (U.S. FDA S, Center for Drug Evaluation and Research, 1997; U.S. FDA S, Center for Drug Evaluation and Research, 2018) as well as in Refs. (Friedel et al., 2018; Siewert et al., 2003).

The dissolution testing was conducted at  $37.0^\circ\text{C}$  in 900 mL releasing bath (sink conditions) stirred at 100 rpm to ensure homogenization. The aerogel was put into a permeable metal basket (Figure 56) and immersed into Simulated Gastric Fluid (SGF) without enzymes (HCl 0.1N - pH1.0) (USP buffer media) during the first hour, and then into Simulated Intestinal Fluids without enzyme (SIF) (NaOH at 0.0112M,  $\text{KH}_2\text{PO}_4$  at 0.05M - pH 6.8) (United States Pharmacopeia n°26 Buffer media). Buffer pharmacopeial solutions suitable for dissolution tests are described in the United States Pharmacopeia.

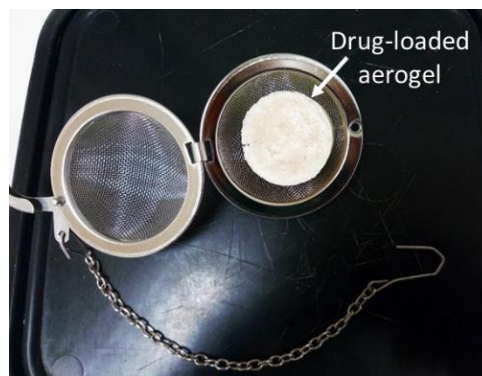


Figure 56. Example of aerogel sample loaded with theophylline placed in a permeable metal basket and maintained completely immersed during the dissolution testing experiment.

Drug release was followed by spectrophotometric measurements at regular time intervals (usually every 5 to 10 minutes) at 271 nm as mentioned above (Lide et al., 2005). Spectrophotometric measurements over time were automatically conducted by coupling a Scanning Spectrophotometer UV-1800 UV/Visible (Shimadzu) to a Peristaltic Sipper Pump 206-23790-91 (Shimadzu) and a Sipper Unit 160C (Shimadzu) with glass cell presenting an optical path length of 10 mm. Figure 57 shows the experimental set-up.

A computer program based on a loop structure was set up with the help of Laurent SCHIATTI DE MONZA (from PERSEE, Mines ParisTech, France) allowing an automatic and continuous execution of the device during the whole experiment time:

- At regular time intervals the sipper unit automatically takes sample solution (around 10 mL) from the release bath (Figure 57 A) to the analysis cell in the spectrophotometer using a stepping motor-driven peristaltic pump (Figure 57 B).
- After a waiting time of 30 seconds, a spectrophotometric measurement is performed.
- The taken volume is then dispensed back into the release bath when a new analysis cycle starts.

By coupling the spectrophotometer to an automatic sipping system, the evolution of theophylline concentration in time into the gastro-intestinal fluids can be followed automatically and continuously at precise time intervals (controlled by developed program) during the whole time of drug release experiment.

After reaching a stable saturation absorbance plateau for more than 30 minutes (no more drug released), the remaining aerogel matrix (if any) was crushed with a mortar and pestle, and the bulk medium was sonicated for 30 min to ensure maximum release of the drug. After sample crushing and sonication treatment, the absorbance of the bulk medium was measured to determine the total theophylline concentration.

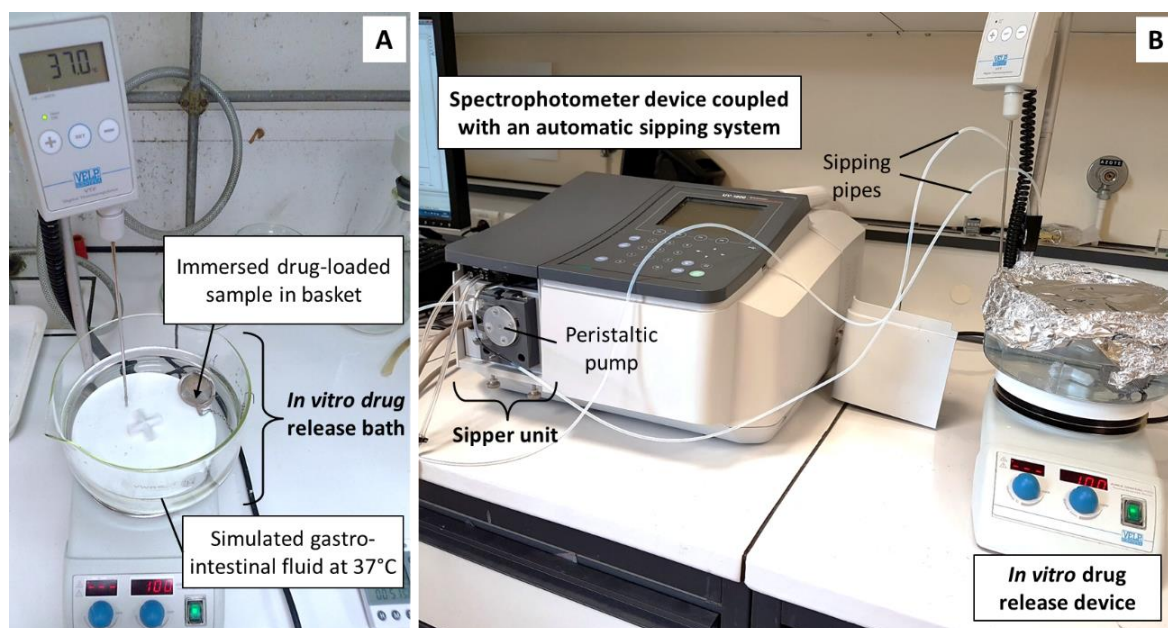


Figure 57. Experimental set-up of *in vitro* drug release experiment: (A) Drug release from a sample into gastro-intestinal fluid at 37.0 °C, (B) Spectrophotometer coupled with drug release device using an automatic sipping system.

Matrix mass and volume were measured in time using digital balance (precision 0.001 g) and caliper (precision 0.1 mm) to estimate water uptake, matrix erosion/dissolution and matrix swelling/shrinkage.

To evaluate the matrices structural and morphological parameters that may impact their drug release behavior, the composition (pectin, cellulose, silica), the sample preparations conditions (wt% of polymer, pH of polymer/starting solution, calcium concentration) and the type of drying (supercritical drying, freeze-drying, evaporative drying) were varied based on the main conclusions presented in Chapter III. Structural properties of pectin aerogels.

### 2.3.5. Cytotoxicity profile of different solid matrices

The cytotoxicity tests were performed at the Intelcentru Lab of “Petru Poni” Institute of Macromolecular Chemistry, Iasi, Romania.

#### ▪ Sample preparation

Prior to cell culture studies, compounds were sterilized by UV exposure with wavelength of 254 nm for 2 hours. Each compound was weighed and mixed with cell culture medium to reach the 1000 µg/ml concentration and allowed to completely solubilize overnight

with the help of a thermoshaker used to assure a thorough mixing at 50°C. Treatment concentrations from 0.49 to 1000 µg/ml were prepared by serial dilutions.

### ▪ MTS assay method

The cytotoxicity of the selected matrices was tested in normal human dermal fibroblasts (NHDF) cells using CellTiter 96®AQueousOne Solution Cell Proliferation Assay (MTS, Promega).

Cells were expanded and maintained in alpha-MEM medium (Lonza) supplemented with 10% fetal bovine serum (FBS, Gibco) and 1% Penicillin-Streptomycin-Amphotericin B mixture (10K/10K/25 µg in 100 ml, Lonza) at 37 °C and 5% CO<sub>2</sub> under humidified atmosphere. For the assay, NHDF cells (PromoCell) were placed in 96-well format (5 x 10<sup>3</sup> cells/well density in 100 µl) for 24 h to ensure cell adhesion; then the media was changed and replaced with the serial dilution of each compound. Control wells received only cell culture medium. A picture of a 96-well format plate used for the cytotoxicity assay of one aerogel sample is shown in Figure 58.

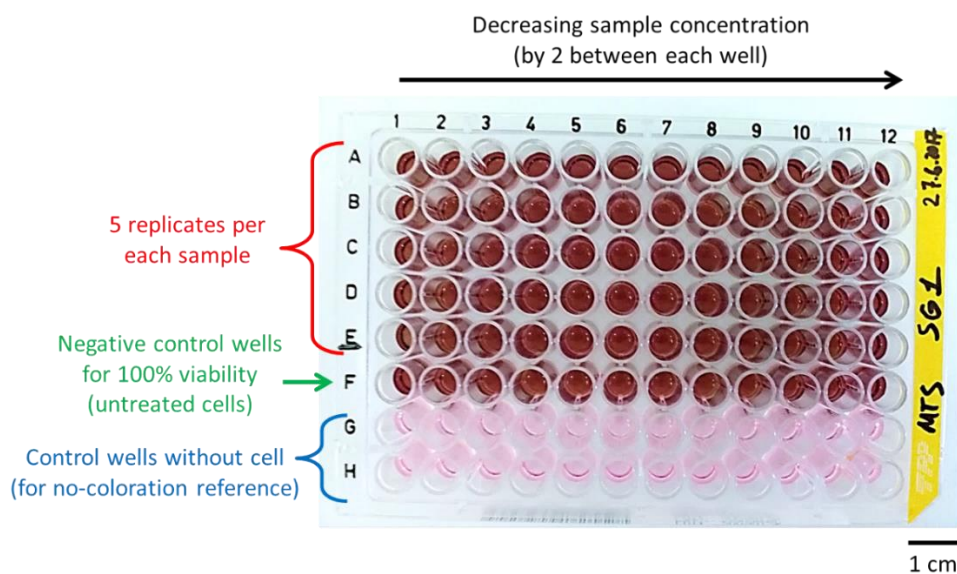


Figure 58. Picture of a 96-well format plate used for the cytotoxicity assay of one sample of aerogel using MTS method. Serial dilutions of sample mixed with culture media were performed and put in contact with NHDF cells (lines A to E). Negative control wells received only untreated cells (without sample) to determine the 100% cell viability (line F), while control wells were filled with cell culture media (without any cell or sample) and were used as coloration reference (lines G and H).

After 44 hours of incubation, a volume of 20 µL of CellTiter 96®AQueousOne Solution reagent was pipetted to each well and the plates were returned to incubator. After another 4 hours the absorbance at 490 nm was recorded with a plate reader (EnSight, PerkinElmer).

Figure 59 shows the visual aspect of NHDF cells within the wells before incubation (Figure 59 A) and after 44 h of incubation (Figure 59 B).

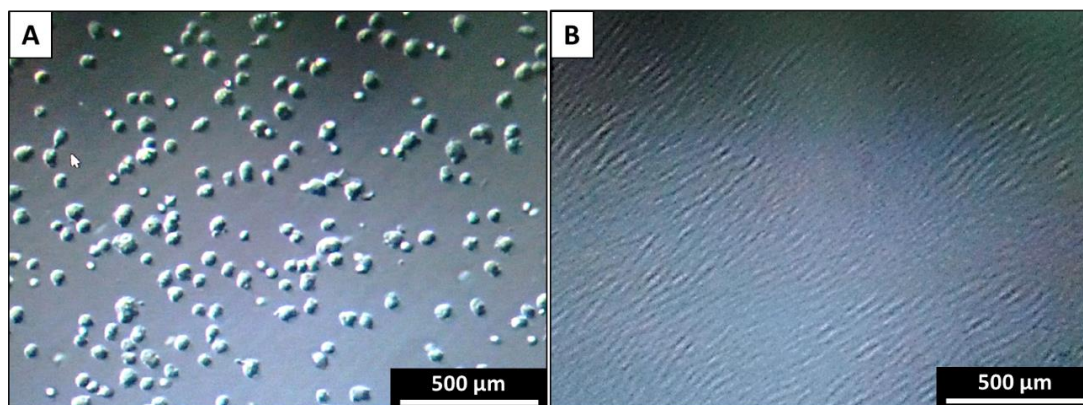


Figure 59. Pictures of NHDF cells in wells observed by phase-contrast microscope (A) before incubation, cells are non-adherent and round-shaped (B) after 44 hours of incubation, a confluent monolayer of elongated adherent cells is obtained.

GraphPad Prism software version 6.04 for Windows (GraphPad Software, San Diego, CA) was used to calculate the relative cell viability. At least 5 replicates were used in the analysis and the experiment was repeated 3 times.

## References

- Buchtová, N., & Budtova, T. (2016). Cellulose aero-, cryo- and xerogels: towards understanding of morphology control. *Cellulose*, 23(4), 2585–2595. <https://doi.org/10.1007/s10570-016-0960-8>
- ChemAxon. (n.d.). Retrieved March 26, 2019, from <https://chemaxon.com/products/marvin>
- FDA/Center for Drug Evaluation and Research. (2019, February). FDA Dissolution Methods Database. Retrieved April 3, 2017, from [https://www.accessdata.fda.gov/scripts/cder/dissolution/dsp\\_SearchResults.cfm](https://www.accessdata.fda.gov/scripts/cder/dissolution/dsp_SearchResults.cfm)
- Fraeye, I., Deroeck, A., Duvetter, T., Verlent, I., Hendrickx, M., & Vanloey, A. (2007). Influence of pectin properties and processing conditions on thermal pectin degradation. *Food Chemistry*, 105(2), 555–563. <https://doi.org/10.1016/j.foodchem.2007.04.009>
- Friedel, H. D., Brown, C. K., Barker, A. R., Buhse, L. F., Keitel, S., Kraemer, J., ... Shah, V. P. (2018). FIP Guidelines for Dissolution Testing of Solid Oral Products. *Journal of Pharmaceutical Sciences*, 107(12), 2995–3002. <https://doi.org/10.1016/j.xphs.2018.08.007>
- Grassi, M., Colombo, I., & Lapasin, R. (2001). Experimental determination of the theophylline diffusion coefficient in swollen sodium-alginate membranes. *Journal of Controlled Release*, 76(1), 93–105. [https://doi.org/10.1016/S0168-3659\(01\)00424-2](https://doi.org/10.1016/S0168-3659(01)00424-2)
- Grassi, Mario, Grassi, G., Lapasin, R., Colombo, I., Grassi, G., Lapasin, R., & Colombo, I. (2006). *Understanding Drug Release and Absorption Mechanisms: A Physical and Mathematical Approach*. <https://doi.org/10.1201/9781420004656>
- Groult, S., & Budtova, T. (2018). Tuning structure and properties of pectin aerogels. *European Polymer Journal*, 108, 250–261. <https://doi.org/10.1016/j.eurpolymj.2018.08.048>
- Gurikov, P., & Smirnova, I. (2018). Non-Conventional Methods for Gelation of Alginate. *Gels*, 4(1), 14. <https://doi.org/10.3390/gels4010014>
- Hayase, G., Kanamori, K., Hasegawa, G., Maeno, A., Kaji, H., & Nakanishi, K. (2013). A Superamphiphobic Macroporous Silicone Monolith with Marshmallow-like Flexibility. *Angewandte Chemie International Edition*, 52(41), 10788–10791. <https://doi.org/10.1002/anie.201304169>
- Hayase, G., Kanamori, K., & Nakanishi, K. (2011). New flexible aerogels and xerogels derived from methyltrimethoxysilane/dimethyldimethoxysilane co-precursors. *Journal of Materials Chemistry*, 21(43), 17077–17079. <https://doi.org/10.1039/C1JM13664J>

- Horvat, G., Xhanari, K., Finšgar, M., Gradišnik, L., Maver, U., Knez, Ž., & Novak, Z. (2017). Novel ethanol-induced pectin-xanthan aerogel coatings for orthopedic applications. *Carbohydrate Polymers*, 166, 365–376. <https://doi.org/10.1016/j.carbpol.2017.03.008>
- Innerlohinger, J., Weber, H. K., & Kraft, G. (2006). Aerocellulose: Aerogels and Aerogel-like Materials made from Cellulose. *Macromolecular Symposia*, 244(1), 126–135. <https://doi.org/10.1002/masy.200651212>
- IUPAC Gold Book. (2017, March 27). Retrieved March 27, 2019, from <https://goldbook.iupac.org/index.html>
- Johannsen, M., & Brunner, G. (1994). Solubilities of the xanthines caffeine, theophylline and theobromine in supercritical carbon dioxide. *Fluid Phase Equilibria*, 95, 215–226. [https://doi.org/10.1016/0378-3812\(94\)80070-7](https://doi.org/10.1016/0378-3812(94)80070-7)
- Krall, S. M., & McFeeters, R. F. (1998). Pectin Hydrolysis: Effect of Temperature, Degree of Methylation, pH, and Calcium on Hydrolysis Rates. *Journal of Agricultural and Food Chemistry*, 46(4), 1311–1315. <https://doi.org/10.1021/jf970473y>
- Lide, D. R., Baysinger, G., Chemistry, S., Berger, L. I., Goldberg, R. N., & Kehiaian, H. V. (2005). *CRC Handbook of Chemistry and Physics*. Boca Raton : CRC Press.
- Malfait, W. J., Zhao, S., Verel, R., Iswar, S., Rentsch, D., Fener, R., ... Koebel, M. M. (2015). Surface Chemistry of Hydrophobic Silica Aerogels. *Chemistry of Materials*, 27(19), 6737–6745. <https://doi.org/10.1021/acs.chemmater.5b02801>
- Masuelli, M. A. (2014). Mark-Houwink Parameters for Aqueous-Soluble Polymers and Biopolymers at Various Temperatures. *Journal of Polymer and Biopolymer Physics Chemistry, Journal of Polymer and Biopolymer Physics Chemistry*, 2(2), 37–43. <https://doi.org/10.12691/jpbpc-2-2-2>
- Renard, C. M. G. C., & Thibault, J.-F. (1996). Degradation of pectins in alkaline conditions: kinetics of demethylation. *Carbohydrate Research*, 286, 139–150. [https://doi.org/10.1016/0008-6215\(96\)00056-0](https://doi.org/10.1016/0008-6215(96)00056-0)
- Robitzer, M., Renzo, F. D., & Quignard, F. (2011). Natural materials with high surface area. Physisorption methods for the characterization of the texture and surface of polysaccharide aerogels. *Microporous and Mesoporous Materials*, 140(1–3), 9–16. <https://doi.org/10.1016/j.micromeso.2010.10.006>
- Rudaz, C. (2013). *Cellulose and Pectin Aerogels: Towards their nano-structuration* (PhD Thesis, Ecole Nationale Supérieure des Mines de Paris). Retrieved from <https://pastel.archives-ouvertes.fr/pastel-00957296/document>

- Rudaz, C., Courson, R., Bonnet, L., Calas-Etienne, S., Sallée, H., & Budtova, T. (2014). Aeropectin: Fully Biomass-Based Mechanically Strong and Thermal Superinsulating Aerogel. *Biomacromolecules*, *15*(6), 2188–2195. <https://doi.org/10.1021/bm500345u>
- Shimizu, T., Kanamori, K., Maeno, A., Kaji, H., & Nakanishi, K. (2016). Transparent Ethylene-Bridged Polymethylsiloxane Aerogels and Xerogels with Improved Bending Flexibility. *Langmuir*, *32*(50), 13427–13434. <https://doi.org/10.1021/acs.langmuir.6b03249>
- Siewert, M., Dressman, J., Brown, C. K., Shah, V. P., Aiache, J.-M., Aoyagi, N., ... Williams, R. (2003). FIP/AAPS guidelines to dissolution/in vitro release testing of novel/special dosage forms. *AAPS PharmSciTech*, *4*(1), 43–52. <https://doi.org/10.1208/pt040107>
- Sing, K. S. W. (1985). Reporting physisorption data for gas/solid systems with special reference to the determination of surface area and porosity (Recommendations 1984). *Pure and Applied Chemistry*, *57*(4), 603–619. <https://doi.org/10.1351/pac198557040603>
- Strøm, R. A., Masmoudi, Y., Rigacci, A., Petermann, G., Gullberg, L., Chevalier, B., & Einarsrud, M.-A. (2007). Strengthening and aging of wet silica gels for up-scaling of aerogel preparation. *Journal of Sol-Gel Science and Technology*, *41*(3), 291–298. <https://doi.org/10.1007/s10971-006-1505-7>
- Tkalec, G., Knez, Ž., & Novak, Z. (2015a). Fast production of high-methoxyl pectin aerogels for enhancing the bioavailability of low-soluble drugs. *The Journal of Supercritical Fluids*, *106*, 16–22. <https://doi.org/10.1016/j.supflu.2015.06.009>
- Tkalec, G., Knez, Ž., & Novak, Z. (2015b). Formation of polysaccharide aerogels in ethanol. *RSC Advances*, *5*(94), 77362–77371. <https://doi.org/10.1039/C5RA14140K>
- U.S. FDA S, Center for Drug Evaluation and Research. (1997). *Extended Release Oral Dosage Forms: Development, Evaluation, and Application of In Vitro/In Vivo Correlations* [FDA Drugs Guidance for Industry]. Retrieved from <https://www.fda.gov/downloads/drugs/guidances/ucm070237.pdf>
- U.S. FDA S, Center for Drug Evaluation and Research. (2018). *Dissolution Testing and Specification Criteria for Immediate-Release Solid Oral Dosage Forms Containing Biopharmaceutics Classification System Class 1 and 3* [FDA Drugs Guidance for Industry]. Retrieved from <https://www.fda.gov/downloads/Drugs/GuidanceComplianceRegulatoryInformation/Guidances/UCM456594.pdf>
- Wijmans, J. G., Altena, F. W., & Smolders, C. A. (1984). Diffusion during the immersion precipitation process. *Journal of Polymer Science: Polymer Physics Edition*, *22*(3), 519–524. <https://doi.org/10.1002/pol.1984.180220313>



# **CHAPTER III. TUNING STRUCTURE AND PROPERTIES OF PECTIN AEROGELS**

---

## CONTENTS

### CHAPTER III. TUNING STRUCTURE AND PROPERTIES OF PECTIN AEROGELS

<b>INTRODUCTION: IMPORTANCE OF AEROGELS' STRUCTURAL PROPERTIES</b>	<b>157</b>
<b>1. CHARACTERIZATION OF PECTINS.....</b>	<b>159</b>
1.1. CHARACTERIZATION OF PECTINS' DEGREE OF ESTERIFICATION.....	159
1.2. DETERMINATION OF PECTIN MOLECULAR WEIGHTS.....	161
<b>2. TUNING STRUCTURE AND PROPERTIES OF LOW METHYLATED PECTIN AEROGELS .....</b>	<b>162</b>
2.1. INFLUENCE OF NON-SOLVENT TYPE AND PECTIN P35 CONCENTRATION ON AEROGEL STRUCTURE AND PROPERTIES .....	163
2.2. INFLUENCE OF PH ON LOW-METHYLATED PECTIN AEROGEL STRUCTURE AND PROPERTIES.....	167
2.3. EFFECT OF CALCIUM IONS ON LOW-METHYLATED PECTIN AEROGEL STRUCTURE AND PROPERTIES .....	172
2.4. EFFECT OF MONOVALENT IONS (NaCl) ON LOW-METHYLATED PECTIN AEROGEL STRUCTURE AND PROPERTIES	175
2.5. DISCUSSION ON THE CORRELATIONS BETWEEN THE PROCESSING PARAMETERS AND THE AEROPECTIN PHYSICAL PROPERTIES.....	178
2.6. MECHANICAL PROPERTIES OF LOW-METHYLATED PECTIN AEROGELS.....	182
2.6.1. <i>Effect of pectin concentration .....</i>	<i>182</i>
2.6.2. <i>Effect of pH of starting pectin solution on the mechanical properties.....</i>	<i>184</i>
2.6.3. <i>Effect of addition of calcium into pectin solution.....</i>	<i>186</i>
2.7. CONCLUSIONS ON THE PROPERTIES OF LOW-METHYLATED PECTIN AEROGELS .....	191
<b>3. EFFECTS OF PECTIN DEGREE OF ESTERIFICATION ON PECTIN AEROGELS STRUCTURAL PROPERTIES.....</b>	<b>191</b>
3.1. IMPACT OF DE ON AEROPECTIN STRUCTURAL PROPERTIES VARYING THE PH.....	192
3.1.1. <i>Impact of pectin DE on the viscosity of pectin solutions while varying the pH .....</i>	<i>193</i>
3.1.2. <i>Impact of pectin DE on aropectin properties while varying the pH.....</i>	<i>194</i>
3.2. IMPACT OF DE ON AEROPECTIN STRUCTURAL PROPERTIES VARYING R(Ca) RATIO .....	198
3.2.1. <i>Effect of DE on gel state at different R(Ca) .....</i>	<i>199</i>
3.2.2. <i>Effect of pH on calcium sensitivity for various DE .....</i>	<i>199</i>
3.3. CONCLUSIONS ON THE INFLUENCE OF PECTIN DE ON AEROPECTINS PROPERTIES .....	204
<b>CONCLUSIONS .....</b>	<b>205</b>
<b>REFERENCES.....</b>	<b>206</b>

## Introduction: importance of aerogels' structural properties

In addition to their biodegradability and biocompatibility, bio-aerogels present very attractive structural properties in terms of high specific surface area, low density, network morphology and pore size. Thus, they are versatile promising materials for a wide range of “classical” aerogel potential applications (from thermal insulation (Druel, Bardl, Vorweg, & Budtova, 2017; Gabrijela Horvat, Fajfar, Uzunalić, Knez, & Novak, 2017; Rudaz et al., 2014) to matrices for catalysis (Chtchigrovsky et al., 2009) and in electro-chemistry when pyrolyzed (Budarin, Clark, Luque, Macquarrie, & White, 2008; Guilminot et al., 2008)). They are also suitable for advanced life science applications, *e.g.* medical devices, biotechnology, pharmaceuticals, cosmetics and food industry. For all these applications, it is well known that the internal structure and physical characteristics of aerogels are determining for their final application properties. The requirements towards aerogel chemical, mechanical and structural properties are dictated by the application. Thus, the understanding of how formulation and external conditions (polymer ionization and concentration, solution pH, presence of ions, *etc.*) influence aerogel properties is a key issue (Aegerter, Leventis, & Koebel, 2011). As an illustration, bio-aerogel density, specific surface area or pore size are critical structural parameters for thermal insulation application (Druel et al., 2017; Rudaz, 2013; Rudaz et al., 2014) or for biomedical uses as drug delivery systems (De Cicco et al., 2016; García-González, Jin, Gerth, Alvarez-Lorenzo, & Smirnova, 2015; Lovskaya, Lebedev, & Menshutina, 2015; Tkalec, Knez, & Novak, 2015) and as 3D cellular scaffolds (G. Horvat et al., 2017; Martins et al., 2015; Quraishi et al., 2015) for tissue engineering.

Despite the importance of morphology control, little is known about the correlations between the type of polysaccharide, processing conditions and aerogel structure and properties. The goal of this work was to show why and how pectin aerogel morphology and properties vary as a function of pectin intrinsic parameters and external conditions. Here we focused on the correlations between the initial polymer characteristics - processing parameters –aerogel structural and mechanical properties.

In the present study, we used three pectins with different Degree of Esterification (DE) of 35%, 59% and 70%, to produce pectin aerogels obtained by polymer dissolution in water, exchange of water to a fluid miscible with CO<sub>2</sub> and supercritical drying with CO<sub>2</sub>. The present investigation provides wide and detailed overview on how and why aerogel structure and mechanical properties vary as a function of external processing conditions and intrinsic pectin characteristics. Pectin concentration, solution pH, type and concentration of metal salts (CaCl<sub>2</sub> and NaCl), nature of non-solvent and pectin's degree of esterification were varied. The role of solution gelation or not, and of the mechanisms of network formation in aerogel precursor are

suggested and discussed. This study demonstrates the ways of controlling structure formation in pectin-based aerogels, and presumably, in other gelling polyelectrolyte polysaccharides. The emphasis is made on the multiscale correlations between the properties of dissolved polymer, mechanisms of network formation and the final structure and properties of pectin aerogels.

The chapter is organized as follows:

- The first part is dedicated to the characterization of three different pectins used in the study.
- Then we selected only the low-methylated pectin (DE = 35%) to finely and deeply study the impact of the external processing parameters on the structural, morphological and mechanical properties of pectin aerogels.
- Finally, we open up the study to different pectins to investigate the influence of pectin DE on aerogel properties regarding to different pH and calcium conditions.

Part of the results presented in the Chapter are published in (Groult & Budtova, 2018).

## 1. Characterization of pectins

### 1.1. Characterization of pectins' degree of esterification

In native pectins, the acid functions are either in form of carboxylic acids (COOH) or are methyl-esterified (COOCH<sub>3</sub>). The Degree of Esterification (DE) corresponds to the molar proportion (%) of methoxy-groups in the pectin. In our study, we used three different citrus pectins, kindly donated by Cargill: a low-methylated pectin with DE of 35% (designed as “P35”), a high/intermediate-methylated pectin with DE of 59% (designed as “P59”) and high-methylated pectin with DE of 70% (designed as “P70”); the values of DE were provided by Cargill. We checked the DE of pectin powders using FTIR technique.

Based on FTIR spectroscopic measurements, major pectin signals can be easily attributed. As shown in Figure 60, a band centered at 1740-1745 cm<sup>-1</sup> is assigned to C=O stretching of esterified groups -COOCH<sub>3</sub> and the band at 1605-1610 cm<sup>-1</sup> is assigned to carboxylate (carboxyl ion) COO<sup>-</sup> (Walter, 2012). In order to completely dissociate carboxylic acid functions (COOH) of galacturonic units of pectin into carboxylates (COO<sup>-</sup>), pectin was dissolved at pH 4.5 (> pK<sub>a</sub>) and dried overnight (at 50°C under vacuum) prior to FTIR analysis. By using the bands height or the peaks area, the pectins' DE can be estimated with the following equations:

$$\textit{Estimated DE (\%)} = \frac{\text{Height peak}_{\text{COOCH}_3}}{(\text{Height peak}_{\text{COOCH}_3} + \text{Height peak}_{\text{COO}^-})} \quad (3.1)$$

$$\textit{Estimated DE (\%)} = \frac{\text{Area peak}_{\text{COOCH}_3}}{(\text{Area peak}_{\text{COOCH}_3} + \text{Area peak}_{\text{COO}^-})} \quad (3.2)$$

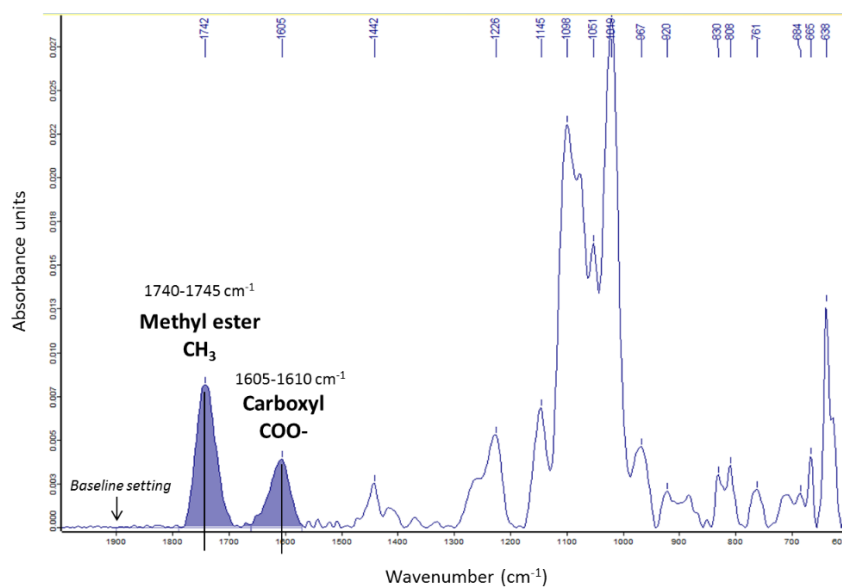


Figure 60. Example of FTIR spectrum of pectin P70. Pectin powder was dissolved at pH 4.5 and dried overnight prior to analysis.

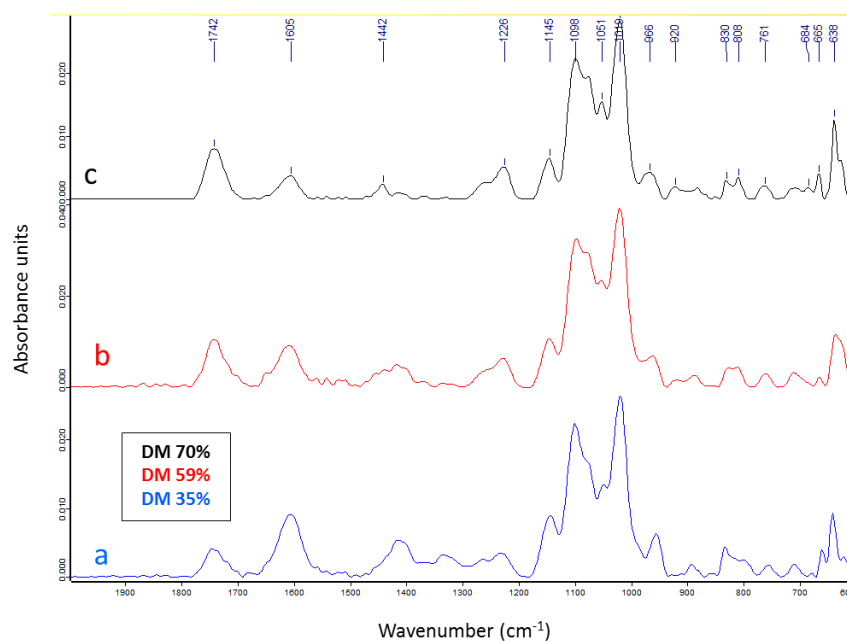


Figure 61. FTIR spectra of pectin (a) P35, (b) P59 and (c) P70. Pectin powders were dissolved at pH 4.5 and dried overnight prior to analysis.

Table 2. FTIR peaks area and band height for methyl-ester and carboxylate signals used for DE estimations of P35, P59 and P70 based on Eq (3.1) and Eq (3.2).

Pectin code	Peaks	Peak wavelenghts range (cm-1)	Peak band (cm-1)	Peak height (u.a.)	Peak area (u.a.)	DE estimation from height ratio (%)	DE estimation from area ratio (%)
						Eq(3.1)	Eq(3.2)
<b>P35</b> (pH 4.5)	Methyl-ester peak (COOCH <sub>3</sub> )	1795 - 1664	1746	0.0047	0.2380	33%	31%
	Carboxylate peak (COO <sup>-</sup> )	1664 - 1566	1606	0.0096	0.5290		
<b>P59</b> (pH 4.5)	Methyl-ester peak (COOCH <sub>3</sub> )	1798 - 1660	1748	0.0108	0.4810	55%	53%
	Carboxylate peak (COO <sup>-</sup> )	1660 - 1571	1607	0.0087	0.4220		
<b>P70</b> (pH 4.5)	Methyl-ester peak (COOCH <sub>3</sub> )	1790 - 1663	1742	0.0082	0.3480	70%	68%
	Carboxylate peak (COO <sup>-</sup> )	1663- 1571	1605	0.0036	0.1660		

As determined from FTIR spectra, the DE of the three citrus pectins of the study were around DE ~ 33-31% for pectin P35, DE ~ 55-53% for pectin P59 and DE ~ 70-68% for pectin P70, all being consistent with the values given by the manufacturer.

## 1.2. Determination of pectin molecular weights

Huggins method was used to determine pectin intrinsic viscosity  $[\eta]$  in 0.01 M NaCl at 26.6 °C (Masuelli, 2014). These conditions were used as far as they allow the calculation of pectin molecular weight  $M$  according to Mark-Houwink equation:

$$[\eta] = KM^a \quad (3.3)$$

where  $K = 0.0234$  and  $a = 0.8221$  (Masuelli, 2014). The dependence of reduced viscosity on pectin concentration for three pectins studied is shown in Figure 62 (a). The intrinsic viscosities of pectins P35, P59, P70 in these conditions were 347 mL/g, 502 mL/g and 566 mL/g, respectively. Their molecular weights were estimated around  $1.15 \cdot 10^5$  g/mol,  $1.86 \cdot 10^5$  g/mol and  $2.15 \cdot 10^5$  g/mol, respectively.

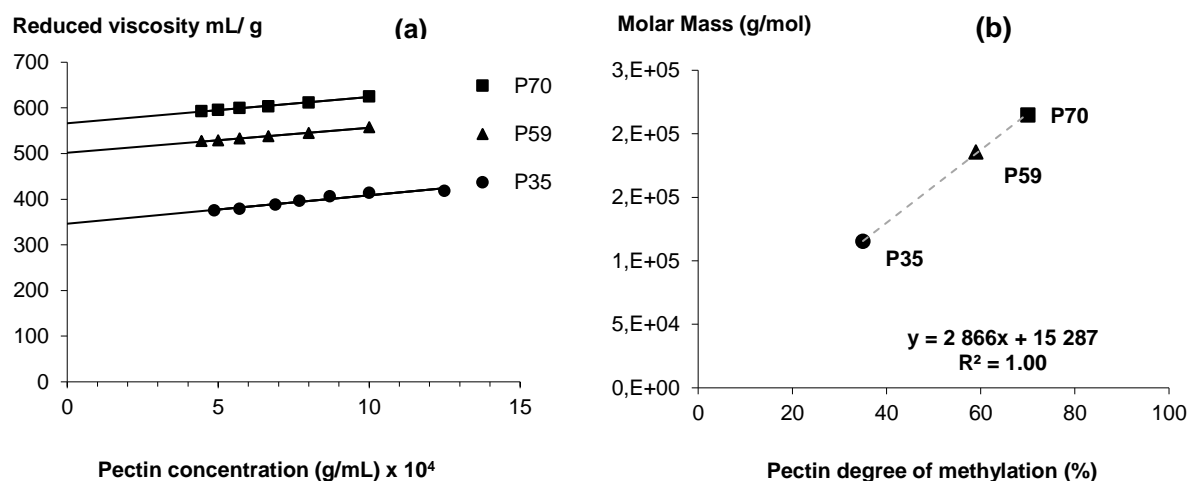


Figure 62. (a) Reduced viscosity of pectin P35, P59 and P70 dissolved in 0.01 M NaCl at 26.6 °C. Solid line is linear approximation. The intersection with Y axis gives intrinsic viscosity. (b) Estimation of pectins' molar mass as a function of their DE.

Figure 62b shows the molecular weight of pectin as a function of its degree of methylation, obtained by capillary viscometry (Masuelli, 2014). Such differences in pectins' molecular weights are known and can be attributed mainly to chemical demethylation treatment of native pectin to obtain low-methylated pectins, the latter are obtained by pectin  $\beta$ -depolymerization with reduction of the neutral sugars, thus reducing Mw (Ilse Fraeye, Duvetter, Doungra, Van Loey, & Hendrickx, 2010; Garnier, Axelos, & Thibault, 1993; Thakur, Singh, Handa, & Rao, 1997).

## 2. Tuning structure and properties of low methylated pectin aerogels

Pectin is a polyelectrolyte, and thus the changes of solution pH and/or addition of ions influence solution viscosity and may induce gelation. Gelation mechanism, in turn, depends on the type of the external parameter. This is well known and described in literature. The open question is how pH, ions' concentration, type of non-solvent influence pectin aerogel morphology and properties. As explained in Chapter II: Material and Methods (see Equation 2.12), when metal cations ( $\text{Na}^+$  or  $\text{Ca}^{2+}$ ) were added to pectin solution, the molar ratio the molar ratio R between pectin carboxyl moieties and metal cations (both expressed in  $\text{mol.L}^{-1}$ ) was used in order to understand of the impact of ions concentration on the properties of pectin. As an illustration, Figure 63 shows examples of different pectin aerogels whose physical properties are controlled by pectin concentration and state of the matter before solvent exchange (solution or gel), pH conditions of the starting solution, presence of  $\text{CaCl}_2$ , etc.

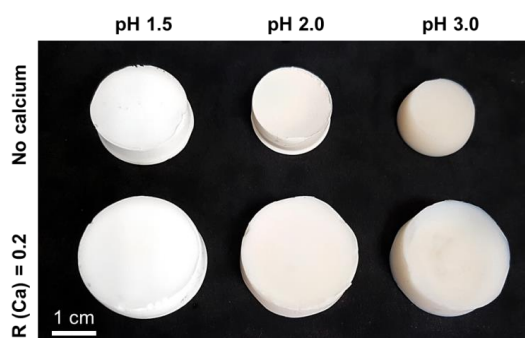


Figure 63. Photos of pectin aerogels from 3 wt% P35 solutions prepared in different conditions at pH 1.5, pH 2.0 and 3.0, without the addition of salts and with addition of calcium at  $R(\text{Ca}) = 0.2$ . Without calcium at pH 1.5 the sample before solvent exchange was weak gel, at pH 2.0 it was high viscosity solution and at pH 3.0 low viscosity solution. At  $R(\text{Ca}) = 0.2$  strong ionic gels were obtained at all pH. Non-solvent was ethanol.

The following sections are structured as follows. We describe the effect of pectin concentration, solution pH, and concentrations of calcium and sodium ions, and the Degree of Esterification of pectin (DE) (from 35% to 70%) on aerogel morphology and properties, keeping one parameter varied and the other constant. Finally, we summarize all findings and make general suggestions on the influence of external and intrinsic parameters and state of the matter, solution or gel, on pectin aerogel properties.

## 2.1. Influence of non-solvent type and pectin P35 concentration on aerogel structure and properties

To study the influence of non-solvent type, acetone vs ethanol, and of pectin concentration on aerogel properties, several batches of pectin P35 solutions from 2 to 8 wt% at pH 3 were prepared. pH 3 was selected because  $pK_a$  is around 3–3.5 for low methylated pectin (Plaschina, Semenova, Braudo, & Tolstoguzov, 1985; Ralet, Dronnet, Buchholt, & Thibault, 2001).

Sample volume shrinkage (see Equation (2.3) from Chapter II) was monitored before and after sc drying and volume shrinkage. As presented in Figure 64, at the end of solvent exchange, the shrinkage is around 10 - 20 vol%, with highest shrinkage for 2% solution (40 vol%), and it is similar for both non-solvents. The overall shrinkage after drying is around 50 – 80 %, it is slightly higher for ethanol as compared to acetone. Shrinkage decreases with the increase of pectin concentration. This phenomenon had already been reported for other bio-aerogels: higher polymer concentration makes the network more “resistant” to solvent exchange and drying (Buchtová & Budtova, 2016; Hoepfner, Ratke, & Milow, 2008).

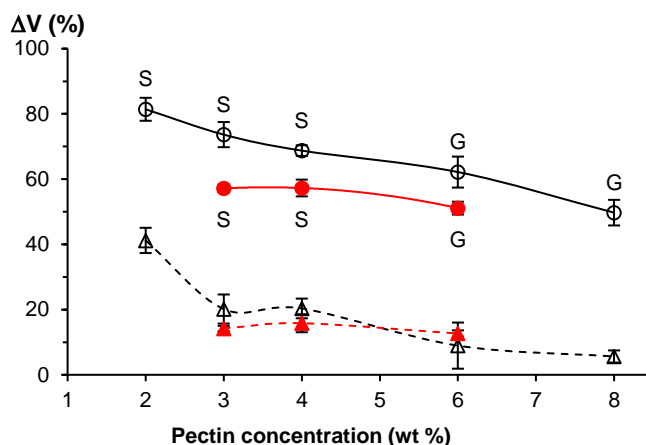


Figure 64. Volumetric shrinkage  $\Delta V$  after solvent exchange (triangles) and after sc drying (circles) as a function of pectin concentration. Pectin P35 was dissolved at pH 3; non-solvent was either ethanol (open points) or acetone (filled points). If not visible, the errors are smaller or of the size of symbols. The state of the matter before solvent exchange, solution (S) or gel (G), is indicated for each case. Lines are given to guide the eye. From (Groult & Budtova, 2018)

Figure 65a and b present pectin aerogel density and specific surface area as a function of pectin concentration and type of non-solvent at pH 3. The use of acetone resulted in lower density and higher specific surface area. For example, for the initial solutions of 3 wt%, aerogel density was around  $0.11 \text{ g/cm}^3$  and specific surface around  $570 \text{ m}^2/\text{g}$  when using ethanol as the non-solvent, whereas while using acetone the density was  $0.065 \text{ g/cm}^3$  and specific surface reached the values up to  $630 \text{ m}^2/\text{g}$ . Similar phenomena were recorded for aerogels made at pH 2 (Figure 66).

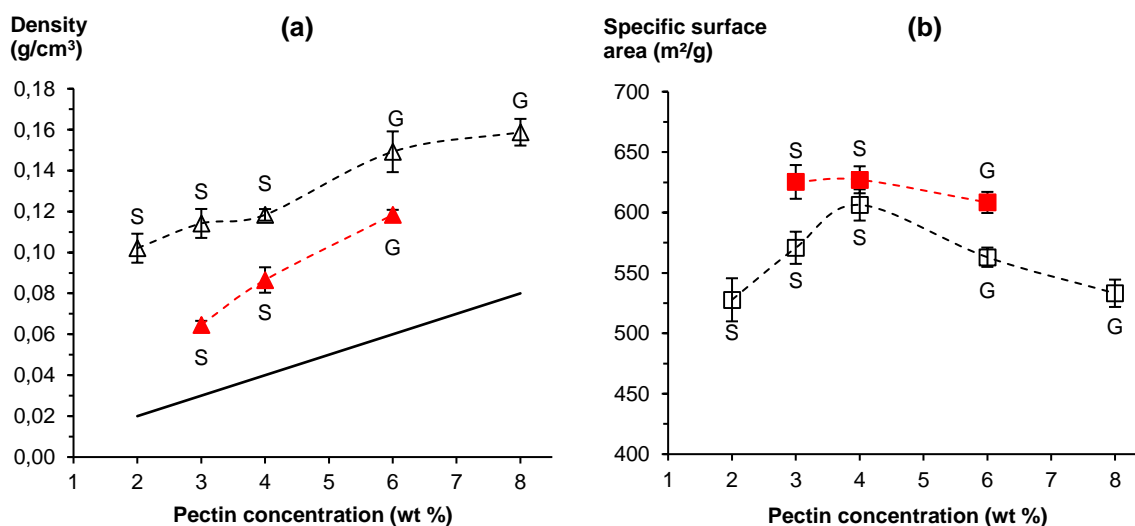


Figure 65. Density (a) and specific surface area (b) as a function of pectin concentration for solvent exchange performed in ethanol (open points) and acetone (filled points). Pectin P35 was dissolved at pH 3.0, the state of the matter before solvent exchange, solution (S) or gel (G), is

indicated for each case. Solid line is theoretical density for no-shrinkage case; dashed lines are given to guide the eye.

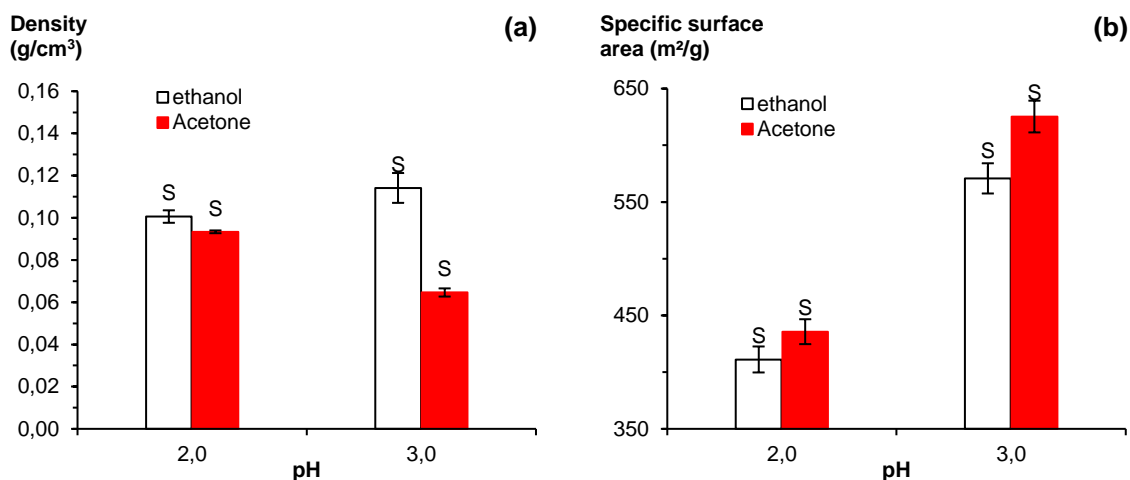


Figure 66. Comparison of (a) density and (b) specific surface area of pectin aerogels made from 3 wt% P35 solution at pH 2 and 3, using either ethanol (open) or acetone (filled) as the non-solvent. The state of the matter before solvent exchange, solution (S) or gel (G), is indicated for each case.

Some works on bio-aerogels suggest that the larger the difference in Hansen solubility parameters between the polymer and non-solvent, the higher is sample shrinkage (Gavillon & Budtova, 2007; Subrahmanyam, Gurikov, Dieringer, Sun, & Smirnova, 2015). However, pectin is heteroglycan and Hansen parameter(s) are not known. It may be possible that the miscibility of non-solvent and CO<sub>2</sub> also plays a role: acetone is better miscible with CO<sub>2</sub> than ethanol according to Hansen solubility parameters (of ethanol it is 26.5 MPa<sup>1/2</sup>, of acetone 19.9 MPa<sup>1/2</sup> and of CO<sub>2</sub> 17.4 MPa<sup>1/2</sup>) (Hansen, 2007). In all the cases studied density of pectin aerogels was from two (for acetone) to more than three (for ethanol) times higher than that of the theoretical no-shrinkage case (Figure 65a.). As expected, density increases with the increase of polymer concentration in solution.

It is difficult to conclude now on the influence of pectin concentration on specific surface area. The reason is that at pH 3, pectin dissolved at 2, 3 and 4 % is solution, and at 6 and 8 % it is gel. Previous studies on cellulose aerogels (Buchtová & Budtova, 2016; Trygg, Fardim, Gericke, Mäkilä, & Salonen, 2013) reported the increase of specific surface area with the increase of polymer concentration which is also the case for pectin aerogels made from 2, 3 and 4 % solutions. The result for cellulose aerogels was interpreted by the decrease of pore size and not increase of pore wall thickness with the increase of polymer concentration (Buchtová & Budtova, 2016). In the case of cellulose, the state of the matter before solvent exchange was the same through all experiments: it was a solution for cellulose dissolved in ionic liquid and in NaOH-urea-water (Buchtová & Budtova, 2016; Trygg et al., 2013). As it will be shown later,

the state of the matter before solvent exchange strongly influences pectin shrinkage and thus aerogel density and morphology.

Pectin aerogel porosity and pore volume (see Equations 2.4 and 2.5 of Chapter II, respectively) of the same samples as shown in Figure 65 are shown in Figure 67. All values are lower for aerogels prepared with ethanol as non-solvent as compared to those prepared with acetone, which is expected from the values of density and specific surface area. The increase of pectin concentration leads to the decrease in porosity and pore volume for both types of non-solvents used. Pore volume varies from 5.6 to 9.1 cm<sup>3</sup>/g for aerogels made with ethanol as non-solvent and it is 30 to 80 % higher for acetone case.

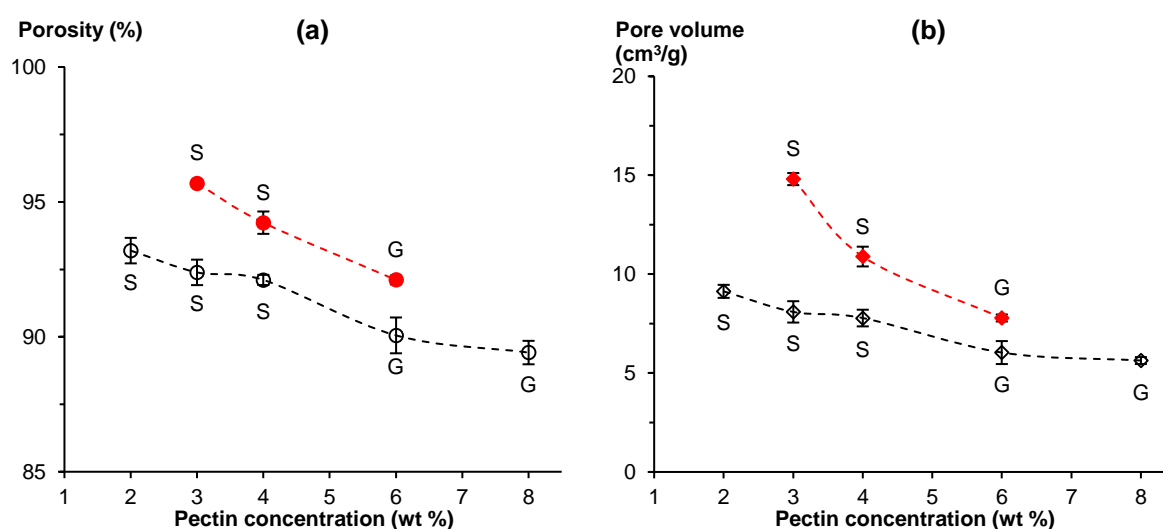


Figure 67. (a) Pectin aerogel porosity and (b) specific pore volume as a function of pectin concentration for solvent exchange performed in ethanol (open points) and acetone (filled points). Pectin P35 was dissolved at pH 3.0, the state of the matter before solvent exchange, solution (S) or gel (G), is indicated for each case. Dashed lines are given to guide the eye.

SEM images of pectin aerogel morphology are presented in Figure 69, for two pectin concentrations and two non-solvents. Solvent exchange with acetone resulted in slightly larger pores with less agglomerated pore walls compared to ethanol. The increase of pectin concentration makes the network denser and with smaller pores. The thickness of pore walls is around 7 to 14 nm as estimated from Figure 69, with some rare chain agglomerates/packages from around 20 to 30 nm of thickness, see an example on Figure 68.

Average fibril size  $D$  can also be roughly calculated as  $D = 4/(\rho_{\text{bulk}}S_{\text{BET}})$  assuming that fibrils are ideal rods of uniform thickness and the same skeletal density. With  $S_{\text{BET}}$  varying from 530 to 630 m<sup>2</sup>/g,  $D$  is around 4 to 5 nm, which fits well the experimental observations after subtracting from the latter few nanometers of sputtered platinum.

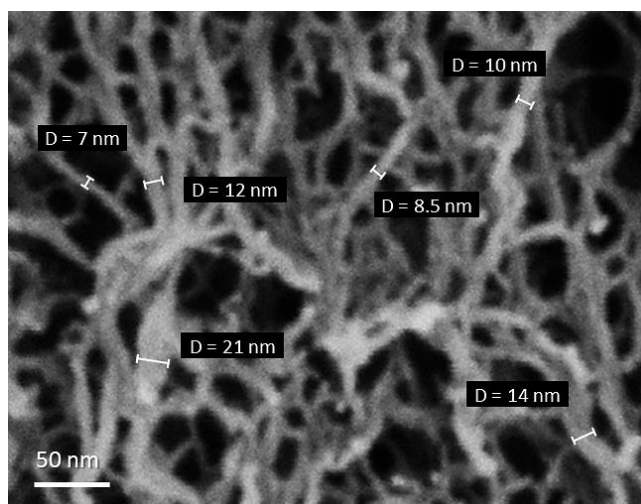


Figure 68. High magnification SEM image of pectin aerogel made from 3 wt% pectin P35 made at pH 3 using acetone as non-solvent. Fibril thicknesses  $D$  (in nm) were estimated using SEM software.

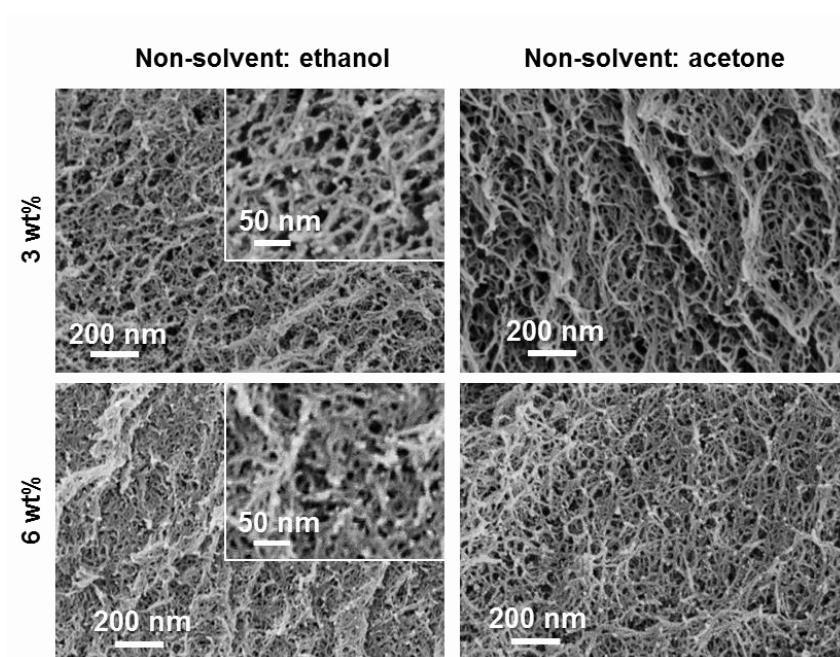


Figure 69. SEM images of pectin aerogels made from 3 wt% and 6 wt% pectin P35 solutions at pH 3, with ethanol (a) or acetone (b) as non-solvent.

## 2.2. Influence of pH on low-methylated pectin aerogel structure and properties

It is known that dissolved pectin, being a polyelectrolyte, is very sensitive to pH. At low pH chains associate and are stabilized by hydrogen bonding between un-dissociated free carboxylic acids and secondary alcohol groups, and by hydrophobic interactions between

methyl esters (Oakenfull, 1991). This is reflected by change of solution viscosity at lower polymer concentration, and may lead to so-called acid gelation if the number of junction zones is sufficient, the latter depending on solution temperature and pectin concentration (Garnier et al., 1993; Kar & Arslan, 1999; Paoletti, Cesaro, Delben, & Ciana, 1986; Voragen, Schols, & Visser, 2013).

To better understand the influence of pH on pectin aerogel structure and properties, we illustrate the effect of pH on pectin chains' interactions via viscosity  $\eta$  of semi-dilute pectin solutions (0.9 wt%) as a function of shear rate  $\dot{\gamma}$  (Figure 70). At pH below  $pK_a \approx 3$ , solutions showed a strong shear-thinning behavior, and viscosity increases with decreasing pH due to macromolecules association. This is especially pronounced at pH below 2.5 when ionization of pectin chains is significantly reduced. At higher pectin concentrations and below pH 2 solutions may form a gel. The increase of pH above  $pK_a$  leads to progressive deprotonation of carboxylic acids into carboxylates. The coulombic repulsion and high hydration of pectin macromolecules prevent polymer aggregation (Paoletti et al., 1986). Beyond pH 4 practically no evolution of viscosity as a function of pH was observed, as ionization of carboxylates is supposed to be complete. In this case, pectin solutions exhibit stable and low viscosity as each polysaccharide chain is hydrated, extended and independent (Paoletti et al., 1986).

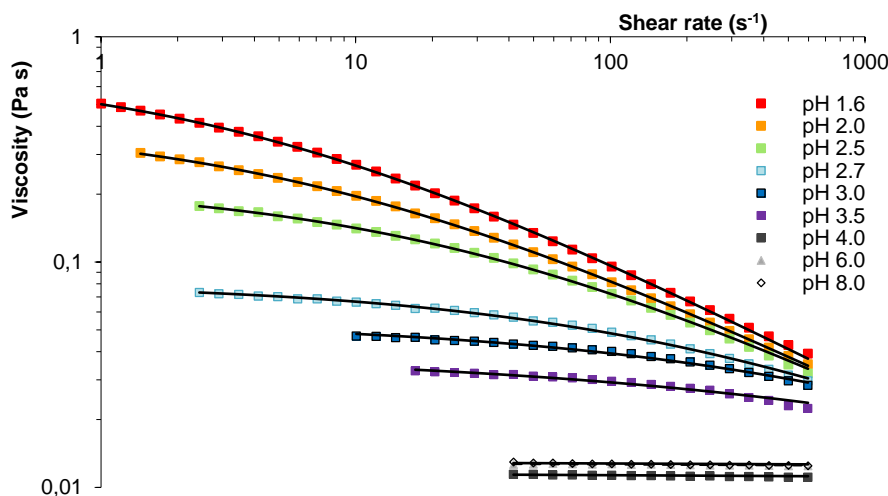


Figure 70. Viscosity as a function of shear rate of 0.9 wt% pectin P35 solutions at different pH at 20 °C. Solid lines correspond to viscosity approximated with Cross model. From (Groult & Budtova, 2018).

The flow curves were fitted using simplified Cross model:

$$\frac{\eta(\dot{\gamma})}{\eta_0} = \frac{1}{1+(\alpha \cdot \dot{\gamma})^n} \quad (3.4)$$

where  $\eta_0$  is zero shear rate viscosity,  $\alpha$  is constant and  $n$  is flow index (or Cross exponent). The fitting parameters are presented in Table 3. Zero shear rate viscosity and flow index as a function of pH are shown in Figure 71. These results confirm what was qualitatively deduced from Figure 70: a strong drop of zero shear rate viscosity and of flow index with the increase of pH and the independence of these parameters on pH at pH > 4.

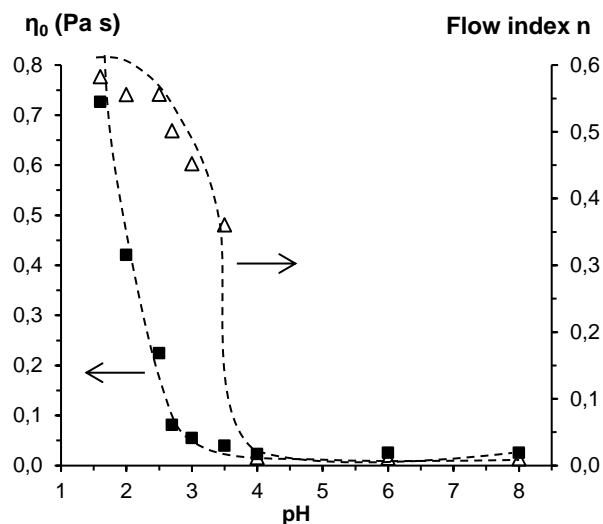


Figure 71. Zero shear rate viscosity (squares) and flow index (triangles) (see Eq. (3.4)) of 0.9 wt% pectin P35 solutions as a function of pH at 20 °C. Dashed lines are given to guide the eye. From (Groult & Budtova, 2018).

Table 3. Fitting parameters for flow curves (Figure 71) according to Eq.(3.4)

pH	1.6	2	2.5	2.7	3	3.5	4	6	8
<b>n</b>	0.5824	0.5556	0.5562	0.5016	0.4519	0.3606	0.0116	0.0110	0.0100
<b><math>\eta_0</math> (Pa s)</b>	0.7262	0.4202	0.2240	0.0810	0.0546	0.0394	0.0226	0.0252	0.0254
<b><math>\alpha</math> (s)</b>	0.2507	0.1279	0.0378	0.0046	0.0012	0.0005	0.0048	0.0043	0.0046

Next pectin aerogels were made from 3 wt% solutions at various pH. Acid-induced gels were obtained at room temperature and pH of 0.5, 1.0, 1.5 and pH 1.8. At higher pH solutions were not gelling and aerogel precursors were obtained by direct solvent exchange with ethanol. In this case, viscosity of pectin solutions had to be sufficiently high for not deformed 3D network to be formed; for example, it was not possible to obtain homogenous aerogels from solutions at pH > 5.

Figure 72a shows the shrinkage of pectin samples after solvent exchange and after drying and Figure 72b corresponds to density and specific surface area of the prepared pectin aerogels.

A very interesting trend was obtained: all parameters show a convex shape as a function of pH, with the highest values of density and specific surface area almost tripled in the maximum.

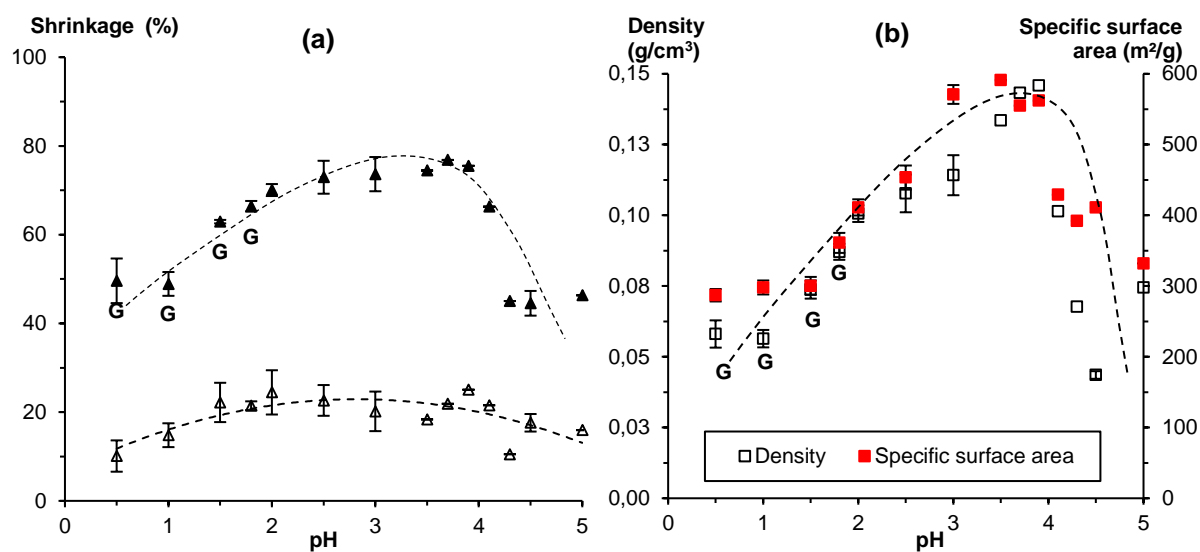


Figure 72. Influence of pH on (a) volumetric shrinkage after solvent exchange (open points) and after sc-drying (filled points) and (b) density (open points) and specific surface area (filled points) of pectin aerogels made from 3 wt% P35 solutions. The state of the matter before solvent exchange is noted “G” for gel, the rest are solutions. Non-solvent used was ethanol. Dashed lines are given to guide the eye. From (Groult & Budtova, 2018).

Shrinkage is around 10 – 20 vol% after solvent exchange and it strongly increases after sc drying, especially for non-gelled solutions at pH > 2. The lower pH, the stronger pectin network (Capel, Nicolai, Durand, Boulenger, & Langendorff, 2006), providing better mechanical resistance to solvent exchange and drying. Gel state prevents shrinkage and preserves gel porous structure resulting in lower density and lower specific surface area (Figure 72b.).

Pectin aerogels at pH 0.5, 1 and 1.5 display large pores and thick pore walls (Figure 73). Porosity is around 95 – 96 % and pore volume around 13 – 17 cm<sup>3</sup>/g (Figure 74). It should be noted that at very low pH (pH ≤ 1) pectin acid degradation may have occurred as reported in Ref. (I Fraeye et al., 2007; Krall & McFeeters, 1998; Renard & Thibault, 1996), resulting in partly damaged morphology as observed by SEM (Figure 73).

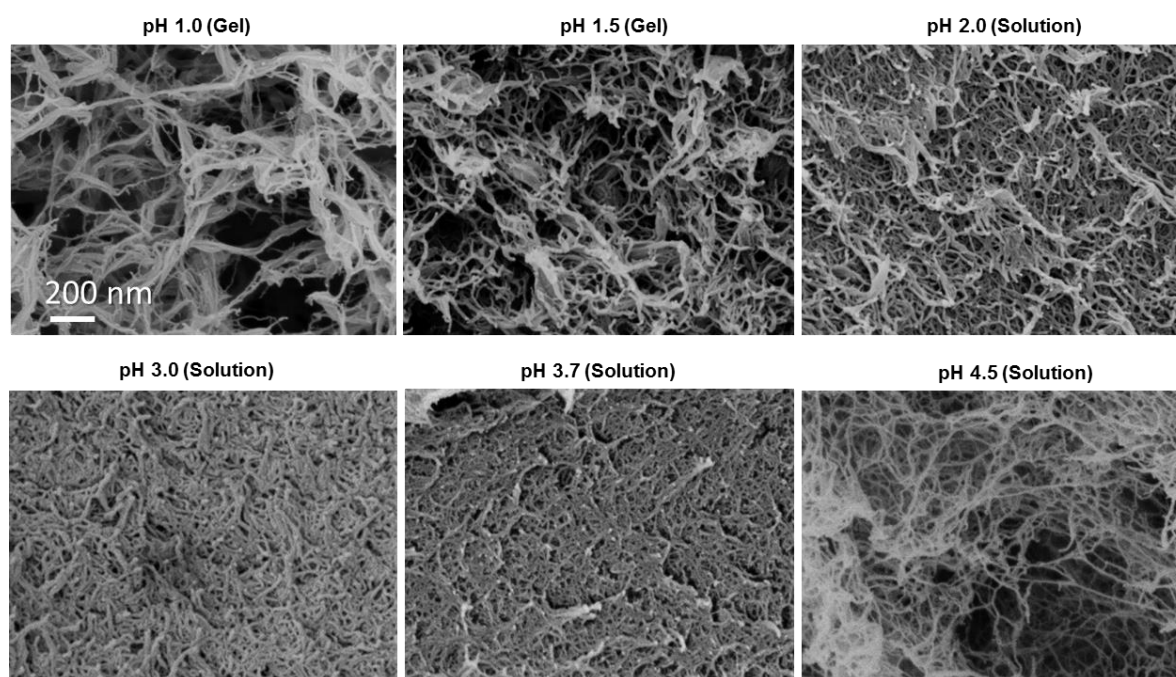


Figure 73. SEM images of pectin aerogel morphology made from 3 wt% P35 solutions at different pH. The state of the matter before solvent exchange is indicated for each case. Non-solvent used was ethanol. The scale is the same for all SEM images. From (Groult & Budtova, 2018).

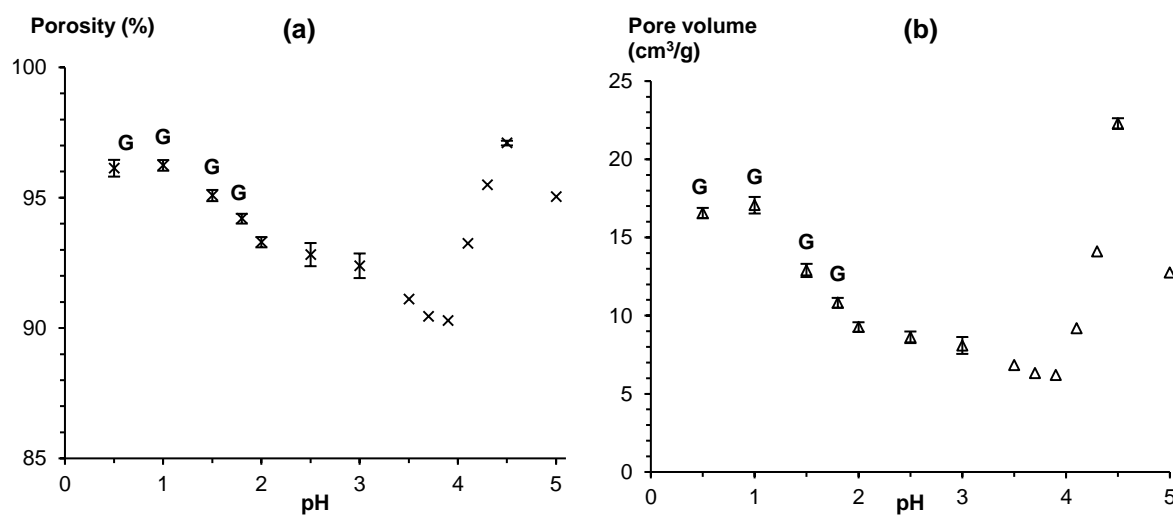


Figure 74. (a) Porosity and (b) pore volume of pectin aerogels made from 3 wt% P35 solutions at different pH, non-solvent was ethanol. The state of the matter before solvent exchange is noted “G” for gel, the rest are solutions. From (Groult & Budtova, 2018).

With the increase of pH from 1.8 to 3 – 3.5, progressive ionization of pectin chains occurred decreasing the probability of their association, and gelation was inhibited. This induced high sample shrinkage, up to 75 vol% (Figure 72a), resulting in the increase of pectin aerogel density (Figure 72b). As a consequence, aerogel porosity and pore volume decreased

to 90% and 6 cm<sup>3</sup>/g, respectively (Figure 74). High shrinkage led to denser morphology and decrease of pore size (Figure 73): for example, pore size varied from 50 – 300 nm at pH 1 to much more homogeneous sizes around 30 – 50 nm at pH 3 as estimated from SEM images. Because at pH 3 – 3.5 aerogel density still remained low and pore size decreased as compared to pH 1 - 2, specific surface area strongly increased as pH increased, from around 300 m<sup>2</sup>/g at pH 1.5 to almost 600 m<sup>2</sup>/g at pH 3. We assume that at pH 3 – 3.5 due to the repulsion between charged chains their agglomeration was inhibited which led to higher specific surface area. Finally, due to complete pectin ionization at pH above 4, viscosities of pectin solutions were too low to lead to monolithic “non-damaged” samples during solvent exchange. After sc drying, pectin aerogels appeared to have very heterogeneous morphology, as can be seen in Figure 73, with lower mean bulk density and specific surface as compared to pH 3 – 3.5.

### **2.3. Effect of calcium ions on low-methylated pectin aerogel structure and properties**

The addition of divalent cations strongly impacts pectin gelation mechanism and thus potentially allows the variation of aerogel properties (Dronnet, Renard, Axelos, & Thibault, 1996; Thibault & Rinaudo, 1986). As described by the so-called “egg-box model” (Grant, Morris, Rees, Smith, & Thom, 1973), the ionized groups of non-methylated galacturonic acid on pectin backbone can create successive ionic bonds with divalent cations such as calcium (Dronnet et al., 1996; Rudolf Kohn, 1987). The ionic bonding results from non-covalent electrostatic interactions between free divalent cations and the oxygen atoms of the hydroxyl groups, the oxygen atoms of the glucosidic ring and the bridging oxygen atoms of dissociated galacturonic acids through their free-electron pairs (Rudolf Kohn, 1987). Besides, the cross-linking formed by ionic bonds between carboxylate functions and divalent cations, such as calcium, produce strong, brittle and less elastic pectin gels than those formed by hydrogen and hydrophobic interactions in acidic condition (Sriamornsak, 2003). The properties and mechanisms of pectin ionic gelation are detailed in Chapter I – Section 1.3.2.

In order to understand the influence of calcium ions on the morphology and properties of pectin aerogels, we varied calcium concentration (or the molar ratio of calcium to pectin, R(Ca)) at fixed pectin concentration 3 wt% and pH 3 which is pK<sub>a</sub> of LM pectin. The photos of the obtained pectin aerogels with increasing R(Ca) ratio are given in Figure 75.

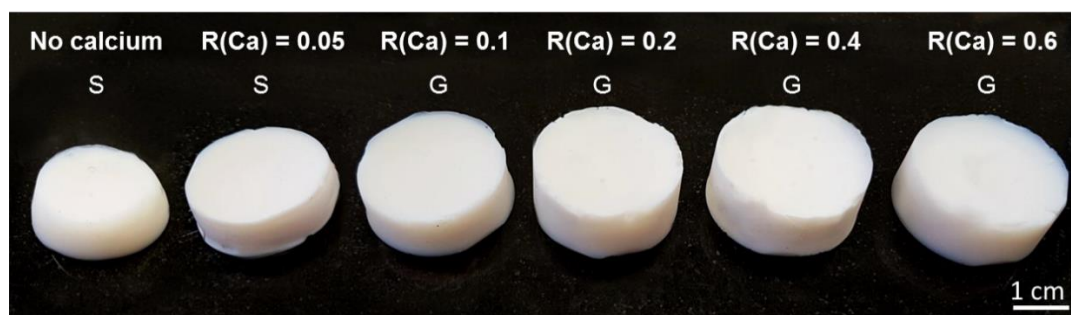


Figure 75. Pectin aerogels made from 3 wt% P35 dissolved at pH 3, with increasing  $R(\text{Ca})$  from 0 to 0.6, non-solvent was ethanol. The state of the matter before solvent exchange, solution (S) or gel (G), is indicated for each case. From (Groult & Budtova, 2018).

The addition of even low amount of calcium increases pectin solution viscosity; at  $R(\text{Ca}) = 0.1$  a weak gel and at  $R(\text{Ca}) \geq 0.2$  strong gels are formed. The influence of  $R(\text{Ca})$  on samples' volumetric shrinkage is shown in Figure 76a and on aerogel density and specific surface area in Figure 76b. Shrinkage of pectin samples decreases with the increase of  $R(\text{Ca})$  as calcium reinforces the network by the formation of large amount of strong ionic junction zones (Cárdenas, Goycoolea, & Rinaudo, 2008; Ilse Fraeye et al., 2009; Grosso & Rao, 1998; Löfgren, Walkenström, & Hermansson, 2002). As a result, density of aerogels strongly decreases from  $0.11 \text{ g/cm}^3$  without calcium to more than twice lower value, around  $0.05 \text{ g/cm}^3$ , for  $R(\text{Ca})$  above 0.2 (Figure 76b). Consequently, porosity and pore volume increase with the increase of calcium concentration (Figure 77).

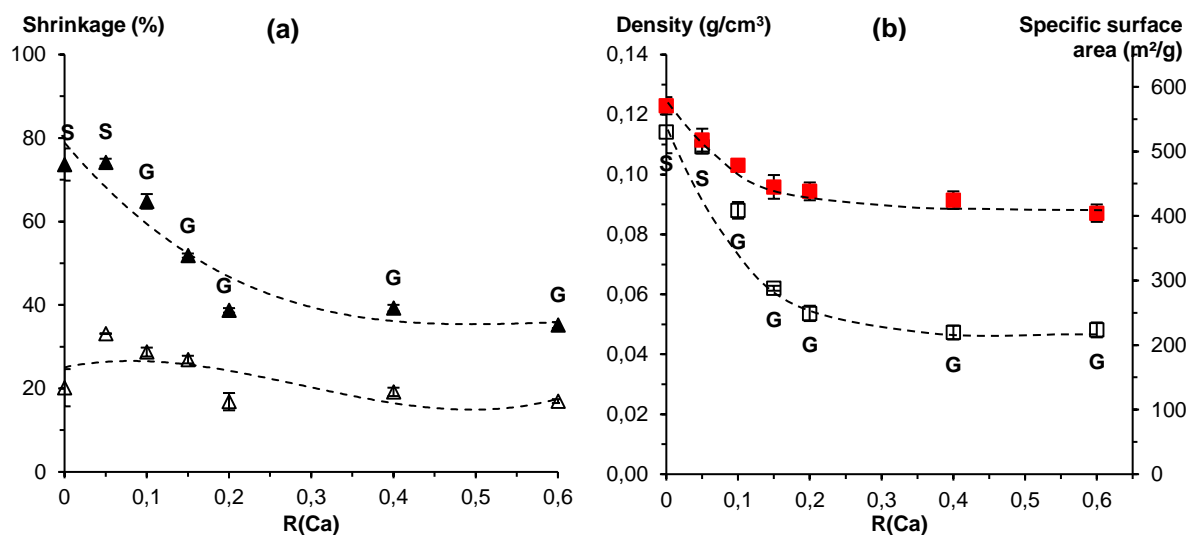


Figure 76. Influence of calcium to pectin molar ratio  $R(\text{Ca})$  on (a) shrinkage after solvent exchange (open points) and after solvent drying (filled points) and (b) density (open points) and specific surface area (filled points) of pectin aerogels made from 3 wt% P35 solutions at pH 3, non-solvent was ethanol. The state of the matter before solvent exchange, solution (S) or gel (G), is indicated for each case. Lines are given to guide the eye. From (Groult & Budtova, 2018).

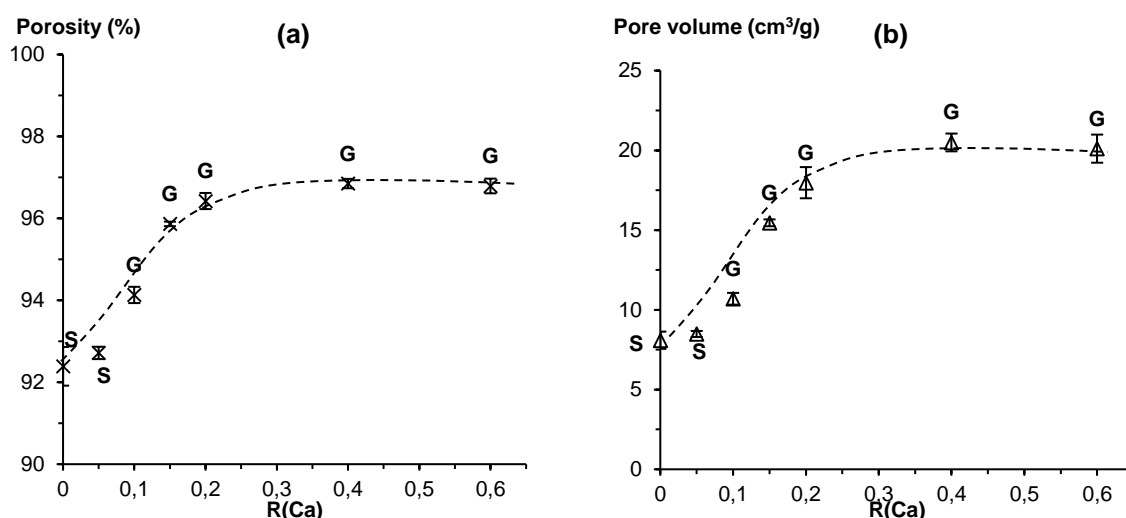


Figure 77. Influence of calcium to pectin molar ratio on (a) porosity and (b) pore volume for pectin aerogels made from 3 wt% P35 at pH 3, non-solvent was ethanol. The state of the matter before solvent exchange, solution (S) or gel (G), is indicated for each case. From (Groult & Budtova, 2018).

Specific surface areas of pectin aerogels decreased from around 600 to around 400 m<sup>2</sup>/g with R(Ca) increase from 0 to 0.2, respectively (Figure 76b). The same trend for shrinkage, density and specific surface area was also found at pH 2 (Figure 78). It has to be noted that at pH 2 the addition of calcium had a smaller impact on pectin aerogel properties as far as carboxyl deprotonation of galacturonic groups is lower at pH 2 than at pH 3 (Gidley, Morris, Murray, Powell, & Rees, 1980).

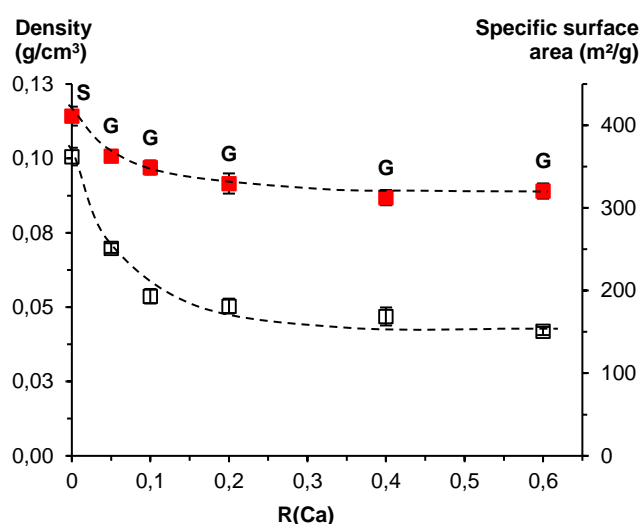


Figure 78. Density (open points) and specific surface area (filled points) of pectin aerogels made from 3 wt% P35 solutions at pH 2 as a function of calcium to pectin molar ratio R(Ca). The state of the matter before solvent exchange, solution (S) or gel (G), is indicated for each case. Non-solvent was ethanol. Lines are given to guide the eye. From (Groult & Budtova, 2018).

The addition of calcium has a strong impact on pectin aerogel morphology, as shown on the representative SEM images in Figure 79. The higher the  $R(\text{Ca})$ , the stronger the gels with less shrinkage and larger pores, from around 30-50 nm (as estimated from SEM images) without calcium to 100 - 150 nm at  $R(\text{Ca}) > 0.2$ . Similarly to acid gelation by lowering pH (see Section 2.2), calcium induced gelation leads to better preservation of network morphology and of macropores, as observed by SEM. Beyond  $R(\text{Ca}) = 0.2$ , the morphology of aerogels is quite similar, except that very fast gelation at  $R(\text{Ca}) > 0.4$  led to heterogeneities due to unevenly dispersed calcium ions. The reason is that the maximum amount of calcium possible to be bound to pectin is around stoichiometric ratio, 0.3 to 0.6 depending on pectin degree of methylation (Dronnet et al., 1996; Garnier, Axelos, & Thibault, 1994; Siew, Williams, & Young, 2005), which corresponds to molar ratio  $R(\text{Ca})$  from 0.15 to 0.3 as used in this work.

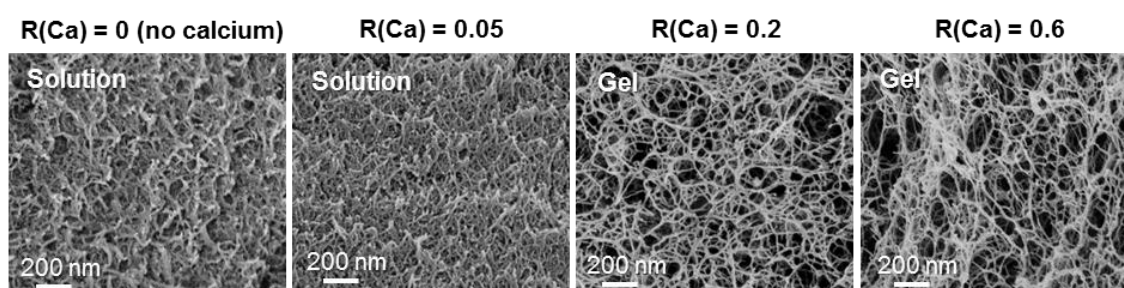


Figure 79. SEM images of pectin aerogels made from 3 wt% P35 solutions at pH 3 with calcium chloride at  $R(\text{Ca}) = 0.05$ , 0.2 and 0.6. The state of the matter before solvent exchange is indicated for each case. Non-solvent used was ethanol. From (Groult & Budtova, 2018).

#### 2.4. Effect of monovalent ions (NaCl) on low-methylated pectin aerogel structure and properties

Monovalent metal ions also influence pectin solution viscosity and may induce solution gelation (Agoda-Tandjawa, Durand, Gaillard, Garnier, & Doublier, 2012; Ström, Schuster, & Goh, 2014; Yoo, Fishman, Savary, & Hotchkiss, 2003). Although ions as sodium cannot create ionic bonds with pectin, they decrease electrostatic repulsions between dissociated carboxyl groups by screening (Agoda-Tandjawa et al., 2012; M. a. V. Axelos, 1990). This allows chains approaching each other and promotes hydrogen bonding and hydrophobic interactions potentially leading to a sort of acid-induced gelation (Agoda-Tandjawa et al., 2012). Here we demonstrate the impact of the presence of sodium ions on pectin aerogel properties and morphology (see photos of aerogels in Figure 80). The molar ratio of sodium to pectin  $R(\text{Na})$  was varied from 0 to 2; at  $R(\text{Na}) \geq 1$  (NaCl concentration 0.1 M) strong turbid gels were obtained.

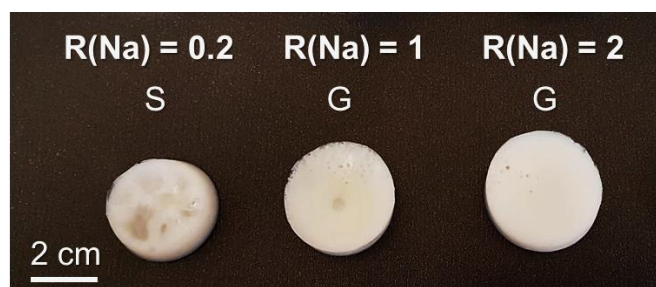


Figure 80. Photos of pectin aerogels made from 3 wt% P35 solutions at pH 3 with different amount of NaCl added. Samples were solutions at  $R(\text{Na}) = 0.2$  and strong gels at  $R(\text{Na}) = 1$  and  $R(\text{Na}) = 2$ . Non-solvent was ethanol. From (Groult & Budtova, 2018).

Figure 81a shows samples' shrinkage as a function of sodium to pectin molar ratio for solutions of 3 wt% at pH 3. As for the case of the addition of calcium (Figure 76a), the presence of sodium ions resulted in lower shrinkage due to solution gelation.

As a consequence, the increase in sodium concentration led to pectin aerogel lower density, from of  $0.114 \pm 0.007 \text{ g/cm}^3$  at  $R(\text{Na}) = 0$  to  $0.069 \pm 0.001 \text{ g/cm}^3$  at  $R(\text{Na}) = 2$  (Figure 81b), higher porosity and pore volume (Figure 82). Specific surface area (Figure 81b) decreased with the increase of  $R(\text{Na})$ , also as in the case of the addition of calcium. Similar trends were recorded for pectin aerogels made from higher pectin concentration, 6 wt% (Figure 83).

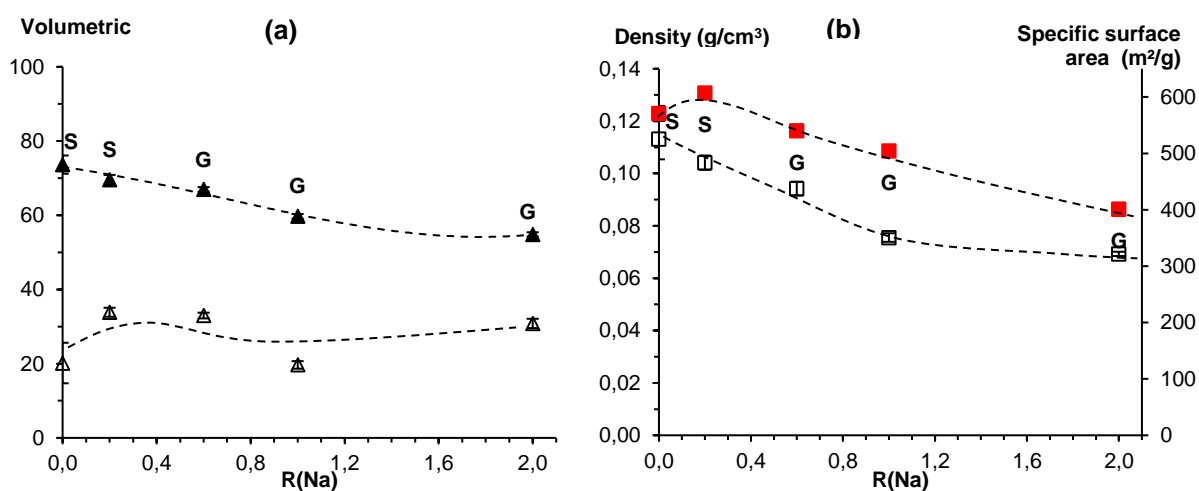


Figure 81. Influence of sodium to pectin molar ratio  $R(\text{Na})$  on (a) shrinkage after solvent exchange (open points) and after drying (filled points) and (b) density (open points) and specific surface area (filled points) of pectin aerogels made from 3 wt% P35 solutions at pH 3, non-solvent was ethanol. The state of the matter before solvent exchange, solution (S) or gel (G), is indicated for each case. Lines are given to guide the eye. From (Groult & Budtova, 2018).

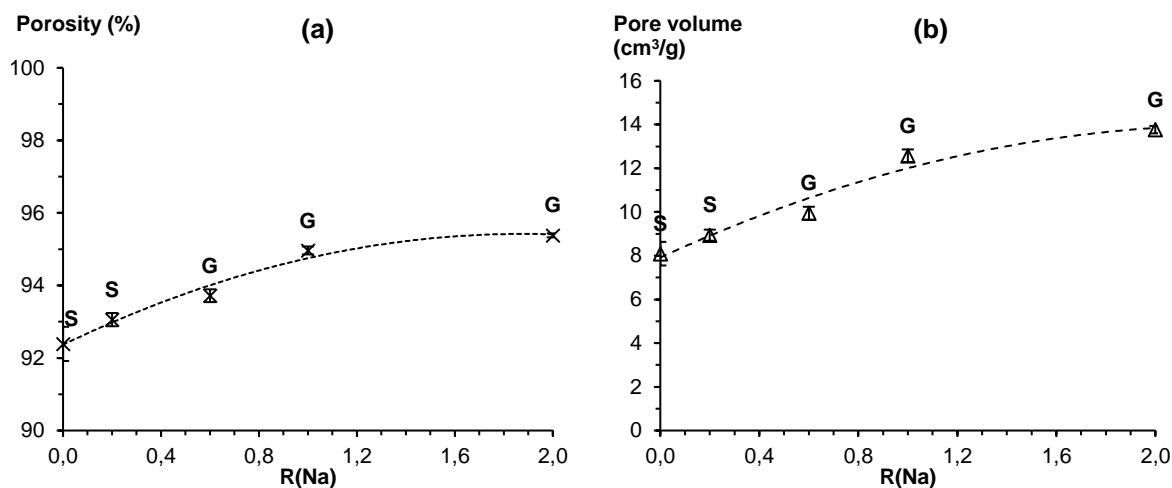


Figure 82. Influence of sodium to pectin molar ratio on (a) porosity and (b) pore volume for pectin aerogels made from 3 wt% at pH 3 (same as in Figure 81). The state of the matter before solvent exchange, solution (S) or gel (G), is indicated for each case. Non-solvent was ethanol. Lines are given to guide the eye. From (Groult & Budtova, 2018).

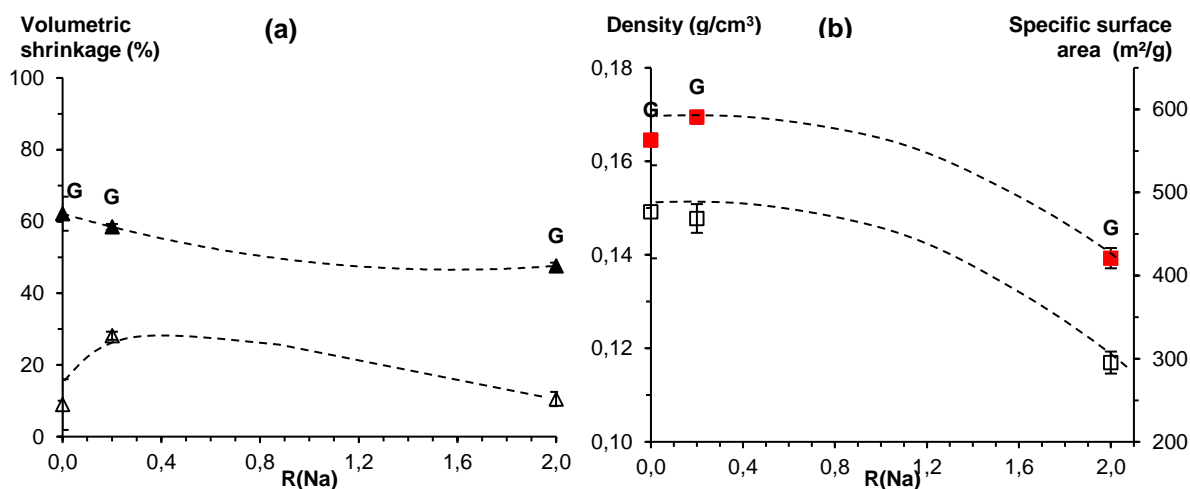


Figure 83. Influence of sodium to pectin molar ratio  $R(\text{Na})$  on (a) shrinkage after solvent exchange (open points) and after drying (filled points) and (b) density (open points) and specific surface area (filled points) of pectin aerogels made from 6 wt% P35 solutions at pH 3, non-solvent was ethanol. The state of the matter before solvent exchange, solution (S) or gel (G), is indicated for each case. Lines are given to guide the eye. From (Groult & Budtova, 2018).

The morphology of pectin aerogels depends on sodium concentration, see Figure 84. Non-gelled aerogel, in the absence of sodium, has compact morphology with the majority of mesopores while at  $R(\text{Na}) = 2$  the morphology is similar to that in the presence of calcium, with rather large macropores.

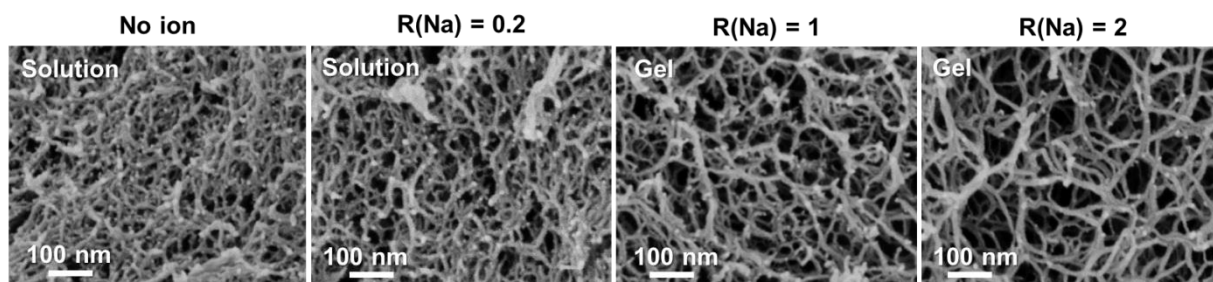


Figure 84. SEM images of pectin aerogels made from 3 wt% P35 solutions at pH 3 with NaCl at  $R(\text{Na}) = 0, 0.2, 1$  and  $2$ . The state of the matter, solution or gel, is indicated for each case. Non-solvent was ethanol. From (Groult & Budtova, 2018).

## 2.5. Discussion on the correlations between the processing parameters and the aeropectin physical properties

The results presented above on the influence of pH and concentration of di- and monovalent metal ions on pectin aerogel morphology and properties show that the main factor governing aerogel characteristics is the mechanism of structure stabilization, or, in other words, the state of the matter before solvent exchange, solution or gel. Gelation, whatever is the mechanism, leads to lower shrinkage upon the addition of non-solvent and sc drying and thus to aerogels with lower density and lower specific surface area, as macropores are preserved. When a non-solvent is added to non-gelled pectin solution, phase separation occurs (also known as “immersion precipitation”) leading to a strong contraction of macromolecules. The particularity of polysaccharides is that above the overlap concentration coagulated pectin still forms porous 3D network structure. This network continues contracting during drying because of a huge difference in polarity of water-soluble pectin and highly apolar  $\text{CO}_2$ . Due to high volume shrinkage the density of aerogels increases (but still remains low, below  $0.2 \text{ g/cm}^3$ ) and specific surface area increases as macropores disappear.

An example of how pectin aerogel morphology and properties can be tuned by varying pH and calcium concentration is shown in Figure 85, where aerogel characteristics are modified with pH (below  $\text{pK}_a$ ) and with calcium at  $R(\text{Ca}) = 0.2$  (concentration  $0.020 \text{ mM}$ ). Strong gels were obtained either by acid-induced gelation at  $\text{pH} < 1.5$ , or by ionic gelation with addition of calcium at pH close to pectin  $\text{pK}_a$  [43], both resulting in low-density pectin aerogels ( $\approx 0.05 \text{ g/cm}^3$ ) with specific surface area around  $300 - 450 \text{ m}^2/\text{g}$ . At pH close to  $\text{pK}_a \approx 3 - 3.5$  and without calcium, non-gelled pectin solutions consisting of dissociated chains were obtained, leading to aerogels with more than twice higher density (around  $0.12 - 0.14 \text{ g/cm}^3$ ) and high specific surface area ( $560 - 590 \text{ m}^2/\text{g}$ ) as compared to low pH. The closer pH was to  $\text{pK}_a$ , the more significant was this difference between samples with or without calcium, gels vs solutions, respectively.

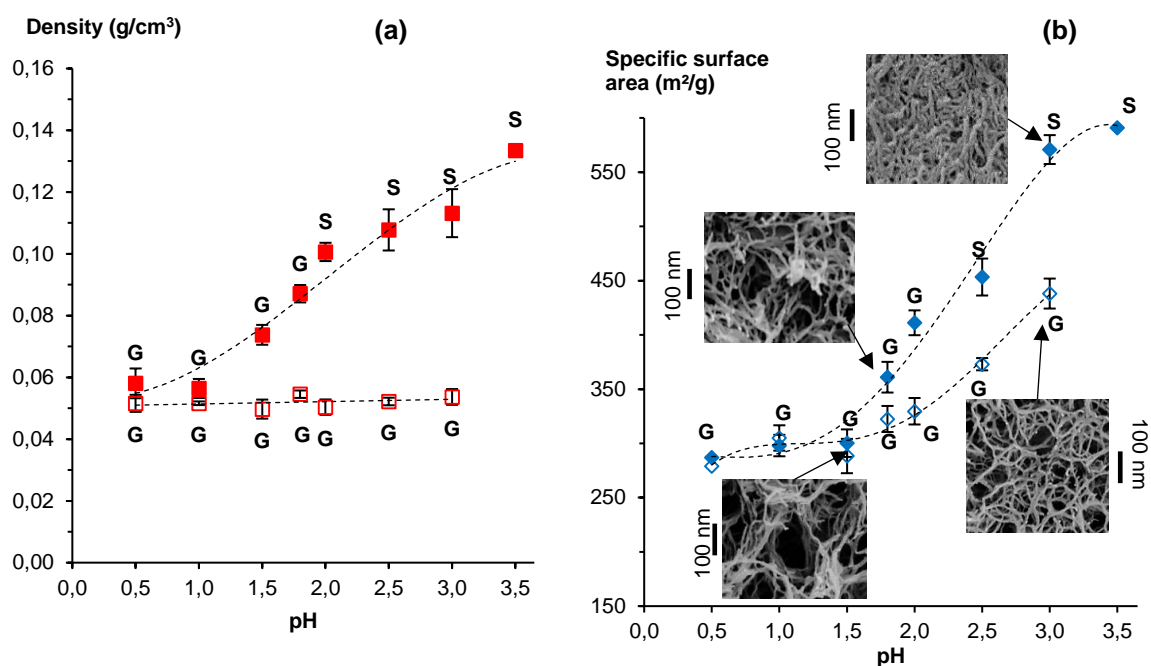


Figure 85. (a) Density and (b) specific surface area of pectin aerogels made from 3 wt% P35 solution in absence (filled symbols) or with addition of calcium at  $R(\text{Ca}) = 0.2$  (empty symbols) at different pH. At pH 3.5 gelation in the presence of calcium was too quick to obtain a homogeneous sample. The state of the matter before solvent exchange, solution (S) or gel (G), is indicated for each case. Dashed lines are given to guide the eye.

The second factor governing pectin aerogel morphology (less important than the state of the matter but still noticeable) is the type of gelation mechanism, acid vs ionic gelation. Here we only compare aerogels obtained from gelled solutions. One example is shown in Figure 85 for the case  $R(\text{Ca}) = 0.2$ : at low pH gelation is mainly acid-induced and at pH around 3 it is ionic. At low pH pectin chains interact by assembling their non-dissociated galacturonic acid domains into intermolecular junction zones involving successive physical bonds. The latter are formed due to hydrogen and hydrophobic interactions. At low pH pectin ionization is very low, and thus acid-induced gelation is relatively unaffected by the addition of calcium. Because acid-induced gelation is a cooperative reaction, aerogel morphology is rather heterogeneous, with large pores and “blocks” of agglomerated chains (see SEM image in Figure 85 at pH 1.5 and  $R(\text{Ca}) = 0.2$ ). At pH around 3 – 3.5 ionic gelation occurs: aerogel density is the same as for acid-induced gelation (Figure 85a) but the morphology is much more homogeneous due to highly dissociated separated chains (see SEM image in Figure 85b at pH 3 and  $R(\text{Ca}) = 0.2$ ). In this case, specific surface area is higher than that at pH 1 – 1.5,  $450 \text{ m}^2/\text{g}$  vs  $290 \text{ m}^2/\text{g}$ , respectively, reflecting the larger fraction of mesopores which can also be seen on SEM images (Figure 85 b.).

Another example illustrating the influence of the type of gelation mechanism on aerogel morphology is shown in Figure 86 for the case of ionic (calcium-induced) vs acid (sodium

induced) induced gelation. The first one results in ionic bonding between pectin chains [22], whereas the latter leads to screening of negative charges allowing acid gelation. The effect of the addition of sodium ions on gelation and pectin aerogel morphology and properties is similar to what was observed for calcium ions, but sodium cations had to be added in much higher concentration than calcium to influence the state of the matter and aerogel properties. When calcium is added, strong gels are formed from 3 wt% solutions at very low ion concentration,  $R(\text{Ca}) = 0.2$ . On the contrary, at  $R(\text{Na}) < 1$  weak gels are formed, resulting in higher density (Figure 86a) and higher specific surface area (Figure 86b); this case resembles non-gelled solutions. However, when  $R(\text{Na})$  is ten times higher than calcium molar concentration,  $R(\text{Na}) = 2$ , acid gelation occurs leading to strong gels and aerogels with low density and rather low specific surface area, similar to those formed via ionic gelation.

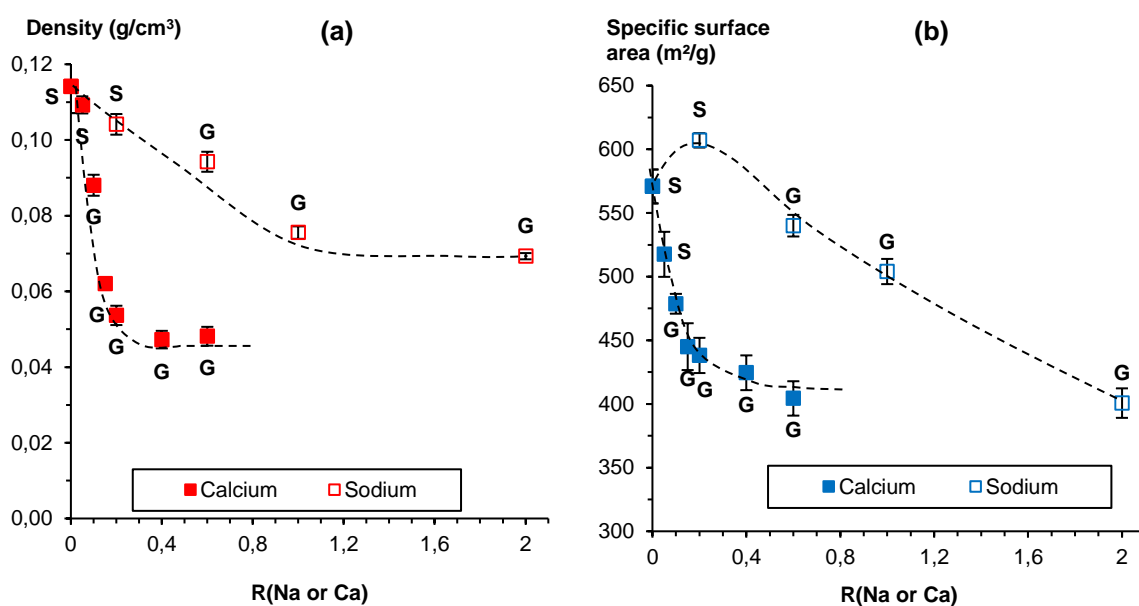


Figure 86. (a) Density and (b) specific surface area of pectin aerogels made from 3 wt% P35 solutions pH 3.0 with either calcium (filled symbols) or sodium (open symbols), as a function of R molar ratio. The state of the matter, solution (“S”) or gel (“G”), is given for each case. Dashed lines are shown to guide the eye.

The correlation between the state of the matter and aerogel density and specific surface area is summarized in Figure 87. Overall, density and specific surface area increase from roughly  $0.05 \text{ g/cm}^3$  and  $300 \text{ m}^2/\text{g}$  to  $0.15 \text{ g/cm}^3$  and  $600 \text{ m}^2/\text{g}$ , respectively, with the following evolution of the state of the matter before solvent exchange: strong gels  $\rightarrow$  weak gels  $\rightarrow$  high viscosity solutions  $\rightarrow$  low viscosity solutions. Figure 87 shows results only for aerogels made from 3 wt% solution with non-solvent ethanol; the properties can be tuned even more if varying pectin concentration and non-solvent. A schematic presentation of structure evolution from pectin solution to aerogel, involving either gelation or phase separation, is shown in Figure 88.

We hypothesize that this approach may be valid for other gelling polysaccharides such as carrageenans and alginate.

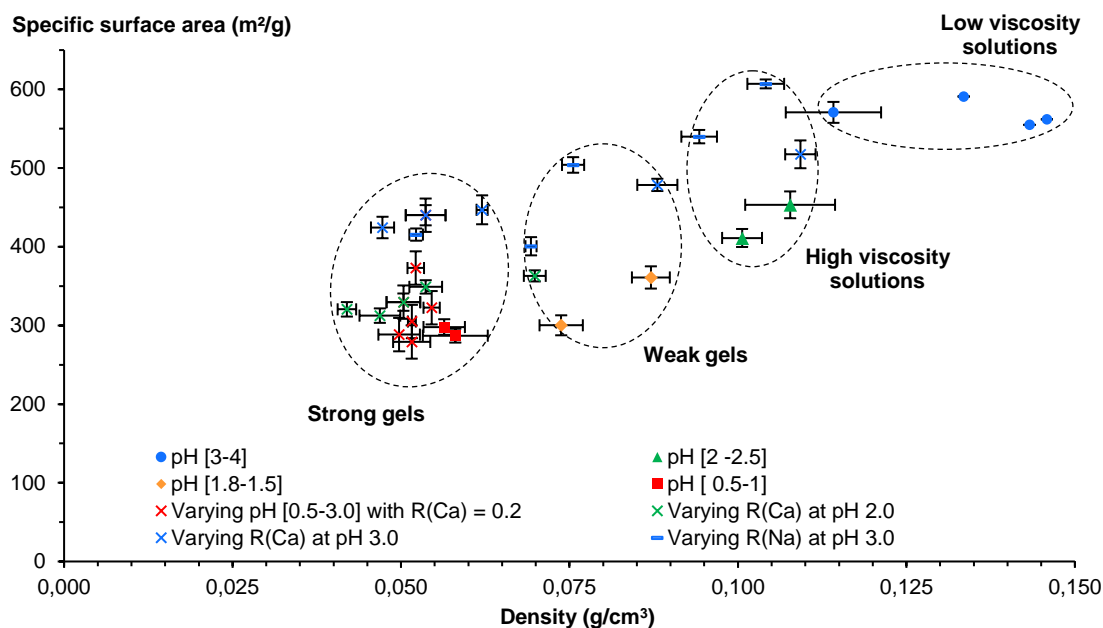


Figure 87. Density and specific surface area of pectin aerogels made from 3 wt% P35 solutions, non-solvent was ethanol. From (Groult & Budtova, 2018).

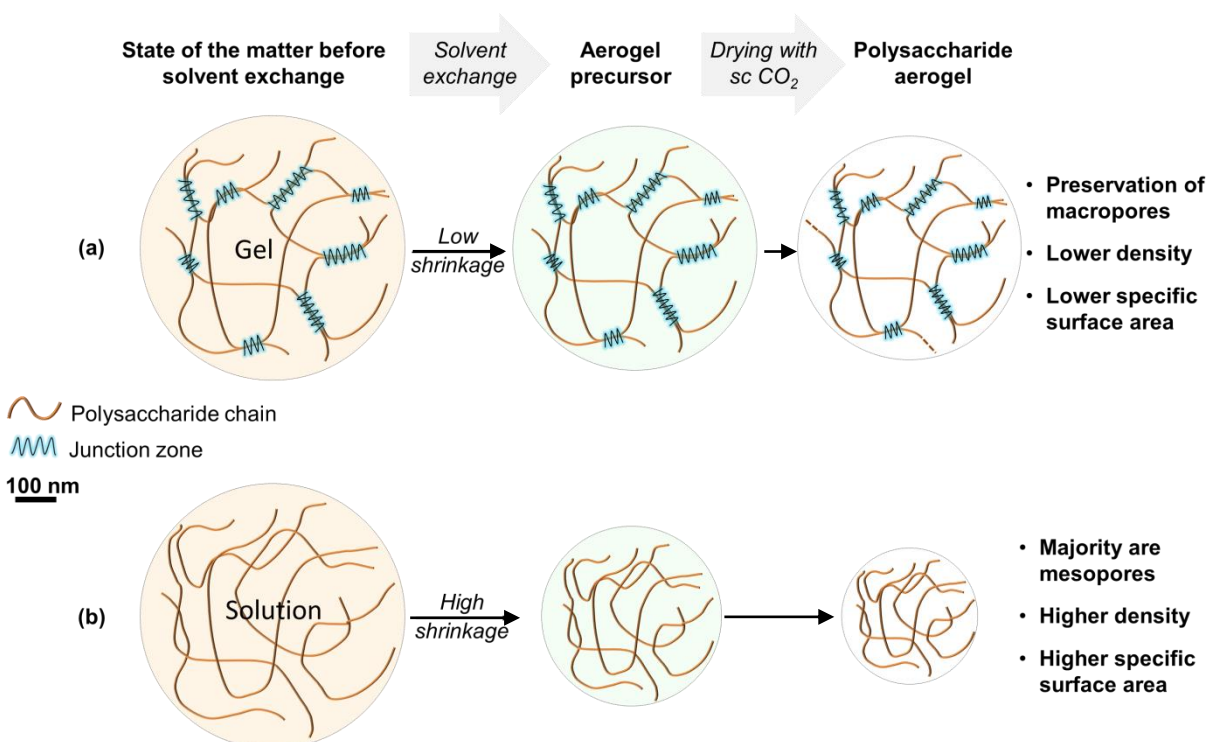


Figure 88. Schematic presentation of two main ways of structure formation, from solution to aerogel. From (Groult & Budtova, 2018).

## 2.6. Mechanical properties of low-methylated pectin aerogels

The mechanical properties of aeropectins were studied by uniaxial compression under high loads and high deformations varying the strain up to 90% to obtain full stress–strain curves. Young’s modulus ( $E$ ) (linear viscoelastic regime), yield stress ( $\sigma_{\text{yield}}$ ) and densification strain (beginning of the plastic region) were determined from the compression strain–stress curves. During the compression testing, no radius increases and no buckling effects were observed. We studied the impact of pectin concentration, pH of pectin solution during dissolution step, and of calcium addition ( $R(\text{Ca}) = 0.2$ ) in pectin solution on aeropectins’ mechanical behavior.

### 2.6.1. Effect of pectin concentration

An example of the compression curves of aeropectins made from solutions of different pectin concentrations (from 2 wt% to 6 wt%) is presented in Figure 89. The corresponding mechanical parameters and network morphologies of the corresponding aeropectins are presented in Table 4 and in Figure 90, respectively. The stress–strain curves presented in Figure 89 are typical for bio-aerogels such as cellulose aerogels (dissolved in NaOH or in ionic liquid) (Demilecamps, 2015; Gavillon, 2007; Sescousse, 2010) and pectin aerogels (acid-gelled (Rudaz et al., 2014) or cross-linked with calcium (Demilecamps, 2015)). All pectin aerogels of the study were found to be extremely compressible with no breakage up to 85% deformation, and present a high stress above 75 % of deformation.

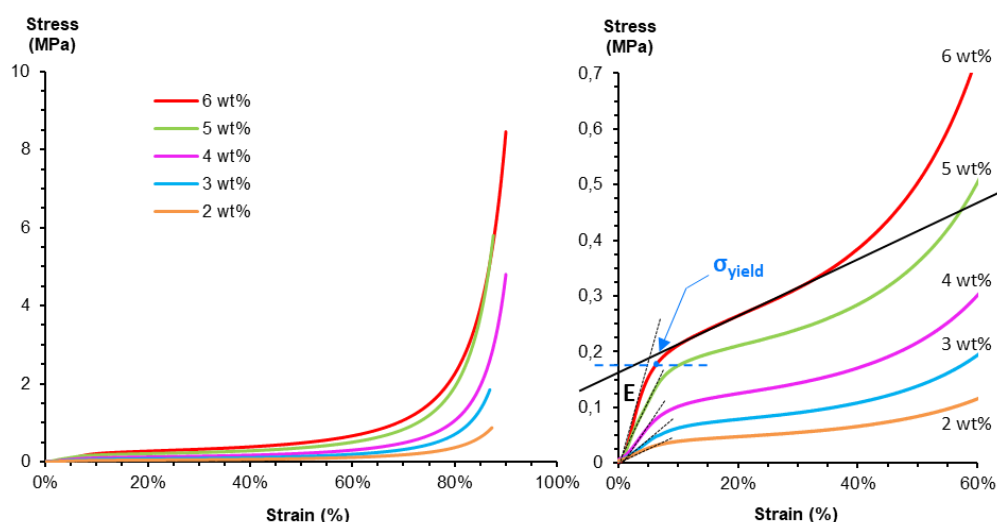


Figure 89. Examples of stress–strain curves for aeropectins made from pectin P35 dissolved at pH 2.0 with calcium added ( $R(\text{Ca}) = 0.2$ ) while increasing pectin concentration of the starting solution from 2 wt% to 6 wt%. The corresponding densities are  $0.037 \text{ g/cm}^3$ ,  $0.045 \text{ g/cm}^3$ ,  $0.060 \text{ g/cm}^3$ ,  $0.074$  and  $0.085 \text{ g/cm}^3$ .

Table 4. Mechanical properties of aeropectins made from pectin P35 dissolved at pH 2.0 with calcium added ( $R(\text{Ca}) = 0.2$ ) while increasing pectin concentration of the starting solution from 2 wt% to 6 wt% (data are from Figure 89).

Pectin concentration (wt%)	Aerogel density after polishing ( $\text{g}/\text{cm}^3$ )	Young modulus E (MPa)	Yield stress $\sigma_{\text{yield}}$ (MPa)	Yield strain (%)	Stress at 85% of deformation (MPa)
2 wt%	0.037	0.50	0.031	6.3%	0.63
3 wt%	0.045	0.81	0.053	7.4%	1.35
4 wt%	0.058	1.41	0.087	7.3%	1.97
5 wt%	0.074	2.10	0.136	7.3%	3.77
6 wt%	0.085	4.04	0.186	6.6%	6.20

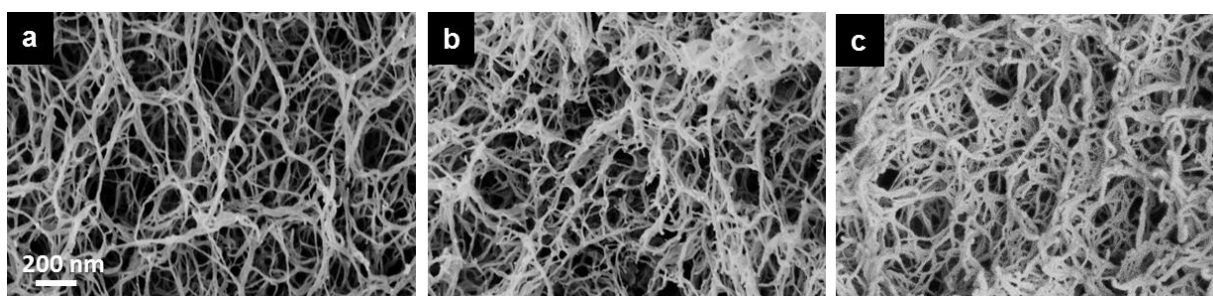


Figure 90. SEM morphologies of aeropectins made from (a) 2 wt% pectin, (b) 4 wt% pectin and (c) 6wt% pectin P35 dissolved at pH 2.0 with calcium added at  $R(\text{Ca}) = 0.2$ . The scale is the same for all pictures.

We found that the increase of pectin concentration (from 2 wt% to 6 wt%) and, as a consequence, the increase of aerogel density, led to the increase of Young's moduli, yield stress and stress measured at 85% deformation, while yield strains remained nearly constant around 6 – 7.5 % (Table 4). The increase of modulus with aerogel bulk density plotted in Figure 91, was also reported for various polysaccharides-based and silica aerogels (Gavillon, 2007; Rege, Schestakow, Karadagli, Ratke, & Itskov, 2016; Rudaz, 2013; Sescousse, 2010). Per analogy with other aerogels made from cellulose, pectin or silica, we can assume that the variation of modulus with bulk density follows a power law. Plotting Young's modulus as a function of density, we found that pectin aerogels follow a power law trend ( $E \sim \rho^n$ ) using the model of Ashby and Gibson (Gibson & Ashby, 1999) with a  $n$  exponent around 2 in the case of pectin aerogels with calcium and made at pH 2.0 (Figure 91).

As it will be shown in the following, it appeared that the value of the  $n$  exponent seems to vary as a function of the pectin aerogels' preparation conditions (*e.g.* pH and calcium concentration) as they strongly impact the network morphology and aerogels physical properties. In order to compare different  $n$  values obtained depending on aerogels preparations conditions, the results are discussed all together at the end of the section 2.6.

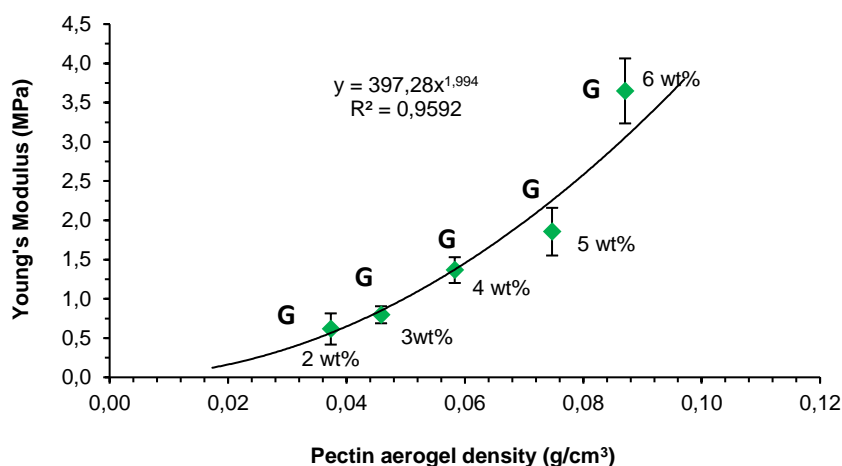


Figure 91. Young's modulus as a function of density of pectin aerogel made from pectin P35 dissolved at pH 2.0 with calcium added ( $R(\text{Ca}) = 0.2$ ) while increasing pectin concentration of the starting solution from 2 wt% to 6 wt%. All samples were pectin ionic gels (calcium-induced) before solvent exchange. Solid line represents the trendline power law.

### 2.6.2. Effect of pH of starting pectin solution on the mechanical properties

As the internal structure of pectin aerogels was found to be strongly impacted by pH of pectin starting solution (see Section 2.2.), we found interesting to compare the mechanical properties of aeropectins varying the pH conditions (from 1.5 to 3.0). The examples of compression curves and mechanical properties of pectin aerogels made at different pH are presented in Figure 92 and Table 5, respectively. SEM pictures of the network morphology are shown in Figure 93.

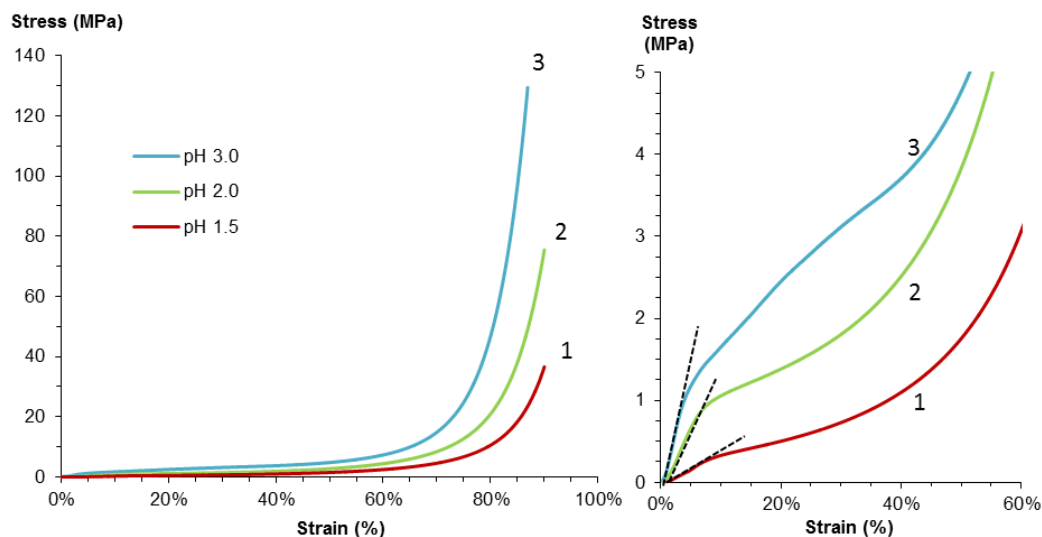


Figure 92. Examples of stress–strain curves for aerogels made from 6 wt% pectin P35 dissolved without calcium at pH 1.5 (1), pH 2.0 (2) and pH 3.0 (3). The corresponding densities are 0.165, 0.215, and 0.260 g/cm<sup>3</sup>, respectively. All samples were pectin acid-induced gels before solvent exchange.

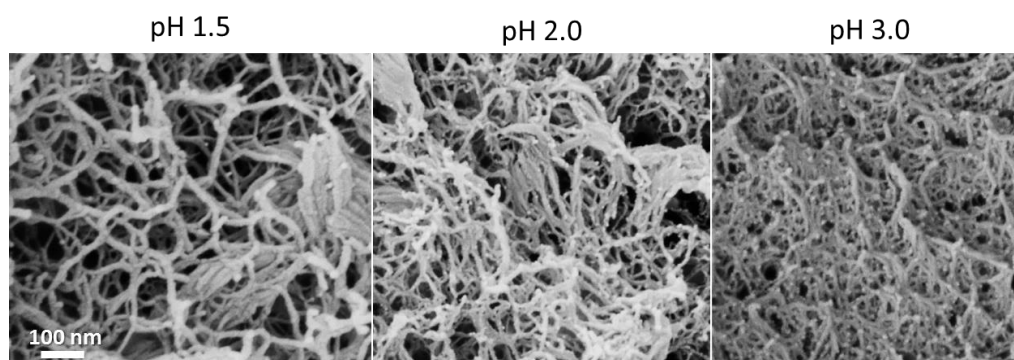


Figure 93. SEM morphologies of aerogels made from 6 wt% pectin P35 dissolved without calcium at pH 1.5, pH 2.0 and pH 3.0, non-solvent was ethanol. The scale is the same for all pictures.

Table 5. Mechanical properties of aerogels made from 6 wt% pectin P35 dissolved without calcium at pH 1.5, pH 2.0 and pH 3.0. (stress-strain curves are in Figure 92).

pH of pectin solution	Aerogel density after polishing (g/cm <sup>3</sup> )	Young modulus E (MPa)	Yield stress $\sigma_{\text{yield}}$ (MPa)	Yield strain (%)	Stress at 85% of deformation (MPa)
1.5	0.165	2.8	0.261	7.6%	7.2
2.0	0.215	16.3	0.891	7.0%	72.1
3.0	0.260	32.1	1.19	5.0%	98.6

As it can be seen in Table 5, the change of network morphology induced by pH of the starting solution of pectin strongly influences the mechanical properties of the pectin aerogels. Indeed, increasing pH from 1.5 to 3.0 resulted in more than 10 times higher Young's moduli and stress measured at 85% of deformation in correlation with higher bulk density (Figure 94). Setting the pectin solution pH at 3.0 instead of 1.5 decreased pectin chains interactions due to coulombic repulsions, leading to weaker acid-gels at "high" pectin concentrations ( $\geq 5$  wt%) and even inhibiting acid gelation at lower pectin concentration ( $\leq 4.5$  wt%). Higher volume shrinkage underwent by pectin sample during the process route resulted in aeropectins with improved mechanical properties as they present more compact and homogenous network morphology, higher density and smaller pores. The exponent  $n$  obtained here is around 4.

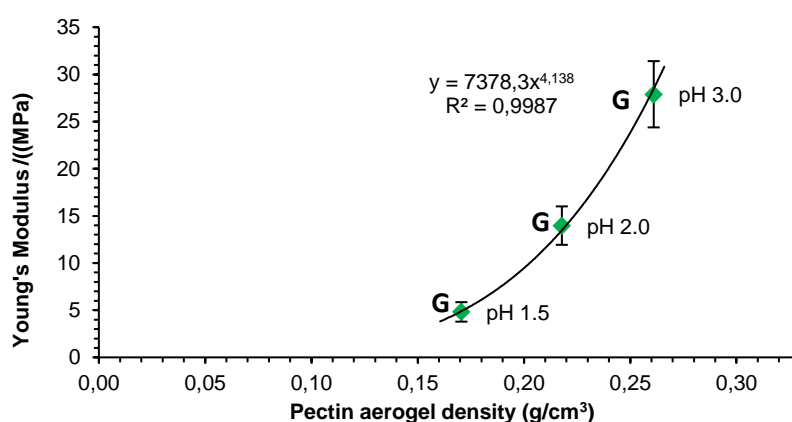


Figure 94. Young's modulus as a function of density of pectin aerogel made from 6 wt% pectin P35 dissolved without calcium at pH 1.5, pH 2.0 and pH 3.0. All samples were pectin acid gels before solvent exchange, non-solvent was ethanol. Solid line represents the trend line power law.

### 2.6.3. Effect of addition of calcium into pectin solution

Finally, we studied the impact of the addition of calcium to pectin solution on the mechanical behavior of aeropectins as calcium addition was also found to be key-process parameter to tune aeropectin structural properties (see section 2.3.).

For this purpose, we compared the mechanical properties of aeropectins made from 6 wt% pectin dissolved at pH 1.5 or pH 2.0 without calcium or with calcium added in pectin solution at  $R(\text{Ca}) = 0.2$ . The examples of compression curves and mechanical properties of the different pectin aerogels at these pH and calcium conditions are presented in Figure 95 and Table 6, respectively. SEM pictures of the corresponding network morphology are shown in Figure 96.

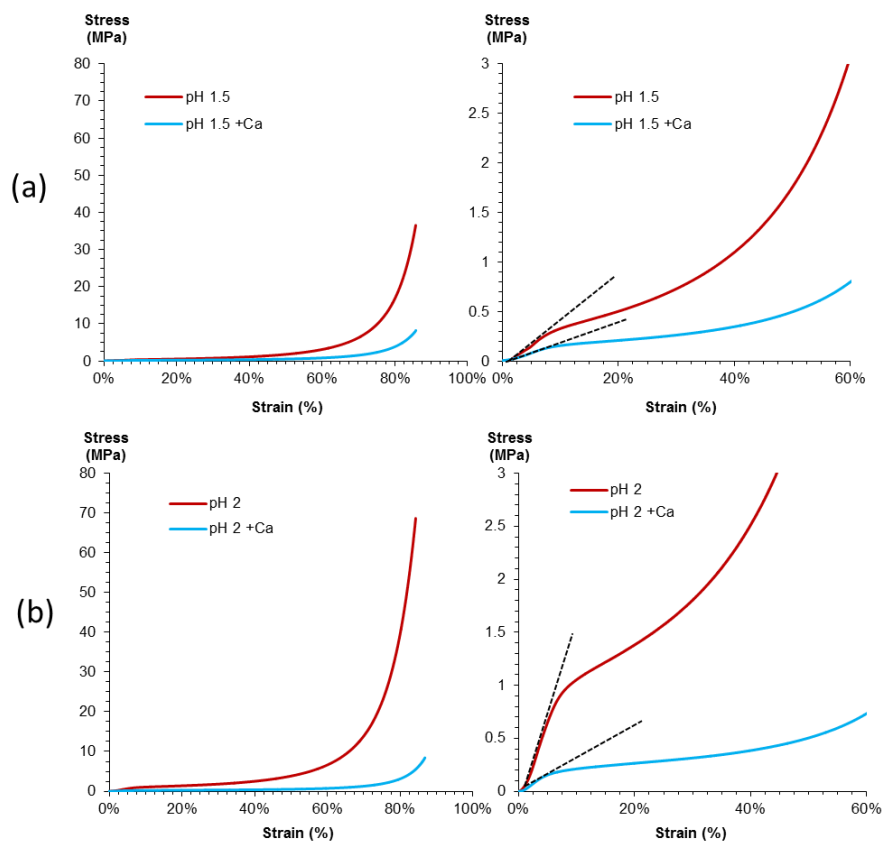


Figure 95. Examples of stress–strain curves for aerogellectins made from 6 wt% pectin P35 dissolved (a) at pH 1.5 or (b) at pH 2.0 in absence of calcium or with calcium added at  $R(\text{Ca}) = 0.2$ . Non-solvent was ethanol.

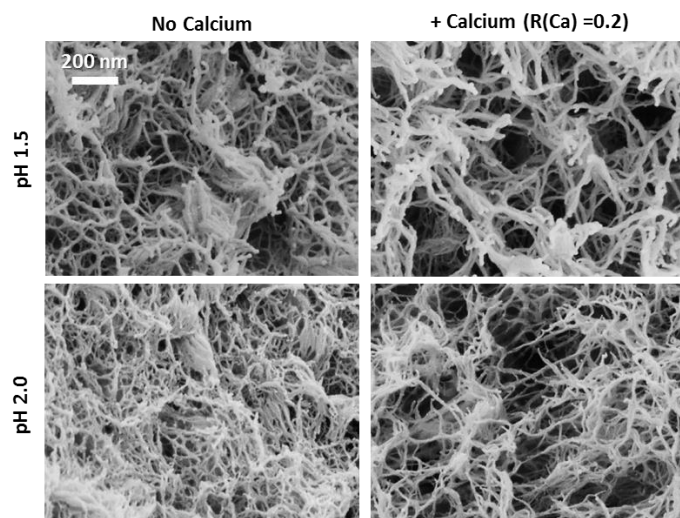


Figure 96. SEM characterization of aerogellectins made from 6 wt% pectin P35 dissolved at pH 1.5 or 2.0 in the absence of calcium or with calcium added at  $R(\text{Ca}) = 0.2$ , non-solvent was ethanol. The scale is the same for all pictures.

Table 6. Mechanical properties of aeropectins made from 6 wt% pectin P35 dissolved at pH 1.5 or 2.0 in the absence of calcium or with calcium added at  $R(\text{Ca}) = 0.2$  (from Figure 95).

pH of pectin solution	Calcium R(Ca) ratio	Aerogel density after polishing ( $\text{g}/\text{cm}^3$ )	Young modulus E (MPa)	Yield stress $\sigma_{\text{yield}}$ (MPa)	Yield strain (%)	Stress at 85% of deformation (MPa)
1.5	–	0.165	4.7	0.261	7.6%	32.6
1.5	0.2	0.091	2.1	0.132	7.1%	7.2
2.0	–	0.215	16.3	0.891	7.0%	72.1
2.0	0.2	0.085	2.8	0.179	6.2%	6.0

As we could expect from aerogels densities, the addition of calcium to pectin solutions ( $R(\text{Ca}) = 0.2$ ) drastically decreased the mechanical parameters of pectin aerogels (Young's modulus, yield stress, stress measured at 85 % of deformation) as it also strongly reduced aerogel density compared to aeropectins without calcium.

Similarly to the effect of decrease of pH discussed just above, the addition of calcium also led to highly porous network morphologies with larger pores (Figure 96), and thus was actually found to significantly weaken the mechanical properties. In addition to the change in aeropectins structural properties, the calcium concentration of pectin solution is known to make pectin hydrogels more brittle due to the “stiffness” of the ionic bonds (Basak & Bandyopadhyay, 2014; Capel et al., 2006, p. 006; Ilse Fraeye, Colle, et al., 2010; Ilse Fraeye, Duvetter, et al., 2010). Thus, we can assume that it could also have an impact on the mechanical properties of supercritically dried pectin aerogels. This effect was also observed by Arnaud Demilecamps during his PhD work on calcium crosslinked aeropectins (Demilecamps, 2015).

As it can be noticed in Figure 97 and Table 6, the effect of calcium addition on the mechanical properties of aeropectins is more pronounced at pH 2.0 than at 1.5. As an illustration, aeropectin Young's modulus is divided by 2 when calcium was added at pH 1.5, and divided by 4 when calcium was added at pH 2.0. This difference is due to a much lower amount of deprotonated functions (carboxylates) available to interact with calcium ions at pH 1.5 compared to pH 2.0, minimizing the effect of calcium on network formation and so on the mechanical properties of pectin aerogels. Without calcium, more “weaker” acid-induced pectin gels were obtained at “high” pectin concentration ( $\geq 5$  wt%) via the formation of hydrogen bonds between protonated functions promoted by low pH ( $\text{pH} \leq 3.0$ ), while much firmer and more porous pectin ionic gels were obtained at “low” and “high” pectin concentrations ( from 2 wt% to 6 wt%) due to strong ionic bonds when calcium was added ( $R(\text{Ca}) = 0.2$ ). As a result, acid gels (without calcium) were more prone to higher volume shrinkage during solvent exchange and sc-drying, which significantly increased the aerogels' density and so their Young 's Modulus. Besides, it can be noticed that even at very low pH (pH 1.5), calcium concentration

still had an effect on the pectin network formation as aerogels density and Young's modulus were much smaller than without calcium. As a conclusion, the structure formation of the pectin network via hydrogen interactions or ionic (by changing pH and calcium conditions) has a direct impact on the level of sample shrinkage, on the final textural properties of aerogels and thus on their mechanical properties.

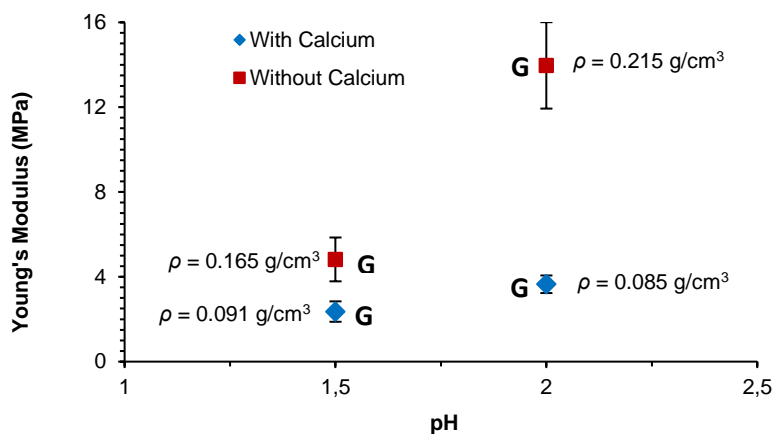


Figure 97. Calcium effect on Young's modulus of aeropectins made from 6 wt% pectin P35 dissolved at pH 1.5 or 2.0 in the absence of calcium (square) or with calcium added at  $R(\text{Ca}) = 0.2$  (diamonds). Non-solvent was ethanol. All samples were pectin gels (acid-induced or calcium-induced) before solvent exchange.

As a conclusion, it seems that mechanical properties of pectin aerogels are mainly controlled by their bulk density, the latter being impacted by the process parameters (pH, concentration of pectin and calcium concentration, all influencing the way of network formation, via acid-induced gelation, ionic gelation or phase separation). As it was also observed with other aerogels made from polysaccharides, silica or inorganic polymers, the variation of modulus with bulk density seems to follow a power law trend ( $E \sim \rho^n$ ) as described using the model of Ashby and Gibson (Gibson & Ashby, 1999). An interesting thing to note is that the  $n$  exponent is equal to 2 (Figure 91) for pectin aerogels crosslinked with calcium ( $R(\text{Ca}) = 0.2$ ) while it is around 4.1 for pectin aerogels without calcium (Figure 98). As a comparison, the exponent  $n$  is around 2.8 as reported for pectin aerogels made without calcium by acid gelation in strong acid (using HCl at 0.5M, pH ~ 0.3) (Rudaz et al., 2014). Those pectin aerogels presented lower density and Young's modulus (between 4 to 10 MPa) for similar pectin concentration (3-5 wt%) (Rudaz, 2013) than the pectin aerogels without calcium of this study (pH varying from 1.5 to 3.0).

Comparatively to other polysaccharide-based aerogels and cryogels, the  $n$  exponents were found to be around 2.8-2.9 for cellulose aerogels (Gavillon & Budtova, 2008; Sescousse, 2010; Sescousse, Gavillon, & Budtova, 2011), and for nanofibrillated cellulose foams (freeze-dried) the  $n$  values were around 2.3 and 3.1 for TEMPO-oxidized or enzymatically pre-treated

nanofibrillated cellulose, respectively (Maroia et al., 2016). For aerogels made from synthetic polymers,  $n$  values were reported to be in general around 2 – 3: for instance,  $n \sim 2$  for polyurea aerogels (Weigold & Reichenauer, 2014),  $n \sim 2.7$  for resorcinol– formaldehyde aerogels (Pekala, Alviso, & LeMay, 1990) and even up to 3.7 for polyurethane aerogels (Diascorn, Calas, Sallee, Achard, & Rigacci, 2015). Finally,  $n$  exponents were reported around 2.9-3.0 for silica aerogels (Alaoui, Woignier, Scherer, & Phalippou, 2008).

Contrary to other types of aerogels, calcium-crosslinked pectin aerogels present much lower  $n$  exponent ( $\sim 1.7$ ), whereas the trend for pectin aerogels without calcium was found to have significantly higher  $n$  exponent ( $\sim 4.1$ ) than for other aerogels. It should be noted that the interval of densities of cross-linked pectin aerogels is rather small, and thus to conclude on the trend for the mechanical properties is a bit delicate. Different power law trends of aeropectins depending on calcium conditions can be explained by the differences between the junction zones made from successive strong ionic bonds (pectin-Ca), as compared to the more flexible and weaker hydrogen bonds between pectin chains in the absence of calcium. The physico-chemical characteristics of junction zones building the pectin network may have also modified chain rigidity and spatial conformation and thus influence the mechanical properties.

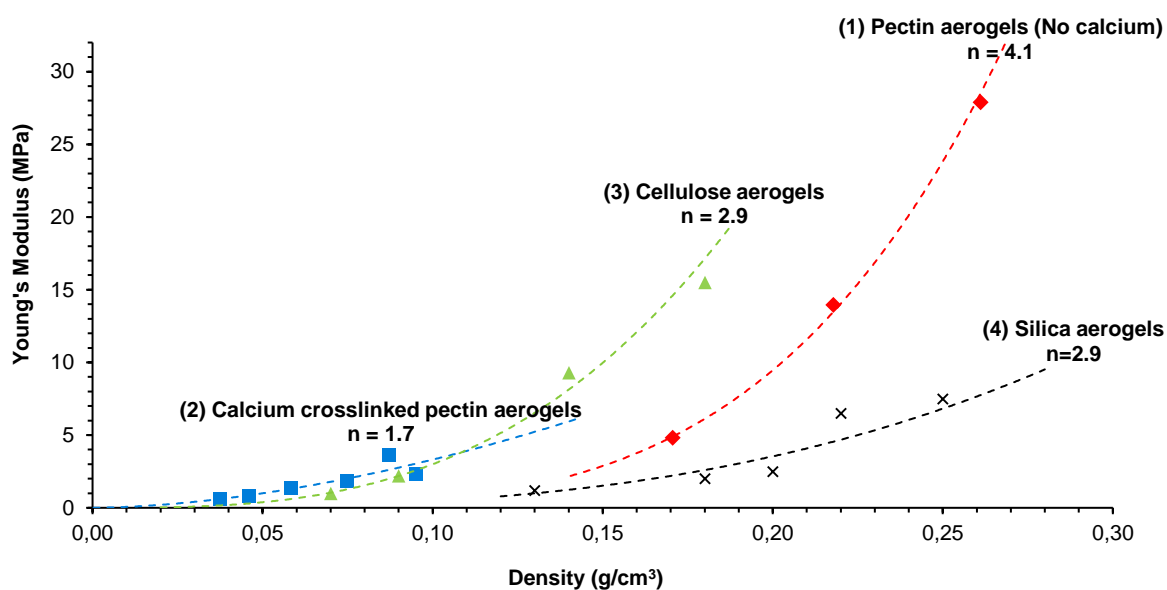


Figure 98. Comparison of Young's moduli and scaling exponents  $n$  as a function of bulk density for different aerogels using power law model  $E \sim \rho^n$  (Gibson & Ashby, 1999): pectin aerogels were either without calcium (1) or cross-linked with calcium  $R(\text{Ca}) = 0.2$  (2), non-crosslinked cellulose aerogels (data taken from (Sescousse, 2010)) (3), and silica aerogels (data taken from (Alaoui et al., 2008)) (4).

## 2.7. Conclusions on the properties of low-methylated pectin aerogels

Low methylated pectin aerogels were synthesized and characterized. A systematic variation of the external parameters (pH, polymer concentration, type of non-solvent, concentration of mono- and polyvalent metal ion salts) allowed modulating solution viscosity and gelation mechanisms, which in turn influenced aerogel structure and mechanical properties. The density of pectin aerogels varied from 0.05 to 0.25 g/cm<sup>3</sup> and specific surface area from 270 to 600 m<sup>2</sup>/g. As expected, the aeropectin mechanical properties were strongly governed by their density but were also impacted by the type of junction zones and network morphology involved in the formation of pectin aerogel network (ionic or hydrogen interactions).

Strong ionic gels formed in the presence of calcium around pectin pK<sub>a</sub> “resisted” shrinkage during solvent exchange and drying. As a result, aerogels with high proportion of macropores, low density, around 0.05 g/cm<sup>3</sup>, and rather low specific surface area, around 300 m<sup>2</sup>/g, were formed. Aerogels with similar morphology and density were obtained at low pH: solutions gelled due to hydrogen bonding between protonated carboxyl groups and hydrophobic interactions between methylated groups. The increase of pH led to carboxylate groups’ ionization preventing gelation. The state of the matter before solvent exchange was solution, and pectin network was formed during solvent exchange, via non-solvent induced phase separation (or coagulation). In this case shrinkage during solvent exchange and supercritical drying was high as far as 3D structure was not “stabilized” by gelation. The resulting pectin aerogels were mesoporous, of density around 0.12 -0.25 g/cm<sup>3</sup> and high specific surface area, around 600 m<sup>2</sup>/g. Weak gels were formed upon the addition of sodium salt which was screening the electrostatic repulsion between charged carboxylates and leading to aerogels with properties intermediate to those described above. The mechanism of structure stabilization, *i.e.* gelation or non-solvent induced phase separation, was shown to be the key parameter controlling aerogel structure and mechanical properties.

## 3. Effects of pectin degree of esterification on pectin aerogels structural properties

In addition to the influence of extrinsic process parameters on aeropectins structural properties, we found interesting to also investigate the impact of intrinsic parameters. Indeed, pectin’s Degree of Esterification (DE) (%), of Acetylation (DAc) (%), of Amidation (DA) (%) as well as the distribution of the specific functions along the pectin chain (random-like or block-wise) depends on pectin source and chemical treatments and are known to be the main factors dictating the gelling ability and their mechanisms. In particular, pectin DE impacts

intermolecular chain interactions (hydrogen/hydrophobic), the internal charge distribution within the backbone of the pectin, and the availability of charged groups to interact with metal ion cations. In the absence of ions and at pH lower than  $pK_a$ , gelation of Low-Methylated pectins (LM) (*i.e.* for DE < 50%) is known to occur mostly through hydrogen bonds, while for High-Methylated pectins (*i.e.* for DE > 50%) gelation occurs via hydrophobic interactions and require a high co-solute content (typically, a high content (> 60%)) of low molecular weight sugar to reduce water activity and stabilize hydrophobic interactions between pectin chains (Dumitriu, 2004; Oakenfull, 1991). In this work we did not add any co-solute in pectin preparations which will impact the structure formation and gelling ability of HM pectin solutions as compared to what is known in literature.

In the previous section on low-methylated pectin aerogel (Section 2) we showed that by varying pH conditions and cations' concentration in low-methylated pectin solutions, we were able to control the build-up of pectin network and state of the matter (gel or solution) by varying acid dissociation/protonation of galacturonic acid. This was found, in turn, to strongly impact the final structural and morphological properties of aeropectins made from low methylated pectin (P35). Now, we open up the question of the influence of pectin DE on pectin gels and aerogels properties while varying the pH and calcium conditions. Are the processing-structure-properties correlations previously observed with low-methylated pectin applicable to higher-methylated ones? At a given preparation and process conditions, does the variation of pectin DE significantly impacts soft matter structuration and the final physical properties of pectin aerogels?

To answer these questions, we used three different citrus pectins to produce aerogels from low- to high-methylation degree (with DE of 35%, 59% and 70%). The pH and R(Ca) ratio were varied in a systematic way, and the obtained pectin gels and aerogels were characterized.

The section is organized as follows:

- We first study the impact of pectin DE on pectin solutions or gels and aerogels properties at different pH conditions.
- Then we examine the influence of pectin DE at different calcium R(ratio) coupled with different pH conditions.

### **3.1. Impact of DE on aeropectin structural properties varying the pH**

As we already know, increasing pH close to and above pectin  $pK_a$  (~ 2.9 - 3.5) (Plaschina et al., 1985; Ralet et al., 2001) results in progressive dissociation of acid functions on non-methylated galacturonic acid groups (Gal.A). The appearance of negative charges is known to lead to coulombic repulsion between pectin chains, which reduces the interactions and may inhibit gelation. On the opposite, as the pH decreases, the protonation of carboxylates into

carboxylic acids of the non-methylated Gal.A occurs, resulting in progressive decrease of the number of negative charges along the pectin backbone. This not only decreases electrostatic repulsions between pectin molecules, but also reduces hydration of carboxylic groups with water molecules (low-water-activity) which allows the formation of physical junctions' zones between pectin chains (Paoletti et al., 1986). Such junction zones are based on chain associations stabilized by hydrogen bonding between un-dissociated carboxylic acids and secondary alcohol groups, and by hydrophobic interactions between methyl esters groups. The build-up of a 3-D network can lead to acid-gelation if chain interactions are sufficient at given conditions of temperature and pectin concentration.

### 3.1.1. Impact of pectin DE on the viscosity of pectin solutions while varying the pH

To investigate the influence of pectin DE, we first study the evolution of viscosity of pectin solutions while varying the pH. Pectin aqueous solutions were made from 0.90 wt% of pectin P35, P59 or P70 with pH varying from 1.5 to 3.0. As it can be seen on Figure 99, viscosity of 0.90 wt% pectin solutions increased when pH was progressively decreasing from 3.0 to 1.5, as already demonstrated for P35 (Section 3.2). The viscosity of LM pectin solutions made from P35 were highly impacted by lowering pH below  $pK_a$  ( $\sim 2.9$  -3.5) contrary to HM pectins P59 and P70. Indeed, pectins sensitivity to pH seemed to be directly correlated to DE, the latter determining the amount of non-methylated carboxyl functions whose dissociation depends on pH conditions. The lower is the pectin DE, the more numerous are the carboxylic functions likely to be dissociated into carboxylates when pH increases, which results in a decrease of solution viscosity with appearance of repulsive charges between the chains. This explained why for HM-pectins solutions (P59 and P70) the appearance of negative charges has a minor impact on viscosity, as the majority of galacturonic acids are methylated, *i.e.* not pH-sensitive.

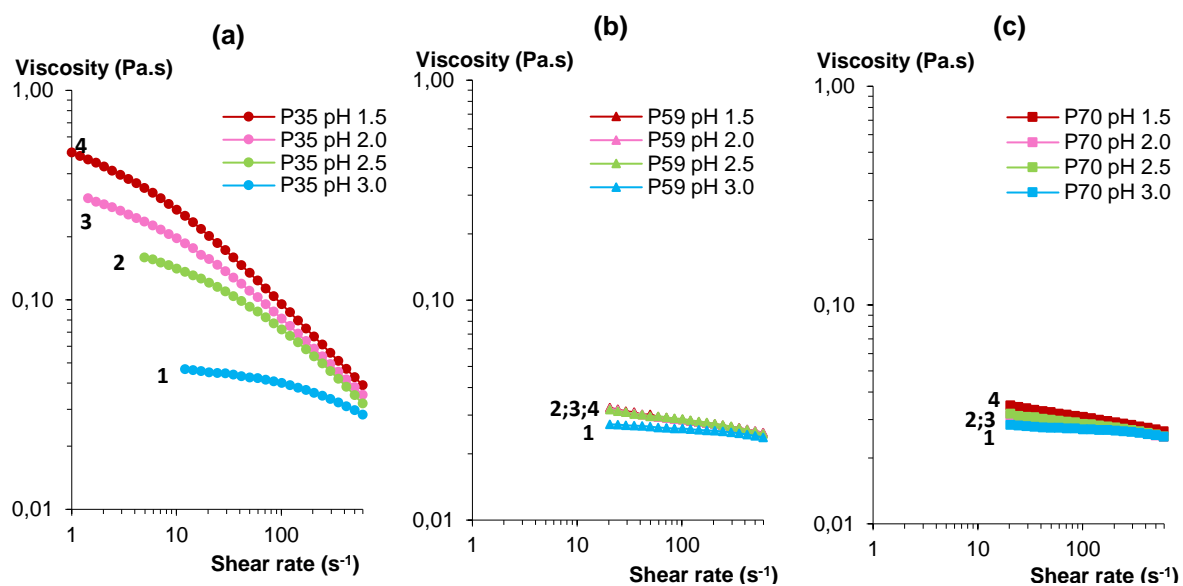


Figure 99. Viscosity as a function of shear rate of 0.9 wt.% pectin solutions of (a) P35 (b) P59 and (c) P70 at pH 3.0 (1), pH 2.5 (2), pH 2.0 (3) and pH 1.5 (4).

Moreover, contrary to what could be expected from the influence of pectin molecular weight (see Section 1.2 of this chapter) on viscosity, *i.e.* higher viscosity for the polymer of higher molecular weight, it can be noticed that viscosity of HM pectin (higher mol. weight) solutions was significantly lower than that of LM P35 (lower mol. weight) in the same conditions of pH and ionic strength. The reason is that LM pectin (P35) has much larger amount of carboxyl groups as compared to HM pectins, and at the same low pH LM pectin possess much larger number of protonated carboxyl groups involved in the formation of hydrogen bonds, which in turn increases solution viscosity. This effect is dominating the potential decrease of solution viscosity expected for polymer of lower molecular weight. We can assume that in absence of co-solute (which enhances hydrophobic interactions), chain-solvent interactions dominated over chain-chains interactions especially for pectins with high DE, resulting in lower viscosity solutions as DE increases. Indeed, it is well known that HM pectins require a significant co-solute content to reduce water activity (typically, high sugar content  $\sim 60\%$ ) and pH lower than 3.5, allowing pectin chains to interact. More precisely, the presence of co-solutes enhances hydrophobic interactions through a solvent ordering effect (Dumitriu, 2004; Oakenfull, 1991), and their amount required increases with increasing DE (Hui, Sherkat, & Sherkat, 2005).

### 3.1.2. Impact of pectin DE on aeropectin properties while varying the pH

As demonstrated in Section 2.2 for LM pectin P35, pH controls the formation of the pectin network influencing the level of acid dissociation of Gal.A. We obtained different states of matter at different pH: strong pectin gels at very low pH ( $\leq 1.0$ ), weak gels (pH  $\sim 1.5$ ), high viscosity solutions (pH  $\sim 2.0$ ) and low viscosity solutions (pH  $\geq 2.5$ ). We showed that un-gelled solutions were resulting in sample higher volume shrinkage during solvent exchange and sc-drying, which led to higher aeropectin density compared to the ones obtained from a mechanically stronger gel. Gel state was found to efficiently prevent volume shrinkage due to a strong network, and very low density aeropectins ( $\sim 0.05\text{g/cm}^3$ ) were obtained after sc-drying.

In this study, this observation is confirmed and generalized for all pectins with different DE. As shown in Figure 100a for all 3 wt% pectin-based aerogels, volume shrinkage decreased while lowering pH from 3.0 ( $\sim 63\%$  -  $75\%$  of shrinkage) to 0.5 ( $\sim 45\%$  -  $53\%$  of shrinkage). The formation of a gel at low pH prevented pectin samples from volume shrinkage during solvent exchange and sc drying, and lower density aeropectins were obtained at low pH for all pectins, as presented in Figure 100b.

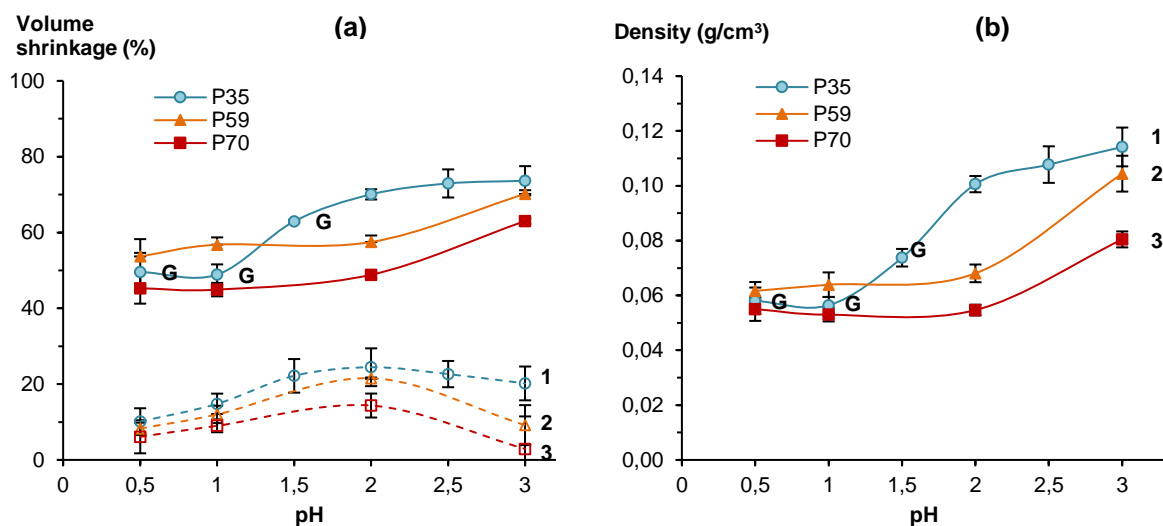


Figure 100. (a) Volume shrinkage after solvent exchange (open symbols) and after sc-drying (filled symbols) and (b) density of aerogel samples made from 3 wt% pectins P35 (1), P59 (2), P70 (3) dissolved at different pH without calcium. Non-solvent was ethanol. Gel state before solvent exchange is indicated with “G”, otherwise samples were solutions. Lines are given to guide the eye.

For especially low viscosity solutions obtained from 3 wt% of HM pectins P59 and P70 at pH 3.0 (Figure 99), we noticed an unexpected swelling phenomenon of the samples during solvent exchange during the first addition of a water / ethanol mixture at ratio 50 / 50 (v). The swelling was observed in the longitudinal direction (around +10-20% of longitudinal swelling as compared to initial sample thickness) as the radial direction was maintained by the mold. This swelling artificially reduced the overall volume shrinkage undergone by HM pectin samples, as shown in Figure 100. As a result, the aerogel samples made from HM pectins (P59 and P70) presented much lower densities after sc-drying than aerogel samples made from LM pectin (P35) as shown in Figure 102. Thus, the viscosities of pectin solution and pectin DE were found to have an opposite influence on pectin aerogel properties, leading to lower aerogel densities as DE was high and pH was low. Swelling was lower with increasing pectin viscosity by lowering pH or by adding calcium to pectin solutions. No swelling was observed once gels or “sufficiently high” viscosity solutions were formed. Contrary to HM pectins (P59, P70), no swelling was observed for LM pectin solution (P35) thanks to their higher viscosity in the pH range (0.5 – 3.0) (Figure 99), resulting in higher aerogel density than HM pectins at a given pH.

As shown in Section 3.1.1., HM pectins are much less sensitive to pH than LM pectin as the latter presents a larger proportion of non-methylated galacturonic acids which are subjected to acid dissociation. For example, HM pectin solutions are not gelling in the pH conditions in which LM pectin does. This difference is also reflected by volume shrinkage and density increase as a function of pH (figure 41): the increase of pH leads to a much higher

variation in shrinkage and density as compared to LM pectin aerogels, especially if comparing P35 and P70. The same is valid for pore volume and porosity, as shown in Figure 101.

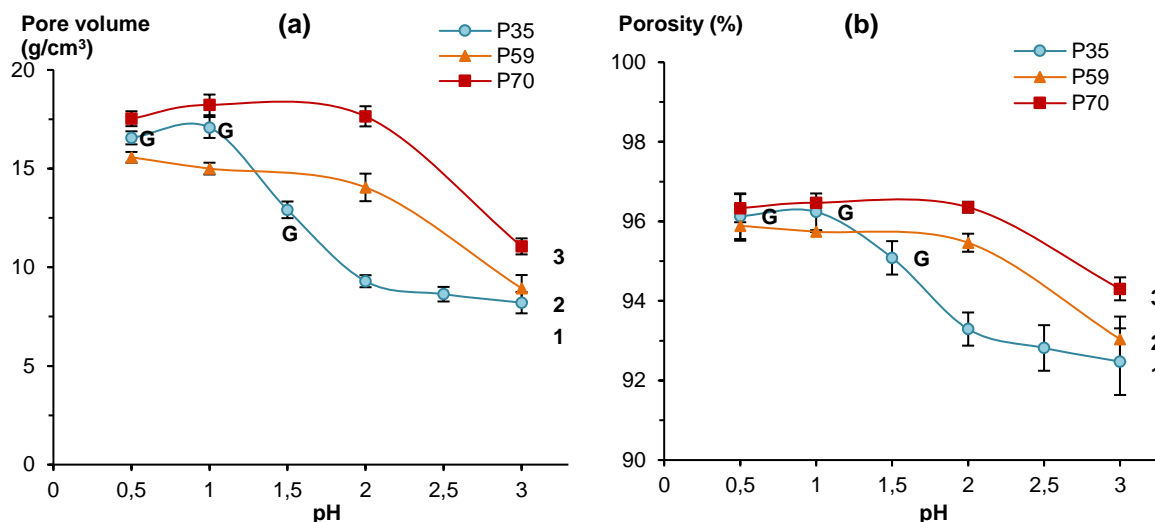


Figure 101. (a) Pore volume and (b) porosity of aerogellectins made of 3 wt% of pectins P35 (1), P59 (2), P70 (3) dissolved at different pH conditions and without calcium. Non-solvent was ethanol. Gel state before solvent exchange is indicated with “G”, otherwise samples were solutions. Lines are given to guide the eye.

Finally, in the previous study on LM pectin (Section 3.2.), we observed a progressive decrease of aerogellectin specific surface area ( $S_{BET}$ ) as the pH of the pectin starting solution was reduced lower than  $pK_a$  ( $\sim 3 - 3.5$ ). The same occurs for all types of pectin aerogels prepared, but in a different manner (Figure 102 (a)). We explained the progressive reduction of  $S_{BET}$  by the formation of non-porous junction zones between pectin chains (hydrogen bonds / hydrophobic interactions) which are favored at low acidic pH solutions. We assume that more numerous junction zones should be formed in LM pectin due to higher proportion of hydrogen bonding compared to HM pectins whose hydrophobic interactions were not adequately stabilized without a high co-solute content (*e.g.* sugars) within pectin solutions. Indeed, gelation and subsequent stability of HM pectin acidic gels depends on a complex “mixture” of hydrogen bonds and hydrophobic interactions (Rosenbohm, Lundt, Christensen, & Young, 2003). Contrary to hydrogen bonds, it is known that hydrophobic interactions require a certain co-solute content to form stable junction zones and to induce gelation (typically  $> 60$  wt% of sugar in pectin solution) (Dumitriu, 2004; Oakenfull, 1991).

In the absence of co-solutes, we assume that aerogellectins’  $S_{BET}$  can be used as a “characterization tool” to highlight the level of chain interactions that were formed in the aqueous state, and might reflect pectin major macromolecular properties. In (Figure 102 (b)), we compared the percentage of decrease of  $S_{BET}$  with pH, starting from pH 3.0 as the “reference point” to pH 1. Higher is pectin degree of methylation, smaller is the variation of  $S_{BET}$ . Indeed,

P35 aerogels presents the widest variation of  $S_{BET}$  with pH (from 570 to 290  $m^2/g$ ) than P59 and P70 (from 430 – 320  $m^2/g$ ).

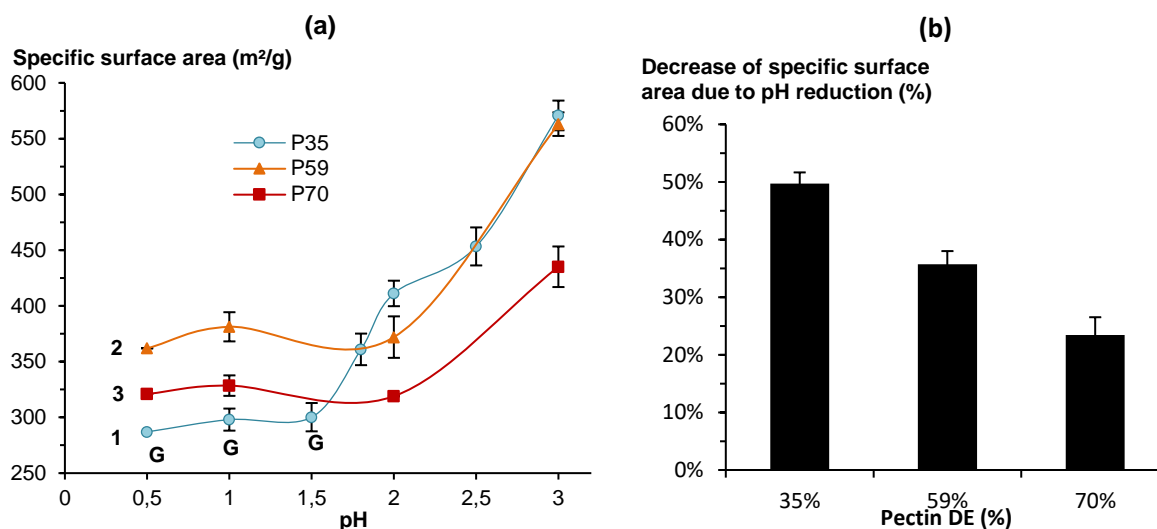


Figure 102. (a) Specific surface area ( $S_{BET}$ ) of aerogels made from 3 wt% of pectins P35 (1), P59 (2), P70 (3) dissolved at different pH and without calcium. Non-solvent was ethanol. Gel state before solvent exchange is indicated with “G”, otherwise samples were solutions. Lines are given to guide the eye.

(b) Reduction of  $S_{BET}$  (%) of aerogels made from 3 wt% when pH of pectin solutions is reduced from 3.0 to 1.0.

SEM characterization, presented on Figure 103, confirms the change of aerogels structural properties when pH was reduced below pH 3.0, with larger pores for all pectin studied at pH 1.0 than at pH 3.0, in correlation with lower density (Figure 100). The changes in network morphology with pH were clearly much more impacting P35 than P59, and were practically not noticeable for P70.

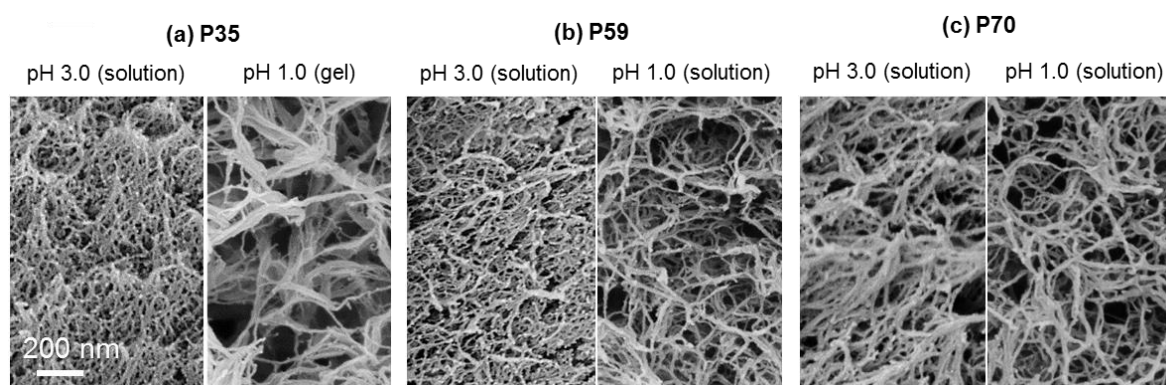


Figure 103. SEM pictures of aerogels made of 3 wt% of (a) P35, (b) P59 and (c) P70 dissolved at pH 3.0 or pH 1.0 without calcium. Non-solvent was ethanol. The state of the matter

(solution or gel) before solvent exchange is indicated for each case. The scale is the same of all images.

As a conclusion, not only we confirmed, but also, we generalized our previous conclusions about the influence of pH of pectin starting solutions on the structural properties of aeropectin (shrinkage, density,  $S_{BET}$ , morphology) made from different pectins from low to high degree of esterification. Moreover, the impacts of pH of pectin solution on aerogel morphology and properties were found to be more pronounced as the DE was lower in direct correlation with the intrinsic physico-chemical properties of each pectin of the study.

### 3.2. Impact of DE on aeropectin structural properties varying R(Ca) ratio

In this part, we focus on the impact of pectin DE in the presence of calcium at given pH on aeropectin final properties.

As it can be seen on Figure 104, viscosities of 0.90 wt% pectin solutions were more or less impacted by calcium addition depending on pectin DE and calcium R(Ca) ratio. Indeed, DE directly determines the proportion of non-methylated functions that can be ionized to interact with calcium ions. The formation of ionic bonds between pectin chains increases the viscosity of solutions and participates in the build-up of the pectin network.

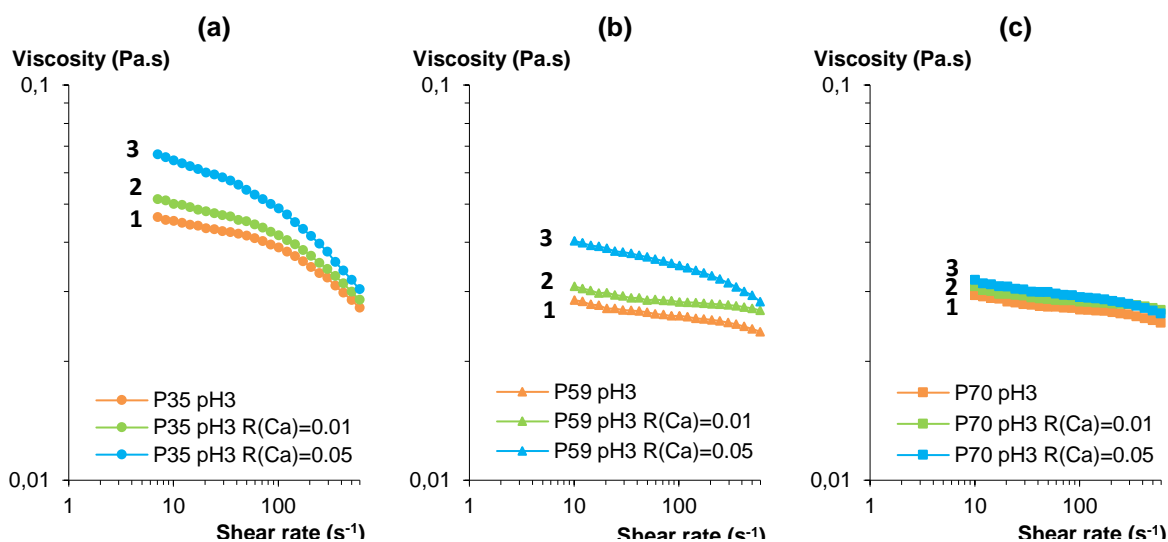


Figure 104. Viscosity as a function of shear rate of 0.9 wt% pectin solutions of (a) P35 (b) P59 and (c) P70 without calcium (1), at R(Ca) = 0.01 (2) or at R(Ca) = 0.05 (3). Viscosities were measured 30 min after calcium addition and homogenization.

As expected, at pH 3.0 close to  $pK_a$ , LM pectin P35 showed a high sensitivity to calcium. In the presence of calcium, viscosity increased with a more pronounced shear-thinning behavior

even at a very low  $R(\text{Ca})$  value ( $R(\text{Ca}) = 0.01$ ). On the opposite, viscosity of solutions of HM pectin P70 was not significantly impacted by addition of small amounts of calcium ( $R(\text{Ca}) = 0.01$  and  $R(\text{Ca}) = 0.05$ ), in correlation with its high proportion of methylated Gal.A which are not available to interact with cation. Due to its intermediate methylation degree, P59 showed a moderate but significant calcium-response similar to LM pectin P35, with solutions viscosity increase by around 25% - 30%. However, at the same  $R(\text{Ca})$  ratio value and polymer concentration, viscosity of solutions of P35 was always higher than P59 and P70. These results highlight the influence of pectin DE on the affinity of pectic chains towards calcium ions and on pectin gel strength in the presence of calcium, in agreement with literature (Garnier et al., 1993, 1994; R. Kohn & Luknár, 1975; Ström et al., 2007).

To investigate the impact of the degree of methylation in the presence of calcium on pectin aerogels structural properties, we added calcium to pectin concentrated solutions made of P35, P59 and P70, at two pH conditions: around  $\text{pK}_a$  at pH 3.0, and lower than  $\text{pK}_a$  at pH 2.0 at which acid dissociation is supposed to be low. Depending on i) the DE, ii) the pH iii) and the  $R(\text{Ca})$  value, we noticed different “calcium effects” on the state of the matter of aqueous pectin samples (solution or gel) before solvent exchange, and on final aeropectins structural properties after sc-drying (density, specific surface area).

### 3.2.1. Effect of DE on gel state at different $R(\text{Ca})$

At pH 3.0, no gel was obtained for P35 if  $R(\text{Ca}) < 0.1$ , for P59 if  $R(\text{Ca}) < 0.2$  and for P70 if  $R(\text{Ca}) < 0.4$ . These observations underline the critical role of the DE in the ionic gelation mechanism (M. A. V. Axelos & Thibault, 1991, p. 6; Garnier et al., 1993). The reactivity and gel forming ability of pectins increase with decreasing the degree of methylation, as the proportion of ionized free carboxylic groups available to create electrostatic bonds with cations is higher (M. A. V. Axelos & Thibault, 1991; Bayarri, Oulahal, Degraeve, & Gharsallaoui, 2014). In other words, the lower the pectin DE, the higher was the affinity of pectin chains towards calcium ions (Garnier et al., 1993, 1994; R. Kohn & Luknár, 1975; Ström et al., 2007). Moreover, this indicates that even HM pectins can interact with calcium, despite that their sensitivity to calcium depends on DE and calcium concentration.

### 3.2.2. Effect of pH on calcium sensitivity for various DE

Gel transition (determined by a “tilting test”) was more shifted to higher  $R(\text{Ca})$  values when pH was decreased to pH 2.0, as dissociation of carboxylates is significantly reduced compared to pH 3.0. Besides,  $R(\text{Ca})$  values where gelation occurred also was depending on the DE of each pectin. The low-methylated pectin P35 remained highly sensitive to calcium even

at pH 2.0, with a strong gelation induced at  $R(\text{Ca}) = 0.05$ , as under  $\text{pK}_a$  hydrogen interactions were contributing to build up the gel network (M. A. V. Axelos & Thibault, 1991; Rudolf Kohn, 1987; Yuliarti, Hoon, & Chong, 2017).

On the contrary, higher calcium concentration was needed to induce gelation of HM pectins solutions (P59 and P70). For P59 no gel transition was observed if  $R(\text{Ca}) < 0.4$  at pH 2.0 (in comparison to gel transition for  $R(\text{Ca}) = 0.2$  at pH 3.0). This indicates that pectin P59, which presents a moderate degree of methylation, kept certain “sensitivity” to calcium even at pH slightly below  $\text{pK}_a$ , but its gelling ability requires doubling calcium concentration to induce gelation. For P70 no gelation was observed within the entire range of  $R(\text{Ca})$  tested (up to  $R(\text{Ca}) = 0.6$ ). Due to its high degree of methylation, P70 required a major dissociation of non-methylated carboxylic groups at higher pH, to be able to efficiently form ionic junctions with calcium, contrary to P59 and P35.

As it was shown previously, the addition of calcium resulted in strengthening the pectin network, which was more pronounced at higher  $R(\text{Ca})$  and lower DE. Consequently, increasing calcium concentration reduced shrinkage during solvent exchange and sc-drying, which led to lower aeropectin density and porosity after drying, as it is shown in Figure 105 and Figure 106. The higher was the sensitivity to calcium reflected by the DE, the stronger were the gels (Ström et al., 2007), preserving samples from shrinkage.

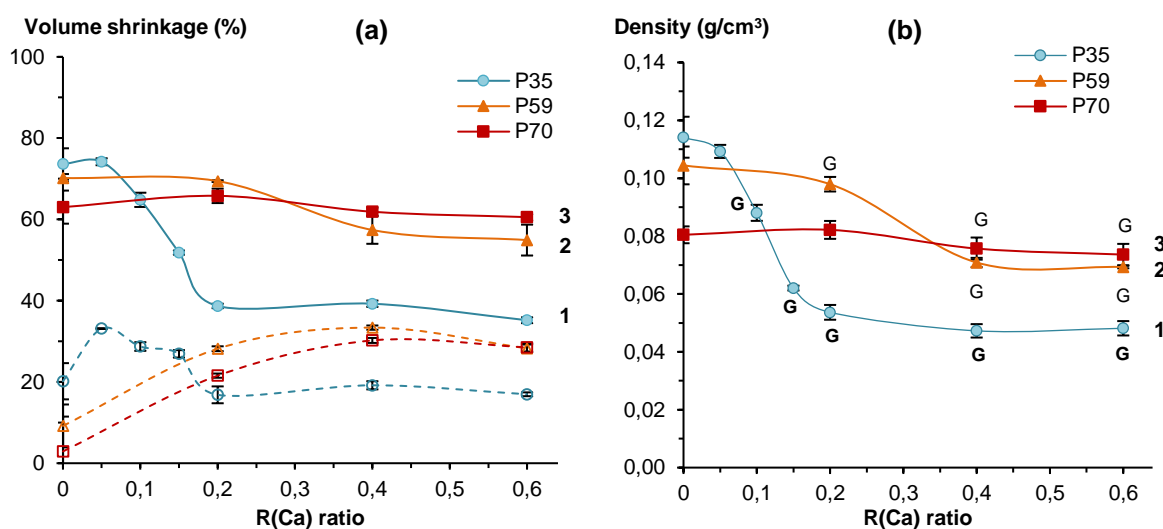


Figure 105. (a) Volume shrinkage after solvent exchange (open symbols) and after sc-drying (filled symbols) and (b) density of aeropectins made from 3 wt% of pectins P35 (1), P59 (2), P70 (3) dissolved at pH 3.0 with addition of calcium at different  $R(\text{Ca})$  ratio from  $R(\text{Ca}) = 0$  (no calcium) to  $R(\text{Ca}) = 0.6$ . Non-solvent was ethanol. Gel state before solvent exchange is indicated with “G”, otherwise samples were solutions.

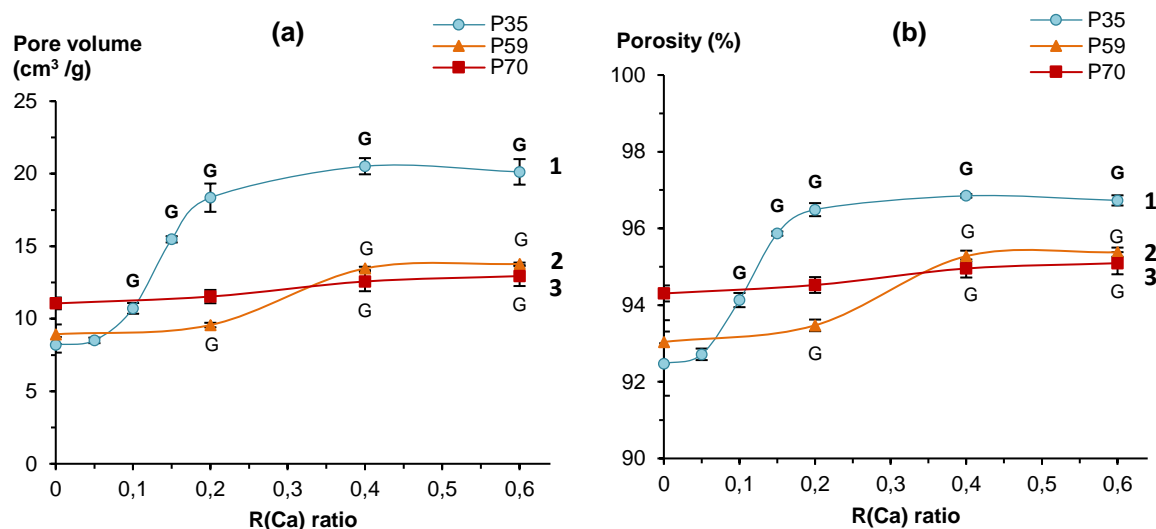


Figure 106. (a) Pore volume and (b) porosity (%) of aerogellectins made of 3 wt% of pectins P35 (1), P59 (2), P70 (3) dissolved at pH 3.0 and with increasing calcium ratio R(Ca) from 0 to 0.6. Non-solvent was ethanol. Gel state before solvent exchange is indicated with “G”, otherwise samples were solutions.

As shown in Figure 107 (a), we observe a progressive reduction of specific surface area while increasing the amount of calcium added in all pectin aerogels, as it was already observed in aerogels made from LM pectin P35 (see Section 2.3.). The lower was the DE and the higher was R(Ca), the more ionic junction zones between pectin chains were formed, resulting in the decrease of specific surface area as shown in Figure 107 (a). The “sensitivity” of the specific surface area to DE is demonstrated in Figure 107 (b) as the percentage of  $S_{BET}$  decrease from R(Ca) = 0 to R(Ca) = 0.6.

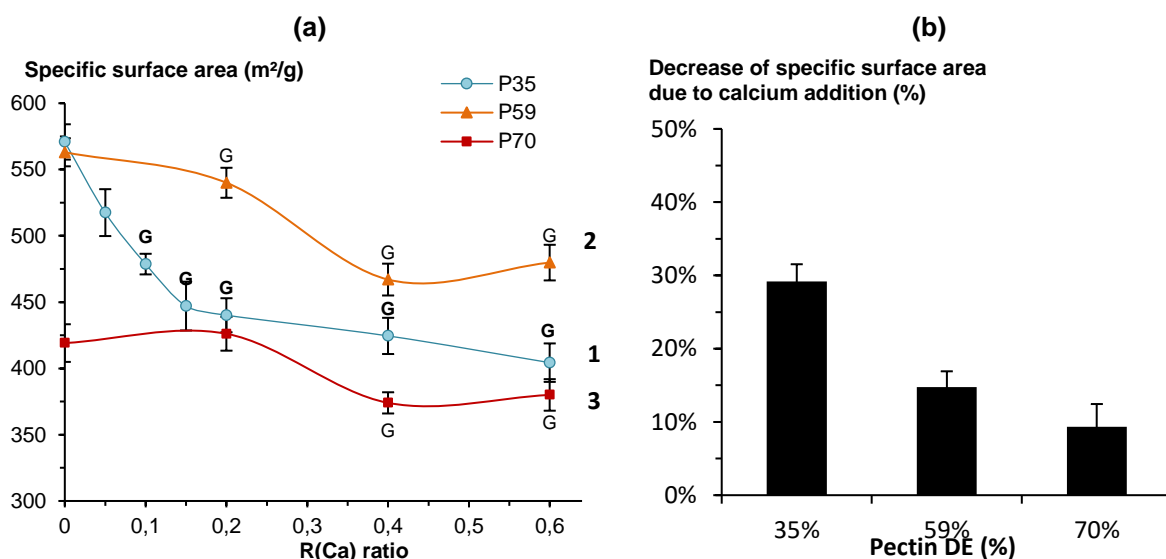


Figure 107. (a) Specific surface area ( $S_{BET}$ ) of aerogellectins made of 3 wt% of pectins P35 (1), P59 (2), P70 (3) dissolved at pH 3.0 and with increasing calcium ratio R(Ca) from 0 to 0.6.

Non-solvent was ethanol. Gel state before solvent exchange is indicated with “G”, otherwise samples were solutions.

(b) Reduction of  $S_{\text{BET}}$  (%) of aeropectins made from 3 wt% of pectin P35, P59, P70 from no calcium to  $R(\text{Ca}) = 0.6$  at pH 3.0. Non-solvent was ethanol.

The impact of the addition of calcium on aeropectin morphologies observed by SEM follows the same tendency as previously explained. The lower was the DE and the higher was  $R(\text{Ca})$ , the stronger was pectin network with better resistance to shrinkage, and the more preserved network morphologies were obtained, as it is shown on Figure 108 with the example of addition of high  $R(\text{Ca})$  ratio ( $R = 0.2$ ) at pH 3.0. In the presence of calcium, network morphology of LM pectin P35 was significantly less dense, with larger macropores in correlation with its structural properties. On the opposite, the network morphology of pectin aerogels from HM pectin P70 was not found to be strongly impacted, with similar morphologies without or with calcium at  $R(\text{Ca}) = 0.2$ . For moderately methylated HM pectin P59, the effect of calcium on morphology and structural properties are in an intermediate level between P35 and P70.

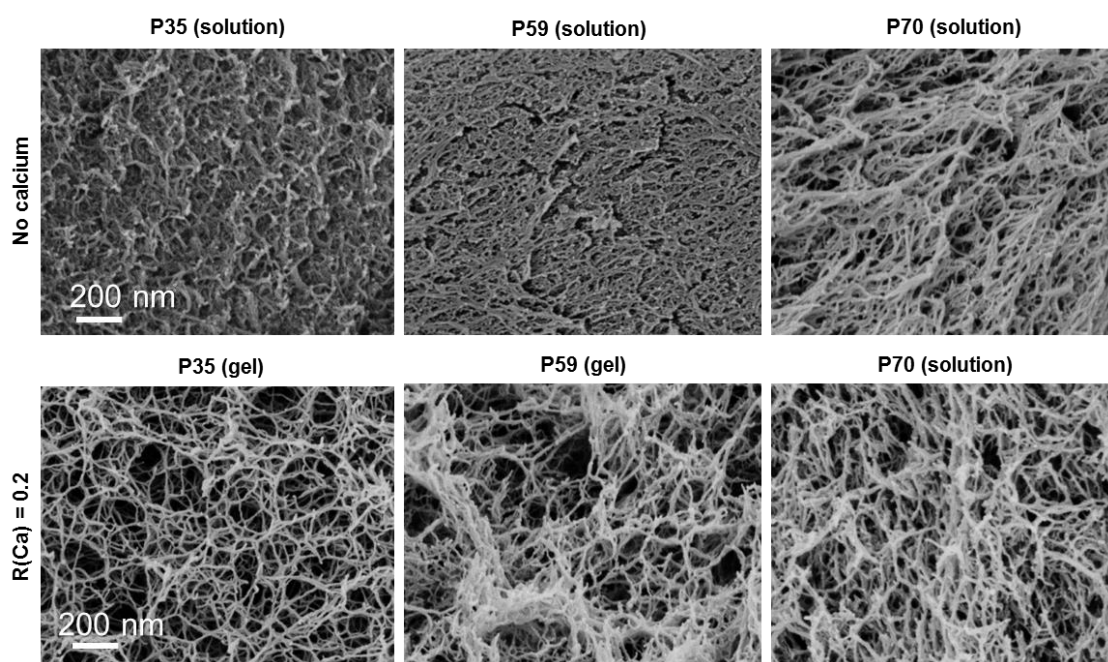


Figure 108. SEM pictures of aeropectins made of 3 wt% of P35, P59 and P70 (from left to right) dissolved at pH 3.0 and in absence of calcium or with addition of calcium at  $R(\text{Ca}) = 0.2$ . Non-solvent was ethanol. The scale is the same of all images.

Finally, we compared the increase of calcium  $R(\text{Ca})$  ratio on aeropectin structural properties but at pH 2.0 which is significantly lower than  $\text{pK}_a$ . Indeed, as pH was decreased from pH 3.0 to pH 2.0, only a small proportion of non-methylated carboxyl groups were still dissociated and thus were chemically available to interact with calcium ions. As a result, we found logical that the “calcium impact” on aeropectins structural properties was significantly

less pronounced than at pH 3.0. Moreover, as it was found for aerogels made from all pectins at pH 3.0, the “calcium impact” at pH 2.0 on aeropectin properties was dependent on pectin DE. Structural properties of aeropectins made from P35, P59 and P70 at pH 2.0 while varying calcium conditions are presented on Figure 109.

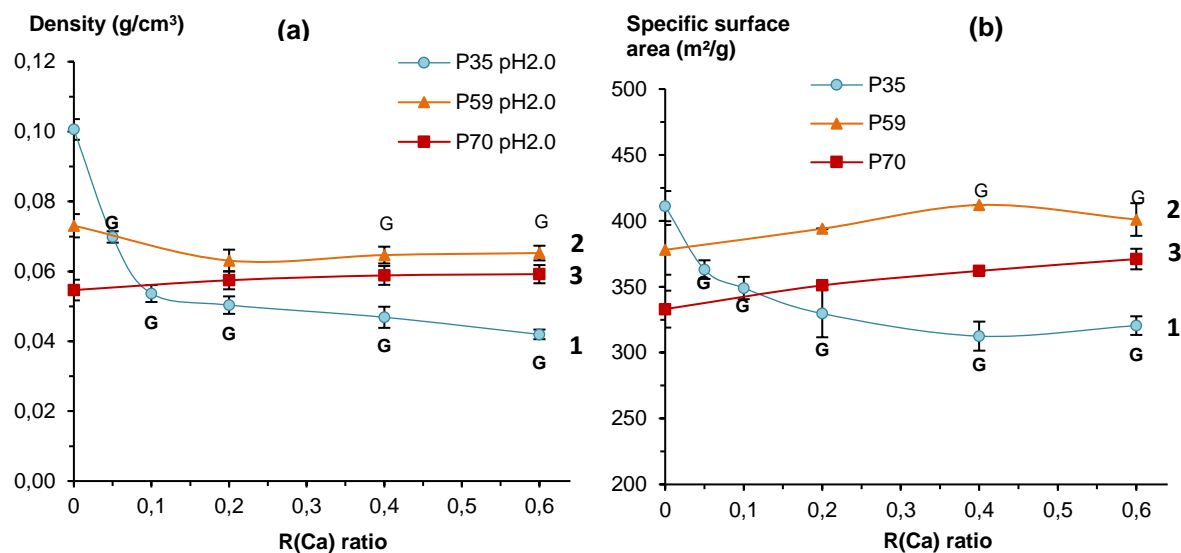


Figure 109. (a) Density and (b) specific surface area of aeropectins made of 3 wt% of pectins P35 (1), P59 (2), P70 (3) dissolved at pH 2.0 with increasing calcium ratio R(Ca) from 0 to 0.6. Non-solvent was ethanol.

Logically, LM pectin P35 exhibiting the lowest degree of methylation showed a significant sensitivity to calcium, as revealed by the strong decrease of density and specific surface area as R(Ca) was increased. On the contrary, the highest methylated pectin P70 exhibited similar properties independently of R(Ca) ratio and no significant calcium impact was found at pH 2.0. Finally, P59 showed an “intermediate” calcium impact on its structural properties in correlation with its DE. Picture of aeropectins made of 3 wt% of pectin P35, P59 and P70 at R(Ca) = 0.4 at pH 3.0 and 2.0 are given for illustration on Figure 110.

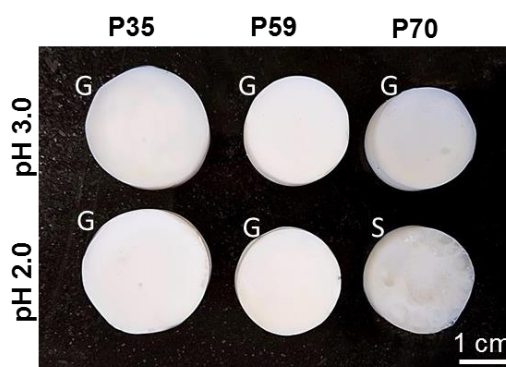


Figure 110. Aeropectins made of 3 wt% of P35, P59 and P70 dissolved at pH 3.0 or pH 2.0 with addition of calcium at R(Ca) = 0.4. Non-solvent was ethanol. The state of the matter before solvent exchange, gel (“G”) or solution (“S”), is indicated in each case.

### 3.3. Conclusions on the influence of pectin DE on aeropectins properties

In this study, we were able to highlight the influence of pectin DE on pectin solution characteristics (viscosity, gelling ability) and pectin aerogel properties (density, porosity, specific surface area, morphology). To our knowledge, this is the first time that the properties of pectin aerogels were correlated to pectin DE. As each pectin presents its “own” initial intrinsic properties (inter-individual variation), we found interesting to compare them by monitoring the evolution of properties of pectin samples (solution, gels, aerogels) while varying the process parameters (pH, calcium R(Ca) ratio).

- We confirmed and generalized the influence of pH and calcium concentration in pectin solutions on the final properties of aeropectins made from low-, medium- and high-methylated pectins.
- We observed that “pH-response” and a “calcium-response” of pectin solutions have a direct influence on pectin aerogel properties which are directly dependent on pectin DE. Low methylated pectin, P35, displayed high “pH-sensitivity” and “Ca-sensitivity”, while high methylated pectin P70 had the lowest sensitivity, and P59 was found to be intermediate. “High sensitivity” was reflected by the significant change of aerogel density and specific surface area as a function of pH and calcium concentration.

In this work, we used supercritical drying process as a tool to correlate physico-chemical phenomena which occurred in pectin aqueous solutions with aerogel properties. We showed that we can tune aeropectin properties not only by varying the process parameters, but also by changing the pectin type. Coupled to the first part of this chapter, we provided a complete study of the influence of extrinsic and intrinsic pectin parameters on pectin-based aerogels characteristics.

## Conclusions

In this chapter, we produced pectin aerogels of various structural and mechanical properties. For this purpose, polymer concentration, pH, concentration of mono- and divalent metal ions, non-solvent type and pectin degree of esterification were varied. The mechanism of structure formation, *i.e.* gelation or phase separation, is the key in aeropectins structure control. More precisely, we explained why and how pectin intrinsic properties (such as degree of methylation) and extrinsic parameters (such as pH condition, type of non-solvent, salt type and concentration) tune aeropectin properties. The multi-scale correlations from macromolecular aspects (polymer ionization with pH, calcium sensitivity and binding), to the morphological, structural and mechanical properties of pectin aerogels are built.

The results obtained provide the guidelines for making aerogel matrices with fully controlled morphology and properties. Fine structure control and tuning of aerogels is critical to adapt them to a specific application. We assume this study provides “recipes” of controlling structure formation of aerogels based on other gelling polyelectrolyte polysaccharides such as alginates and carrageenans.

## References

- Aegerter, M. A., Leventis, N., & Koebel, M. M. (Éd.). (2011). *Aerogels Handbook*. Consulté à l'adresse <http://link.springer.com/10.1007/978-1-4419-7589-8>
- Agoda-Tandjawa, G., Durand, S., Gaillard, C., Garnier, C., & Doublier, J.-L. (2012). Rheological behaviour and microstructure of microfibrillated cellulose suspensions/low-methoxyl pectin mixed systems. Effect of calcium ions. *Carbohydrate Polymers*, 87(2), 1045-1057. <https://doi.org/10.1016/j.carbpol.2011.08.021>
- Alaoui, A. H., Woignier, T., Scherer, G. W., & Phalippou, J. (2008). Comparison between flexural and uniaxial compression tests to measure the elastic modulus of silica aerogel. *Journal of Non-Crystalline Solids*, 354(40), 4556-4561. <https://doi.org/10.1016/j.jnoncrysol.2008.06.014>
- Axelos, M. a. V. (1990). Ion complexation of biopolymers: Macromolecular structure and viscoelastic properties of gels. *Makromolekulare Chemie. Macromolecular Symposia*, 39(1), 323-328. <https://doi.org/10.1002/masy.19900390128>
- Axelos, M. A. V., & Thibault, J.-F. (1991). CHAPTER 6 - The Chemistry of Low-Methoxyl Pectin Gelation. In R. H. Walter (Éd.), *The Chemistry and Technology of Pectin* (p. 109-118). <https://doi.org/10.1016/B978-0-08-092644-5.50011-X>
- Basak, R., & Bandyopadhyay, R. (2014). Formation and rupture of Ca<sup>2+</sup> induced pectin biopolymer gels. *Soft Matter*, 10(37), 7225-7233. <https://doi.org/10.1039/C4SM00748D>
- Bayarri, M., Oulahal, N., Degraeve, P., & Gharsallaoui, A. (2014). Properties of lysozyme/low methoxyl (LM) pectin complexes for antimicrobial edible food packaging. *Journal of Food Engineering*, 131, 18-25. <https://doi.org/10.1016/j.jfoodeng.2014.01.013>
- Braccini, I., & Pérez, S. (2001). Molecular Basis of Ca<sup>2+</sup> -Induced Gelation in Alginates and Pectins: The Egg-Box Model Revisited. *Biomacromolecules*, 2(4), 1089-1096. <https://doi.org/10.1021/bm010008g>
- Buchtová, N., & Budtova, T. (2016). Cellulose aero-, cryo- and xerogels: towards understanding of morphology control. *Cellulose*, 23(4), 2585-2595. <https://doi.org/10.1007/s10570-016-0960-8>
- Budarin, V. L., Clark, J. H., Luque, R., Macquarrie, D. J., & White, R. J. (2008). Palladium nanoparticles on polysaccharide-derived mesoporous materials and their catalytic performance in C-C coupling reactions. *The Royal Society of Chemistry*, 10, 382-387.

- Capel, F., Nicolai, T., Durand, D., Boulenguer, P., & Langendorff, V. (2006). Calcium and acid induced gelation of (amidated) low methoxyl pectin. *Food Hydrocolloids*, 20(6), 901-907. <https://doi.org/10.1016/j.foodhyd.2005.09.004>
- Cárdenas, A., Goycoolea, F. M., & Rinaudo, M. (2008). On the gelling behaviour of ‘nopal’ (*Opuntia ficus indica*) low methoxyl pectin. *Carbohydrate Polymers*, 73(2), 212-222. <https://doi.org/10.1016/j.carbpol.2007.11.017>
- Chtchigrovsky, M., Primo, A., Gonzalez, P., Molvinger, K., Robitzer, M., Quignard, F., & Taran, F. (2009). Functionalized chitosan as a green, recyclable, biopolymer-supported catalyst for the [3+2] Huisgen cycloaddition. *Angewandte Chemie (International Ed. in English)*, 48(32), 5916-5920. <https://doi.org/10.1002/anie.200901309>
- De Cicco, F., Russo, P., Reverchon, E., García-González, C. A., Aquino, R. P., & Del Gaudio, P. (2016). Prilling and supercritical drying: A successful duo to produce core-shell polysaccharide aerogel beads for wound healing. *Carbohydrate polymers*, 147, 482–489.
- Demilecamps, A. (2015). *Synthesis and characterization of polysaccharides-silica composite aerogels for thermal superinsulation*. (PhD Thesis, Ecole Nationale Supérieure des Mines de Paris).
- Diascorn, N., Calas, S., Sallee, H., Achard, P., & Rigacci, A. (2015). Polyurethane aerogels synthesis for thermal insulation – textural, thermal and mechanical properties. *Journal of Supercritical Fluids*, 106, 76–84. <https://doi.org/10.1016/j.supflu.2015.05.012>
- Dronnet, V. M., Renard, C. M. G. C., Axelos, M. A. V., & Thibault, J.-F. (1996). Characterisation and selectivity of divalent metal ions binding by citrus and sugar-beet pectins. *Carbohydrate Polymers*, 30(4), 253-263. [https://doi.org/10.1016/S0144-8617\(96\)00107-5](https://doi.org/10.1016/S0144-8617(96)00107-5)
- Druel, L., Bardl, R., Vorwerg, W., & Budtova, T. (2017). Starch Aerogels: A Member of the Family of Thermal Superinsulating Materials. *Biomacromolecules*, 18(12), 4232-4239. <https://doi.org/10.1021/acs.biomac.7b01272>
- Dumitriu, S. (2004). *Polysaccharides: Structural Diversity and Functional Versatility, Second Edition*. CRC Press.
- Fraeye, I., Deroeck, A., Duvetter, T., Verlent, I., Hendrickx, M., & Vanloey, A. (2007). Influence of pectin properties and processing conditions on thermal pectin degradation. *Food Chemistry*, 105(2), 555-563. <https://doi.org/10.1016/j.foodchem.2007.04.009>
- Fraeye, Ilse, Colle, I., Vandevenne, E., Duvetter, T., Van Buggenhout, S., Moldenaers, P., ... Hendrickx, M. (2010). Influence of pectin structure on texture of pectin–calcium gels.

- Innovative Food Science & Emerging Technologies*, 11(2), 401-409.  
<https://doi.org/10.1016/j.ifset.2009.08.015>
- Fraeye, Ilse, Doungha, E., Duvetter, T., Moldenaers, P., Van Loey, A., & Hendrickx, M. (2009). Influence of intrinsic and extrinsic factors on rheology of pectin–calcium gels. *Food Hydrocolloids*, 23(8), 2069-2077. <https://doi.org/10.1016/j.foodhyd.2009.03.022>
- Fraeye, Ilse, Duvetter, T., Doungha, E., Van Loey, A., & Hendrickx, M. (2010). Fine-tuning the properties of pectin–calcium gels by control of pectin fine structure, gel composition and environmental conditions. *Trends in Food Science & Technology*, 21(5), 219-228. <https://doi.org/10.1016/j.tifs.2010.02.001>
- García-González, C. A., Jin, M., Gerth, J., Alvarez-Lorenzo, C., & Smirnova, I. (2015). Polysaccharide-based aerogel microspheres for oral drug delivery. *Carbohydrate Polymers*, 117, 797-806. <https://doi.org/10.1016/j.carbpol.2014.10.045>
- Garnier, C., Axelos, M. A. V., & Thibault, J.-F. (1993). Phase diagrams of pectin-calcium systems: Influence of pH, ionic strength, and temperature on the gelation of pectins with different degrees of methylation. *Carbohydrate Research*, 240, 219-232. [https://doi.org/10.1016/0008-6215\(93\)84185-9](https://doi.org/10.1016/0008-6215(93)84185-9)
- Garnier, C., Axelos, M. A. V., & Thibault, J.-F. (1994). Selectivity and cooperativity in the binding of calcium ions by pectins. *Carbohydrate Research*, 256(1), 71-81. [https://doi.org/10.1016/0008-6215\(94\)84228-0](https://doi.org/10.1016/0008-6215(94)84228-0)
- Gavillon, R. (2007). *Preparation and characterization of ultra porous cellulosic materials* (École Nationale Supérieure des Mines de Paris). Consulté à l'adresse <https://pastel.archives-ouvertes.fr/tel-00173409/>
- Gavillon, R., & Budtova, T. (2007). Kinetics of cellulose regeneration from cellulose--NaOH-water gels and comparison with cellulose--N-methylmorpholine-N-oxide--water solutions. *Biomacromolecules*, 8(2), 424-432. <https://doi.org/10.1021/bm060376q>
- Gavillon, R., & Budtova, T. (2008). Aerocellulose: new highly porous cellulose prepared from cellulose-NaOH aqueous solutions. *Biomacromolecules*, 9(1), 269-277. <https://doi.org/10.1021/bm700972k>
- Gibson, L. J., & Ashby, M. F. (1999). *Cellular Solids: Structure and Properties*. Cambridge University Press.
- Gidley, M. J., Morris, E. R., Murray, E. J., Powell, D. A., & Rees, D. A. (1980). Evidence for two mechanisms of interchain association in calcium pectate gels. *International Journal of Biological Macromolecules*, 2(5), 332-334. [https://doi.org/10.1016/0141-8130\(80\)90060-4](https://doi.org/10.1016/0141-8130(80)90060-4)

- Grant, G. T., Morris, E. R., Rees, D. A., Smith, P. J. C., & Thom, D. (1973). Biological interactions between polysaccharides and divalent cations: The egg-box model. *FEBS Letters*, 32(1), 195-198. [https://doi.org/10.1016/0014-5793\(73\)80770-7](https://doi.org/10.1016/0014-5793(73)80770-7)
- Grosso, C. R. F., & Rao, M. A. (1998). Dynamic rheology of structure development in low-methoxyl pectin+Ca<sup>2+</sup>+sugar gels. Based on a paper presented at the 3rd International Hydrocolloids Conference, 11–16 August 1996, Sydney, Australia. *Food Hydrocolloids*, 12(3), 357-363. [https://doi.org/10.1016/S0268-005X\(98\)00034-4](https://doi.org/10.1016/S0268-005X(98)00034-4)
- Groult, S., & Budtova, T. (2018). Tuning structure and properties of pectin aerogels. *European Polymer Journal*, 108, 250-261. <https://doi.org/10.1016/j.eurpolymj.2018.08.048>
- Guilminot, E., Gavillon, R., Chatenet, M., Berthon-Fabry, S., Rigacci, A., & Budtova, T. (2008). New nanostructured carbons based on porous cellulose: Elaboration, pyrolysis and use as platinum nanoparticles substrate for oxygen reduction electrocatalysis. *Journal of Power Sources*, 185(2), 717-726. <https://doi.org/10.1016/j.jpowsour.2008.08.030>
- Hansen, C. M. (2007). *Hansen Solubility Parameters: A User's Handbook, Second Edition*. <https://doi.org/10.1201/9781420006834>
- Hoepfner, S., Ratke, L., & Milow, B. (2008). Synthesis and characterisation of nanofibrillar cellulose aerogels. *Cellulose*, 15(1), 121-129. <https://doi.org/10.1007/s10570-007-9146-8>
- Horvat, G., Xhanari, K., Finšgar, M., Gradišnik, L., Maver, U., Knez, Ž., & Novak, Z. (2017). Novel ethanol-induced pectin-xanthan aerogel coatings for orthopedic applications. *Carbohydrate Polymers*, 166, 365-376. <https://doi.org/10.1016/j.carbpol.2017.03.008>
- Horvat, G., Fajfar, T., Uzunalić, A. P., Knez, Ž., & Novak, Z. (2017). Thermal properties of polysaccharide aerogels. *Journal of Thermal Analysis and Calorimetry*, 127(1), 363-370. <https://doi.org/10.1007/s10973-016-5814-y>
- Hui, Y. H., Sherkat, F., & Sherkat, F. (2005). *Handbook of Food Science, Technology, and Engineering - 4 Volume Set*. <https://doi.org/10.1201/b15995>
- Kar, F., & Arslan, N. (1999). Effect of temperature and concentration on viscosity of orange peel pectin solutions and intrinsic viscosity–molecular weight relationship. *Carbohydrate Polymers*, 40(4), 277-284. [https://doi.org/10.1016/S0144-8617\(99\)00062-4](https://doi.org/10.1016/S0144-8617(99)00062-4)
- Kohn, R., & Luknár, O. (1975). Calcium and strontium ion activity in solutions of the corresponding pectinates and its dependence on their degree of esterification. *Collection of Czechoslovak Chemical Communications*, 40(4), 959-970. <https://doi.org/10.1135/cccc19750959>

- Kohn, Rudolf. (1987). Binding of divalent cations to oligomeric fragments of pectin. *Carbohydrate Research*, 160, 343-353. [https://doi.org/10.1016/0008-6215\(87\)80322-1](https://doi.org/10.1016/0008-6215(87)80322-1)
- Krall, S. M., & McFeeters, R. F. (1998). Pectin Hydrolysis: Effect of Temperature, Degree of Methylation, pH, and Calcium on Hydrolysis Rates. *Journal of Agricultural and Food Chemistry*, 46(4), 1311-1315. <https://doi.org/10.1021/jf970473y>
- Löfgren, C., Walkenström, P., & Hermansson, A.-M. (2002). Microstructure and Rheological Behavior of Pure and Mixed Pectin Gels. *Biomacromolecules*, 3(6), 1144-1153. <https://doi.org/10.1021/bm020044v>
- Lovskaya, D. D., Lebedev, A. E., & Menshutina, N. V. (2015). Aerogels as drug delivery systems: In vitro and in vivo evaluations. *The Journal of Supercritical Fluids*, 106, 115-121. <https://doi.org/veron>
- Martins, M., Barros, A. A., Quraishi, S., Gurikov, P., Raman, S. P., Smirnova, I., ... Reis, R. L. (2015). Preparation of macroporous alginate-based aerogels for biomedical applications. *The Journal of Supercritical Fluids*, 106, 152-159. <https://doi.org/10.1016/j.supflu.2015.05.010>
- Martoia, F., Cochereau, T., Dumont, P. J. J., Orgéas, L., Terrien, M., & Belgacem, M. N. (2016). Cellulose nanofibril foams: Links between ice-templating conditions, microstructures and mechanical properties. *Materials & Design*, 104, 376-391. <https://doi.org/10.1016/j.matdes.2016.04.088>
- Masuelli, M. A. (2014). Mark-Houwink Parameters for Aqueous-Soluble Polymers and Biopolymers at Various Temperatures. *Journal of Polymer and Biopolymer Physics Chemistry, Journal of Polymer and Biopolymer Physics Chemistry*, 2(2), 37-43. <https://doi.org/10.12691/jpbpc-2-2-2>
- Morris, E. R., Powell, D. A., Gidley, M. J., & Rees, D. A. (1982). Conformations and interactions of pectins: I. Polymorphism between gel and solid states of calcium polygalacturonate. *Journal of Molecular Biology*, 155(4), 507-516. [https://doi.org/10.1016/0022-2836\(82\)90484-3](https://doi.org/10.1016/0022-2836(82)90484-3)
- Oakenfull, D. G. (1991). CHAPTER 5 - The Chemistry of High-Methoxyl Pectins. In R. H. Walter (Éd.), *The Chemistry and Technology of Pectin* (p. 87-108). <https://doi.org/10.1016/B978-0-08-092644-5.50010-8>
- Paoletti, S., Cesaro, A., Delben, F., & Ciana, A. (1986). Ionic Effects on the Conformation, Equilibrium, Properties, and Rheology of Pectate in Aqueous Solutions and Gels. In *ACS Symposium Series: Vol. 310. Chemistry and Function of Pectins* (Vol. 310, p. 73-87). <https://doi.org/10.1021/bk-1986-0310.ch007>

- Pekala, R. W., Alviso, C. T., & LeMay, J. D. (1990). Organic aerogels: microstructural dependence of mechanical properties in compression. *Journal of Non-Crystalline Solids*, *125*(1), 67-75. [https://doi.org/10.1016/0022-3093\(90\)90324-F](https://doi.org/10.1016/0022-3093(90)90324-F)
- Plaschina, I. G., Semenova, M. G., Braudo, E. E., & Tolstoguzov, V. B. (1985). Structural studies of the solutions of anionic polysaccharides. IV. Study of pectin solutions by light-scattering. *Carbohydrate Polymers*, *5*(3), 159-179. [https://doi.org/10.1016/0144-8617\(85\)90020-7](https://doi.org/10.1016/0144-8617(85)90020-7)
- Quraishi, S., Martins, M., Barros, A. A., Gurikov, P., Raman, S. P., Smirnova, I., ... Reis, R. L. (2015). Novel non-cytotoxic alginate–lignin hybrid aerogels as scaffolds for tissue engineering. *The Journal of Supercritical Fluids*, *105*, 1-8. <https://doi.org/10.1016/j.supflu.2014.12.026>
- Ralet, M.-C., Dronnet, V., Buchholt, H. C., & Thibault, J.-F. (2001). Enzymatically and chemically de-esterified lime pectins: characterisation, polyelectrolyte behaviour and calcium binding properties. *Carbohydrate Research*, *336*(2), 117-125. [https://doi.org/10.1016/S0008-6215\(01\)00248-8](https://doi.org/10.1016/S0008-6215(01)00248-8)
- Rege, A., Schestakow, M., Karadagli, I., Ratke, L., & Itskov, M. (2016). Micro-mechanical modelling of cellulose aerogels from molten salt hydrates. *Soft Matter*, *12*(34), 7079-7088. <https://doi.org/10.1039/C6SM01460G>
- Renard, C. M. G. C., & Thibault, J.-F. (1996). Degradation of pectins in alkaline conditions: kinetics of demethylation. *Carbohydrate Research*, *286*, 139-150. [https://doi.org/10.1016/0008-6215\(96\)00056-0](https://doi.org/10.1016/0008-6215(96)00056-0)
- Rosenbohm, C., Lundt, I., Christensen, T. I. E., & Young, N. G. (2003). Chemically methylated and reduced pectins: preparation, characterisation by <sup>1</sup>H NMR spectroscopy, enzymatic degradation, and gelling properties. *Carbohydrate Research*, *338*(7), 637-649. [https://doi.org/10.1016/S0008-6215\(02\)00440-8](https://doi.org/10.1016/S0008-6215(02)00440-8)
- Rudaz, C. (2013). *Cellulose and Pectin Aerogels: Towards their nano-structuration* (PhD Thesis, Ecole Nationale Supérieure des Mines de Paris). Consulté à l'adresse <https://pastel.archives-ouvertes.fr/pastel-00957296/document>
- Rudaz, C., Courson, R., Bonnet, L., Calas-Etienne, S., Sallée, H., & Budtova, T. (2014). Aeropectin: Fully Biomass-Based Mechanically Strong and Thermal Superinsulating Aerogel. *Biomacromolecules*, *15*(6), 2188-2195. <https://doi.org/10.1021/bm500345u>
- Sescousse, R. (2010). *Nouveaux matériaux cellulose ultra-poreux et leurs carbones à partir de solvants verts* (Phdthesis, École Nationale Supérieure des Mines de Paris). Consulté à l'adresse <https://pastel.archives-ouvertes.fr/pastel-00618528/document>

- Sescousse, R., Gavillon, R., & Budtova, T. (2011). Aerocellulose from cellulose–ionic liquid solutions: Preparation, properties and comparison with cellulose–NaOH and cellulose–NMMO routes. *Carbohydrate Polymers*, 83(4), 1766-1774. <https://doi.org/10.1016/j.carbpol.2010.10.043>
- Siew, C. K., Williams, P. A., & Young, N. W. G. (2005). New Insights into the Mechanism of Gelation of Alginate and Pectin: Charge Annihilation and Reversal Mechanism. *Biomacromolecules*, 6(2), 963-969. <https://doi.org/10.1021/bm0493411>
- Sriamornsak, P. (2003). Chemistry of pectin and its pharmaceutical uses: A review. *Silpakorn University International Journal*, 3(1-2), 206–228.
- Ström, A., Ribelles, P., Lundin, L., Norton, I., Morris, E. R., & Williams, M. A. K. (2007). Influence of Pectin Fine Structure on the Mechanical Properties of Calcium–Pectin and Acid–Pectin Gels. *Biomacromolecules*, 8(9), 2668-2674. <https://doi.org/10.1021/bm070192r>
- Ström, A., Schuster, E., & Goh, S. M. (2014). Rheological characterization of acid pectin samples in the absence and presence of monovalent ions. *Carbohydrate Polymers*, 113, 336-343. <https://doi.org/10.1016/j.carbpol.2014.06.090>
- Subrahmanyam, R., Gurikov, P., Dieringer, P., Sun, M., & Smirnova, I. (2015). On the Road to Biopolymer Aerogels—Dealing with the Solvent. *Gels*, 1(2), 291-313. <https://doi.org/10.3390/gels1020291>
- Thakur, B. R., Singh, R. K., Handa, A. K., & Rao, M. A. (1997). Chemistry and uses of pectin — A review. *Critical Reviews in Food Science and Nutrition*, 37(1), 47-73. <https://doi.org/10.1080/10408399709527767>
- Thibault, J. F., & Rinaudo, M. (1986). Chain association of pectic molecules during calcium-induced gelation. *Biopolymers*, 25(3), 455–468.
- Tkalec, G., Knez, Ž., & Novak, Z. (2015). Fast production of high-methoxyl pectin aerogels for enhancing the bioavailability of low-soluble drugs. *The Journal of Supercritical Fluids*, 106, 16-22. <https://doi.org/10.1016/j.supflu.2015.06.009>
- Trygg, J., Fardim, P., Gericke, M., Mäkilä, E., & Salonen, J. (2013). Physicochemical design of the morphology and ultrastructure of cellulose beads. *Carbohydrate Polymers*, 93(1), 291-299. <https://doi.org/10.1016/j.carbpol.2012.03.085>
- Voragen, F., Schols, H., & Visser, R. G. F. (2013). *Advances in Pectin and Pectinase Research*. Springer.
- Walter, R. H. (2012). *The Chemistry and Technology of Pectin*. Academic Press.

- Weigold, L., & Reichenauer, G. (2014). Correlation between mechanical stiffness and thermal transport along the solid framework of a uniaxially compressed polyurea aerogel. *Journal of Non-Crystalline Solids*, 406, 73-78. <https://doi.org/10.1016/j.jnoncrysol.2014.09.040>
- Yoo, S.-H., Fishman, M. L., Savary, B. J., & Hotchkiss, A. T. (2003). Monovalent Salt-Induced Gelation of Enzymatically Deesterified Pectin. *Journal of Agricultural and Food Chemistry*, 51(25), 7410-7417. <https://doi.org/10.1021/jf030152o>
- Yuliarti, O., Hoon, A. L. S., & Chong, S. Y. (2017). Influence of pH, pectin and Ca concentration on gelation properties of low-methoxyl pectin extracted from *Cyclea barbata* Miers. *Food Structure*, 11, 16-23. <https://doi.org/10.1016/j.foostr.2016.10.0>



**CHAPTER IV. THERMAL  
CONDUCTIVITY-STRUCTURE  
PROPERTIES CORRELATIONS OF  
PECTIN AEROGELS**

---

**CONTENTS**

**CHAPTER IV. THERMAL CONDUCTIVITY-STRUCTURE PROPERTIES  
CORRELATIONS OF PECTIN AEROGELS**

<b>INTRODUCTION.....</b>	<b>217</b>
<b>1. THERMAL CONDUCTIVITY AS A FUNCTION OF PECTIN AEROGEL DENSITY: SUMMARY OF ALL RESULTS .....</b>	<b>218</b>
<b>2. INFLUENCE OF PECTIN CONCENTRATION AND NON-SOLVENT TYPE ON AEROGEL THERMAL CONDUCTIVITY .....</b>	<b>222</b>
2.1. INFLUENCE OF PECTIN CONCENTRATION .....	222
2.2. INFLUENCE OF NON-SOLVENT TYPE ON AEROGEL THERMAL CONDUCTIVITY .....	226
<b>3. INFLUENCE OF CA-INDUCED CROSS-LINKING AND PH ON PECTIN AEROGEL PROPERTIES .....</b>	<b>228</b>
3.1. INFLUENCE OF PH AT R(CA) = 0 AND 0.2 .....	228
3.2. INFLUENCE OF CALCIUM CONCENTRATION AT PH 3 .....	232
<b>CONCLUSIONS .....</b>	<b>236</b>
<b>REFERENCES.....</b>	<b>237</b>

## Introduction

Silica aerogels are known to be materials with the lowest thermal conductivity in ambient conditions, *i.e.* with thermal conductivity below that of air, 0.013 – 0.014 vs 0.025 W/(m.K), respectively. Some synthetic polymer aerogels, for example, based on polyurethanes, are also super-insulating materials but with slightly higher conductivity, around 0.017 W/(m.K) (Diascorn, Calas, Sallee, Achard, & Rigacci, 2015). Compared to the first silica aerogels (*i.e.* non chemically-modified) which are extremely fragile, polymer-based aerogels, and bio-aerogels in particular, do not break under compression (Rudaz et al., 2014). Moreover, the synthesis of bio-aerogels does not involve any toxic compounds which is the case of many synthetic polymer aerogels (for example, based on resorcinol formaldehyde or polyurethanes cross-linked with isocyanate) (Pekala, 1989). Bio-aerogels from medium and high methylated pectins were shown to be thermal super-insulating materials with conductivity increasing from 0.018 W/(m.K) to 0.03 W/(m.K) for densities from 0.05 to 0.15 g/cm<sup>3</sup> (Rudaz et al., 2014). Very few is known about the thermal conductivity of bio-aerogels, and practically nothing on conductivity-structure correlations.

The goal of this work is to correlate thermal conductivity with aerogel morphology and properties in order to understand how to obtain a thermal super-insulating material with the lowest possible conductivity. In the whole chapter, the focus will be made on the relationship between the characteristics of the initial polymer, the processing parameters, the structural properties of the pectin aerogels and their thermal conductivity.

We finely tuned pectin aerogels properties and morphology by adjusting polymer concentration, non-solvent type, pH and calcium concentration, and correlated them with material thermal conductivity. As the relationships between the process parameters and the structural properties of aerogel were established and discussed in detail in the Chapter III, in this chapter we will rather focus on the structure-thermal properties correlations of pectin aerogels. The chapter is organized as follows:

- The first part is dedicated to the influence of pectin concentration and non-solvent on aerogel density and morphology, and then on the resulting thermal properties.
- As pectin is a polyelectrolyte, the influence of pH conditions on pectin aerogel properties was evaluated, in the presence ( $R(\text{Ca}) = 0.2$ ) or in absence of calcium ions.
- Then, we set the pH, and we studied the influence of Ca-induced cross-linking by increasing calcium ratio from  $R(\text{Ca}) = 0$  to  $R(\text{Ca}) = 0.2$ .

Most of the results presented in this Chapter were published in (Groult & Budtova, 2018).

## 1. Thermal conductivity as a function of pectin aerogel density: summary of all results

As mentioned in the state of the art (Chapter I), thermal conductivity of aerogels is strongly impacted by network morphology and density. Guided by the main results presented in the previous Chapter III about aeropectins' structure-properties correlations, polymer concentration, solution pH, concentration of calcium ions and the type of non-solvent used for solvent-exchange were varied to tune pectin gelation mechanism and the state of matter, solution or gel, which strongly impacted the final structural and thermal properties of pectin aerogels after sc-drying. All results on thermal conductivity obtained in this work are summarized in Figure 111 as a function of aeropectin bulk density and all characteristics of aerogels are in Table 7. Figure 111 shows a U-shape curve obtained for this type of bio-aerogels. The general trends known for thermal conductivity of classical aerogels are thus applicable to bio-aerogels. The minimal thermal conductivity is very low, 0.015 W/(m.K), and comparable with that of silica aerogels; it corresponds to pectin aerogel density of 0.1 g/cm<sup>3</sup> (Figure 111).

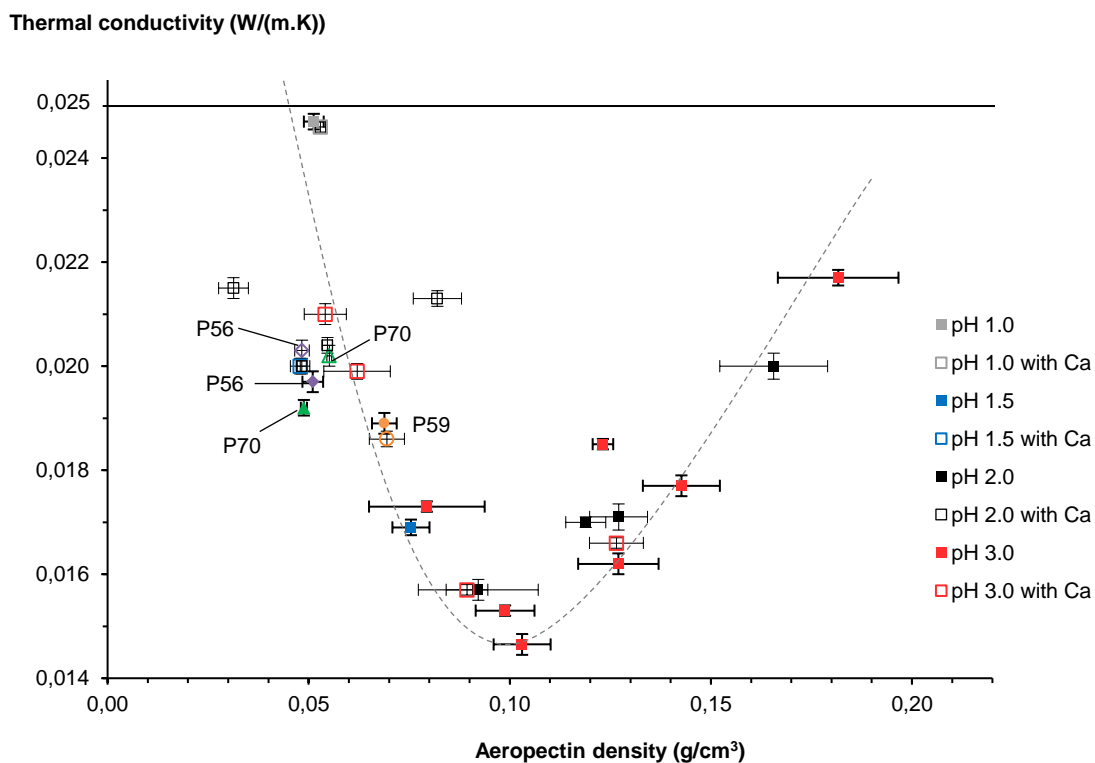


Figure 111. Aeropectin thermal conductivity as a function of density. Open points correspond to samples cross-linked with calcium. Not-marked samples are from P35 (squares). P56 (diamonds), P59 (circles) and P70 (triangles) were made from 3 wt% pectin solutions at pH 1. Solid line is conductivity of air in ambient conditions; dashed line is given to guide the eye.

Figure 111 shows that density is one of the key parameters controlling thermal conductivity, as expected. Thus, the first question to answer is what are the experimental conditions which control the density of aeropectin? For example, when density varies from 0.05 to 0.10 g/cm<sup>3</sup>, thermal conductivity decreases from 0.024 to 0.015 W/(m.K). Obviously, the morphology of aerogels also plays a very important role.

Thus, the second question to answer is how to control the morphology of aeropectins to obtain the lowest thermal conductivity? To answer these questions, we studied the influence of P35 concentration, pH, concentration of Ca<sup>2+</sup> ions, the state of matter (gel or solution) before solvent exchange, and the type of non-solvent on aeropectin density and specific surface area to finally correlate with thermal conductivity.

## CHAPTER IV.

## Thermal conductivity-structure properties correlations of pectin aerogels

Table 7. Characteristics of all aeropectins synthesised in the work. The state of matter solution before solvent-exchange “S” or gel “G” is given in each case.

Pectin DE (%)	Pectin wt%	pH	R(Ca) ratio	State of matter	Type of non-solvent	Shrinkage after solvent-exchange (%)		Total volume shrinkage (%)		Bulk density (g/cm <sup>3</sup> )		Porosity (%)		Pore volume (cm <sup>3</sup> / g)		Specific surface area (m <sup>2</sup> /g)		Thermal conductivity (W/(m.K))	
70	3	1.0	0	S	Ethanol	9.0	± 1.7	46.0	± 1.8	0.049	± 0.002	96.7	± 0.2	18.23	± 0.52	329	± 9	0.01920	± 0.00015
70	3	1.0	0.20	S	Ethanol	12.0	± 1.3	48.3	± 2.5	0.055	± 0.004	96.3	± 0.3	18.18	± 0.66	326	± 9	0.02020	± 0.00015
59	3	1.0	0	S	Ethanol	10.0	± 2.3	57.8	± 1.9	0.069	± 0.006	95.4	± 0.6	15.00	± 0.30	396	± 13	0.01890	± 0.00020
59	3	1.0	0.20	S	Ethanol	16.0	± 1.1	53.9	± 1.9	0.069	± 0.003	95.4	± 0.4	15.37	± 0.16	371	± 6	0.01860	± 0.00020
56	3	1.0	0	S	Ethanol	17.8	± 1.2	54.5	± 1.0	0.051	± 0.001	96.6	± 0.1	18.93	± 0.24	326	± 13	0.01970	± 0.00015
56	3	1.0	0.20	S	Ethanol	18.7	± 1.3	40.4	± 1.8	0.048	± 0.001	96.8	± 0.1	20.02	± 0.26	321	± 20	0.02030	± 0.00010
35	3	1.0	0	G	Ethanol	17.0	± 0.8	50.8	± 2.7	0.051	± 0.003	96.6	± 0.5	17.08	± 0.53	238	± 10	0.02470	± 0.00020
35	3	1.0	0.20	G	Ethanol	20.2	± 0.5	38.6	± 1.6	0.053	± 0.001	96.5	± 0.2	18.73	± 0.30	219	± 9	0.02460	± 0.00020
35	3	1.5	0	G	Ethanol	30.3	± 1.2	65.4	± 1.2	0.075	± 0.005	95.0	± 0.5	12.34	± 0.81	249	± 24	0.01690	± 0.00015
35	3	1.5	0.20	G	Ethanol	20.1	± 0.6	41.4	± 1.4	0.048	± 0.002	96.8	± 0.1	19.60	± 0.18	257	± 21	0.02000	± 0.00015
35	2	2.0	0	S	Ethanol	39.0	± 2.9	80.6	± 3.6	0.092	± 0.015	93.9	± 2.0	10.20	± 0.27	274	± 33	0.01570	± 0.00020
35	3	2.0	0	S	Ethanol	28.1	± 3.5	73.8	± 2.5	0.127	± 0.007	91.5	± 1.0	9.29	± 0.30	399	± 6	0.01710	± 0.00025
35	4	2.0	0	G	Ethanol	33.3	± 1.9	69.8	± 1.7	0.119	± 0.005	92.1	± 0.4	7.98	± 0.31	416	± 28	0.01700	± 0.00010
35	6	2.0	0	G	Ethanol	17.4	± 2.1	67.3	± 1.0	0.166	± 0.013	89.0	± 1.2	5.77	± 0.35	444	± 21	0.02000	± 0.00025

## CHAPTER IV.

## Thermal conductivity-structure properties correlations of pectin aerogels

35	2	2.0	0.20	G	Ethanol	20.9 ± 2.8	40.4 ± 2.5	0.031 ± 0.004	97.9 ± 0.3	30.01 ± 1.79	267 ±	0.02150 ± 0.00020
35	3	2.0	0.20	G	Ethanol	7.3 ± 1.2	34.5 ± 3.0	0.048 ± 0.001	96.8 ± 0.5	19.22 ± 1.08	317 ± 12	0.02000 ± 0.00015
35	4	2.0	0.20	G	Ethanol	11.0 ± 2.0	29.9 ± 0.6	0.055 ± 0.001	96.4 ± 0.9	17.12 ± 0.38	342 ± 22	0.02040 ± 0.00015
35	6	2.0	0.20	G	Ethanol	8.0 ± 1.8	32.6 ± 2.7	0.082 ± 0.006	94.5 ± 0.7	12.85 ± 0.98	357 ± 18	0.02130 ± 0.00015
35	2	3.0	0	S	Ethanol	44.2 ± 1.4	81.4 ± 2.3	0.103 ± 0.007	93.1 ± 0.3	9.15 ± 0.33	541 ± 24	0.01465 ± 0.00020
35	3	3.0	0	S	Ethanol	23.1 ± 4.8	79.7 ± 3.9	0.143 ± 0.010	90.5 ± 0.5	7.97 ± 0.60	552 ± 18	0.01770 ± 0.00020
35	4	3.0	0	S	Ethanol	20.6 ± 5.3	68.4 ± 2.8	0.127 ± 0.010	91.5 ± 0.9	7.68 ± 0.48	601 ± 16	0.01620 ± 0.00020
35	6	3.0	0	G	Ethanol	6.8 ± 1.4	71.5 ± 0.5	0.182 ± 0.015	87.9 ± 1.7	5.98 ± 0.32	529 ± 22	0.02170 ± 0.00015
35	3	3.0	0.05	S	Ethanol	40.0 ± 5.6	75.4 ± 3.4	0.127 ± 0.007	91.6 ± 0.2	8.51 ± 0.19	522 ± 23	0.01660 ± 0.00010
35	3	3.0	0.10	G	Ethanol	33.1 ± 1.0	63.9 ± 1.8	0.089 ± 0.005	94.0 ± 0.2	10.71 ± 0.37	499 ± 10	0.01570 ± 0.00010
35	3	3.0	0.15	G	Ethanol	26.9 ± 0.9	51.8 ± 1.5	0.062 ± 0.008	95.9 ± 0.1	15.48 ± 0.21	444 ± 21	0.01990 ± 0.00015
35	3	3.0	0.20	G	Ethanol	16.8 ± 2.1	39.2 ± 2.8	0.054 ± 0.005	96.4 ± 0.2	18.35 ± 0.98	455 ± 32	0.0210 ± 0.00020
35	3	3.0	0	S	Acetone	27.2 ± 4.8	62.7 ± 5.2	0.08 ± 0.018	94.7 ± 0.6	12.9 ± 0.63	614 ± 24	0.0173 ± 0.0001
35	4	3.0	0	S	Acetone	24.7 ± 3.3	57.9 ± 3.3	0.099 ± 0.007	93.4 ± 0.7	10.9 ± 0.07	621 ± 8	0.01530 ± 0.0001
35	6	3.0	0	G	Acetone	14.7 ± 1.8	50.2 ± 1.6	0.123 ± 0.003	91.8 ± 0.2	7.8 ± 0.17	594 ± 21	0.01850 ± 0.0001

## 2. Influence of pectin concentration and non-solvent type on aerogel thermal conductivity

### 2.1. Influence of pectin concentration

The influence of pectin concentration on samples' shrinkage after solvent exchange and after drying is shown in Figure 112 for solutions at pH 2. The effect of pectin concentration on aerogel density and specific surface area is illustrated in Figure 113.

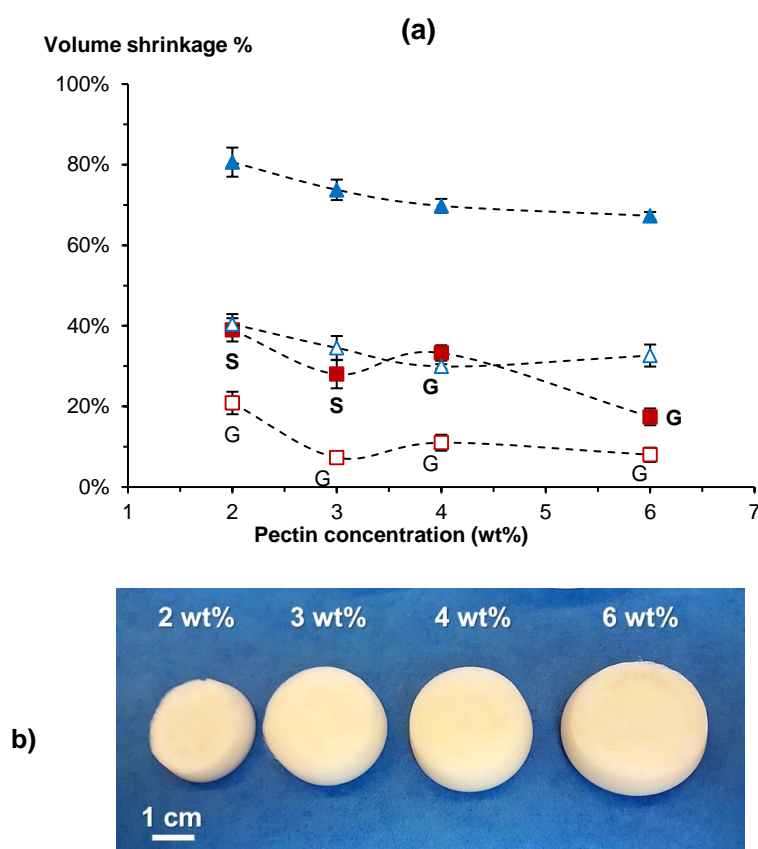


Figure 112. (a) Volume shrinkage of pectin aerogels after solvent exchange (squares) and overall volume shrinkage after sc drying (triangles) as a function of P35 concentration at pH 2. Filled points correspond to non-cross-linked sample, open points – when calcium was added ( $R(\text{Ca}) = 0.2$ ). The state of matter before solvent exchange is indicated for each case (solution “S” or gel “G”). Non-solvent was ethanol. Lines are given to guide the eye. From (Groult & Budtova, 2018).

(b) Pictures of pectin aerogels made from pectin P35 at different pectin concentration (wt%) dissolved at pH 3.0 without calcium.

Increasing pectin concentration decreased shrinkage, as already reported for other bio-aerogels (Buchtová & Budtova, 2016; Hoepfner, Ratke, & Milow, 2008). The values obtained in this work are from 65 % to 80 % for non-cross-linked samples, and from 30 % to 50 % for cross-linked with calcium.

As expected from the Chapter III, despite lower shrinkage at higher polymer concentration, aeropectin density increased with the increase of pectin concentration in both cases, when pectin was cross-linked with calcium and not. It should be noted that the density of cross-linked aeropectins ( $R(\text{Ca}) = 0.2$ ) was twice lower than that of the corresponding non-cross-linked ones, and it was very close to the theoretical density calculated for the case of zero volume shrinkage (solid line in Figure 113).

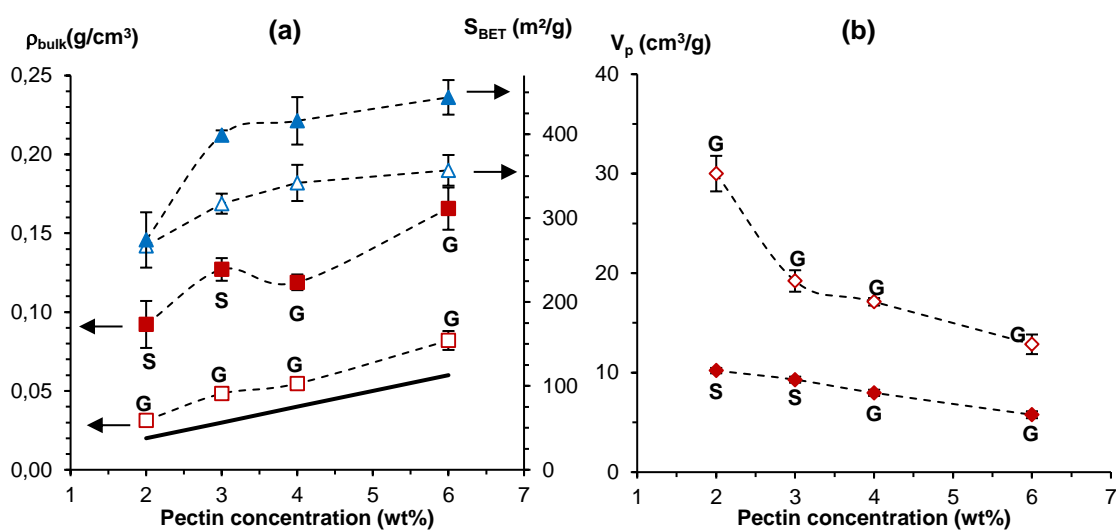


Figure 113. (a) Density (squares) and specific surface area (triangles) and (b) pore volume of aeropectins based on P35 dissolved at pH 2 as a function of polymer concentration in solution. Filled points correspond to non-cross-linked samples, open points – when calcium was added ( $R(\text{Ca}) = 0.2$ ). Solid line is theoretical density corresponding to zero volume shrinkage. The state of matter before solvent exchange is indicated for each case (solution “S” or gel “G”). Dashed lines are given to guide the eye. From (Groult & Budtova, 2018).

As shown in Figure 114, similar results and trends on pectin aerogels structural properties were obtained at pH 3 while varying pectin concentration.

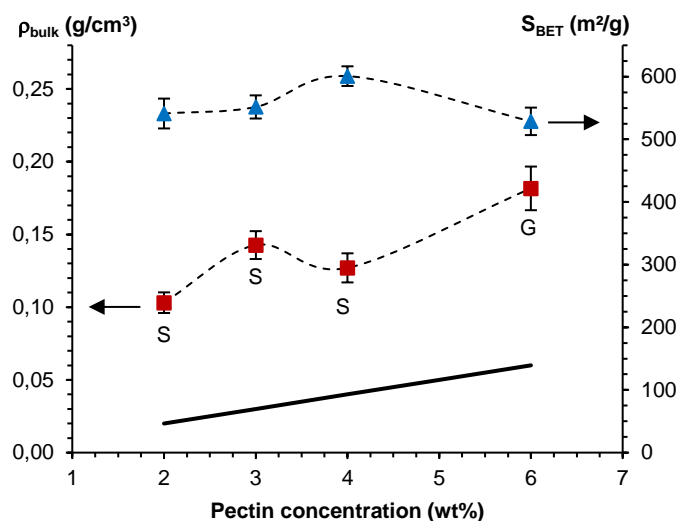


Figure 114. Influence of non-crosslinked pectin concentration and state of the matter before solvent exchange (solution “S” or gel “G”) on bulk density (squares) and specific surface area (triangles) of aeropectins based on P35 dissolved at pH 3. Solid line is theoretical density corresponding to zero volume shrinkage. Dashed lines are given to guide the eye. From (Groult & Budtova, 2018).

As it was already shown in the Chapter III, at low pH (pH = 2 which is lower than  $pK_a = 3$ ) specific surface area increased with pectin concentration (Figure 113, triangles) with highest values being around 360 and 440 m<sup>2</sup>/g for cross-linked and non-cross-linked pectins, respectively. As suggested in (Buchtová & Budtova, 2016), the increase of polymer concentration leads to the decrease of pore size without significant evolution of pore walls’ thickness.

As shown by SEM characterization of aeropectin morphologies in Figure 115, with the increase of pectin concentration, the network becomes denser and pores smaller, confirming the trend obtained on specific surface area (Figure 113).

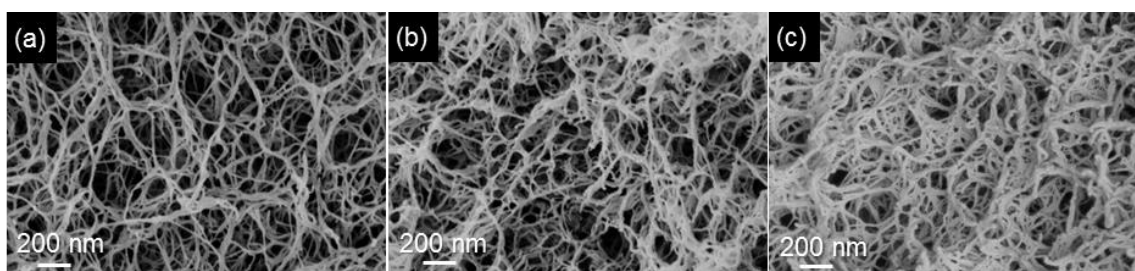


Figure 115. SEM images of P35 based aeropectins from 2 wt% (a), 4 wt% (b) and 6 wt% (c) solutions at pH 2 cross-linked with calcium ( $R(\text{Ca}) = 0.2$ ), non-solvent was ethanol. All samples were gels before solvent exchange. From (Groult & Budtova, 2018).

The results presented above show that the increase of pectin concentration leads to the increase in density and decrease of network pore size. The first trend, *i.e.* increase in aerogel

CHAPTER IV.

Thermal conductivity-structure properties correlations of pectin aerogels

density, should logically result in the enhancing of heat conduction via the solid backbone, and thus in the overall increase in thermal conductivity. The second trend, *i.e.* decrease of pore size, leads to the increase of the amount of mesopores which contribute to Knudsen effect, and thus is supposed to decrease the conduction of gaseous phase. These two oppositely acting trends may result in different behaviour of thermal conductivity as a function of polymer concentration (or aerogel density) depending which input is dominating. The expected increase of thermal conductivity as a function of density is given as an example for pH 2 and 3 in Figure 116 (a) for non-cross-linked pectin. Figure 116 (b) shows that for aeropectins cross-linked with calcium thermal conductivity weakly depends on polymer concentration, with a small minimum corresponding to 3 wt%, indicating that density increase is counterbalanced by pore's size decrease in their inputs in the overall conductivity.

It is thus clear that in addition to polymer concentration, cross-linking strongly influences aeropectin morphology and thus thermal conductivity. The effect of pH and presence of calcium on aeropectin properties is presented and discussed in the Section 3.

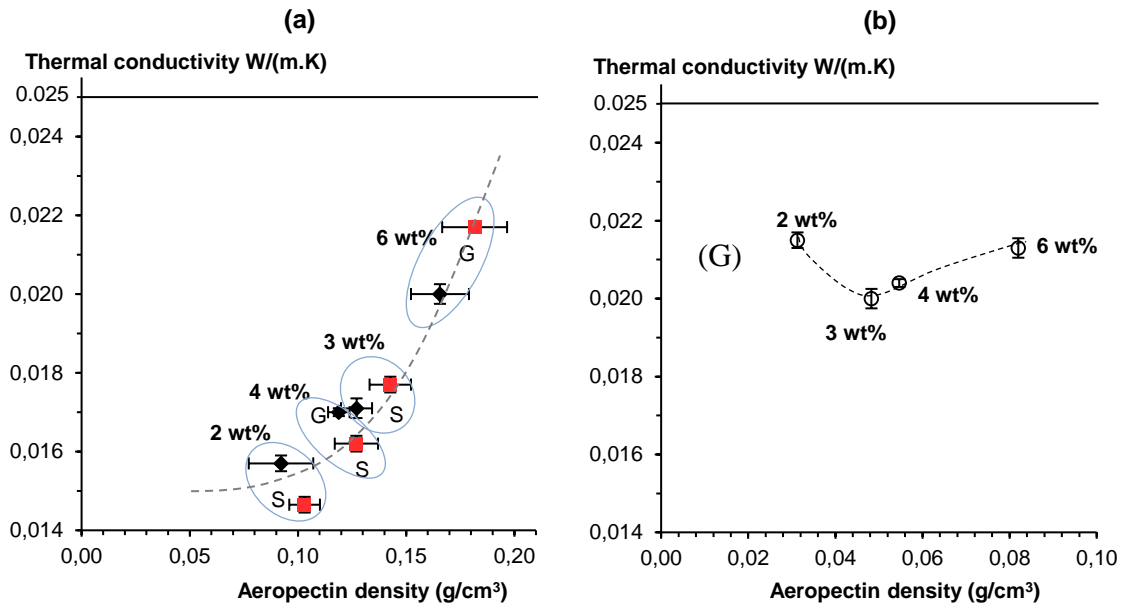


Figure 116. Thermal conductivity in ambient conditions of aeropectins from P35 as a function of density, with pectin concentration varying from 2 wt% to 6 wt%, non-solvent was ethanol

at pH 3 (squares) and pH 2 (diamonds), all without calcium. The state of matter before solvent exchange is indicated for each case (solution “S” or gel “G”).

at pH 2, cross-linked with calcium (open points) at  $R(Ca) = 0.2$ , all were gels before solvent exchange

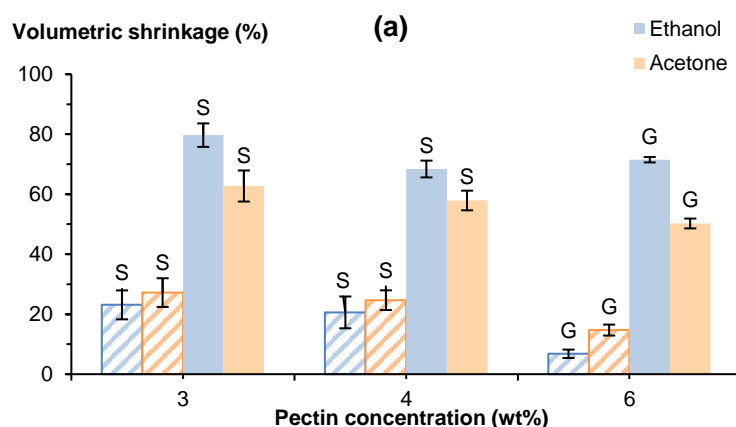
. Dashed line is given to guide the eye. Solid line corresponds to the conductivity of air.

## 2.2. Influence of non-solvent type on aerogel thermal conductivity

As it was shown in Chapter III, the type of non-solvent used for solvent exchange is important for the aerogels' structure formation. Indeed, when a non-solvent is added to non-gelled pectin solution, phase separation occurs (also known as "immersion precipitation" process) (Wijmans, Altena, & Smolders, 1984; Wijmans, Baaij, & Smolders, 1983), leading to a strong contraction of macromolecules. When non-solvent is added to a pectin gel, this leads to coagulation and network contraction. In both cases, solvent exchange leads to sample shrinkage. We used ethanol and acetone to study the influence of non-solvent type on pectin aerogel structural and thermal properties.

As we saw in the Chapter III, using acetone as the non-solvent significantly decreased the total volume shrinkage of pectin samples compared to ethanol (see Figure 117 (a)). As a direct consequence of a better-preserved network from collapsing, aeropectins present lower densities with higher specific surface areas when using acetone compared to ethanol as shown in Figure 117 (b, c). This is a rather unusual trend as often a material with lower density is supposed to have larger pores and thus lower specific surface area.

We hypothesize here that when coagulated in acetone, samples are not only collapsing less, but also chains are agglomerating less, thus creating a network with a finer structure. SEM characterization of aeropectins in Figure 118 shows that all aerogels exhibited a finer mesoporous network when acetone was used instead of ethanol, independently of the state of state of matter before solvent exchange or pectin concentration.



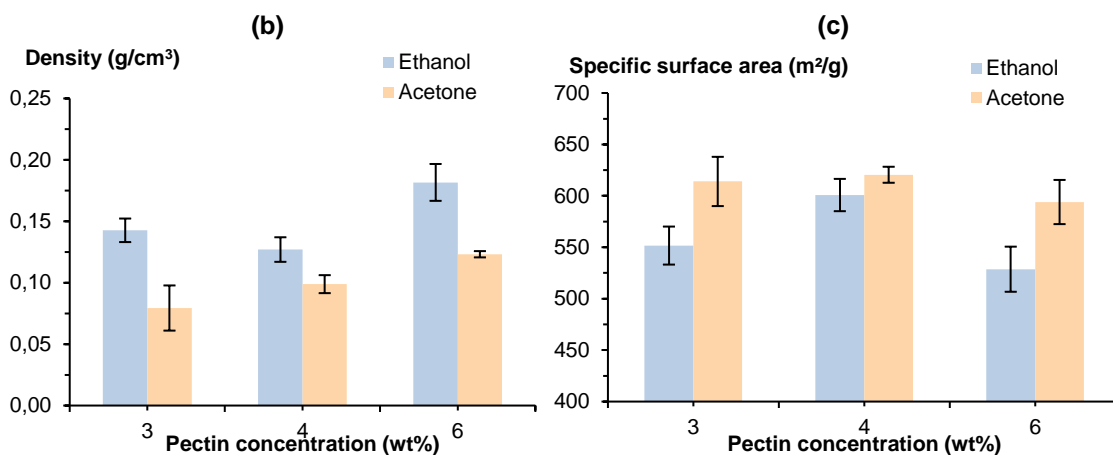


Figure 117. (a) Volumetric shrinkage measured after solvent exchange (crossed bars) and after sc-drying (full bars), (b) density and (c) specific surface area of pectin aerogels made from pectin P35 dissolved at pH 3 without calcium at different pectin concentration, using either ethanol (blue) or acetone (orange) as the non-solvent. The state of matter before solvent exchange is indicated for each case (solution “S” or gel “G”).

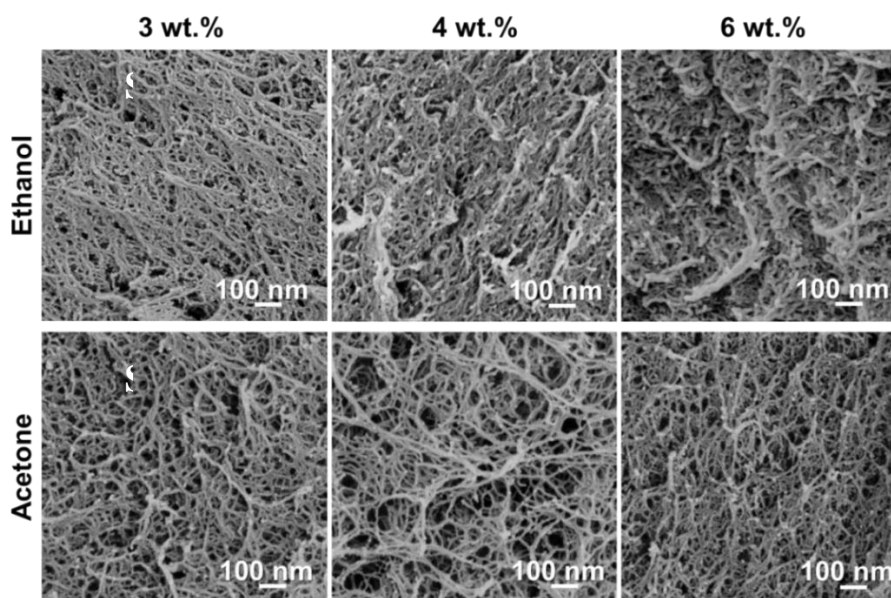


Figure 118. Network morphology of aeropectins made from pectin P35 at different pectin concentration (wt%) dissolved a pH 3.0 without calcium, and using either ethanol or acetone as the non-solvent. The state of matter before solvent exchange is indicated for each case (solution “S” or gel “G”).

Regardless the concentration of pectin solutions and state of matter before solvent exchange, we noticed lower thermal conductivity when acetone was used instead of ethanol; the results are presented in Figure 119.

As suggested above, lower density (thus lower input in solid conduction) and finer network morphology (higher input of Knudsen effect) after coagulation in ethanol results in lower thermal conductivity.

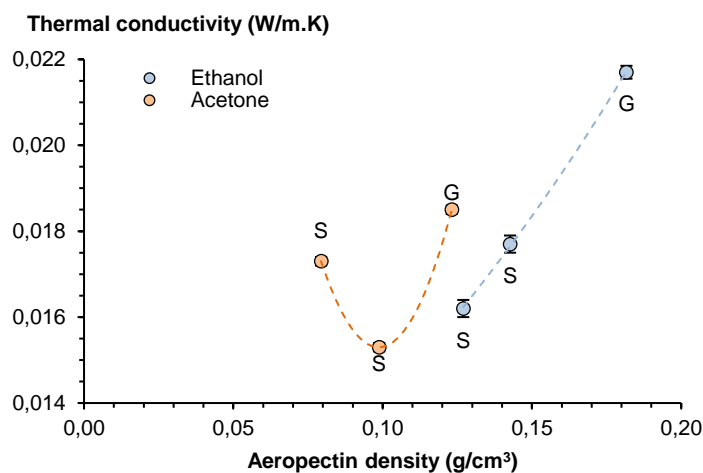


Figure 119. Thermal conductivity in ambient conditions of aeropectins made from pectin P35 at different pectin concentration dissolved at pH 3.0 without calcium and using either ethanol or acetone as the non-solvent. Dashed lines are given to guide the eye.

### 3. Influence of Ca-induced cross-linking and pH on pectin aerogel properties

It is well known that pH and presence of metal ions, especially bivalent, influence pectin solution viscosity and gelation (Thakur, Singh, Handa, & Rao, 1997; Walkinshaw & Arnott, 1981). As we already studied in the Chapter III, changes in calcium concentration and solution pH were found to induce strong variations in terms of aeropectins' density and morphology. Based on the work performed on the tuning of aeropectins structure (Chapter III), we will first, examine how aeropectin thermal conductivity changes with solution pH keeping pectin and calcium concentration constant, and then calcium content will be varied at constant pectin concentration and pH.

#### 3.1. Influence of pH at $R(\text{Ca}) = 0$ and 0.2

To understand the influence of pH, presence of calcium and state of matter (solution or gel) on aerogel morphology and thermal conductivity we varied pH, from 1 to 3, and for each pH two types of samples were prepared, without and with calcium ( $R(\text{Ca}) = 0.2$ ).

## CHAPTER IV.

### Thermal conductivity-structure properties correlations of pectin aerogels

Pectin shrinkage after solvent exchange and after drying as a function of pH is presented in Figure 120, and aeropectin density and specific surface area in Figure 121a and Figure 121b, respectively. For the samples cross-linked with calcium no influence of pH on shrinkage was recorded (around 40 %), within the experimental errors. The total shrinkage of non-cross-linked samples shows a strong dependence on pH, from 50% to 80 % for pH from 1 to 3, respectively. For P35 3 wt% solutions when calcium was added the solutions became gels before solvent exchange while non-cross-linked pectins were gels only at low pH, 1 and 1.5, and solutions at pH 2 and 3 (Figure 121a).

As mentioned in Chapter 3, the highest shrinkage upon the addition of non-solvent occurs for non-gelled solutions (non-solvent induced phase separation), less in physically gelled solutions and even less in calcium cross-linked pectin. This trend is reflected by density which does not vary with pH for cross-linked pectin aerogels and increases with pH in almost 3 times for non-crosslinked ones (Figure 121a). As it was detailed in the Chapter III, this is due to the strength of the bonds, ionic gelation leads to more firm and brittle gels than their physical counterparts (Djabourov, Nishinari, & Ross-Murphy, 2013).

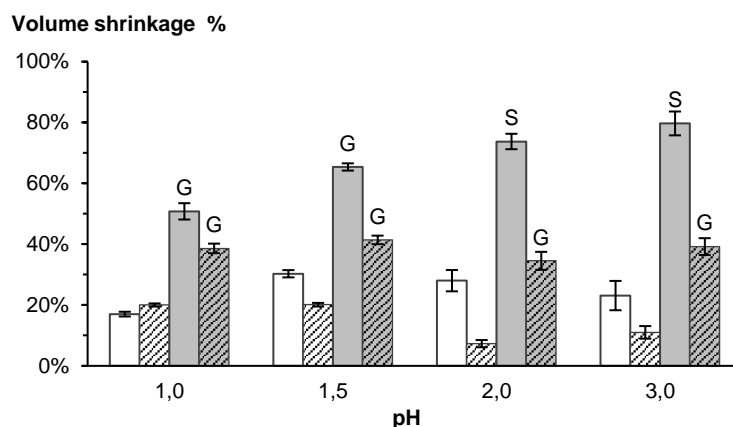


Figure 120. Influence of pH, presence of calcium ( $R(\text{Ca}) = 0.2$ ) (shaded bars) and state of matter before solvent exchange (solution “S” or gel “G”) on P35 shrinkage after solvent exchange (white bars) and after sc drying (grey bars). Initial polymer concentration was 3 wt%.

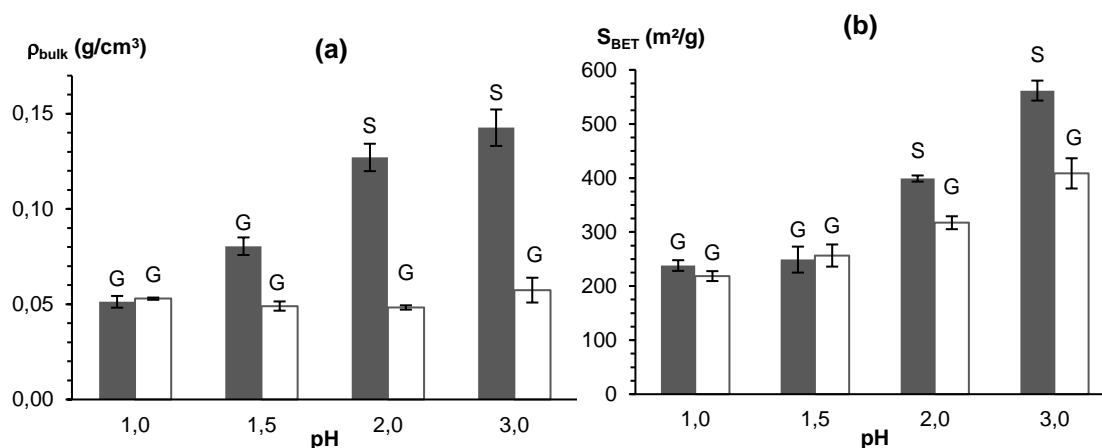


Figure 121. Aeropectin density (a) and specific surface area (b) as a function of pH for 3 wt% P35 solutions cross-linked with calcium ( $R(\text{Ca}) = 0.2$ ) (white bars) or not (black bars). The state of matter before solvent exchange is indicated for each case (solution “S” or gel “G”).

In particular, it is well known that low methylated pectins undergo a strong ionic gelation in the presence of calcium due to their high sensitivity to  $\text{Ca}^{2+}$  ions; these pectins were also reported to form weak acid gels in the absence of cations at pH values below  $\text{pK}_a$  (Capel, Nicolai, Durand, Boulenger, & Langendorff, 2006; Gilsenan, Richardson, & Morris, 2000; Löfgren, Walkenström, & Hermansson, 2002; Morris, Gidley, Murray, Powell, & Rees, 1980; Ström, Schuster, & Goh, 2014).

Figure 121b represents specific surface area of pectin aerogels which density is shown in Figure 121a. As expected (see Chapter III),  $S_{\text{BET}}$  significantly increases with pH for both cross-linked and non-cross-linked aeropectins, and aerogels from non-gelled solutions at pH 2 and 3 show  $S_{\text{BET}}$  much higher than that from cross-linked pectins. These results are explained by the dissociation/protonation of pectin galacturonic acids depending on pH conditions, which in turn directly impacts the number, the strength and the type of pectin chains interactions (*i.e.* ionic bonds with cations, hydrogen bonds, hydrophobic interactions) (Fraeye, Duvetter, Doungra, Van Loey, & Hendrickx, 2010; Löfgren, Guillotin, Evenbratt, Schols, & Hermansson, 2005):

The representative examples of the morphology and pore volume of aerogels from 3 wt% P35 are demonstrated in Figure 122 and Figure 123, respectively. As expected from the Chapter III, in the case of non-crosslinked pectin the increase of pH led to aerogels with a denser morphology and lower pores' size: from around 50-150 nm at pH 1.5 (acid gels) to around 10-50 nm at pH 3 (solutions) (Figure 122). The difference between aerogels made from gels or solutions is significant: contrary to aerogels made from a solution, all aerogels made from gels had macropores. Aerogel from non-cross-linked solution at pH 3 looks very dense but it has porosity around 90 % and is mesoporous, as reflected by high specific surface area (Figure 121b). Strong shrinkage (Figure 120) clearly induced the decrease pores' size. Cross-linking

with calcium led to the presence of macropores and thus low density and moderate specific surface area (Figure 121a and Figure 121b).

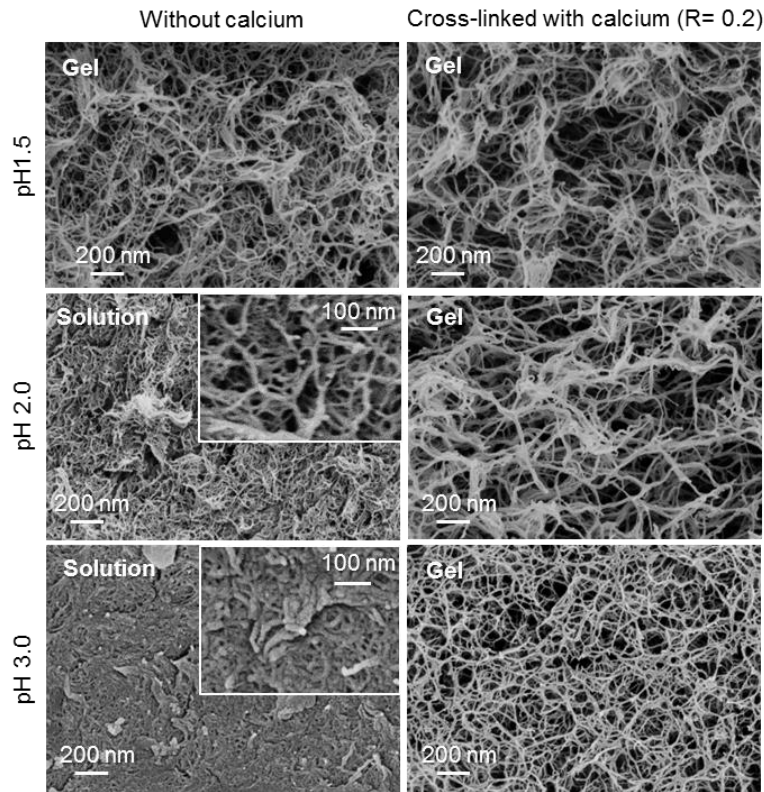


Figure 122. Morphology of aeropectins from P35 dissolved at 3 wt% at various pH, cross-linked with calcium ( $R(\text{Ca}) = 0.2$ ) and not. From (Groult & Budtova, 2018).

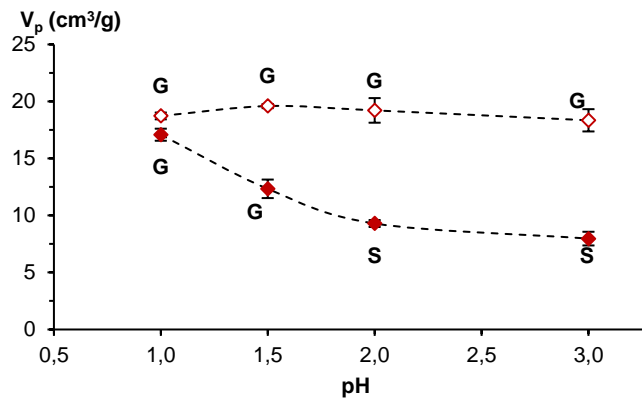


Figure 123. Pore volume of aeropectins made from 3 wt% of P35 dissolved at different pH. Filled points correspond to non-cross-linked samples, open points – when calcium was added ( $R(\text{Ca}) = 0.2$ ). The state of matter before solvent exchange is indicated for each case (solution “S” or gel “G”). Dashed lines are given to guide the eye. From (Groult & Budtova, 2018).

Thermal conductivity of aeropectins as a function of pH is summarized in Figure 124 for 3 wt% pectin, cross-linked with calcium ( $R(\text{Ca}) = 0.2$ ) and not. In both cases the dependences

have a U-shape as in Figure 111 for thermal conductivity vs density. All values are in thermal super-insulating region (conductivity below 0.025 W/(m.K)). When decreasing pectin concentration to 2 wt% at pH 3, it was possible to obtain the lowest value ever reported for bio-aerogels,  $0.0147 \pm 0.0002$  W/(m.K). Aeropectins cross-linked with calcium show conductivity higher than that of non-cross-linked ones, except at pH 1 when they are equal. The reason of this difference is in the microstructure of aeropectins: despite lower density of all cross-linked aerogels as compared to their non-cross-linked counterparts (Figure 121a), the macropores, clearly visible on SEM images (Figure 122), significantly contribute to heat transfer via gaseous phase and are thus unfavorable for the thermal conductivity. Overall, strong gels (at pH 1 and when cross-linked with calcium) that resist shrinkage may be highly porous but are too macroporous for having thermal conductivity below 0.02 W/(m.K).

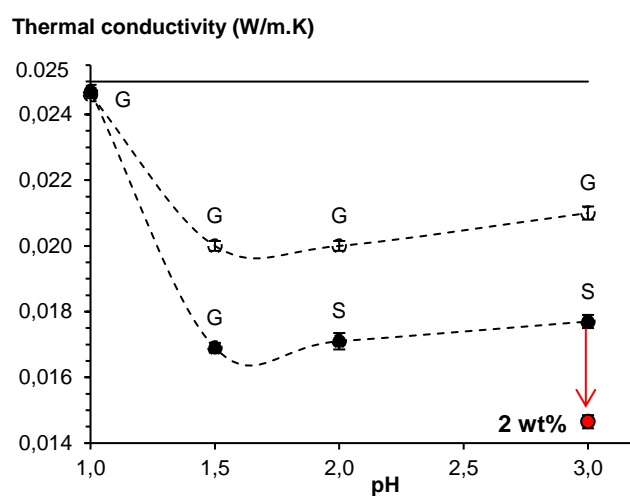


Figure 124. Thermal conductivity in ambient conditions of aeropectins from P35 as a function of pH at pectin concentration 3 wt% and for non-cross-linked pectin (filled points) and at  $R(\text{Ca}) = 0.2$  (open points). One point at pH 3 is for 2 wt% solution. The state of matter before solvent exchange is indicated for each case (solution “S” or gel “G”). Dashed lines are given to guide the eye. Solid line corresponds to the conductivity of air. From (Groult & Budtova, 2018).

Thermal conductivity can be thus used as a measure of structure “finesse”. U-shape curve for both types of aeropectins reflects a competition between solid and gaseous phases conduction which depend on aerogel density and morphology, which in turn are controlled by pectin concentration, state of matter before solvent exchange and sample shrinkage.

### 3.2. Influence of calcium concentration at pH 3

Next, we varied calcium concentration keeping pectin at 3 wt% and pH 3 and changing  $R(\text{Ca})$  ratio from 0.05 to 0.2. As it was already demonstrated in the Chapter III, the pectin

network was reinforced due to higher cross-linking with the increase of calcium concentration (Fraeye et al., 2009; Löfgren et al., 2002) and thus it became more resistant leading to lower shrinkage (see Figure 125) and thus lower aeropectins' density (Figure 126).

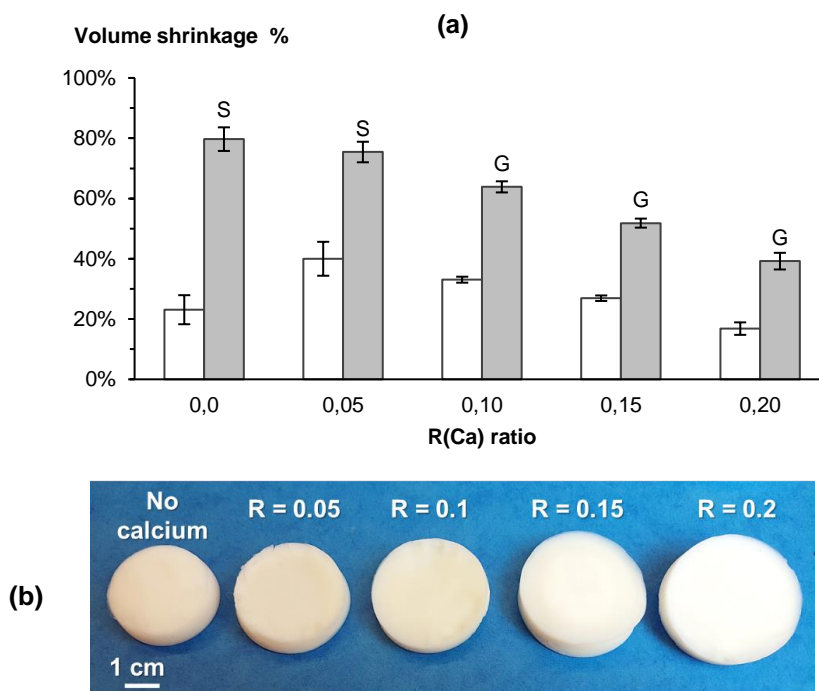


Figure 125. (a) Influence of calcium concentration (R(Ca) ratio) and state of matter before solvent exchange (solution “S” or gel “G”) on P35 shrinkage after solvent exchange (white bars) and after sc drying (grey bars). Polymer concentration in solution was 3 wt% and pH was 3. From (Groult & Budtova, 2018). (b) Pictures of the corresponding pectin aerogels.

Specific surface area also decreased with R(Ca) (Figure 126), most probably due to increasing amount of ionic non-porous junction zones. It is interesting to see that at R(Ca) = 0.05 the amount of calcium added was not sufficient to induce strong ionic gelation, however, calcium influence on density and specific surface area was noticeable.

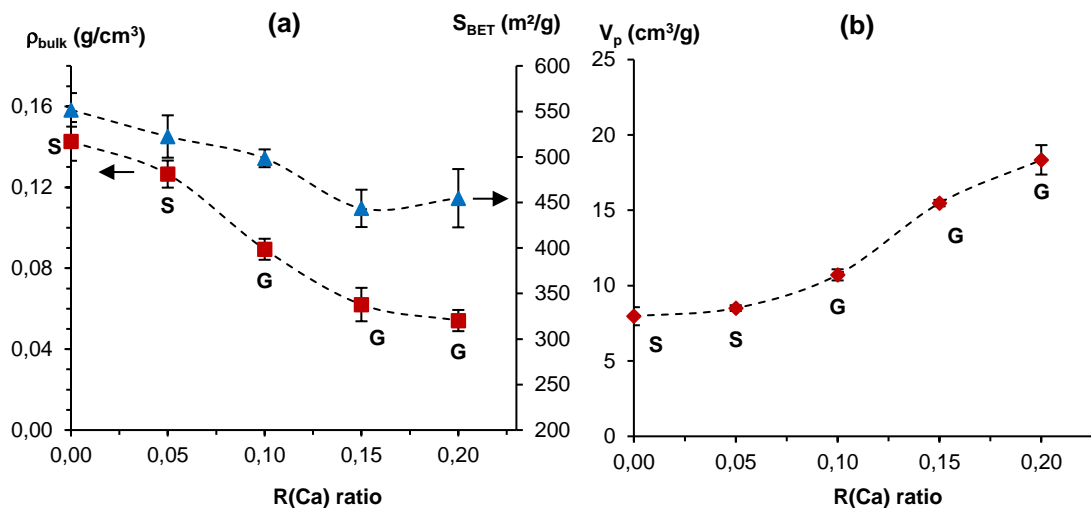


Figure 126. (a) Density (squares) and specific surface area (triangles), (b) pore volume of aeropectins based on P35 dissolved at 3 wt% and pH 3 as a function calcium R(Ca) ratio. The state of matter before solvent exchange is indicated for each case (solution “S” or gel “G”). Dashed lines are given to guide the eye. From (Groult & Budtova, 2018).

As we already know, the addition of calcium has a strong impact on pectin morphology as observed by SEM (Figure 127). The higher was R(Ca) value, the larger were pore sizes due to lower shrinkage. Aeropectin morphology and properties were thus finely tuned by varying calcium concentration: from very low density with macropores to higher density and compact morphology.

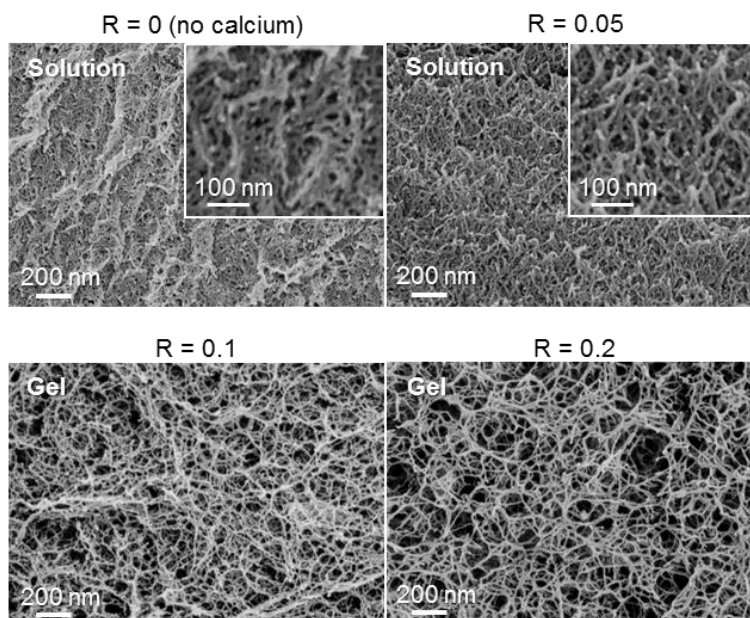


Figure 127. Morphology of aeropectins from P35 dissolved at 3 wt% and pH 3, cross-linked with calcium at different R(Ca) ratio from R(Ca) = 0 (no calcium added) to R(Ca) = 0.2. From (Groult & Budtova, 2018).

Finally, the influence of calcium concentration on thermal conductivity of aeropectins is presented in Figure 128 (a). The same data but as a function of density at various R(Ca) ratio is shown in Figure 128 (b). As for the overall dependence of conductivity vs density (Figure 111) and pH (Figure 124), here also U-shape curves are recorded. The minimal value obtained was  $0.0157 \pm 0.0001$  W/(m.K). The U-shape for calcium cross-linked pectin aerogels shows again that a balance between density and morphology is needed to obtain the lowest thermal conductivity.

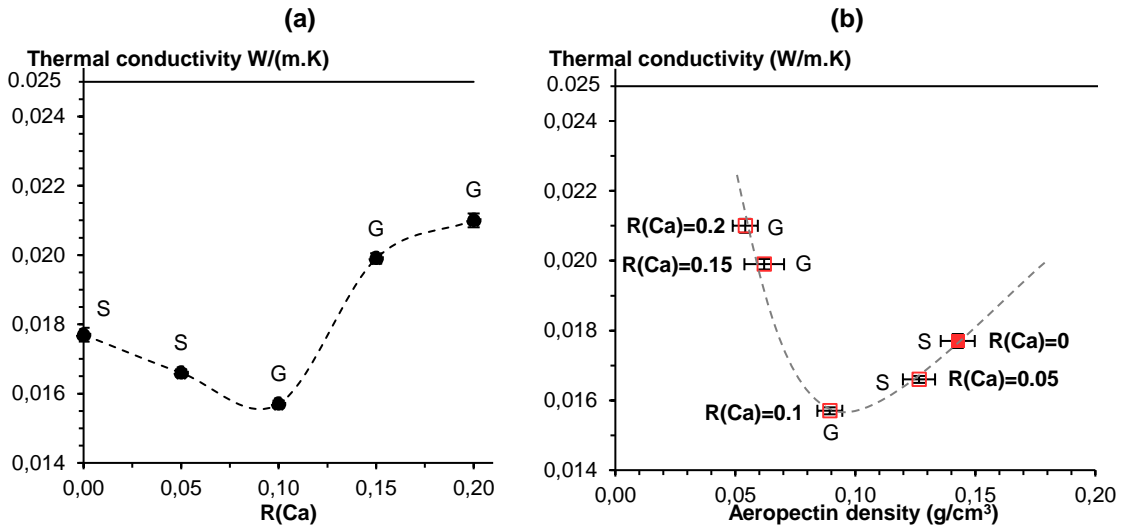


Figure 128. Thermal conductivity in ambient conditions of aeropectins from P35 at pectin concentration 3 wt% and pH 3

(a) as a function of R(Ca).

(b) P35 as a function of density at various R(Ca)

The state of matter before solvent exchange is indicated for each case (solution “S” or gel “G”). Dashed line is given to guide the eye. Solid line corresponds to the conductivity of air. From (Groult & Budtova, 2018).

## Conclusions

Pectin aerogels with thermal superinsulating properties were synthesized. To modify aerogel density and morphology and thus understand their influence on aerogel thermal conductivity, pH, concentration of calcium, pectin concentration and type of non-solvent were varied in a systematic way. Aerogel density was from 0.05 to 0.2 g/cm<sup>3</sup> and specific surface was from 220 to 620 m<sup>2</sup>/g.

For the first time a U-shape curve of thermal conductivity vs density was obtained for bio-aerogels synthesized via dissolution-solvent exchange-sc drying route. It shows that the type of pectin chains' interactions and physical state of matter (solution or gel) are crucial to understand and predict aerogel morphology and properties. More numerous and stronger pectin chains' interactions (ionic vs hydrogen) led to stronger gels (at pH 1 and cross-linked with calcium at all pH studied) which shrank less during solvent exchange and drying.

As a result, aerogels with lower density and high proportion of macropores were obtained. The contribution of the gaseous phase to thermal conductivity was thus higher leading to higher thermal conductivity. On the contrary, chains' repulsion at higher pH prevented gelation leading to higher shrinkage and density but also to the reduction of pore size to the level of mesopores. In this case the conduction of the gaseous phase is low thanks to Knudsen effect, but the contribution of the solid backbone increases.

A delicate compromise in aeropectin morphology and density is thus needed to get the lowest thermal conductivity. This minimal value of  $0.0147 \pm 0.0002$  W/(m.K) was found for non-gelled solution at pH 2 and pectin concentration of 2 wt%. Thermal conductivity is a very sensitive parameter reflecting aerogel morphology and can be used to characterize the finesse bio-aerogel structure.

## References

- Buchtová, N., & Budtova, T. (2016). Cellulose aero-, cryo- and xerogels: towards understanding of morphology control. *Cellulose*, 23(4), 2585-2595. <https://doi.org/10.1007/s10570-016-0960-8>
- Capel, F., Nicolai, T., Durand, D., Boulenger, P., & Langendorff, V. (2006). Calcium and acid induced gelation of (amidated) low methoxyl pectin. *Food Hydrocolloids*, 20(6), 901-907. <https://doi.org/10.1016/j.foodhyd.2005.09.004>
- Diascorn, N., Calas, S., Sallee, H., Achard, P., & Rigacci, A. (2015). Polyurethane aerogels synthesis for thermal insulation – textural, thermal and mechanical properties. *Journal of Supercritical Fluids*, 106, 76–84. <https://doi.org/10.1016/j.supflu.2015.05.012>
- Djabourov, M., Nishinari, K., & Ross-Murphy, S. B. (2013). *Physical gels from biological and synthetic polymers*. Cambridge: Cambridge Univ. Press.
- Fraeye, I., Doungla, E., Duvetter, T., Moldenaers, P., Van Loey, A., & Hendrickx, M. (2009). Influence of intrinsic and extrinsic factors on rheology of pectin–calcium gels. *Food Hydrocolloids*, 23(8), 2069-2077. <https://doi.org/10.1016/j.foodhyd.2009.03.022>
- Fraeye, I., Duvetter, T., Doungla, E., Van Loey, A., & Hendrickx, M. (2010). Fine-tuning the properties of pectin–calcium gels by control of pectin fine structure, gel composition and environmental conditions. *Trends in Food Science & Technology*, 21(5), 219-228. <https://doi.org/10.1016/j.tifs.2010.02.001>
- Gilsenan, P. M., Richardson, R. K., & Morris, E. R. (2000). Thermally reversible acid-induced gelation of low-methoxy pectin. *Carbohydrate Polymers*, 41(4), 339-349. [https://doi.org/10.1016/S0144-8617\(99\)00119-8](https://doi.org/10.1016/S0144-8617(99)00119-8)
- Groult, S., & Budtova, T. (2018). Thermal conductivity/structure correlations in thermal super-insulating pectin aerogels. *Carbohydrate Polymers*, 196, 73-81. <https://doi.org/10.1016/j.carbpol.2018.05.026>
- Hoepfner, S., Ratke, L., & Milow, B. (2008). Synthesis and characterisation of nanofibrillar cellulose aerogels. *Cellulose*, 15(1), 121-129. <https://doi.org/10.1007/s10570-007-9146-8>
- Löfgren, C., Guillotin, S., Evenbratt, H., Schols, H., & Hermansson, A.-M. (2005). Effects of Calcium, pH, and Blockiness on Kinetic Rheological Behavior and Microstructure of HM Pectin Gels. *Biomacromolecules*, 6(2), 646-652. <https://doi.org/10.1021/bm049619+>
- Löfgren, C., Walkenström, P., & Hermansson, A.-M. (2002). Microstructure and Rheological Behavior of Pure and Mixed Pectin Gels. *Biomacromolecules*, 3(6), 1144-1153. <https://doi.org/10.1021/bm020044v>

## CHAPTER IV.

### Thermal conductivity-structure properties correlations of pectin aerogels

---

- Morris, E. R., Gidley, M. J., Murray, E. J., Powell, D. A., & Rees, D. A. (1980). Characterization of pectin gelation under conditions of low water activity, by circular dichroism, competitive inhibition and mechanical properties. *International Journal of Biological Macromolecules*, 2(5), 327-330. [https://doi.org/10.1016/0141-8130\(80\)90058-6](https://doi.org/10.1016/0141-8130(80)90058-6)
- Pekala, R. W. (1989). Organic aerogels from the polycondensation of resorcinol with formaldehyde. *Journal of Materials Science*, 24(9), 3221-3227. <https://doi.org/10.1007/BF01139044>
- Rudaz, C., Courson, R., Bonnet, L., Calas-Etienne, S., Sallée, H., & Budtova, T. (2014). Aeropectin: Fully Biomass-Based Mechanically Strong and Thermal Superinsulating Aerogel. *Biomacromolecules*, 15(6), 2188-2195. <https://doi.org/10.1021/bm500345u>
- Ström, A., Schuster, E., & Goh, S. M. (2014). Rheological characterization of acid pectin samples in the absence and presence of monovalent ions. *Carbohydrate Polymers*, 113, 336-343. <https://doi.org/10.1016/j.carbpol.2014.06.090>
- Thakur, B. R., Singh, R. K., Handa, A. K., & Rao, M. A. (1997). Chemistry and uses of pectin — A review. *Critical Reviews in Food Science and Nutrition*, 37(1), 47-73. <https://doi.org/10.1080/10408399709527767>
- Walkinshaw, M. D., & Arnott, S. (1981). Conformations and interactions of pectins: II. Models for junction zones in pectinic acid and calcium pectate gels. *Journal of Molecular Biology*, 153(4), 1075-1085. [https://doi.org/10.1016/0022-2836\(81\)90468-X](https://doi.org/10.1016/0022-2836(81)90468-X)
- Wijmans, J. G., Altena, F. W., & Smolders, C. A. (1984). Diffusion during the immersion precipitation process. *Journal of Polymer Science: Polymer Physics Edition*, 22(3), 519-524. <https://doi.org/10.1002/pol.1984.180220313>
- Wijmans, J. G., Baaij, J. P. B., & Smolders, C. A. (1983). The mechanism of formation of microporous or skinned membranes produced by immersion precipitation. *Journal of Membrane Science*, 14(3), 263-274. [https://doi.org/10.1016/0376-7388\(83\)80005](https://doi.org/10.1016/0376-7388(83)80005)

# **CHAPTER V. PECTIN AEROGELS AS DRUG DELIVERY SYSTEMS**

---

## CONTENTS

### CHAPTER V. PECTIN AEROGELS AS DRUG DELIVERY SYSTEMS

<b>INTRODUCTION.....</b>	<b>241</b>
<b>1. PRODUCTION AND CHARACTERIZATION OF THE DRUG-LOADED AEROPECTINS.....</b>	<b>242</b>
1.1. METHOD OF INCORPORATION OF THEOPHYLLINE INTO AEROGEL PRECURSORS .....	242
1.2. CHARACTERIZATION OF LOADED AEROPECTINS .....	244
1.2.1. <i>Aeropectins drug loading efficiency.....</i>	<i>244</i>
1.2.2. <i>Structural characterization of theophylline loaded aeropectins .....</i>	<i>247</i>
1.2.3. <i>Determination of crystalline structure of theophylline incorporated in pectin aerogels, xerogels and cryogels by X-rays diffraction .....</i>	<i>248</i>
<b>2. STUDY OF THEOPHYLLINE RELEASE FROM PECTIN, AEROGELS, CRYOGELS AND XEROGELS .....</b>	<b>251</b>
2.1. STRUCTURAL PROPERTIES OF PECTIN MATRIX MADE WITH DIFFERENT DRYINGS .....	252
2.2. THEOPHYLLINE RELEASE PROFILES AS A FUNCTION OF DRYING METHOD .....	254
2.3. COMPARISON OF RELEASE PROPERTIES OF PECTIN HYDROGELS AND AEROGELS .....	259
<b>3. BACKGROUND ANALYSIS OF AEROPECTIN BEHAVIOUR AND THEOPHYLLINE RELEASE.....</b>	<b>261</b>
3.1. INFLUENCE OF PH OF RELEASE MEDIUM ON AEROPECTIN EROSION, SWELLING AND DRUG RELEASE .....	261
3.2. SELECTION OF A MODEL TO DESCRIBE RELEASE KINETICS.....	264
3.2.1. <i>Mathematical models fitting drug release profiles.....</i>	<i>265</i>
3.2.2. <i>Overview of drug release from aeropectins .....</i>	<i>269</i>
<b>4. CASE STUDIES: INFLUENCE OF VARIOUS PARAMETERS ON THE KINETICS OF THEOPHYLLINE RELEASE FROM PECTIN AEROGELS.....</b>	<b>272</b>
4.1. INFLUENCE OF PH OF PECTIN SOLUTIONS ON RELEASE KINETICS OF THEOPHYLLINE FROM AEROPECTIN .....	272
4.2. IMPACT OF CALCIUM CONCENTRATION ON RELEASE KINETICS OF THEOPHYLLINE FROM AEROPECTIN.....	278
<b>CONCLUSIONS .....</b>	<b>284</b>
<b>REFERENCES.....</b>	<b>286</b>

## Introduction

The goal of this work is to study the release of theophylline from different pectin aerogel matrices in order to find out structure-properties correlations explaining drug release mechanisms. In the whole chapter, the focus will be made on the relationship between the specificity of the initial polymer, the characteristics of the pectin aerogel carrier and its release properties in aqueous media. For this purpose, structural and physico-chemical properties of the aerogel carrier were varied by adjusting the preparation conditions and gelation mechanisms (pectin concentration, calcium concentration, pH of pectin solution). Matrix swelling, erosion and drug release profiles from different aerogels matrices were characterized and compared. Kinetics models based on mathematical functions will be used to identify the main physical mechanism governing the release (*e.g.* diffusion, dissolution, erosion, swelling...*etc.*). This approach will be used in the following chapter (VI) for pectin-cellulose and pectin-silica composite-aerogels.

The chapter is organized as follows:

First, the way of incorporation of theophylline, as model drug used in this work, is presented. Then the main correlations between aeropectin loading efficiency and loading capacity and aerogel density and specific surface area are demonstrated. The detailed study of release kinetics is discussed in two parts:

- a) The impact of the drying methods (supercritical, evaporative or freeze drying) on release properties of the different pectin matrices (hydrogel, aerogels, cryogels, xerogels).
- b) A step by step examination of the impacts of aeropectins' preparation conditions on their release properties:

In the first instance, general trends of the release properties of aeropectin will be deeply examined and discussed, taking one example of aeropectin.

Then, we study the effect of aeropectin density on the release, varying the pH of pectin solutions.

Finally, we examine the effect of cross-linking on the release, varying calcium concentration of pectin solutions.

## 1. Production and characterization of the drug-loaded aeropectins

### 1.1. Method of incorporation of theophylline into aerogel precursors

Theophylline (1,3-dimethylxanthine) is a bronchodilator drug widely used to treat the symptoms of chronic airway diseases (persistent asthma, emphysema, chronic bronchitis). In this study, we have selected theophylline as a model drug for both its pharmaceutical and chemical (solubility) properties. Indeed, theophylline is a polar and hydrophilic alkaloid drug well soluble in water (8.3 g/L at 25°C) (Yalkowsky, He, Jain, He, & Jain, 2016) and presents a  $pK_a$  around 8.81 (Kortüm, Vogel, & Andrussow, 1960). It belongs to Class 1 drugs of the Biopharmaceutics Classification System (BCS), that is to say it is a highly soluble and highly permeable drug, subject to immediate and complete absorption after oral administration.

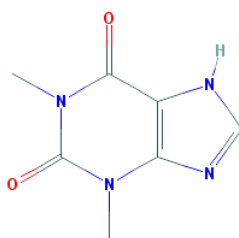


Figure 129. Theophylline 2D-chemical structure, from National Center for Biotechnology Information. PubChem Database. Theophylline, CID=2153, <https://pubchem.ncbi.nlm.nih.gov/compound/2153> (accessed on Mar. 26, 2019)

However, theophylline has a narrow therapeutic window of 10 – 20 µg of theophylline/mL in serum, above which adverse effects may be observed including serious cardiovascular toxic effects due to over-dosage (tachycardia, circulatory failure, ventricular arrhythmias). In other words, theophylline has to be chronically and constantly administrated in the right dosage maintained into the therapeutic window, with avoidance of both over-dosage (toxicity) and under-dosage (inefficiency). Thus, extending and controlling its release into gastro-intestinal tracks is an important issue, and that is why it must be administrated orally using controlled release preparations.

Theophylline is moderately soluble in ethanol (3.5 g/L at 25°C) allowing its impregnation into pectin aerogel precursor (pectin coagulated in ethanol) through diffusion. Due to its high polarity and low octanol-water partition coefficient  $K_{ow}$  from -0.02 (experimental value (Martin, 1996)) to -0.7 (predicted) (calculation module developed by ChemAxon (« ChemAxon », s. d.)) theophylline is practically insoluble in non-polar solvent such as supercritical CO<sub>2</sub>, with solubility lower than 0.04 g/kg at 313 K and 19.9 MPa (Johannsen & Brunner, 1994), thus avoiding its dissolution in CO<sub>2</sub> during sc drying.

Theophylline dissolved in ethanol was impregnated into pectin aerogel precursor which itself carries ethanol. To minimize the dilution effect due to the presence of ethanol within the aerogel precursors, the samples were immersed in theophylline solution 25 to 30 times larger than the volume of pectin, and ethanol solution bath was changed for fresh one after 48 h. As shown in Figure 53, pectin aerogel precursors were immersed for 7 days (the reason of this duration is explained below) into either an ethanol solution at a concentration of theophylline of 2.5 g/L or in a theophylline suspension in ethanol at 3.4 g/L, depending on the case.

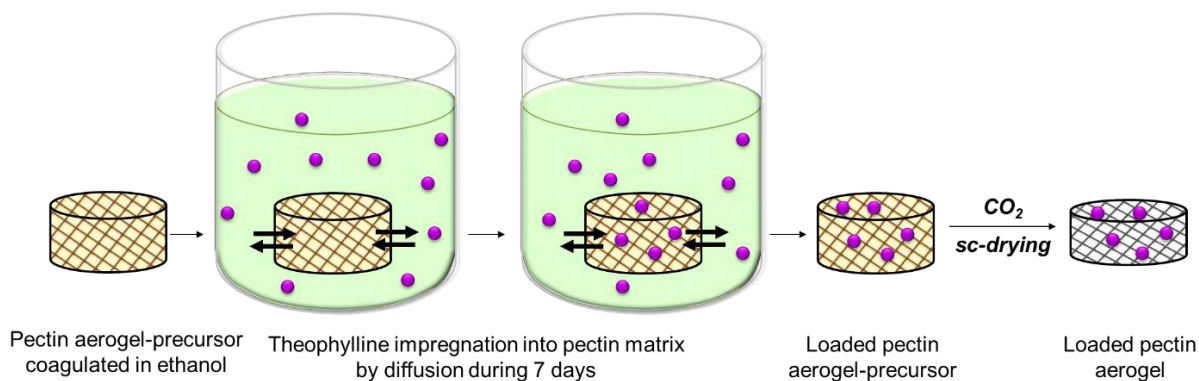


Figure 130. Schematic representation of the impregnation method of theophylline into pectin aerogel-precursor by diffusion through ethanol.

To evaluate the time needed to completely impregnate aerogel precursor samples with theophylline, we estimated the diffusion coefficient of theophylline in ethanol. The diffusion coefficient ( $D$ ) of a solute through a medium in a dilute state is given by Stokes-Einstein Equation (5.1):

$$D = \frac{k_{Bz} \cdot T}{6\pi R \eta} \quad (5.1)$$

Where  $k_{Bz}$  is the Boltzmann constant,  $T$  the temperature,  $R$  the hydrodynamic Stokes radius of the solute, and  $\eta$  the viscosity of the medium. As theophylline concentration in ethanol is lower than 0.44 wt% (3.5 g/L), we considered that it is in dilute state.

Theophylline's Stokes radius is estimated between 3.7 Å (experimental estimation) (M. Grassi, Colombo, & Lapasin, 2001) and 3.5 Å (numerical estimation) (Grassi et al., 2006) in water at 37°C. Using  $\eta_{\text{ethanol}} = 1.20 \cdot 10^{-3}$  Pa.s, theophylline diffusion coefficient in ethanol at 25°C is estimated to be around  $4.92 \cdot 10^{-10}$  m<sup>2</sup>/s in the absence of pectin network. The diffusion of theophylline through ethanol is expected to be slowed down in the presence of a network porous structure. By analogy with the previous work on diffusion of other molecules (NaOH, ionic liquid) through cellulose matrix as a function of cellulose concentration (Gavillon & Budtova, 2007; Sescousse, Gavillon, & Budtova, 2011), we divided the diffusion coefficient

by a factor 10 for 6 wt% pectin matrices. This roughly gives  $D_{\text{Theophylline}} \sim 4.92 \cdot 10^{-11} \text{ m}^2/\text{s}$  in pectin aerogel-precursor.

The diffusion of theophylline in ethanol medium through a porous matrix results from Brownian motion. The distance  $L$  made by theophylline molecule during time  $t$  is given by:

$$L = \sqrt{D_{\text{Theophylline}} \cdot t} \quad (5.2)$$

In 24 h, a theophylline molecule diffuses through a distance of  $\sim 2.1$  mm in such porous system. Considering that half thickness of the matrix samples was 5 mm maximum, the time needed to diffuse to the center of the material is estimated to be around 5.9 days. Thus, we consider that theophylline impregnation through the pectin-precursor was complete in 7 days.

After theophylline impregnation, the pectin aerogel precursors loaded with theophylline were directly freeze dried using  $\text{CO}_2$  to obtain drug loaded pectin aerogels.

## 1.2. Characterization of loaded aeropectins

### 1.2.1. Aeropectins drug loading efficiency

As shown in Figure 131, drug loading efficiency (%) (see Equation (2.12) from Chapter II) obtained for theophylline loaded aeropectins (all data for all formulations) reached variable values (from  $\sim 40$  to 80%) depending on sample preparation conditions (pectin concentration, pH of pectin solution, addition of calcium) which were impacted by aeropectins properties ( $S_{\text{BET}}$ , density, porosity, *etc.*). These values compare well with literature on polysaccharide aerogels, with loading efficiency usually from 15% to 80% (García-González, Jin, Gerth, Alvarez-Lorenzo, & Smirnova, 2015; Mehling, Smirnova, Guenther, & Neubert, 2009; Tkalec, Knez, & Novak, 2016; Veronovski, Tkalec, Knez, & Novak, 2014). Especially high loading efficiencies up to 70-80% were achieved for high density aeropectins ( $0.16 < \rho < 0.20 \text{ g/cm}^3$ ) (Figure 131 (a)).

Moreover, we noticed that drug loading efficiency (%) was positively correlated with the specific surface area of aeropectins for a given pectin concentration (3 wt% or 6 wt %) (Figure 131 (b)). This confirms that the higher the specific surface area offered by the polysaccharide network, the higher the drug deposition onto the chains and thus the higher the aerogel loading efficiency, as reported in (Alnaief & Smirnova, 2010; García-González et al., 2015; Mehling et al., 2009; I. Smirnova, Mamic, & Arlt, 2003; I. Smirnova, Suttiruengwong, & Arlt, 2005; Veronovski et al., 2014). In correlation with literature, this also suggests that apart specific surface area other parameters might be involved in the loading efficiency, such as pectin

concentration and/or aerogel density. Indeed, Figure 131 (a) shows the high correlation between loading efficiency and aeropectin density regardless pectin concentration or addition of calcium.

As it was suggested by (Mehling et al., 2009; I. Smirnova, Suttiruengwong, & Arlt, 2004), high aerogel density, which also reflects smaller pore size in the case of aeropectins, might be an important parameter for loading efficiency. One of the possible reasons is that a denser network with smaller pores and higher tortuosity might physically better prevent from theophylline wash off during sc-drying process. This assumption was confirmed by comparing the loading efficiency of aerogel obtained from the same sample preparation (6% pectin P35 solution dissolved at pH 2.0 with calcium addition at  $R(\text{Ca}) = 0.2$ ), and impregnated by diffusion of the same solution of theophylline in ethanol (3.4g/L) but dried either by evaporation (xerogel) or by sc-drying (aerogel). Pectin xerogel exhibited a high loading efficiency around 94% while aerogel showed lower loading efficiency around 62% (more detailed discussion will be given in Section 2.1). First, this proves that diffusion time was sufficient to completely load the sample to the core. However, even not being soluble in  $\text{CO}_2$ , a certain portion of the drug can be physically washed out because of the miscibility of ethanol with  $\text{CO}_2$  and flow during the sc drying process. The influence of drying is detailed in the following Section 2.1

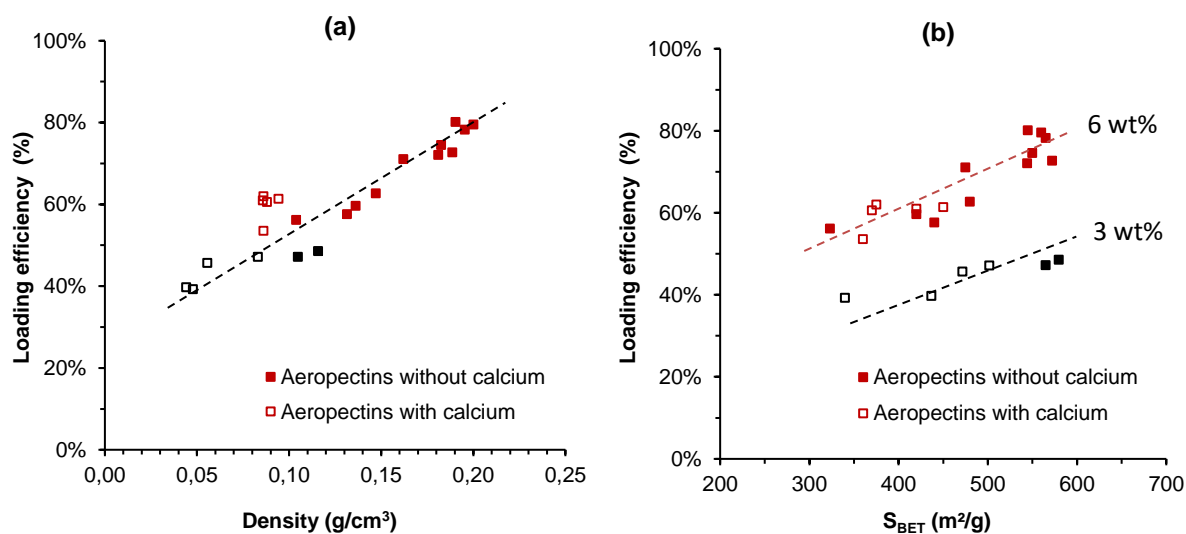


Figure 131. Plot of loading efficiency (a) as a function aerogel density and (b) as a function of  $S_{\text{BET}}$  for all pectin-based aerogels studied in this work. Aeropectins were made from pectin solutions of either 3 wt% of pectin P35 (black squares) or 6 wt% (red squares), in the absence of calcium (filled symbols) or cross-linked with calcium (open symbols). Pectin samples were impregnated in ethanol at theophylline concentration of 2.5 or 3.4 g/L. Dashed line is given to guide the eye.

The drug loading capacity of aeropectins (see Equation (2.13) from Chapter II) presented in Figure 132 shows its increase with the specific surface area (a) but no clear trend as a function of density (b). Even if aerogel density was found to be strongly correlated to drug loading

efficiency (Figure 131 (a)), it can be seen on Figure 132 (b) that density is not sufficient to fully explain the loading capacity.

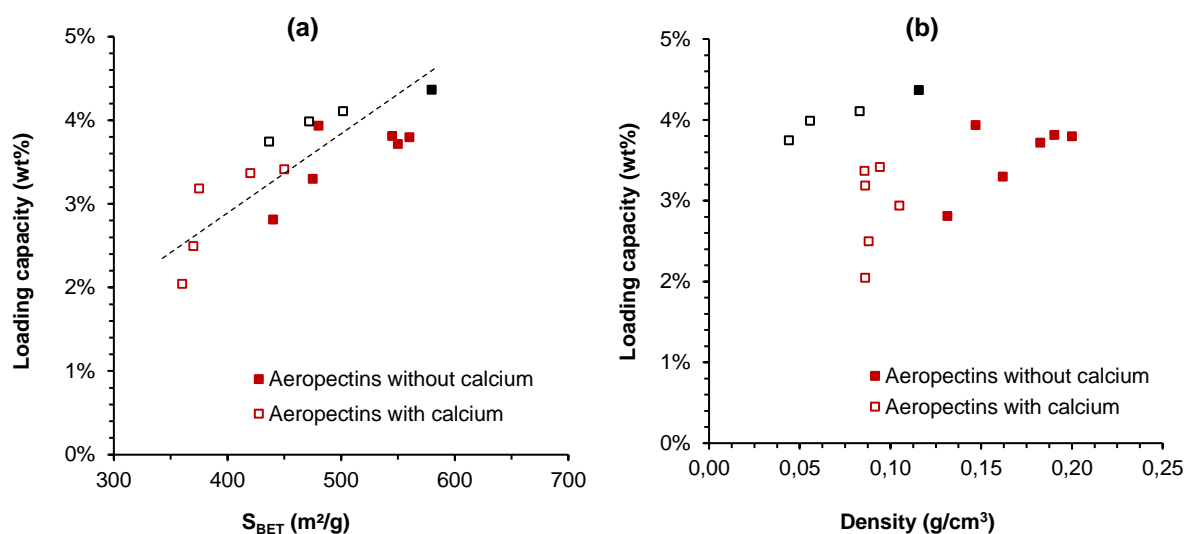


Figure 132. Plot of aerogel loading capacity (a) as a function of  $S_{BET}$  and (b) of density. Aerogels were made from solutions of either 3 wt% of pectin P35 (black squares) or 6 wt% (red squares), in the absence of calcium (filled symbols) or cross-linked with calcium (open symbols). Pectin samples were impregnated in ethanol at theophylline concentration of 3.4 g/L. Dashed line is given to guide the eye.

The change of pH, addition of calcium at various concentrations and pectin concentration were found to have a major impact on loading capacity due to aerogel structure change, but influenced differently the specific surface area and density. Indeed, decreasing pectin concentration from 6 wt to 3 wt% did not decrease much specific surface area (around 550-580 m<sup>2</sup>/g) and thus the drug deposition onto pectin chain, but artificially increase the mass contribution (wt%) of the drug regarding to the twice lower mass pectin carrier. Besides, the increase of calcium concentration or the decrease of pH progressively reduced specific surface area (and thus the surface of deposition) but not necessarily the density. As a result, some 6 wt% pectin aerogels can present density in the same range of values ( $\sim 0.9$  g/cm<sup>3</sup>) but with high variation of the loading capacities (2 wt% - 3.4 wt%) due to wide variations of their  $S_{BET}$  (from 360 – 450 m<sup>2</sup>/g).

The obtained theophylline loading capacities around 2 to 4.5 wt% (Figure 132) were much lower than what was reported for pectin aerogels ( $\sim 10 - 40$  wt%) and more generally for polysaccharide aerogels (García-González et al., 2015; Mehling et al., 2009; Tkalec, Knez, & Novak, 2015; Tkalec et al., 2016; Veronovski et al., 2014), however, in these publications, other drugs and/or other impregnation methods were used. Indeed, it has to be noted that the results of drug loading efficiency are highly dependent on the method of drug impregnation (*e.g.* impregnation before gelation, during solvent exchange or by impregnation under supercritical CO<sub>2</sub>) and drug properties (solubility in solvent and in scCO<sub>2</sub>). Aerogel's loading capacity is

directly limited by the maximum solubility of the drug in the impregnating media and by the weight of the carrier. Low drug loading capacity we have obtained are in correlation with rather low solubility of theophylline in ethanol ( $\sim 3.5$  g/L at  $25$  °C) and with rather high concentration of pectin solutions (6 wt%) to produce the aeropectin carriers.

### 1.2.2. Structural characterization of theophylline loaded aeropectins

SEM observations presented in Figure 133 show that the external surface of the aeropectins was covered by particles of the micrometric scale, which is typical for theophylline. For comparison, pictures of pure theophylline particles precipitated from ethanol are shown in Figure 134.

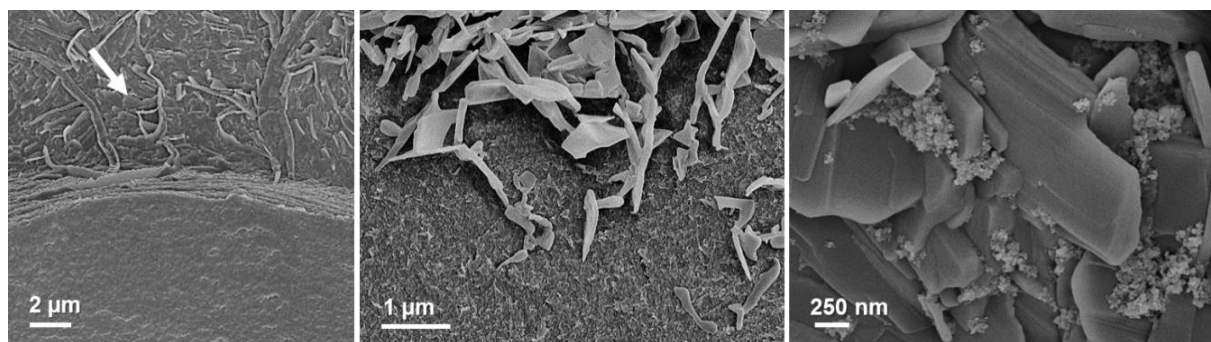


Figure 133. SEM pictures of the external surface of aeropectin matrix (white arrow) loaded with theophylline. Micrometric theophylline elongated particles are covering the external surface of aerogel.

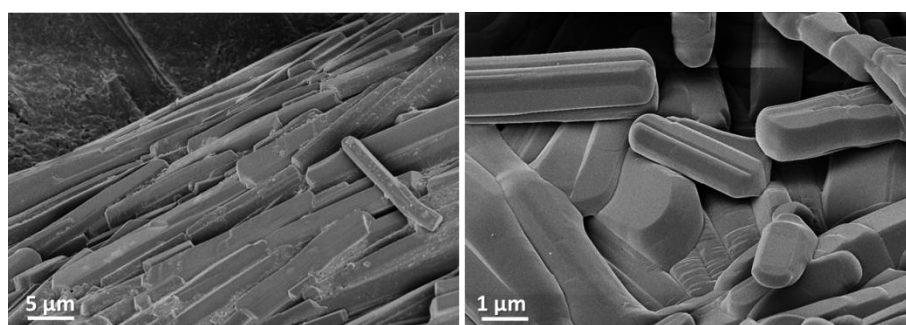


Figure 134. SEM pictures of pure theophylline elongated particles precipitated from ethanol by solvent evaporation.

We suggest that solidification of theophylline on the external surface of aerogel is due to evaporation of ethanol during the lag time between sample removal from ethanol and the launch of sc-drying. This was also observed by Haimer et al. after sc-drying of cellulose aerogels which were loaded with a drug by diffusion in ethanol prior to drying (Haimer et al., 2010). According to them, this was due to the spilling out of the drug solution in ethanol out of the matrix.

However, none of those sharp geometrical structures were found in the core of the aerogel as shown in Figure 135. Even if we were not able to visually observe the presence of theophylline inside the materials, the fact that theophylline was released over 10 h while aeropectin matrix was progressively dissolved due to surface erosion confirmed its presence not only on the external surface but also in the core of the material. Finally, network morphology, density and specific surface area of aeropectins loaded with drug remained unchanged when compared with non-loaded aeropectins, as the mass content of drug in aeropectins was low.

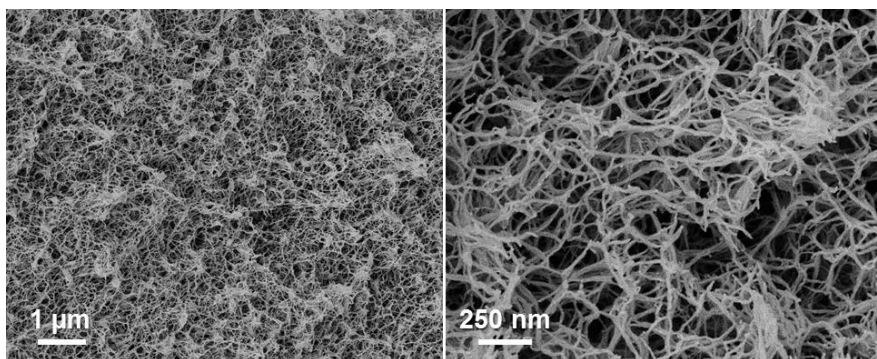


Figure 135. SEM pictures of the internal structure of aeropectin matrix loaded with theophylline.

### 1.2.3. Determination of crystalline structure of theophylline incorporated in pectin aerogels, xerogels and cryogels by X-rays diffraction

To determine if theophylline is in the crystalline or amorphous form within pectin aerogels, cryogels and xerogels, X-ray diffraction (XRD) analysis<sup>2</sup> was conducted on the external surface and in the core of the drug loaded samples. We also characterized theophylline drug particles as the raw powder in order to compare with drug-loaded pectin samples.

The X-ray diffractogram of pure theophylline as the raw powder (Figure 136 (A)) clearly shows the presence of sharp and intense diffraction peaks which reflects its crystalline structure. The diffractograms obtained from neat pectin aerogels and with theophylline inside (Figure 136 (B) and (C), respectively) present a similar broad hump without any sharp diffraction peaks, which is an indication for an amorphous structure of both pectin aerogel and the theophylline-pectin aerogel. These qualitative results suggest that initially crystalline theophylline is transformed into amorphous solids once incorporated into pectin aerogels.

---

<sup>2</sup> We thank Dr. Daniel Timpu from P. Poni Institute of Macromolecular Chemistry, Iasi, Romania, for performing XRD on pectin xerogels and cryogels

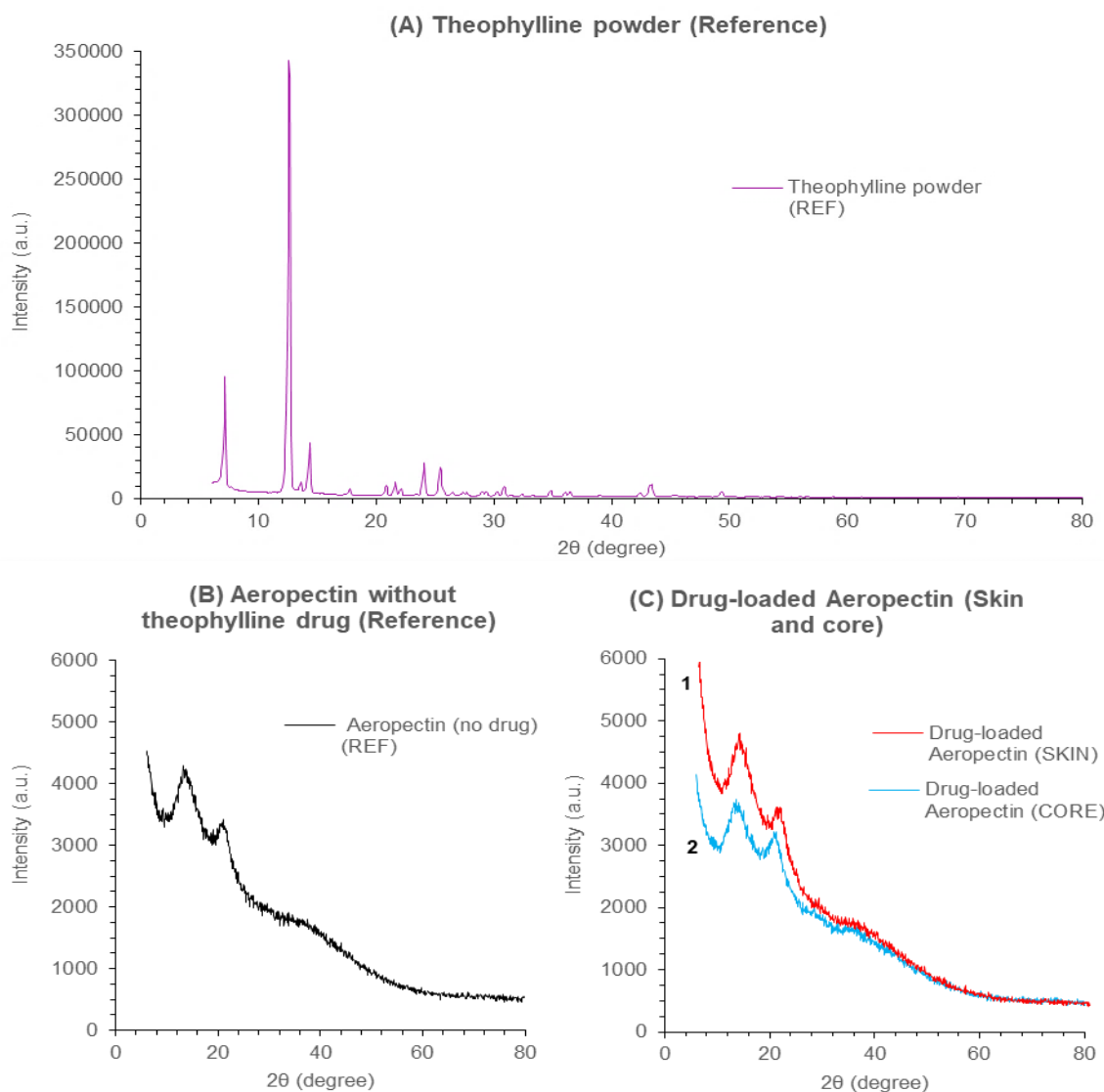


Figure 136. X-ray diffraction spectra (A) of theophylline raw powder, (B) of neat aerogel and (C) of an aerogel loaded with theophylline: on the external surface (curve 1) and in the core of the aerogel (curve 2). Both pectin aerogels were made from 6 wt% of pectin P35 dissolved at pH 2.0 without calcium. Pectin samples were impregnated by theophylline-ethanol solution at concentration of 3.4 g/L.

We investigated the impact (if any) of the drying method on the crystalline form of theophylline incorporated into pectin samples by comparing the X-ray diffractograms of drug-loaded pectin aerogels, xerogels and cryogels. Similarly to non-drug-loaded pectin aerogels (Figure 136 B), the diffractograms of neat pectin xerogels (Figure 137 A) and cryogels (Figure 137 C) present a wide hump without diffraction peaks, reflecting the amorphous form of the pectin dry samples. However, some sharp diffraction peaks in drug-loaded pectin xerogels (Figure 137 A vs B) and cryogels (Figure 137 C vs D) were recorded. In particular, specific diffraction peaks corresponding to crystalline theophylline located at around  $7.1^{\circ}$  and  $12.7^{\circ}$  (Figure 136 (A)) were found.

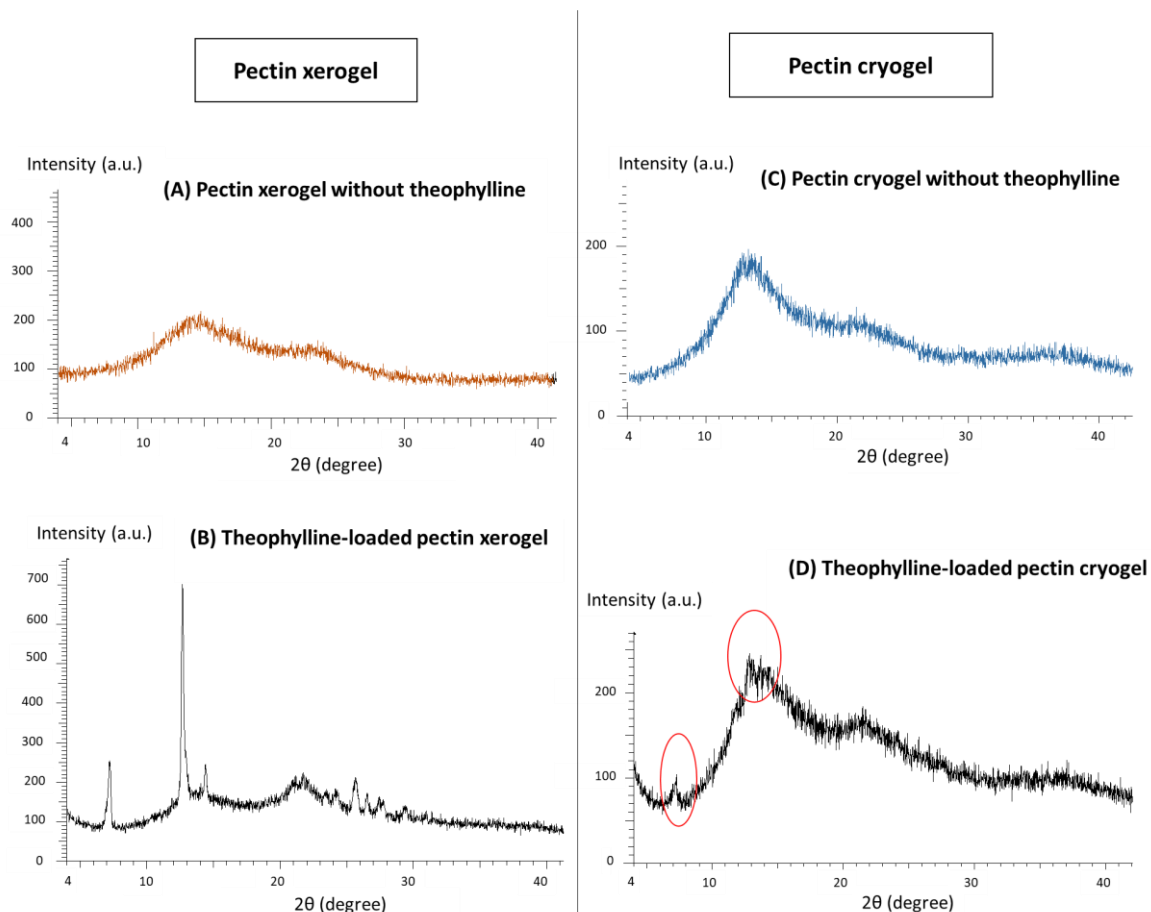


Figure 137. X-ray diffraction spectra of:

(A) Pectin xerogels without theophylline and (B) loaded with theophylline.

(C) Pectin cryogels without theophylline and (D) loaded with theophylline.

Both pectin xerogels and cryogels were made from 6 wt% of pectin P35 dissolved at pH 2.0 without calcium. Pectin xerogels were impregnated in ethanol at theophylline concentration of 3.4 g/L and dried by evaporation at 60°C in low vacuum conditions and pectin loaded cryogels were made by mixing pectin aqueous solution with theophylline at concentration of 3.4 g/L followed by gelation and freeze-drying.

These qualitative results show that drying method may have an impact on the final form (crystalline or not) of theophylline.

## 2. Study of theophylline release from pectin, aerogels, cryogels and xerogels

This part is dedicated to a detail study of the use of aropectins as oral drug delivery system, with theophylline as drug model. We remind that sample was first placed in acid medium Simulated Gastric Fluid (SGF) (pH 1.0) for one hour, and then in neutral medium Simulated Intestinal Fluid (SIF) (pH 6.8) until the end of release. As an illustration, Figure 138 shows an example of drug release curves obtained from theophylline released *in vitro* into simulated physiological fluids (37°C) as a free drug, or incorporated into a pectin hydrogel or pectin aerogel. Pectin hydrogel and aerogel were produced from the same initial pectin acid gel, based on 6 wt% pectin dissolved at pH 2.0 without calcium. The drug incorporation methods into the different pectin matrices are detailed in the Chapter II, Section 2.

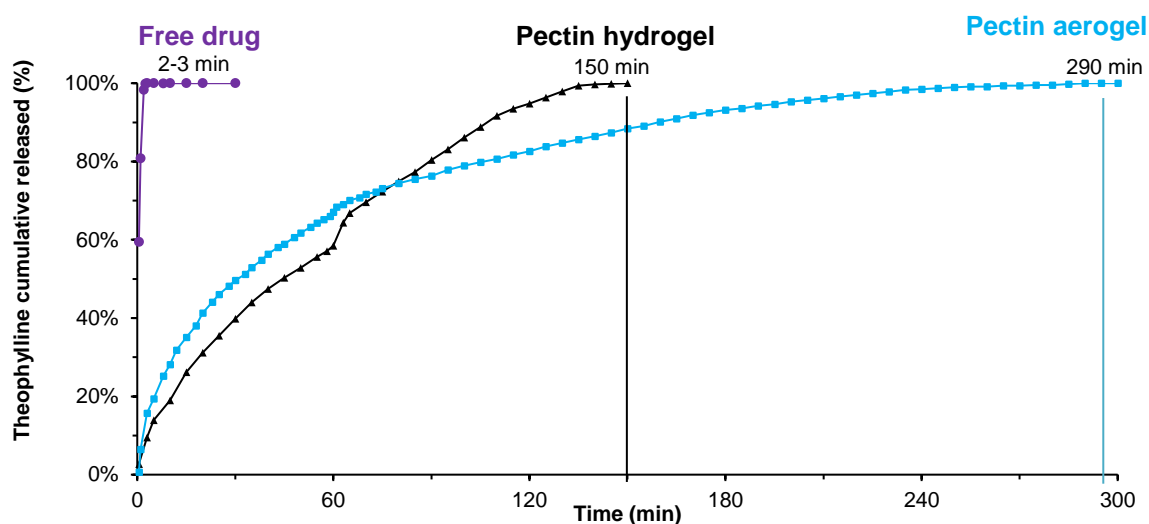


Figure 138. (a) Theophylline cumulative release (%) over time as free drug (anhydrous powder) versus release from pectin hydrogel or from pectin aerogel matrix. Pectin hydrogel and aerogel were made from 6 wt% of pectin P35 dissolved at pH 2.0 without calcium.

As expected, theophylline as free drug was immediately dissolved in correlation with its high solubility in the releasing media. In contrast, its release was significantly slowed down when embedded into the polymer matrix which acted as a physical barrier to theophylline instant release into the bath. Indeed, full drug release occurred in 150 minutes from pectin hydrogel and twice longer, around 300 minutes, from pectin aerogel. The difference in release time between the two pectin matrices is significant and is correlated to the much slower erosion of the pectin aerogel than of pectin hydrogel (both in the absence of calcium). This example illustrates the interest for the use of aerogels as drug carriers and their potential for prolonged-drug delivery applications.

Next, step by step examination of release kinetics from various pectin matrices is presented and discussed.

First, we compare drug release from pectin matrices based on the same formulation but dried in different ways: non-dried (pectin hydrogel) and dried using either sc-drying (pectin aerogel), or freeze drying (pectin cryogel) or evaporative drying at 60°C (pectin xerogel). The initial solutions were the same: aqueous 6% pectin P35 dissolved at pH 2.0, and calcium was added at  $R(\text{Ca}) = 0.2$  to induce ionic gelation. A strong ionic gelation induced by calcium was found to be necessary to prevent structure collapse during the drying of xerogels and cryogels.

To obtain theophylline loaded hydrogels and cryogels, the drug was added to pectin aqueous solution at 3.4 g/L which was then gelled for 48 h. Pectin cryogel was made by freeze-drying of a hydrogel. To produce xerogels and aerogels, theophylline was impregnated at the same dose into the coagulated samples at the very last step prior drying. The drug incorporation methods into the different pectin matrices are presented in the Chapter II, Section 2.

## 2.1. Structural properties of pectin matrix made with different dryings

As expected, pectin hydrogel and cryogel presented around 100% of loading efficiency. Pectin xerogel also exhibited a high loading efficiency around 94%, proving that diffusion time was sufficient to completely load the sample to the core (Figure 139). On the contrary, aerogel showed the lowest loading efficiency (~62%) due to theophylline being washed out because of the flow during sc-drying process, as previously discussed in the Section 1.2.1.

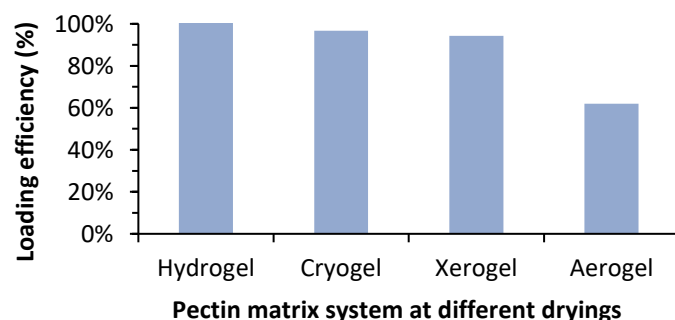


Figure 139. Theophylline loading efficiency (%) depending on pectin matrix drying: hydrogel, cryogel, xerogel or aerogel. All samples were made from the same initial pectin solution of 6% pectin P35 dissolved at pH 2.0 cross-linked with calcium at  $R(\text{Ca}) = 0.2$ .

The matrices dried in different ways presented very different internal structures, as expected, as shown in Figure 140 and Table 8. Cryogels were obtained by immersing pectin hydrogel in liquid nitrogen bath (-196°C) for 5 minutes in order to freeze water prior its removal by sublimation (freeze-drying). We observed very low sample shrinkage (around 10 - 13 vol

%) which might be due to sample contraction when they were immersed in nitrogen bath. During freezing, ice crystals were growing within the sample (Job et al., 2005), compressing the walls of pectin network and creates large pores. As a result, freeze dried samples present a highly porous rather damaged morphology with cracks and very large macropores in the micrometric scale (Figure 140). Its characteristics are shown in Table 8.

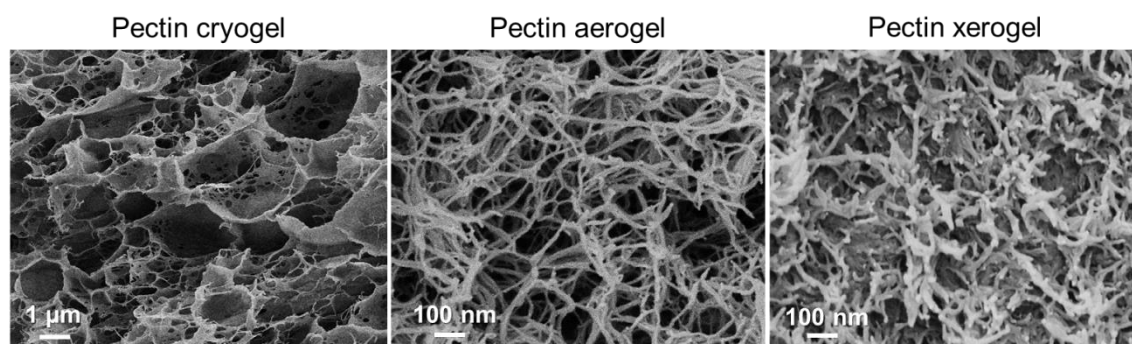


Figure 140. SEM observations of pectin cryogel, aerogel and xerogel. All samples were made from the same initial pectin preparation of 6% pectin P35 dissolved at pH 2.0 cross-linked with calcium at  $R(\text{Ca}) = 0.2$ .

Table 8. Structural properties of pectin hydrogel, cryogel, aerogel and xerogel matrix (the skeletal density of pectin is around is  $1.5 \text{ g/cm}^3$  (Groult & Budtova, 2018)). All samples were made from the same initial pectin preparation of 6% pectin P35 dissolved at pH 2.0 cross-linked with calcium at  $R(\text{Ca}) = 0.2$ . The size of pores was estimated from SEM images.

Matrix	Hydrogel	Cryogel	Aerogel	Xerogel
Density ( $\text{g/cm}^3$ )	$1.076 \pm 0.009$ (wet material)	$0.073 \pm 0.003$ (dry material)	$0.083 \pm 0.005$ (dry material)	$1.057 \pm 0.021$ (dry material)
Porosity (%)	–	$95.1 \pm 0.2$	$94.6 \pm 0.3$	$29.6 \pm 1.4$
Pore volume ( $\text{cm}^3/\text{g}$ )	–	$13.04 \pm 0.53$	$11.63 \pm 0.75$	$0.28 \pm 0.02$
$S_{\text{BET}}$ ( $\text{m}^2/\text{g}$ )	–	10 to 20	$362 \pm 14$	Non-measurable
Network morphological aspect	–	Large macropores of around 0.5 to 5 $\mu\text{m}$ of diameter	Mesopores and small macropores of around 50 to 150 nm of diameter	Highly dense network

The evaporative drying (xerogels) performed at 60°C in low vacuum conditions induced massive shrinkage over 90 vol% of pectin sample. Structure collapse occurred due to important capillary forces and led to high density xerogels ( $> 1 \text{ g/cm}^3$ ) displaying low porosity ( $\sim 30\%$ ) and compact morphology after drying (Figure 140).

In the supercritical state (aerogels), the supercritical fluid has properties midway between a liquid and a gas. As there is no meniscus, the capillary forces were avoided and the samples were dried without damaging the structure. However, volume shrinkage ( $\sim 30 \text{ vol}\%$ ) occurred due to contraction during solvent exchange step and sc-drying, as detailed in Chapter III. After sc-drying, low density aerogels were obtained ( $\sim 0.080 - 0.085 \text{ g/cm}^3$ ), displaying high porosity with mesopores and small macropores (around 50 to 150 nm of diameter as deduced from SEM images).

## 2.2. Theophylline release profiles as a function of drying method

Theophylline release profiles and matrix mass and volume evolution in time for hydrogel, cryogel, xerogel or aerogel are plotted in Figure 141 and Figure 142, respectively.

As expected, we observed that the drying method of the matrix had a strong impact on its drug release properties, as it drastically changed the internal structure even if the initial composition was the same. In this work, we used kinetic mathematical models based on the fitting with experimental data to determine the main drug release mechanisms governing theophylline release (see Annex for the description of each model).

The methodology to select the most accurate models to describe the release kinetics will be given in detail in the Section 3.2 based on one example of drug release experiment from a pectin aerogel. Here, we used Korsmeyer-Peppas and Peppas-Sahlin models (See equations (A.12) and (A.14) of the Annex, respectively) as they were found to be the most suitable models based on their good fitting to data with the highest  $R^2$  values ( $R^2 > 0.99$ ), and their ability to discriminate different release behaviour. The calculated parameters are presented in Figure 141.

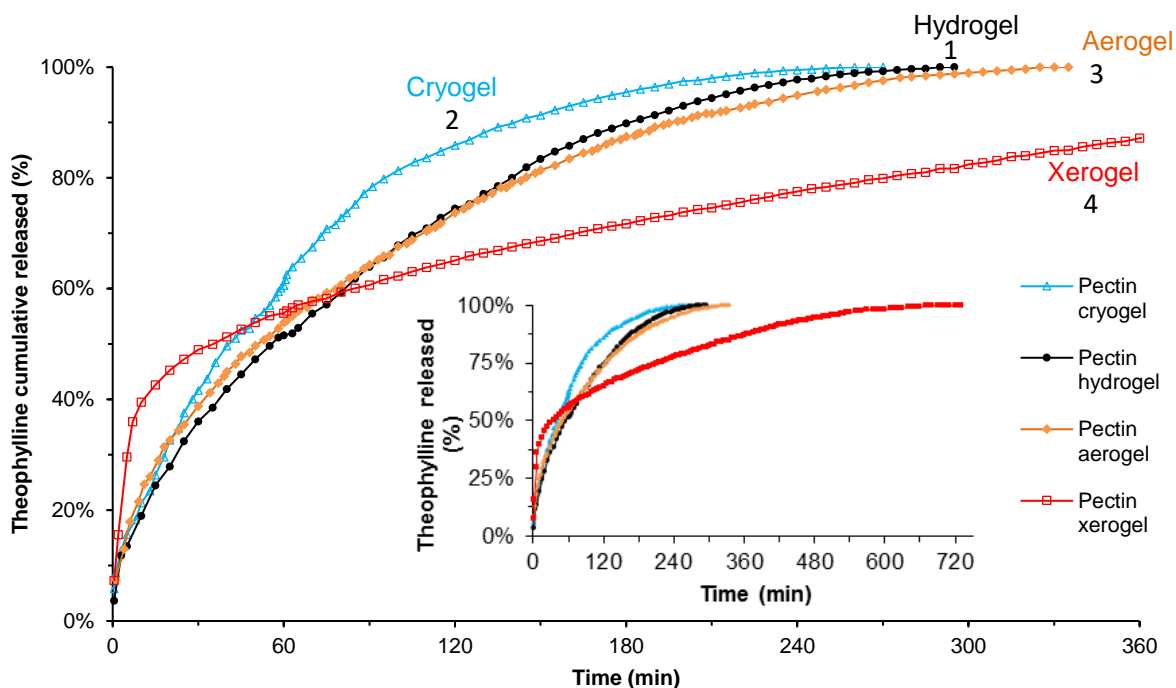


Figure 141. Theophylline cumulative release (%) over time depending on pectin matrix system: hydrogel (1), cryogel (2), aerogel (3) and xerogel (4). All matrices were produced from the same aqueous pectin solution: 6 wt% pectin dissolved at pH 2.0 cross-linked with calcium at  $R(\text{Ca}) = 0.2$ .

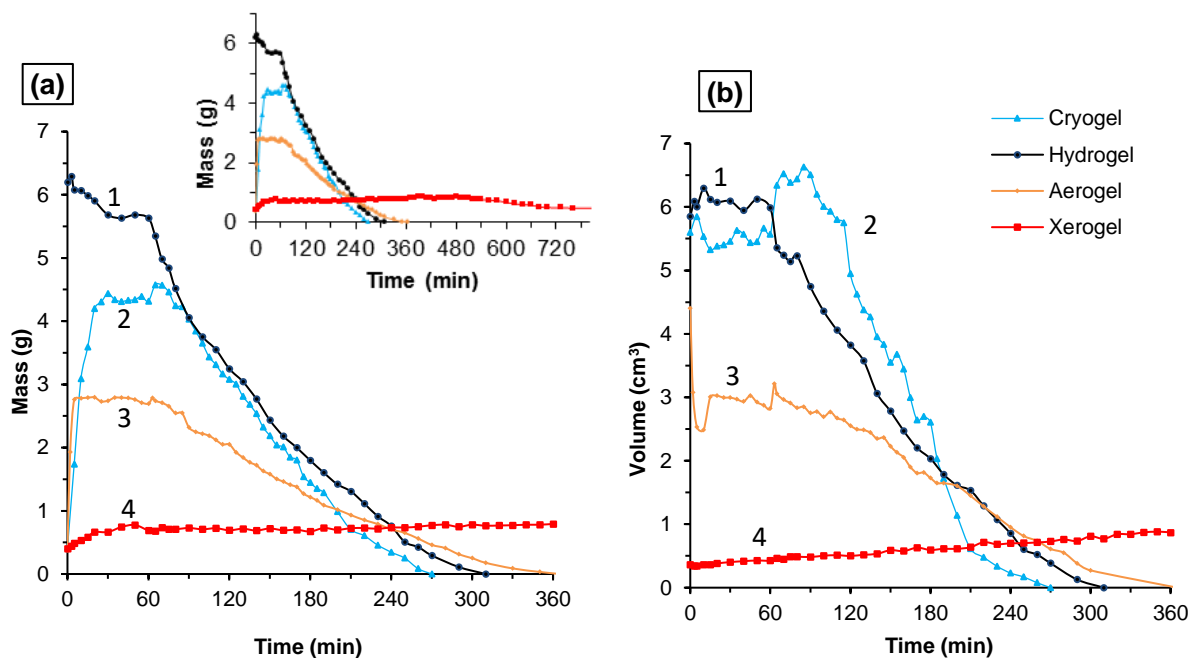


Figure 142. (a) Mass (g) and (b) volume (cm<sup>3</sup>) evolution over release time of each pectin matrix depending on the drying method: hydrogel (1), cryogel (2), aerogel (3) and xerogel (4).

Table 9. Estimation of the parameters from Korsmeyer-Peppas and Peppas-Sahlin models for theophylline release from pectin hydrogel, cryogel, aerogel, and xerogel (Peppas & Sahlin, 1989; Ritger & Peppas, 1987a, 1987b).

Matrix	Hydrogel	Cryogel	Aerogel	Xerogel
<b>Korsmeyer-Peppas model</b>	n = 0.542 K <sub>kp</sub> = 0.743 R <sup>2</sup> = 0.999	n = 0.603 K <sub>kp</sub> = 0.778 R <sup>2</sup> = 0.996	n = 0.500 K <sub>kp</sub> = 0.756 R <sup>2</sup> = 0.997	n = 0.230 K <sub>kp</sub> = 0.758 R <sup>2</sup> = 0.967
<b>Peppas-Sahlin model</b>	Diffusional K <sub>F</sub> = 0.362 h <sup>-0.43</sup>  Relaxational K <sub>R</sub> = 0.151 h <sup>-0.86</sup>  R <sup>2</sup> = 0.998	Diffusional K <sub>F</sub> = 0.371 h <sup>-0.43</sup>  Relaxational K <sub>R</sub> = 0.240 h <sup>-0.86</sup>  R <sup>2</sup> = 0.997	Diffusional K <sub>F</sub> = 0.460 h <sup>-0.43</sup>  Relaxational K <sub>R</sub> = 0.085 h <sup>-0.86</sup>  R <sup>2</sup> = 0.998	Diffusional K <sub>F</sub> = 0.979 h <sup>-0.43</sup>  Relaxational K <sub>R</sub> < 0  R <sup>2</sup> = 0.979

Pectin hydrogel release profile can be considered as a “reference” to evaluate the impact of drying. As shown in Figure 141, full theophylline release from hydrogel occurred in around 290 min, correlating with hydrogel erosion by dissolution as shown in Figure 142. The Korsmeyer-Peppas *n* exponent was estimated to be around 0.54 for release from hydrogel, which is related to anomalous transport of drug (non Fickian), governed by the coupling of diffusional and relaxational (polymer swelling and erosion) phenomena.

Thus, Peppas-Sahlin model was used to estimate the Fickian diffusion contribution to the release, as shown by the Fickian release fraction over time in Figure 143. At the beginning of release, diffusion dominates and drug release is mainly due to drug diffusion through the first layers of the hydrogel. With time, polymer relaxation becomes significantly involved in the delivery of drug particles located deeper in the hydrogel matrix. Polymer swelling and dissolution occurred resulting in larger “free spaces” in the matrix, which in turn increases diffusivity of solvent and drug through the matrix.

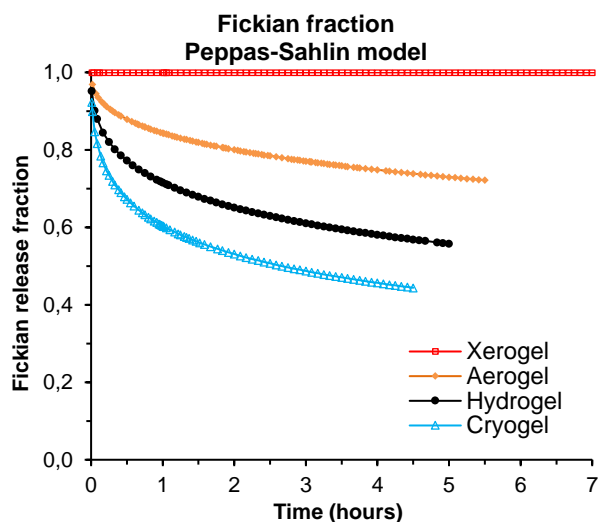


Figure 143. Fickian release fraction ( $F$ ) as a function of release time, from a flat cylinder model with  $m$  value of 0.430, based on Peppas-Sahlin model (Peppas & Sahlin, 1989).

As it can be seen in Figure 13, pectin cryogel showed the fastest full release which was completed in about 260 min, governed by coupling of diffusional and relaxational phenomena as revealed by Korsmeyer  $n = 0.6$  (between 0.45 and 0.89). This rapid release is in correlation with highly macroporous morphology due to water ice crystals growth during freeze-drying (Figure 140), which resulted in the formation of micrometric channels, poor mechanical properties and low-density material. We assume that this particular open structure enabled high solvent velocity and drug diffusivity through the system. The fast solvent penetration and low-density network might have promoted rapid matrix erosion (Figure 142), which in turn accelerated drug release. Our assumptions are confirmed by the high relaxational contribution to the release using Peppas-Sahlin model, as shown in Figure 143.

Pectin aerogel showed a full release in around 330 min, also driven by diffusion and polymer swelling / dissolution according to Korsmeyer  $n = 0.5$  (between 0.45 and 0.89) Despite a low density similar to pectin cryogel, the microstructure of aerogel presented much smaller pores in the nanometric scale (Figure 140) which made the difference in matrix erosion and release rates as compared with cryogel. Even slightly higher density (+13-15%) coupled to smaller pore sizes may also limit free spaces and mass transport phenomena. Indeed, as shown in Figure 142, aerogel matrix erosion was more than one hour and half longer than that of cryogel, and one hour longer than of hydrogel. We visually noted that a dry core in aerogel was maintained during the first hours of release experiment, confirming low solvent velocity through the dry system (Figure 144). As a result, matrix erosion and drug release were slowed down. This is also confirmed by higher Fickian contribution to the release as compared with cryogel and hydrogel (Figure 143).

Xerogel exhibited the small initial matrix volume due to ~ 93-95% shrinkage during drying, which led to high density and low porosity. We assume that the compactness of the structure prevented both diffusion and matrix dissolution and thus the release of drug. This was visually confirmed by the maintenance of a dry core in the center of the matrix, as shown in Figure 144. As it can be seen in Figure 142, matrix volume and mass were maintained during a long period of time ( $t > 800$  min) and no matrix erosion was observed until 500 min of experiment. According to Korsmeyer-Peppas model, we obtained  $n$  value of 0.23 which was lower than 0.45 (Case I Fickian diffusion) but suggested a diffusion-based mechanism. This  $n$  value indicates a deviation from Fick's law, which can be due to the polydispersity of pore sizes, potentially presence of closed pores and overall heterogeneity within the material. It is known that when pores of a dried polysaccharide are closed during drying, they may not re-open during wetting, this phenomenon known for cellulose as "hornification". Similar behaviour was already reported in the work of Horvat et al. on pectin-xanthan composite aerogels (Horvat et al., 2017), and also in ref (Rezaei, Nasirpour, Tavanai, & Fathi, 2016; Sauri et al., 2014; Sengupta, 2016).

As the xerogel matrix showed good durability and stability in the releasing media, with no erosion observed during 97% of total drug released (Figure 142 (a)), we assumed that the release of the drug occurred only due to diffusion, meaning that the soluble drug might have diffused out of the sample before matrix erosion occurred. This is also confirmed using Peppas-Sahlin model (Figure 143) revealing that all drug release was due to diffusional transport. Thus, we assume that the extremely slow xerogel erosion coupled with slow diffusion through the dense and compact network resulted in extended release up to about 10 hours. For illustration, pictures of each matrix after 120 minutes of dissolution testing experiments are presented in Figure 144.



Figure 144. Pictures of pectin hydrogel, cryogel, aerogel, and xerogel after 120 minutes of release experiment in simulated gastric fluid (SGF, pH 1.0) the first hour, then in simulated intestinal fluid (SIF, pH 6.8) at 37°C. All matrices were produced from the same initial aqueous 6 wt% pectin solution dissolved at pH 2.0 cross-linked with calcium at  $R(\text{Ca}) = 0.2$ . The scale is the same for all pictures.

It is interesting to see how drying of hydrogel matrix to make either xerogel (evaporation), or cryogel (freeze drying) or aerogel (sc-drying) results in various internal structures, leading to very slow (more than 10 h) to faster (5 h) drug release, respectively. The variation of network

morphology due to drying process was shown to balance the contribution of both diffusional and relaxational mechanisms, as summarized in Figure 143.

### 2.3. Comparison of release properties of pectin hydrogels and aerogels

As stated above, we noted that twice slower complete drug release time occurred from aerogels as compared to hydrogel (Figure 138), however, Figure 141 shows that total release time from hydrogel and aerogel is very similar. The reason is that release properties are strongly dependent on matrix formulation and, as a consequence, material properties.

As shown in Figure 145, in absence of cross-linking by calcium, the difference in drug release behavior between the two pectin matrices is significant, with complete release of theophylline in around 150 minutes from pectin hydrogel, and twice longer, around 300 minutes, from pectin aerogels. This stems from the dramatic difference in matrix “stability” and erosion, hydrogel vs aerogel (both without calcium) in the releasing media. As it can be seen in Figure 146 (a), the erosion by dissolution of pectin hydrogel was twice faster (in 160 min) than that of pectin aerogel (in 320 min) in absence of calcium. In contrast, when calcium was added to pectin solution ( $R(\text{Ca}) = 0.2$ ) to produce hydrogel and aerogel samples, the two matrices displayed much more similar drug release profiles, with complete theophylline release in around 300 and 330 min, for pectin hydrogel and aerogel, respectively. This prolonged drug release behavior from hydrogel is in correlation with slow matrix erosion which is practically the same for the both matrixes when calcium was added. Pectin hydrogel was completely dissolved within 310 min, and the pectin aerogel within 365 min.

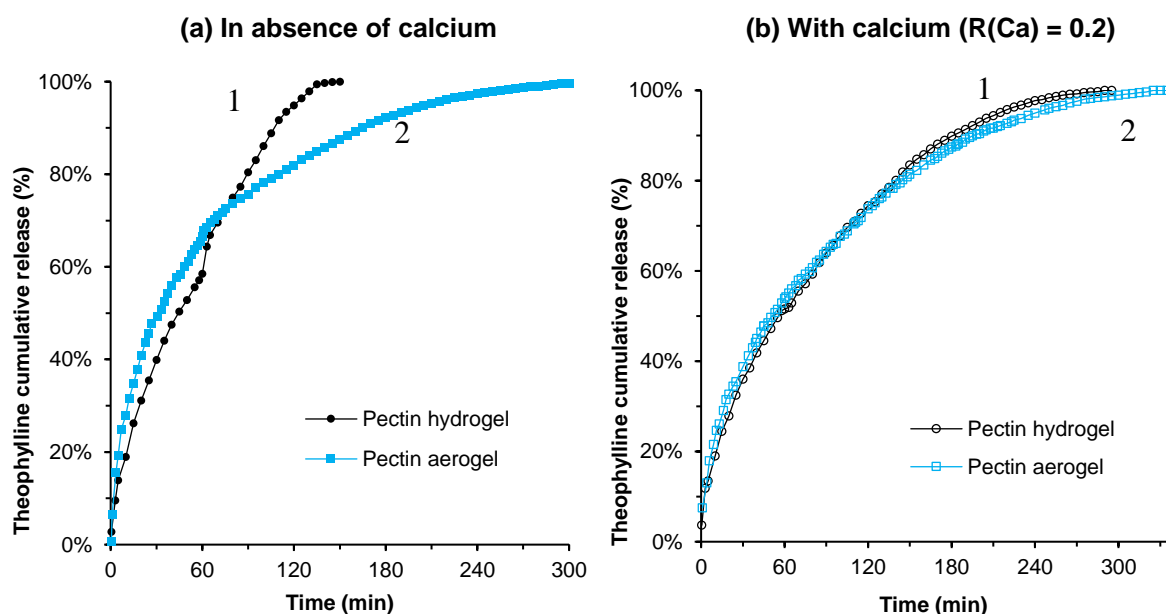


Figure 145. Theophylline cumulative release (%) over time from pectin hydrogel (1) or from pectin aerogel (2) based on the same formulation made from 6wt% of pectin at pH2.0, (a) in absence of calcium or (b) cross-linked with calcium at  $R(\text{Ca}) = 0.2$ .

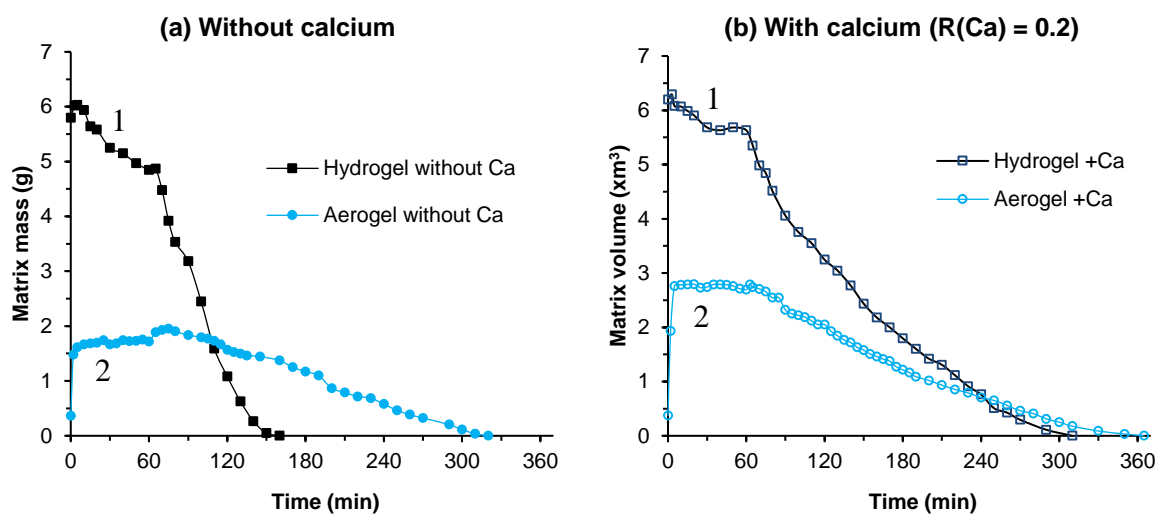


Figure 146. Comparison of matrix mass (g) evolution over time for hydrogels (1) and aeropectins (2) based on the same formulation made from 6 wt% of pectin at pH2.0, (a) in absence of calcium or (b) cross-linked with calcium at  $R(\text{Ca}) = 0.2$ .

As shown above, supercritical drying has a slowing down effect on the release properties of pectin matrix, and this effect is much more pronounced when no cross-linking with calcium was used. There are two significant differences between hydrogel and aerogel matrices:

- One is that aeropectins are dried materials in contrast to hydrogels. When aerogel is placed in aqueous medium, only chains on sample surface start to be hydrated and a dry core remained visually intact, as revealed by the floating of the aeropectin and estimated density lower than 1 throughout the whole dissolution test. Thus, we can assume that the gradient of water penetration through the dry matrix might have played a role in liquid diffusion and dissolutions mechanisms.
- Another reason is that aeropectin network became denser with smaller pores due to high shrinkage (from 60% to 75 vol %) during the processing route. The increased tortuosity of the pectin network might have decreased diffusion coefficient restraining water and drug diffusion processes. The volume of aeropectin matrix was around three times lower than that of hydrogel matrix, confining mass transport into smaller free spaces offered by the matrix.

In the absence of calcium, pectin acidic hydrogels were soft and fragile, made of labile reversible chain interactions (hydrogen bonds and hydrophobic interactions) that were easily destabilized. When re-hydrated, the coagulated network from pectin aerogel led to stronger and more stable system which was less easily dissolved than acidic hydrogel. In contrast, when calcium was added ( $R(\text{Ca}) = 0.2$ ) into pectin solutions, both ionic hydrogels and aeropectins

present strong crosslinked network, resulting in more “similar” properties (shrinkage of calcium cross-linked pectin is around twice smaller than that of acid gel): it is slow matrix erosion which governs slow theophylline release.

### 3. Background analysis of aeropectin behaviour and theophylline release

This section is making a background for the further detailed analysis of the release of theophylline for pectin aerogels. Here a reference sample is considered: aeropectin based on 6 wt% of pectin P35 at pH 3.0 without calcium. Before performing “real” tests placing aeropectin in simulated gastric fluids (SGF, pH 1.0) for one hour and then in the simulated intestinal fluid (SIF, pH 6.8) as it was described in Section 2, here we evaluate aerogel behaviour in each fluid separately to understand the influence of pH. Then release kinetics from this aeropectin is analyzed in physiological condition (one hour in SGF and then in SIF) using models to select the best one fitting experimental data. The main drug release mechanisms governing theophylline release will be determined and discussed.

#### 3.1. Influence of pH of release medium on aeropectin erosion, swelling and drug release

To illustrate aeropectin pH sensitivity to the release bath media, the experiments of theophylline release were performed either in Simulated Gastric Fluid (pH 1.0) (SGF) only or in Simulated Intestinal Fluid (pH 6.8) (SIF) only, until full release. The results are presented in Figure 147. Volume and mass of aeropectin matrices as a function of time (in Figure 148) were systematically followed to correlate drug release profile and matrix swelling and erosion.

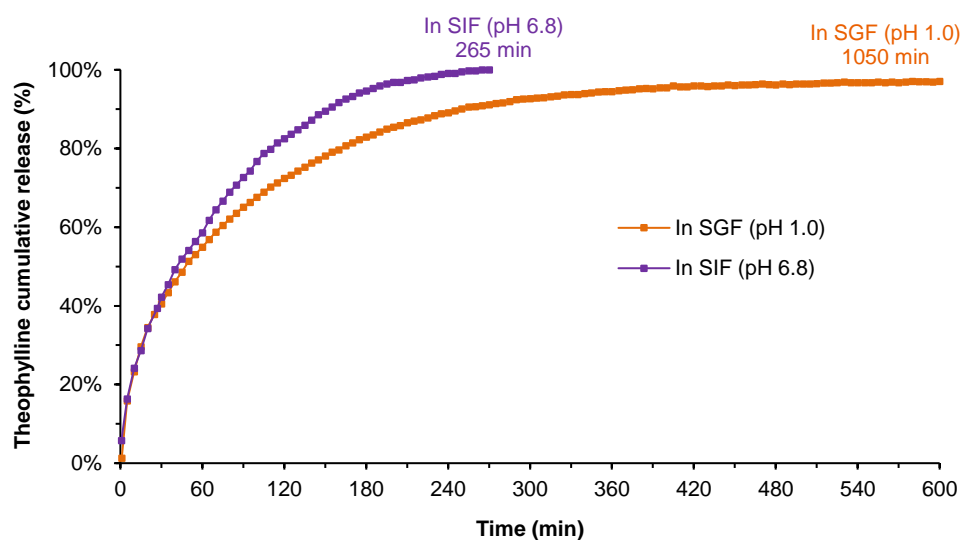


Figure 147. Theophylline cumulative release (%) from aeropectins over time in either SGF medium (pH 1.0) or in SIF medium (pH 6.8) at 37 °C during the whole dissolution testing. Aeropectins were made from 6 wt% of P35 dissolved at pH 3.0 without calcium.

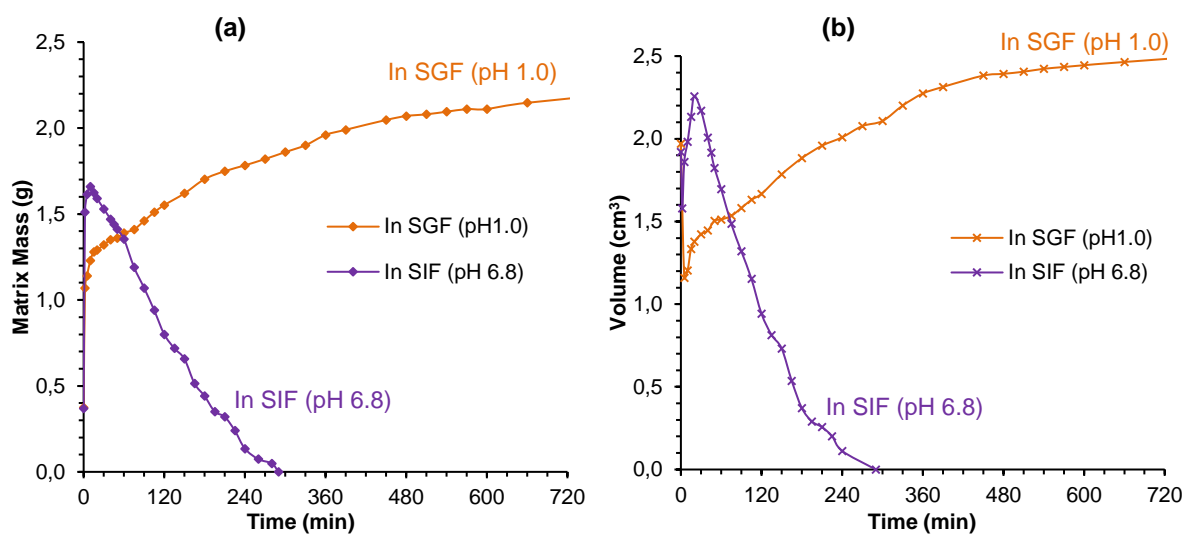


Figure 148. (a) Aeropectin matrix mass (g) and (b) volume (cm<sup>3</sup>) evolution when immersed either in SGF (pH 1.0) or SIF (pH 6.8) bath at 37 °C. Aeropectins were made from 6 wt% P35 dissolved at pH 3.0 without calcium.

As shown in Figure 148, aeropectins instantly contracted in contact with liquid media (from 20% to 30%, as compared with dry state). As also observed in the work of Marin et al., this initial shrinkage can be due to collapse of macropores by capillary forces exerted from fast water penetration into the system (Marin, Mallepally, & McHugh, 2014). During the first 10 minutes of immersion in releasing media, aeropectin exhibited a fast mass increase, from +230% in SGF (pH 1.0) to +350% (as compared with dry state). This mass increase is simply due to water uptake by a porous matter.

As explained in the Annex (Section 1), the velocity of diffusion of a liquid depends on the structural characteristics of the matrix network, the physical and chemical properties of the polymer, as well as the properties of liquid. As pectin is a polyelectrolyte with  $pK_a$  around 3-3.5, pectin-based aerogels were expected to be pH-sensitive materials and react in different ways when immersed either into SGF (pH 1.0) or SIF (pH 6.8). Indeed, it can be seen in Figure 148 that aeropectins' mass and volume evolution differ depending on the liquid pH. In acidic media ( $\ll pK_a$ ), strong interactions between pectin chains due to hydrogen bonding are promoted, as Gal.A exhibited protonated acid functions and chain hydration of pectin is low. In SGF (pH 1.0) we observed that re-hydration of aeropectin resulted in the formation of a “resistant” external gel layer surrounding the dry core (as shown in Figure 150).

The strong gelled network prevented chain relaxation, which hindered matrix swelling and inhibited polymer dissolution. As a consequence, pectin gel was strongly resistant to dissolution and the matrix did not dissolve for more than 24 hours of immersion in SGF. In the

absence of erosion, the matrix was slowly swelling for 24 h in SGF (+40 vol% after 24 h of immersion). This resistant gel layer might also have acted like a “barrier” to water and drug diffusion due to reduced diffusion coefficient.

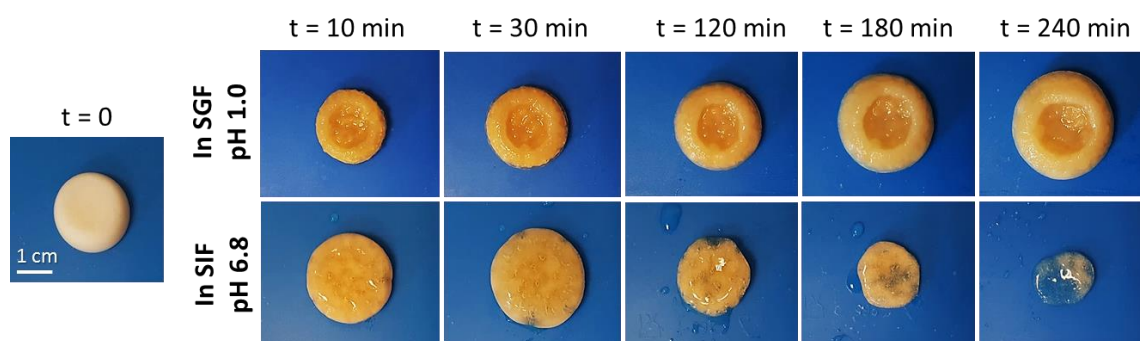


Figure 149. Pictures of aeropectins from 6 wt% P35 dissolved at pH 3.0 without calcium, at different time after immersion into SGF (pH 1.0) or in SIF (pH 6.8) at 37°C. All pictures are at the same scale.

In SIF (pH 6.8) medium, ionization of carboxylate groups of pectin occurred; pectin chains repelled each other due to coulombic repulsion and chain hydration increased leading to chain disentanglements and dissolution. As a result, the hydrated network tended to dissociate and expand as revealed by strong matrix swelling immediately followed by dramatic erosion by dissolution (Figure 148). The pH sensitivity of pectin-based materials is known and widely used to design effective gastro-resistant drug delivery systems (Liu, Fishman, Kost, & Hicks, 2003).

Figure 149 presents the evolution of aeropectin macroscopic dimensions with time in SGF and in SIF. It can be seen that immersion in media with pH higher than  $pK_a$  promotes quick swelling and erosion of the matrix, while erosion is inhibited when pH is lower than  $pK_a$ , as schematized in Figure 150.

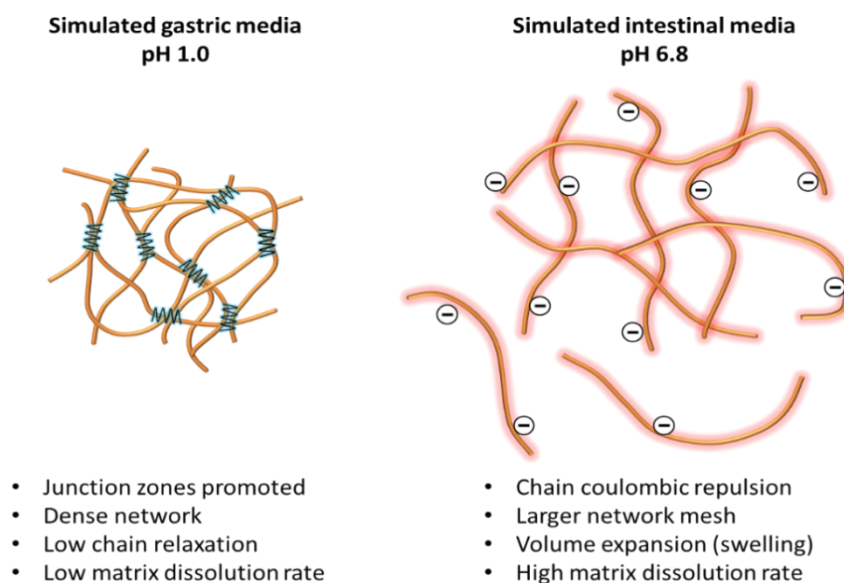


Figure 150. Schematic representation of the pectin network either in simulated gastric media (pH 1.0) or simulated intestinal media (pH 6.8)

As a result of matrix swelling/erosion sensitivity to pH, theophylline release from aeropectins was directly impacted by the pH of the releasing media. As shown in Figure 147, full theophylline release occurred rapidly in SIF media (in 265 min) driven by fast matrix erosion, while the release in SGF was 4 times longer, with slow release prolonged for more than 1000 minutes (17.5h) in correlation with matrix resistance to dissolution. Indeed, in the intestinal media (SIF)  $\text{pH} \gg \text{pK}_a$ , the important matrix erosion promoted water penetration and drug diffusivity in the system, resulting in faster drug release, while in gastric media (SGF)  $\text{pH} \ll \text{pK}_a$ , matrix erosion was inhibited and drug slowly diffused out of the swollen network.

These results confirm that aeropectins are gastro-resistant materials that can be used to protect drug from gastric degradation and to prevent full drug release in the stomach. The change of liquid media from gastric to intestinal conditions during dissolution testing experiments is expected to promote matrix erosion and thus drug release.

Based on pectin polyelectrolyte property, aeropectins can be used as pH-responsive drug delivery systems. Similar results were found for drug-loaded bio-aerogels in the shape of microparticles made from polyelectrolyte polysaccharides such as alginate, pectin and carrageenan and cross-linked with calcium ( $\text{CaCl}_2$  or  $\text{CaCO}_3$ ) (Gonçalves et al., 2016; Veronovski et al., 2014).

### 3.2. Selection of a model to describe release kinetics

To mimic the physiological release conditions, the reference theophylline loaded pectin aerogel (6 wt% of pectin P35 dissolved at pH 3.0 without calcium) was first immersed into SGF (pH 1.0) during the first hour and then in SIF (pH 6.8) during the following hours. Drug cumulative release over time and matrix mass and volume erosion are presented in Figure 151.

As it can be seen, full theophylline release occurred in around 360 min, and was correlated with the slow erosion of the aerogel matrix over time. Based on our previous observations, we could clearly notice that matrix erosion was promoted when releasing media was changed from SGF (pH 1.0) to SIF (pH 6.8) after 1 hour of experiment, as revealed by rapid matrix swelling immediately followed by a strong decrease of matrix mass and volume over time, as presented in Figure 151 (b) (c).

In the following, we use these data to select the suitable mathematical model describing release kinetics and to better understand the physical mechanisms involved in the drug release.

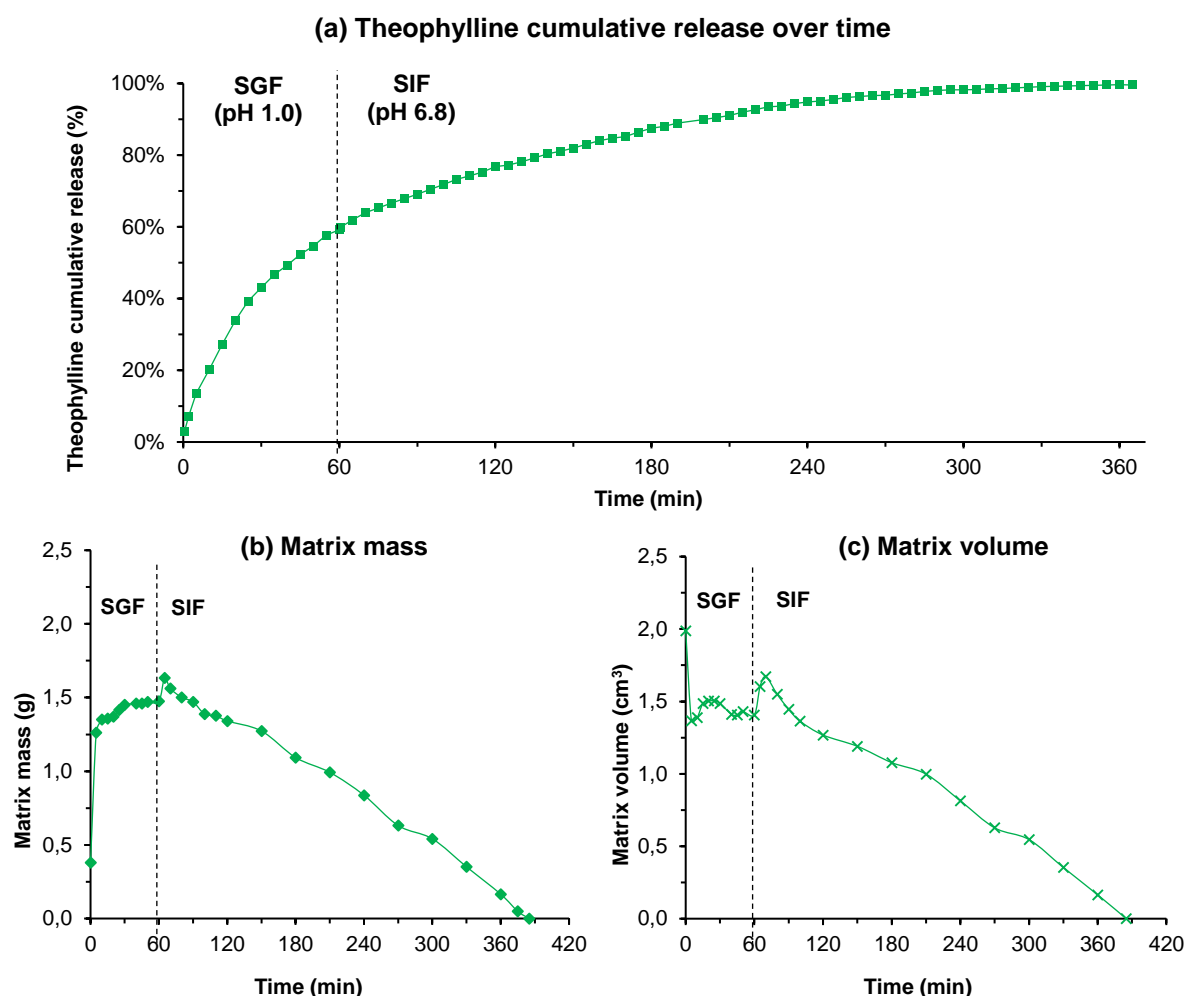


Figure 151. (a) Theophylline cumulative release (%) over time from pectin aerogel made from 6 wt% of pectin pH 3.0 and (b) matrix mass and (c) matrix volume evolution in time. The aeropectin was immersed into SGF (pH 1.0) the first hour and in SIF the following hours (pH 6.8) at 37°C. The vertical dashed lines indicate the change of releasing media at  $t = 60$  min.

### 3.2.1. Mathematical models fitting drug release profiles

We have tested the fitting of the several currently used mathematical models to the data obtained from theophylline release experiment from aeropectin. Only the models applicable for solid polymeric matrix were selected which include: Zero-order kinetics, First-order kinetics, Higuchi, Korsmeyer-Peppas, Peppas-Sahlin, Hixson-Crowell, Hopfenberg, Gallagher-Corrigan models. The description, equations and assumptions of each model are presented in the Annex (Section 2). Correlation coefficient  $R^2$  was chosen to define the accuracy of each model. Release constants from Hopfenberg and Gallagher-Corrigan models were determined through least squares fitting, otherwise the release constants were obtained by linear regression. “Acceptable” model fitting to data are achieved when  $R^2$  values  $> 0.970$ , and “high” correlations for  $R^2 > 0.990$ .

The experimental data and the corresponding fits together with the table of correlation coefficient and release constants are presented in Figure 152 and Table 10, respectively.

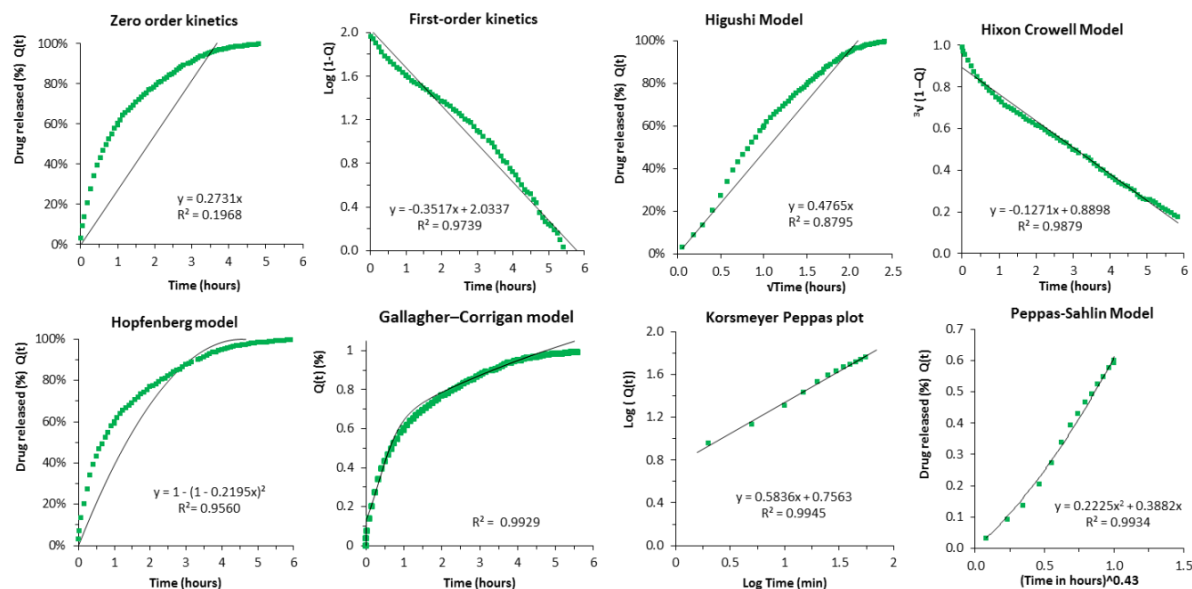


Figure 152. Experimental data and the corresponding fits for theophylline release data. Theophylline release occurred in SGF (pH 1.0) the first hour and in SIF (pH 6.8) during the following hours. Aeropectin was made from 6% of P35 dissolved at pH 3.0 without calcium.  $Q(t)$  is the percentage of cumulative drug released in time  $t$ . Solids lines are the model plots.

Table 10. Table of correlation coefficients and release rate constants of each model:  $k_0$ ,  $k_1$ ,  $k_H$ ,  $K_{HC}$ ,  $K_G$ ,  $n$ ,  $K_{kp}$ ,  $K_F$ ,  $K_R$ ,  $k_e$ ,  $k_b$ . (See the equations (A.5), (A.6), (A.8), (A.9), (A.11), (A.12), (A.14) and (A.17), respectively, in the Annex to the manuscript.)

Model	Zero order kinetics	First order kinetics	Higuchi (simplified)	Hixson Crowell	Hopfenberg	Korsmeyer Peppas For $Q_t < 60\%$	Peppas-Sahlin For $Q_t < 60\%$	Gallagher-Corrigan
$R^2$	0.1968	0.9739	0.8795	0.9879	0.9560	0.9945	0.9934	0.9912
Release rate constant	$K_0$ 0.2731	$K_1$ 0.153	$K_H$ 0.477	$K_{HC}$ 0.127	$K_G = \frac{k_0}{C_0 a_0}$ = 0.220	$n = 0.584$ $K_{kp} = 0.328$	$K_F$ 0.388 $K_R$ 0.223	$F_b = 0.384$ $k_e = 3.10$ $k_b = 0.101$ $t_{max} = 0.350$

As expected, Zero-order kinetics did not fit the obtained data ( $R^2 \sim 0.2$ ) as the release from aeropectin exhibit a strong initial burst followed by variable theophylline release rates over time. Indeed, a zero-order kinetics system releases the drug at a (nearly) constant release

rate over time independently on the remaining drug concentration. This kind of kinetics reflects the ideal case of controlled release and did not fit release from aeropectins matrix.

Intermediate correlation ( $0.8 < R^2 < 0.9$ ) was found for Higuchi model, which is applied to describe drug release based on Fickian diffusion of both solvent and the drug throughout the pores of the matrix. The Higuchi model assumes that dissolution and swelling of the matrix are negligible, maintaining drug diffusivity constant. Our results suggest that the release is due to non-Fickian transport, meaning that other mass transports than diffusion is involved. Indeed, aeropectin are soluble matrices and pectin chain relaxation and matrix swelling and erosion are expected to impact the drug release.

Good model fitting ( $0.95 > R^2 > 0.99$ ) were found for Hopfenberg model, Hixson-Crowell models and first order kinetics. Both Hopfenberg and Hixson-Crowell models are applicable when drug release is controlled only by the dissolution rate of the core material (matrix erosion). Thus, in these models only matrix erosion and time are limiting factors, excluding any diffusive phenomena. However, we assume that diffusion has to be taken in account, as it can occur through the pores and channels of the hydrated network.

First order equation describes dissolution of drug particles which are not efficiently entrapped in polymeric matrix and are ready to be dissolved. A quite good correlation with first order kinetics ( $R^2 \sim 0.97$ ) is due to the burst phase obtained just after immersing the aeropectin in bulk media. As explained previously, the strong initial burst stage is explained by the presence of theophylline particles covering the external surface of the aeropectin. However, the model does not perfectly determine all release processes over time.

Finally, the highest correlations ( $R^2 > 0.99$ ) were found for Korsmeyer-Peppas plot, Peppas-Sahlin model and Gallagher-Corrigan models, which have in common the consideration of several potential physical mechanisms involved in the drug release.

Korsmeyer-Peppas plot shows the highest correlation with the experimental data ( $R^2 \sim 0.993$ ), and allows finding out the mass transport mechanisms governing the drug release using the  $n$  exponent value (based on the first 60% drug release data). We obtained  $n$  value around 0.60 which is characteristic to an anomalous transport (non-Fickian diffusion) for cylindrical shaped matrices. This indicates that solvent diffusion and polymer relaxation have similar time rates. Thus, as the solvent diffuses through the matrix, polymer relaxation does not occur immediately which significantly influences the diffusive transport of the drug out of the matrix. Thereby, drug release is governed by coupling the diffusion and polymer relaxation (matrix swelling or erosion). To find the contribution of each of mechanisms involved in the anomalous

transport we used Peppas-Sahlin model to estimate the Fickian release contribution over time (Peppas & Sahlin, 1989).

In this work, aerogels with aspect ratio (diameter to thickness ratio) from 2.3 to 2.5 were made, corresponding to a Fickian diffusional exponent  $m$  around 0.430, as referred in the work of Peppas and Sahlin (Peppas & Sahlin, 1989).

The results are presented in Figure 153 using a Fickian diffusional exponent  $m$  of 0.430 which corresponds to cylindrical matrix with aspect ratio around 2.5. We obtained diffusional and relaxational constants  $K_F \sim 0.388 \text{ min}^{-0.43}$  and  $K_R \sim 0.223 \text{ min}^{-0.86}$  respectively. As it can be seen, at the beginning of drug release, the diffusional mechanism predominates until  $t \sim 2.0 \text{ h}$ , with drug release being mostly due to Fickian diffusion. Then, it can be seen that relaxational and diffusional mechanisms have similar contributions to drug release changing the drug diffusion to non-Fickian transport.

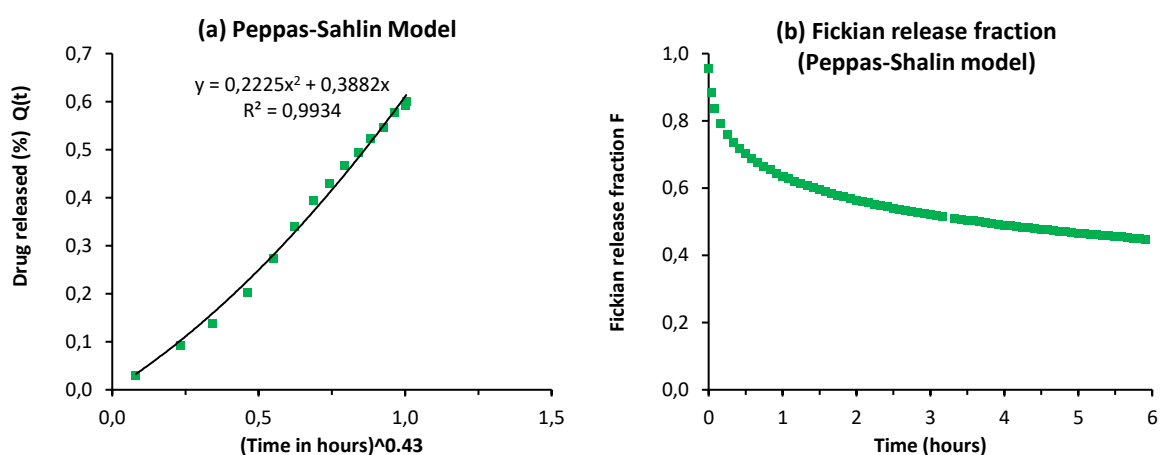


Figure 153. (a) Peppas-Sahlin model of the first 60% release data using Fickian diffusional exponent  $m$  of 0.430. Solid line is the model plot.

(b) Fickian release fraction ( $F$ ) as a function of release time, from a flat cylinder with  $m$  value of 0.43, when  $K_F$  (diffusional) =  $0.388 \text{ min}^{-0.43}$ , and  $K_R$  (relaxational) =  $0.223 \text{ min}^{-0.86}$

These findings coincide with the high correlation obtained using the Gallagher-Corrigan model ( $R^2 > 0.99$ ) as presented in Figure 154. The Gallagher-Corrigan model described a two-phase drug release profile (anomalous transport), starting with an initial burst phase and followed by a slower matrix erosion-controlled release phase (Gallagher & Corrigan, 2000). The release is highly dependent on matrix erosion as revealed by the higher value of erosion kinetics constant ( $k_e \sim 3.10 \text{ h}^{-1}$ ) as compared with the burst constant ( $k_b \sim 0.101 \text{ h}^{-1}$ ) of Gallagher-Corrigan model. The high value of the erosion kinetics constant can be explained by the high hydrophilicity of pectin and the rapid matrix degradation in releasing media with  $\text{pH} > \text{pK}_a$ . These assumptions were confirmed experimentally, with significant matrix erosion observed especially in SIF media ( $\text{pH} 6.8$ ), as previously shown in Figure 148.

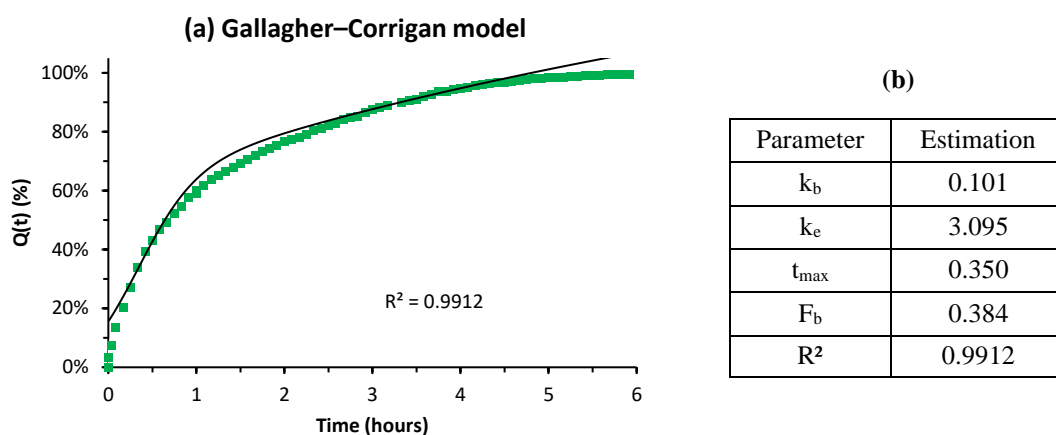


Figure 154. (a) Plot of the Gallagher–Corrigan model for the percentage of cumulative drug released (%) in time  $t$  and (b) the parameters of the model with  $F_b$  being the fraction of drug released during the initial burst phase,  $t_{max}$  the time to the maximum drug release rate, and  $k_b$  and  $k_e$  the burst and erosion constants in  $h^{-1}$ , respectively. Solid line is the model plot and points are experimental values.

### 3.2.2. Overview of drug release from aeropectins

Based on mathematical analysis and taking into account the correlations with experimental data found above, it is possible to precisely explain different steps in the release of theophylline from an aeropectin, characterized by variable drug release rates over time, as schematized in Figure 155. To illustrate the kinetics phases, release rates are given in Figure 157 by extracting slope values from the curve plotted in Figure 151(a). In this example, 14.2 mg of theophylline was embedded into 360 mg of aeropectin matrix.

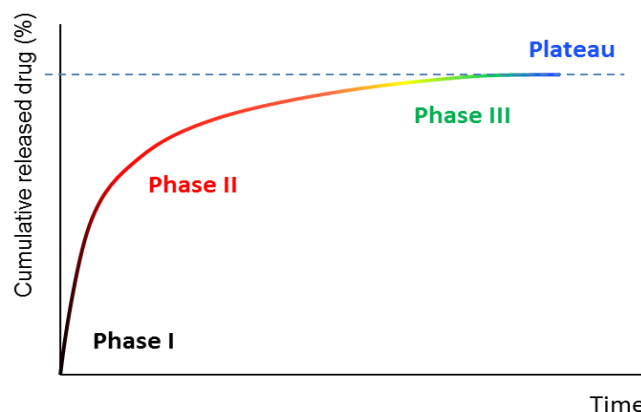


Figure 155. Schematic representation of the different phases of the release from aeropectin matrix over time.

The kinetics of theophylline release from aeropectins can be explained as follows:

**Phase I:** Once the aeropectin matrix is put into contact with the liquid media, the drug particles that are covering the surface of aeropectin (as shown in Figure 133) are immediately dissolved due to theophylline high solubility. This initial burst phase is also fed by rapid release of the drug located close to the surface. It leads to a typical initial burst of release during which a high quantity of the drug is released in a short period of time. It is logically characterized by the highest theophylline release rate around 0.15 to 0.40 mg theophylline.min<sup>-1</sup> (~ 1.1 to 2.8 wt%.min<sup>-1</sup> of total theophylline). In this example (in Figure 151), around 20% of the total amount of theophylline was released in the first 10 minutes of the experiment. The release of the accessible fraction of drug close to the surface is governed by Fickian diffusion, as the chemical gradient is the only driving force. Indeed, the drug particles on and close to the surface are freely accessible, and the impact of polymer relaxation is considered to be negligible. Thus, under sink conditions the diffusion/surface burst phase may be described by a first-order process. This burst phase is therapeutically necessary in order to quickly achieve the therapeutic efficiency range (Huang & Brazel, 2001).

**Lag time:** The first step is followed by a lag time before the actual matrix erosion phase starts. Indeed, for drug particles that are located deeper in the matrix, the time of diffusion to get out of the matrix is significantly longer due to the quadratic relation between the distance and time, see equation 5.2. As the diffusion times of both the solvent and theophylline become longer due to longer distances, the release of theophylline over time is slowed down. It is characterized by lower theophylline release rates from 0.06 to 0.11 mg.min<sup>-1</sup> (~ 0.5 to 0.8 wt%.min<sup>-1</sup> of total theophylline), which marks the end of the burst phase.

In parallel, the impact of chain relaxation on diffusion transport becomes significant as the remaining drug is less accessible and requires polymer swelling and dissolution to diffuse out of the matrix. In SGF media, the network is poorly hydrated and slightly dissolved as a resistant acidic pectin gel layer is formed. But after the first hour, the matrix is put in SIF medium which promotes ionization of pectin chain. Pectin aerogel matrix dissolves (erosion) which in turn increases diffusion of liquid and drug, and thus drives the release.

**Phase II:** This second phase concerned around 60 wt% of the total drug that is embedded into pectin matrix and is not freely accessible. During this step, progressive pectin chain relaxation, re-arrangement, swelling and dissolution occur, which may significantly impact the release kinetics. At the interface of the matrix and the liquid a viscous pectin gel layer is formed which acts as a physical “barrier” that limits mass transport of both drug and liquid, as shown in Figure 156. Due to lower diffusion coefficient, the release of theophylline through the viscous hydrated network is slowed down. In parallel, aeropectin matrix is progressively dissolved, starting from erosion front on the outer surface which gradually moves inward, as revealed by the decrease of volume and mass of aeropectins shown in Figure 151 (b) (c).

Usually, the slowest mechanism (*i.e.* diffusion, relaxation, dissolution, and swelling) becomes the determining step that drives the drug release. In the case of aeropectin, this phase is mainly characterized by simultaneous diffusion and matrix swelling followed by erosion (non-Fickian transport) phenomena, as confirmed by  $n$  value ( $0.45 > n > 0.89$ ) used by Korsmeyer-Peppas model

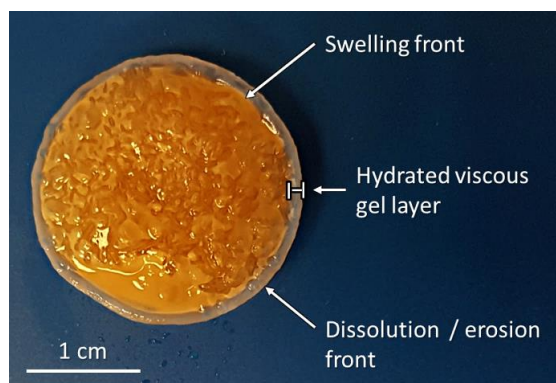


Figure 156. Picture of an aeropectin after being immersing in SGF (37 °C) for 45 min. Aeropectin was prepared from 6 wt% pectin P35 solution dissolved at pH 3.0 without calcium.

After one hour, the aeropectin is transferred from SGF medium (pH 1.0) to SIF medium (pH 6.8). In reaction to medium pH change, liquid penetration into the aeropectin is promoted and the matrix instantly swells (Figure 151) resulting in a “boost” of release rate observed at 60 minutes of experiment (Figure 157). When immersed in SIF (pH 6.8), the release of drug from aeropectin is significantly impacted by matrix erosion as it was observed experimentally (Figure 151) and in adequacy with high value relaxational constant ( $k_R \sim 0.223 \text{ h}^{-0.86}$ ) of Peppas-Sahlin model and high erosion kinetic constants ( $k_e \sim 3.10 \text{ h}^{-1}$ ) of Gallagher-Corrigan model. This can be explained by the high hydrophilicity of pectin and sample “instability” in releasing media with  $\text{pH} > \text{pK}_a$  leading to rapid matrix erosion. This was experimentally confirmed by the strong matrix erosion by dissolution especially observed in SIF (pH 6.8), as previously presented in Figure 147.

After the burst phase and a lag time, all mass transport phenomena reach an “equilibrium” leading to a nearly steady release phase (or controlled release phase) that lasts the major part of the release. Theophylline is then released at rates between  $0.02$  to  $0.04 \text{ mg} \cdot \text{min}^{-1}$  ( $\sim 0.11 - 0.25 \text{ wt} \cdot \text{min}^{-1}$  of total theophylline). This quasi controlled-release phase is especially desirable for pharmaceutical industry as it delivers a certain dose maintained over a prolonged period of time.

**Phase III:** Finally, a slowing down of theophylline release rate occurs due to less amount of remaining drug inside the matrix, as revealed by the lowest theophylline release rate  $0.003$ - $0.010 \text{ mg} \cdot \text{min}^{-1}$  ( $\sim 0.02$ -  $0.07 \text{ wt} \cdot \text{min}^{-1}$  of total theophylline). Release then reaches a plateau (**Phase IV**) when no more accessible or free drug is remaining. For aeropectin, full theophylline release occurs just before the end of matrix dissolution, as dissolution and diffusion phenomena

are completed. As it will be shown later, for a non-soluble matrix such as cellulose or certain silica-based aerogels, a mechanical treatment is necessary to destroy the matrix and achieve 100 % theophylline released.

Finally, it is possible to conclude that theophylline release profile from aeropectin matrix is thus governed by coupling burst dissolution/diffusion and erosion mechanisms, and corresponds to a complex anomalous transport (non-Fickian). Similar trends and experimental observations on pectin aerogels crosslinked with calcium were reported in (García-González et al., 2015; Tkalec et al., 2015) and correlate with our results and analysis.

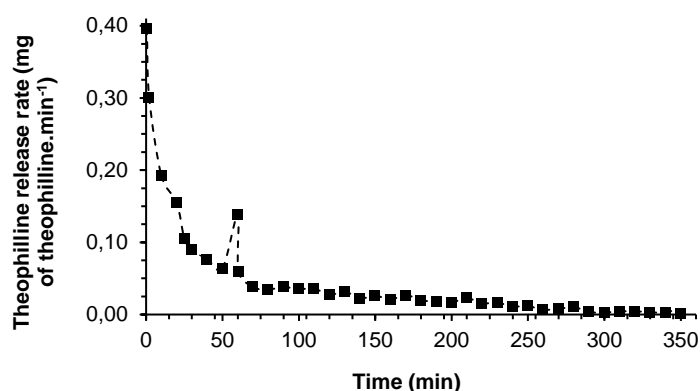


Figure 157. Theophylline release rate (mg of theophylline released.min<sup>-1</sup>) over time from aeropectin made from 6 wt% pectin P35 solution dissolved at pH 3.0 without calcium. Release rates were estimated by calculation of the slopes from theophylline release curve (Figure 151) considering a linear function between two points separated by 5 or 10 minutes. Dashed line is given to guide the eye.

## 4. Case studies: influence of various parameters on the kinetics of theophylline release from pectin aerogels

In the Chapter III, we have shown that we were able to tune aeropectin structure and properties in a large range of network morphologies and structural parameters (density, porosity,  $S_{BET}$ ...). Below we demonstrate and discuss how internal structure and physical properties of aeropectin matrices impact their drug release properties.

### 4.1. Influence of pH of pectin solutions on release kinetics of theophylline from aeropectin

As explained in Chapter III Section 3.2, lowering pH below pH 3.0 (~ pKa value) results in reducing ionization of pectin Gal.A which reduces coulombic repulsions and promotes chains

interactions (hydrogen and hydrophobic interactions). By lowering pH, weak pectin gels were obtained at pH 3.0 and stronger acidic gel were obtained at pH lower than pH 2.0 as Gal.A dissociation is low. The lower the pH, the stronger the pectin network (up to certain pH when pectin degradation occurs), and the more resistant it is to volume shrinkage during the process route. Thus, strong gelation led to a lower density and more porous aeropectin after sc-drying, but with lower  $S_{BET}$ .

Here, we have compared 3 aerogels obtained by dissolution of 6 wt% pectin P35 at different pH. Weak gels were obtained at pH 3.0 and led to denser materials ( $\rho \sim 0.18 - 0.19 \text{ g/cm}^3$ ) with small pores ( $< 50 \text{ nm}$  as deduced from SEM images, Figure 158), whereas stronger gels at pH 2.0 and even stronger at pH 1.2 led to less dense materials ( $\rho \sim 0.13 - 0.10 \text{ g/cm}^3$ ) with higher porosity and larger pores (50 to 150 nm). Network morphologies of aeropectins are shown in Figure 158 and their structural characteristics are reported in Table 11. Aeropectins were loaded with 2.5 g/L theophylline.

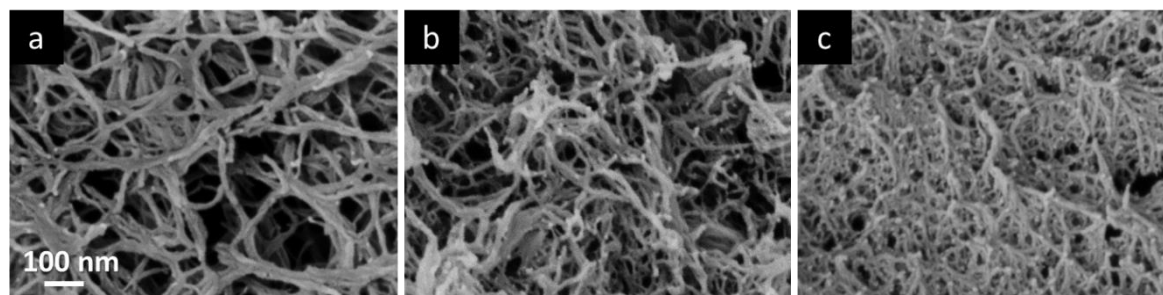


Figure 158. Network morphologies observed by SEM of theophylline-loaded aeropectins made from 6 wt% of pectin P35 dissolved without calcium at (a) pH 1.2, (b) pH 2.0 and (c) pH 3.0

Table 11. Characteristics of aeropectins made from 6 wt% of pectin P35 dissolved without calcium at pH 3.0, pH 2.0 and pH 1.2. Aeropectins were loaded by diffusion of theophylline dissolved in ethanol at 2.5 g/L.

pH of pectin solution:	pH 1.2	pH 2.0	pH 3.0
Aerogel-precursor volume during theophylline impregnation ( $\text{cm}^3$ )	$5561 \pm 62$	$5307 \pm 69$	$5129 \pm 75$
Aerogel volume after sc-drying ( $\text{cm}^3$ )	$3487 \pm 71$	$2660 \pm 48$	$2052 \pm 44$
Aerogel density ( $\text{g/cm}^3$ )	$0.105 \pm 0.03$	$0.136 \pm 0.03$	$0.181 \pm 0.05$
Porosity (%)	$93.0 \pm 0.2$	$90.9 \pm 0.2$	$87.9 \pm 0.3$

<b>Aerogel <math>S_{BET}</math> (<math>m^2/g</math>)</b>	$323 \pm 17$	$421 \pm 16$	$544 \pm 19$
<b>Drug loading efficiency (%)</b>	56.1	59.6	71.9
<b>Drug loading capacity (wt%)</b>	2.14	2.20	2.51
<b>Specific drug loading (<math>\times 10^{-5} g/m^2</math>)</b>	6.63	5.21	4.59

As it can be seen from Table 11, the drug loading capacity (wt%) and drug loading efficiency (%) were higher for the matrix with higher density, which is the consequence of higher initial solution pH. In the Section 1 of this Chapter, we showed a high positive correlation between  $S_{BET}$  area and the loading capacity. The loading efficiency was found to be correlated with density but not with  $S_{BET}$ . Thus, specific surface area determines the maximum amount of drug that can cover pore walls and thus drug loading, while the efficiency of impregnation is governed by matrix density as denser network may prevent from the drug wash out during secondary drying. The large difference of  $S_{BET}$  depending on pH value explains the decrease of specific drug loading with pH increase.

Figure 159 shows how pH of pectin solutions, and as a consequence, the differences in aeropectin structural properties, impact their drug release properties. Lower density aerogels are significantly faster drug delivery systems, with a complete theophylline release in 250 min for pH 1.2 matrix, 290 min for pH 2.0 matrix, and 350 min for pH 3.0 matrix (Figure 159 (a)). These results are correlated with faster and easier matrix erosion (dissolution) over time presented in Figure 159 (b) and (c). We assume that denser network with smaller pores network slowed down the diffusion of liquid into aeropectin, which in turn slowed down matrix dissolution and thus the release of theophylline. On the contrary, lower density matrices were more “permeable” to mass transport phenomena; their large pores provided lower “resistance” to water penetration through the system and larger free volume increased solvent and drug diffusivity and promoted matrix dissolution. As an illustration, aeropectin matrices produced at pH 1.2 were completely dissolved in ~ 280 min compared to ~ 400 minutes when pH was 3.0. Pictures of pH 1.2, pH 2.0 and pH 3.0 aeropectins after 180 minutes of dissolution experiment are presented in Figure 160 for comparison of matrix dissolution.

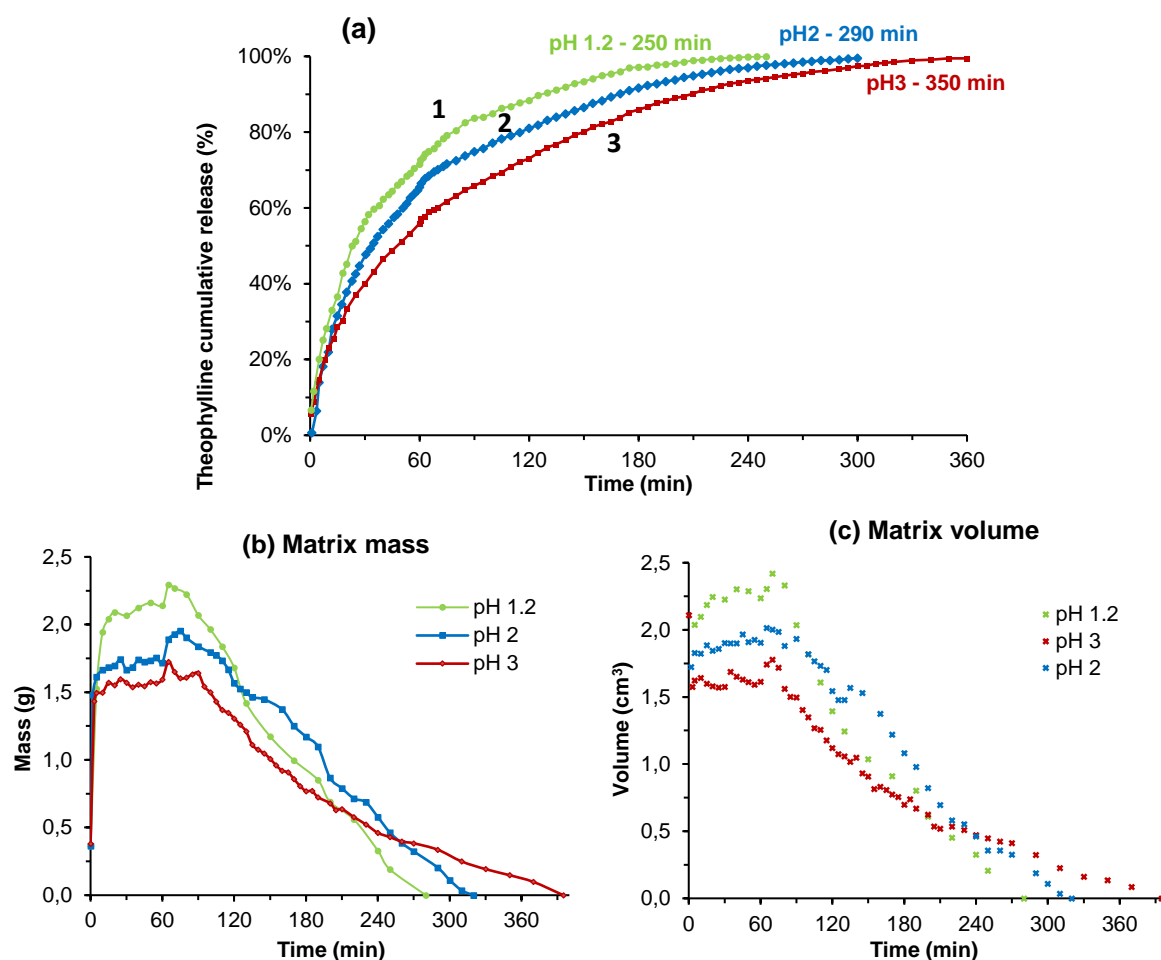


Figure 159 (a) Theophylline cumulative release over time (%) and (b) matrix mass (g) and (c) volume (cm<sup>3</sup>) evolution in time for aerogels made from 6 wt% of pectin P35 dissolved without calcium at pH 1.2 (1), pH 2.0 (2) and pH 3.0 (3). Aerogels were all loaded with theophylline at 2.5 g/L.



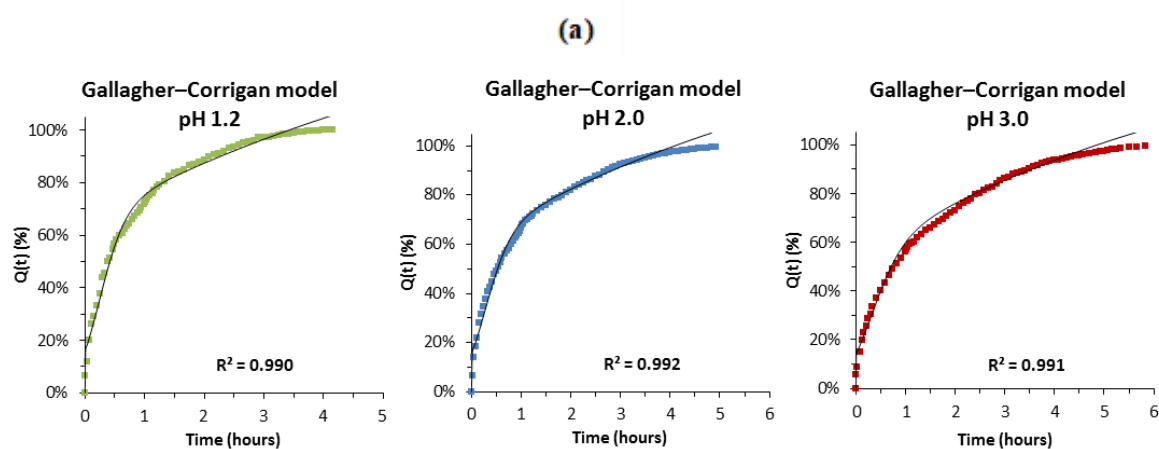
Figure 160. Pictures of theophylline loaded aerogels during dissolution testing experiment at time  $t = 180$  minutes. Aerogels were made from 6 wt% pectin P35 dissolved without calcium at pH 1.2, pH 2.0 and pH 3.0. The scale is the same for all the pictures.

Lower density aerogels present a higher sample volume than higher density ones, around 3600 cm<sup>3</sup> for pH 1.2 matrix vs around 2100 cm<sup>3</sup> at pH 3.0. This resulted in a higher liquid intake at lower density, for instance + 500% for pH 1.2 aerogel and + 350% for pH 3.0 aerogel. We assume that higher volume and mass liquid intake even more promoted solvent penetration, drug diffusion and pectin dissolution, and resulted in a faster drug release.

To conclude, by adjusting aeropectin densities by varying pH conditions of pectin solutions, we were able to modify the kinetics of drug release. We assume that higher density has a retarding effect on drug delivery kinetics, as it may prevent matrix dissolution and solvent and drug diffusion through the system.

Our observations stated above were analyzed by mathematical models. As expected, release from the three matrices are due to anomalous transport, as revealed by  $n$  exponents values higher than 0.45 using Korsmeyer-Peppas model, with high correlation to the data ( $R^2 > 0.995$ ). Thus, Gallagher-Corrigan models and Peppas-Sahlin models were chosen to investigate the differences in the coupling of diffusion and matrix erosion/swelling between matrices.

Figure 161 shows the experimental data and the corresponding plots of Gallagher-Corrigan model together with fitting parameters, with high correlation  $R^2 > 0.99$ . As it can be seen, the first order constants  $k_b$  slightly increased from  $0.10 \text{ h}^{-1}$  to  $0.13 \text{ h}^{-1}$ , while the erosion constant  $k_e$  clearly increases from around  $3.01 \text{ h}^{-1}$  to  $4.61 \text{ h}^{-1}$  when pectin solution pH decreased from 3.0 to 1.2. This confirms that diffusion rate at the beginning and matrix erosion rate are higher due to lower density obtained at low pH. In addition, the plot of the Fickian release contribution of Peppas-Sahlin model in Figure 162 illustrates the decreasing contribution of Fickian mechanisms to the release depending on pH.



Parameter	Estimation		
	pH 1.2	pH 2.0	pH 3.0
$k_b$	0.129	0.121	0.104
$k_e$	4.612	3.907	3.005
$F_b$	0.324	0.390	0.414
$t_{\max}$	0.242	0.2823	0.340
$R^2$	0.990	0.992	0.991

Figure 161. (a) Experimental release data and Gallagher-Corrigan model plot and (b) estimation of the corresponding Gallagher-Corrigan parameters of theophylline release experiments from aeropectins made from 6 wt% of pectin P35 dissolved without calcium at pH 1.2 (green), pH 2.0 (blue) or pH 3.0 (red). Solids lines are the model plots.

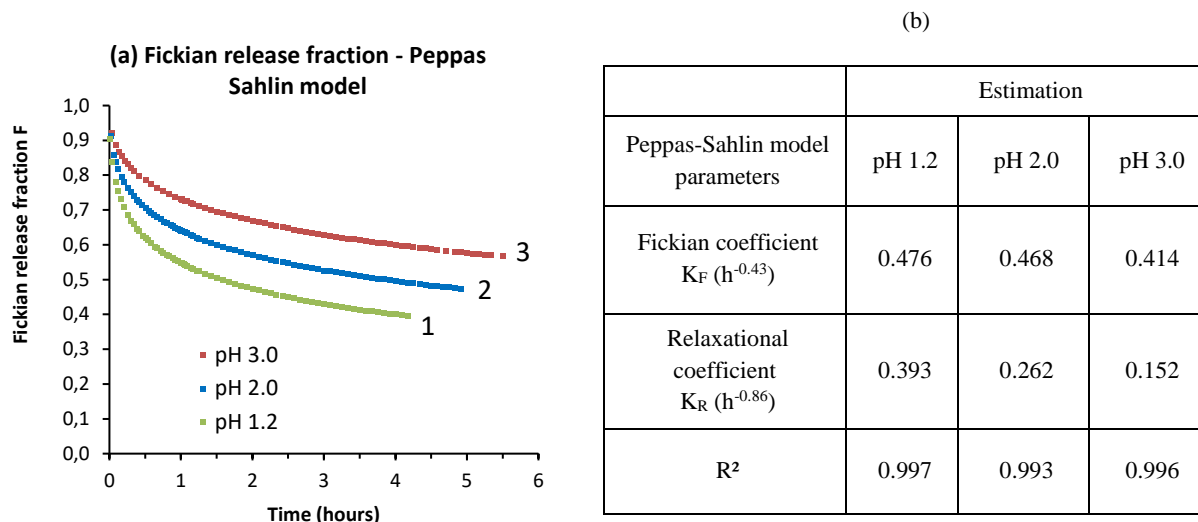


Figure 162. (a) Fickian release fraction according to Peppas-Sahlin model for the first 60% of released drug from aeropectins based of 6 wt% of pectin P35 dissolved without calcium at pH 1.2 (1), pH 2.0 (2) or pH 3.0 (3) and (b) Estimation of the corresponding Peppas-Sahlin parameters performed using Fickian diffusional exponent  $m$  of 0.43.

It has to be noticed that the three mathematical models used (Korsmeyer-Peppas, Peppas-Sahlin and Gallagher-Corrigan models) led to similar and consistent conclusions on aeropectins' drug release behaviour. We found out that the release was governed by the coupling of diffusional and relaxational phenomena whose relative contributions to the release could be tuned by changing the density of the matrix.

Besides, the mathematical models allowed the quantification of release kinetics parameters which can be used for the comparison with other systems. In comparison with literature, we obtained exponent  $n$  values in the same range of values ( $0.45 < n < 0.89$ ) (Anomalous transport case) using Korsmeyer-Peppas model, and similar values of erosion kinetics constants  $k_e$  ( $\sim 3 - 4.5 \text{ h}^{-1}$ ) using Gallagher-Corrigan model as in other works on aerogels based on pectin or based on alginate both crosslinked with calcium (De Cicco et al., 2016; Veronovski, Knez, & Novak, 2013a, 2013b).

## 4.2. Impact of calcium concentration on release kinetics of theophylline from aeropectin

The goal of this section is to demonstrate the impact of calcium concentration on aeropectin drug release behaviour. As already explained in Chapter III, the addition of calcium into pectin solution led to the formation of strong ionic bonds resulted in ionic gelation following the egg-box model (Grant, Morris, Rees, Smith, & Thom, 1973). The resulting aeropectins have lower density and a high proportion of large macropores as they underwent lower volume shrinkage (~ 40 vol% to 50 vol%) compared to aeropectin obtained from a weak gel or un-gelled solutions (~ 60 vol% to 80 vol%).

Increasing calcium concentration in 3 wt% pectin solutions at pH 3.0 from  $R(\text{Ca}) = 0$  to  $R(\text{Ca}) = 0.6$  promoted the formation of ionic bridges between pectin chains, leading to aeropectins with decreasing densities with more macroporous network morphology, as presented in Table 12 and Figure 163. Aeropectins were loaded with 3.4 g/L theophylline.

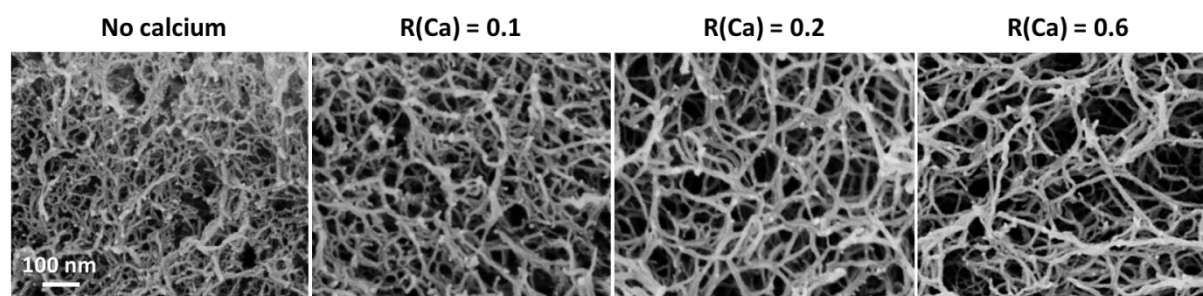


Figure 163. Network morphologies of theophylline-loaded aeropectins made from 3 wt% of pectin P35 dissolved at pH 3.0 with increasing calcium R ratio  $R(\text{Ca})$  from 0 to 0.6. Aeropectins were loaded with 3.4 g/L theophylline. The scale is the same on all images.

Table 12. Characteristics of aeropectins loaded with theophylline made from 3 wt% of pectin P35 dissolved at pH 3.0 with increasing calcium R ratio  $R(\text{Ca})$  from 0 to 0.6.

<b>R(Ca) value:</b>	<b>R(Ca) = 0 (no calcium)</b>	<b>R(Ca) = 0.1</b>	<b>R(Ca) = 0.2</b>	<b>R(Ca) = 0.6</b>
<b>Aerogel volume during theophylline impregnation (cm<sup>3</sup>)</b>	4450	5010	5540	6100
<b>Aerogel density (g/cm<sup>3</sup>)</b>	0.118	0.085	0.056	0.044
<b>Aerogel <math>S_{\text{BET}}</math> (m<sup>2</sup>/g)</b>	574	502	472	437
<b>Drug loading efficiency (%)</b>	48.8	47.1	45.6	39.7

<b>Drug loading capacity (wt%)</b>	4.29	4.10	3.98	3.74
<b>Specific drug loading (<math>\times 10^{-5}</math> g/m<sup>2</sup>)</b>	7.48	8.17	8.44	8.56

As shown previously, release from aeropectin is governed by diffusion and polymer relaxation (swelling / erosion) mechanisms. Despite of lower density and much larger pores which enable quicker diffusion of both water inside and drug outside the matrix, the presence of calcium slows down theophylline release over time (Figure 164). We observed that the higher calcium concentration in the matrix, the slower the drug release. As an example, total theophylline release occurred in about 190 min without calcium and in about 440 min for R(Ca) = 0.6.

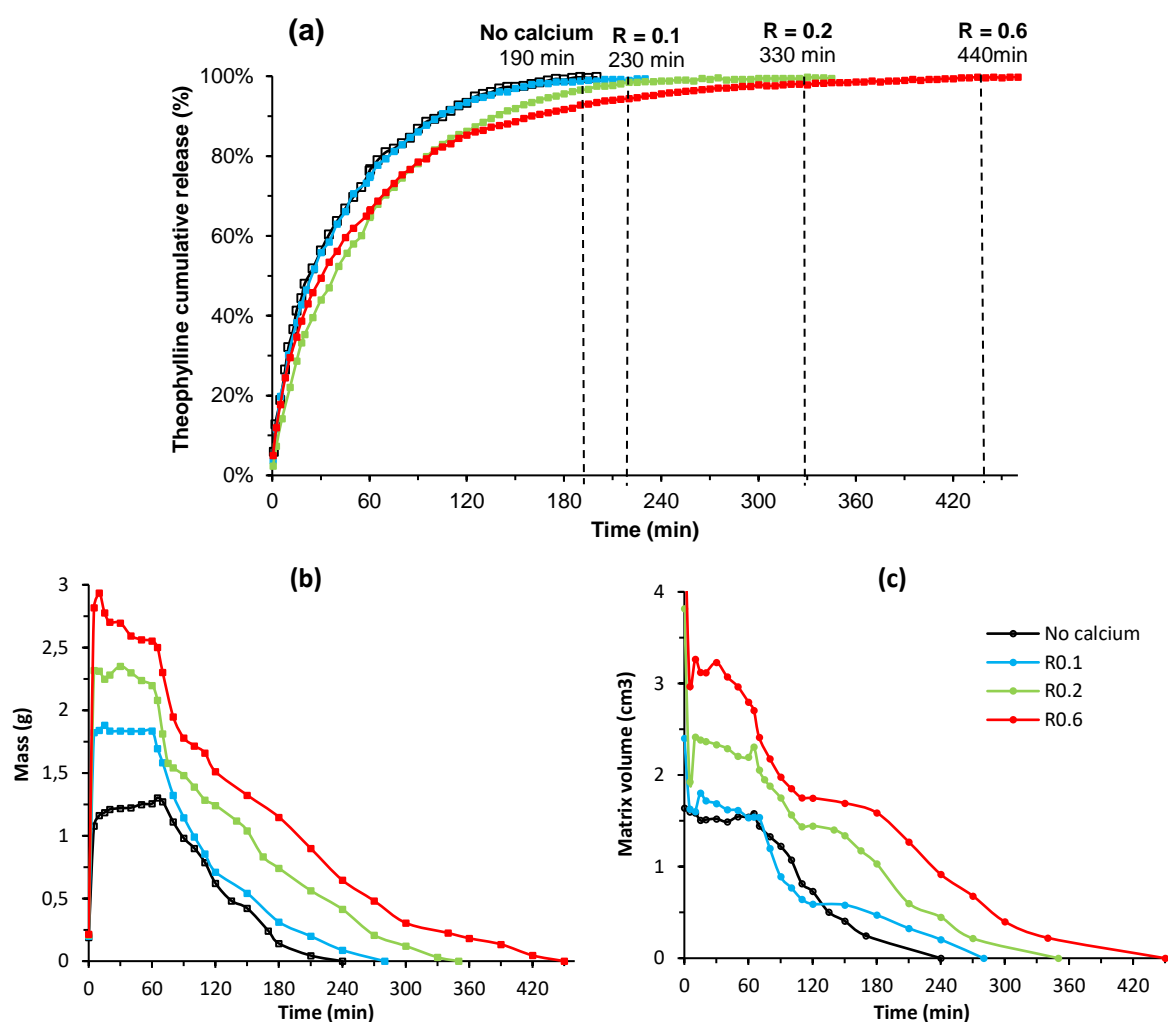


Figure 164. (a) Theophylline cumulative release (%), (b) matrix mass (g) and (c) matrix volume (cm<sup>3</sup>) evolution in time for aeropectins made from 3 wt% pectin P35 dissolved at pH 3.0 and R(Ca) = 0, 0.1, 0.2 and 0.6.

The formation of ionic junctions is promoted by increasing calcium concentration as explained in Chapter III. As a result, pectin network is reinforced by the presence of intermolecular bridges between chains, making them more resistant to polymer dissolution and inhibiting matrix erosion as it can be seen in Figure 165.

On the opposite, without calcium or at low R(Ca) matrix erosion occurred easier and faster, facilitating water penetration and drug diffusivity, and promoting drug release. Similar trends were found by studying the influence of calcium crosslinking on the drug release properties of pectin hydrogels (Dupuis, Chambin, G nelot, Champion, & Pourcelot, 2006; Liu et al., 2003; Rubinstein, Radai, Ezra, Pathak, & Rokem, 1993). As in the case of the influence of solution pH, we assume that lower matrix erosion rates inhibited solvent and drug diffusion through the network which led to slower drug release, as it can be seen in Figure 164 (a).

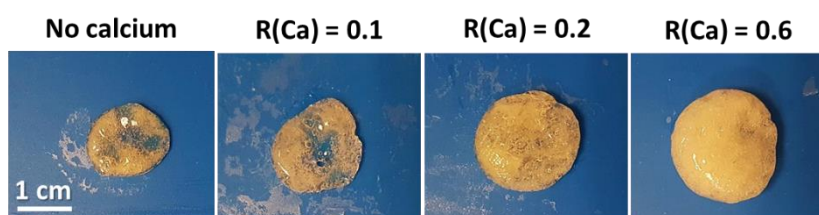


Figure 165. Pictures of theophylline loaded pectin aerogel during dissolution testing experiment at time  $t = 180$  minutes. Pectin aerogel was made from 3 wt% pectin P35 dissolved at pH 3.0 with increasing calcium R ratio from  $R(\text{Ca}) = 0$  to  $R(\text{Ca}) = 0.6$ . The scale is the same for all the pictures.

Peppas-Sahlin model showed high correlation ( $R^2 > 0.99$ ) to the data (Figure 166) allowing the estimation of diffusional and relaxational coefficients  $K_F$  and  $K_R$  presented in Figure 167.

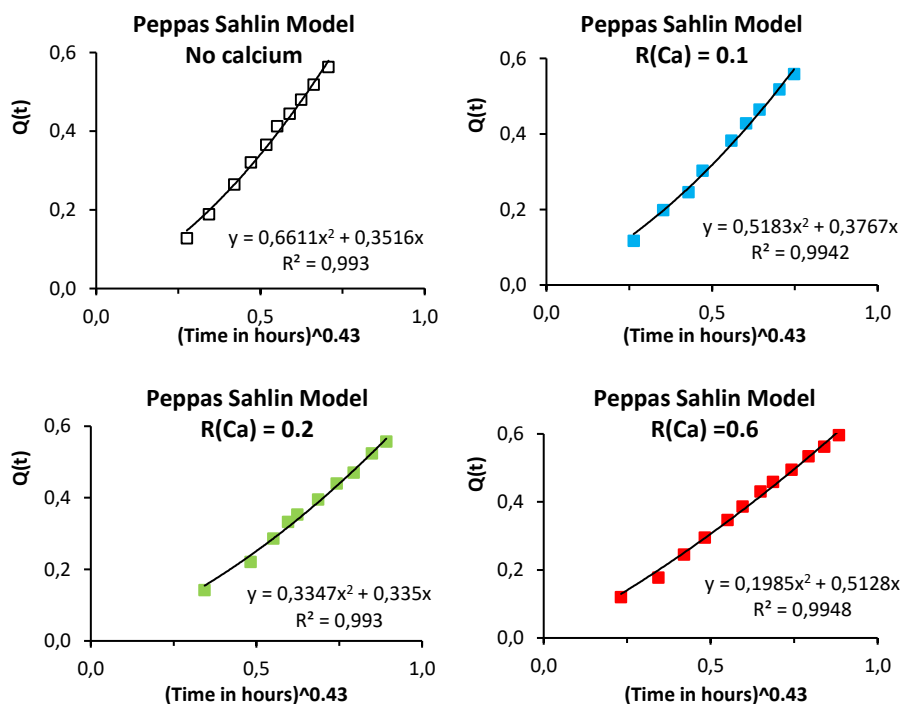


Figure 166. Peppas-Sahlin model of the first 60% release data from aerogel pectins made from 3 wt% of pectin dissolved at pH 3.0 without calcium and with R(Ca) ratio from 0.1 to 0.6, using Fickian diffusional exponent  $m$  of 0.430. Solid lines are the model plots.

As it can be seen, the value of the relaxational coefficient  $K_R$  decreases with the increase of calcium concentration (Figure 167). The plot of the Fickian fraction over time in Figure 167 illustrates the increasing contribution of diffusion to the release and decreasing erosion contribution as R(Ca) increases.

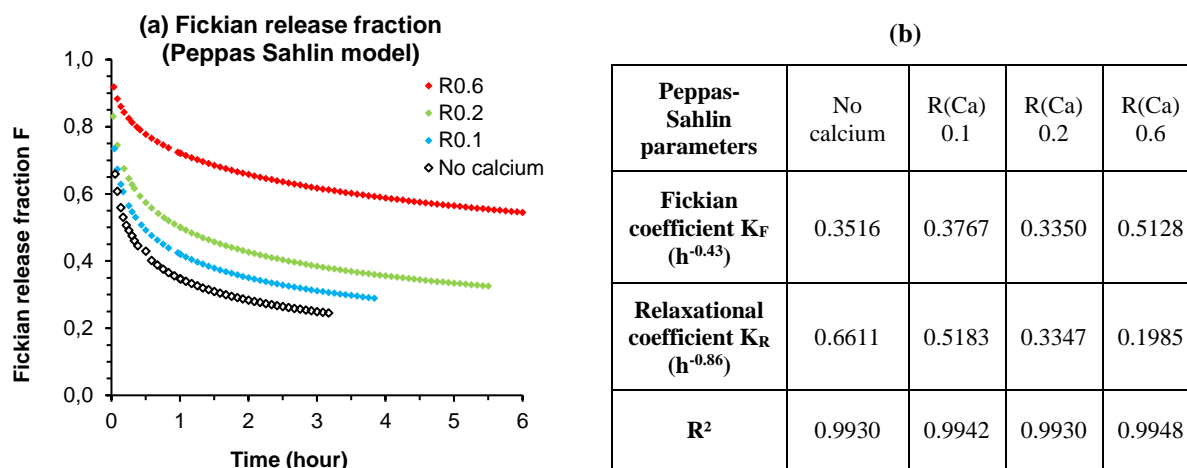


Figure 167. (a) Fickian release fraction (F) from theophylline release data of aerogel pectins made from 3 wt% of pectin dissolved at pH 3.0 without calcium and with R(Ca) ratio from 0.1 to 0.6. (b) Estimation of the corresponding Peppas-Sahlin parameters, using Fickian diffusional exponent  $m$  of 0.43.

As calcium concentration increases, matrix dissolution rate is reduced and diffusion mechanism predominates in the coupling diffusion-erosion release. As matrix erosion is very slow, liquid and drug slowly diffuse into the hydrated network which reduces drug release rate and prolongs release time.

This is in correlation with data fitting with Gallagher-Corrigan model with high correlation ( $R^2 > 0.99$ ) as shown in Figure 168. The estimation of parameters presented in Table 13 clearly shows a decrease of the erosion constant value  $k_e$  with the increase of calcium concentration. It can be noted that the burst constant  $k_b$  is also reduced with calcium concentration, as the drug release is slowed down.

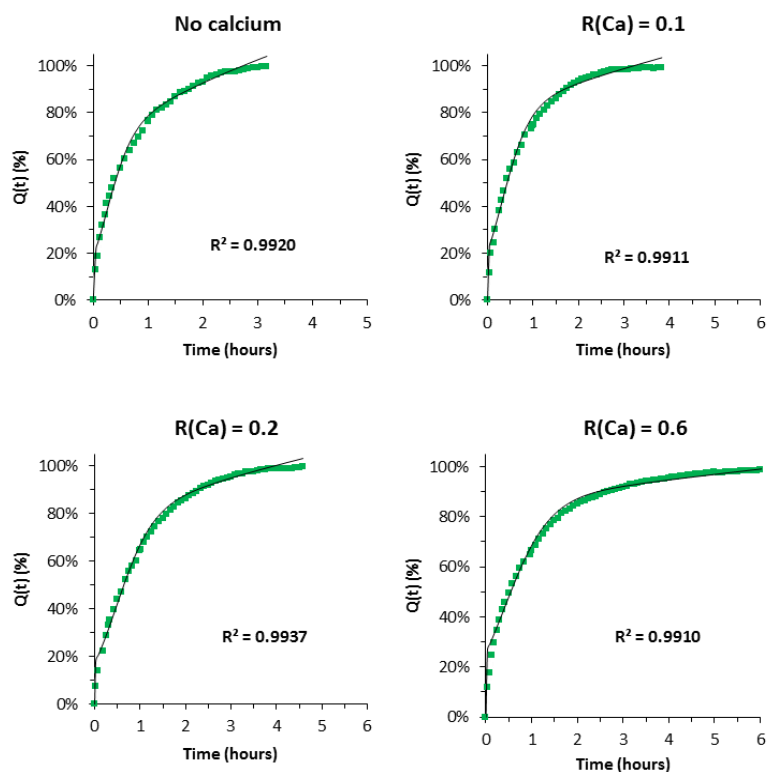


Figure 168. Gallagher-Corrigan model plot for theophylline release from aerogel systems made from 3 wt% of pectin dissolved at pH 3.0 without calcium or with calcium with R(Ca) ratio from 0.1 to 0.6. Solid lines are the model plots.

Table 13. Parameters from Gallagher-Corrigan model for theophylline release data for aerogel systems made from 3 wt% of pectin dissolved at pH 3.0 without calcium or with calcium with R(Ca) ratio from 0.1 to 0.6.

Parameter	Estimation			
	No calcium	R(Ca) = 0.1	R(Ca) = 0.2	R(Ca) = 0.6
$k_b$	0.1402	0.0718	0.0651	0.0241
$k_e$	4.1889	3.3080	2.5492	2.0625
$F_b$	0.3164	0.2049	0.2286	0.1444
$t_{max}$	0.2413	0.3169	0.4905	0.4076
$R^2$	0.9920	0.9911	0.9935	0.9910

Once again, good data fitting with different mathematical models based on diffusion-erosion controlled release shows that matrix erosion and drug release over time could be slowed down by adjusting calcium concentration in pectin solutions. In addition to matrix density governed by pH of pectin solution, ionic crosslinking driven by calcium concentration of pectin solution was found to significantly impact the release properties of aerogel systems.

The impact of crosslinking on release properties of aerogels was also studied for chitosan aerogels crosslinked with salbutamol at various concentrations (Obaidat, Tashtoush, Bayan, T. Al Bustami, & Alnaief, 2015) or using different crosslinkers (Chang, Chen, & Jiao, 2008) to change matrix erosion properties.

In the same way, drug-loaded alginate and pectin aerogels were prepared by crosslinking with different divalent cations ( $\text{Ca}^{2+}$ ,  $\text{Sr}^{2+}$ ,  $\text{Zn}^{2+}$ ) to tune matrix structure and stability which eventually impacted drug release profile (Tkalec et al., 2016). It was shown that once immersed in the simulating intestinal medium (pH 6.8) both alginate and pectin aerogels cross-linked with calcium underwent a quick bulk erosion by dissolution, leading to the fastest drug release. Oppositely, slower matrix degradation was observed for zinc cross-linked aerogels as a result of more extensive ionic bridges with  $\text{Zn}^{2+}$  ions, which led to more stable matrices and retarded the drug release from the carriers.

## Conclusions

In this chapter, a detailed and systematic study was performed to evaluate the potential of pectin aerogels to be used as oral drug delivery system using theophylline as drug model. Theophylline was successfully incorporated before drying by diffusion into aerogel precursors via ethanol. Drug loading efficiency and loading capacity were shown to depend on aeropectin matrix structure (specific surface area and density). When immersed into simulated physiological media, aeropectin matrix showed a prolonged drug release behavior, with matrix resistance in gastric media followed by dissolution into intestinal media.

Drug release was found to be governed by diffusive mass transports through the system coupled with relaxational phenomena induced by matrix swelling and erosion, in correlation with the polyelectrolyte and hydrosoluble characteristics of pectin. Sustained drug release from pectin aerogel fitted well Korsmeyer-Peppas, Peppas-Sahlin and Gallagher-Corrigan ( $R^2 > 0.99$ ) models, showing different contributions of erosion and diffusion mechanisms depending on matrix internal structure. By finely tuning the structural parameters of the aeropectins (specific surface, density and ionic crosslinking), adjusting sample formulation and drying method, we were able to determine their impacts on the drug loading and release kinetics.

Overall, our results point out the possibility to tailor aeropectin drug release properties by adjusting the process route to target the therapeutic indications. Aeropectins show high potential for drug release applications as biodegradable, biocompatible and bio-based carriers.

Depending on their chemical structure, bio-polymers and silica aerogels display different properties such as hydrophilicity, solubility, mechanical properties in a given release media, which in turn are known to impact their release properties. In contrast to hydrophilic silica aerogels, whose brittle matrix instantly disintegrates upon contact with the liquid due to capillary forces leading to immediate drug release (in several minutes) (Caputo, Scognamiglio, & De Marco, 2012; Mehling et al., 2009; I. Smirnova et al., 2004), aeropectins present higher matrix integrity, allowing release of the drug for a prolonged period of time (in several hours). Aeropectins were found to have similar extended drug release behaviour (diffusion-erosion controlled) to aerogels made from other polyelectrolyte polysaccharides such as alginate (De Cicco et al., 2016; García-González et al., 2015; Gonçalves et al., 2016; Mehling et al., 2009; Veronovski et al., 2013b) and  $\kappa$ -carrageenans (Gonçalves et al., 2016)

As they are all highly hydrosoluble and pH-sensitive polysaccharides, strong matrix erosion occurred by dissolution in phosphate buffer simulating intestinal fluid (pH 6.5 to pH 7.2) accelerating the release. Due to their “rigid” aerogel structure, higher stability in releasing media and stronger resistance against hydration, starch aerogels (García-González et al., 2015;

Garcia-Gonzalez & Smirnova, 2013) or chitosan aerogels (Mehling et al., 2009; Obaidat et al., 2015) appeared to be more stable aerogels matrix in releasing media. In those cases, extended drug release profile was achieved (in several hours, depending on the matrix size and the type of drug), governed by diffusion and assisted by a slow erosion process. On the opposite, bio-aerogels made from water non-soluble polymer such as bacterial cellulose (Haimer et al., 2010) or silk fibroin (Mallepally et al., 2015; Marin et al., 2014) release drug by pure Fickian diffusion as these aerogels were not subjected to matrix erosion in aqueous releasing media.

As it will be shown in the following chapter, the release kinetics of pectin aerogels can be additionally modified by making interpenetrating networks with cellulose and silica.

## References

- Alnaief, M., & Smirnova, I. (2010). Effect of surface functionalization of silica aerogel on their adsorptive and release properties. *Journal of Non-Crystalline Solids*, 356(33), 1644-1649. <https://doi.org/10.1016/j.jnoncrysol.2010.06.027>
- Caputo, G., Scognamiglio, M., & De Marco, I. (2012). Nimesulide adsorbed on silica aerogel using supercritical carbon dioxide. *Chemical Engineering Research and Design*, 90(8), 1082-1089. <https://doi.org/10.1016/j.cherd.2011.11.011>
- Chang, X., Chen, D., & Jiao, X. (2008). Chitosan-Based Aerogels with High Adsorption Performance. *The Journal of Physical Chemistry B*, 112(26), 7721-7725. <https://doi.org/10.1021/jp8011359>
- ChemAxon. (s. d.). Consulté 26 mars 2019, à l'adresse <https://chemaxon.com/products/marvin>
- De Cicco, F., Russo, P., Reverchon, E., García-González, C. A., Aquino, R. P., & Del Gaudio, P. (2016). Prilling and supercritical drying: A successful duo to produce core-shell polysaccharide aerogel beads for wound healing. *Carbohydrate polymers*, 147, 482–489.
- Dupuis, G., Chamblin, O., Génelot, C., Champion, D., & Pourcelot, Y. (2006). Colonic drug delivery: influence of cross-linking agent on pectin beads properties and role of the shell capsule type. *Drug Development and Industrial Pharmacy*, 32(7), 847-855. <https://doi.org/10.1080/03639040500536718>
- Gallagher, K. M., & Corrigan, O. I. (2000). Mechanistic aspects of the release of levamisole hydrochloride from biodegradable polymers. *Journal of Controlled Release*, 69(2), 261-272. [https://doi.org/10.1016/S0168-3659\(00\)00305-9](https://doi.org/10.1016/S0168-3659(00)00305-9)
- García-González, C. A., Jin, M., Gerth, J., Alvarez-Lorenzo, C., & Smirnova, I. (2015). Polysaccharide-based aerogel microspheres for oral drug delivery. *Carbohydrate Polymers*, 117, 797-806. <https://doi.org/10.1016/j.carbpol.2014.10.045>
- Garcia-Gonzalez, C. A., & Smirnova, I. (2013). Use of supercritical fluid technology for the production of tailor-made aerogel particles for delivery systems. *Journal of Supercritical Fluids*, 79, 152-158. <https://doi.org/10.1016/j.supflu.2013.03.001>
- Gavillon, R., & Budtova, T. (2007). Kinetics of cellulose regeneration from cellulose--NaOH--water gels and comparison with cellulose--N-methylmorpholine-N-oxide--water solutions. *Biomacromolecules*, 8(2), 424-432. <https://doi.org/10.1021/bm060376q>
- Gonçalves, V. S. S., Gurikov, P., Poejo, J., Matias, A. A., Heinrich, S., Duarte, C. M. M., & Smirnova, I. (2016). Alginate-based hybrid aerogel microparticles for mucosal drug delivery. *European Journal of Pharmaceutics and Biopharmaceutics: Official Journal*

- of Arbeitsgemeinschaft Fur Pharmazeutische Verfahrenstechnik e.V.*, 107, 160-170.  
<https://doi.org/10.1016/j.ejpb.2016.07.003>
- Grant, G. T., Morris, E. R., Rees, D. A., Smith, P. J. C., & Thom, D. (1973). Biological interactions between polysaccharides and divalent cations: The egg-box model. *FEBS Letters*, 32(1), 195-198. [https://doi.org/10.1016/0014-5793\(73\)80770-7](https://doi.org/10.1016/0014-5793(73)80770-7)
- Grassi, M., Colombo, I., & Lapasin, R. (2001). Experimental determination of the theophylline diffusion coefficient in swollen sodium-alginate membranes. *Journal of Controlled Release*, 76(1), 93-105. [https://doi.org/10.1016/S0168-3659\(01\)00424-2](https://doi.org/10.1016/S0168-3659(01)00424-2)
- Grassi, Mario, Grassi, G., Lapasin, R., Colombo, I., Grassi, G., Lapasin, R., & Colombo, I. (2006). *Understanding Drug Release and Absorption Mechanisms: A Physical and Mathematical Approach*. <https://doi.org/10.1201/9781420004656>
- Groult, S., & Budtova, T. (2018). Thermal conductivity/structure correlations in thermal super-insulating pectin aerogels. *Carbohydrate Polymers*, 196, 73-81. <https://doi.org/10.1016/j.carbpol.2018.05.026>
- Haimer, E., Wendland, M., Schlufter, K., Frankenfeld, K., Miethe, P., Potthast, A., ... Liebner, F. (2010). Loading of Bacterial Cellulose Aerogels with Bioactive Compounds by Antisolvent Precipitation with Supercritical Carbon Dioxide. *Macromolecular Symposia*, 294(2), 64-74. <https://doi.org/10.1002/masy.201000008>
- Horvat, G., Xhanari, K., Finšgar, M., Gradišnik, L., Maver, U., Knez, Ž., & Novak, Z. (2017). Novel ethanol-induced pectin-xanthan aerogel coatings for orthopedic applications. *Carbohydrate Polymers*, 166, 365-376. <https://doi.org/10.1016/j.carbpol.2017.03.008>
- Huang, X., & Brazel, C. S. (2001). On the importance and mechanisms of burst release in matrix-controlled drug delivery systems. *Journal of Controlled Release*, 73(2), 121-136. [https://doi.org/10.1016/S0168-3659\(01\)00248-6](https://doi.org/10.1016/S0168-3659(01)00248-6)
- Job, N., Théry, A., Pirard, R., Marien, J., Kocon, L., Rouzaud, J.-N., ... Pirard, J.-P. (2005). Carbon aerogels, cryogels and xerogels: Influence of the drying method on the textural properties of porous carbon materials. *Carbon*, 43(12), 2481-2494. <https://doi.org/10.1016/j.carbon.2005.04.031>
- Johannsen, M., & Brunner, G. (1994). Solubilities of the xanthines caffeine, theophylline and theobromine in supercritical carbon dioxide. *Fluid Phase Equilibria*, 95, 215-226. [https://doi.org/10.1016/0378-3812\(94\)80070-7](https://doi.org/10.1016/0378-3812(94)80070-7)
- Kortüm, G., Vogel, W., & Andrussow, K. (1960). Dissociation constants of organic acids in aqueous solution. *Pure and Applied Chemistry*, 1(2-3), 187-536. <https://doi.org/10.1351/pac196001020187>

- Liu, L., Fishman, M. L., Kost, J., & Hicks, K. B. (2003). Pectin-based systems for colon-specific drug delivery via oral route. *Biomaterials*, *24*(19), 3333-3343. [https://doi.org/10.1016/S0142-9612\(03\)00213-8](https://doi.org/10.1016/S0142-9612(03)00213-8)
- Mallepally, R. R., Marin, M. A., Surampudi, V., Subia, B., Rao, R. R., Kundu, S. C., & McHugh, M. A. (2015). Silk fibroin aerogels: potential scaffolds for tissue engineering applications. *Biomedical Materials*, *10*(3), 035002. <https://doi.org/10.1088/1748-6041/10/3/035002>
- Marin, M. A., Mallepally, R. R., & McHugh, M. A. (2014). Silk fibroin aerogels for drug delivery applications. *Journal of Supercritical Fluids*, *91*, 84-89. <https://doi.org/10.1016/j.supflu.2014.04.014>
- Martin, Y. C. (1996). Exploring QSAR: Hydrophobic, Electronic, and Steric Constants. *Journal of Medicinal Chemistry*, *39*(5), 1189-1190. <https://doi.org/10.1021/jm950902o>
- Mehling, T., Smirnova, I., Guenther, U., & Neubert, R. H. H. (2009). Polysaccharide-based aerogels as drug carriers. *Journal of Non-Crystalline Solids*, *355*(50-51), 2472-2479. <https://doi.org/10.1016/j.jnoncrysol.2009.08.038>
- Obaidat, R. M., Tashtoush, B. M., Bayan, M. F., T. Al Bustami, R., & Alnaief, M. (2015). Drying Using Supercritical Fluid Technology as a Potential Method for Preparation of Chitosan Aerogel Microparticles. *AAPS PharmSciTech*, *16*(6), 1235-1244. <https://doi.org/10.1208/s12249-015-0312-2>
- Peppas, N. A., & Sahlin, J. J. (1989). A simple equation for the description of solute release. III. Coupling of diffusion and relaxation. *International Journal of Pharmaceutics*, *57*(2), 169-172. [https://doi.org/10.1016/0378-5173\(89\)90306-2](https://doi.org/10.1016/0378-5173(89)90306-2)
- Rezaei, A., Nasirpour, A., Tavanai, H., & Fathi, M. (2016). A study on the release kinetics and mechanisms of vanillin incorporated in almond gum/polyvinyl alcohol composite nanofibers in different aqueous food simulants and simulated saliva. *Flavour and Fragrance Journal*, *31*(6), 442-447. <https://doi.org/10.1002/ffj.3335>
- Ritger, P. L., & Peppas, N. A. (1987a). A simple equation for description of solute release I. Fickian and non-fickian release from non-swellable devices in the form of slabs, spheres, cylinders or discs. *Journal of Controlled Release*, *5*(1), 23-36. [https://doi.org/10.1016/0168-3659\(87\)90034-4](https://doi.org/10.1016/0168-3659(87)90034-4)
- Ritger, P. L., & Peppas, N. A. (1987b). A simple equation for description of solute release II. Fickian and anomalous release from swellable devices. *Journal of Controlled Release*, *5*(1), 37-42. [https://doi.org/10.1016/0168-3659\(87\)90035-6](https://doi.org/10.1016/0168-3659(87)90035-6)
- Rubinstein, A., Radai, R., Ezra, M., Pathak, S., & Rokem, J. S. (1993). In vitro evaluation of calcium pectinate: a potential colon-specific drug delivery carrier. *Pharmaceutical Research*, *10*(2), 258-263.

- Saurí, J., Millán, D., Suñé-Negre, J. M., Colom, H., Ticó, J. R., Miñarro, M., ... García-Montoya, E. (2014). Quality by Design approach to understand the physicochemical phenomena involved in controlled release of captopril SR matrix tablets. *International Journal of Pharmaceutics*, 477(1), 431-441.
- Sengupta, N. (2016). *SMART Technologies for Natural Resource Conservation and Sustainable Development*. Allied Publishers.
- Sescousse, R., Gavillon, R., & Budtova, T. (2011). Aerocellulose from cellulose–ionic liquid solutions: Preparation, properties and comparison with cellulose–NaOH and cellulose–NMMO routes. *Carbohydrate Polymers*, 83(4), 1766-1774. <https://doi.org/10.1016/j.carbpol.2010.10.043>
- Smirnova, I., Mamic, J., & Arlt, W. (2003). Adsorption of Drugs on Silica Aerogels. *Langmuir*, 19(20), 8521-8525. <https://doi.org/10.1021/la0345587>
- Smirnova, I., Suttiruengwong, S., & Arlt, W. (2004). Feasibility study of hydrophilic and hydrophobic silica aerogels as drug delivery systems. *Journal of Non-Crystalline Solids*, 350, 54-60. <https://doi.org/10.1016/j.jnoncrysol.2004.06.031>
- Smirnova, I., Suttiruengwong, S., & Arlt, W. (2005). Aerogels: Tailor-made Carriers for Immediate and Prolonged Drug Release. *KONA Powder and Particle Journal*, 23, 86-97. <https://doi.org/10.14356/kona.2005012>
- Tkalec, G., Knez, Ž., & Novak, Z. (2015). Fast production of high-methoxyl pectin aerogels for enhancing the bioavailability of low-soluble drugs. *The Journal of Supercritical Fluids*, 106, 16-22. <https://doi.org/10.1016/j.supflu.2015.06.009>
- Tkalec, G., Knez, Ž., & Novak, Z. (2016). PH sensitive mesoporous materials for immediate or controlled release of NSAID. *Microporous and Mesoporous Materials*, 224, 190-200. <https://doi.org/10.1016/j.micromeso.2015.11.048>
- Veronovski, A., Knez, Ž., & Novak, Z. (2013a). Comparison of ionic and non-ionic drug release from multi-membrane spherical aerogels. *International Journal of Pharmaceutics*, 454(1), 58-66. <https://doi.org/10.1016/j.ijpharm.2013.06.074>
- Veronovski, A., Knez, Ž., & Novak, Z. (2013b). Preparation of multi-membrane alginate aerogels used for drug delivery. *The Journal of Supercritical Fluids*, 79, 209-215. <https://doi.org/10.1016/j.supflu.2013.01.025>
- Veronovski, A., Tkalec, G., Knez, Ž., & Novak, Z. (2014). Characterisation of biodegradable pectin aerogels and their potential use as drug carriers. *Carbohydrate Polymers*, 113, 272-278. <https://doi.org/10.1016/j.carbpol.2014.06.054>
- Yalkowsky, S. H., He, Y., Jain, P., He, Y., & Jain, P. (2016). *Handbook of Aqueous Solubility Data*. <https://doi.org/10.1201/EBK1439802458>



**CHAPTER VI. ORGANIC-ORGANIC  
AND ORGANIC-INORGANIC  
PECTIN-BASED COMPOSITE  
AEROGELS FOR DRUG RELEASE  
APPLICATIONS**

---

**CONTENTS****CHAPTER VI. ORGANIC-ORGANIC AND ORGANIC-INORGANIC PECTIN-BASED COMPOSITE AEROGELS FOR DRUG RELEASE APPLICATIONS**

<b>INTRODUCTION.....</b>	<b>294</b>
<b>1. CELLULOSE-PECTIN COMPOSITE AEROGELS .....</b>	<b>295</b>
1.1. PRODUCTION AND CHARACTERIZATION OF CELLULOSE-PECTIN COMPOSITES.....	296
1.1.1. <i>Production of cellulose-pectin composites.....</i>	296
▪ Production of cellulose matrix samples.....	296
▪ Impregnation of cellulose matrix by pectin solution .....	296
1.1.2. <i>Structure and properties of cellulose-pectin composite aerogels .....</i>	299
▪ Formation of interpenetrated network cellulose-pectin and density of composite aerogels .....	299
▪ Morphology of composite aerogels.....	304
1.2. CELLULOSE-PECTIN COMPOSITES AS DRUG DELIVERY SYSTEM .....	306
1.2.1. <i>Characteristics of drug-loaded composite cellulose-pectin aerogels .....</i>	306
1.2.2. <i>Theophylline release profiles from cellulose-pectin aerogels.....</i>	309
▪ Comparison of theophylline release from neat reference pectin-based versus neat reference cellulose-based aerogel matrices.....	310
▪ Influence of pectin/cellulose composition on release kinetics of theophylline from composite aerogels.....	315
➤ Cellulose-pectin composite aerogels without calcium .....	315
➤ Cellulose-pectin composite aerogels with calcium .....	322
1.3. CONCLUSIONS ON PECTIN-CELLULOSE COMPOSITE AEROGELS.....	326
<b>2. PECTIN-SILICA COMPOSITE AEROGELS.....</b>	<b>328</b>
2.1. PRODUCTION AND CHARACTERIZATION OF PECTIN-SILICA COMPOSITES .....	329
2.1.1. <i>Materials.....</i>	329
2.1.2. <i>Sol-gel synthesis of neat silica aerogels using either TEOS or PEDS.....</i>	329
▪ Production of silica aerogels made from TEOS.....	329
▪ Production of silica aerogels made from PEDS.....	330
1.1.1. <i>Production of pectin-silica composite aerogels.....</i>	330
▪ Process route of pectin-silica composite aerogels .....	330
▪ Calculation of silica diffusion time inside pectin matrix .....	332
▪ Estimation of the silica impregnation efficiency into pectin matrices.....	333
2.2. CHARACTERIZATION OF PECTIN-SILICA COMPOSITE AEROGELS .....	334
2.2.1. <i>Influence of the type of silica sol on the properties of neat silica aerogels (TEOS vs PEDS) .....</i>	334
2.2.2. <i>Distribution and impregnation efficiency of silica in pectin matrix.....</i>	339
2.2.3. <i>Structural properties of pectin-silica composite aerogels and loading with theophylline ..</i>	342
2.2.4. <i>Theophylline loading in pectin-silica composite aerogels .....</i>	346
2.3. THEOPHYLLINE RELEASE PROFILES FROM PECTIN-SILICA AEROGEL MATRICES.....	348

CHAPTER VI.

Organic-organic and organic-inorganic pectin-based composite aerogels for drug release applications

---

2.3.1.	<i>Comparison of theophylline release from neat silica and pectin aerogels matrices</i> .....	349
2.3.2.	<i>Theophylline release from pectin-silica composite aerogels</i> .....	354
➤	Without calcium crosslinking .....	355
➤	Pectin cross-linked with calcium .....	358
2.4.	CONCLUSIONS ON PECTIN-SILICA COMPOSITE AEROGELS .....	369
<b>3.</b>	<b>CYTOXOCITY PROFILE OF DIFFERENT AEROGELS AND CRYOGELS</b>	
	<b>MATRICES</b> .....	<b>371</b>
	<b>CONCLUSIONS</b> .....	<b>373</b>
	<b>REFERENCES</b> .....	<b>374</b>

## Introduction

The goal of this work is to produce organic-organic and organic-inorganic pectin-based composite aerogels, with one component being pectin and the other either cellulose or silica.

The main question to answer is “can we modify the release kinetics from pectin aerogel by making composite material?”, and then, “what is the influence of the second component on drug release kinetics and matrix behaviour?”. The synergy of properties brought by the different components is expected to result in new physical and chemical properties of composite aerogels and to offer new prospects in composite aerogels used as drug carrier.

Cellulose-pectin and pectin-silica composite aerogels were produced and characterized. Theophylline, used as drug model, was incorporated into the samples in order to study its release behaviour and correlate to the matrices' composition. In this work, focus is made on the relationships between the intrinsic characteristics of each component of aerogel, the structural and physical properties of the composite network, and the properties of the composite materials used as drug carriers.

First, we study “all polysaccharide” composite aerogels, based on cellulose and pectin. In the second part, we present our work on organic-inorganic composite aerogels, based on pectin and silica.

## 1. Cellulose-pectin composite aerogels

Cellulose-pectin composite aerogels were produced by impregnation of cellulose “wet” matrix (cellulose coagulated in water) with pectin solution. The aerogel composition was varied by adjusting polymer composition (ratio cellulose/pectin) to produce different composites keeping 6 wt% of polysaccharides in the initial mixtures and 0.300 mg of polysaccharide (dry weight) in total. These two hydrophilic polysaccharides were chosen as they were expected to display dissimilar properties as drug-carrier. Indeed, pectin is soluble in the releasing media (SIF, SGF), thus pectin-based matrices are prone to erosion by dissolution as described in the previous chapter (Chapter V). In contrast, cellulose is known to be non-soluble polymer in the releasing media (SIF, SGF), thus cellulose-based matrices are expected to present different drug release behaviour in comparison to neat pectin. Moreover, we suppose that the “mixture” of the properties of each component may lead to a certain synergy in the properties of composite aerogels.

This section is organized as follows:

- The first part is dedicated to the production and the characterization of theophylline-loaded composite aerogels made from pectin and cellulose. The impact of the cellulose/pectin ratio on the structural properties of the composite aerogels is presented.
- The second part deals with the use of cellulose-pectin composite aerogels as drug delivery systems, using theophylline as drug model. We start with the characterization and comparison of neat cellulose and neat pectin aerogel used as drug-carriers. The impact of the composition of the composite aerogel on their drug loading and release properties are presented and discussed. Matrix swelling ability, erosion properties, drug loading characteristics and release profile are compared.

To the best of our knowledge, this is the first time that cellulose-pectin composite aerogels are produced and used as drug delivery matrices. Only a few works on polysaccharide composite aerogels for drug delivery applications are reported in literature and the large majority deals with composites obtained by coating of one polymer by another. Here, we propose an original method of making organic-organic interpenetrated aerogel network by impregnation of one component with another.

## 1.1. Production and characterization of cellulose-pectin composites

We first present the process route to produce cellulose-pectin composite aerogels. Their structural and morphological properties are characterized and discussed regarding to pectin/cellulose composition.

### 1.1.1. Production of cellulose-pectin composites

#### ▪ **Production of cellulose matrix samples**

Microcrystalline cellulose was dried overnight at 50°C under vacuum and let swelling in water for 2 hours at 5°C prior to its dissolution. Cellulose solutions were prepared at cellulose concentrations from 2.5 wt% to 6 wt% by mixing swollen cellulose with NaOH-water and urea to reach final solvent concentration 8 wt% NaOH-12 wt% urea. The whole was pre-cooled at -12.3°C and mixed during 3 minutes at 1000 RPM (Luo & Zhang, 2010). After dissolution, cellulose solutions were poured into cylindrical molds and let gelled (when possible) 24 h at 50°C. Gelled and non-gelled cellulose samples were gently coagulated with distilled water and were extensively washed with water until pH neutralization.

#### ▪ **Impregnation of cellulose matrix by pectin solution**

The coagulated cellulose samples were immersed into pectin solution at pH 3.0 of different concentrations depending on the desired ratio cellulose/pectin. Impregnation of cellulose matrix by pectin occurred by diffusion of pectin solution into the cellulose coagulated network, at 60 °C during 5 days. A schematic illustration of the preparation route of the composite matrices is given in Figure 169.

The coagulated cellulose matrices were filled with pectin in order to obtain 6 wt% of polysaccharides in total and to obtain aerogels made of 0.300 mg of polysaccharides (dry weight). The wet concentration (wt%) of each cellulose matrix and the corresponding pectin concentration in the impregnation bath are shown in Table 14. The theoretical mass ratios cellulose/pectin are compared with the experimental ratio obtained in each case.

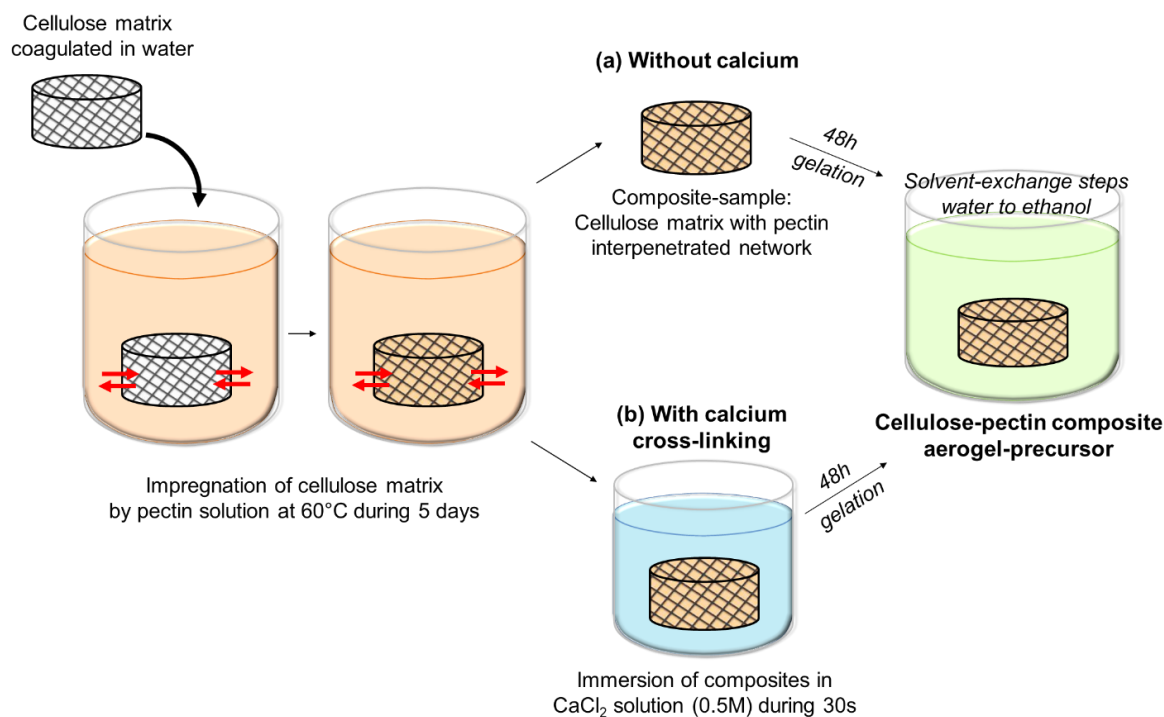


Figure 169. Process route of cellulose matrix impregnation by pectin solution to produce cellulose-pectin composite sample (a) without calcium or (b) cross-linked with calcium.

Table 14. Composition of composites cellulose – pectin aerogels

Initial matrix composition in solution (wt%)	State of matter of cellulose matrix before solvent-exchange	Pectin concentration in the impregnation bath (wt%)	Theoretical ratios cellulose / pectin	Experimental Ratio of cellulose	Experimental Ratio of pectin	CaCl <sub>2</sub> [0.5M] solution for pectin gelation
6 wt% cellulose	Gel	-	1 / 0	1	0	-
5.5 wt% cellulose	Gel	1.3	0.92 / 0.08	0.883 ±0.006	0.117 ±0.006	-
5 wt% cellulose	Gel	2.4	0.83 / 0.17	0.798 ±0.006	0.202 ±0.006	-
4 wt% cellulose	Solution	5.6	0.66 / 0.34	0.637 ±0.007	0.363 ±0.007	-
3 wt% cellulose	Solution	7.5	0.5 / 0.5	0.522 ±0.010	0.478 ±0.010	-
2.5 wt% cellulose	Solution	8.4	0.42 / 0.58	0.429 ±0.004	0.571 ±0.004	-
6 wt% pectin	Solution	-	0 / 1	0	1	-
4 wt% cellulose	Solution	5.6	0.66 / 0.34	0.607 ±0.009	0.393 ±0.009	yes

<b>3 wt% cellulose</b>	Solution	7.5	0.5 / 0.5	0.474 ±0.009	0.526 ±0.009	yes
<b>2.5 wt% cellulose</b>	Solution	8.4	0.42 / 0.58	0.407 ±0.009	0.593 ±0.009	yes
<b>6 wt% pectin</b>	Gel	-	0 / 1	0	1	yes

After pectin impregnation step, cellulose-pectin samples were taken out from pectin solution and let gelling in small sealed containers in ambient conditions for 48 h. To investigate the impact of calcium, some of the cellulose-pectin samples (after pectin impregnation) were directly placed into CaCl<sub>2</sub> solution (0.5 M) during 30 seconds to induce ionic gelation of pectin. After 48 h of gelation time, all cellulose-pectin composites (with or without calcium) went through extensive solvent-exchange steps, in order to exchange water to ethanol. Finally, the composite aerogel precursors were loaded with theophylline by diffusion through ethanol at 3.4 g/L during at least 7 days, as detailed in Materials and Method (Chapter II), prior to CO<sub>2</sub> s-drying.

In addition to cellulose-pectin composite aerogels, we produced aerogels from each separate component, *i.e.* un-filled cellulose matrices (not impregnated by pectin) and the pectin solutions used for impregnation, in order to be used as “references”. These aerogels will be referred as “cellulose-matrix references” (neat cellulose matrices from 2.5 wt% to 6 wt% of cellulose without pectin) and “pectin-bath references” made from pectin solutions of each impregnation bath (from 1.3 wt% to 8.4 wt% of pectin). These reference samples were loaded with theophylline in the same way as composites, by diffusion through ethanol at 3.4 g/L during at least 7 days, as detailed in Material and Method (Chapter II). Each sample was produced at least in duplicate with calcium, and in triplicate without calcium.

In this work, cellulose to pectin ratios were estimated using the masses of the cellulose-pectin composites and of the corresponding cellulose-matrix reference aerogels as follows:

$$Ratio_{Cellulose/pectin} = \frac{mass_{cellulose-matrix\ reference\ aerogel}}{mass_{composite\ aerogel}} \quad (6.1)$$

Thus, the ratio of pectin to cellulose is simply the inverse:

$$Ratio_{Pectin/cellulose} = 1 - Ratio_{Cellulose/pectin} \quad (6.2)$$

The theoretical mass of pectin within the aerogel composite (g) is based on the concentration of the pectin bath (wt%) ( $C_{pectin\ bath}$ ) and the volume of the wet cellulose matrix during pectin impregnation step ( $Volume_{wet\ matrix\ cellulose}$ ), as follows:

$$Pectin\ theoretical\ amount\ (g) = Volume_{wet\ matrix\ cellulose} \times C_{pectin\ bath} \quad (6.3)$$

Here we assume that 100% of the matrix volume is filled with pectin solution and that diffusion was complete.

The actual pectin amount in composite aerogels is obtained by the mass difference between the cellulose-pectin aerogels and cellulose-matrix reference aerogels (not filled with pectin), as given by:

$$\begin{aligned} & \text{Pectin actual amount (g)} \\ &= \text{mass}_{\text{composite aerogels}} - \text{mass}_{\text{cellulose-matrix reference aerogel}} \end{aligned} \quad (6.4)$$

Thus, we define the pectin filling efficiency (%) as follows:

$$\text{Pectin filling efficiency (\%)} = \frac{\text{Pectin actual amount (g)}}{\text{Pectin theoretical amount (g)}} \times (100\%) \quad (6.5)$$

Finally, we determine the theoretical density of composite aerogel ( $\text{g}/\text{cm}^3$ ) which is defined as the ratio of the theoretical mass of the composite to the volume of cellulose coagulated matrix (before pectin impregnation). The theoretical mass of the composite is the sum of cellulose amount (g) and pectin theoretical amount (g) within the system, assuming 100% pectin filling efficiency.

$$\begin{aligned} & \text{Theoretical density}_{\text{composite aerogel}} (\text{g}/\text{cm}^3) \\ &= \frac{\text{mass}_{\text{cellulose-matrix reference aerogel}} + \text{Pectin theoretical amount (g)}}{\text{Volume}_{\text{cellulose coagulated matrix}}} \end{aligned} \quad (6.6)$$

In the same way, we define the composite theoretical specific surface area ( $S_{\text{BET}}$  in  $\text{m}^2/\text{g}$ ) which is based on “mixing law” as follows:

$$\begin{aligned} & \text{Theoretical } S_{\text{BET}} \text{ composite aerogel } (\text{m}^2/\text{g}) = \\ & \left( \text{Experimental ratio}_{\text{pectin/cellulose}} \times S_{\text{BET}} \text{ pectin-bath reference aerogel} \right) + \\ & \left( \text{Experimental ratio}_{\text{cellulose/pectin}} \times S_{\text{BET}} \text{ cellulose-matrix reference aerogel} \right) \end{aligned} \quad (6.7)$$

### 1.1.2. Structure and properties of cellulose-pectin composite aerogels

- **Formation of interpenetrated network cellulose-pectin and density of composite aerogels**

As shown in Figure 170, the filling efficiency (%) of cellulose matrix by pectin solution was around 90 – 95%, and thus the mass ratio cellulose / pectin obtained experimentally was

very close to the theoretical one as shown Table 14. However, it has to be noted that a substantial external layer of pectin was formed on the surface of cellulose matrix, which may have contributed to artificially increased the pectin fraction and make impregnation efficiency (%) slightly above 100% in a few cases. The more concentrated was the pectin solution, the thicker was the external layer, in correlation with pectin solution viscosity.

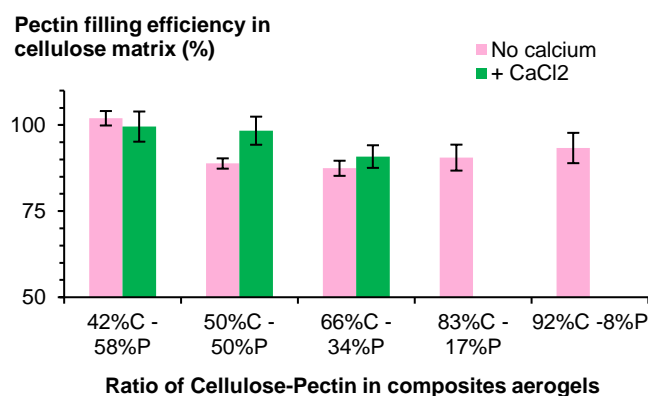


Figure 170. Pectin filling efficiency (%) in coagulated cellulose as a function of cellulose / pectin ratio (%). Cellulose is noted “C” and pectin “P”.

As mentioned in Section 1.1.1 of this chapter, pectin reference aerogels were prepared from solutions which had the same “history” as those which were used for the impregnation of cellulose matrix. The reason is that solution “history” has changed neat pectin aerogel properties. We remind that in order to decrease pectin solution viscosity and thus increase diffusion into cellulose matrix, the impregnation was performed at 60 °C for 5 days. Pectin solutions were taken from the oven, cooled down and used to make aerogels. Surprisingly, we noticed that these solutions did not gel at room temperature, as it was expected at pH 3. Except for the highest pectin concentrations (7.5 and 8.4 wt%), pectin solutions with concentrations from 1.3 wt% to 6 wt% remained viscous solutions (in the absence of calcium). Based on our previous work, we expected to have acidic gelation at pH 3.0 for pectin solutions above 4.5 wt% (Groult & Budtova, 2018). We assume that some degradation of pectin occurred due the impregnation conditions which might have altered pectin gelling ability. However, strong pectin ionic gelation occurred once calcium was added.

Pectin-impregnated cellulose samples were placed in ethanol to perform solvent exchange in order to “fix” pectin inside cellulose, followed by impregnation with theophylline and drying. We noticed the difference between the volume of neat cellulose aerogel precursors and those impregnated with pectin, (from ~ 6 to 17 vol%), as shown in Figure 171. We assume that cellulose shrinkage during pectin-impregnation step was due to osmotic pressure caused by pectin solution outside cellulose matrix filled with water; it may be possible that additional shrinkage is also caused by pectin network contraction during solvent exchange step. The

shrinkage was twice higher (12-17 vol%) for cellulose-matrix which was non-gelled ( $\leq 4$  wt% of cellulose) as compared to that which was gelled (6 - 7 vol%).

Non-gelled cellulose matrices remained fragile even after solvent exchange, and were mechanically less resistant to shrinkage. These matrices were contracting more when placed in concentrated pectin solutions ( $\geq 5.6$  wt% of pectin) than their gelled counterparts. The cellulose-pectin samples which were placed into calcium solution exhibited lower shrinkage due to strong ionic crosslinking of pectin. Besides, pectin-cellulose aerogels with calcium were found to have a slightly higher pectin content inside cellulose matrix (Figure 170) as calcium prevented pectin mass loss during sample manipulation by strongly “fixing” it within the sample.

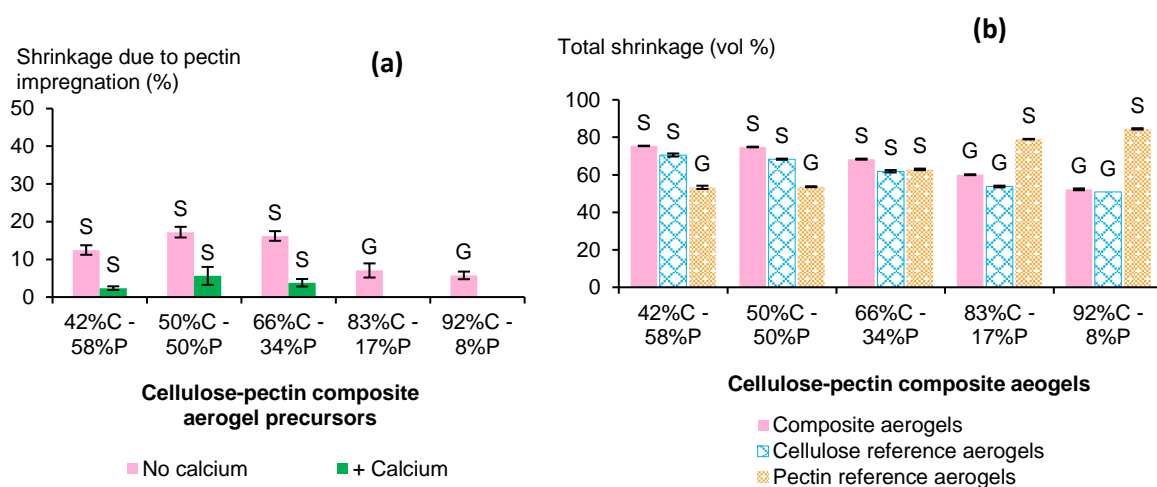


Figure 171. (a) Volume additional shrinkage due to pectin impregnation (measured after solvent exchange) (%) and (b) Total shrinkage obtained after sc-drying of composite samples and of their references at the corresponding polymer concentration in composite matrix. Cellulose is noted “C” and pectin “P”. The state of each sample before coagulation, (‘S’) or gel (‘G’), is indicated.

It has to be noted that concentrations of pectin baths were adjusted taking in account the levels of shrinkage of each cellulose matrix during impregnation. Indeed, the decrease of matrix volume directly reduces the quantity of pectin that can be incorporated, and thus pectin content in the composites.

Pictures of cellulose – pectin composite aerogels and neat matrix cellulose aerogels (not filled with pectin) are given for illustration in Figure 172. As it can be visually seen from the pictures, the volume of aerogels was lower with the decrease of cellulose concentration due to higher volume shrinkage during coagulation and sc-drying steps. When comparing to the neat cellulose reference with its pectin-impregnated counterpart, the additional volume shrinkage of the composite aerogels due to pectin impregnation can be seen.

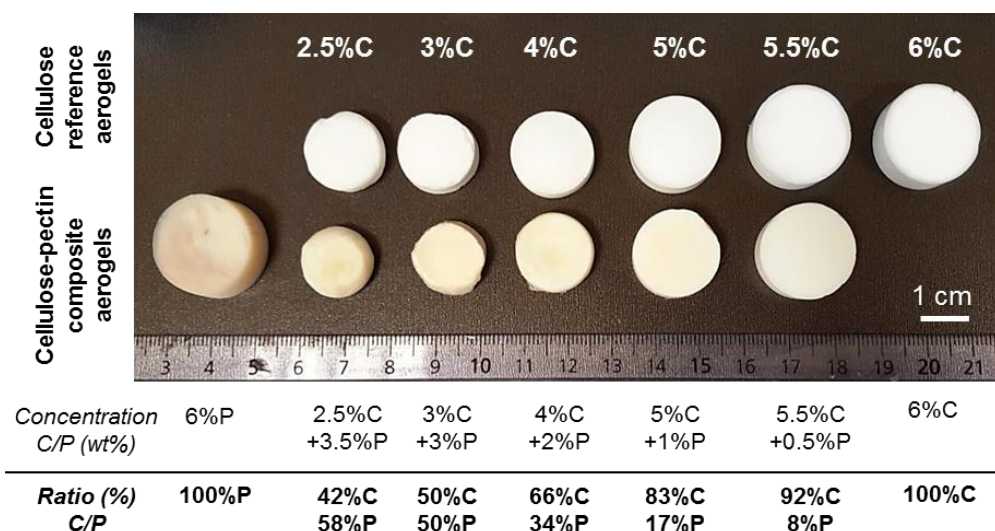


Figure 172. Pictures of neat reference cellulose and pectin aerogels and cellulose-pectin composite aerogels, obtained by impregnation of pectin solution into cellulose matrices, no calcium added. Concentration (wt%) of cellulose ('C') and pectin ('P') at the impregnation step and ratio (%) cellulose/pectin in aerogel corresponding to each image are also given.

On Figure 173 and Figure 174, we can observe that composite aerogels' density and porosity were highly dependent on cellulose / pectin ratio. Indeed, the density of composite aerogels was influenced by the additional volume shrinkage of cellulose matrices due to pectin impregnation. As impregnation efficiencies were similar and exceeded 90% for each composite (Figure 170), the differences between composite aerogels densities of different composition were mostly driven by different matrix shrinkages.

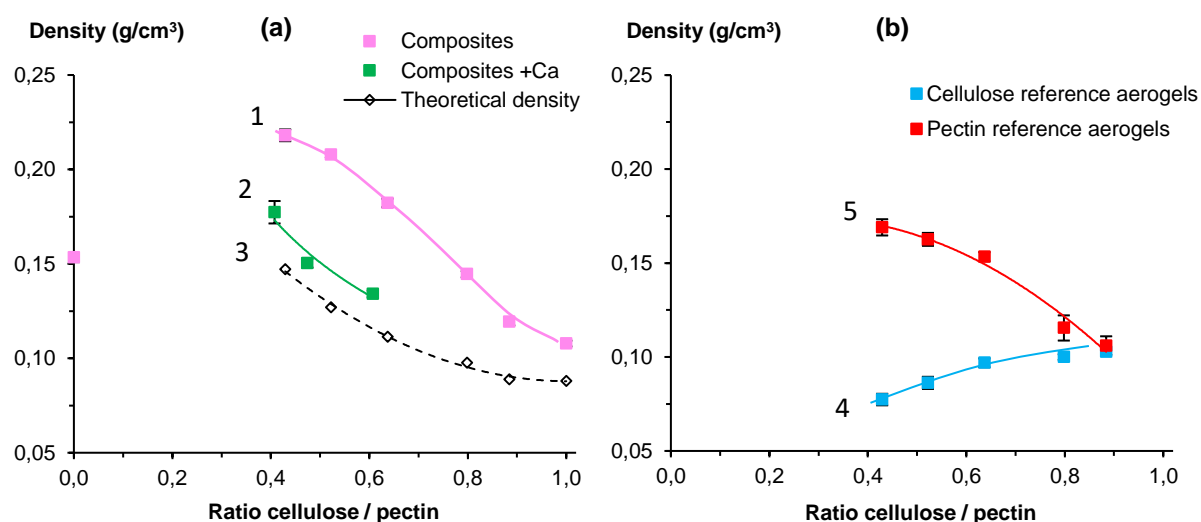


Figure 173. (a) Composite aerogel densities without calcium (1) or with calcium (2), total polymer concentration in the initial solutions was 6 wt %. The theoretical composite densities (3) are given by Equation (4.6).

(b) Density of the “reference” cellulose (5) and pectin (6) aerogels plotted at concentrations corresponding to the ratios they are present in the composites.

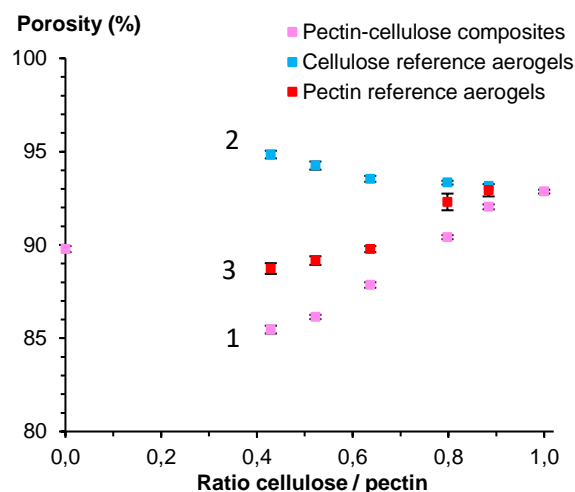


Figure 174. Porosity of composite aerogels (1) and their corresponding references aerogels: cellulose (2) and pectin (3). Porosity of cellulose and pectin reference aerogels are plotted at concentrations corresponding to the ratios they are present in the composites.

As it is presented in Figure 173, composite aerogel density decreases with the increase of cellulose fraction in composite aerogel. The lower cellulose concentration of the initial matrix, the weaker is cellulose network and more it is shrinking during the impregnation of pectin, solvent exchange and sc-drying steps, and thus the higher is aerogel density (Figure 173) and lower aerogel porosity (Figure 174). We underline here the critical role of the initial wet cellulose matrices on the determination of the final density and porosity of composite aerogels. Besides, Figure 173 also shows that composite densities were significantly higher than the estimated theoretical densities (eq. 4.6), as a result of volume shrinkage during the impregnation of cellulose matrices by pectin solution, but also during solvent exchange and sc-drying steps (Figure 171).

Specific surface area of composites was found to more or less follow the “mixing law”, *i.e.* additive sum of the contributions of each neat aerogel. As it can be seen in Figure 175, as pectin aerogels have higher  $S_{\text{BET}}$  than cellulose ones at the same concentration, the specific surface of composite aerogels  $S_{\text{BET}}$  increased with pectin content. Theoretical (additive)  $S_{\text{BET}}$  was estimated for each composite with eq. 5.7. As it can be seen, experimental and theoretical values of  $S_{\text{BET}}$  were similar, revealing that the pectin aerogel has a similar morphology when impregnated in cellulose matrix. However, we observed that neat pectin aerogels made from solutions stored at 60 °C presented lower specific surface by at least 20 to 30% as compared with pectin aerogels from our previous work (Chapter V). These results confirm our assumption on pectin partial degradation in hot conditions and acidic media (pH 3.0).

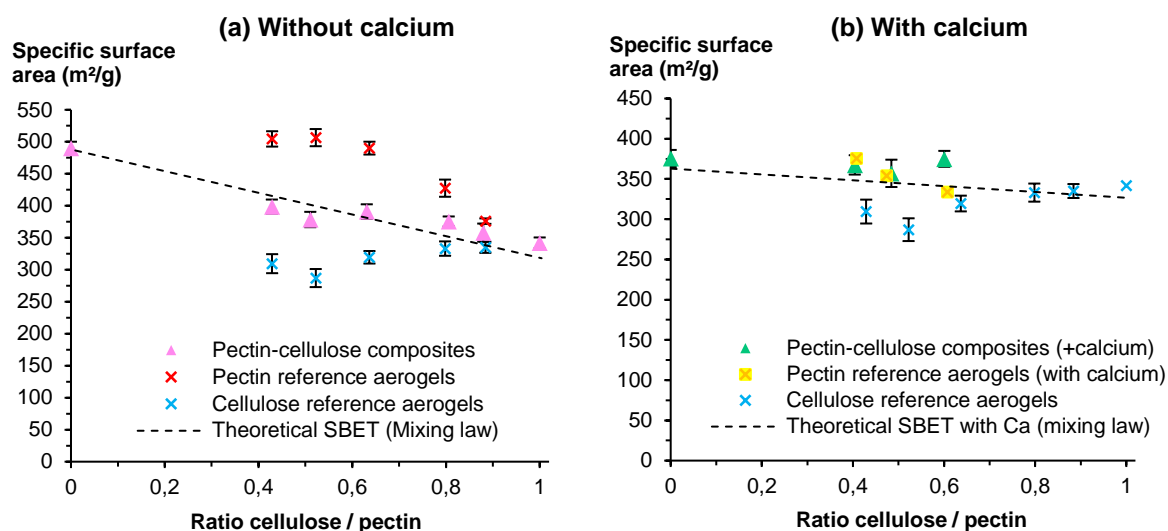


Figure 175. Specific surface areas of composite aerogels (a) without calcium (pink triangles) and (b) with calcium (green triangles) and their corresponding pectin and cellulose reference aerogels. Specific surface areas of cellulose and pectin reference aerogels are plotted at the concentrations corresponding to the fractions they are present in the composites. Theoretical  $S_{BET}$  (dashed line) were estimated using mixing law (Equation (6.7)).

### ▪ Morphology of composite aerogels

SEM observations in Figure 176 (a) confirmed the existence of an external layer of pectin around cellulose matrix, with thickness increasing with pectin solution concentration and when calcium was added to induce ionic gelation. As previously observed for neat aeropectins in Chapter V, the surface of composite aerogels was also covered by sharp “particles” typical for theophylline.

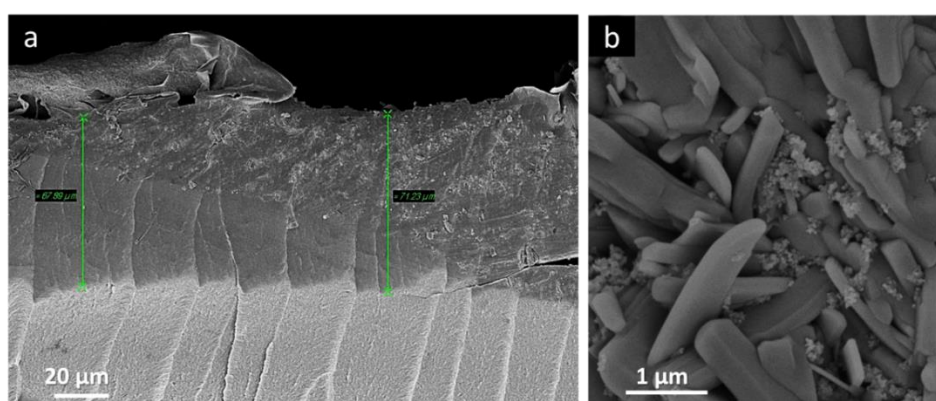


Figure 176. SEM observations of (a) composite aerogel cross section and (b) surface of theophylline loaded composite aerogel made from 42% cellulose-58% pectin without calcium.

The internal structure of cellulose-pectin composite aerogels shows interpenetrated cellulose-pectin network (Figure 177b). Reference neat pectin aerogel (Figure 177a) and reference neat cellulose aerogel (Figure 177c) are also presented: pectin aerogel possesses a

denser and more fine network with smaller pores in the range of 20 to 50 nm as compared to cellulose aerogel thicker pore walls and larger pores. The analysis of Figure 9b for composite aerogel allows assuming that pectin seems to have filled the pores offered by cellulose.

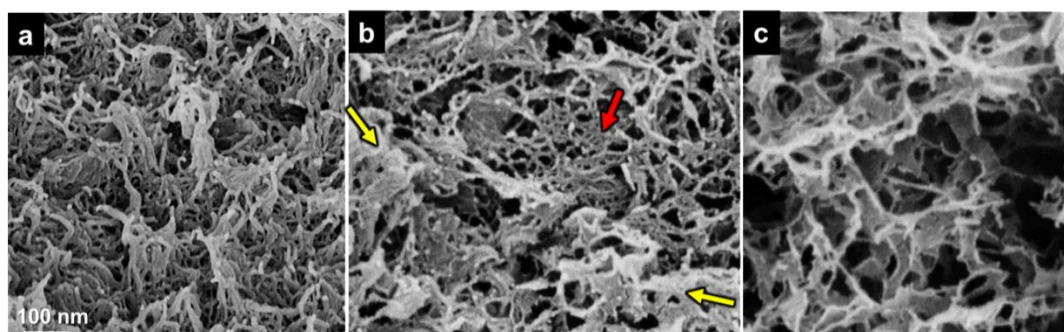


Figure 177. SEM pictures of (a) 5.6 wt% pectin aerogel, (b) 66% C – 34% P composite aerogel sample made from 4 wt% matrix cellulose and impregnated with 5.6 wt% pectin solution (yellow arrows correspond to cellulose network and red to pectin), and (c) 4 wt% cellulose aerogel. No calcium added.

By scanning different fields of view within the samples using SEM (from samples' skin to core), we noticed that that pectin impregnation was not perfectly homogeneous within composites, as we observed less pectin fine network in the center of the material. These observations concerned samples with the highest pectin ratio, and can be explained by the higher viscosity of pectin solution and thus much slower diffusivity within the cellulose matrix. Internal morphologies of cellulose-pectin composite at the core of aerogels and of the corresponding neat reference cellulose aerogels are presented in Figure 178.

As it can be seen, composites' interpenetrated networks are becoming denser with smaller pores while increasing pectin fraction. Composite network tends to be more similar to the typical dense aspect of pectin aerogel as pectin content increases. The increased shrinkage with the increase of pectin concentration (Figure 171 and Figure 173) could also be the reason of a denser morphology.

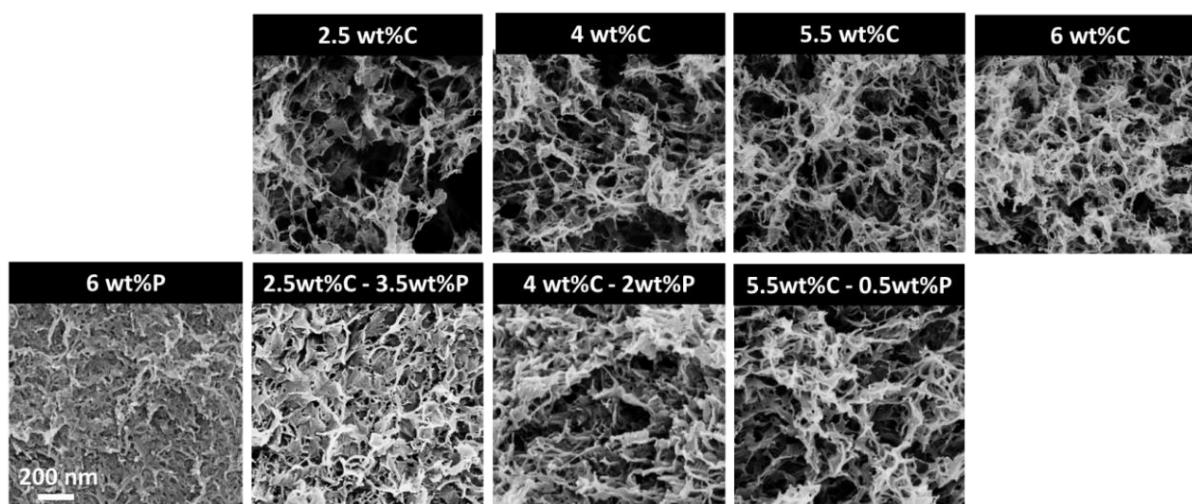


Figure 178. SEM pictures at the core of composite aerogels at different cellulose (C) to pectin (P) ratios and their corresponding neat reference aerogels. No calcium was added

As expected from our previous results on aeropectins (Chapter III), the addition of calcium to the composites “solidified” the structure by strong ionic gelation of the pectin fraction, which reduced volume shrinkage and density of cellulose-pectin composite aerogels as compared to those without calcium. The internal structures were less compact and displayed larger pores as shown in Figure 179.

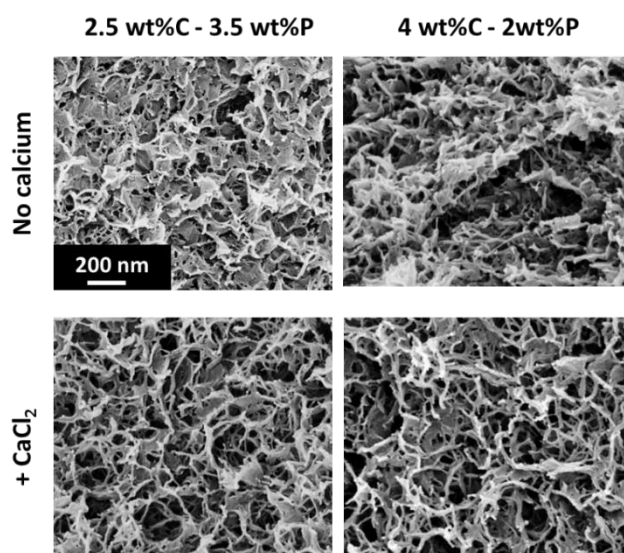


Figure 179. SEM pictures of cellulose-pectin composite aerogels with or without addition of calcium.

## 1.2. Cellulose-pectin composites as drug delivery system

### 1.2.1. Characteristics of drug-loaded composite cellulose-pectin aerogels

Theophylline loading efficiency (%) and loading capacity (wt%) of composites and of reference aerogels are plotted in Figure 180, and their loading and structural properties are summarized in Table 15 and Table 16. All cellulose-, pectin- and cellulose-pectin aerogels were loaded with theophylline at 3.4 g/L.

Table 15. Structural and drug loading properties of cellulose-pectin composite aerogels without calcium as a function of cellulose/pectin ratio (%).

Ratio cellulose/pectin (%)	100% pectin (reference)	42%C 58%P	50%C 50%P	66%C 34%P	83%C 17%P	92%C 8%P	100% cellulose (reference)

## CHAPTER VI.

## Organic-organic and organic-inorganic pectin-based composite aerogels for drug release applications

<b>Aerogel density (g/cm<sup>3</sup>)</b>	0.153 ± 0.002	0.218 ± 0.003	0.208 ± 0.002	0.182 ± 0.003	0.145 ± 0.003	0.119 ± 0.002	0.108 ± 0.002
<b>Porosity (%)</b>	89.8 ± 0.2	85.5 ± 0.2	86.1 ± 0.1	87.8 ± 0.2	90.4 ± 0.2	90.4 ± 0.1	92.9 ± 0.1
<b>Aerogel S<sub>BET</sub> (m<sup>2</sup>/g)</b>	490 ± 10	399 ± 11	379 ± 12	391 ± 11	376 ± 8	358 ± 14	342 ± 9
<b>Pore volume (cm<sup>3</sup>/g)</b>	5.85 ± 0.10	3.92 ± 0.07	4.14 ± 0.04	4.82 ± 0.07	6.29 ± 0.08	7.71 ± 0.14	8.67 ± 0.13
<b>Drug loading efficiency (%)</b>	67.8	108.0	87.8	85.8	77.4	53.4	48.1
<b>Drug loading capacity (wt%)</b>	3.2	3.2	3.0	2.9	2.8	2.1	1.9
<b>Specific drug loading (× 10<sup>-5</sup> g/m<sup>2</sup>)</b>	6.8	8.2	7.8	7.4	7.5	5.9	5.6

Table 16. Structural and loading properties of cellulose-pectin composite aerogels with calcium as a function of cellulose/pectin ratio (%).

<b>Ratio cellulose/pectin (%)</b>	<b>100% pectin +Ca (reference)</b>	<b>42%C 58%P+Ca</b>	<b>66%C 34%P+Ca</b>	<b>100% cellulose (reference)</b>
<b>Aerogel density (g/cm<sup>3</sup>)</b>	0.071 ± 0.002	0.177 ± 0.006	0.134 ± 0.002	0.108 ± 0.002
<b>Porosity (%)</b>	95.3 ± 0.1	88.2 ± 0.4	91.1 ± 0.1	92.9 ± 0.1
<b>Aerogel S<sub>BET</sub> (m<sup>2</sup>/g)</b>	376 ± 11	367 ± 12	375 ± 10	342 ± 9
<b>Pore volume (cm<sup>3</sup>/g)</b>	13.46 ± 0.34	4.98 ± 0.19	6.79 ± 0.10	8.67 ± 0.13
<b>Drug loading efficiency (%)</b>	59.2	102.5	97.2	48.1
<b>Drug loading capacity (wt%)</b>	3.6	3.2	3.1	1.9
<b>Specific drug loading (x10<sup>-5</sup> g/m<sup>2</sup>)</b>	9.5	8.7	7.9	5.6

As previously observed for theophylline loaded aeropectins (Chapter V), the loading efficiency of composite aerogels (Figure 180 a) was also found to be positively correlated with aerogel density. This figure also shows that loading efficiency is not proportional to cellulose/pectin composition as both reference pectin and reference cellulose aerogels had much lower loading efficiency than their composites.

We assume that the higher density of composite aerogels led to the increase drug loading efficiency. As we have already mentioned for aeropectins (see the detailed study in Chapter V), we hypothesize that matrix density prevented theophylline physical wash off with the flow during the  $sc\text{-CO}_2$  drying, even though theophylline is not soluble in  $sc\text{-CO}_2$ . Such effect of density was also reported by Mehling et al. and Smirnova et al. who suggested that smaller pore size in case of high aerogel density might be an important parameter for loading efficiency (Mehling, Smirnova, Guenther, & Neubert, 2009; I. Smirnova, Suttiruengwong, & Arlt, 2004).

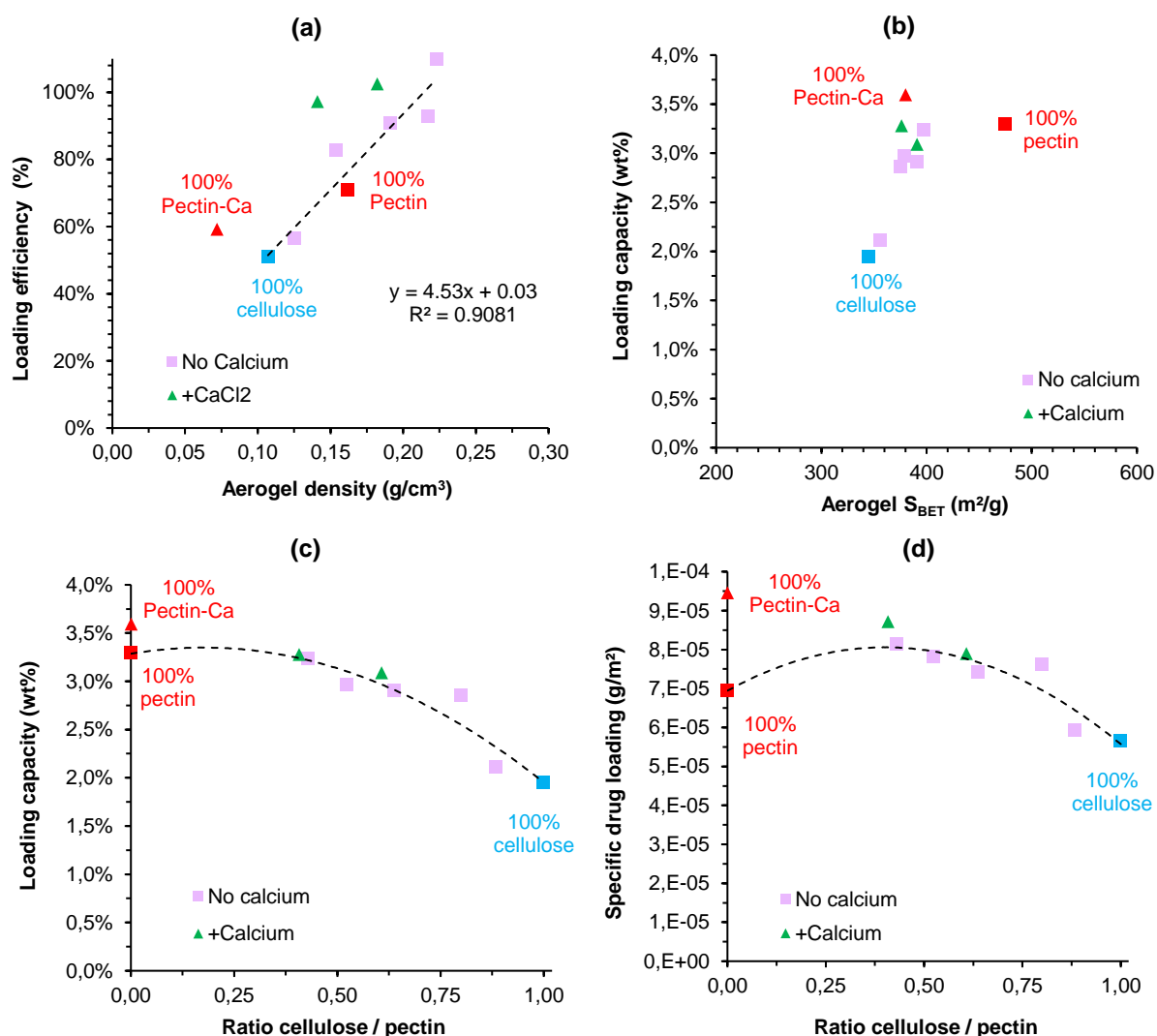


Figure 180. Drug loading characteristics of composite aerogels and of their reference counterparts. (a) Theophylline loading efficiency (%) as a function of aerogel density. A linear trend line was fitted to the data to correlate composite aerogel density to the loading efficiency.

(b) Loading capacity as a function of aerogel  $S_{\text{BET}}$ .

(c) Loading capacity as a function of cellulose/pectin ratio.

(d) Specific loading as a function of cellulose/pectin ratio. Composite aerogels are either without calcium (squares) or with calcium (triangles). Dashed lines in (c) and (d) are given to guide the eye.

As it can be seen in Figure 180a and 12b, the neat reference pectin aerogel with calcium presents lower drug loading efficiency (59%) than without calcium (71%), due to lower density, in correlation with our previous work (Chapter V). However, at the same aerogel density, composite aerogels with calcium have significantly higher loading efficiencies (close to 100%) while displaying similar loading capacities as compared to composites without calcium. This unexpected increase of loading efficiency of composites with calcium is actually due to a thicker external (around cellulose matrix) pectin layer. Indeed, the strong pectin gelation induced by calcium instantly fixed the entire pectin layer preventing from pectin loss. As a result, the addition of calcium increased pectin fraction in aerogel and thus composite aerogel mass by about 7 - 8%, indirectly resulting in higher amount of drug carried by aerogel around +7- 10% as compared to composites without calcium.

The theophylline loading capacity of composite aerogels was found to be correlated to polysaccharides' composition of the samples. Reference pectin and reference cellulose aerogels do not present the same drug loading properties: neat pectin aerogels had the highest loading capacity (~ 3.3 wt% without calcium, ~3.6 wt% with calcium) and neat cellulose aerogel the lowest (~ 1.9 wt%). We assume that this may be due to the combined physico-chemical effects: higher internal surface offered by pectin network ( $S_{\text{BET}} \sim 490 \text{ m}^2/\text{g}$ ) vs cellulose ( $S_{\text{BET}} \sim 340 \text{ m}^2/\text{g}$ ) (Figure 180 b) and higher aerogel density (+ 30%) for pectin as compared to cellulose (Figure 180 a), and possibly different chemical interactions drug-polysaccharide. As a result, the drug loading (Figure 180 c) and specific loading (Figure 180 d) of composite aerogels depend on their cellulose/pectin ratio. As shown in Figure 180 b, the higher pectin proportion, the larger amount of drug can be loaded i) by a given unit of material mass (Figure 180 c) and ii) by a given unit of specific surface area (Figure 180 d).

### 1.2.2. Theophylline release profiles from cellulose-pectin aerogels

In this section, we compare the release of theophylline from aerogels characterized above, made of 6 wt% of polysaccharides (in the initial solutions) while varying their composition. The aerogel with theophylline was first placed in Simulated Gastric Fluid (SGF, pH 1) for 1 hour and then in Simulated Intestinal Fluid (SIF, pH 6.8) until the end of release. Due to the opposite solubility characteristics in the releasing media of cellulose and pectin, they

were expected to present dissimilar matrix erosion properties and release behaviour when used as drug delivery matrix.

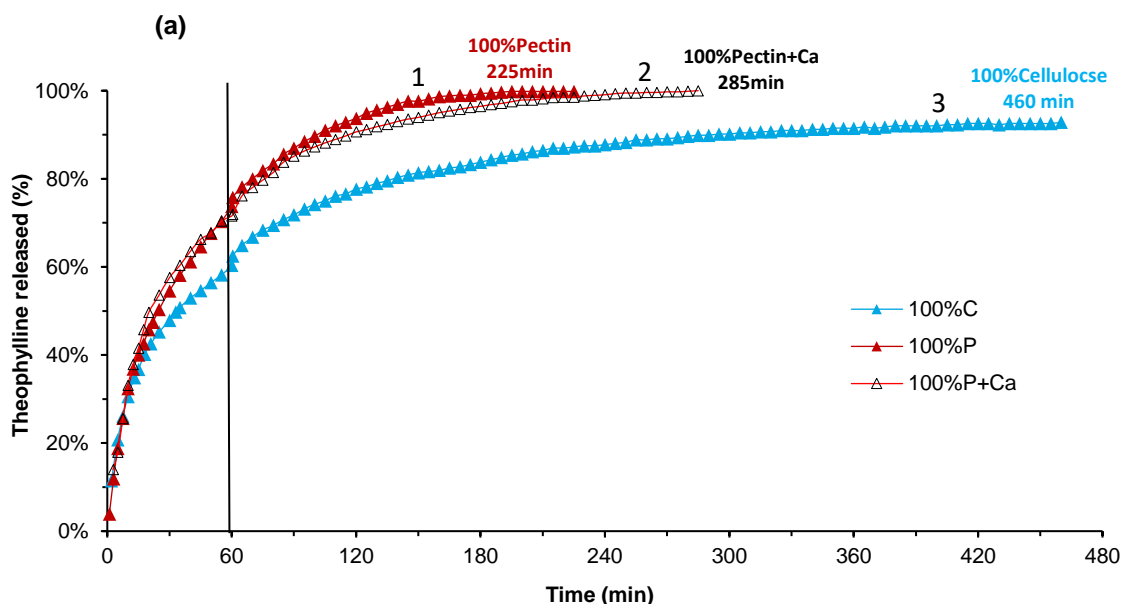
Thus, the emphasis will be placed on the impact of the variation of cellulose/pectin ratio on the release properties of the composite aerogel.

This section is organized as follows:

- The first part is dedicated to the comparison of reference aerogels, cellulose and pectin, used as matrices for drug delivery system using theophylline as drug model.
- Then, matrix composition is varied by adjusting the ratio cellulose/pectin in the system keeping constant a total of 6 wt% of polysaccharide in the initial solution and 0.300 mg of polysaccharide dry mass. The impacts of the cellulose/pectin ratio of the composite aerogels on their release properties are presented and discussed.

### ▪ Comparison of theophylline release from neat reference pectin-based versus neat reference cellulose-based aerogel matrices

As it can be seen in Figure 181 (a), pectin and cellulose aerogels displayed different drug release behaviour and matrix “stability” in the releasing media. Figure 181 (b) and (c) show the evolution of pectin and cellulose aerogel mass and volume in these conditions.



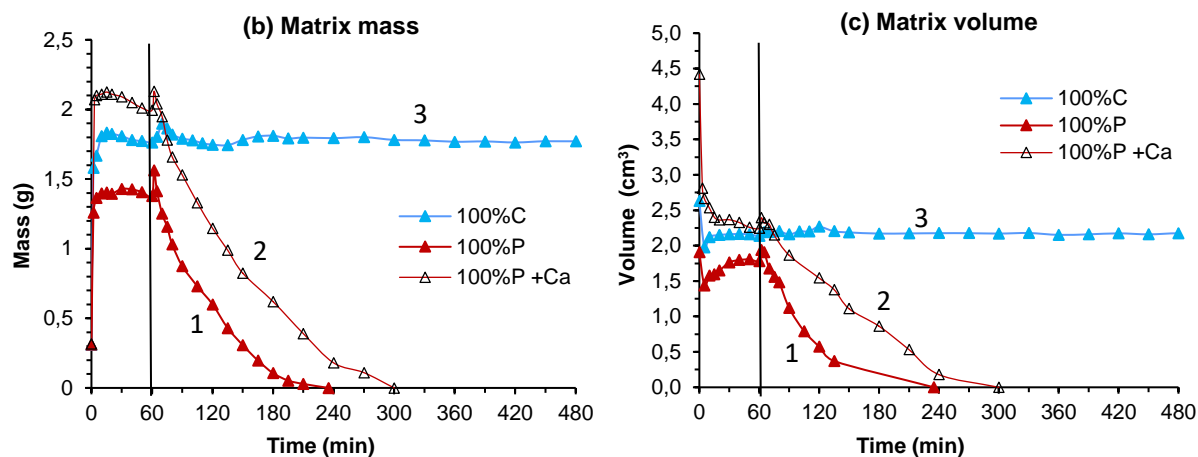


Figure 181. (a) Theophylline cumulative release (%) over time from the reference aerogels based on pectin without calcium (1), pectin with calcium (2), and cellulose (3) aerogels. All aerogels were made from 6% of polysaccharide.

(b) Matrix mass and (c) matrix volume evolution in time. Vertical line shows the change of release medium, from SGF (pH 1.0) the first hour to SIF (pH 6.8) the following hours, both at 37°C

Once immersed into the SGF (pH 1.0), all aerogels presented immediate shrinkage (around 20 to 30 vol%) (Figure 181 c) due to surface tension induced by the surrounding liquid, as also reported in Haimer et al for bacterial cellulose aerogels (Haimer et al., 2010). Simultaneously, pectin and cellulose aerogels showed an initial burst release phase due to the rapid dissolution of the theophylline particles on and close to the surface (Figure 181 a). As shown in Figure 181 (b), the liquid rapidly penetrated into the aerogels in the first minutes of experiment, which dramatically increased their mass by around +350% for pectin aerogels without calcium, +560% for pectin aerogel with calcium, and +480% for cellulose aerogels. The different mass increases between the pectin and cellulose aerogels is simply due to different matrix volume and density. As a reminder, aerogels density was around 0.11 g/cm<sup>3</sup> for cellulose aerogels, 0.15 g/cm<sup>3</sup> for pectin aerogels without calcium and 0.07 g/cm<sup>3</sup> with calcium. Thus, the volume of the pectin aerogel without calcium was 30% lower than that of cellulose matrix, which might have restricted the liquid content in the matrix. But with calcium, volume of pectin aerogel was 40 % higher than that of cellulose, leading to the highest mass increase.

During the first hour in SGF (pH 1.0), as no sign of matrix erosion was observed for both pectin and cellulose matrices, thus we assume that drug release was mainly governed by diffusion. It is interesting to see that even with different properties in terms of aeropectins structure (density, pore size) varying the calcium condition (with/without), pectin aerogels delivered more rapidly the drug than cellulose aerogel. As an illustration, both pectin aerogels (with and without calcium) released ~ 72-73% of total theophylline after one hour in SGF, while

only 60% was released from cellulose aerogel. The different release properties from pectin and cellulose aerogels are discussed below.

As expected, pectin and cellulose aerogels presented significantly different matrix stability in SIF medium (pH 6.8), as revealed by the evolution of matrix mass and volume with time (Figure 181b, c). After one hour when the aerogels were transferred from SGF media (pH 1.0) to SIF media (6.8), both pectin and cellulose aerogels showed a small peak of mass and volume increase, which is attributed to osmotic pressure difference between the interior and exterior of the matrix caused by the change of bath salinity and pH (Grignon & Scallan, 1980). Once in SIF (pH 6.8), pectin aerogels (with and without calcium) started to be dissolved, as revealed by the continuous drop in matrix volume and mass for three hours (Figure 181b, c). As previously detailed in Chapter V, matrix erosion of pectin aerogels is pH-dependent, as pectin is a hydrosoluble polyelectrolyte polymer. We showed that in SGF pectin matrix formed a resistant acidic gel inhibiting its erosion, while in SIF the dissolution of pectin matrix was promoted as media pH exceeded pectin  $pK_a$  (~3.0- 3.5), which in turn accelerated the release of the drug. On the contrary, cellulose aerogel matrix was found to be stable in SGF and in SIF, in correlation with its non-solubility in the releasing medium. Thus, no sign of erosion was observed and cellulose matrix volume and mass remained nearly constant for almost 11 hours. It has to be noted that we did not observe any swelling of the cellulose matrix. In correlation with their different matrix behaviour, drug release profile from pectin and cellulose aerogels matrices considerably differed (Figure 181 a). Full theophylline release from pectin aerogel without calcium occurred in 225 min, driven by fast matrix erosion (in 235 min), which is twice faster than the end of drug release from cellulose aerogel observed at 460 min. As we previously demonstrated (Chapter V), the addition of calcium to pectin aerogels delayed its matrix erosion thanks to network ionic crosslinking. Here, it can be seen that the complete matrix dissolution and full drug release from pectin aerogel with calcium were actually delayed by around 1 h as compared to the case without calcium.

As a direct consequence of their dissimilar solubility properties, 100% of total theophylline was released from pectin aerogels as the matrices were completely dissolved, while only 92% was released from cellulose aerogels which remained physically intact at the end of experiment. Thus, a portion of the drug remained entrapped within the matrix even after 30 h of immersion. We assume the existence of a closed porosity within cellulose aerogel which does not allow complete diffusion of theophylline from cellulose matrix. There can be several reasons of the presence of closed pores in cellulose aerogels: they can be formed either during coagulation step or during rewetting or both. The observed shrinkage of aerogels due to surface tension may lead to capillary contraction and pore enclosure, as reported in Refs. (Haimer et al., 2010; Job et al., 2005). Our assumption was supported by the density of wet cellulose aerogels, 0.82-0.85g/cm<sup>3</sup>, after 30 h of immersion into liquid media, which confirms the

presence of air within the system. Complete release of the drug from cellulose aerogel was only obtained by mechanical destruction of the matrix (grinding), followed by sonication treatment.

The fact that cellulose aerogel displayed a more controlled release behaviour than pectin aerogels results from polysaccharide intrinsic properties, physico-chemical and structural (density, sample thickness, pore size) aspects that differ for pectin and cellulose aerogels. Obviously, the solubility of pectin matrices in SIF (pH 6.8) explained the faster release from pectin aerogels than from cellulose aerogels. But in SGF (pH 1.0), pectin matrices erosion was inhibited and cannot explain why we also observed faster release from pectin aerogels (with and without calcium) than from cellulose aerogels. One of the reasons can be pectin partial degradation as solutions were kept at 60 °C for five days, as mentioned in Refs. (Fraeye et al., 2007; Krall & McFeeters, 1998; Renard & Thibault, 1996). As mentioned above (Section 2.1), we observed that the gelling abilities of pectin solutions and specific surface area of aerogels were altered by extended heating. The potential partial degradation of pectin used for the impregnation of cellulose (and thus used as a reference), is confirmed by the comparison of theophylline release from the reference aerogel with that from the standard one, the latter prepared as described in Chapter II (Figure 182). Reference pectin aerogels (solutions heated at 60 °C for 5 days) releases theophylline more than 2 hours quicker as compared to the standard pectin aerogels made from solution of the same concentration but without heating. This is true for both calcium cross-linked and not pectin aerogels.

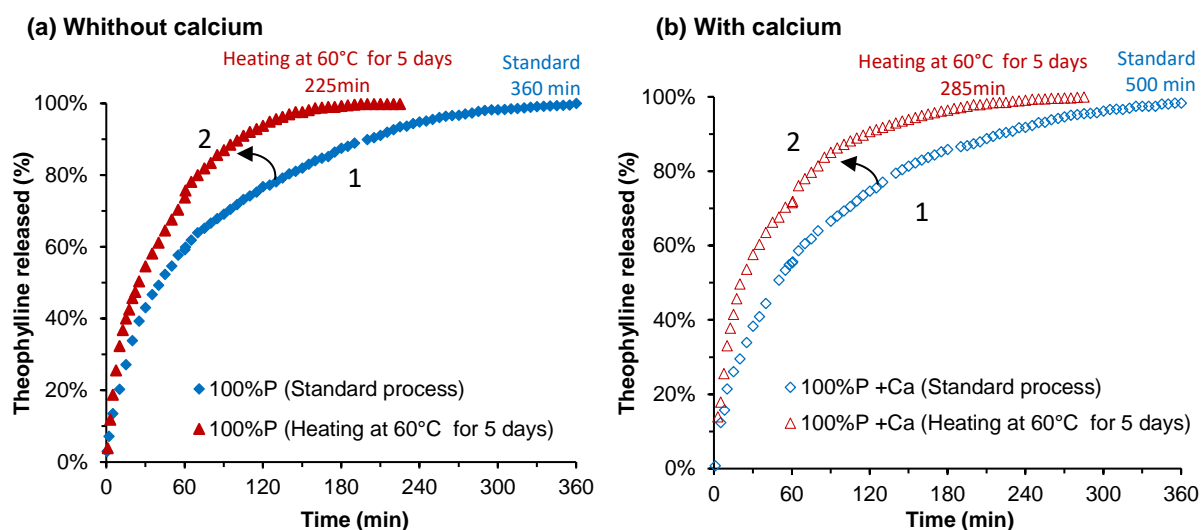


Figure 182. Comparison of theophylline release from aeropectins obtained from standard process route (1) and from process route used for making composite aerogels, heating step at 60 °C for 5 days (2). Aeropectins were made from 6 wt% of pectin P35 solution dissolved at pH 3.0 (a) without calcium or (b) with calcium. All aeropectins were loaded with theophylline at 3.4 g/L.

Korsmeyer-Peppas models were applied (Figure 183) to characterize the release mechanism of drug based on the value of  $n$  exponent. We obtained  $n$  values of 0.66 and 0.62 for both pectin aerogels without calcium and with calcium, respectively, and  $n$  around 0.43 for cellulose aerogel, with high fitting correlation to the data ( $R^2 > 0.99$ ). As expected from the previous results (Chapter V), the  $n$  values between  $0.45 < n < 0.89$  for pectin matrices indicated that drug release was due to an anomalous transport governed by the coupling of diffusion and polymer relaxation mechanisms (*i.e.* swelling and erosion). On the opposite, the  $n$  value close to 0.45 for cellulose aerogel is characteristic to Fickian diffusion of the drug within a stable matrix. In this case, polymer relaxation rate was either negligible or much more rapid as compared to diffusion rate, thus cellulose chains swelling did not interfere with drug diffusivity within the system.

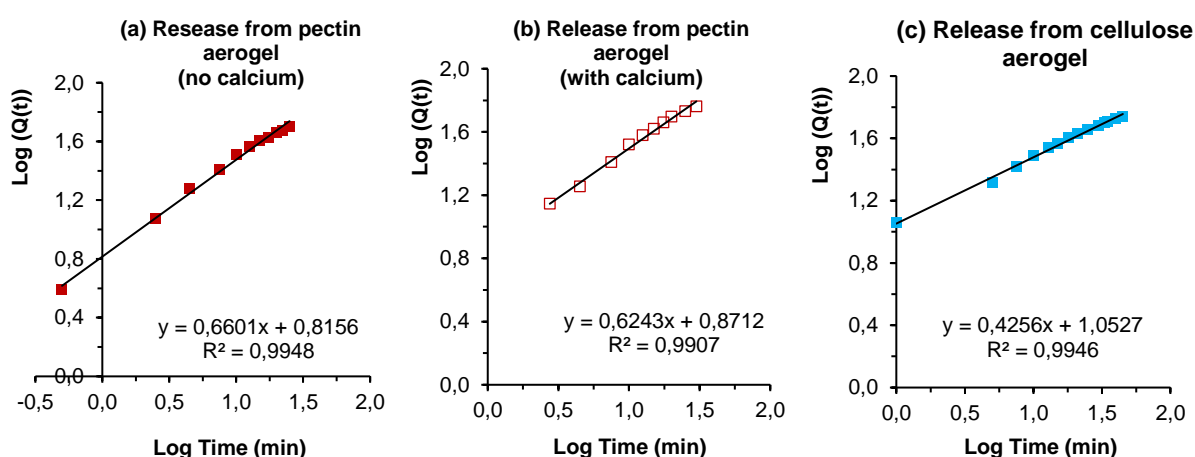


Figure 183. Experimental data and the corresponding fits (Korsmeyer-Peppas plot) for theophylline release from (a) pectin aerogel without calcium, (b) pectin aerogel with calcium or (c) cellulose aerogel. Aerogels were made from 6% of polysaccharide solutions.  $Q(t)$  is the cumulative release in time  $t$ . Solid lines are the plots of Korsmeyer-Peppas model according to Equation (A.12) in the Annex.

To conclude, as we expected, pectin and cellulose aerogels displayed distinct release properties. Cellulose aerogel was found to be a non-erodible matrix displaying diffusion-controlled drug release behaviour (Fickian release). Whereas drug release from pectin aerogels was strongly impacted by matrix erosion due to pectin solubility in the gastro-intestinal media (regardless the calcium conditions), consequently release of theophylline was due to anomalous transport involving polymer swelling and erosion (non-Fickian release). In addition, it clearly appeared that structural and release properties of pectin network were affected by prolonged heating during the impregnation process, as compared to the previously studied pectin aerogels in Chapter V.

The next intriguing question to answer is “what are the release properties of composite aerogels at different cellulose/pectin ratios?”.

### ▪ Influence of pectin/cellulose composition on release kinetics of theophylline from composite aerogels

In this section, we analyze and compare theophylline release from cellulose-pectin composite aerogels while varying the ratio of cellulose and pectin. The influence of composition on aerogels matrix behaviour (swelling and dissolution) and release properties in time is discussed. We first present the composites made without calcium, and then the case when calcium was added. For clarity, we refer to composite aerogels by their composition (%) using “C” for cellulose and “P” for pectin proportions.

#### ➤ *Cellulose-pectin composite aerogels without calcium*

The theophylline release curves from cellulose-pectin composite aerogels with different cellulose/pectin ratios are plotted in Figure 184. The evolution of matrices’ mass and volume with time of each composite are presented in Figure 185 (a) and (b), respectively. Pictures of composite aerogels are presented in Figure 186.

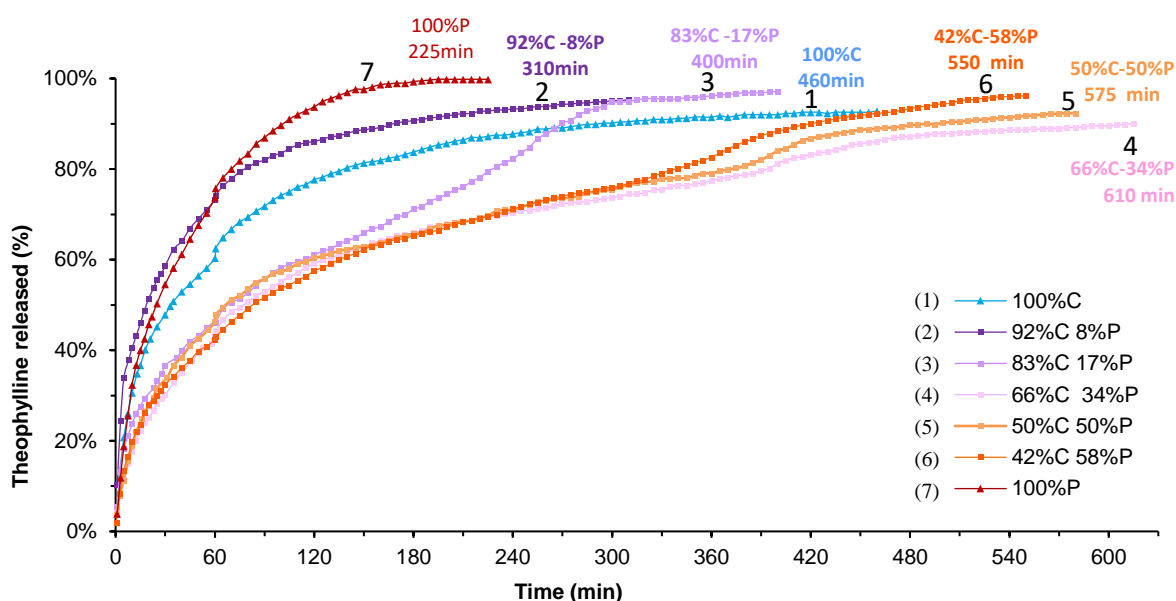


Figure 184. Theophylline cumulated release (%) in time from aerogels made from 6 wt% of polysaccharide solutions without calcium, at different cellulose / pectin ratio: 100%C (1), 92%C-8%P (2) 83%C-17%P (3), 66%C-34%P (4), 50%C-50%P (5) 42%C-58%P (6) and 100%P (7). Aerogels were loaded with theophylline at 3.4 g/L.

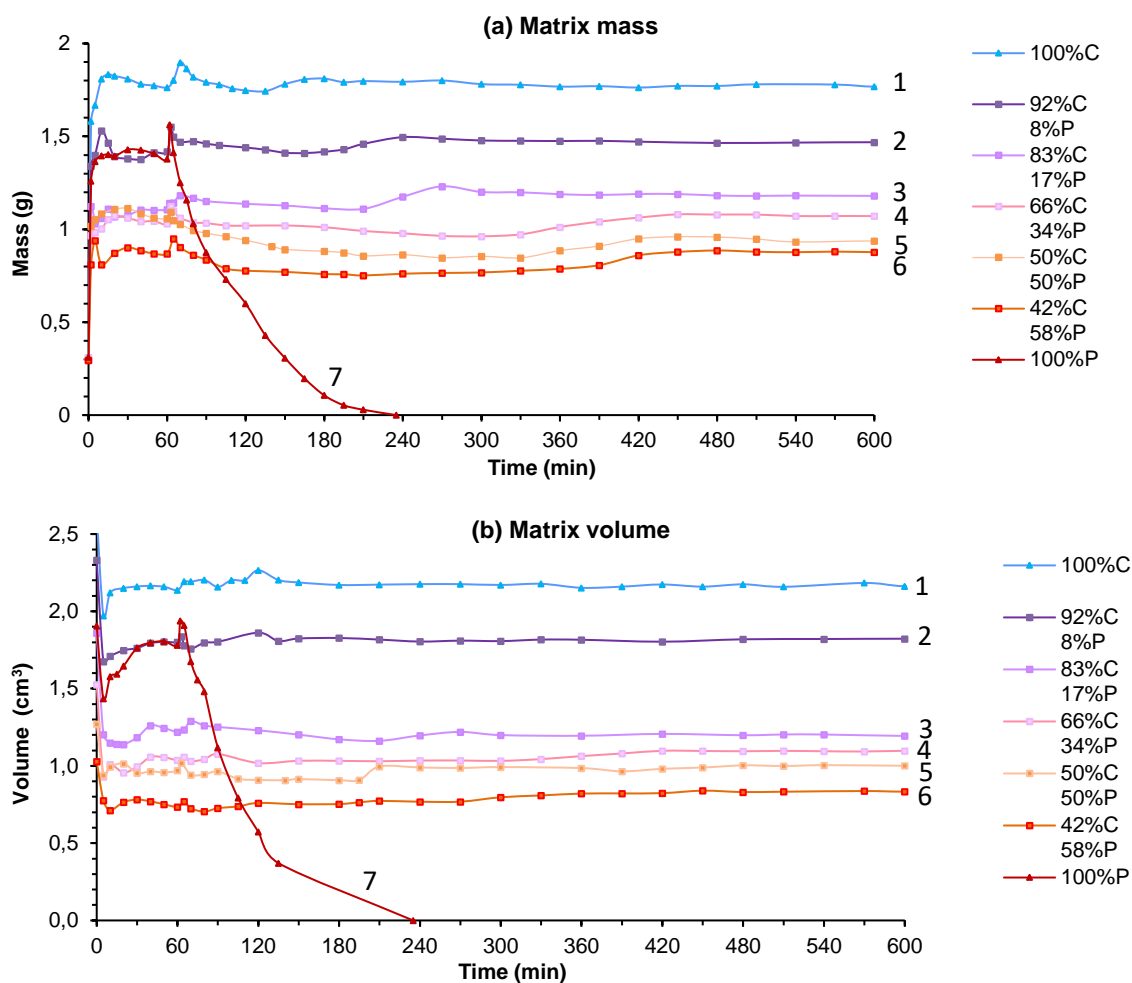


Figure 185. (a) Matrix mass (g) and (b) volume ( $\text{cm}^3$ ) evolution in time of aerogels made from 6 wt% of polysaccharides without calcium while varying cellulose / pectin ratio (noted “C” and “P”, respectively): 100%C (1), 92%C-8%P (2), 83%C-17%P (3), 66%C-34%P (4), 50%C-50%P (5), 42%C-58%P (6) and 100%P (7).



Figure 186. Pictures of cellulose-pectin composite aerogels after 90 minutes of dissolution testing (1 hour in SGF (pH 1.0) and 30 min in SIF (pH 6.8)). Composite aerogels were made without calcium. The scale is the same for all the pictures.

The difference in the initial mass and volume between the composite aerogels simply reflects the different level of volume shrinkage underwent during the preparation route

depending on the formulation. As it is shown in Figure 185 (a) and (b), all composite aerogels presented similar trend in mass and volume evolutions over time except neat pectin aerogel. During the first hour of experiment in SGF (pH 1.0), they all showed an initial “water filling stage”, followed by mass and volume “peaks” when transferred into SIF (pH 6.8) at 60 min of experiment. In correlation with the non-soluble cellulose matrix which did not swell or erode over time, the volume and mass of composites remained nearly constant after being immersed into SIF. We could notice a small increase of mass for all composites before the end of drug release, which may indicate the liquid filling pores in cellulose matrix (“empty” space left after complete dissolution of pectin). As the majority of sample weight increase was due to the liquid filling, pectin dissolution (which corresponds to a mass loss of around 0.050 to 0.170 g) was hard to notice.

However, we can visually follow the progressive disappearance of pectin within the composite with time, as the initially yellow-brown samples (typical of pectin) turned to completely white (cellulose) (see Figure 186). When samples were grinded to have access to the remaining theophylline after the experiment, we noted that composite samples were completely white inside, thus we could deduce that pectin was completely dissolved. Alike neat cellulose aerogels, we noticed that some air remained trapped into closed porosity of the composite (*i.e.* cellulose) matrices, as confirmed by a density around 0.8-0.9 g/cm<sup>3</sup> even after 11 h of immersion into liquid media. This was in correlation with incomplete release of theophylline; depending on the composite composition, from 90% to 97% of the total theophylline was released.

Contrary to similar mass and volume evolutions over time for all composites, a wide range of drug release profiles was obtained at different aerogel compositions, as it can be seen in Figure 184. All drug release from cellulose-pectin composites was significantly longer (from +38% to +170%) than that from neat pectin aerogels. As cellulose is non-soluble, the “stability” of the composite matrices in the release media obviously improved as compared to pectin aerogels. Thus, mixing pectin with cellulose might have slowed down pectin dissolution within the composites and prolonged the release for all cases. To be able to discriminate the different matrices as a function of their composition, we will discuss the results from another perspective. We analyze the composites starting from aerogels made of 100% cellulose and progressively increase the proportion of pectin in order to show the impact of pectin on the release properties of the composites. We will show that depending on pectin content, the release of theophylline from composite aerogels can be either promoted or slowed down as compared to neat cellulose aerogels.

As it can be seen for the composites made from 92% cellulose and 8% pectin, the replacement of a small proportion of cellulose by pectin led to acceleration of release, with end of release in around 310 min from 92%C-8%P composite aerogel versus 460 min for neat

cellulose aerogel (Figure 187). Logically, the partial substitution of cellulose (not soluble in the releasing media) by pectin (hydrosoluble especially in SIF (pH 6.8)), might have led to a less “stable” matrix than neat cellulose. Besides, as pectin network was based on 1.3 wt% pectin solution, we suppose that such small pectin content has been rapidly dissolved, leaving behind the “empty space” in cellulose matrix which promoted mass transports phenomena. This “accelerating effect” (as compared to cellulose aerogel) on the release due to the presence of pectin was also found when doubling the pectin proportion to make 83%cellulose-17% pectin composite aerogels. As it can be seen in Figure 187, drug release from 83%cellulose-17% pectin occurred in 410 min, which is still faster than from neat cellulose (460 min), but surprisingly longer than from 92%cellulos-8%pectin composite with smaller pectin proportion (310 min).

By increasing pectin proportion within the composite, the total matrix certainly became more soluble, but it also led to the increase the composite density as compared to neat cellulose aerogels. Indeed, while composite aerogels with the smallest pectin proportion (92%C-8%P) presented density ( $\sim 0.12 \text{ g/cm}^3$ ) similar to that of neat cellulose aerogels, the 83%C-17%P composite aerogels displayed higher density (+30%),  $0.145 \text{ g/cm}^3$ . This explains why even with a higher solubility (higher pectin proportion), the release of the drug from 83%C-17%P was actually longer than from 92%C-8%P composite aerogel.

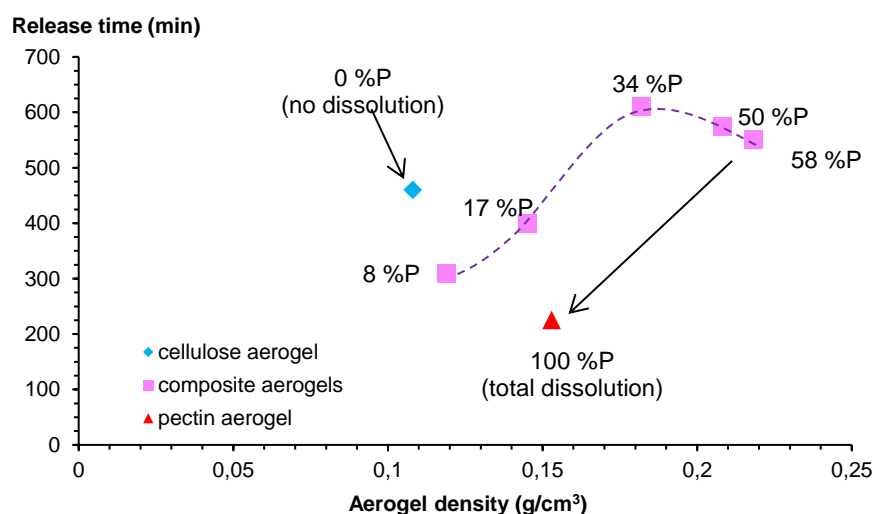


Figure 187. Release time needed to reach the plateau (equilibrium) in drug release experiment (data extracted from Figure 184) as a function of the aerogel density, no calcium added. Depending on sample composition (neat pectin, neat cellulose or pectin-cellulose composite aerogels), this time corresponds to 92% - 100% of total theophylline released. Dashed line is given to guide the eye.

This observation was also found to be valid when increasing even more pectin content (Figure 187): 66%C-34%P, 50%C-50%P and 42%C-58%P composite aerogels were respectively +70%, +93% and +100% denser than neat cellulose aerogels, and the release of the drug was +33%, +26% and +20% longer, respectively, than from neat cellulose aerogels.

As we described in Section 1.1. of this chapter, the increase of pectin content in cellulose matrix leads to density increase (Figure 173) and also denser morphology (Figure 178) which decreased liquid and drug diffusivity within the system. The results obtained show that there is a balance between the acceleration of release due to pectin dissolution and slowing down of release due to the increase of aerogel density. Composite aerogels based on interpenetrated network cellulose-pectin do not follow “mixing rule” in what concerns the kinetics and total release time of theophylline.

The release results were analyzed by several mathematical models. As the matrices were complex and partially erodible, most of the models used previously did not fit release kinetics from composites. The best model fittings to data were obtained by plotting Korsmeyer-Peppas model (Figure 188 and Table 17) and Peppas-Sahlin models (Figure 189 and Figure 190) with high correlation ( $R^2 \geq 0.98$ ). As expected, the release from the composite aerogels with low pectin content  $\leq 17\%$  (92%C-8%P and 83%C-17%P composites) were governed by Fickian diffusion as revealed by  $n$  exponent values close to 0.45 using Korsmeyer-Peppas model with high correlation to the data ( $R^2 \geq 0.994$ ). For higher pectin contents (66%C-34%P, 50%C-50%P and 42%C-58%P composites), the  $n$  exponents values between 0.45 and 0.89 suggest that drug release was due to anomalous transport, involving both diffusion and polymer relaxation. It can be noted that the value of  $n$  exponent continuously increases with pectin fraction.

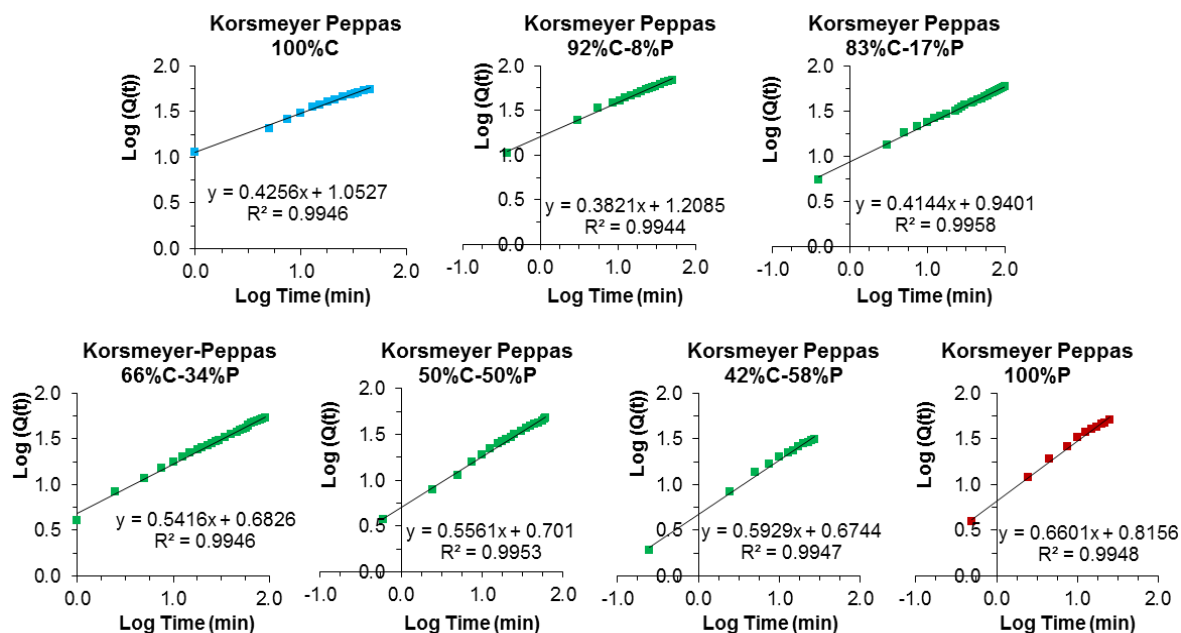


Figure 188. Korsmeyer-Peppas model for the first 60% release data of theophylline release from composite aerogels made from 6 wt% of polysaccharides without calcium while varying cellulose / pectin ratio (noted “C” and “P”, respectively): 100%C, 92%C-8%, 83%C-17%P, 66%C-34%P, 50%C-50%P, 42%C-58%P and 100%P. Solid lines are the theoretical plots.

Table 17. Korsmeyer-Peppas parameters of theophylline release experiments from composite aerogels made from 6 wt% of polysaccharides without calcium while varying the cellulose / pectin ratio: 100%C, 92%C-8%, 83%C-17%P, 66%C-34%P, 50%C-50%P, 42%C-58%P and 100%P.

Ratio (%) Cellulose / Pectin	100%C	92%C 8%P	83%C 17%P	66%C 34%P	50%C 50%P	42%C 58%P	100%P
<i>n</i> exponent	0.43	0.38	0.41	0.54	0.56	0.59	0.66
<b>R<sup>2</sup></b>	0.995	0.994	0.996	0.995	0.995	0.995	0.995

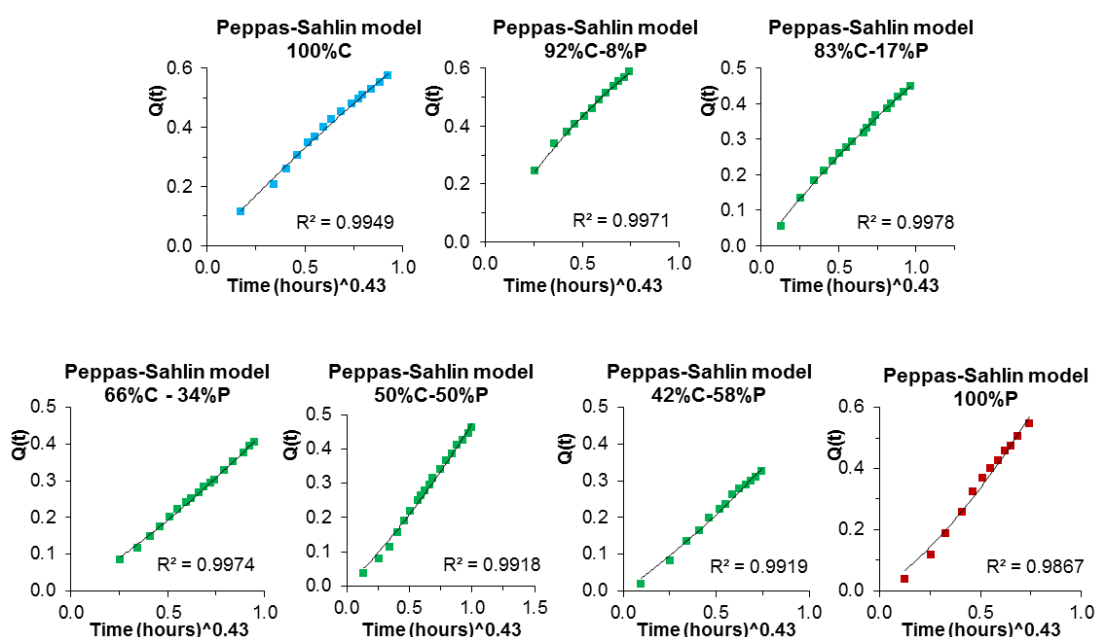


Figure 189. Peppas-Sahlin model for the first 60% release data of theophylline release from composite aerogels made from 6 wt% of polysaccharides without calcium while varying the cellulose / pectin ratio: 100%C, 92%C-8%, 83%C-17%P, 66%C-34%P, 50%C-50%P, 42%C-58%P and 100%P, using Fickian diffusional exponent *m* of 0.430. Solid lines are the theoretical plots.

Table 18. Peppas-Sahlin parameters using Fickian diffusional exponent *m* of 0.430 of theophylline release experiments from composite aerogels made from 6 wt% of polysaccharides without calcium while varying the cellulose / pectin ratio: 100%C, 92%C-8%, 83%C-17%P, 66%C-34%P, 42%C-58%P and 100%P.

<b>Ratio (%) Cellulose / Pectin</b>	<b>100%C</b>	<b>92%C 8%P</b>	<b>83%C 17%P</b>	<b>66%C 34%P</b>	<b>50%C 50%P</b>	<b>42%C 58%P</b>	<b>100%P</b>
<b>Fickian coefficient <math>K_F</math> (<math>h^{-0.43}</math>)</b>	0.700	1.03	0.547	0.342	0.363	0.352	0.480
<b>Relaxational coefficient <math>K_R</math> (<math>h^{-0.86}</math>)</b>	< 0	< 0	< 0	0.089	0.110	0.129	0.386
<b><math>R^2</math></b>	0.995	0.997	0.998	0.997	0.992	0.992	0.987

We thus demonstrated that the ratio of polysaccharides in the composite aerogels actually drive the main physical mechanisms involved in the release of the drug. Release behavior from composites is more “cellulose-like” (diffusion-controlled) if cellulose is strongly predominant, and turned into “pectin-like” (diffusion erosion-controlled) once pectin content exceeds 34% within the composite.

Peppas-Sahlin model was applied to highlight the differences in the coupling of diffusion and matrix erosion in composite aerogels of various compositions. The estimations of Peppas-Sahlin parameters and the model plots are presented in Figure 189 and Table 18, respectively, with high correlation to the data ( $R^2 \geq 0.987$ ). The calculation of the Fickian contribution to the release over time based on the estimated parameters is plotted Figure 190.

As it was found with Korsmeyer-Peppas plot, the value for the composites with low pectin content (92%C-8%P and 83%C-17%P composites) and neat cellulose aerogels present negative  $K_R$  coefficient, meaning that relaxational phenomena (swelling or matrix erosion) had negligible or no effect on the release as compared to diffusional phenomena. Thus, in low pectin-content matrices theophylline was mainly released by diffusion mechanism. However, for pectin content  $\geq 34\%$ , diffusion and erosion co-exist. As presented in Figure 190, we found logical that the values of  $K_R$  coefficient increase (from 0.089 to 0.129  $h^{-0.86}$ ) with pectin content (from 34% to 58%), revealing the increase of erosion contribution to the drug release as the matrices are becoming more erodible. As shown in Figure 21, the release of the drug from composites with high pectin content ( $\geq 34\%$ ) start with a main diffusion-controlled phase at the beginning of experiment, followed by a diffusion-erosion controlled phase until the end of the release.

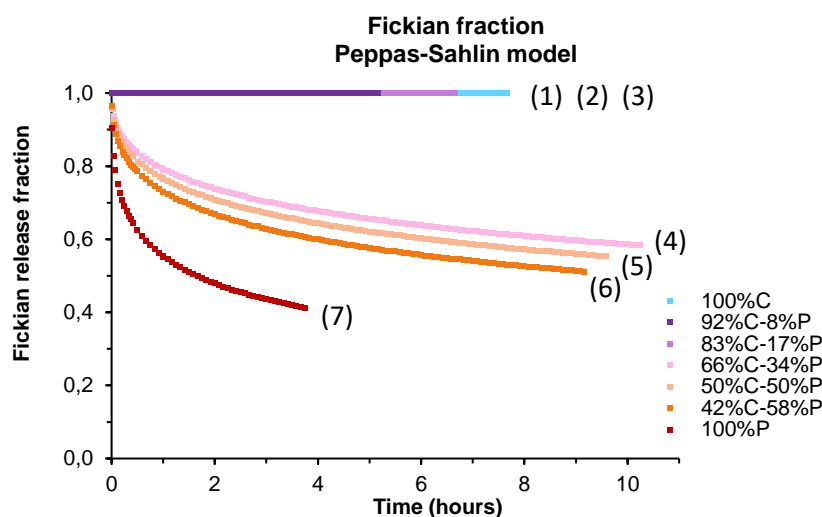


Figure 190. Fraction of Fickian release according to Peppas-Sahlin model using Fickian diffusional exponent  $m$  of 0.430, for the first 60% of released drug from composite aerogels made from 6 wt% of polysaccharides aerogels without calcium while varying the cellulose / pectin ratio: 100%C (1), 92%C-8%P (2), 83%C-17%P (3), 66%C-34%P (4), 50%C-50%P (5), 42%C-58%P (6) and 100%P (7).

### ➤ Cellulose-pectin composite aerogels with calcium

In this section the release of theophylline from cellulose-pectin aerogels and matrices' mass and volume over time were studied in which pectin was cross-linked with calcium (Figure 191 and Figure 192, respectively). Few release profiles for composite aerogels with non-cross-linked pectin (open symbols) are also shown for comparison.

As shown in Figure 191, we observed that the addition of calcium changed the theophylline release profile of cellulose-pectin composite aerogels. When calcium was added to cellulose-pectin composites (66%C-34%P<sub>Ca</sub> and 42%C-58%P<sub>Ca</sub> samples), composites showed a more controlled-release behaviour and a significant increase of the time needed to reach the plateau (release equilibrium)<sup>3</sup> was observed compared to composites without calcium (compare curve 2 with 3 and 4 with 5).

<sup>3</sup> In some cases, a small portion of the drug remained "entrapped" into the matrix, and the equilibrium was not reached at 100% of theophylline released.

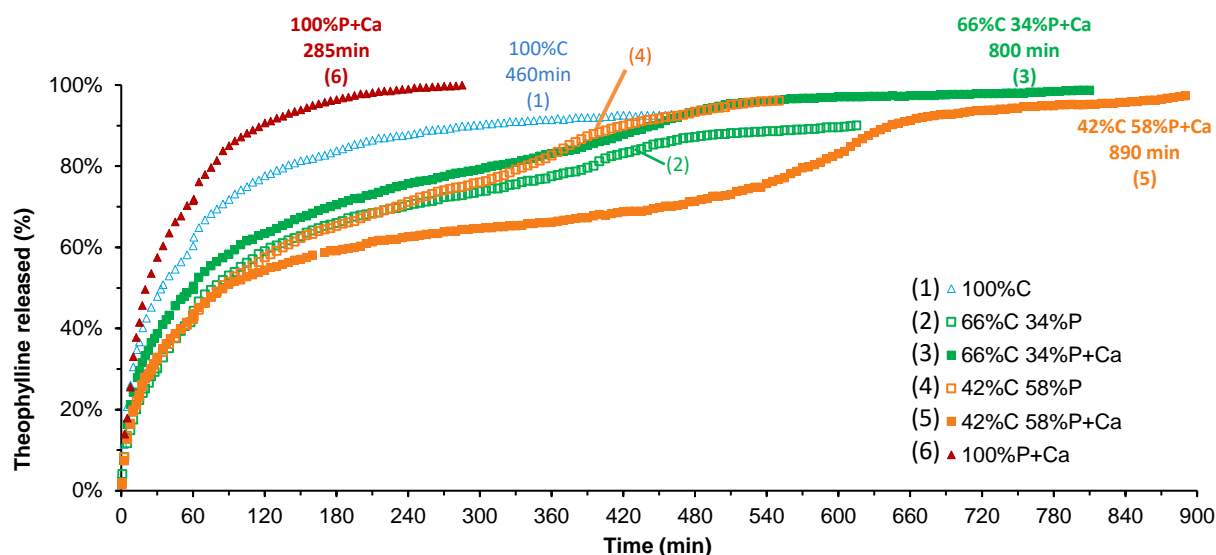


Figure 191. Theophylline release over time (%) from aerogels made from 6 wt% of solutions (pectin cross-linked with calcium) while varying the cellulose / pectin ratio (filled symbols correspond to pectin cross-linked with calcium and open symbols to pectin without calcium): 100%C (1), 66%C-34%P without calcium (2) and with calcium (3), 42%C-58%P without calcium (4) and with calcium (5) and 100%P with calcium (6). Aerogels were loaded with theophylline at 3.4g/L.

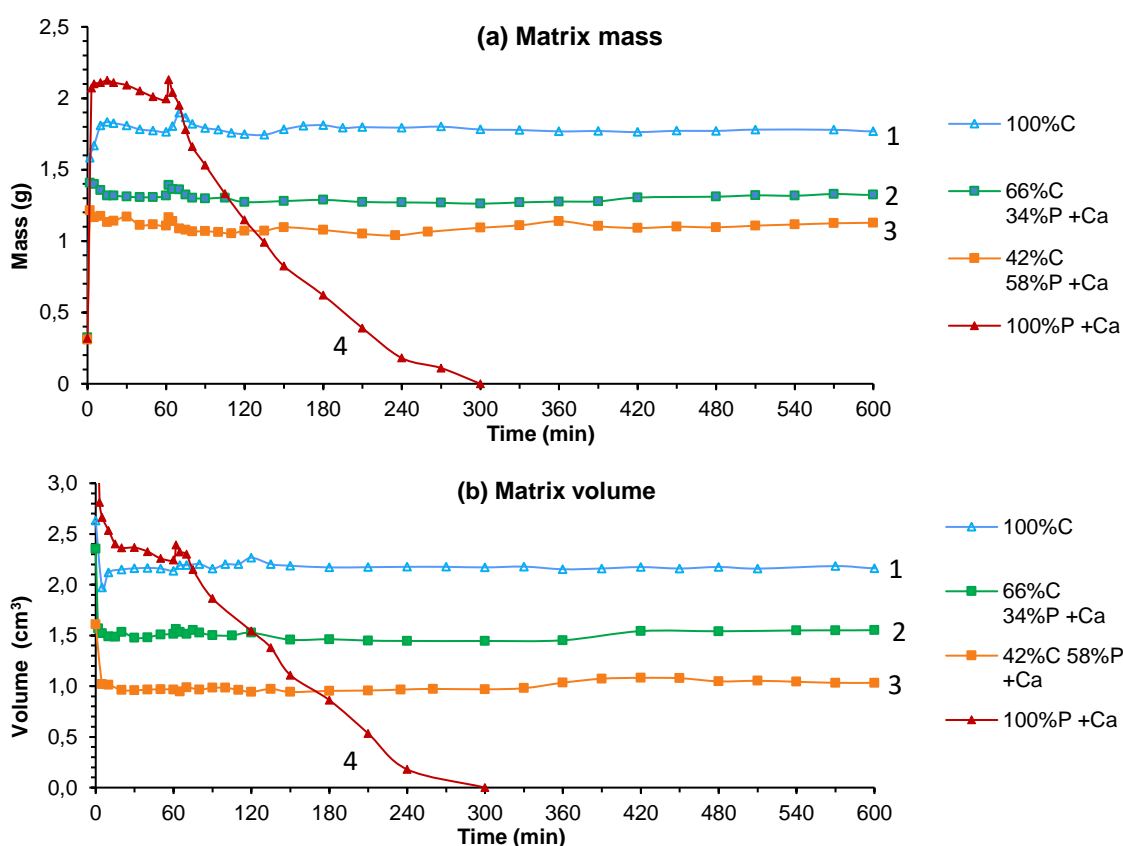


Figure 192. (a) Matrix mass (g) and (b) volume (cm<sup>3</sup>) evolution in time of aerogels made from 6 wt% of polysaccharides with calcium while varying the cellulose / pectin ratio: 100%C (1),

66%C-34%P +Ca (2), 42%C-58%P +Ca (3) and 100%P +Ca (4). Aerogels were loaded with theophylline at 3.4g/L.

Indeed, drug release from 66%C-34%P<sub>Ca</sub> composite was prolonged up to 800 min when calcium was added versus 610 minutes without calcium, which correspond to a 30% longer release of drug. This effect of calcium was even more pronounced when the pectin content was higher; drug release from 42%C-58%P<sub>Ca</sub> composite aerogel was prolonged up to 890 min instead of 550 min without calcium, which corresponds to +60% longer drug release.

As stated above for neat pectin aerogels with calcium (Figure 181) and discussed in detail in Chapter V, we already demonstrated that pectin cross-linked with calcium led to a stronger and less soluble network, inhibiting polymer dissolution which delays the full release of the drug. Here, we similarly assume that ionic crosslinking of pectin network hindered dissolution within the composite. As pectin fraction in the composites was dissolved more slowly, the cellulose-pectin matrix remained stable longer and better prevented liquid and theophylline diffusion, which finally slowed down the release of drug. The increase of the release time from composites with calcium (from +30% to +60% as compared to without calcium) was actually dependent on pectin content in the composite (as ionic crosslinking only concerns pectin portion of the composite).

As it can be observed in Figure 191 on which two examples of release from composites with non-crosslinked pectin are also shown, theophylline release curves from pectin-cellulose composites (with or without calcium) displayed an “S-shape” (sigmoidal curve), distinct from the typical asymptotic curves obtained from neat cellulose and neat pectin aerogels. The “S shape” appeared at the end of the drug release and is even more pronounced with the increase of pectin fraction within the composite. This change of slope is a sign of an acceleration of the release rate at the end of the experiment and reflects either an increase in solvent velocity within the system and/or a sudden increase of drug diffusivity. In our case, it can be explained by the complete dissolution of the pectin fraction of the composite matrix which certainly boosted all the diffusional phenomena of the drug and liquid within the system.

The evolution of matrix mass and volume of the composites over time in Figure 192 shows the same tendency as composites without calcium, except the fact than matrices with calcium had higher volume (and mass increase) due to lower shrinkage during aerogel preparation compared to the case without calcium. As composite aerogels without calcium, matrices mass and volume with calcium were nearly constant after the initial liquid filling step and during the first 60 min.

The prediction given by the mathematical models was consistent with our interpretation of release data. Using Korsmeyer-Peppas plot with high correlation to the data ( $R^2 > 0.995$ ) (Figure 193) we obtained smaller  $n$  exponent values when calcium was added to composites.

For 66%C-34%P<sub>Ca</sub> composite aerogels,  $n$  value decreased from 0.54 (anomalous transport case) without calcium to 0.44 (Fickian diffusion case) with calcium. In the same way,  $n$  value obtained from release data from 42%C-58%P<sub>Ca</sub> composite aerogels decreased from 0.59 (anomalous transport case) without calcium, to 0.47 (Fickian diffusion case) with calcium. This suggests that the release of theophylline from composites, which was originally governed by the coupling diffusion and matrix erosion, turned to be mainly diffusion-controlled when calcium was added due to the higher pectin resistance to dissolution.

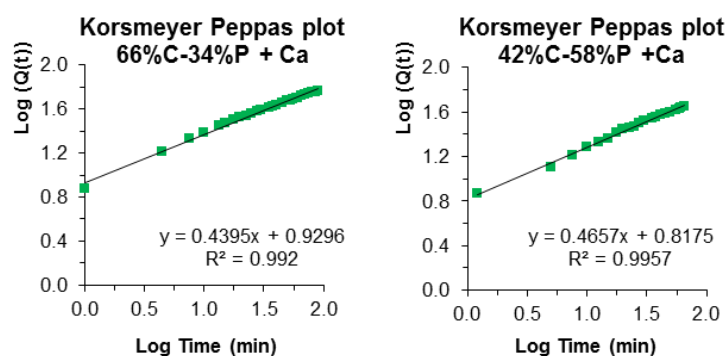


Figure 193. Example of Korsmeyer-Peppas model for the first 60% release data of theophylline release from composite aerogels made from 6 wt% of polysaccharides with calcium while varying the cellulose / pectin ratio: 66%C-34%P and 42%C-58%P. Solid lines are the model plots.

Peppas-Sahlin model was applied with good data fitting ( $R^2 \geq 0.984$ ) (Table 19) and the calculation of the Fickian contribution to the release over time based on the estimated parameters is plotted in Figure 194. In line with Korsmeyer-Peppas model, it can be clearly seen that the relaxational coefficient coefficients  $K_R$  were drastically reduced when calcium was added, as pectin dissolution within the composite was prevented due to ionic crosslinking (lower pectin solubility). As a consequence, pectin-cellulose composites with calcium (66%C-34%P<sub>Ca</sub> and 42%C-58%P<sub>Ca</sub>) even exhibit relaxational coefficients close to or equal to 0 (Table 19), reflecting a very low contribution of erosion phenomena to the release and the predominance of Fickian diffusion phenomena in the release from more stable composite matrices.

Table 19. Peppas-Sahlin parameters using Fickian diffusional exponent  $m$  of 0.430 of theophylline release experiments from composite aerogels made from 6 wt% of polysaccharides with and without calcium while varying cellulose / pectin ratio: 100%C, 66%C-34%P without and with calcium, 42%C-58%P without and with calcium and 100%P without and with calcium.

Ratio (%) Cellulose / Pectin	100%C	66%C 34%P	66%C 34%P +Ca	42%C 58%P	42%C 58%P +Ca	100%P	100%P +Ca

<b>Fickian coefficient</b> $K_F (h^{-0.43})$	0.700	0.342	0.5528	0.352	0.423	0.480	0.579
<b>Relaxational coefficient</b> $K_R (h^{-0.86})$	< 0	0.089	< 0	0.129	0.0115	0.386	0.278
<b>R<sup>2</sup></b>	0.995	0.997	0.998	0.992	0.996	0.987	0.984

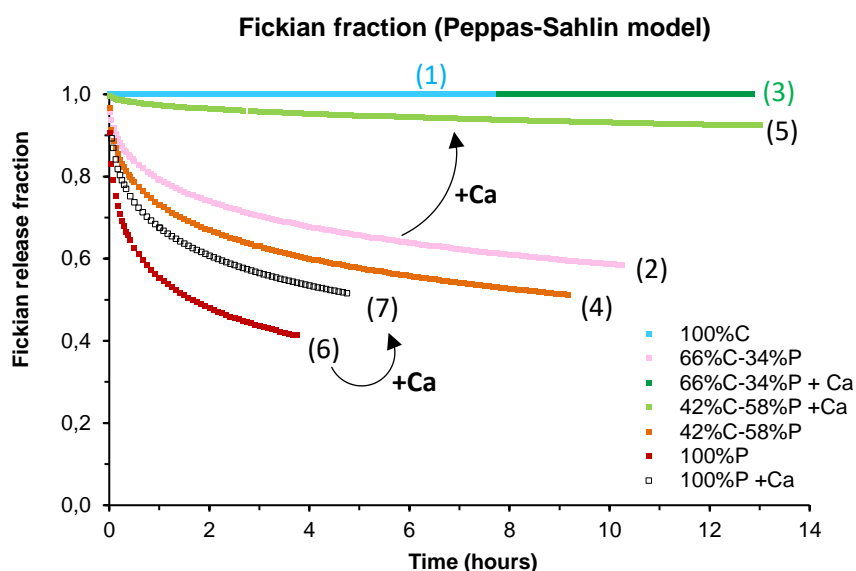


Figure 194. Fickian release fraction according to Peppas-Sahlin model using Fickian diffusional exponent  $m$  of 0.430, for the first 60% of released drug from composite aerogels made from 6 wt% of polysaccharides aerogels with and without calcium, while varying the cellulose / pectin ratio: 100%C (1), 66%C-34%P without calcium (2) and with calcium (3), 42%C-58%P without calcium (4) and with calcium (5), 100%P without (6) and with calcium (7).

### 1.3. Conclusions on pectin-cellulose composite aerogels

Composite cellulose-pectin aerogels are new material produced by making interpenetrated network of pectin and cellulose. Used as complex matrices for drug delivery, their physical and release properties were characterized and correlated to their composition, and also compared to neat cellulose and pectin reference aerogels. We found that by varying cellulose and pectin fractions, it was possible to vary their contributions to the structural and release properties of the composite aerogels.

We demonstrated that depending on the fraction of pectin in the composite aerogels, the release can be either significantly accelerated or slowed down as compared to the case of neat

cellulose aerogels. The presence of pectin in the composite aerogel had two opposite impacts on the physico-chemical characteristics of the composites, which in turn influenced drug release properties. On the one hand, the addition of pectin increases matrix “instability” (in the sense of dissolution in the release media) which is promoting drug release. On the other hand, the presence of pectin increased composite density due to volume shrinkage which slowed down drug release. Depending on pectin fraction, it is either the physico-chemical (*i.e.* matrix dissolution) or the structural (high density) impact on the release that outweighed one the other. To demonstrate this phenomenon, the time needed to reach the equilibrium of drug release for composite aerogels is plotted as a function of their composition in Figure 195.

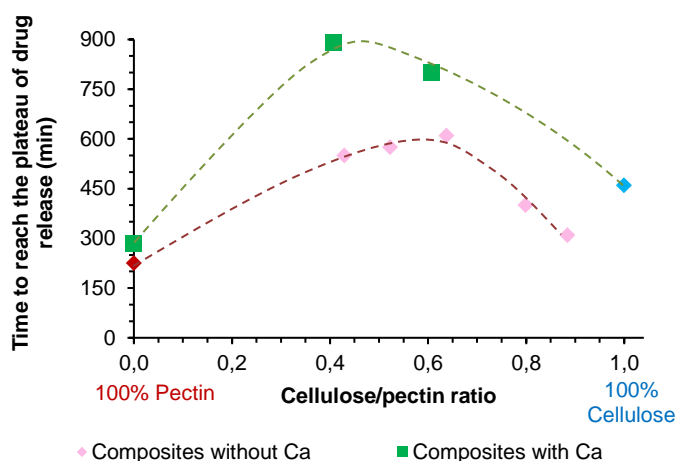


Figure 195. Release time needed to reach the plateau (equilibrium) in drug release experiment (data extracted from Figure 184 and Figure 191). Depending on sample composition, this time corresponds to 92% - 100% of total theophylline released. Dashed lines are given to guide the eye.

We showed that pectin ionic gelation within cellulose matrix drastically increased release time and also changed the drug release profile because of different physical mechanisms involved in the release. Even if the addition of calcium only impacted the pectin part of the composite, it finally changed the properties of the overall composite.

Thanks to their different intrinsic properties, both cellulose and pectin parts of the composites contributed to obtain drug extended-release behaviour.

- Cellulose greatly improved the stability of the matrix due to its non-solubility in the release media, which also slowed down pectin dissolution.
- Cellulose aerogel presents larger pores than pectin aerogels which tends to facilitate diffusional phenomena.

- The addition of pectin increased the density of the composites and significantly decreased pore size (especially at high pectin content), which in turn hindered the diffusion of both liquid and drug through the system.
- Pectin also increased drug loading efficiency and loading capacity probably due to the higher matrix density and maybe higher chemical affinity with theophylline.
- Pectin also contributed to chemical “instability” of the matrix due to its solubility in aqueous medium, even if the latter could be attenuated by ionic cross-linking with calcium.

Based on the results and trends obtained, we can now provide the “recipes” on how to control and tune different contributions of the two dissimilar polysaccharides on the structural and release properties of composite aerogels.

## 2. Pectin-Silica composite aerogels

The goal of this section is to prepare and characterize pectin-silica composite aerogels and study the kinetics of theophylline release from these samples.

- The first part of this section presents the synthesis of silica aerogels by sol-gel method using either polyethoxydisiloxane (PEDS) or tetraethylorthosilicate (TEOS) as two sources of silica. Then, we describe the process route to produce pectin-silica composite aerogels by silica sol impregnation within pectin aerogel precursor (wet pectin matrix after coagulation).
- In a second part, we present the structural and morphological characterization of neat silica and neat pectin aerogels, used as “reference”. Then the structural properties of pectin-silica aerogels are studied and discussed in correlation with the type of silica-precursor (TEOS vs PEDS) and with the pectin/silica composition.
- Finally, the release theophylline from pectin, silica and pectin-silica aerogels are investigated, and correlated to the matrices’ composition and structural aspects.

## 2.1. Production and characterization of pectin-silica composites

### 2.1.1. Materials

In order to produce silica aerogels and pectin-silica composite aerogels, we synthesized silica alcogels by sol-gel polymerization of two different silica sols:

- Tetraethylorthosilicate (TEOS) (98 wt%).
- Polyethoxydisiloxane (PEDS, also called P75E20 by the provider (Enersens), 20 w/w% SiO<sub>2</sub> content in ethanol) was used as pre-polymerized oligomers of TEOS.

Solutions of hydrochloric acid (HCl) (32%) and of ammonium hydroxide (NH<sub>4</sub>OH) (30wt%) were used as catalysts for hydrolysis and condensation reactions, respectively. TEOS and PEDS were diluted with ethanol when needed.

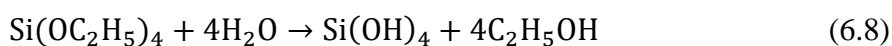
### 2.1.2. Sol-gel synthesis of neat silica aerogels using either TEOS or PEDS

#### ▪ **Production of silica aerogels made from TEOS**

TEOS gels were synthesized by sol-gel polymerization process of tetraethylorthosilicate (Si(OC<sub>2</sub>H<sub>5</sub>)<sub>4</sub>) using ethanol and water. As it was presented in the Chapter I (Section 2.2.1), the process is divided into two steps; the first is acid-catalyzed hydrolysis which leads to the production of reactive groups silanol (SiOH) with hydroxyl function bound to silicon. This step is then followed by acid or base-catalyzed polycondensation reactions leading to the creation of silicon-oxygen-silicon bridges and further polymerization. Depending on the chemistry of the reaction solution, gelation may happen rapidly, or may require additional catalyst, water, temperature or time.

In this study, we used HCl and NH<sub>4</sub>OH as hydrolysis and condensation catalysts, respectively, to synthesize TEOS alcogel by the sol-gel polymerization. The synthesis route was inspired from the mix of several works on TEOS aerogels (Assifaoui, Bouyer, Chambin, & Cayot, 2013; Błaszczński, Śłosarczyk, & Morawski, 2013; Błaszczński et al., 2013; Buckley & Greenblatt, 1994; Laudise & Johnson, 1986).

The hydrolysis of TEOS can be represented as follows:



In order to promote the reaction to the right, water was added in excess as compared to stoichiometric ratio of Equation (6.8). For the acid hydrolysis step, TEOS, water and ethanol were mixed together at the molar ratio 1/4/6 (TEOS/Ethanol/Water) in order to produce TEOS solution at  $0.4 \text{ mol.L}^{-1}$ , which corresponds to 8 wt% of TEOS (Assifaoui et al., 2013). Ethanol and water were first mixed and TEOS was added while stirring. Small quantity of HCl (32 wt%) was added to reduce pH to around 2. The two solutions were non-miscible at the beginning, but mixed up after 10 minutes of stirring. The sol was let under stirring for 2 h of hydrolysis time in ambient conditions. To induce polymerization by condensation reaction, small quantity of  $\text{NH}_4\text{OH}$  catalyst solution was added to obtain 0.06 % wt of  $\text{NH}_4\text{OH}$  in the mix. After 5 minutes of homogenization by stirring, the sol was poured into molds. We noticed an increase of the viscosity of the sol after few hours at room temperature. Samples were let gelled and aged for 7 days at room conditions, and were intensively washed with ethanol (Laudise & Johnson, 1986). Then, TEOS-alcogels were loaded with theophylline by impregnation at 3.4 g/L in ethanol for 2 weeks, and finally supercritically dried using  $\text{CO}_2$ .

#### ▪ **Production of silica aerogels made from PEDS**

As PEDS was already hydrolyzed precursors (silica-sol), they were are therefore very prone to acid- or base-catalysed condensation reactions as described by (Malfait et al., 2015; Pajonk et al., 1995; Strøm et al., 2007). Thus, we directly mixed 8 wt% of PEDS in ethanol and basic catalyst solution ( $\text{NH}_4\text{OH}$ , 0.6 wt% in ethanol:water = 96:4 w/w) during 5 minutes before being poured the silica-sol into molds, as described in (Demilecamps, Beauger, Hildenbrand, Rigacci, & Budtova, 2015). Due to PEDS pre-hydrolysis, we noticed an increase of sol viscosity in less than 10 minutes, and transition to the gel state occurred (via tilting test) in less than three hours at room temperature. Samples were let gelled and aged for 3 days at room conditions, and were intensively washed with ethanol. Then, PEDS-alcogels were loaded with theophylline by impregnation at 3.4 g/L in ethanol for 2 weeks, and finally supercritically dried using  $\text{CO}_2$ .

For the sake of simplification, silica aerogel produced using PEDS (*resp.* TEOS) as silica-precursors will be called “PEDS aerogels” (*resp.* TEOS aerogels).

#### 1.1.1. Production of pectin-silica composite aerogels

#### ▪ **Process route of pectin-silica composite aerogels**

The production of pectin-silica composites consists of impregnation and gelation of silica-precursors within a pre-existing “wet” coagulated pectin matrix, as illustrated in Figure 196.

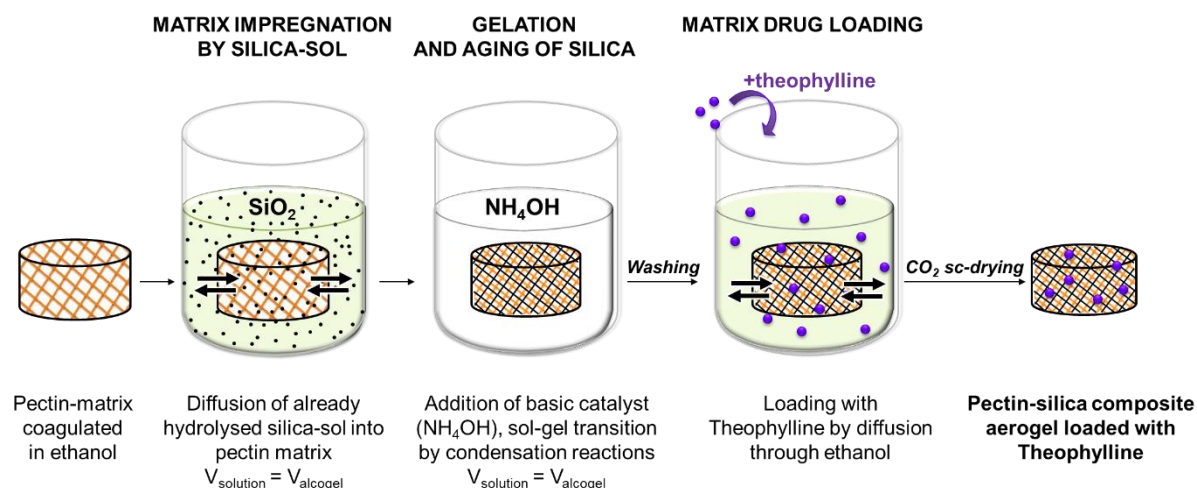


Figure 196. Schematic representation of the fabrication process of pectin-silica composite aerogels (silica here is PEDS, for TEOS the process is the same except catalyst) loaded with theophylline.

Pectin matrices were made from 6 wt% of pectin P35 dissolved at pH 3.0 or at pH 2.0 with  $R(\text{Ca})$  varying from 0 (no calcium) to 0.6, and were then coagulated in ethanol as described in Chapter II. The concentration of silica and catalyst were calculated taking into account the volume of ethanol inside pectin “wet” matrix. Coagulated pectin in ethanol was immersed into twice its own volume of 16 wt% of pre-hydrolyzed silica sol in order to obtain 8 wt% silica after diffusion into pectin, supposing a homogeneous distribution of silica all over the system (which will be checked further).

Pectin samples were let to be impregnated by silica sol by diffusion for 15 days in ambient conditions. Pectin-silica samples were then extracted and placed in twice their volume of basic catalyst solution ( $\text{NH}_4\text{OH}$ , 1.3 wt% in ethanol:water = 96:4 w/w) (Demilecamps et al., 2015), resulting in *in situ* silica gelation. Samples were let gelled and aged for 3 days for PEDS and 7 days for TEOS. After intensive washing with ethanol, the pectin-silica composite alcogels were loaded with theophylline at 3.4 g/L in ethanol for 2 weeks, before being supercritically dried using  $\text{CO}_2$ .

In parallel, non-impregnated pectin matrices were also drug-loaded and  $\text{CO}_2$  supercritically dried to be used as a ‘reference’. The pectin matrices were loaded with theophylline at 3.4 g/L in ethanol for 2 weeks, prior to  $\text{CO}_2$  sc-drying.

In each section, the type of silica-sol and the formulation of the pectin matrices will be specified.

### ▪ Calculation of silica diffusion time inside pectin matrix

To evaluate the time needed to completely impregnate coagulated pectin with silica sol, we estimated the diffusion coefficient of silica in ethanol using the same “diffusion” approach as described in Chapter V, Section 1.1, Equations (5.1) and (5.2). The Stokes radius of pre-polymerized silica (PEDS) was estimated previously to be around 1 nm (Rudaz, 2013). Using  $\eta_{\text{ethanol}} = 1.20 \cdot 10^{-3}$  Pa.s, silica diffusion coefficient in ethanol at 25°C is estimated to be around  $1.82 \cdot 10^{-10}$  m<sup>2</sup>/s in the absence of pectin network. Being slowed down in pectin network, the diffusion of silica in coagulated pectin network filled with ethanol is approximately  $D_{\text{silica}} \sim 1.82 \cdot 10^{-11}$  m<sup>2</sup>/s. The distance made by silica PEDS particle as a function of time is shown in Table 7.

As TEOS is non pre-polymerized silica precursor, its Stokes radius is expected to be smaller as compared to PEDS (pre-polymerized). As a consequence, the time to diffuse through a given distance should be normally shorter for TEOS than for PEDS.

Table 20. Distance made by silica molecules (from PEDS) by diffusion as free molecules in ethanol, or through a 6 wt% pectin matrix, in ambient conditions.

$D_{\text{silica}}$ (m <sup>2</sup> /s)	t (days)	L (mm)
<b>1.82 10<sup>-10</sup></b> (free diffusion in ethanol)	1	4.0
	2	5.6
	10	12.5
	15	15.4
<b>1.82 10<sup>-11</sup></b> (diffusion through a 6 wt% pectin matrix)	1	1.2
	2	1.7
	10	4.4
	15	4.9

In 24 h, silica (from PEDS) diffuses through a distance of ~ 1.2 mm in such porous system. Considering that half thickness of the pectin matrix samples was 5 mm maximum, and that diffusion is slowed down as soon as pectin is progressively filled with silica, we consider that silica impregnation of coagulated pectin should be completed in 15 days.

▪ **Estimation of the silica impregnation efficiency into pectin matrices**

To estimate silica impregnation efficiency (%) into the pectin matrices, we compared the amount of silica actually present in the matrices with the theoretical maximum amount of 100% impregnated case. For this purpose, we considered that silica impregnated the “free” volume offered by pectin sample, *i.e.* the volume of the pores ( $V_{pores}$ ) within pectin matrices, which is obtained from pectin aerogel porosity (Equation (6.11)).

$$\epsilon (\%) = \frac{V_{pores}}{V_{total}} = \left(1 - \frac{\rho_{bulk}}{\rho_{skeletal}}\right) \times 100\% \quad (6.11)$$

Besides, we assume that the density of silica aerogel formed inside pectin matrix is the same as of neat silica aerogel. We obtained neat silica aerogels density ( $\rho_{silica\ aerogel}$ ) around  $0.111 \pm 0.002$  g.cm<sup>-3</sup> from PEDS, and around  $0.124 \pm 0.002$  g.cm<sup>-3</sup> from TEOS. As the skeletal density of silica aerogels is known to be around 2.0 g/cm<sup>3</sup> (Phalippou & Kocon, 2004), we can calculate the maximum amount of silica that can impregnate pectin matrices as follows (Equation (6.12)):

$$m_{max\ silica} = \rho_{silica\ aerogel} \times V_{pores\ pectin\ aerogel} \quad (6.12)$$

Then, we can evaluate the theoretical density of pectin-silica composite aerogel, as defined by:

$$\rho_{theoretical\ composite} = \frac{m_{max\ silica}}{V_{total}} + \frac{m_{pectin}}{V_{total}}$$

$$\rho_{theoretical\ composite} = \frac{\rho_{silica\ aerogel} \times V_{pores\ pectin\ aerogel}}{V_{total}} + \rho_{pectin\ aerogel}$$

Thus, we have:

$$\rho_{theoretical\ composite} = \rho_{silica\ aerogel} \times \epsilon (\%)_{pectin\ aerogel} \times \left(\frac{1}{100\%}\right) + \rho_{pectin\ aerogel} \quad (6.13)$$

We can therefore estimate silica impregnation efficiency (%) within pectin matrices as the ratio of the experimental bulk density of composite aerogel  $\rho_{composite}$  and the theoretical one (from Equation (6.13)):

$$\%_{Si\ impregnation} = \frac{\rho_{composite}}{\rho_{theoretical\ composite}} \times 100\% \quad (6.14)$$

Using the mixing law, we define the composite theoretical specific surface area ( $S_{BET}$  in m<sup>2</sup>/g) also according to the mixing rule:

$$\begin{aligned} & \textit{Theoretical } S_{BET} \textit{ Pectin-silica composite aerogel } \left( m^2/g \right) \\ = & \left( \textit{Ratio}_{pectin/silica} \times S_{BET} \textit{ pectin aerogel} \right) + \left( \textit{Ratio}_{silica/pectin} \times S_{BET} \textit{ silica aerogel} \right) \end{aligned} \quad (6.15)$$

In the same way, we calculated the theoretical drug loading capacity (in wt%) as the weighted average of loading capacity of each component of the composite (mixing law):

$$\begin{aligned} & \textit{Theoretical loading capacity}_{pectin-silica composite aerogel} \text{ (wt\%)} \\ = & \left( \textit{Ratio}_{pectin/silica} \times \textit{Loading capacity}_{pectin aerogel} \right) \\ + & \left( \textit{Ratio}_{silica/pectin} \times \textit{Loading capacity}_{silica aerogel} \right) \end{aligned} \quad (6.16)$$

## 2.2. Characterization of pectin-silica composite aerogels

### 2.2.1. Influence of the type of silica sol on the properties of neat silica aerogels (TEOS vs PEDS)

Silica aerogels made from TEOS or PEDS were produced but were extremely fragile (half of samples were presenting cracks after sc-drying) and mildly transparent materials. Pictures of PEDS and TEOS aerogels are shown in Figure 197. We noted that TEOS aerogels had lower mass by 6 – 8 % as compared to PEDS aerogels, which can indicate that not all silica from TEOS was completely polymerized and monomers/oligomers were washed out before sc-drying.

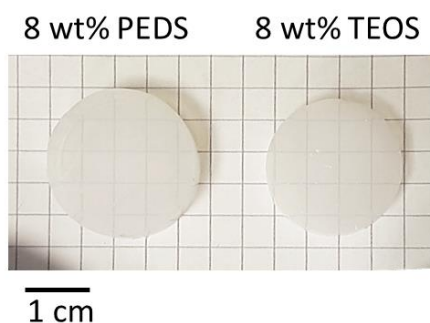


Figure 197. Picture of silica aerogels made from 8 wt% of PEDS or from 8 wt% TEOS

The structural properties and drug loading characteristics of 8 wt% silica aerogels based on TEOS and PEDS are presented in Table 21, neat 6 wt% pectin aerogels (not filled with silica) are also given for comparison. PEDS- and TEOS- and pectin-based aerogels presented similar bulk density, porosity and pore volume, but silica aerogels have significantly higher specific

surface from +50% to +115% (depending on the pectin and silica aerogels formulations) in correlation with literature.

Table 21. Structural and drug loading properties of neat pectin (with and without calcium) and neat silica aerogels using PEDS or TEOS as silica sol. All aerogels were loaded with theophylline at 3.4 g/L, as described in Chapter II.

<b>Aerogel composition</b>	<b>6wt% pectin without calcium</b>	<b>6wt% pectin with calcium R<sub>Ca</sub>=0.2</b>	<b>8wt% silica from PEDS</b>	<b>8wt% silica from TEOS</b>
<b>Volume shrinkage (%)</b>	61.1 ± 0.6	30.5 ± 0.7	39.9 ± 0.5	50.6 ± 0.4
<b>Density (g/cm<sup>3</sup>)</b>	0.157 ± 0.003	0.088 ± 0.001	0.106 ± 0.001	0.123 ± 0.001
<b>Porosity (%)</b>	89.5 ± 0.2	94.1 ± 0.1	94.7 ± 0.01	93.8 ± 0.02
<b>Pore volume (cm<sup>3</sup>/g)</b>	5.71 ± 0.12	10.69 ± 0.19	8.75 ± 0.13	7.46 ± 0.08
<b>S<sub>BET</sub> (m<sup>2</sup>/g)</b>	554 ± 16	479 ± 14	1011 ± 34	834 ± 32
<b>Network morphological aspect</b>	Mesopores and small macropores of around 30 to 70 nm of diameter	Mesopores and small macropores of around 50 to 150 nm of diameter	Small mesoporous network	Small mesoporous network
<b>Loading efficiency (%)</b>	80.1	61.3	15.8	33.4
<b>Aerogel loading capacity (wt%)</b>	3.81	3.41	0.70	1.58
<b>Specific loading (x 10<sup>5</sup> g/m<sup>2</sup>)</b>	7.0	7.6	0.7	1.8

We noticed that the source of silica-precursors (TEOS or PEDS) significantly affected the aerogel structural and morphological properties. Indeed, TEOS aerogels underwent a higher shrinkage (~ 51 vol%) than PEDS (~ 40 vol%) which led to higher density for TEOS aerogels (~ 0.123 g/cm<sup>3</sup>) as compared to PEDS aerogels (~ 0.106 g/cm<sup>3</sup>).

In Figure 198, SEM observation of TEOS aerogel network morphology shows some silica aggregates and non-uniform pore size (5 – 70 nm). On the contrary, morphology of PEDS aerogel was found to be homogenous with smaller pore sizes (< 40 nm). Besides, PEDS aerogels presented +20% higher specific surface area (~ 1000 m<sup>2</sup>/g) compared to that of TEOS aerogels (~ 830 m<sup>2</sup>/g). This can be attributed to the pre-polymerization of silica in PEDS. These

dissimilar structural properties (density, pore size,  $S_{\text{BET}}$ ) between TEOS and PEDS aerogels were also reported (Wagh, Begag, Pajonk, Rao, & Haranath, 1999).

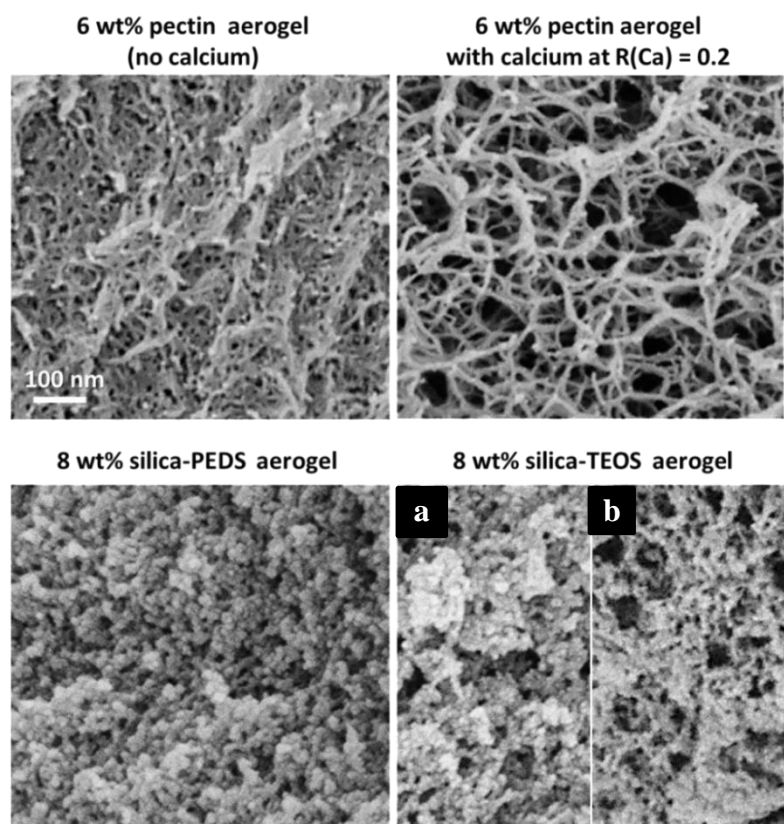


Figure 198. SEM pictures of neat pectin aerogels (with and without calcium made from 6 wt% pectin P35 solutions at pH 3.0) and neat silica aerogels from PEDS and from TEOS, 8 wt% sol. We present two different fields of view from the core of TEOS aerogels (a) and (b) to highlight their morphological heterogeneity. All images are at the same scale.

As stated above (*cf.* Section 1 of this chapter), cellulose- and pectin-based aerogels were found to display high drug loading efficiency from 50 to 80%, and their drug loading properties were found to be positively correlated to the structural parameters such as density and  $S_{\text{BET}}$ . It is interesting to see that even if silica aerogels displayed similar density, pore volume, porosity and much higher  $S_{\text{BET}}$  than pectin and cellulose aerogels, the loading of theophylline within silica aerogels was significantly weaker, around 15-30% (Table 21). As a direct consequence of a low drug loading efficiency, drug loading capacity and specific loading of both types of silica aerogels were significantly lower than of polysaccharides aerogels.

Moreover, we highlight here another major difference between PEDS- and TEOS aerogels concerning their drug loading properties. It is interesting to see that loading efficiency, capacity and specific loading was twice higher in TEOS aerogels ( $\sim 30\%$ ) than in PEDS aerogels ( $\sim 15\%$ ). As their physical and structural properties were similar, we suppose that this is due to different physico-chemical characteristics of TEOS- and PEDS- aerogels, impacting drug-matrix interactions and the loading process.

One of the differences between TEOS and PEDS can be aerogel hydrophilic/hydrophobic properties. To check this, the simplest test to do is to measure the contact angle with water. The results are presented in Figure 199 and Figure 200.

As it is well known, pectin aerogel showed extremely high hydrophilicity as revealed by immediate absorption of the water droplet in less than 0.4 s. As expected, due to the high hydrophilicity of TEOS aerogels, water contact angle values could not be measured, as the droplet was immediately absorbed ( $< 0.2$  s) when placed on the surface of the aerogel. Once in contact with water, TEOS aerogels immediately cracked due to capillary forces inside the pores and lost its physical integrity, as it is commonly reported for non-hydrophobized silica aerogels (Caputo, Scognamiglio, & De Marco, 2012; I. Smirnova et al., 2004). However, surprisingly we noticed the opposite for PEDS aerogels which appeared to be rather hydrophobic, as revealed by the contact angle with water around  $140$  to  $130^\circ$  in the first 15 seconds of experiment.

We could not continue following of the contact angle evolution longer than for 15 seconds as evaporation of water from the droplet was becoming noticeable. But we visually noticed a progressive drop spreading with time, and after 15 min in contact with a water droplet, PEDS aerogels started to fracture due to capillary forces in the pores. This means that PEDS aerogels are much more hydrophobic as compared to its TEOS-based counterpart.

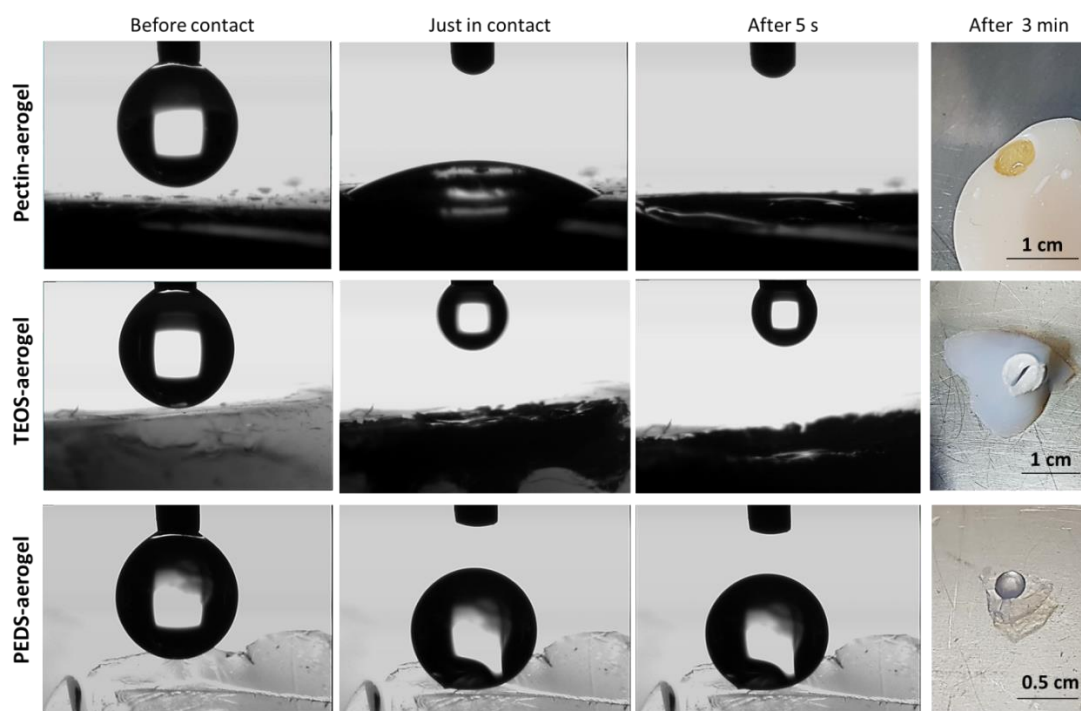


Figure 199. Pictures of pectin (made from P35 6 wt% solution at pH 3.0), TEOS and PEDS aerogels during contact angle experiments at different times, and visual aspect of the surface of aerogels after the experiment.

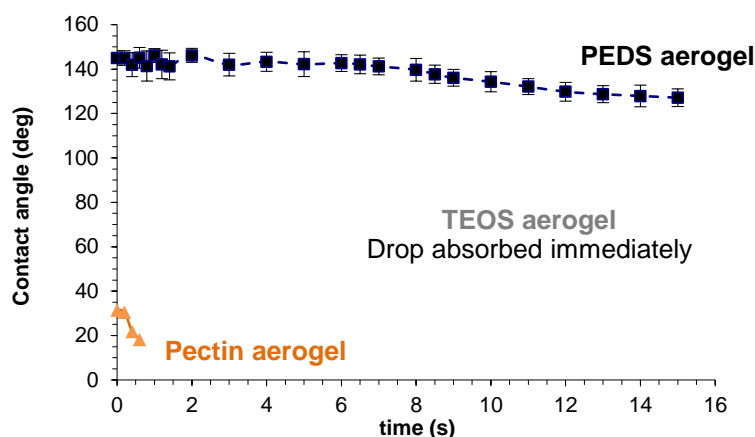


Figure 200. Contact angle with water of the surface of pectin, TEOS and PEDS aerogels as a function of time.

Non-functionalized silica aerogels usually contain some un-reacted silanol (Si-OH) groups on the surface of their backbone. Even if silanol groups are not numerous, water molecules can readily interact with the hydroxyl functions, explaining the high hydrophilicity of silica. We assume that the difference in hydrophilicity between PEDS and TEOS aerogels is due to the partial hydrolysis and pre-polymerization of silica in PEDS. We assume that in the case of PEDS, a higher portion of the silanol groups interacted with each other to form connective silicon-oxygen-silicon bridges, which led to lower amount of un-reacted silanol groups than in TEOS. The apparent hydrophobicity of PEDS aerogels might stem from the practically absence of un-reacted hydroxyl groups on the surface of their silica skeleton, contrary to TEOS aerogels.

We can imagine that the hydrophobicity of PEDS network could also have increased its compatibility with  $sc\text{-CO}_2$  (non-polar fluid) during  $sc$ -drying resulting in lower volume shrinkage and aerogel density. The significantly higher specific surface area of PEDS aerogels may be explained by a possible higher network ramification due to silica pre-hydrolysis and by a better network preservation from moisture thanks to its hydrophobicity. Finally, we assume that this major difference in terms of surface chemistry affects theophylline loading in PEDS aerogels and TEOS aerogels. Indeed, theophylline is a highly polar drug due to the numerous number nitrogen and oxygen atoms (Yalkowsky, He, Jain, He, & Jain, 2016). Contrary to TEOS aerogels, higher hydrophobicity of PEDS aerogels might have prevented drug deposition within the silica matrix. This is in correlation with the work of Smirnova et al. who obtained higher ketoprofen loading into hydrophilic than into hydrophobic silica aerogels (I. Smirnova, Mamic, & Arlt, 2003; I. Smirnova et al., 2004). This assumption about the influence of the hydrophilicity of the carrier material on drug (here, theophylline) loading also explained the high loading efficiency (50 - 80%) obtained for polysaccharide aerogels (cellulose and pectin) as they present numerous polar functions (carboxyl- and hydroxyl-) promoting the loading of

theophylline, while less polar functions of silica aerogels (SiOH) significantly reduced drug loading efficiency (15%-30%).

### 2.2.2. Distribution and impregnation efficiency of silica in pectin matrix

Pectin-silica composite aerogels were obtained by impregnation of a 6 wt% pectin matrix by 8 wt% silica-precursors (TEOS or PEDS) (as described in Section 2.1). We studied pectin-silica aerogels by SEM with Energy-dispersive X-ray spectroscopy (EDS) to characterize the elemental composition alongside the sample thickness.

The X-rays energy emitted by an element from a sample directly depends on the atomic number, and thus is characteristic of an element. An example of X-ray spectrum from the surface cross-section of pectin-silica composite obtained by EDS is given in Figure 201. The different peaks correspond to calcium ( $K_{\alpha}$  3.692 KeV), sodium ( $K_{\alpha}$  1.040 KeV) and silicon ( $K_{\alpha}$  1.740 and  $K_{\beta}$  1.837 keV). The peak height gives the mass proportion of each element detected in the sample at the selected point (Figure 202). To obtain the atomic percentage (noted %<sub>atomic</sub>) of each element, the mass proportions are divided by the atomic mass of the corresponding atom. As a result, we are able to obtain the atomic composition (in %<sub>atomic</sub>) of all the elements present in the sample at the selected point on the surface.

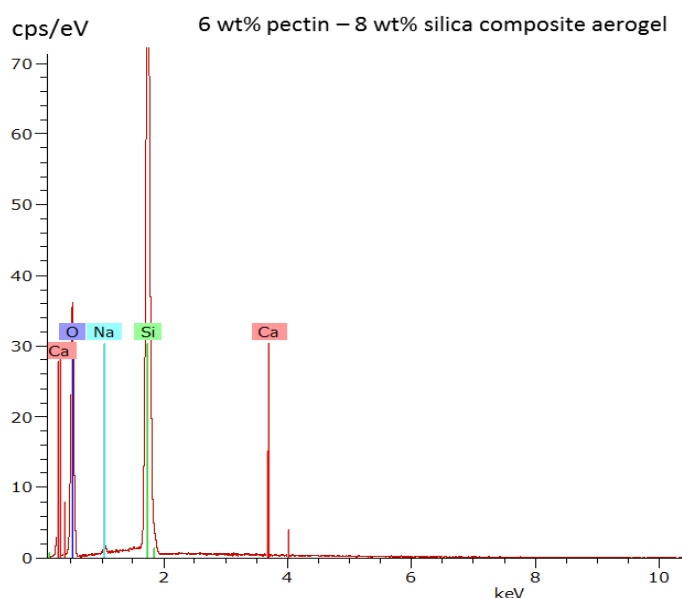


Figure 201. Example of EDS spectrum from a selected point on the internal cross-section of pectin-silica aerogel, pectin was from 6wt% pectin P35 (pH 2.0, R(Ca) = 0.2), silica was from 8 wt% PEDS.

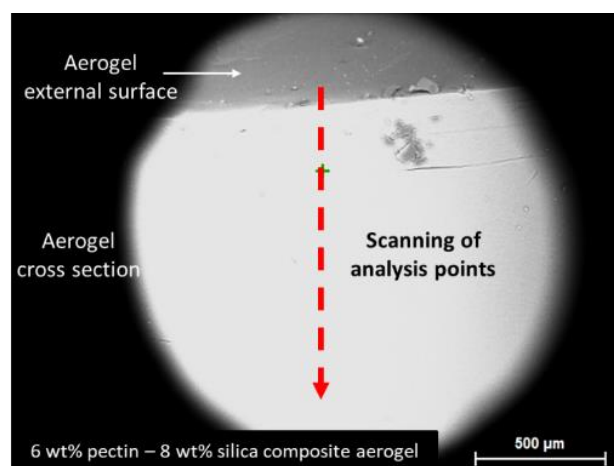


Figure 202. SEM images of EDS analysis: illustration of the EDS analysis along the internal cross-section of pectin-silica aerogel, pectin was from 6 wt% pectin P35 (pH 2.0,  $R(\text{Ca}) = 0.2$ ), silica was from 8 wt% PEDS.

Based on the method shown in Figure 201 and Figure 202 (see details in Chapter II), we were able to follow the atomic proportion of Si (%<sub>atomic</sub>) all over the internal cross-section of pectin-silica aerogel.

We know that depending on the formulation of the pectin matrix (pH and calcium conditions), pectin aerogel density and pore size vary which impacted silica impregnation as shown in Figure 203. We observed that silica had penetrated within the entire thickness of pectin network in all cases. However, silica spatial distribution was not homogenous. Indeed, for pectin matrix made from 6 wt% pectin solution at pH 3.0 without calcium, we could observe slightly less silica in the center of the material as compared to other 6 wt% pectin matrices with lower density and larger pores (pH 2.0 with and without calcium). This can be attributed to the higher pectin network density and small pore size in the case when coagulated pectin was made from solutions at pH 3 without calcium, which might have slowed down silica diffusion.

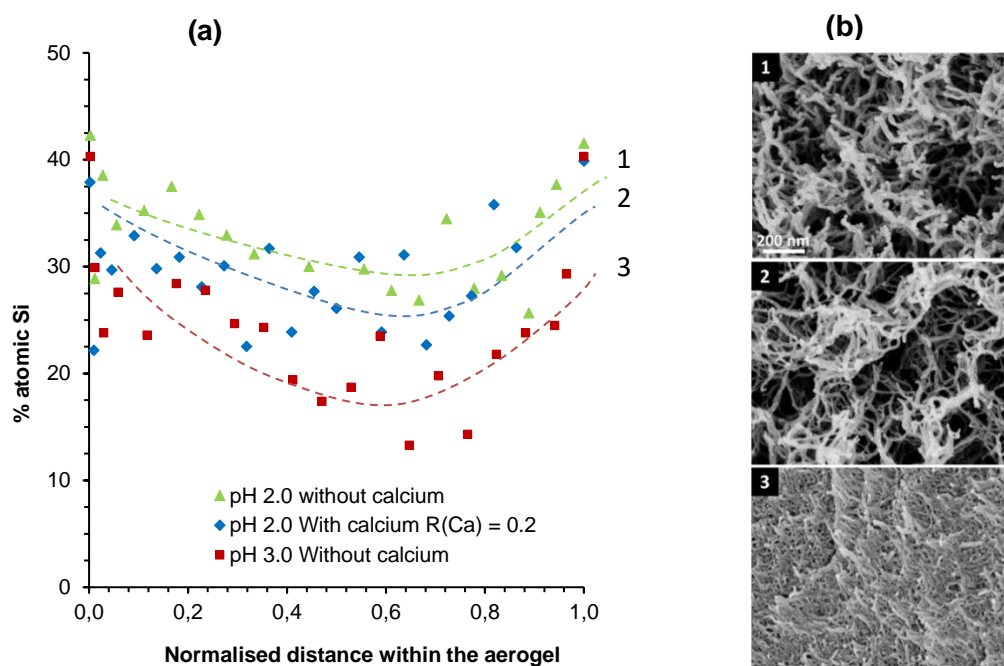


Figure 203.

(a) Distribution of silica (from PEDS) over the cross-section of composite pectin-silica aerogel; pectin was from 6 wt% solutions at (1) pH 2 and  $R(\text{Ca}) = 0$  (without calcium), (2) pH 2 and  $R(\text{Ca}) = 0.2$  and (3) pH 3 and  $R(\text{Ca}) = 0$  (without calcium). Lines are given to guide the eye.

(b) SEM images of the corresponding neat pectin aerogels which wet precursors were used for the impregnation by silica.

Silica impregnation efficiencies (%) (eq. 6.14) obtained for different pectin matrices as a function of  $R(\text{Ca})$  ratio are presented in Figure 204. As it can be seen, silica impregnation efficiency was high ( $> 75\%$ ) but lower than 100% for all composites, despite the fact that we have set a long impregnation time (15 days) to let silica sol diffusing into pectin matrix. As shown in Figure 204, we noticed an impact of calcium concentration in pectin solution ( $R(\text{Ca})$  ratio) on silica impregnation efficiency. As explained in Chapter III, the structural properties of pectin aerogels (in particular density and pore size) are strongly influenced by calcium addition. We assume that larger pores and lower density obtained due to pectin cross-linking with might have facilitated the diffusion of silica sol into the core of pectin network. As it can be seen in Figure 204, impregnation efficiency of silica from PEDS increases from 82 ( $R(\text{Ca}) = 0$ ) to 91% ( $R(\text{Ca}) = 0.4$ ) due to pectin cross-linking with calcium.

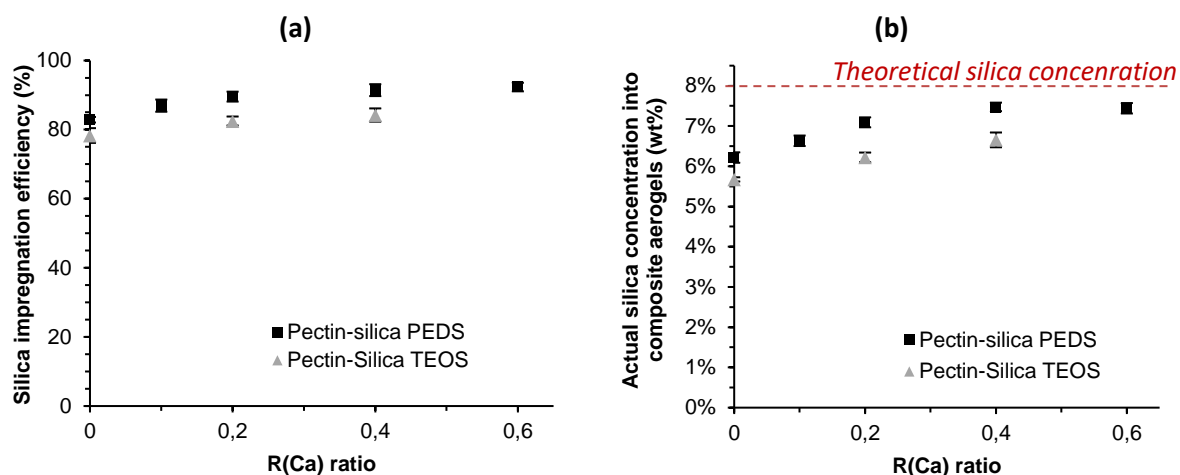


Figure 204. (a) Silica impregnation efficiency (%) in pectin matrices and (b) actual silica concentration (wt%) within pectin-silica composite aerogels. Pectin matrices were made from 6 wt% of P35 dissolved at pH 3.0 at different R(Ca).

As a result of different impregnation efficiencies, the mass concentration of silica in pectin matrices was actually lower than 8 wt%. Based on aerogels' mass without (neat pectin aerogels) and with silica (composite aerogels), we estimated that the actual concentrations of silica within pectin matrices (wt%) were varying from 6.2 to 7.5 wt% for pectin-PEDS aerogels and from 5.7 wt% to 6.7 wt% for pectin-TEOS aerogels (Figure 204 b).

### 2.2.3. Structural properties of pectin-silica composite aerogels and loading with theophylline

6wt%pectin-8wt%TEOS and 6wt%pectin-8wt%PEDS composite aerogels were produced while varying the R(Ca) of the pectin matrix from 0 (no calcium) to 0.6. Pictures of pectin-TEOS aerogels are given as an illustration in Figure 205.

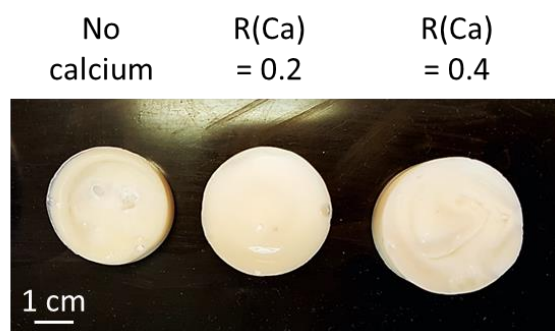


Figure 205. Pictures of 6 wt% pectin- 8 wt% TEOS composite aerogels. The pectin matrix was made from 6 wt% of pectin P35 dissolved at pH 3.0 without calcium or with calcium (R(Ca) 0.2 and 0.4).

As presented in Figure 206, the presence of a rigid silica network within pectin matrices slightly prevented volume shrinkage during sc-drying compared to neat pectin aerogels in the case of low R(Ca). Cross-linking of pectin with calcium was shown to “stabilize” the network and thus to decrease the shrinkage, and the presence of silica did not influence shrinkage anymore.

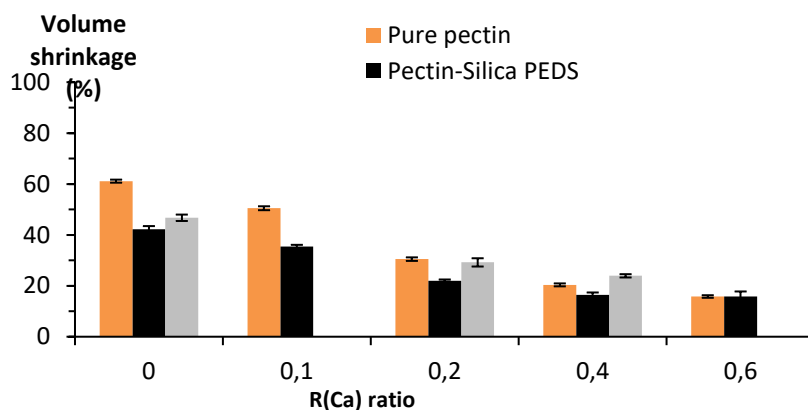


Figure 206. Volume shrinkage (%) of 6 wt% pectin aerogels (not impregnated with silica), and 6 wt% pectin – 8 wt% silica composite aerogels made from PEDS or TEOS as a function of R(Ca) ratio. All pectin matrices were produced from 6 wt% of pectin P35 dissolved at pH 3.0.

As expected, the addition of around 6 wt% to 7.5 wt% of silica into 6 wt% pectin matrices increased the density (from +30% to +100% depending on the sample) and specific surface area (from +24% to +115% depending on the sample) of the pectin-silica composite aerogels (Figure 207).

As might be expected from the study of neat silica aerogels from TEOS or PEDS, pectin-PEDS composite aerogels presented significantly higher specific surface area than pectin-TEOS aerogels while their densities were the same.

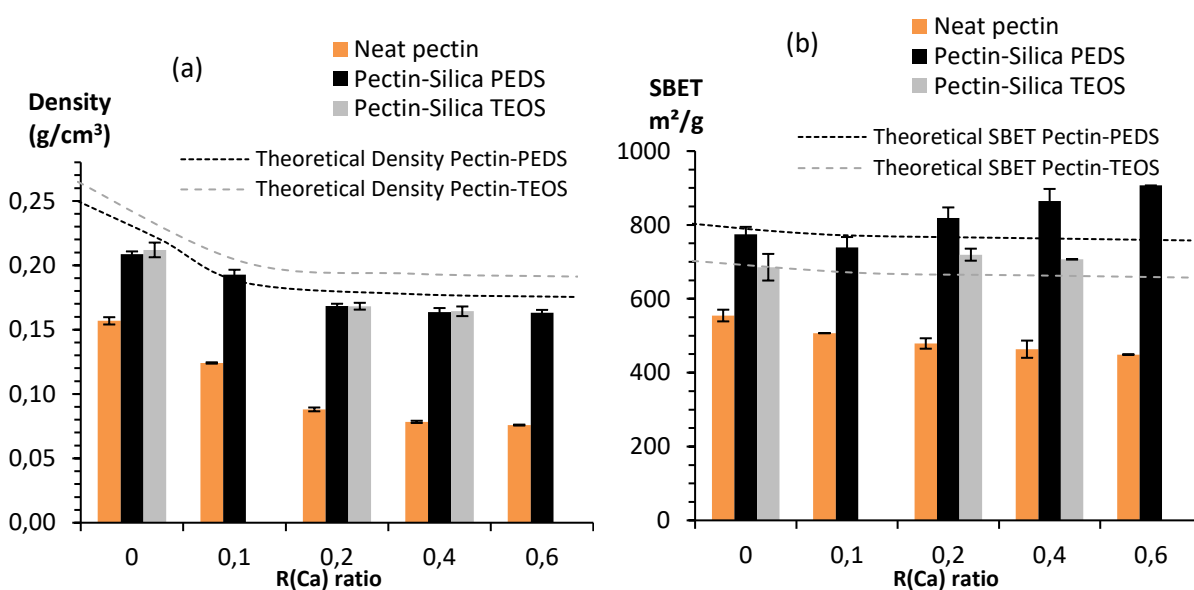


Figure 207. (a) Aerogel density and (b) specific surface area  $S_{\text{BET}}$  of neat 6 wt% pectin aerogels and 6 wt% pectin – 8 wt% silica composite aerogels made from PEDS or TEOS as a function of  $R(\text{Ca})$ . Dashed lines represent theoretical density (eq. 6.13) and theoretical  $S_{\text{BET}}$  (eq. 6.15) of pectin-silica composite aerogels. All pectin matrices were produced from 6 wt% of pectin P35 dissolved at pH 3.0.

SEM observation at high magnification allows the understanding of the organization of silica network within the pectin matrix. As shown in Figure 208, in the absence of silica pectin aerogels present a typical “smooth” fibril organized in a network, while when silica (TEOS or PEDS) was added pectin fibrils are covered by nanometric “granules”. We suppose that pectin-silica composite aerogel was formed by deposition and polymerization of silica particles directly upon the pre-existing wet network of pectin, which led to partially covered surface of pectin fibrils. Once pectin fibrils are fully covered, silica filled the pores within pectin network.

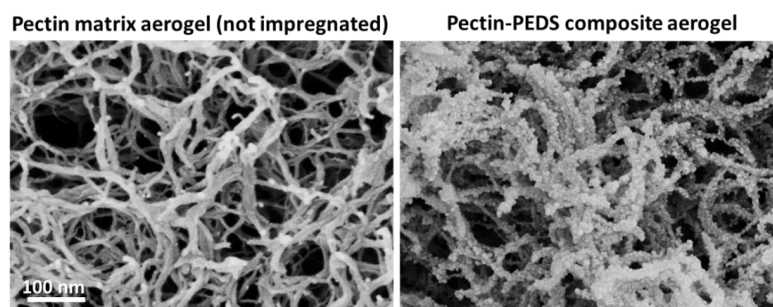


Figure 208. SEM observations of neat pectin aerogel and pectin-PEDS composite aerogel. Pectin matrix was made from 6 wt% of pectin P35 dissolved at pH 3.0 with calcium at  $R(\text{Ca}) = 0.2$ . The scale is the same for both pictures.

The observation of the composite aerogels’ morphologies in Figure 209 clearly shows the covering of pectin fibrils and “filling” of the pectin network pores when compared to neat pectin aerogel. Due to the addition of silica into pectin matrices, the pores of the composite aerogels were systematically smaller than those in the corresponding pectin aerogel references, in correlation with their higher bulk densities and confirmed by higher specific surface area (Figure 207).

In correlation with a high silica impregnation efficiency into pectin matrices (Figure 204), the experimental values of density and  $S_{\text{BET}}$  of pectin-TEOS and pectin-PEDS composite aerogels were found to be close to the theoretical ones estimated using mixing law (see eq. (6.13) and (6.15)) (Figure 207). This also suggests that the structuration of the silica networks within pectin matrices was similar to the ones forming neat silica aerogels. However, it is clear that the pores of composite aerogels were not completely filled with silica which was expected from silica impregnation efficiency around 80 – 90 % (Figure 204 a.). In the absence of calcium,

composite aerogels present small mesopores in the same range as neat pectin and silica aerogels (< 50 nm), while increasing calcium ratio pores of the composites were progressively becoming larger (10-80 nm) but still smaller than in the neat corresponding pectin aerogels.

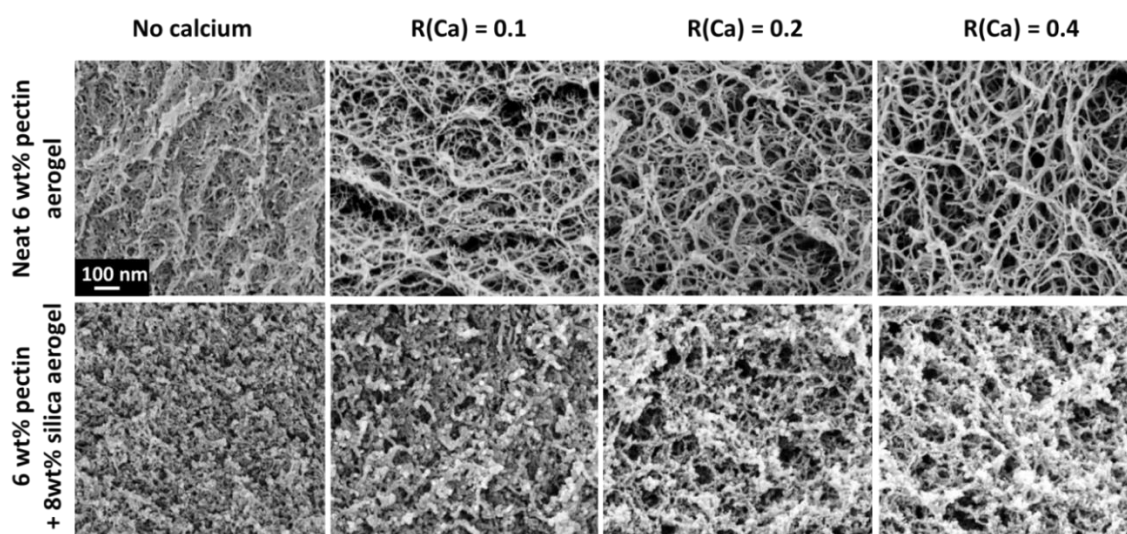


Figure 209. SEM pictures of neat 6 wt% pectin aerogels and 6 wt% pectin-8 wt% silica (PEDS) composite aerogels. The pectin matrices were made from 6 wt% pectin P35 dissolved at pH 3.0 without calcium or with calcium at different R(Ca) ratio from 0.1 to 0.4. All images are at the same scale.

Finally, we observed that pectin-silica aerogels using either TEOS or PEDS present different morphology depending on the type of silica sol. As we already observed for neat silica aerogels using TEOS or PEDS, pectin-PEDS composite aerogels displayed more homogenous network and pore size distribution than pectin-TEOS aerogels.

Besides, similar to what was observed for neat TEOS aerogels (Figure 198), large silica aggregates were formed within pectin matrix. We can correlate higher  $S_{BET}$  of pectin-PEDS aerogels (Figure 207) to their finer network morphology of smaller silica particles as compared to pectin-TEOS aerogels.

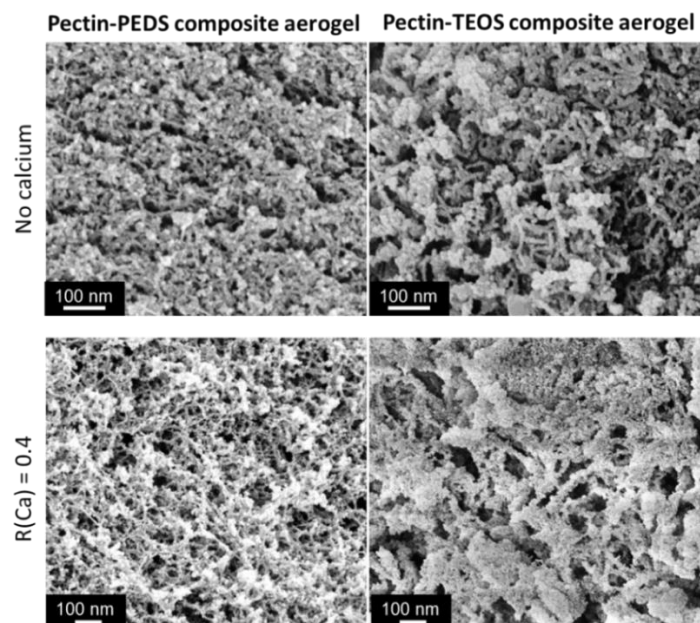


Figure 210. SEM pictures of 6 wt% pectin-8 wt% silica composite aerogels using either PEDS or TEOS as silica sol. The pectin matrices were made from 6 wt% of pectin P35 dissolved at pH 3.0 without calcium or with calcium at a R(Ca) ratio of 0.4.

#### 2.2.4. Theophylline loading in pectin-silica composite aerogels

The drug loading properties of the 6 wt% pectin-8 wt% silica composite aerogels, *i.e.* drug loading efficiency, drug loading capacity and specific loading, are plotted in Figure 211. Neat 6 wt% neat pectin aerogels “references” are shown for comparison. All aerogels were loaded with theophylline at 3.4g/L.

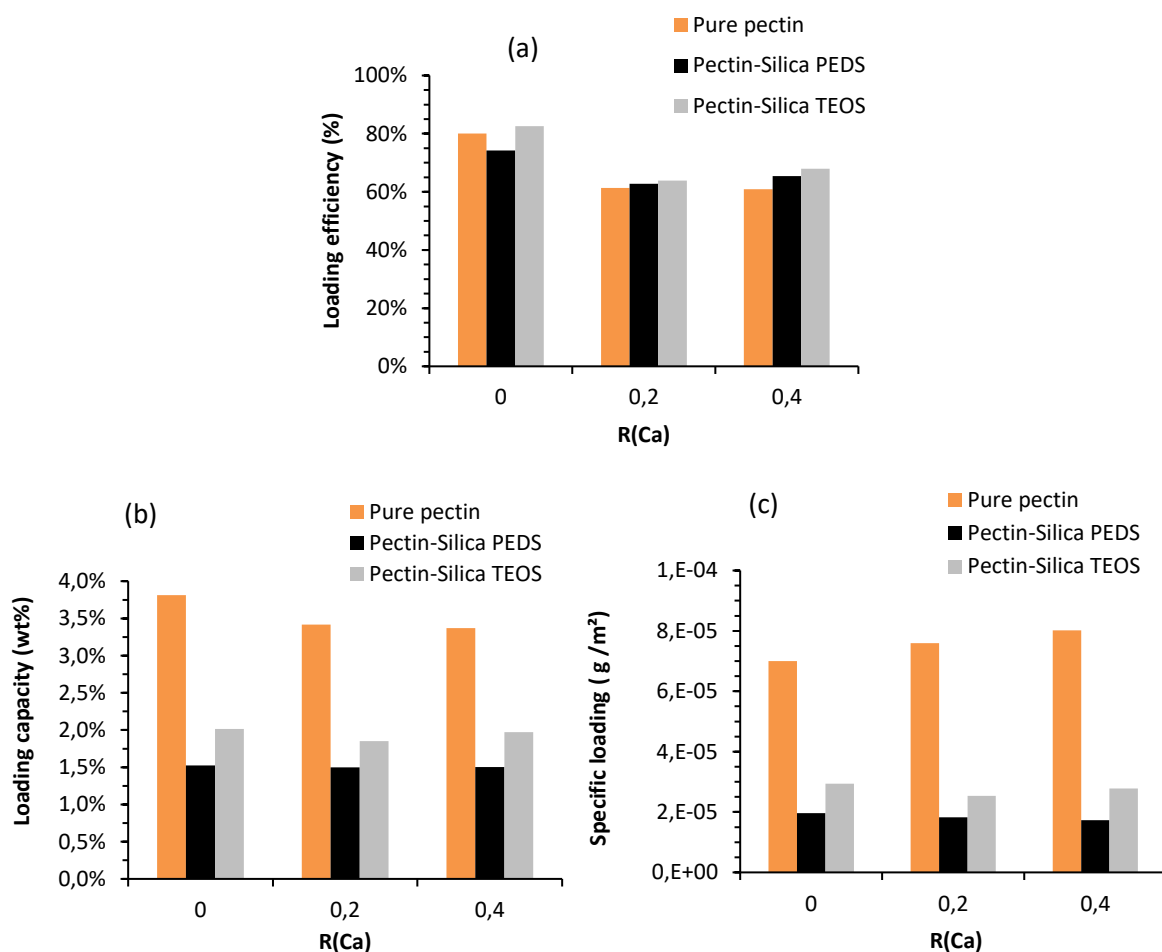


Figure 211. (a) Drug loading efficiency, (b) loading capacity and (c) specific loading of neat 6 wt% pectin aerogels and 6 wt% pectin – 8 wt% silica composite aerogels made from PEDS or TEOS as a function of R(Ca) ratio. All pectin matrices were produced from 6 wt% of pectin P35 dissolved at pH 3.0 with R(Ca) ratio from 0 to 0.4.

We found that the loading efficiency of composite aerogels was similar to that of neat pectin aerogels, from 60 to 80% depending on R(Ca) ratio, and thus was much higher than that of neat TEOS aerogels (~30%) and of PEDS aerogels (~15%) (Table 21). This means that the pectin part of the composite (which represents 40-45% of the composite mass) actually governed the drug loading properties of pectin-silica composite, even if pectin network was partially covered by silica (Figure 208, Figure 209).

As we showed in Chapter V, the increase in specific surface area and density of aerogels improves their drug loading properties as higher surface area is supposed to provide larger surface for drug deposition and higher density prevents drug wash off during sc-drying. Thus, we could expect that addition of silica to pectin matrices could have improved the loading of the drug into composite aerogels, as their density, specific surface area and the mass of solid content were considerably increased compared to neat pectin aerogels.

However, theophylline loading capacity and specific loading were more than twice lower when silica was added to pectin matrices (Figure 211 b and c). We assume that silica part of the composites (~ 55-60% of total composite mass) practically did not contribute to theophylline loading properties compared to pectin part. Finally, we noticed that all drug loading characteristics of pectin-silica composite aerogels were slightly better when TEOS was used instead of PEDS, in correlation with their own drug loading properties (Table 21) and different hydrophilicity (Figure 200).

To highlight the impact of aerogels' composition on their drug loading properties, we plotted the respective drug loading capacity for neat silica (using TEOS or PEDS) aerogels, for neat pectin aerogel, and for pectin-silica composite aerogels (using TEOS or PEDS) in Figure 212, all for non-crosslinked pectin. It is interesting to see how the composition influenced the loading of the drug while their structural properties would have suggested the opposite. We underline here the important influence of the physico-chemical characteristics of the matrices on the loading of drug, with aerogel properties being not the only controlling parameters.

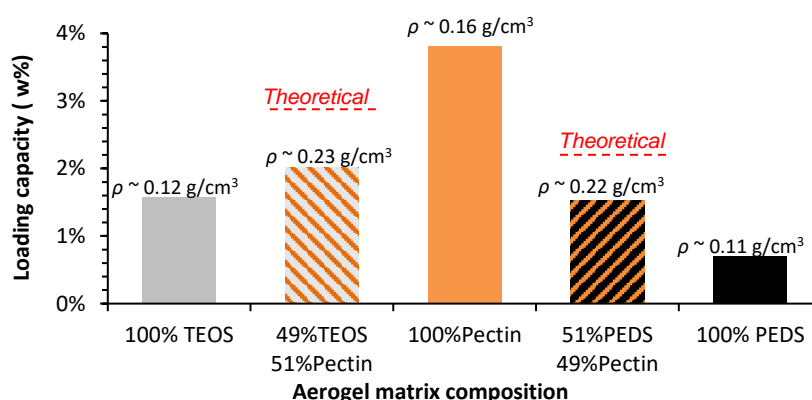


Figure 212. Theophylline loading capacity (wt%) of aerogels made from different formulations. All pectin matrices were produced from 6 wt% of pectin P35 dissolved at pH 3.0 without calcium. Silica was from TEOS or PEDS at 8 wt%. All aerogels were loaded with theophylline at 3.4 g/L. Aerogel density is indicated in each case. Dashed lines represent the theoretical loading capacity of pectin-silica composites, obtained using mixing law (eq (6.16)).

### 2.3. Theophylline release profiles from pectin-silica aerogel matrices

We first analyze the release kinetics from neat pectin and neat silica aerogels (from TEOS and from PEDS) using theophylline as drug model.

Then, we study the drug release behaviour from pectin-silica aerogels varying the calcium R(Ca) ratio (from 0 to 0.4) and the type of silica sol used for impregnation (TEOS and PEDS).

The impact of the composition of the composite aerogels on their release properties are presented and discussed.

### 2.3.1. Comparison of theophylline release from neat silica and pectin aerogels matrices

Figure 213 (a) shows a comparison of release kinetics from TEOS, pectin and PEDS based reference aerogels, and Figure 213 (b) their stability into gastro-intestinal simulated media. As shown in Figure 214, contrary to pectin aerogel which was demonstrating progressive surface erosion by dissolution, both silica aerogels were prone to bulk erosion with matrix disintegration into small pieces in contact with releasing media, and thus the evolution of matrix volume over time could not be followed in this study. These different matrix erosion properties were found to strongly impact the release of theophylline from each aerogel:

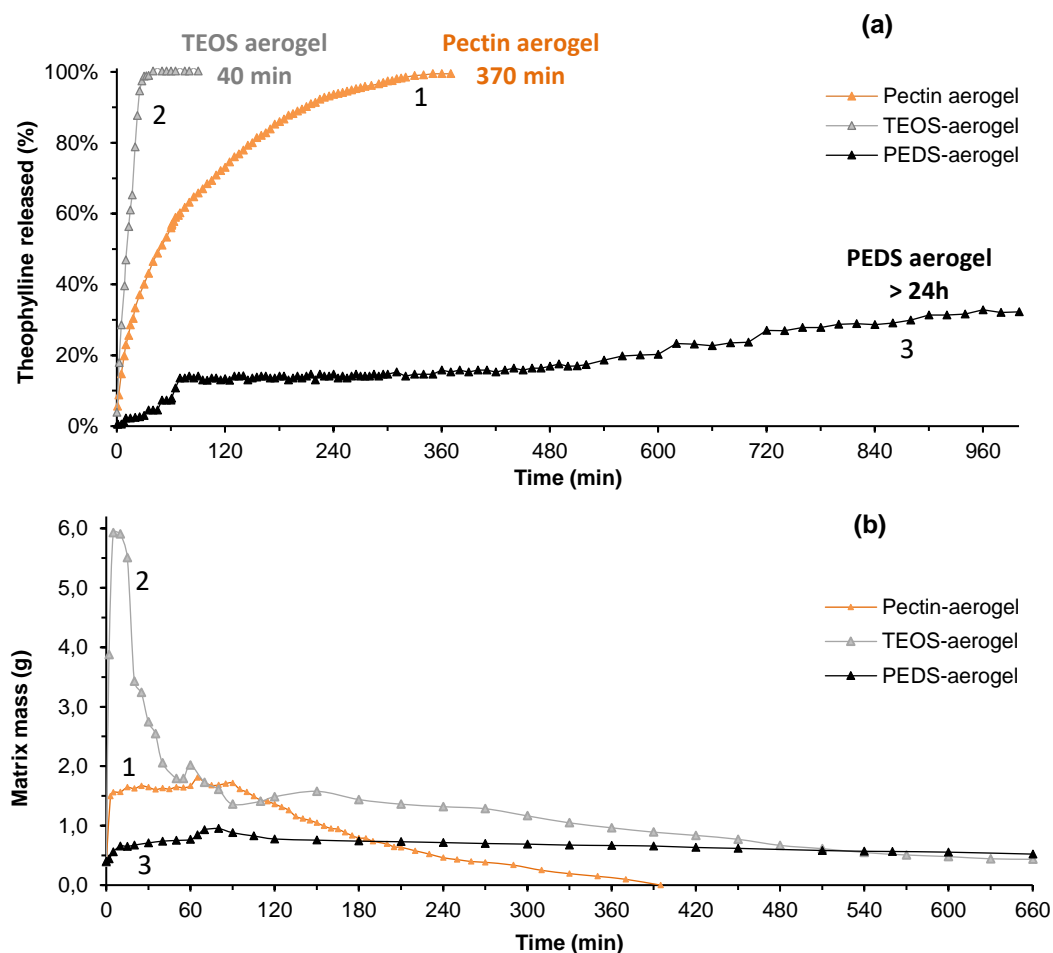


Figure 213. (a) Theophylline cumulative release (%) over time from 6 wt% pectin aerogel (without calcium at pH 3.0) (1), silica aerogel from 8 wt% TEOS (2) and silica aerogel from 8 wt% PEDS (3). (b) Aerogel mass evolution over time. The weight of all aerogels was around 0.380 - 400 mg.

- As it was already known in the previous chapters (Chapter IV and V), pectin aerogel presented a full and extended release of theophylline over 370 min, which was governed by the coupling of diffusion phenomena and matrix erosion in correlation with its “instability” in SIF media (pH 6.8) (Figure 213 b and Figure 214).
- We observed that TEOS aerogel instantly burst into several pieces once put in contact with liquid due to its high hydrophilicity and brittle characteristics (Figure 214). As shown in Figure 213 b, TEOS aerogel displayed a high and rapid mass intake (+ 1420 % in 5 min, as compared to dry mass) due to high liquid penetration into the matrix. Then, we observed that sample mass strongly dropped due to the progressive loss of physical integrity by erosion of the matrix into smaller particles which went out the testing permeable basket. The dramatic disintegration of the matrix allowed the drug to be immediately surrounded by the liquid and quickly dissolved due to high solubility of theophylline in aqueous media. As a result, TEOS aerogels showed immediate release behaviour with 95% of total theophylline released in around 25 min, and full drug release occurring in around 40 min. Similar matrix behaviour and immediate drug release profile was also reported in several studies on hydrophilic silica aerogels (Caputo et al., 2012; Mehling et al., 2009; Mohammadian, Jafarzadeh Kashi, Erfan, & Soorbaghi, 2018; I. Smirnova et al., 2004; I. Smirnova, Suttiruengwong, & Arlt, 2005; I. Smirnova, Suttiruengwong, Seiler, & Arlt, 2004).
- On the contrary, PEDS aerogels showed extended release behaviour with an extremely slow release of the drug over time. As an illustration, only 30% of the total drug was released after 16 hours of immersion into release media. We noted that PEDS aerogels also cracked into pieces due to its mechanical brittleness, but much more slowly than TEOS aerogels. Besides, we noticed that the increase of the mass of the PEDS matrix was low (~ + 90% of mass increase in 60 min) and it slowly decreased over time. Moreover, we visually observed that sample pieces were floating in the basket which reveals that they were not completely filled with liquid and air was remaining in the sample even after 10 h of immersion into the liquid. We assume that the low wettability of PEDS aerogel is due to its hydrophobicity (Figure 200) preventing water penetration into the system, which led to inhibited diffusion, delay of erosion and drastically slowed down the release of the drug. Due to its extreme fragility, we do not exclude the possibility of having impacted matrix erosion process by simple placing the sample in/out of liquid media for regular mass monitoring. An interesting observation is the correlation between the major cracks and fractures of the PEDS aerogel and the sudden peaks of theophylline release. A detailed plot of the first 150 minutes of release experiment

from PEDS aerogel (extracted from Figure 213 (a)) shows the correlation between major sample cracks and release profile (Figure 215).

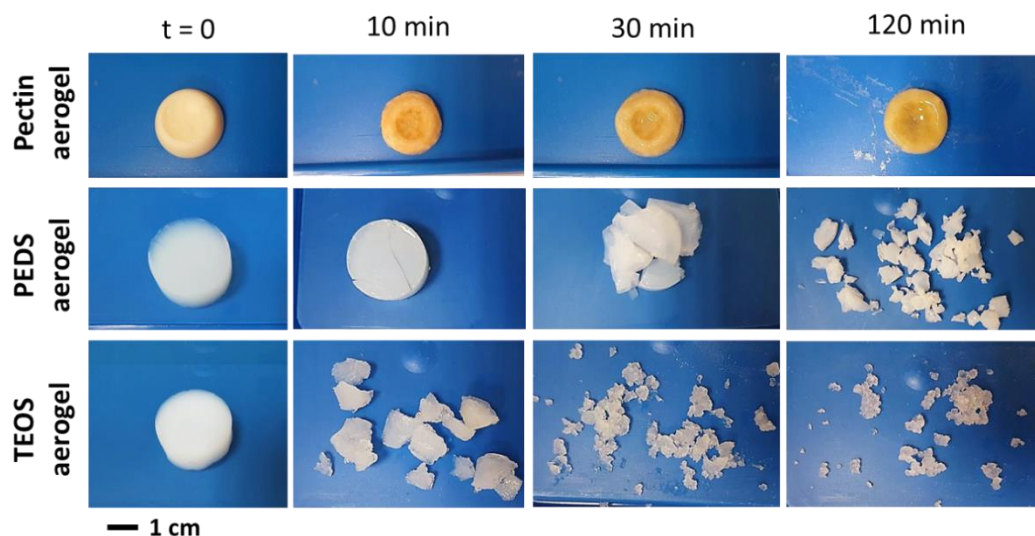


Figure 214. Pictures of pectin, PEDS and TEOS aerogels at different times during release experiment. Aerogels were immersed into SGF (pH 1.0) the first hour and in SIF (pH 6.8) the following hours, at 37°C.

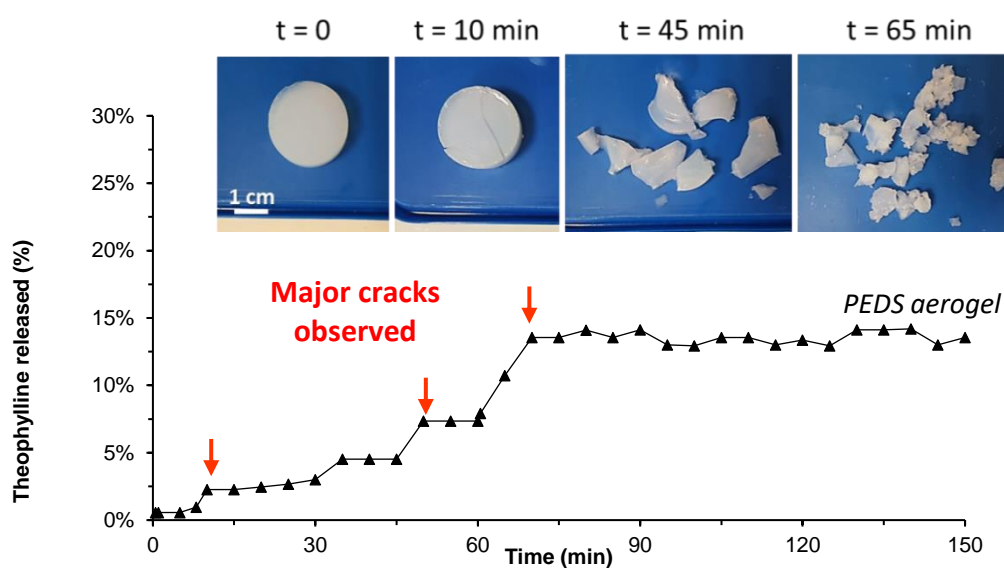


Figure 215. First two hours of release kinetics from PEDS aerogel (taken from Figure 213). The appearance of the major cracks is indicated by red arrows. The corresponding pictures of the PEDS aerogel are shown to illustrate the progressive degradation of the matrix over time.

Mathematical models such as Korsmeyer-Peppas and Peppas-Sahlin models consider both diffusional and relaxational phenomena as physical mechanisms involved in the release of a drug. We know that polymer relaxation does not occur in silica network like in pectin aerogels. Indeed, neat silica and silica-pectin aerogels are prone to physical bulk matrix erosion due to

cracks and pieces detachments. Despite knowing that, we choose to keep these models as they were used previously (Chapters V and VI) in order to provide a comparison between different matrices studied in the whole work. Thus, we will compare the kinetic coefficients obtained from Korsmeyer-Peppas and Peppas-Sahlin models, assuming that “relaxational” phenomena refers to matrix physical disintegration in case of silica aerogels.

Korsmeyer-Peppas mathematical models were applied with high fitting correlation to the data ( $R^2 \geq 0.90$ ) (Figure 216) to characterize the release mechanism of drug based on the value of  $n$  exponent (Table 22). We obtained  $n$  values of 0.54 and 0.56 for pectin aerogel and PEDS aerogels, respectively. As previously discussed,  $n$  values between  $0.45 < n < 0.89$  indicate that drug release was due to an anomalous transport governed by the coupling of diffusion and erosion mechanisms. On the opposite, the  $n$  value close to 0.89 for TEOS aerogels is characteristic to a Case II (which can turn into Super-case II) (see the detailed description of the models in the Section 2 of the Annex). In this case, solvent diffusion is much faster than erosion process. The rapid penetration to the center of the matrix occurs when solvent has a high affinity to the matrix or in the case of erosion-controlled release. In the case of TEOS aerogels, it is explained by TEOS high hydrophilicity (Figure 199 and Figure 200) coupled with rapid matrix disintegration (Figure 214).

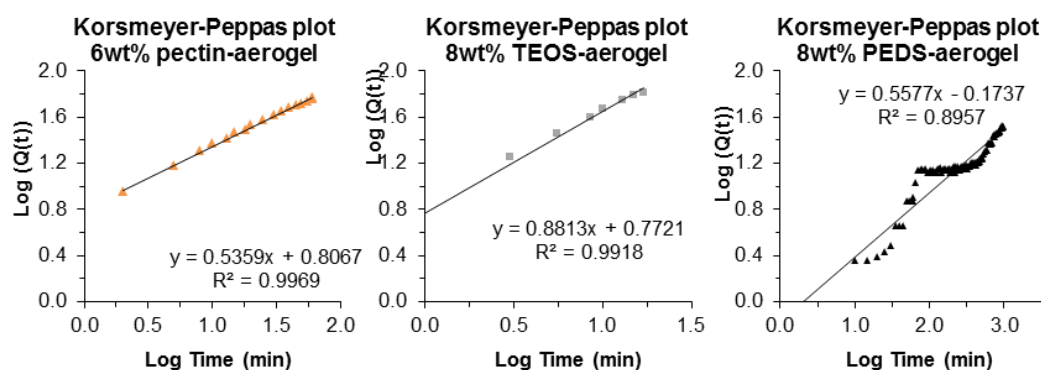


Figure 216. Korsmeyer-Peppas model on the first 60% release data of theophylline release from pectin aerogel, TEOS aerogel and PEDS aerogel.

Table 22. Korsmeyer-Peppas parameters of theophylline release from pectin aerogel, TEOS aerogel and PEDS aerogel.

Aerogel matrix composition	6wt% pectin aerogel	8wt% TEOS aerogel	8wt% PEDS aerogel
$n$ exponent	0.54	0.88	0.56
$R^2$	0.997	0.992	0.896

To explain different drug release behavior from pectin aerogel and PEDS aerogel, Peppas-Sahlin model was applied to highlight the differences in the coupling of diffusion and matrix erosion phenomena. The model plots and the estimations of Peppas-Sahlin parameters with good correlation to the data ( $R^2 \geq 0.89$ ) are presented in Figure 217 and Table 23, respectively. The calculation of the Fickian contribution to the release over time based on the estimated parameters is presented in Figure 218.

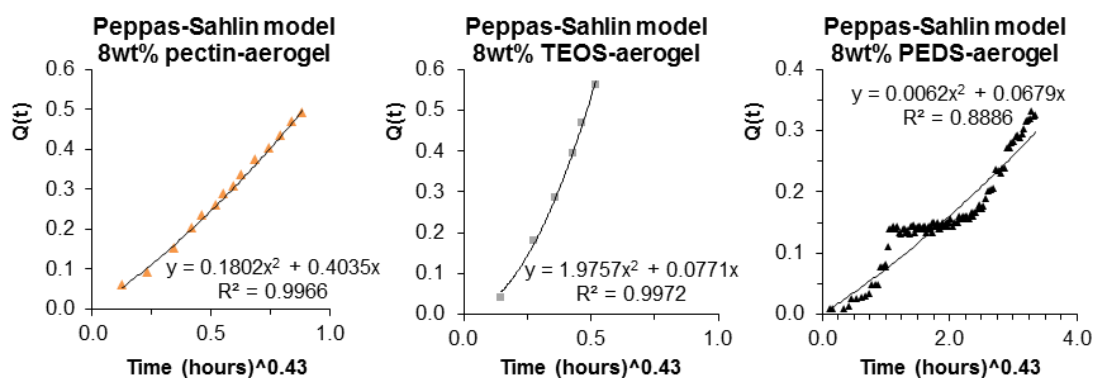


Figure 217. Peppas-Sahlin model for the first 60% release data from pectin aerogel, TEOS aerogel and PEDS aerogel.

Table 23. Peppas-Sahlin parameters using Fickian diffusional exponent  $m$  of 0.430 of theophylline release from pectin aerogel, TEOS aerogel and PEDS aerogel.

Aerogel matrix composition	6wt% pectin aerogel	8wt% TEOS aerogel	8wt% PEDS aerogel
Fickian coefficient $K_F$ ( $h^{-43}$ )	0.404	0.077	0.068
“Relaxational” coefficient $K_R$ ( $h^{-86}$ )	0.180	1.976	0.006
$R^2$	<b>0.997</b>	<b>0.997</b>	<b>0.889</b>

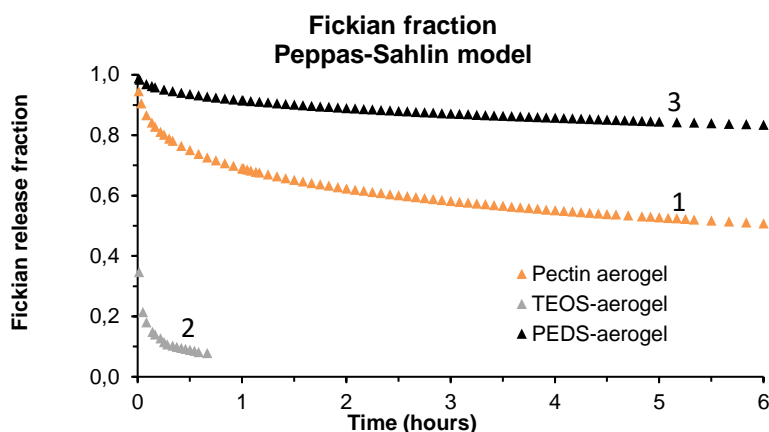


Figure 218. Fickian release fraction according to Peppas-Sahlin model using Fickian diffusional exponent  $m$  of 0.430, for the first 60% of released drug from pectin aerogel (1), TEOS aerogel (2) and PEDS aerogel (3).

In correlation with previous characterization (Chapter IV), theophylline release from pectin aerogels without calcium is diffusion-dissolution controlled, according to Peppas-Sahlin model, with nearly equivalent contributions of diffusion and matrix dissolution phenomena to drug release over time.

According to Peppas-Sahlin model, TEOS aerogel presents a high value of erosion coefficient ( $K_R \sim 1.976 \text{ h}^{-86}$ ) which is 25 times higher than diffusional coefficient ( $K_D \sim 0.077 \text{ h}^{-43}$ ). As it was found with Korsmeyer-Peppas plot, drug release from TEOS aerogel is clearly erosion-controlled with major contribution of matrix disintegration to drug release, as is it shown in Figure 218. On the opposite, PEDS aerogel presents the lowest erosion ( $K_R \sim 0.006 \text{ h}^{-86}$ ) and diffusional ( $K_D \sim 0.068 \text{ h}^{-43}$ ) coefficients, in relation with the extremely slow release of the drug observed over time (Figure 213). In addition, it has to be noted that the erosion coefficient ( $K_R$ ) is ten times lower than the diffusional one ( $K_D$ ), meaning that matrix erosion phenomena had only a small contribution to the release as compared to slow but continuous diffusion phenomena within the system (determining step). We assume that apart from the aerogel breaking which rapidly release around 20% of the drug especially in the first hours of experiment, the release was actually mostly governed by the slow liquid diffusion within the system limited by the hydrophobicity of the PEDS network.

### 2.3.2. Theophylline release from pectin-silica composite aerogels

This section is organized as follows:

- First, we investigate the release of theophylline from pectin-silica composite aerogels with either TEOS or PEDS. The influence of the R(Ca) ratio on release properties of pectin-silica composite aerogels is investigated. The release behaviour and matrix “stability” of pectin-silica are compared to neat pectin and neat silica aerogels.
- Then, we use the same mathematical models as previously to characterize and compare the main physical mechanisms involved in the release of theophylline out of the different matrices.

➤ Without calcium crosslinking

The dependence of theophylline release over time from 6 wt% pectin-8 wt% TEOS and from 6 wt% pectin-8 wt% PEDS composite aerogels without calcium and the evolution of the matrix mass over time are presented in Figure 219 and Figure 220, respectively. Release from neat 6 wt% pectin (without calcium) and neat 8 wt% silica aerogels (TEOS and PEDS) are also plotted for comparison. Visual aspects of aerogels matrices during the release experiments are presented for illustration on Figure 221.

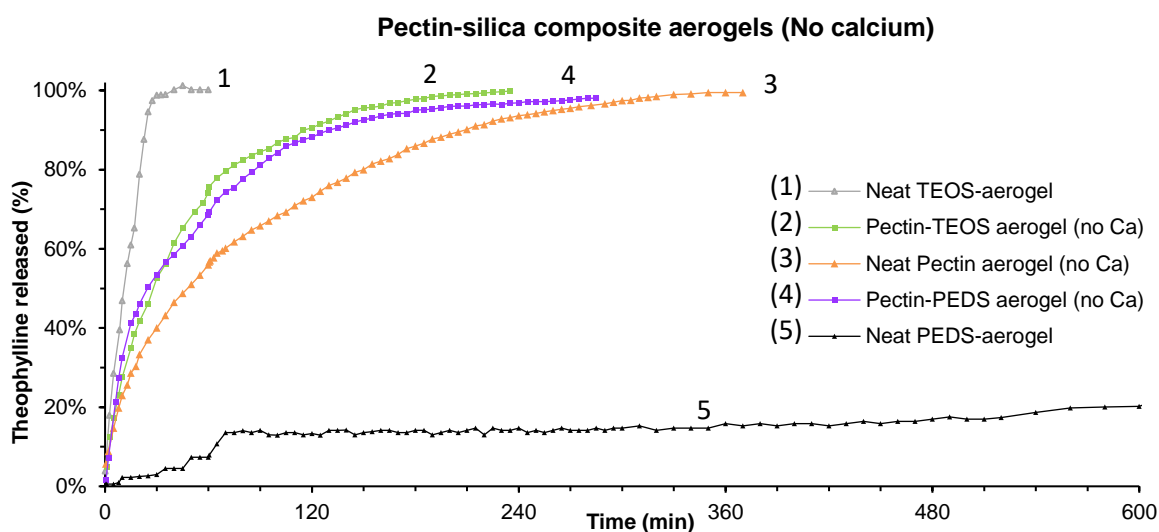


Figure 219. Theophylline cumulative release (%) over time from 8 wt% TEOS aerogel (1), 6 wt% pectin-8 wt% TEOS aerogel (2), 6 wt% pectin aerogel (3), 6 wt% pectin-8 wt% PEDS aerogel (4) and from 8 wt% PEDS aerogel (5). All pectin matrices were produced without calcium.

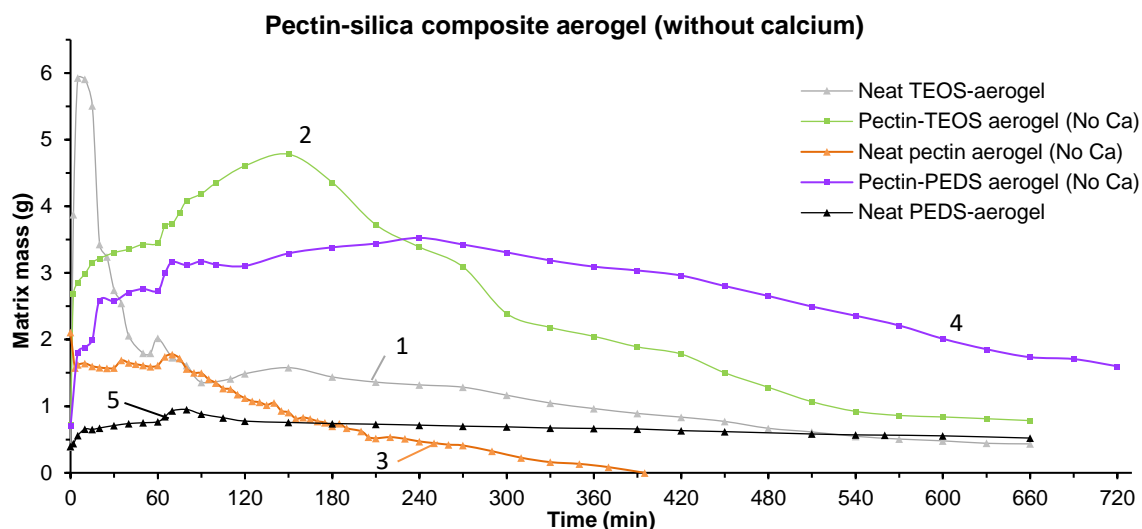


Figure 220. Matrix mass evolution over time: 8 wt% TEOS aerogel (1), 6 wt% pectin-8 wt% TEOS aerogel (2), 6 wt% pectin aerogel (3), 6 wt% pectin-8 wt% PEDS aerogel (4) and from 8 wt% PEDS aerogel (5). All pectin matrices were produced without calcium.

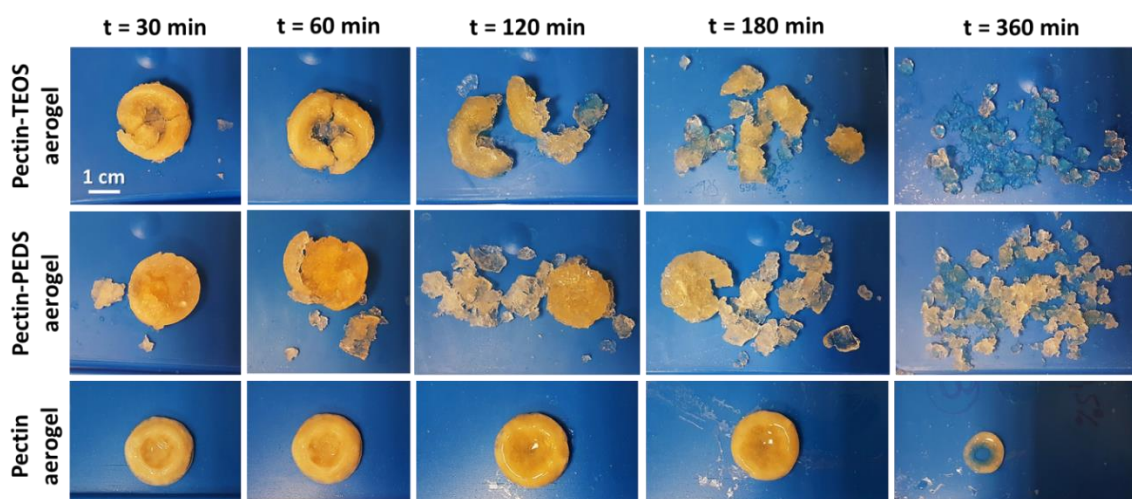


Figure 221. Pictures of neat pectin aerogel and 6 wt% pectin – 8 wt% silica composite aerogels over time during release experiment using either TEOS or PEDS as silica sol. Pectin matrices were produced without calcium at pH 3.0.

Unexpectedly, both pectin-silica composite aerogels (using either TEOS or PEDS as silica sol) showed similar release behaviour, as shown in Figure 219. Indeed, full release occurred rapidly in around 235 min from pectin-TEOS aerogel and in 285 min for pectin-PEDS aerogel. In both cases, the release of theophylline from pectin-silica composites was significantly faster than from neat pectin aerogel, despite that pectin content was the same in the three matrices, and that the total amount of “solids” (pectin + silica) (14 wt%) in the composite aerogels and their density was more than doubled as compared to neat pectin aerogel

(6 wt%). Higher density was supposed to slow down the release. This means that the addition of TEOS or PEDS to pectin matrices actually promoted and accelerated the release of theophylline from the system. Given the opposite physico-chemical and drug release properties of neat TEOS and PEDS aerogels (see Figure 200 and Figure 213), we found surprising that their composites with pectin displayed such similar drug release profile once put in gastrointestinal simulated liquid media.

By observing the visual aspects and physical integrity (Figure 221) and by following the matrix mass (Figure 220) over time of pectin-silica aerogels, we conclude that the release profile actually resulted from the same brittle characteristic of silica aerogels based on either PEDS or TEOS. We could observe that once in contact with release liquids, both pectin-TEOS and pectin-PEDS composite aerogels fractured and progressively cracked into pieces because of silica phase, which promoted solvent penetration, dissolution of pectin and the release of theophylline.

The contact angle of water with composite is presented in Figure 222; it reveals that all pectin-silica composites were hydrophilic, explaining the wettability and fast solvent penetration into the system observed during release experiments. Indeed, pectin-TEOS composite was found to be highly hydrophilic materials (contact angle non-measurable) as both pectin and TEOS are highly hydrophilic components. Pectin-PEDS composite aerogels presented an intermediate hydrophilicity (contact angle around  $75^\circ - 60^\circ$ ) between the highly hydrophilic pectin aerogels and rather hydrophobic PEDS aerogels. We assume that the hydrophilicity of the pectin fraction dominates in the pectin-PEDS composite aerogels, leading to the overall hydrophilic composite.

Due to the hydrophobicity of PEDS, pectin-PEDS composite aerogels were significantly less hydrophilic than pectin-TEOS aerogels. Finally, we noticed that the external surface of the pectin-PEDS aerogel was more hydrophobic than its core, which can be related to the external layer richer in silica than the core due to the impregnation process route.

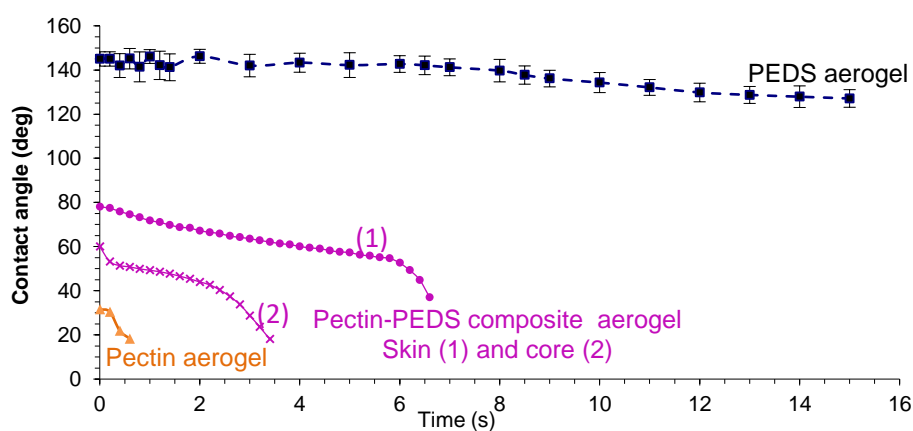


Figure 222. Contact angle with water of neat pectin aerogels, neat silica aerogels and pectin-silica composite aerogels, using TEOS or PEDS as silica sol, as a function of time. For TEOS aerogel and pectin-TEOS aerogel water droplet was immediately absorbed.

Due to their hydrophilicity, the pectin-silica composite aerogels were all rapidly penetrated by the aqueous media (regardless to the type of silica sol), resulting in a strong and fast mass intake for both pectin-PEDS (+200 % in 5 minutes as compared to dry weight) and pectin-TEOS (+300 % in 5 minutes as compared to dry weight) composite aerogels (Figure 220). The highly re-hydrated pectin-silica aerogels progressively cracked due to the brittleness of silica network and capillary forces due to liquid filling. It has to be noted that pectin-TEOS composite aerogels fractured more rapidly and eroded faster than pectin-PEDS aerogels (Figure 221 and Figure 220) leading to an even faster drug release than from pectin-PEDS aerogels (Figure 219).

To conclude, in the absence of calcium, a quite fast release of theophylline from pectin-silica composite aerogels occurred due to the breakage of silica part, inducing breakage of the whole composite aerogel and inducing high solvent velocity and matrix erosion. While the release from pectin-TEOS is in-between the release of the corresponding neat compounds, this is not the case for pectin-PEDS composite aerogels which do not obey the “mixing rule”. As it will be shown below, theophylline release profile from pectin-silica composite and matrix “stability” in liquid media turned to be different when calcium was cross-linking pectin.

➤ *Pectin cross-linked with calcium*

Based on our previous results on pectin aerogels and pectin-cellulose composite aerogels, the addition of calcium to pectin is expected to impact theophylline release from pectin-silica composite aerogels. Here we first study the release kinetics from neat pectin aerogels (the same trends as shown in Chapter V), pectin-TEOS and pectin-PEDS composite aerogels separately, each type at different R(Ca) ratio, up to 0.4. Then we set a high calcium ratio  $R(\text{Ca}) = 0.4$  and compare the influence of the type of silica sol (TEOS vs PEDS) on the release properties of pectin-silica composite aerogels in presence of calcium.

Theophylline release over time from 6 wt% pectin aerogels, 6 wt% pectin – 8 wt% TEOS and from 6 wt% pectin – 8 wt% PEDS composite aerogels at different R ratio are presented in Figure 223, Figure 224 and Figure 225, respectively. The evolution of the mass of the corresponding matrices over time is presented in Figure 226 (A), (B), and (C), respectively, and their visual aspects during the release experiments on Figure 226(D).

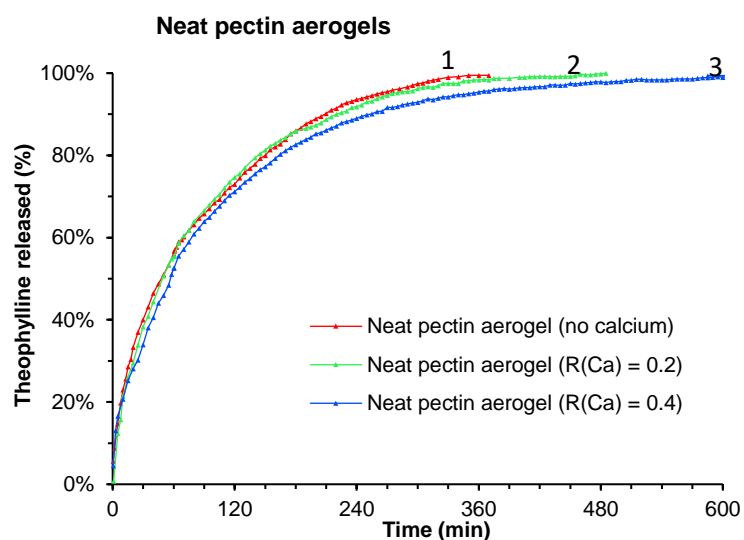


Figure 223. Theophylline cumulative release (%) over time from 6 wt% pectin aerogels while varying R(Ca) ratio of pectin matrices from 0 (no calcium) (1), to 0.2 (2), and to 0.4 (3). All pectin matrices were produced from 6 wt% pectin P35 dissolved at pH 3.0.

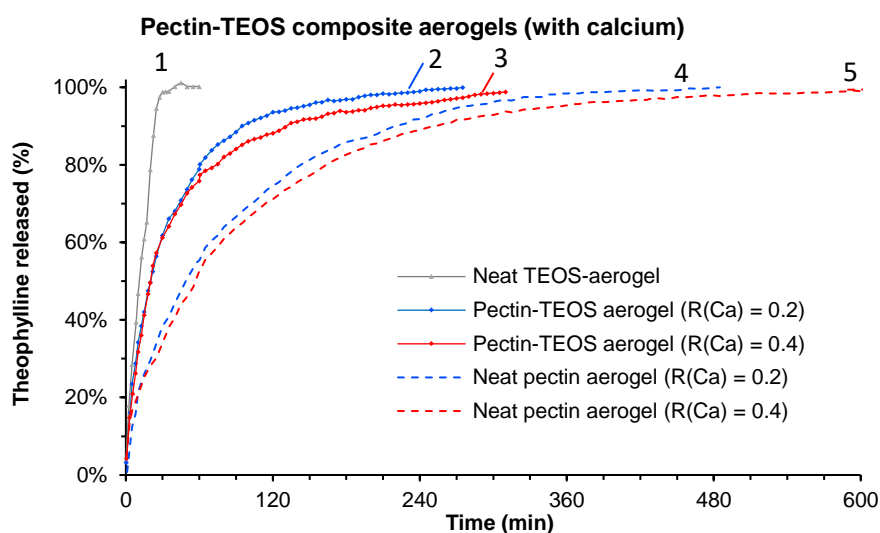


Figure 224. Theophylline cumulative release (%) over time from: 8 wt% TEOS aerogel (1), 6 wt% pectin-8 wt% TEOS aerogel with R(Ca) = 0.2 (2), 6 wt% pectin-8 wt% TEOS aerogel with R(Ca) = 0.4 (3), and 6 wt% pectin aerogels with R(Ca) = 0.2 (4) and R(Ca) = 0.4 (5). All pectin matrices were produced from 6 wt% pectin P35 dissolved at pH 3.0.

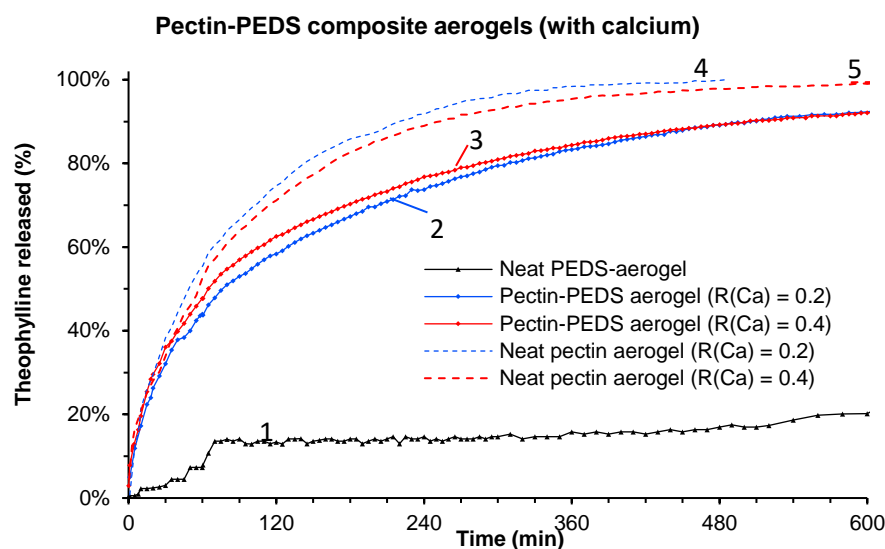
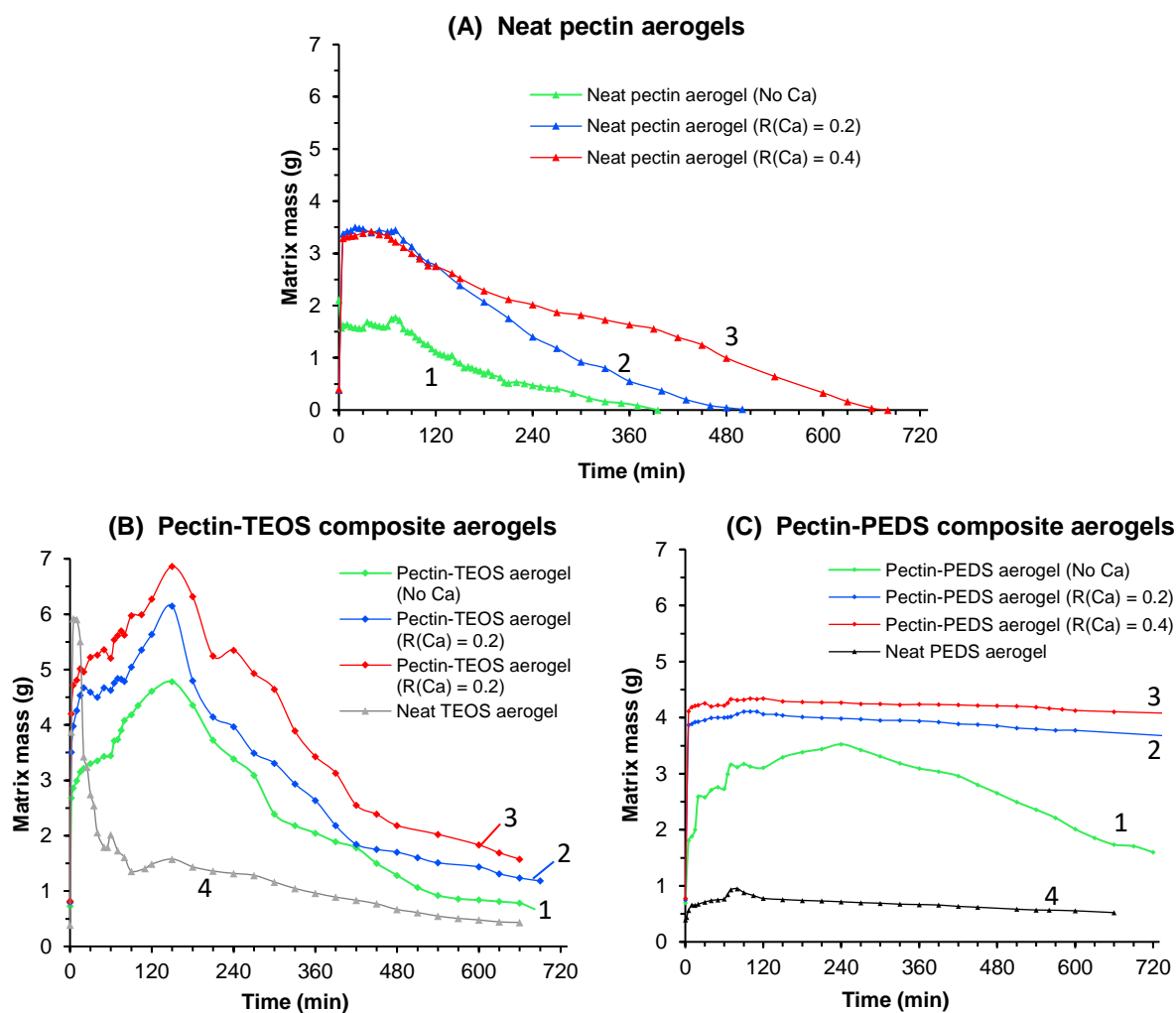


Figure 225. Theophylline cumulative release (%) over time from: 8 wt% PEDS aerogel (1), 6 wt% pectin-8 wt% PEDS aerogel with  $R(\text{Ca}) = 0.2$  (2), 6 wt% pectin-8 wt% PEDS aerogel with  $R(\text{Ca}) = 0.4$  (3), and 6 wt% pectin aerogels with  $R(\text{Ca}) = 0.2$  (4) and  $R(\text{Ca}) = 0.4$  (5). All pectin matrices were produced from 6 wt% pectin P35 dissolved at pH 3.0.



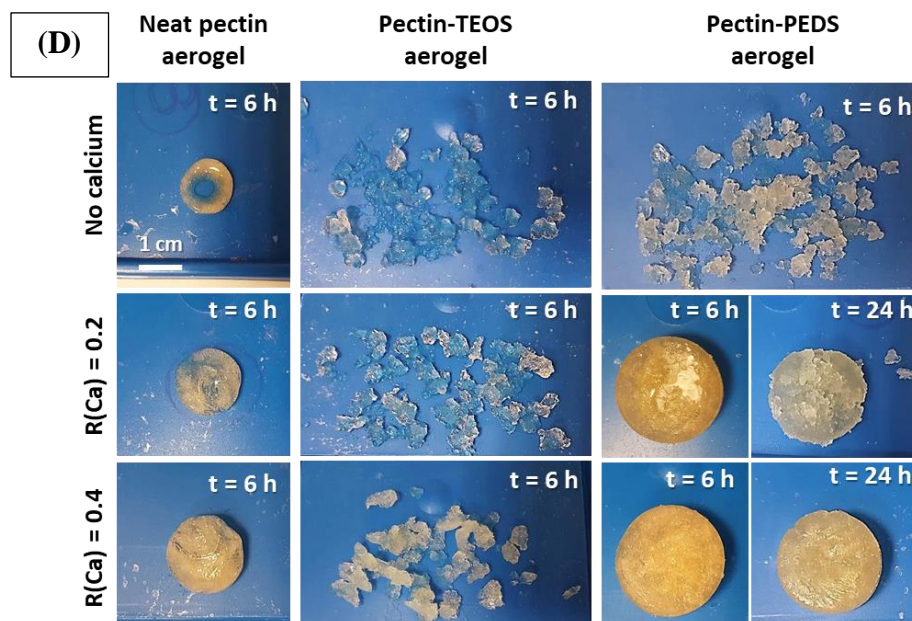


Figure 226. Aerogel mass evolution over time of (A) neat pectin aerogels, (B) 6 wt% pectin-8 wt% TEOS and (C) 6 wt% pectin-8 wt% PEDS composite aerogels while varying  $R(\text{Ca})$  ratio from 0 (no calcium) (curve 1), to 0.2 (curve 2), to 0.4 (curve 3). In (B) and (C), neat silica aerogels (using TEOS or PEDS) are plotted as reference (curve 4).

(D) Pictures of neat pectin aerogels and 6 wt% pectin – 8 wt% silica composite aerogels after 6 and 24 hours of release experiment, using either TEOS or PEDS as silica sol. Pectin matrices were produced either without calcium or with calcium at  $R(\text{Ca}) = 0.2$  or  $R(\text{Ca}) = 0.4$ . Neat pectin aerogels are shown as references.

As it was previously discussed, the addition of calcium to pectin solutions increased the “stability” of pectin aerogels when immersed into simulated physiological fluids (Chapter V and VI Section 1.), slowing down matrix erosion (Figure 226 A) and thus the release of the drug (Figure 223). As shown in Figure 226 (B), (C) and (D), the erosion of pectin-silica composite aerogels was also clearly impacted by pectin cross-linking with calcium.

For comparison, we plotted the time needed to release 100% of total theophylline as a function of the composition of the aerogel matrix in Figure 227. As it can be seen, the duration of drug release out of the matrix was prolonged by increasing calcium  $R(\text{Ca})$  ratio and was also strongly influenced by the matrix composition (neat pectin or pectin-silica composites, type of silica). Depending on matrix composition and calcium concentration, theophylline release out of aerogels immersed into simulated gastro-intestinal fluids at  $37^\circ\text{C}$  could be either immediate (40 min from TEOS aerogels), extended to several hours (neat pectin aerogels with and without calcium), or prolonged up to more than 24 hours (Pectin-PEDS composite aerogels with  $R(\text{Ca}) = 0.4$ ).

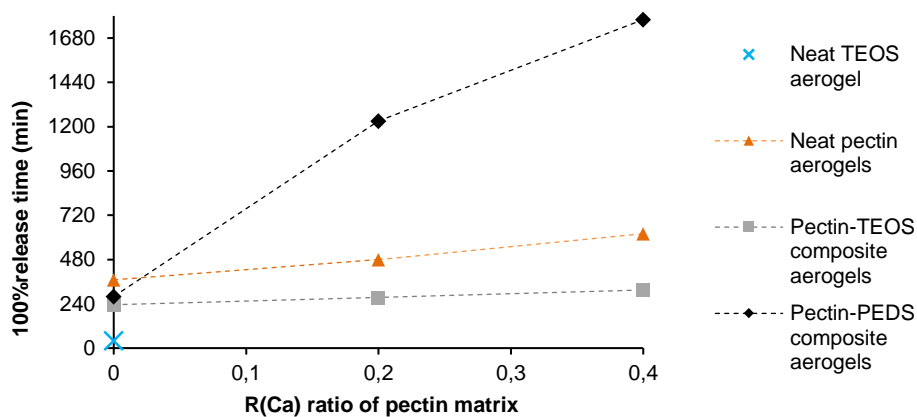


Figure 227. Time needed to release 100% of total theophylline from neat 8 wt% silica (from TEOS), neat 6 wt% pectin, and 6 wt% pectin – 8 wt% silica (from TEOS or PEDS) composite aerogels immersed into simulated gastro-intestinal fluids at 37°C while varying their composition (pectin, TEOS, PEDS) and calcium R(Ca) ratio. All pectin matrices were produced from 6 wt% pectin P35 dissolved at pH 3.0.

As presented in Figure 226 (B), the highly hydrophilic pectin-TEOS composite aerogels were quickly filled with release medium with mass uptake up to +700% (as compared to the dry weight) due to liquid penetration. In the same way as neat TEOS aerogels (Figure 214) and pectin-TEOS aerogels without calcium (Figure 221), pectin-TEOS composite with calcium rapidly fractured and cracked into many pieces (Figure 226). As already known, increasing calcium concentration in pectin matrices leads to aerogels of lower density due to higher volume, which results in higher mass uptake when filled by release media. Both the addition of TEOS and pectin cross-linking with calcium strongly promoted liquid diffusion inside composite aerogel. Even if matrix erosion was slightly slowed down by pectin cross-linking with calcium and thus slightly delaying the complete drug release (from 240 min without calcium to 310 min with  $R(\text{Ca}) = 0.4$ ), all pectin-TEOS aerogels rapidly lost their physical integrity and completely broke into pieces in less than 3 hours, independently of calcium concentration (Figure 226 D). As a result, whatever calcium concentration, the release of theophylline from pectin-TEOS composite aerogels was significantly accelerated and promoted as compared to that from neat cross-linked pectin aerogels. As well as in the case without calcium, matrix erosion properties and drug release profiles from pectin-TEOS composite with calcium displayed intermediate properties between neat cross-linked pectin aerogels and neat TEOS aerogel.

On the opposite, the use of PEDS as silica sol was found to drastically change the release of theophylline from pectin-PEDS composite aerogels when pectin was cross-linked with calcium. As shown in Figure 226 (C), the presence of calcium in pectin-PEDS composite aerogels strongly stabilized the pectin-PEDS matrices and slowed down matrix bulk erosion process as compared to that observed for the same composites but without calcium. In the

absence of calcium, the pectin-PEDS composite aerogel quickly fractured and was completely broken into pieces in 3 hours of immersion into release medium (Figure 221), completely releasing theophylline in 280 min (Figure 225). When pectin was cross-linked with calcium, the liquid filling composite aerogels was slowed down because of hydrophobic PEDS and matrix erosion inhibited because of pectin cross-linking, as it is revealed by their nearly constant mass and low density around  $1.065$  to  $1.07$  g/cm<sup>3</sup> over the first 11 hours of experiment, for both calcium concentrations. Even if pectin-PEDS aerogels with calcium presented small surface cracks once immersed into release medium, the physical integrity of the composite aerogels with calcium was maintained up to 11 h for  $R(\text{Ca}) = 0.2$  and up to 30 h for  $R(\text{Ca}) = 0.4$ , contrary to composites without calcium (disintegration in less than 1 h). As a result, the complete release of theophylline from pectin-PEDS matrices was strongly slowed down from 280 min without calcium, to around 1230 min for  $R(\text{Ca}) = 0.2$  and 1780 min for  $R(\text{Ca}) = 0.4$ , which is more than 3 and 5 times longer, respectively, than from pectin-PEDS aerogels without calcium.

As it can be seen in Figure 228, the pectin-PEDS composite silica which was initially yellow due to the presence of pectin at the beginning of release testing, was progressively turning transparent (which is typical for silica aerogel) starting from the external layer of the composite to its core. After 11 h of experiment, we were still able to note the maintenance of a denser yellowish core, most likely richer in pectin than the external layer of the composite. These observations suggest the progressive disappearance of pectin by dissolution within the pectin-silica composite while the silica network remained nearly intact during 11 h of immersion due to its non-solubility in the release aqueous media. When pectin concentration became too low after a certain time of dissolution, we assume that the remaining pectin network became too weak to physically maintain and stabilize the brittle silica network which started to erode into pieces (after at least 11 h of experiment). This assumption is in accordance with the gradual and very low reduction of the composite mass over time (Figure 226 (C)).

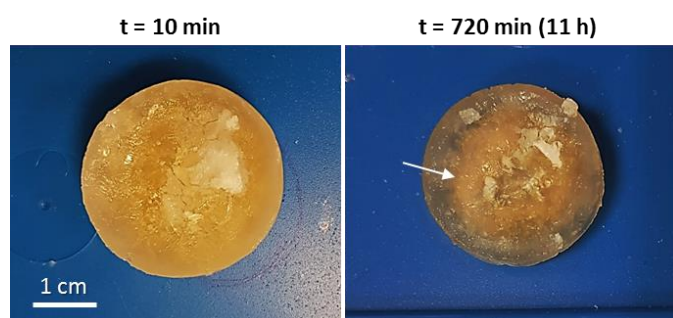


Figure 228. Pictures of 6 wt% pectin-8 wt% PEDS composite aerogel with calcium at  $R(\text{Ca}) = 0.2$  after 10 minutes and 720 min of immersion into gastro-intestinal simulated fluids. The arrow shows the border between a denser and yellowish core of the composite, which is probably richer in pectin, and transparent external layer (typical for silica). The scale is the same for both pictures.

We assume that covering of pectin chains by PEDS (Figure 208) protected the matrix from liquid penetration within the system and pectin dissolution, while ionic junctions between pectin chains and calcium ions significantly increased i) the “stability” of pectin network delaying even more its dissolution and ii) mechanical resistance of the overall network to physical breakage once immersed into gastro-intestinal liquid. Cross-linking of pectin with calcium delayed pectin dissolution and improved the mechanical properties of pectin network, as compared to non-cross-linked case. As a result, the release properties of pectin-PEDS composite aerogels with calcium displayed intermediate properties to neat pectin (with calcium) and neat PEDS aerogels. Contrary to pectin-PEDS composite aerogels without calcium prone to quick physical disintegration in liquid media, the release properties of pectin-PEDS composite were found to follow the “mixing law” when calcium was added ( $R(\text{Ca}) = 0.2$  and  $0.4$ ). Indeed, the presence of calcium prevented physical breakage of composite matrix in gastro-intestinal liquid which delayed the release as compared to non-cross-linked composite aerogel. The release from composite aerogel with cross-linked pectin was governed by the slow dissolution of pectin which even more slowed down because of the presence of “resistant” PEDS part. Each component plays an important role in the release behaviour allowing modulating its kinetics.

Figure 229 and Figure 230 perfectly illustrates the “mixing rule” followed by pectin-TEOS and pectin-PEDS composite aerogels when calcium was added to pectin matrixes (at  $R(\text{Ca}) = 0.2$  and  $0.4$ ). As it can be seen, the release kinetics and matrix erosion over time of pectin-silica composite (using PEDS or TEOS) appeared to be “in-between” as compared to neat pectin (with calcium) and the corresponding neat silica aerogels.

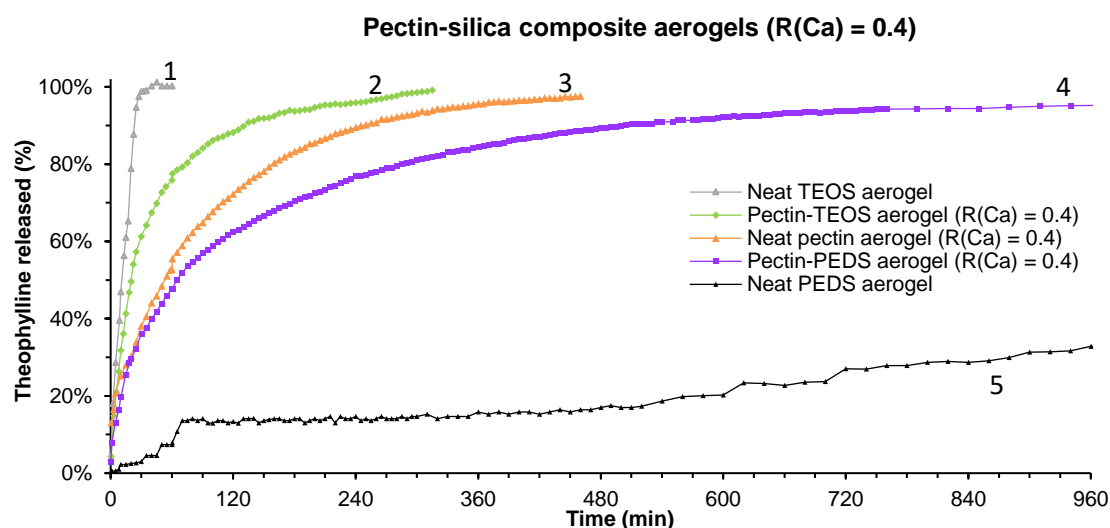


Figure 229. Theophylline cumulative release over time from 8 wt% TEOS aerogel (1) 6 wt% pectin-8 wt% TEOS aerogel (2), 6 wt% pectin-8 wt% PEDS aerogel (3), 6 wt% pectin aerogel (4) and 8 wt% PEDS (5). All pectin matrixes were produced from 6 wt% pectin P35 dissolved at pH 3.0 cross-linked with calcium at  $R(\text{Ca}) = 0.4$ .

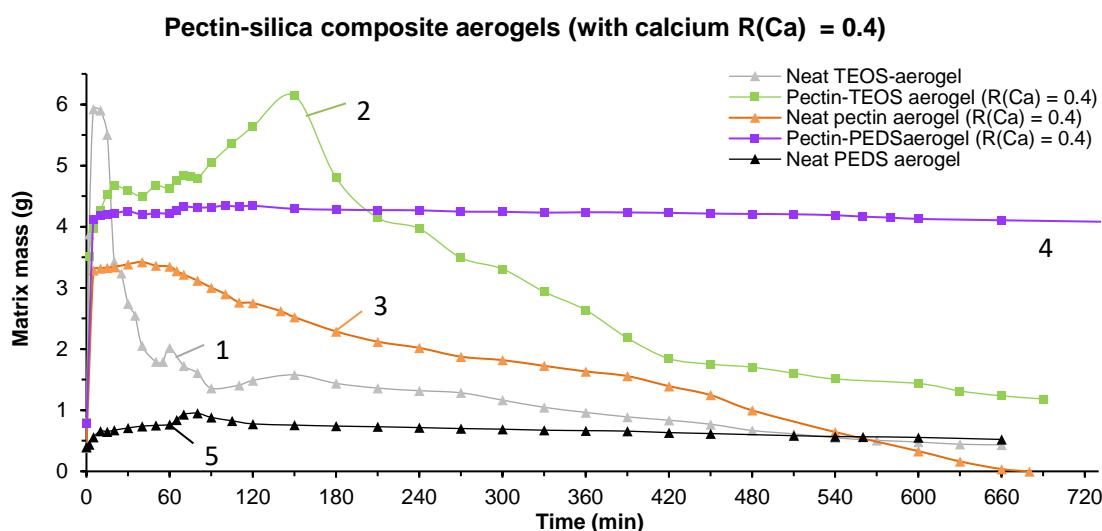


Figure 230. Matrix mass evolution over time: 8 wt% TEOS aerogel (1) 6wt%pectin-8wt%TEOS aerogel (2) 6wt% pectin-8wt% PEDS aerogel (3) 6wt%pectin aerogel (4), from 6wt% pectin-8wt% PEDS aerogel from 8wt% PEDS (5). All pectin matrices were produced from 6wt% pectin P35 dissolved at pH 3.0 with calcium at R(Ca) = 0.4.

The release of theophylline from pectin-silica composite aerogels with and without pectin cross-linked by calcium was analyzed by mathematical models. Best model fittings to data were obtained by plotting Korsmeyer-Peppas model (Figure 231 and Table 24) and Peppas-Sahlin models (Figure 232 and

Table 25) to the data with high correlation ( $R^2 \geq 0.99$ ). As a reminder, we will compare the kinetics coefficients obtained from Korsmeyer-Peppas and Peppas-Sahlin models, assuming that “relaxational” phenomena from the two models also refer to matrix physical disintegration by pieces detachment. We know that polymer relaxation does not occur in silica network like in pectin aerogels.

Table 24. Korsmeyer-Peppas parameters of theophylline release experiments from pectin aerogel, pectin-TEOS composite aerogels, and pectin-PEDS composite aerogels while varying R(Ca) ratio.

Aerogel matrix composition	Pectin aerogel			Pectin-TEOS composite aerogel			Pectin-PEDS composite aerogel		
	0	0.2	0.4	0	0.2	0.4	0	0.2	0.4
Calcium ratio R(Ca) of the pectin matrix									
<i>n</i> exponent	0.54	0.52	0.48	0.64	0.66	0.69	0.69	0.46	0.46
$R^2$	<b>0.997</b>	<b>0.997</b>	<b>0.987</b>	<b>0.997</b>	<b>0.994</b>	<b>0.998</b>	<b>0.994</b>	<b>0.995</b>	<b>0.996</b>

Table 25. Peppas-Sahlin parameters using Fickian diffusional exponent  $m$  of 0.430 of theophylline release from pectin aerogel, pectin-TEOS composite aerogels and pectin-PEDS composite aerogels while varying R(Ca) ratio.

Aerogel matrix composition	Pectin aerogel			Pectin-TEOS composite aerogel			Pectin-PEDS composite aerogel		
	0	0.2	0.4	0	0.2	0.4	0	0.2	0.4
Calcium ratio R(Ca) of the pectin matrix									
Fickian coefficient $K_F$ ( $h^{-43}$ )	0.404	0.362	0.363	0.337	0.453	0.301	0.444	0.375	0.426
“Relaxational” coefficient $K_R$ ( $h^{-86}$ )	0.180	0.196	0.154	0.515	0.558	0.799	0.472	0.066	0.054
$R^2$	0.997	0.999	0.994	0.995	0.994	0.998	0.989	0.997	0.997

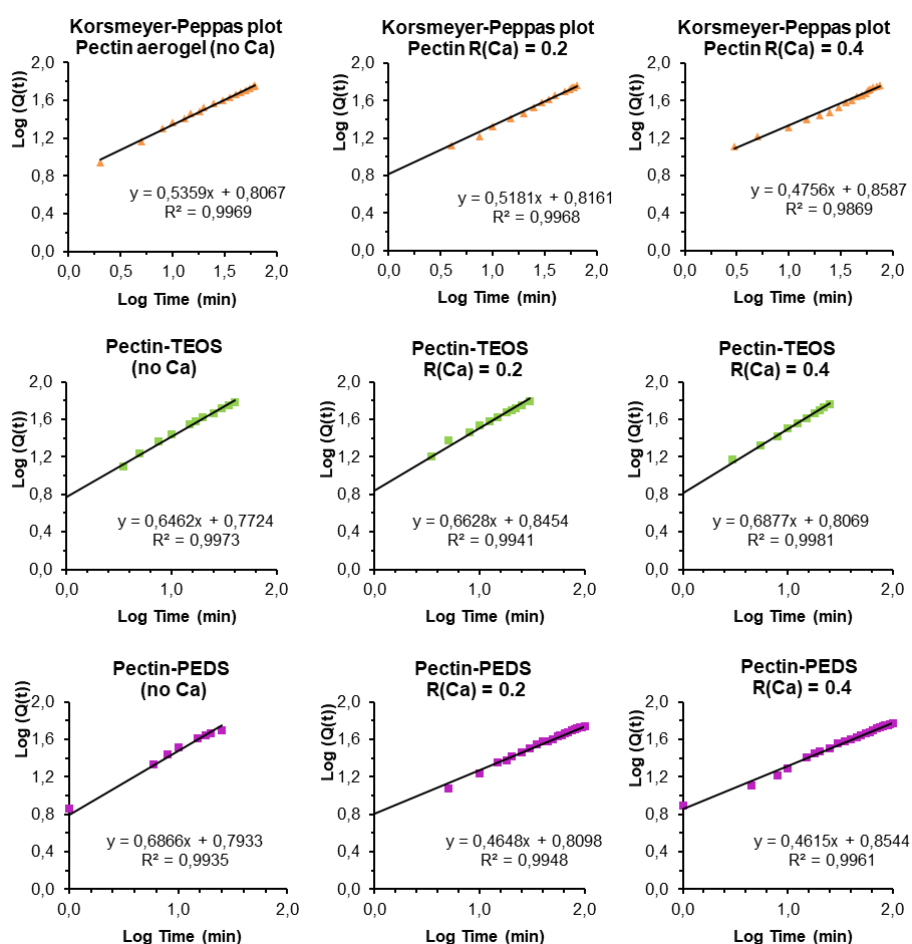


Figure 231. Korsmeyer-Peppas plot of theophylline release from pectin aerogel, pectin-TEOS composite aerogels and pectin-PEDS composite aerogels while varying R(Ca).

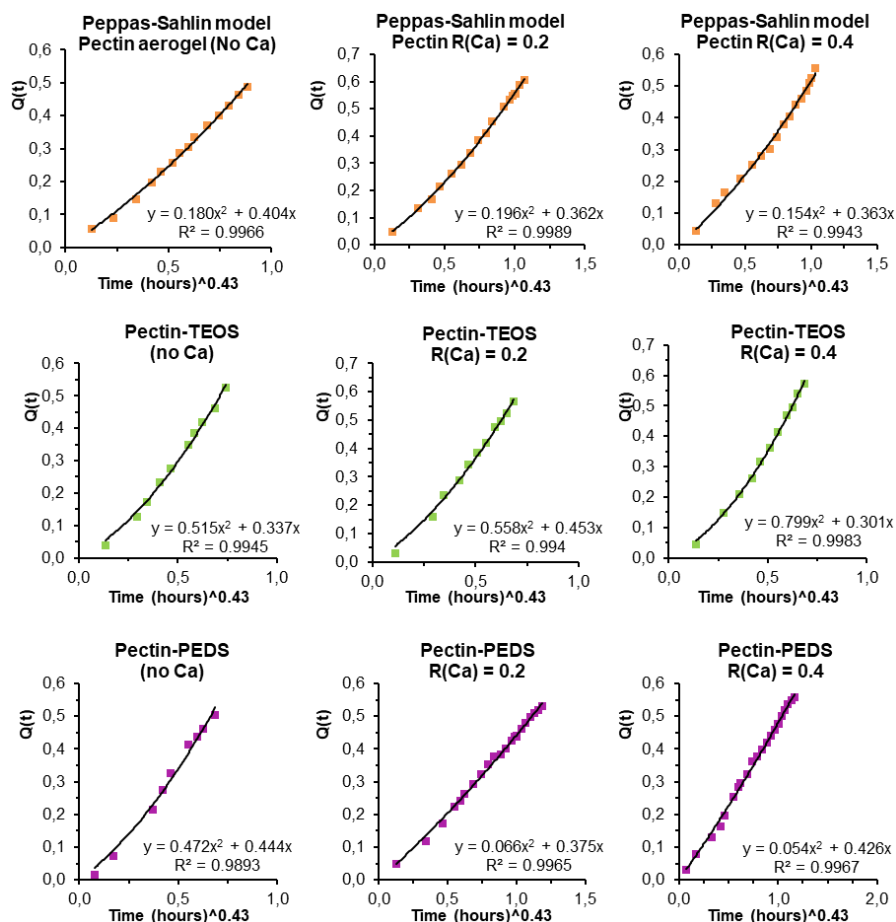


Figure 232. Peppas-Sahlin plot of theophylline release from pectin aerogel, pectin-TEOS composite aerogels and pectin-PEDS composite aerogels while varying  $R(\text{Ca})$ .

The results of the application of mathematical models are consistent with our observations and assumptions about the release properties of pectin-silica composite aerogels varying the type of silica sol and calcium concentration.

- As already found in Chapter V, we obtained  $n$  exponent values around 0.50- 0.55 (between  $0.45 < n < 0.89$ ) for all pectin aerogels with or without calcium added, which is characteristic of an anomalous transport of the drug, governed by the coupling of matrix erosion and diffusion phenomena. As a result of a high pectin concentration and a relatively “high” aerogel density, diffusional phenomena had a higher contribution to the release of the drug than relaxational phenomena (slow matrix dissolution), as revealed by the twice higher Fickian coefficient ( $K_F \sim 0.40 \text{ h}^{-43}$ ) than relaxational coefficient ( $K_R \sim 0.18 \text{ h}^{-86}$ ) using Peppas-Sahlin model (Table 25).

For both pectin-TEOS and pectin-PEDS composite aerogels without calcium, we obtained similar  $n$  values around 0.65 - 0.7 (anomalous transport case using Korsmeyer-Peppas model)

despite the different type of silica sol. As we already mentioned, the strong bulk erosion observed over time due to the brittleness of both types of the silica networks (TEOS and PEDS) might have predominately governed the release of theophylline out of the matrix.

This interpretation is also supported by the higher values of  $K_R$  coefficients (erosion) than  $K_F$  coefficients (diffusion) using Peppas-Sahlin model for both pectin-silica composite matrices without calcium. The plot of Fickian release fraction over time on Figure 233 clearly shows the predominance of the contribution of erosion phenomena in the release the drug from composite aerogels made from pectin-silica (from TEOS and PEDS) and in absence of calcium. The interpretation of this case is consistent with what is commonly reported in literature for non-hydrophobized classical silica aerogels, whose physical degradation of the structure promotes the release of the drug (Caputo et al., 2012; Mehling et al., 2009; Mohammadian et al., 2018; I. Smirnova et al., 2004; I. Smirnova et al., 2005, 2004).

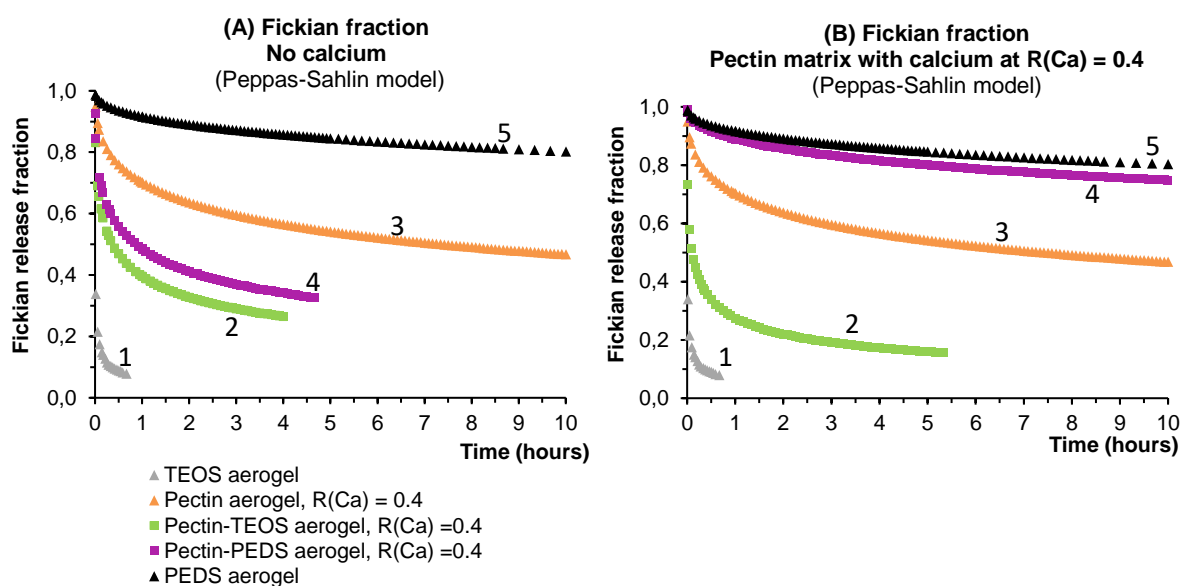


Figure 233. Fickian release fraction over time from 8 wt% TEOS aerogel (1), 6 wt% pectin-8 wt% TEOS aerogel (2), 6 wt% pectin aerogel (3), 6 wt% pectin-8 wt% PEDS aerogel (4) and 8 wt% PEDS (5). All pectin matrices were produced from 6 wt% pectin P35 dissolved at pH 3.0 without calcium (A) or with calcium at  $R(\text{Ca}) = 0.4$  (B).

Finally, when calcium was added to cross-link pectin in pectin-silica composites (with  $R(\text{Ca}) \geq 0.2$ ), the release of the drug from pectin-PEDS composite aerogels with calcium was found to be “in-between” between the release properties of neat cross-linked pectin and neat silica aerogels. We obtained two significantly different release behaviours depending on the type of silica sol:

- For theophylline release from pectin-TEOS aerogels with calcium, we obtained the same range of  $n$  values around 0.65 - 0.7 (anomalous transport case using Korsmeyer-Peppas model) similar to composite without calcium and independent of calcium  $R$  ratio. The use of Peppas-Sahlin model shows that the

contribution of erosion phenomena to the release of the drug was highly predominant ( $K_R > K_F$ ) and pectin-TEOS aerogels regardless the calcium conditions, similarly to neat TEOS aerogels (Table 22 and Table 23).

- On the opposite, cross-linking of pectin by calcium in PEDS-pectin composite aerogels strongly reduced the  $n$  exponents values from  $\sim 0.69$  without calcium (diffusion-erosion control) to around 0.46 with calcium added, which is characteristic to a Fickian diffusion-controlled release of the drug. This strong change in drug release behaviour was also obtained using Peppas-Sahlin model as revealed by very low erosion coefficients ( $K_R < 0.07 \text{ h}^{-86}$ ) and the predominance of diffusional contribution to the release of the drug (Figure 233) when calcium was added. It has to be noted that drug release profile from pectin-PEDS with calcium with slow Fickian diffusion over time is similar to the release behaviour of neat PEDS aerogels (Table 22 and Table 23). Thus, we assume that calcium crosslinking of the pectin strengthened and maintained the physical integrity of the overall composite structure which counterbalanced the brittleness of the silica part. As a result, theophylline release was promoted by pectin hydrophilicity and solubility, while the hydrophobicity of the PEDS network slowed down all mass transport phenomena within the composite matrix. Overall, it led to very slow Fickian diffusion of theophylline from a nearly stable matrix.

It is interesting to see that in the absence of calcium, the high brittleness of both pectin-TEOS and pectin-PEDS composite aerogels due to silica prevailed and governed the release by strong bulk erosion (Figure 219). However, pectin-silica composite with calcium were perfectly following the “mixing rule”, with properties in between those of neat pectin aerogels (with calcium) and neat silica aerogels. The type of silica sol was found to drastically influence the erosion and release properties from the pectin-silica aerogels when calcium was used to cross-link pectin as it completely changed the “stability” (in terms of dissolution) of the overall matrix.

## 2.4. Conclusions on pectin-silica composite aerogels

In this work, we investigated the impact of composition on the structural, physico-chemical and release properties of pectin-silica composite aerogels. We separately explored and tuned the properties of the silica fraction (nature of silica sol) and of the pectin fraction (calcium concentration) of the organic-inorganic composite. By varying the process parameters and composition, we obtained different aerogels with a wide range of structural, physical and physico-chemical properties, which in turn were strongly influencing the release properties of

pectin-silica composites used as drug delivery system. Interestingly, the nature of silica-precursors turned out to be a determining factor as well as the calcium conditions of the pectin matrix.

Independently of calcium concentration of the pectin, the drug release properties and matrix erosion behaviour of pectin-TEOS composites followed the “mixing rule” as compared to neat pectin and neat TEOS aerogels. The release of the drug was driven by pronounced matrix bulk erosion over time due to the brittleness characteristic brought by TEOS. Surprisingly, this mixing rule was not applicable for pectin-PEDS aerogels without calcium: PEDS brittleness prevailed the “strength” of pectin network leading to a quicker release than each of the neat aerogels. Changing the formulation and composition factors not only influenced the main physical mechanisms involved in the release of the drug (erosion and/or diffusion controlled) but also the kinetics release parameters. As an illustrative summary, different aspects of composition of pectin-silica aerogels impacting the time needed to completely release the drug are presented in Figure 234 and Table 26.

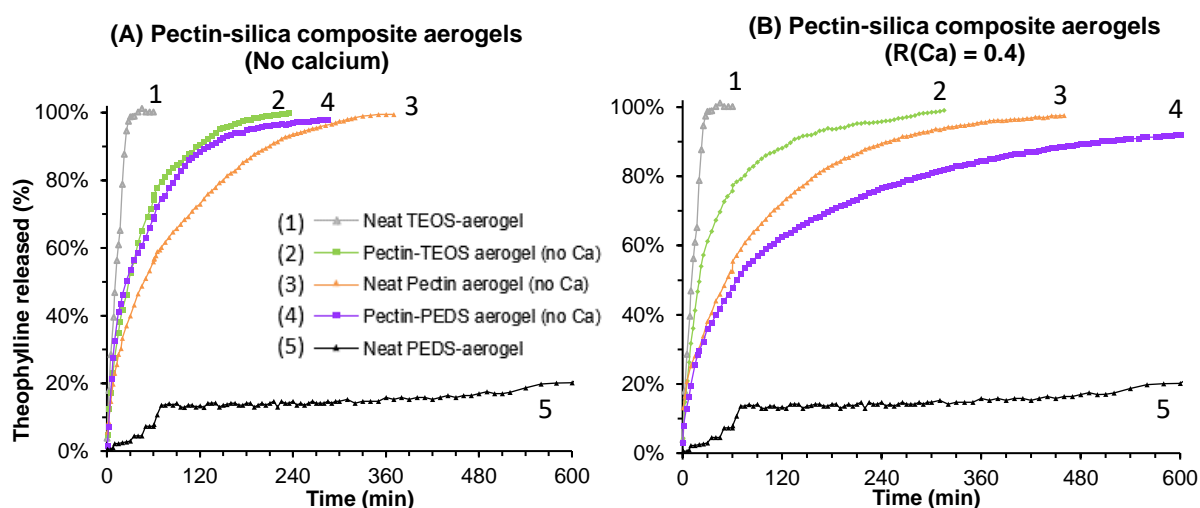


Figure 234. Theophylline cumulative release over time from 8 wt% TEOS aerogel (1) 6 wt% pectin-8 wt% TEOS aerogel (2), 6 wt% pectin-8 wt% PEDS aerogel (3), 6 wt% pectin aerogel (4) and 8 wt% PEDS (5). All pectin matrices were produced from 6 wt% pectin P35 dissolved at pH 3.0, either (A) without calcium, or (B) cross-linked with calcium at  $R(\text{Ca}) = 0.4$ .

Table 26. Summary of the time needed to release 100% of total theophylline from aerogel immersed into simulated gastro-intestinal fluids at 37°C while varying their composition and calcium  $R(\text{Ca})$  ratio.

Aerogel matrix composition	Neat TEOS aerogel	Neat PEDS aerogel	Neat pectin aerogel			Pectin-TEOS composite aerogel			Pectin-PEDS composite aerogel		
Calcium ratio $R(\text{Ca})$	-	-	0	0.2	0.4	0	0.2	0.4	0	0.2	0.4

<b>Time to release 100% of total theophylline (min)</b>	40	> 1500	370	490	640	240	275	315	280	1230	1780
---	----	--------	-----	-----	-----	-----	-----	-----	-----	------	------

### 3. Cytotoxicity profile of different aerogels and cryogels matrices

This work was performed in collaboration with P. Poni Institute of Macromolecular Chemistry (Iasi, Romania) and we are very grateful to Gabriela Pricope and Dragos Peptanariu for their welcome and help.

We selected different aerogels and cryogels matrices, varying their formulations (drying process, composition, pH of pectin solution, addition of calcium, presence of theophylline) in order to evaluate their cytotoxicity for the purpose of being used as a matrix for oral drug delivery. We chose to test pectin cryogels made from pectin solutions at low pH and with calcium as the samples did not undergo any washing steps (solvent-exchange steps) prior to freeze-drying contrary to pectin aerogels. The selected samples are presented in Table 27. To evaluate the toxicity of aerogel/cryogel matrices, we used a metabolic assay (MTS) which measures the mitochondrial reductase activity in NHDF cells incubated with matrices SG1-6 at various concentrations from 1 mg/mL to 0.49  $\mu$ g/mL.

As shown in Figure 235, all samples, except “SG4” (cryogel made from 6 wt% pectin loaded with theophylline at a high dose of 8.3 g/L), and with all treatments at matrix concentrations up to 1000  $\mu$ g/ml did not reduce cell survival after 48 h, whereas at 1000  $\mu$ g/ml of SG4 caused a 20% reduction in the cell number vs. control. The latter effect is attributed to the high content of theophylline loaded in the SG4 matrix.

All pectin-based, cellulose-based and silica-based aerogel matrices did not exhibit any cytotoxicity, regardless the composition of the matrix, pH adjustment or presence of calcium salts. Thanks to their ability to modify drug release over time and their low toxicity profile required for biocompatibility, these aerogels show promising potential to be used as biomedical devices.

**Table 27 Matrix composition and formulations parameters of the aerogel and cryogel samples used for cytotoxicity test.**

<b>Sample</b>	<b>SG1</b>	<b>SG2</b>	<b>SG3</b>	<b>SG4</b>	<b>SG5</b>	<b>SG6</b>
<b>Matrix</b>	Aerogel	Composite aerogel	Cryogel	Cryogel	Aerogel	Microcrystalline cellulose
	6 wt% pectin		6wt% pectin	6wt% pectin	5 wt% cellulose	(Avicel) (raw powder)

CHAPTER VI.

Organic-organic and organic-inorganic pectin-based composite aerogels for drug release applications

		6wt% pectin +8wt% silica from PEDS					
<b>pH of pectin solution</b>		2.0	2.0	2.0	2.0	NA	NA
<b>Calcium R(Ca) ratio of pectin solution</b>		0.2	0.2	0.2	0.2	NA	NA
<b>Theophylline loading (g/L)</b>		-	-	-	8.3 g/L	-	-
<b>Tested factors</b>		Cytotoxicity of pectin Influence of low pH (pH 2) and of the presence of calcium	Cytotoxicity of PEDS	Influence of low pH (pH 2) and of the presence of calcium (without any solvent exchange steps)	Cytotoxicity of theophylline (highest dose)	Cytotoxicity of cellulose	Cytotoxicity of cellulose as a homogeneous suspension of cellulose particles

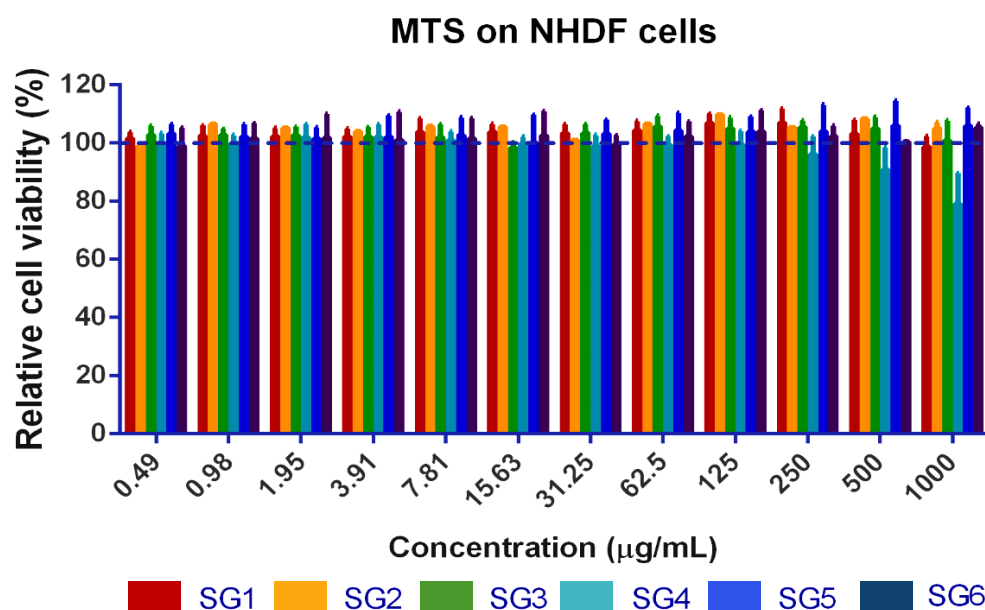


Figure 235. Dose-response for SG1-SG6 samples. NHDF cells were treated for 48 h with various concentrations of compounds as mentioned in the Materials and methods. MTS assay was then used to determine the relative cell viability (%).

## Conclusions

We have proposed original approaches of interpenetrating networks to produce organic-organic and organic-inorganic composite aerogels based on pectin. Pectin-cellulose aerogels (Part 1) were made by the impregnation of pectin solution in cellulose matrix, and the second part of the work dealt with the impregnation of organic silica particles in pectin network (Part 2). Making composite interpenetrated aerogels as drug delivery matrices is a new approach in the field.

The process route and formulation were varied in order to modulate the structural, physical and physico-chemical properties of pectin-cellulose and pectin-silica composite aerogels, which in turn were influencing their release properties when used as drug delivery systems. It is interesting to note that both kinetic parameters as well as the main physical mechanisms involved in the drug release (diffusion and/or erosion) could be tuned by adjusting the process route and composition.

We demonstrated that matrix physico-chemical and structural properties, governed by matrix composition and process parameters, not only influence the drug loading properties but also strongly impact the kinetics release characteristics. In particular, we tuned the release kinetics of theophylline in gastro-intestinal release media from an immediate release profile, to a prolonged release for several hours, up to an extended release for more than 24 h. The overall work presented in this chapter proves that not only by changing composition (pectin, cellulose, silica source) but also by finely combining different physico-chemical, structural and physical properties brought by each component of a composite, it is possible to tune all characteristics of aerogels when used as drug carrier.

The whole study presented and discussed within the Chapters V and VI contributes to the understanding of the physical phenomena involved in the release of drugs from aerogels and to correlating them to their structural and physico-chemical properties of the matrix. Finally, the low toxicity profile of different aerogels based on pectin, and/or cellulose and/or silica opens up possibilities and offers promising potential for their use as solid matrices for sorption/desorption of compounds at the interface with life sciences.

## References

- Assifaoui, A., Bouyer, F., Chambin, O., & Cayot, P. (2013). Silica-coated calcium pectinate beads for colonic drug delivery. *Acta Biomaterialia*, 9(4), 6218–6225. <https://doi.org/10.1016/j.actbio.2012.11.031>
- Błaszczczyński, T., Śłosarczyk, A., & Morawski, M. (2013). Synthesis of Silica Aerogel by Supercritical Drying Method. *Procedia Engineering*, 57, 200–206. <https://doi.org/10.1016/j.proeng.2013.04.028>
- Buckley, A. M., & Greenblatt, M. (1994). The Sol-Gel Preparation of Silica Gels. *Journal of Chemical Education*, 71(7), 599. <https://doi.org/10.1021/ed071p599>
- Caputo, G., Scognamiglio, M., & De Marco, I. (2012). Nimesulide adsorbed on silica aerogel using supercritical carbon dioxide. *Chemical Engineering Research and Design*, 90(8), 1082–1089. <https://doi.org/10.1016/j.cherd.2011.11.011>
- Demilecamps, A., Beauger, C., Hildenbrand, C., Rigacci, A., & Budtova, T. (2015). Cellulose–silica aerogels. *Carbohydrate Polymers*, 122, 293–300. <https://doi.org/10.1016/j.carbpol.2015.01.022>
- Fraeye, I., Deroeck, A., Duvetter, T., Verlent, I., Hendrickx, M., & Vanloey, A. (2007). Influence of pectin properties and processing conditions on thermal pectin degradation. *Food Chemistry*, 105(2), 555–563. <https://doi.org/10.1016/j.foodchem.2007.04.009>
- Grignon, J., & Scallan, A. M. (1980). Effect of pH and neutral salts upon the swelling of cellulose gels. *Journal of Applied Polymer Science*, 25(12), 2829–2843. <https://doi.org/10.1002/app.1980.070251215>
- Groult, S., & Budtova, T. (2018). Tuning structure and properties of pectin aerogels. *European Polymer Journal*, 108, 250–261. <https://doi.org/10.1016/j.eurpolymj.2018.08.048>
- Haimer, E., Wendland, M., Schlufte, K., Frankenfeld, K., Miethe, P., Potthast, A., ... Liebner, F. (2010). Loading of Bacterial Cellulose Aerogels with Bioactive Compounds by Antisolvent Precipitation with Supercritical Carbon Dioxide. *Macromolecular Symposia*, 294(2), 64–74. <https://doi.org/10.1002/masy.201000008>
- Job, N., Théry, A., Pirard, R., Marien, J., Kocon, L., Rouzaud, J.-N., ... Pirard, J.-P. (2005). Carbon aerogels, cryogels and xerogels: Influence of the drying method on the textural properties of porous carbon materials. *Carbon*, 43(12), 2481–2494. <https://doi.org/10.1016/j.carbon.2005.04.031>

- Krall, S. M., & McFeeters, R. F. (1998). Pectin Hydrolysis: Effect of Temperature, Degree of Methylation, pH, and Calcium on Hydrolysis Rates. *Journal of Agricultural and Food Chemistry*, 46(4), 1311–1315. <https://doi.org/10.1021/jf970473y>
- Laudise, R. A., & Johnson, D. W. (1986). Supercritical drying of gels. *Journal of Non-Crystalline Solids*, 79(1), 155–164. [https://doi.org/10.1016/0022-3093\(86\)90043-8](https://doi.org/10.1016/0022-3093(86)90043-8)
- Luo, X., & Zhang, L. (2010). Creation of regenerated cellulose microspheres with diameter ranging from micron to millimeter for chromatography applications. *Journal of Chromatography A*, 1217(38), 5922–5929. <https://doi.org/10.1016/j.chroma.2010.07.026>
- Malfait, W. J., Zhao, S., Verel, R., Iswar, S., Rentsch, D., Fener, R., ... Koebel, M. M. (2015). Surface Chemistry of Hydrophobic Silica Aerogels. *Chemistry of Materials*, 27(19), 6737–6745. <https://doi.org/10.1021/acs.chemmater.5b02801>
- Mehling, T., Smirnova, I., Guenther, U., & Neubert, R. H. H. (2009). Polysaccharide-based aerogels as drug carriers. *Journal of Non-Crystalline Solids*, 355(50–51), 2472–2479. <https://doi.org/10.1016/j.jnoncrysol.2009.08.038>
- Mohammadian, M., Jafarzadeh Kashi, T. S., Erfan, M., & Soorbaghi, F. P. (2018). Synthesis and characterization of silica aerogel as a promising drug carrier system. *Journal of Drug Delivery Science and Technology*, 44, 205–212. <https://doi.org/10.1016/j.jddst.2017.12.017>
- Pajonk, G. M., Elaloui, E., Achard, P., Chevalier, B., Chevalier, J.-L., & Durant, M. (1995). Physical properties of silica gels and aerogels prepared with new polymeric precursors. *Journal of Non-Crystalline Solids*, 186, 1–8. [https://doi.org/10.1016/0022-3093\(95\)00210-3](https://doi.org/10.1016/0022-3093(95)00210-3)
- Phalippou, J., & Kocon, L. (2004). Aérogeles Aspects fondamentaux. *Techniques de l'ingénieur. Matériaux Fonctionnels*, 1(AF3609). Retrieved from <http://cat.inist.fr/?aModele=afficheN&cpsidt=20744134>
- Renard, C. M. G. C., & Thibault, J.-F. (1996). Degradation of pectins in alkaline conditions: kinetics of demethylation. *Carbohydrate Research*, 286, 139–150. [https://doi.org/10.1016/0008-6215\(96\)00056-0](https://doi.org/10.1016/0008-6215(96)00056-0)
- Rudaz, C. (2013). *Cellulose and Pectin Aerogels: Towards their nano-structuration* (PhD Thesis, Ecole Nationale Supérieure des Mines de Paris). Retrieved from <https://pastel.archives-ouvertes.fr/pastel-00957296/document>
- Smirnova, I., Mamic, J., & Arlt, W. (2003). Adsorption of Drugs on Silica Aerogels. *Langmuir*, 19(20), 8521–8525. <https://doi.org/10.1021/la0345587>

- Smirnova, I., Suttiruengwong, S., & Arlt, W. (2004). Feasibility study of hydrophilic and hydrophobic silica aerogels as drug delivery systems. *Journal of Non-Crystalline Solids*, 350, 54–60. <https://doi.org/10.1016/j.jnoncrysol.2004.06.031>
- Smirnova, I., Suttiruengwong, S., & Arlt, W. (2005). Aerogels: Tailor-made Carriers for Immediate and Prolonged Drug Release. *KONA Powder and Particle Journal*, 23, 86–97. <https://doi.org/10.14356/kona.2005012>
- Smirnova, I., Suttiruengwong, S., Seiler, M., & Arlt, W. (2004). Dissolution rate enhancement by adsorption of poorly soluble drugs on hydrophilic silica aerogels. *Pharmaceutical Development and Technology*, 9(4), 443–452.
- Strøm, R. A., Masmoudi, Y., Rigacci, A., Petermann, G., Gullberg, L., Chevalier, B., & Einarsrud, M.-A. (2007). Strengthening and aging of wet silica gels for up-scaling of aerogel preparation. *Journal of Sol-Gel Science and Technology*, 41(3), 291–298. <https://doi.org/10.1007/s10971-006-1505-7>
- Wagh, P. B., Begag, R., Pajonk, G. M., Rao, A. V., & Haranath, D. (1999). Comparison of some physical properties of silica aerogel monoliths synthesized by different precursors. *Materials Chemistry and Physics*, 57(3), 214–218. [https://doi.org/10.1016/S0254-0584\(98\)00217-X](https://doi.org/10.1016/S0254-0584(98)00217-X)
- Yalkowsky, S. H., He, Y., Jain, P., He, Y., & Jain, P. (2016). *Handbook of Aqueous Solubility Data*. <https://doi.org/10.1201/EBK1439802458>

# **GENERAL CONCLUSIONS AND PERSPECTIVES**

---

## General conclusions

The overall goal of this PhD work was to develop versatile and multi-functional bio-based materials. We have demonstrated that bio-aerogels based on pectin are indeed such materials as they can be used for very different and not connected applications: as matrices for drug delivery and for thermal insulation.

In this framework, we have prepared, characterized and studied various pectin-based aerogels and composite aerogels with different properties. As the structure control and fine tuning of aerogels are critical to adapt them to a specific application, the main question we asked was “**How can we tune pectin aerogels properties?**”. Therefore, the focus of this work was placed on the understanding of the relationships between the characteristics of the initial polymer (pectin), the preparation conditions, the internal structure of aerogel and the final “application properties” *i.e.* their thermal conductivity and drug loading/release properties.

Each chapter of the manuscript is devoted to the preparation of various types of pectin aerogels and pectin-based composite aerogels via dissolution-solvent exchange route followed by supercritical drying using CO<sub>2</sub>. The systematic variation of the external parameters (composition, pH, polymer concentration, type of non-solvent, concentration of mono- and polyvalent metal ion salts) allowed fine modulating solution viscosity and gelation mechanisms, which in turn influenced aerogel structure and properties.

In the first chapter describing the results obtained (**Chapter III**), we have performed a complete study on the fine tuning of the structural, physical and morphological properties of pectin aerogels by varying the process routes. More precisely, we explained why and how pectin intrinsic properties (such as degree of methylation) and extrinsic parameters (such as pH condition, type of non-solvent, salt type and concentration) tune aeropectin properties. The mechanism of structure formation, *i.e.* gelation or phase separation, was found to be the key in aeropectins’ control of structure. The multi-scale correlations from macromolecular aspects (polymer ionization with pH, calcium sensitivity and binding) to the morphological, structural and mechanical properties of pectin aerogels are now built and the results obtained will provide the guidelines for making aerogel matrices (potentially, based on other gelling polyelectrolytes) with fully controlled morphology and properties.

In the **Chapter IV**, we have studied in details the thermal properties of pectin aerogels. The process route was varied in a systematic way in order to modify aerogel density and morphology and thus understand their influence on aerogel thermal conductivity. For the first time a U-shape curve of thermal conductivity vs density was obtained for bio-aerogels synthesized via dissolution-solvent exchange-sc drying route. We showed that the type of pectin chains’ interactions and physical state of matter (solution or gel) are crucial to understand and

predict aerogel morphology and properties. A delicate compromise between aeropectin morphology (pore size) and density is thus needed to maximize the Knudsen effect while minimizing heat conduction via the solid backbone in order to get the lowest thermal conductivity. This minimal value of  $0.0147 \pm 0.0002$  W/(m.K) was found for non-gelled solution at pH 2 and pectin concentration of 2 wt%. Thus, pectin aerogels are thermal superinsulating materials and present a high potential for thermal insulation applications as they are fully bio-based and mechanically robust.

In the **Chapter V**, we have explored and evaluated the potential of pectin aerogels to be used as oral drug delivery system using theophylline as drug model. Drug loading efficiency and loading capacity were shown to depend on aeropectin matrix structure and properties (specific surface area and density). When immersed into simulated physiological media, aeropectin matrix showed prolonged drug release behaviour, with matrix resistance in gastric media followed by strong dissolution in intestinal media. Drug release was found to be governed by diffusive mass transports through the system coupled with relaxational phenomena induced by matrix swelling and erosion, in correlation with the polyelectrolyte and hydrosoluble characteristics of pectin. By finely tuning the structural parameters of the aeropectins (specific surface, density and degree of ionic crosslinking with calcium), adjusting sample formulation and drying method, we were able to determine the impacts of these parameters on the drug loading and release kinetics. Overall, our results point out the possibility to tailor aeropectin drug release properties by adjusting the process route to target the therapeutic indications. Aeropectins show high potential for drug release applications as biodegradable, biocompatible and bio-based carriers.

Finally, in the last chapter (**Chapter VI**) we went even further by showing that the release kinetics of pectin aerogels can be additionally modified by making organic-organic and organic-inorganic composite aerogels based on pectin. We proposed original approaches of interpenetrating networks of pectin with cellulose and with silica to produce pectin-based composite aerogels used as drug delivery matrices. Pectin-cellulose aerogels were made by the impregnation of pectin solution in cellulose matrix, while pectin-silica aerogels were produced by the impregnation of organic silica particles in pectin network. The process route and formulation were varied in order to modulate the structural, physical and physico-chemical properties of pectin-cellulose and pectin-silica composite aerogels, which in turn were influencing their release properties. We demonstrated that both kinetic parameters as well as the main physical mechanisms involved in the drug release (diffusion and/or erosion) can be tuned by adjusting the process route and composition. We demonstrated that matrix physico-chemical and structural properties, governed by matrix composition and the process parameters, not only influence the drug loading properties but also strongly impact the kinetics release characteristics. In particular, we tuned the release kinetics of theophylline in gastro-intestinal

release media from immediate release profile to a prolonged release for several hours, up to an extended release for more than 24 h. The overall work presented in this chapter proves that not only by changing composition (pectin, cellulose, silica source) but also by finely combining different physico-chemical, structural and physical properties brought by each component of a composite, it is possible to tune all characteristics of aerogels when used as drug carrier. The whole study presented and discussed within the Chapters V and VI contributes to the understanding of the physical phenomena involved in the release of drugs from aerogels and to correlating them to their structural and physico-chemical properties of the matrix.

As an overall conclusion, we clearly demonstrated that pectin aerogels can be advanced versatile bio-based materials whose physical-chemical, structural and morphological properties can be finely tuned to adapt to the requirement of a specific application. However, all the work performed during the three years of PhD on pectin aerogels is not providing a “turnkey solution” for a specific application as the field of bio-aerogels is quite “young”. The results obtained provide useful directions and guidelines for further study. Thus, in the following, we would like to highlight some limitations and propose perspectives for future work which could inspire the following research on polysaccharide-based aerogels.

### General comments and perspectives

- In this thesis, we were rather focused on low-methylated pectin and using calcium to induce ionic-gelation. However, other options of pectin solution gelation exist. Pectin ionic gelation can also be initiated by different divalent cations (Mn, Mg, St, Zn...) as reported by (Tkalec, Knez, & Novak, 2016). Gelation of high-methylated pectin by efficiently promoting hydrophobic interactions in the proper conditions (pH < 3.5 and high co-solute content > 60%) may also be possible. Changing the counter-ions involved in junction zones or modifying pectin methylation degree may change their internal structure and physico-chemical characteristics (solubility, erosion/swelling ability in liquid) is thus worth investigating.
- In order to achieve industrial feasibility and decrease the production cost, freeze-drying might be a good alternative to supercritical drying, provided the preservation of the network structure during drying. As suggested by literature (Ni, Tesconi, Tabibi, Gupta, & Yalkowsky, 2001; Wittaya-arekul & Nail, 1998), using tert-butanol as a solvent for freeze-drying (tert-butanol/water cosolvent systems) might prevent ice growth and lead to fine-nanostructured cryogel. The best option would be to find the conditions leading to aerogel-like properties but obtained with ambient pressure drying or low vacuum

drying. This was never demonstrated before except for cellulose (Druel & Budtova, n.d.).

➤ **Concerning the use of bio-aerogels as thermal insulating materials:**

- First, the reasons why pectin and some other bio-aerogels are super-insulating materials and why cellulose aerogels are not are still unknown. We point out here the influence of the chemical structure of the polysaccharide's chains on the aerogels' morphology and thus on their thermal properties. The modelling of molecular phenomena of the coagulation process would be extremely attractive to understand (and control) the formation of the wet network during solvent exchange step.
- Besides, as future prospects and technical challenge, hydrophobization of hydrophilic bio-aerogels would be particularly attractive in order to decrease moisture adsorption and avoid aging. Classical hydrophobization techniques of silica aerogels consist in the replacement of hydrophilic groups by non-polar functions (*e.g.* by silylation with trichloromethylsilane or methyltrimethoxysilane). This was never tried before on pectin aerogels. In addition, using natural compound would be a much better option for bio-aerogels in adequation with their low-toxicity profile, environmentally friendly and human friendly characteristics.

➤ **Concerning the use of bio-aerogels as oral drug delivery systems:**

- As a reminder, the dissolution testing experiments were conducted *in vitro* and at the laboratory scale, which might strongly differ from *in vivo* conditions. To be closer to real physiological conditions, we suggest in the first instance the addition of the digestive enzymes (pepsin and pancreatin) in the *in vitro* release baths prior to *in-vivo* tests step.
- As we showed in this thesis, the release properties of polysaccharide-based aerogels as drug matrix can be varied by creating composite aerogels from different components (organic or inorganic). The “mixture” of properties brought by the different components in the same matrix results in new physical and chemical properties and offer new perspectives to polysaccharide aerogels used as drug carrier. “Core-shell” composite aerogels can be good perspective to go further, for example, by coating of a low-hydrosoluble polysaccharide (core) with an external layer of a gastro-resistant polysaccharide (such as pectin or alginate). This would both attenuate the strong burst

release we observed, protect the drug from any acid degradation in the stomach, and delay the drug release in the intestinal tract.

- With the aim of extended-drug release during the longer time possible, we suggest the use of non-hydrosoluble polymer such as cellulose or with lower solubility (such as starch) to make bio-aerogels. Indeed, decrease the solubility of the aerogel would strongly protect the matrix from rapid degradation by solubilization and thus might prolong the release over time. Another possibility could be hydrophobization of the bio-aerogel by natural hydrophobic compounds (wax, fatty acids...).
- Finally, the 3-D printing technology of complex three-dimensional structure with a defined shape open up the potential for innovative food manufacturing or for creating bio-artificial tissue (regenerative medicine) (Markstedt et al., 2015). Alginate (another polyelectrolyte polysaccharide) is already commonly used as bio-ink to produce 3-D printed hydrogels thanks to its fast gelation property with multivalent cations (Axpe & Oyen, 2016; Song et al., 2011). Recently, pectin gels were found to be also printable materials in order to encapsulate alive plant cells (Vancauwenberghe, Baiye Mfortaw Mbong, et al., 2017) or to produce tunable food stimulants (Vancauwenberghe, Katalagarianakis, et al., 2017). The supercritical drying of 3-D printed pectin gels would allow the design of customizable highly porous aerogels with specific structures and textures, in order use them as dry cellular-scaffold for tissue engineering.

## References

- Axpe, E., & Oyen, M. L. (2016). Applications of Alginate-Based Bioinks in 3D Bioprinting. *International Journal of Molecular Sciences*, *17*(12). <https://doi.org/10.3390/ijms17121976>
- Druel, L., & Budtova, T. (n.d.). *Patent FR1902812, submitted.*
- Markstedt, K., Mantas, A., Tournier, I., Martínez Ávila, H., Hägg, D., & Gatenholm, P. (2015). 3D Bioprinting Human Chondrocytes with Nanocellulose–Alginate Bioink for Cartilage Tissue Engineering Applications. *Biomacromolecules*, *16*(5), 1489–1496. <https://doi.org/10.1021/acs.biomac.5b00188>
- Ni, N., Tesconi, M., Tabibi, S. E., Gupta, S., & Yalkowsky, S. H. (2001). Use of pure t-butanol as a solvent for freeze-drying: a case study. *International Journal of Pharmaceutics*, *226*(1), 39–46. [https://doi.org/10.1016/S0378-5173\(01\)00757-8](https://doi.org/10.1016/S0378-5173(01)00757-8)
- Song, S.-J., Choi, J., Park, Y.-D., Hong, S., Lee, J. J., Ahn, C. B., ... Sun, K. (2011). Sodium Alginate Hydrogel-Based Bioprinting Using a Novel Multinozzle Bioprinting System: THOUGHTS AND PROGRESS. *Artificial Organs*, *35*(11), 1132–1136. <https://doi.org/10.1111/j.1525-1594.2011.01377.x>
- Tkalec, G., Knez, Ž., & Novak, Z. (2016). PH sensitive mesoporous materials for immediate or controlled release of NSAID. *Microporous and Mesoporous Materials*, *224*, 190–200. <https://doi.org/10.1016/j.micromeso.2015.11.048>
- Vancauwenberghe, V., Baiye Mfortaw Mbong, V., Vanstreels, E., Verboven, P., Lammertyn, J., & Nicolai, B. (2017). 3D printing of plant tissue for innovative food manufacturing: Encapsulation of alive plant cells into pectin based bio-ink. *Journal of Food Engineering*. <https://doi.org/10.1016/j.jfoodeng.2017.12.003>
- Vancauwenberghe, V., Katalagianakis, L., Wang, Z., Meerts, M., Hertog, M., Verboven, P., ... Nicolai, B. (2017). Pectin based food-ink formulations for 3-D printing of customizable porous food simulants. *Innovative Food Science & Emerging Technologies*, *42*, 138–150. <https://doi.org/10.1016/j.ifset.2017.06.011>
- Wittaya-areekul, S., & Nail, S. L. (1998). Freeze-Drying of tert-Butyl Alcohol/Water Cosolvent Systems: Effects of Formulation and Process Variables on Residual Solvents. *Journal of Pharmaceutical Sciences*, *87*(4), 491–495. <https://doi.org/10.1021/js9702832>



**ANNEX. FUNDAMENTALS AND  
CONCEPTS FOR DRUG DELIVERY  
APPLICATIONS**

---

**CONTENTS**

**ANNEX. FUNDAMENTALS AND CONCEPTS FOR DRUG DELIVERY APPLICATIONS**

<b>1. DRUG RELEASE MECHANISMS FROM POLYMER MATRIX SYSTEMS .....</b>	<b>387</b>
1.1. WATER DIFFUSION AND POLYMER RELAXATION (SWELLING) .....	387
1.2. MATRIX EROSION .....	388
1.3. DRUG DISSOLUTION .....	389
1.4. DRUG DIFFUSION .....	390
<b>2. MATHEMATICAL MODELS OF RELEASE KINETICS .....</b>	<b>391</b>
2.1. ZERO-ORDER KINETICS .....	393
2.2. FIRST-ORDER RELEASE KINETICS .....	394
2.3. HIGUCHI RELEASE MODEL .....	394
2.4. HIXSON-CROWELL RELEASE MODEL .....	396
2.5. HOPFENBERG MODEL .....	397
2.6. RITGER-KORSMEYER-PEPPAS (POWER LAW) MODEL .....	397
2.7. PEPPAS-SAHLIN MODEL .....	400
2.8. GALLAGHER-CORRIGAN MODEL .....	401
<b>REFERENCES .....</b>	<b>402</b>

The annex section presents an overview on drug release fundamentals and concepts. It is organized as follows:

- First, we introduce and define the main physical mechanisms involved in the release of a drug from a polymer matrix delivery system (*e.g.* dissolution, diffusion, matrix erosion and swelling, polymer relaxation...*etc.*).
- Then, we present in details the most used kinetics mathematical models which are applicable for solid matrix systems (Zero-order, First-order, Higuchi, Korsmeyer-Peppas, Hixson-Crowell, Hopfenberg, Gallagher–Corrigan release models).

## 1. Drug release mechanisms from polymer matrix systems

When studying drug delivery from a solid matrix, different mass transport phenomena are involved successively or simultaneously: water diffusion inside the device, system swelling, system dissolution / erosion, drug dissolution and diffusion through the hydrated system. Usually, the slowest physical phenomenon is the determining step as it plays a significant controlling role on the release. Drug properties (solubility, crystallinity), polymer composition and properties, and system morphology and geometry are known to drive the release characteristics. In the following, the case of a hydrophilic erodible polymer matrix loaded with an instantaneously dissolving drug will be considered as the closest to the case of pectin aerogels.

The case of a system of physical immobilization of the drug will be used as we assume that there is no covalent bonding between the drug and the matrix. Four successive phenomena occur when a dry hydrophilic soluble matrix is put in contact with aqueous media: water diffusion, polymer chain relaxation, polymer swelling and matrix erosion.

### 1.1. Water diffusion and polymer relaxation (swelling)

First water diffuses into the hydrophilic matrix driven by osmotic forces due to the gradient of chemical potential. Water penetration into the system occurs via pores and/or through continuous polymeric networks. These phenomena depend on morphological properties of the system as well as polymer physicochemical characteristics (hydrophilicity, solubility in water, nature and number of interactions between chains, chain length...) and temperature. As soon as a minimum of water content penetrates into the hydrophilic system, polymer chains relaxation occurs. Chains disentangle and reorganize into a three-dimensional hydrated network (gel-like structure). Once hydrated, the system locally swells leading to

volume expansion, which facilitates solvent diffusion and macromolecular mobility. Chain relaxation is a significant step for swellable or soluble system, as it is a prelude swelling or dissolution of the polymer. If chain relaxation is a relatively slow step compared to water diffusion, a narrow swelling front separates the swollen network from the non-swollen region. Drug release is controlled by the formation of a hydrated viscous layer around the matrix which acts as a barrier by opposing penetration of water and drug diffusion out of the matrix (Heller, Helwing, Baker, & Tutte, 1983).

Many hydrophilic materials display a swelling behavior when they are in contact with water due to the interactions between water and polymer chains. However, material swelling might be limited in case of rigid or cross-linked polymers not able to disentangle, or in case of polymers with large chain length (Siegel & Rathbone, 2012). In practice, macroscopic material swelling is observable when diffusion of water into the matrix is a relatively rapid step and polymer dissolution is comparatively slow (Juergen Siepmann, Siegel, & Rathbone, 2012). On the contrary, for “swellable-soluble” matrix, its swelling may not be noticeable as swelling is followed by polymer dissolution (Colombo, 1993).

Once aqueous media has penetrated into the system, two phenomena occur in parallel: drug dissolution and polymer erosion/dissolution (in case of soluble or erodible matrix).

## 1.2. Matrix erosion

Degradation or dissolution effects are termed as the erosion of the matrix. It consists of the loss of structural and physical integrity of the matrix over time, such as its dimensions or shape. Erosion can be caused by physical, chemical or biological reactions in response to matrix immediate environment: such as polymer dissolution, mechanical “corrosion” or breakage, hydrolysis, or enzymatic biodegradation (Bruschi, 2015; Siegel & Rathbone, 2012).

As the solvent diffuses into the matrix, relaxation and rearrangement of polymer chains take place and polymer chains start to disentangle if water content is high enough to be below the critical polymer concentration. In this case, the number of disentanglements exceeds the number of entanglements and the system erodes in the surrounding bulk fluid creating an “erosion front” at the interface with the liquid media. Polymer dissolution occurs according to reptation theory and the dissolved chains start to diffuse, which in turn increases solvent penetration and drug diffusion. The inner structure of the eroding matrix changes significantly with time, becoming more porous (aqueous channels) and less restrictive for diffusion of drug and solvent. Depending on erosion rate regarding to diffusion rate, matrix erosion might be negligible, for example, if all drug has already been released before polymer dissolution (Bruschi, 2015; Siegel & Rathbone, 2012).

Erosion of the matrix can be controlled by varying polymer characteristic (chain length, molecular weight, hydrophilicity, solubility, ionization, cross-linking), matrix properties (porosity, density, composition, wettability) and extrinsic factors (pH, ionic strength, temperature) (Bruschi, 2015). Depending on the velocity of water diffusion and matrix erosion, two main options are possible: erosion on the surface or in the bulk (see Figure 236).

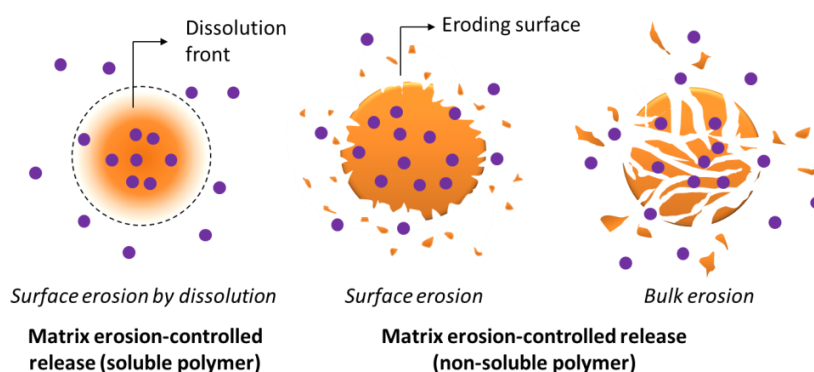


Figure 236. Surface or bulk erosion mechanisms from solid polymer matrix

Surface erosion occurs when the velocity of water penetration is lower than that of matrix degradation, whereas bulk erosion occurs when water invades the system more rapidly compared to matrix dissolution/degradation. Surface erosion of a system leads to progressive reduction of its dimensions with time, resulting in the release of drug that is close to the surface. Bulk erosion starts with water diffusion into the system, causing progressive matrix “degradation” throughout the bulk of the material. In the last stage, it results in network disintegration as a whole, matrix loses its physical integrity and the drug is released (Bruschi, 2015; Siegel & Rathbone, 2012).

### 1.3. Drug dissolution

As the drug is dispersed as solid species in the matrix, its dissolution is a fundamental step for diffusion to start through the system. Upon contact with diffusing liquid, drug starts to dissolve. The higher the solubility of the drug in the liquid media, the more rapid the dissolution rate. But if the local drug concentration exceeds its solubility, the solvating medium is locally saturated and only a portion of the drug can be dissolved. In other words, both dissolved and non-dissolved drugs particles may co-exist in the matrix, and only the dissolved part is able to diffuse outside the matrix (Bruschi, 2015; Siegel & Rathbone, 2012).

Time of drug dissolution may depend on drug particle size and solubility, chemical interactions (if any) with the matrix, temperature, mechanical stirring and local viscosity of the

liquid media. In the case of highly soluble drug, its dissolution can be considered instantaneous as it is more rapid than other mass transport phenomena (water diffusion, matrix dissolution, drug diffusion...). In case of highly soluble drug, drug dissolution may not be the determining step when released from a matrix as compared to matrix dissolution/erosion and diffusion mechanisms (Bruschi, 2015; Siegel & Rathbone, 2012).

#### 1.4. Drug diffusion

Once a portion of the drug is dissolved into the hydrated system, the dissolved part diffuses out through the polymer and aqueous pores towards the bulk fluid. Drug loaded matrix acts both as a drug storage medium and a mediator of diffusion. The process of drug diffusion can be defined as the spatial mass transfer of the drug through a system, driven by gradient concentrations forces (Bruschi, 2015; Siegel & Rathbone, 2012). During this process, differences in drug concentration are progressively reduced by spontaneous flux of matter, which are carried by random molecular motions and governed by the concentration gradient and the distance, as described by Fick's first law (for dispersed drug):

$$J = -D \frac{dC}{dx} \quad (\text{A.1})$$

where J is the rate of mass transfer per unit area of the section, D is the diffusion coefficient, C is the concentration of the diffusing substance, x is the distance between the two points, dC/dx is change in concentration.

The diffusion coefficient D can represent molecule's mobility in a given system. D depends on temperature, pressure, the rheological and chemical properties of the bulk medium, and the characteristics of the drug. The diffusion coefficient of a solute through a medium in a dilute state is given by Stokes-Einstein Equation:

$$D_{solute} = \frac{k_{Bz} \cdot T}{6\pi R \eta} \quad (\text{A.2})$$

where  $k_{Bz}$  is the Boltzmann constant, T the temperature, R the hydrodynamic Stokes radius of the solute, and  $\eta$  the shear viscosity of the medium.

The diffusion of a solute in liquid medium through a porous matrix results from Brownian motion. The distance L made by a solute during a time t is given by:

$$L = \sqrt{D_{solute} \cdot t} \quad (\text{A.3})$$

Thus, matrix geometry and its thickness play a significant role on drug release as the time required to diffuse over a certain distance is proportional to the square of that distance.

In drug release experiments from soluble matrix,  $D$  is not constant as the surrounding system permanently evolves because of other mass transport phenomena such as matrix dissolution, swelling or water diffusion through the matrix. As the matrix is actually a dynamic fluctuating structure,  $D$  may be considered as an illustration of these fluctuations. Indeed,  $D$  increases with drug gradient concentration, with expansion of free volume (matrix erosion and swelling), and with increasing water content (solvent diffusion). On the opposite, it decreases with matrix density, viscosity of the liquid and drug size (Bruschi, 2015; Siegel & Rathbone, 2012).

A schematic illustration of drug loaded-polymeric soluble matrix upon liquid penetration into the system is presented in Figure 237.

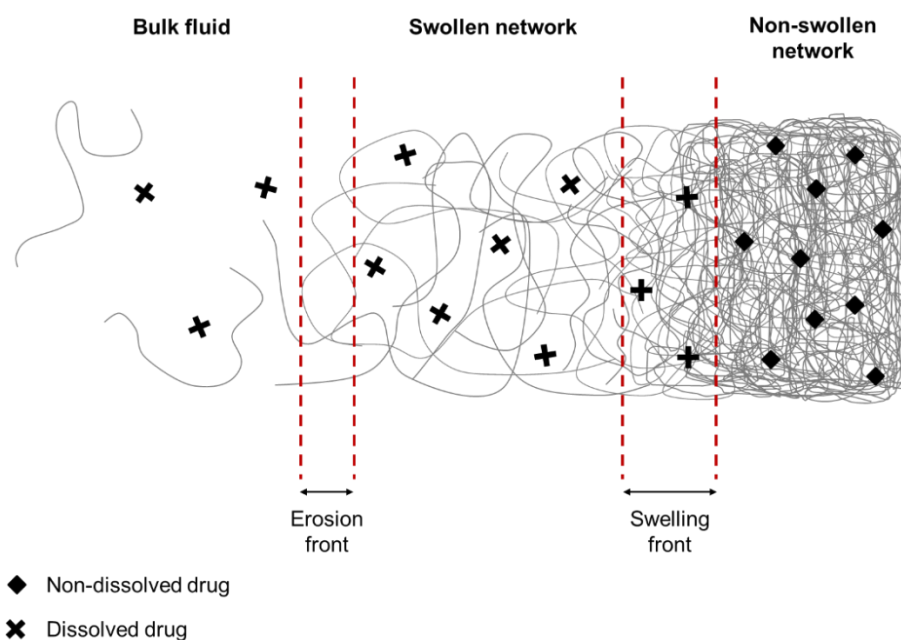


Figure 237. Schematic presentation of drug loaded-polymeric soluble matrix upon liquid penetration into the system. Illustration inspired from (Siegel & Rathbone, 2012).

## 2. Mathematical models of release kinetics

According to what has been described previously, drug release from a solid matrix is known to be impacted by several mass transport mechanisms including diffusion, swelling, dissolution or erosion. It is possible to acquire mathematical equations that describe the dependence of drug delivery as a function of time. Mathematical models are useful tools to

predict release behavior of a system and design optimal pharmaceutical formulations and matrix geometry (Nicholas A. Peppas & Narasimhan, 2014). Fitting release experimental data with various models allows evaluating the main mass transport mechanisms governing the drug release (diffusion, dissolution, swelling, erosion...). Understanding the different factors (composition, polymer chemical structure, drug properties, matrix density ...) that affect each mechanism and how in turn they influence the overall release behavior is a key to adjust therapeutic parameters (drug dose and release rate, time of release) (Juergen Siepmann et al., 2012).

The velocity of drug dissolution in a solvent can be described as:

$$\frac{dC}{dt} = \frac{D.A}{h} (C_s - C(t)) \quad (\text{A.4})$$

where  $dC/dt$  is dissolution rate,  $D$  the diffusion coefficient of drug through the system,  $h$  the thickness of the diffusion layer,  $A$  the surface area of the exposed solid,  $C_s$  the saturated solubility of the drug,  $C(t)$  the drug concentration in the bulk solution at time  $t$ .

Drug release profile can be graphically illustrated from the data obtained from dissolution testing experiments by plotting the drug fraction released  $Q(t) = \frac{M_t}{M_\infty}$  as a function of time. The release profiles of each system can be evaluated and described by model-dependent methods, based on mathematical functions. To determine if the fitting of a model to experimental data is good or bad, statistical coefficients are used such as the higher coefficient of determination  $R^2$  and the lower AIC (Akaike Information Criterion). The most probable physical mechanism(s) (*e.g.* diffusion, swelling and chain relaxation, dissolution, erosion) that predominantly govern drug release can be thus deduced from the best fit.

Below only the most used mathematical equations and models applicable for solid matrix systems will be presented (J. Siepmann & Siepmann, 2008):

- Zero order release model
- First order release model
- Higuchi release model
- Korsmeyer-Peppas release model
- Peppas-Sahlin equation
- Hixson-Crowell model
- Hopfenberg model
- Gallagher–Corrigan model

Equations will be given assuming the initial amount of drug dissolved at time 0 is being 0.

The widely used Baker and Lonsdale release model is not presented as it is based on Higuchi model for drug release from spherical matrices.

It has to be noted that Korsmeyer–Peppas approach and Peppas-Sahlin model are expected to be valid for up to ~60% of the cumulative drug released and not on the full release curve, so fitting with the data has to be restricted to this range.

## 2.1. Zero-order kinetics

Zero-order kinetics represents the “ideal” pharmacokinetic response curve. The drug release is only a function of time and the delivery rate remains constant until the device is exhausted from the drug, independently of the drug concentration in the system (Hsieh, Rhine, & Langer, 1983; Möckel & Lippold, 1993). This release can be found typically in transdermal or osmotic systems, and also for very slow release from a matrix that does not disaggregate in case of very low solubility drug, for example.

$$Q(t) = k_0 t^n, \quad \text{for a cylinder } Q(t) = k_0 t^{0.89} \quad (\text{A.5})$$

where  $Q_t$  is the cumulative fraction of drug released at time  $t$ ,  $k_0$  is a rate constant or apparent dissolution velocity. The value of  $n$  depends on matrix geometry; it is equal to 1.0 for a thin film, 0.89 for a cylinder and 0.85 for sphere (J. Siepmann & Siepmann, 2008). A graphical representation of the model is shown in Figure 238.

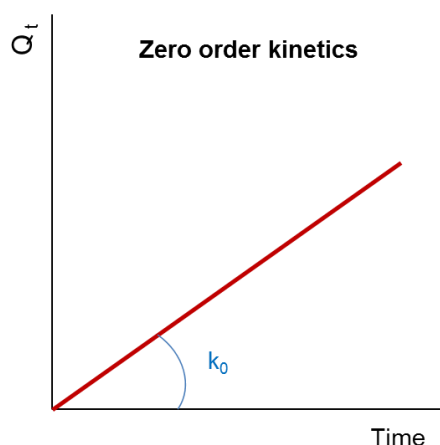


Figure 238. Graphical representation of zero-order kinetics: plot of the cumulative fraction of drug released  $Q_t$  (%) versus time,  $k_0$  is the zero-order rate constant.

## 2.2. First-order release kinetics

The first order kinetics is desirable for sustained release drug delivery systems.

This relationship is found in the cases of water-soluble drugs in porous matrix, exhibiting dissolution-controlled or diffusion-controlled release. The amount of drug released is directly proportional to amount of drug loaded in the device and leads in a constant release of the drug available at  $t$  time, and thus depends only on initial drug concentration (Mulye & Turco, 1995; Schwartz, Simonelli, & Higuchi, 1968).

$$Q_t = 1 - \exp(-k_1 t)$$

$$\text{And linearized as: } \log(1 - Q_t) = \frac{k_1 \cdot t}{2.303} \quad (\text{A.6})$$

where  $(1 - Q_t)$  represents the remaining fraction of drug at time  $t$  in the device, and  $k_1$  is the first-order constant. A graphical representation of the model is shown in Figure 239.

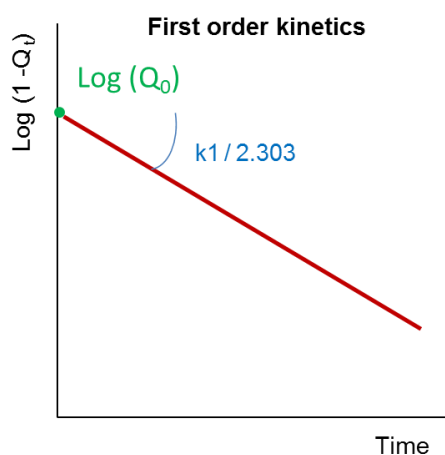


Figure 239. Graphical representation of first-order kinetics: plot of logarithm of the non-released fraction of drug  $(1 - Q_t)$  (%) versus time

## 2.3. Higuchi release model

The most used mathematical model to describe release from a solid matrix is Higuchi model (Higuchi, 1961). It corresponds to a hydrosoluble drug dispersed in a homogeneous solid matrix immersed in a diffusion medium. In this model, drug release only occurs by Fickian diffusion of the solvent and the drug throughout the macromolecular mesh and aqueous pores of the matrix.

The model is based on Fick's law, and considers several assumptions i) drug concentration in the matrix is higher than its solubility, ii) drug diffusion occurs through pores in the matrix based on one-dimensional diffusion, iii) drug particles are smaller than pore walls, iv) drug diffusivity is constant and matrix dissolution and swelling is negligible (constant boundaries); v) the release environment is always perfectly maintained in sink conditions (Brophy & Deasy, 1987; Higuchi, 1961; Juergen Siepmann & Peppas, 2011).

Thus, the model is not theoretically valid if the diffusion coefficient or physical boundaries of the matrix are not constant over time, such as in cases of swellable or soluble delivery systems.

The cumulative released fraction is presented as follows:

$$Q_t = \sqrt{\frac{D\varepsilon}{\tau}}(2m_d - \varepsilon S_d)S_d t \quad (\text{A.7})$$

where  $\varepsilon$  is the porosity of matrix,  $\tau$  is the capillary tortuosity factor,  $m_d$  is the initial amount of drug contained in the dosage form,  $S_d$  is the solubility of active agent in the matrix medium. Tortuosity is defined as the dimensions of radius and branching of the pores and canals in the matrix.

In a simplified model Equation (A.7) becomes:

$$Q_t = k_H \sqrt{t} \quad (\text{A.8})$$

where  $K_H$  is the release constant of Higuchi. With the simplified model, the amount of drug released is proportional to the square root of time, as expected from Fick law. It has to be noted that the simplified Higuchi model was initially built for matrix with thin film geometry, and will be used in this work. A graphical representation of the model is shown in Figure 240.

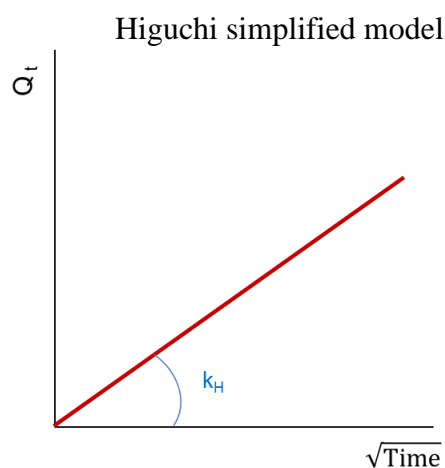


Figure 240. Graphical representation of Higuchi simplified model: plot of the cumulative fraction of drug released  $Q_t$  (%) versus the square root of time.

## 2.4. Hixson-Crowell release model

The Hixson-Crowell assumes that matrix erosion occurs homogeneously in such way that the matrix dimensions decrease keeping the initial shape. In addition, it assumes that drug release is limited only by drug dissolution velocity, neglecting any diffusion phenomena (Hixson & Crowell, 1931).

$$\sqrt[3]{W_0} - \sqrt[3]{W_t} = k_{HC}t. \quad (\text{A.9})$$

where  $W_0$  is the initial amount of the drug in the system;  $W_t$  is the amount remaining in the system at time  $t$ ; and  $k_{HC}$  is the constant of incorporation, which relates surface and volume of the drug.

It is possible to simplify Equation (A.9) dividing by  $\sqrt[3]{W_0}$  :

$$(\sqrt[3]{1 - Q_t}) = 1 - k_{\beta} \cdot t \quad (\text{A.10})$$

where  $(1 - Q_t)$  is the non-released fraction of drug and  $k_{\beta}$  is a release constant. A graphical representation of the model is shown in Figure 241.

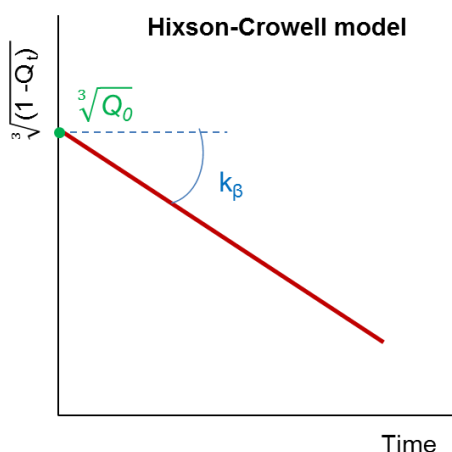


Figure 241. Graphical representation of Hixson-Crowell model: plot of cubic root of fraction of active agent not released  $(1 - Q_t)$  versus time.

## 2.5. Hopfenberg model

Hopfenberg model correlates drug release from the surface of heterogeneously eroding matrix of various geometries. It is applicable where the limiting factors for drug release are matrix erosion and time. It is assumed that surface area is maintained constant during the process (HOPFENBERG, 1976).

$$Q(t) = 1 - \left[ 1 - \frac{k_0 t}{C_0 a_0} \right]^n$$

$$Q(t) = K_G^2 t^2 - K_G t \quad \text{with } K_G = \frac{k_0}{C_0 a_0} \text{ and } n = 2 \quad (\text{A.11})$$

where  $k_0$  is the erosion grade constant,  $C_0$  is the initial concentration of the drug in the matrix, and  $a_0$  is the initial radius of matrix sphere or cylinder or a half thickness of matrix film. According to the geometrical form of the matrix, the  $n$  value is 1, 2 or 3 for a film, a cylinder or a sphere, respectively.

## 2.6. Ritger–Korsmeyer–Peppas (Power law) model

The model is based on an power law relationship between the amount of drug released and the time; it is used to describe drug release from hydrophilic polymeric matrix (Korsmeyer, Gurny, Doelker, Buri, & Peppas, 1983; Ritger & Peppas, 1987a, 1987b). It is presented as follows:

$$Q(t) = \frac{M_t}{M_\infty} = K_{KP} t^n \quad (\text{A.12})$$

where  $K_{kp}$  is the constant comprising the structural and geometrical characteristics of the system (also considered the release velocity constant), and  $n$  is the exponent of release (related to the drug release mechanism).

When the release is characterized by an abrupt burst release, the following equation was proposed by (Kim & Fassihi, 1997):

$$Q(t) = K_{KP} t^n + b \quad (\text{A.13})$$

where  $b$  is the burst effect. A graphical representation of the model is shown in Figure 242.

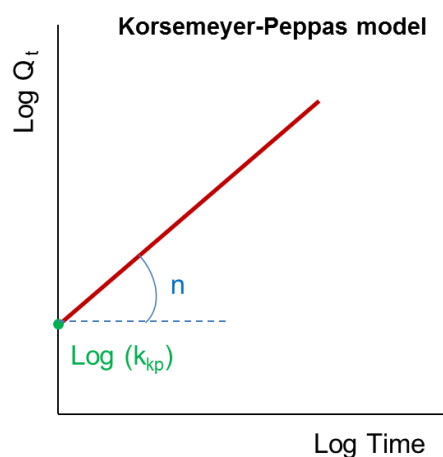


Figure 242. Graphical representation of Korsmeyer-Peppas model: plot of logarithm of the released fraction of drug ( $\text{Log}(Q_t)$ ) versus logarithm of time.

The power law model is used to study the release when the mechanism is not known or when more than one mechanism is involved. By determining the value of the exponent  $n$  according to the best fit with experimental data (for  $Q(t) < 60\%$ ) and depending on the matrix geometry it is possible to estimate the dominant physical mechanism impacting drug release between Fickian diffusion (Case I) or non-Fickian mechanisms (Case II, anomalous transport, Super Case II) in which polymer relaxation (swelling) and/or matrix erosion are impacting diffusion. It has to be noted that the value of  $n$  for each case depends on the geometry of the system (*e.g.* thin film, sphere or cylinder) (Klech & Simonelli, 1989; Kosmidis, Argyrakis, & Macheras, 2003; Kuipers & Beenackers, 1993; N. A. Peppas, 1985; Ritger & Peppas, 1987a), Table 28 summarizes this classification for cylindrical-shaped matrix.

Table 28. Interpretation of release models from polymeric matrices with cylindrical geometry depending on exponent  $n$  value with  $t_{diffusion}$  the solvent diffusion time through the matrix;  $t_{relaxation}$  the polymer relaxation time (Klech & Simonelli, 1989; Kosmidis et al., 2003; Kuipers & Beenackers, 1993; N. A. Peppas, 1985; Ritger & Peppas, 1987a).

Fickian diffusion	Non-Fickian diffusion mechanism		
$n = 0.45$	$n = 0.89$	$0.45 < n < 0.89$	$n > 0.89$
$t_{diffusion} > t_{relaxation}$	$t_{diffusion} < t_{relaxation}$	$t_{diffusion} \approx t_{relaxation}$	High velocity of solvent diffusion

Case I transport (Fickian diffusion)	Case II (relaxational transport)	Anomalous transport	Super Case II transport
Governed by solvent diffusion → Higuchi model	Governed by polymer relaxation (swelling) → Zero order kinetics	Governed by the coupling of diffusion and polymer relaxation (swelling or erosion)	Driven by the acceleration of solvent penetration

Fickian and non-Fickian mechanisms differ with the velocity of solvent diffusion:

**When  $n = 0.45$** , this means that the velocity of solvent diffusion is much slower than polymer relaxation time. In this case, polymer chains have high mobility enabling solvent penetration through tortuous interstitial spaces, and conformational changes in the polymer structure take place instantaneously. Thus, drug release is governed by drug diffusion in the surrounding medium from the matrix and the driving force is drug concentration gradient. It corresponds to Case I or Fickian diffusion as described by Higuchi model.

**When  $n = 0.89$** , the solvent diffusion is much faster than polymer relaxation process, leading to a non-Fickian solvent diffusion through the system as it is relaxation-balanced. The slow re-arrangement of polymer chains induces a gradient of solvent penetration to the center of the matrix. Thus, drug release is driven by polymer relaxation (swelling), and corresponds to a Case II (relaxational) transport as described by Zero order kinetics.

**When  $0.45 < n < 0.89$** , solvent diffusion and polymer relaxation time have comparable rates, and leading to a non-Fickian diffusion. Drug release is due to the combination of diffusion mechanisms and polymer relaxation (or dissolution) (Singh & Fan, 1986), as opposed to simple Fickian diffusion. As the solvent diffuses into the matrix, relaxation and rearrangement of polymer chains do not occur instantaneously. The relaxed chains locally swell (or are dissolved), which in turn promote liquid and drug diffusion. Thus, the relaxation process influences the diffusive transport of the drug (Rabin & Siegel, 2012). As more than one process is involved, it leads to an anomalous transport case and refers to the coupling of solvent diffusion and polymer relaxation (swelling) or matrix erosion.

Finally, the case **when  $n > 0.89$**  constitutes an extreme form of transport (non-Fickian diffusion) and corresponds to a Super Case II transport. It is characterized by a high velocity of solvent diffusion through the matrix and/or an increase of solvent penetration rate at the end. The rapid penetration of the solvent to the center of the matrix occurs when solvent has a high

affinity to the matrix or in the case of erosion-controlled release where channels and aqueous pores are formed promoting solvent penetration.

## 2.7. Peppas–Sahlin model

Peppas-Sahlin model is a power law model used in the case of anomalous drug release process to approximate the contribution of two physical mechanisms: diffusion and polymer chain relaxation (Nikolaos A. Peppas & Sahlin, 1989).

The model considered the two mechanisms as an additive sum:

$$Q_t = K_F t^m + K_R t^{2m} = F + R \quad (\text{A.14})$$

where  $K_F$  is diffusion constant,  $K_R$  relaxation constant and  $m$  is purely Fickian diffusion exponent of a matrix of any geometrical shape. The model postulates that drug release from any matrix, irrespective of its geometric shape, can be written in terms of a Fickian and a relaxational contribution. If the Fickian contribution can be expressed as a function of  $t^m$ , then the relaxational contribution can be expressed as a function of  $t^{2m}$

As it is shown in Figure 243, the Fickian diffusional exponent  $m$  varies with the aspect ratio of the matrix Peppas and Sahlin ; defined as  $2a/l$ , where  $2a$  is the diameter and  $l$  is the thickness (height) (Nikolaos A. Peppas & Sahlin, 1989).

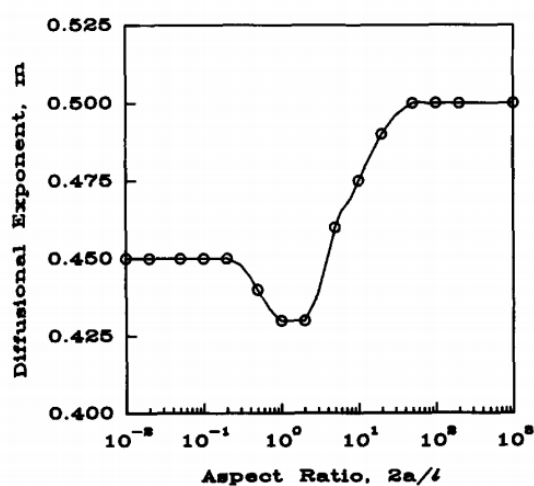


Figure 243 Variation of the Fickian diffusional exponent  $m$  with the aspect ratio of the matrix,  $2a/l$ , the figure is extracted from (Nikolaos A. Peppas & Sahlin, 1989). Reprinted from International Journal of Pharmaceutics, Volume 57, Issue 2, Nikolaos A. Peppas, Jennifer J. Sahlin, A simple equation for the description of solute release. III. Coupling of diffusion and relaxation, Pages 169-172., Copyright (2019), with permission from Elsevier.

As mentioned above, the model is based on a sum of a diffusional contribution ( $F$ ) and a Case II transport involving polymer relaxation ( $R$ ). Once  $K_F$  and  $K_R$  coefficient are obtained, it is possible to estimate the percentage of drug release which is due to the Fickian mechanism,  $F$ , called the Fickian release fraction.

$F$  is calculated as follows:

$$F = \frac{1}{1 + \frac{K_R}{K_F} t^m} \quad (\text{A.15})$$

and the ratio of relaxational over Fickian contribution as:

$$\frac{R}{F} = \frac{K_R}{K_F} t^m \quad (\text{A.16})$$

## 2.8. Gallagher–Corrigan model

The Gallagher-Corrigan model is used to describe release from a solid matrix which includes an initial burst release which results from rapid dissolution of drug close to the surface (first order process) followed by second drug release phase which is controlled by matrix erosion (Gallagher & Corrigan, 2000). Thus, the total released fraction ( $Q_t$ ) is given by the sum of drug released via surface diffusion and that released by erosion:

$$Q_t = F_{max}[1 - \exp(-k_b \cdot t)] + (F_{max} - F_b) \left[ \frac{\exp(k_e \cdot t - k_e \cdot t_{max})}{1 - \exp(k_e \cdot t - k_e \cdot t_{max})} \right] \quad (\text{A.17})$$

where  $F_{max}$  represents the maximum fraction of drug released during the total time period,  $F_b$  fraction of drug released during the initial burst phase,  $t_{max}$  the time to the maximum drug release rate, and  $k_b$  and  $k_e$  are the first order kinetic coefficients of the initial phase (burst phase) and of the second stage (erosion-controlled) in  $\text{min}^{-1}$ , respectively.

## References

- Brophy, M. R., & Deasy, P. B. (1987). Application of the Higuchi model for drug release from dispersed matrices to particles of general shape. *International Journal of Pharmaceutics*, 37(1), 41-47. [https://doi.org/10.1016/0378-5173\(87\)90008-1](https://doi.org/10.1016/0378-5173(87)90008-1)
- Bruschi, M. L. (2015). *Strategies to Modify the Drug Release from Pharmaceutical Systems*. Woodhead Publishing.
- Colombo, P. (1993). Swelling-controlled release in hydrogel matrices for oral route. *Advanced Drug Delivery Reviews*, 11(1), 37-57. [https://doi.org/10.1016/0169-409X\(93\)90026-Z](https://doi.org/10.1016/0169-409X(93)90026-Z)
- Gallagher, K. M., & Corrigan, O. I. (2000). Mechanistic aspects of the release of levamisole hydrochloride from biodegradable polymers. *Journal of Controlled Release*, 69(2), 261-272. [https://doi.org/10.1016/S0168-3659\(00\)00305-9](https://doi.org/10.1016/S0168-3659(00)00305-9)
- Heller, J., Helwing, R. F., Baker, R. W., & Tutte, M. E. (1983). Controlled release of water-soluble macromolecules from bioerodible hydrogels. *Biomaterials*, 4(4), 262-266. [https://doi.org/10.1016/0142-9612\(83\)90025-X](https://doi.org/10.1016/0142-9612(83)90025-X)
- Higuchi, T. (1961). Rate of Release of Medicaments from Ointment Bases Containing Drugs in Suspension. *Journal of Pharmaceutical Sciences*, 50(10), 874-875. <https://doi.org/10.1002/jps.2600501018>
- Hixson, A. W., & Crowell, J. H. (1931). Dependence of Reaction Velocity upon surface and Agitation. *Industrial & Engineering Chemistry*, 23(8), 923-931. <https://doi.org/10.1021/ie50260a018>
- HOPFENBERG, H. B. (1976). Controlled Release from Erodible Slabs, Cylinders, and Spheres. In *ACS Symposium Series: Vol. 33. Controlled Release Polymeric Formulations* (Vol. 33, p. 26-32). <https://doi.org/10.1021/bk-1976-0033.ch003>
- Hsieh, D. S. T., Rhine, W. D., & Langer, R. (1983). Zero-Order Controlled-Release Polymer Matrices for Micro- and Macromolecules. *Journal of Pharmaceutical Sciences*, 72(1), 17-22. <https://doi.org/10.1002/jps.2600720105>
- Kim, H., & Fassihi, R. (1997). Application of binary polymer system in drug release rate modulation. 2. Influence of formulation variables and hydrodynamic conditions on release kinetics. *Journal of Pharmaceutical Sciences*, 86(3), 323-328. <https://doi.org/10.1021/js960307p>
- Klech, C. M., & Simonelli, A. P. (1989). Examination of the moving boundaries associated with non-fickian water swelling of glassy gelatin beads: Effect of solution pH. *Journal of Membrane Science*, 43(1), 87-101. [https://doi.org/10.1016/S0376-7388\(00\)82355-8](https://doi.org/10.1016/S0376-7388(00)82355-8)

- Korsmeyer, R. W., Gurny, R., Doelker, E., Buri, P., & Peppas, N. A. (1983). Mechanisms of solute release from porous hydrophilic polymers. *International Journal of Pharmaceutics*, *15*(1), 25-35. [https://doi.org/10.1016/0378-5173\(83\)90064-9](https://doi.org/10.1016/0378-5173(83)90064-9)
- Kosmidis, K., Argyrakis, P., & Macheras, P. (2003). Fractal kinetics in drug release from finite fractal matrices. *The Journal of Chemical Physics*, *119*(12), 6373-6377. <https://doi.org/10.1063/1.1603731>
- Kuipers, N. J. M., & Beenackers, A. A. C. M. (1993). Non-fickian diffusion with chemical reaction in glassy polymers with swelling induced by the penetrant: a mathematical model. *Chemical Engineering Science*, *48*(16), 2957-2971. [https://doi.org/10.1016/0009-2509\(93\)80041-N](https://doi.org/10.1016/0009-2509(93)80041-N)
- Möckel, J. E., & Lippold, B. C. (1993). Zero-Order Drug Release from Hydrocolloid Matrices. *Pharmaceutical Research*, *10*(7), 1066-1070. <https://doi.org/10.1023/A:1018931210396>
- Mulye, N. V., & Turco, S. J. (1995). A Simple Model Based on First Order Kinetics to Explain Release of Highly Water Soluble Drugs from Porous Dicalcium Phosphate Dihydrate Matrices. *Drug Development and Industrial Pharmacy*, *21*(8), 943-953. <https://doi.org/10.3109/03639049509026658>
- Peppas, N. A. (1985). Analysis of Fickian and non-Fickian drug release from polymers. *Pharmaceutica Acta Helvetiae*, *60*(4), 110-111.
- Peppas, Nicholas A., & Narasimhan, B. (2014). Mathematical models in drug delivery: How modeling has shaped the way we design new drug delivery systems. *Journal of Controlled Release*, *190*, 75-81. <https://doi.org/10.1016/j.jconrel.2014.06.041>
- Peppas, Nikolaos A., & Sahlin, J. J. (1989). A simple equation for the description of solute release. III. Coupling of diffusion and relaxation. *International Journal of Pharmaceutics*, *57*(2), 169-172. [https://doi.org/10.1016/0378-5173\(89\)90306-2](https://doi.org/10.1016/0378-5173(89)90306-2)
- Rabin, C. R., & Siegel, S. J. (2012). Delivery systems and dosing for antipsychotics. *Handbook of Experimental Pharmacology*, (212), 267-298. [https://doi.org/10.1007/978-3-642-25761-2\\_11](https://doi.org/10.1007/978-3-642-25761-2_11)
- Ritger, P. L., & Peppas, N. A. (1987a). A simple equation for description of solute release I. Fickian and non-fickian release from non-swellable devices in the form of slabs, spheres, cylinders or discs. *Journal of Controlled Release*, *5*(1), 23-36. [https://doi.org/10.1016/0168-3659\(87\)90034-4](https://doi.org/10.1016/0168-3659(87)90034-4)
- Ritger, P. L., & Peppas, N. A. (1987b). A simple equation for description of solute release II. Fickian and anomalous release from swellable devices. *Journal of Controlled Release*, *5*(1), 37-42. [https://doi.org/10.1016/0168-3659\(87\)90035-6](https://doi.org/10.1016/0168-3659(87)90035-6)

- Schwartz, J. B., Simonelli, A. P., & Higuchi, W. I. (1968). Drug release from wax matrices I. Analysis of data with first-order kinetics and with the diffusion-controlled model. *Journal of Pharmaceutical Sciences*, 57(2), 274-277. <https://doi.org/10.1002/jps.2600570206>
- Siegel, R. A., & Rathbone, M. J. (2012). Overview of Controlled Release Mechanisms. In Juergen Siepmann, R. A. Siegel, & M. J. Rathbone (Éd.), *Fundamentals and Applications of Controlled Release Drug Delivery* (p. 19-43). [https://doi.org/10.1007/978-1-4614-0881-9\\_2](https://doi.org/10.1007/978-1-4614-0881-9_2)
- Siepmann, J., & Siepmann, F. (2008). Mathematical modeling of drug delivery. *International Journal of Pharmaceutics*, 364(2), 328-343. <https://doi.org/10.1016/j.ijpharm.2008.09.004>
- Siepmann, Juergen, & Peppas, N. A. (2011). Higuchi equation: Derivation, applications, use and misuse. *International Journal of Pharmaceutics*, 418(1), 6-12. <https://doi.org/10.1016/j.ijpharm.2011.03.051>
- Siepmann, Juergen, Siegel, R. A., & Rathbone, M. J. (Éd.). (2012). *Fundamentals and Applications of Controlled Release Drug Delivery*. Consulté à l'adresse [//www.springer.com/us/book/9781461408802](http://www.springer.com/us/book/9781461408802)
- Singh, S. K., & Fan, L. T. (1986). A generalized model for swelling-controlled release systems. *Biotechnology Progress*, 2(3), 145-156. <https://doi.org/10.1002/btpr.5420020309>



## RÉSUMÉ

---

Les aérogels sont des matériaux nano-structurés ultralégers, hautement poreux et présentant une surface spécifique élevée. Les bio-aérogels sont une nouvelle génération d'aérogels entièrement bio-sourcés, offrant de ce fait de grands potentiels pour des applications à l'interface avec le vivant tout en valorisant la biomasse.

Dans le cadre de cette thèse, la pectine a été utilisée pour produire des bio-aérogels. Deux principaux objectifs ont été atteints :

- Le premier était de déterminer et de maîtriser les corrélations existantes entre les caractéristiques de la pectine et les conditions de préparation d'une part, avec la structure interne de l'aérogel et ses propriétés physico-chimiques d'autre part.
- Le second était d'évaluer et développer les aérogels de pectine pour deux applications distinctes : l'isolation thermique et la libération de médicaments.

Il a été établi que les différents mécanismes de formation du réseau, la gélification et la séparation de phase, jouaient un rôle majeur sur la morphologie et les propriétés finales de l'aérogel. La conductivité thermique des aérogels de pectine s'est révélée très faible, de l'ordre de 0,015 à 0,020 W/(m.K), et a présenté une courbe de dépendance en forme de U avec leurs densités. Les aérogels ont également été utilisés en tant que matrices supports de médicament. Les cinétiques de libération du médicament en milieu liquide ont été corrélées aux structures et densités des aérogels de pectine. Des aérogels composites, de type cellulose-pectine et silice-pectine, ont été préparés et utilisés comme supports de médicament menant à une libération prolongée du principe actif dans le temps. Dans cette thèse, nous avons mis en évidence le potentiel élevé des aérogels de pectine utilisés en tant que biomatériaux avancés, versatiles et aux fonctionnalités ajustables.

## MOTS CLÉS

---

Bio-aérogel, pectine, densité, morphologie, libération de médicaments, isolation thermique.

## ABSTRACT

---

Aerogels are ultra-light, highly porous and nano-structured materials with high specific surface area. Bio-aerogels are a new generation of aerogels that are fully biomass-based, which opens up a lot of potentials in biomass valorization and life science applications.

In this work pectin was used to produce bio- aerogels. Two main objectives were achieved:

- The first was to understand and correlate the characteristics of pectin and the preparation conditions with the internal structure of aerogel and its physico-chemical properties.
- The second was to evaluate and develop pectin aerogels as advanced bio-materials for the two different applications: thermal insulation and drug delivery.

Various mechanisms of network formation, gelation and non-solvent induced phase separation, were demonstrated to play a very important role in aerogel morphology and properties. Thermal conductivity of pectin aerogels was very low, around 0.015 - 0.020 W/(m.K), and showing U-shape dependence on density. When used as drug delivery matrices, the kinetics of drug release was correlated with pectin aerogels' structure and density. Composite cellulose-pectin and silica-pectin aerogels were synthesized and also used as drug carriers; a prolonged release was recorded. A high potential of pectin aerogels to be used as versatile bio-materials with advanced tunable functionalities was demonstrated.

## KEYWORDS

---

Bio-aerogel, pectin, density, morphology, drug release, thermal insulation.